NTIA REPORT 01-383

The Temporal and Spectral Characteristics of Ultrawideband Signals

William A. Kissick, Editor

report series

U.S. DEPARTMENT OF COMMERCE ● National Telecommunications and Information Administration

NTIA Report 01-383

The Temporal and Spectral Characteristics of Ultrawideband Signals

William A. Kissick, Editor

U.S. DEPARTMENT OF COMMERCE
Norman Y. Mineta, Secretary

Gregory L. Rohde, Assistant Secretary
for Communications and Information

January 2001

ERRATA

On page C-8 of NTIA Report 01-383, in Equations (C.43) and (C.44), the impedance of free space (377 ohms) should be located in the denominator rather than the numerator.

The correct equations are:

$$\left(P_{\rho}, \mu W / cm^2\right) = \frac{1}{377 \cdot 10^{10}} \left(field\_strength, \mu V / m\right)^2 \qquad \text{(C.43)}$$

$$\left(P_{\rho}, \mu W / cm^2\right) = 2.65 \cdot 10^{-13} \cdot \left(field\_strength, \mu V / m\right)^2 \qquad \text{(C.44)}$$

Disclaimer

Certain equipment and software products are identified in this report to ensure completeness and accuracy in describing the information presented. Such identification, implied or specific, does not represent a recommendation or endorsement of the companies or the products by the National Telecommunications and Information Administration or the National Institute of Standards and Technology.

CONTENTS

EXECUTIVE SUMMARY

Objectives of this Work

A preliminary objective of this study was to develop a description and gain an understanding of the ultrawideband (UWB) signal structure based on current, and hopefully typical, UWB system capabilities and applications. This began with a determination, from specifications and/or direct measurement, of the salient temporal characteristics of UWB signals that included minimal descriptions of their modulation schemes for data and/or voice and detailed descriptions of their pulse shape, width, repetition rate, dithering, and gating characteristics. Then, key fundamental aspects of UWB signal behavior were derived from first principles. This provided a basis for identifying what to measure and the effects certain temporal characteristics have on the spectral characteristics.

The primary objective was to observe and record the temporal and spectral characteristics of various UWB signals using both highly accurate measurement methods and practical approaches with commercial off-the-shelf (COTS) test equipment. The measurements are supported by the theoretical work noted above and confirmed through simulation. Meeting the primary objective has provided the technical information needed by NTIA to develop policies for use of UWB by the Federal government and to work with the Federal Communications Commission (FCC) to develop rules and regulations for UWB emissions. Secondary objectives included the development and description of reliable and repeatable measurement methods using COTS test equipment, and measurement of the effects UWB signals have on several, selected Federal Aviation Administration (FAA) radar systems.

There are unanswered questions and claims regarding UWB. Some say that the 2-GHz bandwidth (nominal, based on a pulse width of 1 ns) is ideal in many applications because the already low total power of a UWB signal is spread so "thinly" that the spectral power density in any conventional (bandwidth limited) channel is inconsequential. The claim goes further to say that the signal is similar to Gaussian, or white, noise and therefore it is like the background noise any communications or radar receiver experiences.

UWB Technology and the Radio Spectrum

UWB technology may offer very effective solutions for various communications and sensing applications; but its uncommon approach of using narrow pulses, or impulses, as a basic signal structure rather than generating and modulating a sinusoidal carrier results in an unusually wide emission bandwidth. Since such a wide signal covers many radio bands and services, the conditions under which it can operate without causing undue interference must be determined before UWB systems are allowed to proliferate.

The use of a carrier signal by nearly all existing services that share the radio spectrum helps ensure that the bandwidth of the emissions of those signals can be kept as narrow as possible for any given application, i.e., the bandwidth required to transmit the information of interest or perform the necessary sensing functions. This approach allows for effective and efficient spectrum management and frequency assignment procedures for sharing of the radio spectrum among diverse applications and users. Can UWB share the radio spectrum with existing users? What frequency-related limits such as emission bandwidth and lower frequency limit should be imposed on UWB signals? Should limits be established for time-related characteristics such as pulse width and pulse repetition rate (PRR)? If UWB systems proliferate, what are the effects of the aggregate of independent UWB signals?

Measurements of Ultrawideband Signals

From over twenty UWB devices available to ITS, five were chosen to be fully measured. This selection represents a sampling of the various UWB signal waveforms in use. This group included communications and sensing devices that used pulse-position and on/off keying modulation methods, some did not incorporate pulse dithering, another used relative dither and yet another used absolute-time-base pulse dithering, one had gated pulse groups.

A very fast transient digitizer was used to capture the individual pulses directly in the time domain (in some cases a sampling oscilloscope was used) at the output of each device (a "conducted" measurement) and "in space" as measured by a known antenna (a "radiated" measurement). Figure ES.1 shows examples: (a) is a narrow impulse about 1.5 ns in length from one of the UWB devices, and (b) is a longer, very complex pulse shape about 15 ns in length from a different device. The former occupies about 3.5 GHz of spectrum and the latter about a fifth or sixth of that. Although some devices generate an impulse like that shown above in ES.1(a), when radiated by an antenna, the impulse may be changed quite dramatically. Figure ES.1(c) shows what the pulse shown in (a) is like after being radiated by an antenna designed to radiate UWB signals.

Measurements of the UWB signal power in various bandwidths were made using spectrum analyzers and it was determined that the measurement of the signal amplitude probability distribution (APD) is a very informative measurand. It shows, sometimes in a dramatic way, the general nature of a UWB source, whether it resembles Gaussian noise or very impulsive noise. Figure ES.2 shows two APD curves on a Rayleigh probability scale. Curve A, actually a straight line, represents a signal that is Gaussian distributed; while curve B is the APD for one of the UWB devices measured. Notice that the signal exceeds about -55 dBm for 1% of the time and exceeds -80 dBm for about 12% of the time that it is on. Both signals here are noise-like; the former, a Gaussian distribution, is a truly random signal and the latter is a highly impulsive signal.

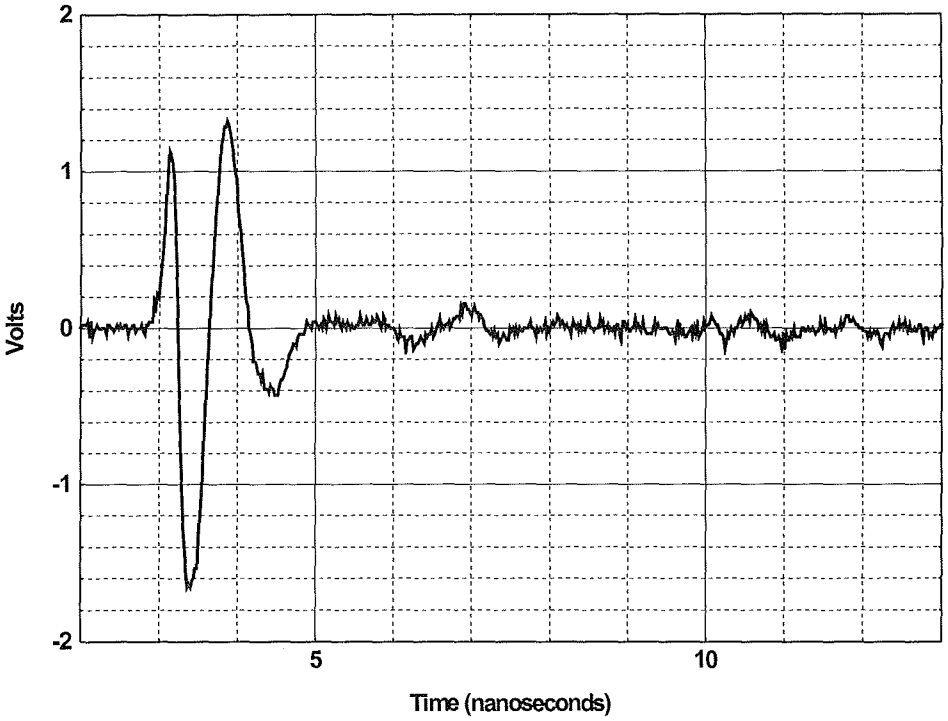

Figure ES.1(a). An example of a short UWB pulse.

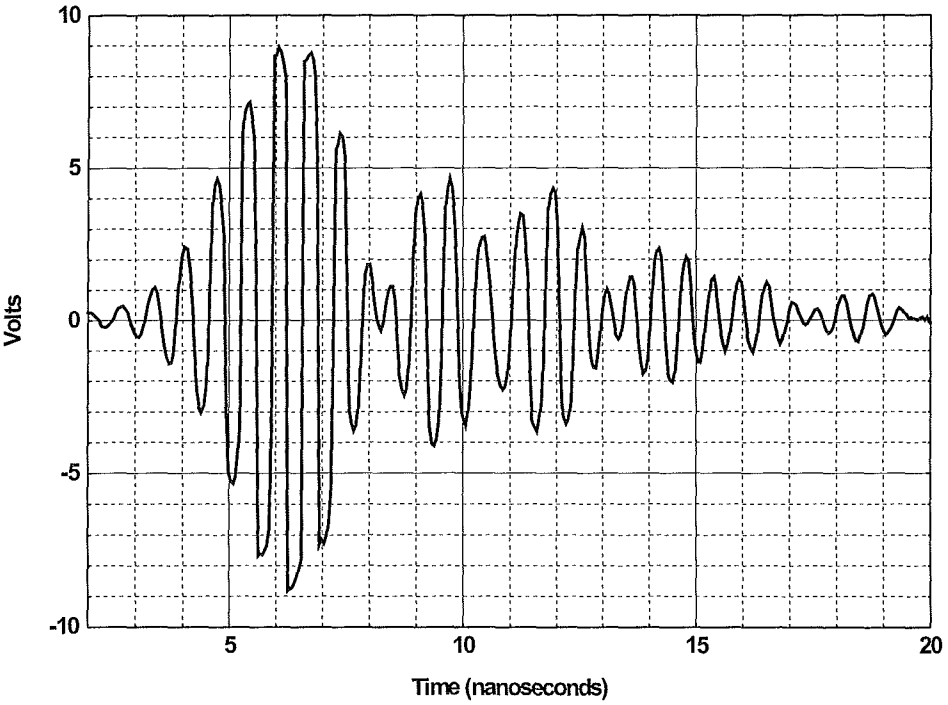

Figure ES.1(b). An example of a long UWB pulse.

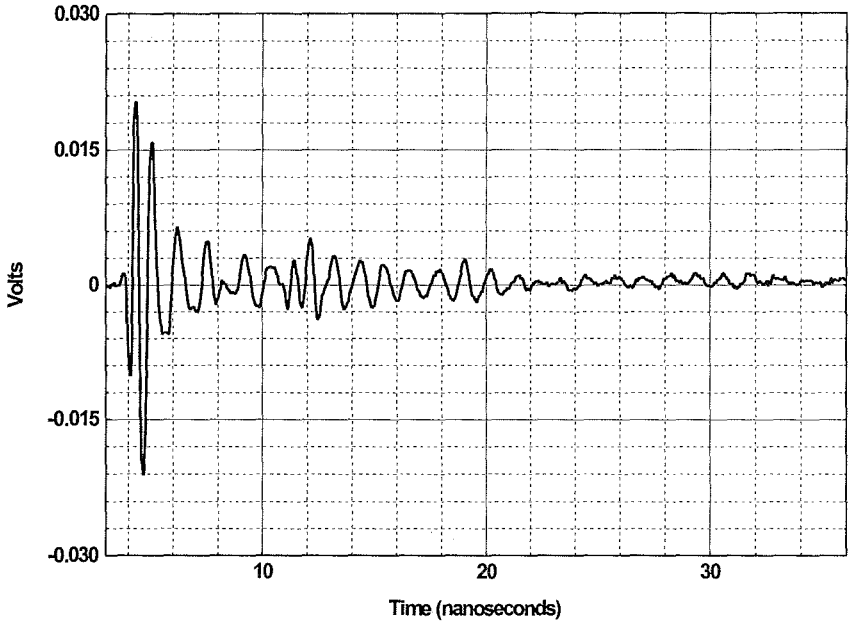

Figure ES.1(c). The shape of the pulse shown in (a) radiated, i.e., "in space."

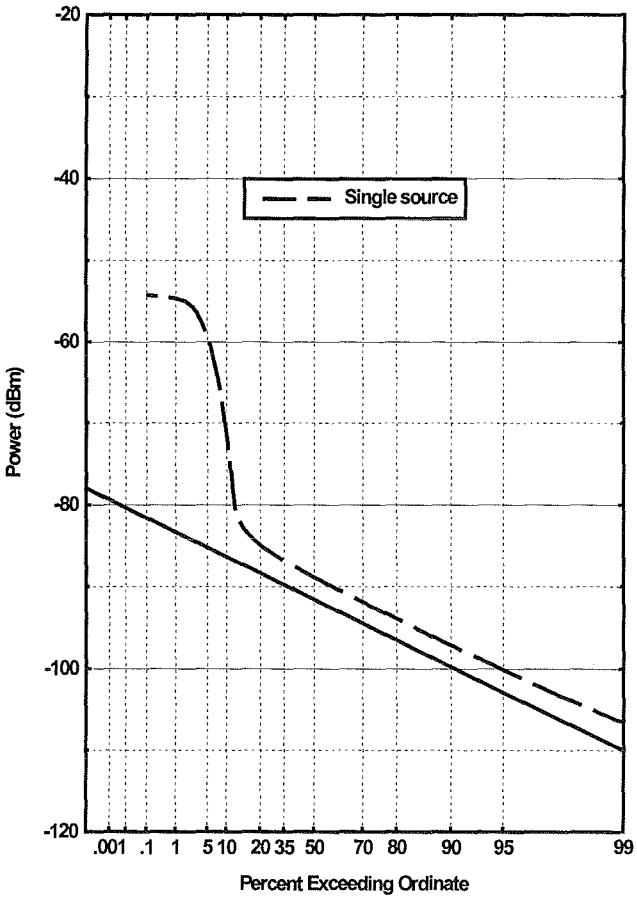

Figure ES.2. APDs for Gaussian noise and a UWB signal.

Companion Report and Other Investigations

The research, observations, measurements, and analyses presented in this report were performed at the NTIA Institute for Telecommunication Sciences (ITS), an independent laboratory located in Boulder, Colorado. The National Institute of Standards and Technology (NIST) Radio Frequency Technology Division, also located in the same building as ITS in Boulder, performed some of the measurements reported herein. The NTIA Office of Spectrum Management (OSM) has used the results of this investigation to examine the options and constraints appropriate for allowing UWB to share the use of the radio spectrum. In their report, a companion to this one, separation distances are developed for widely accepted receiver protection and interference criteria. It discusses the operation of UWB under unlicensed and licensed conditions.

A follow-on research effort at ITS has made use of the knowledge of UWB signal characteristics from this work to develop a test facility to measure the effects of UWB signals on Global Positioning System (GPS) receivers. The results of this GPS interference investigation will be published by ITS in a report similar to this one and OSM will use the GPS receiver performance data to determine the Federal government's position regarding the potential for UWB to share the spectrum, in particular, the GPS band at 1.5 GHz.

THE TEMPORAL AND SPECTRAL CHARACTERISTICS OF ULTRAWIDEBAND SIGNALS

William A. Kissick, Editor[1]

Ultrawideband (UWB) technology, useful for both communication and sensing applications, uses the radio spectrum differently than the vast majority of radiocommunication technologies. UWB systems make use of narrow pulses and time-domain signal processing. Questions regarding how these systems, with their potentially very wide emission bandwidths, might affect the efficient use of the radio spectrum or cause interference to conventional radio and wireless systems must be answered before there is any large-scale deployment of UWB systems. The investigation reported here examined both the temporal and spectral characteristics of UWB signals, since all radio signals exist in both the time and frequency domains. The investigation was approached with theoretical analyses, measurement of actual UWB devices, and computer simulations. The emissions of several UWB transmitters were measured under controlled, and repeatable, laboratory conditions. Those measurement methods useful for routine measurements using commercially-available test equipment were identified. The characteristics of an aggregate of several UWB signals were examined. An initial assessment of the effects of UWB signals on several Federal Government systems was accomplished through field measurements. This report provides a basis for an assessment of the effects of UWB signals on other communication and radar systems, the study of the spectrum efficiency of UWB technologies, and the development of spectrum sharing policies and regulations.

Key words: emissions, aggregate emissions, ultrawideband, UWB, time domain, frequency domain, radio spectrum, average power, RMS power, peak power, signal strength, pulse measurements, spectrum measurements.

1. THE RADIO SPECTRUM AND ULTRAWIDEBAND

William A. Kissick[1]

As the radio spectrum becomes more crowded due to the ever-increasing demand for radio and wireless communications and for sensing, a wide variety of creative approaches have been proposed for allowing more users to share this limited resource. These innovations include new, digital technologies that permit the same amount of information (e.g., an audio signal) to fit into increasingly narrower channels as is occurring in the land mobile radio service; or allow much more information to be transmitted in existing channels as is occurring with high-definition

---

[1]The editor, and author of Section 1, is with the Institute for Telecommunication Sciences, National Telecommunications and Information Administration, U.S. Department of Commerce, Boulder, CO 80305.

television. This investigation is primarily concerned with one such approach called ultrawideband (UWB) technology and its ability to share the spectrum with existing users. There are claims that UWB technology, which uses novel signal generating and processing methods, can use large portions of the already allocated spectrum with minimal or no interference to existing users due to the very low spectral power density of UWB signals. The assessment of that claim is critical to decisions regarding the deployment, and potential ubiquitous use, of UWB devices for both communications and sensing. The radio spectrum, a nondepleting but limited natural resource, is used to support all radio and wireless services for both public and private purposes. Broadcasting, land mobile radio, cellular telephones, radar, satellite communications, remote sensing, and radio astronomy all depend upon the shared use of the radio spectrum which has benefitted mankind for the past century. The rules and regulations that enable this sharing are based on fundamental natural laws (of physics), agreements among proximate users, international treaties, and domestic public law. Spectrum management and frequency assignment represent the disciplines and processes used to allocate bands of the spectrum to various radio services and assign frequencies, each with an associated bandwidth, to individual users. In many cases, users are expected to ensure that their transmitter's emissions do not adversely affect existing users.

This approach is based on the fact that all electromagnetic signals can be both electronically generated and separated by the frequency of those signals. Essentially, all conventional signals use a single-frequency signal – a sinusoidal (sine) wave called a carrier that is modulated with the information it is to "carry." Its amplitude, frequency, or phase is varied according to the information (e.g., voice, video, or data) to be carried.

Radio and wireless communications are managed using tools and techniques that describe signals in the frequency domain; however, it is very important to recognize that every signal exists simultaneously in both the frequency domain and the time domain. These domains are simply alternative ways of describing and processing electronic and electromagnetic (radio) signals. This is easy to visualize. The cycling of a simple sine wave is the time domain perspective and its existence at a single frequency is the frequency domain perspective.

Using a carrier allows good control over the bandwidth any signal occupies and has been an enormously effective approach for dividing the radio spectrum by bands and channels, which has enabled tractable and effective sharing of the spectrum. It has always been possible, however, to generate signals without a carrier. In the case of UWB, these signals are simply pulses of electromagnetic energy shaped by electronic circuitry and a transmitting antenna. Recent advances in electronics and microcircuits have allowed the development of communications and radar systems that use such carrierless pulses. It is a fundamental physical law that the narrower the pulse in the time domain, the wider the emission in the frequency domain.

A classic radar is an example of a device that requires signal processing in both the frequency domain and the time domain. It has a carrier. Pulses of that carrier are transmitted periodically. Reflections of that signal from a target return to the point of origin. The radar receiver uses a filter in the frequency domain to select only that small portion of the spectrum where the radar signal exists. Then, the receiver uses time domain processing to determine how long it took the reflection to return and thus determine the distance to the target.

1.1 Objectives of this Work

The primary objective of this investigation was to develop an understanding of UWB signal characteristics based on several currently available devices. Both temporal and spectral characteristics of the UWB signals were sought, with the latter being of particular interest. The nature of the emission spectrum, whether smooth, comprised of lines, or a combination of both, is needed for interference analyses. How that emission spectrum depends on the temporal characteristics such as UWB pulse width, type of signal modulation, and the use of dithering may be needed to develop sharing policies and regulations. Finally, the nature of the aggregate of many individual UWB signals is important in understanding how the radio spectrum might be affected if and when large numbers of UWB devices are deployed.

Practical and repeatable measurement methods to obtain values for particularly useful UWB signal parameters with available commercial-off-the-shelf (COTS) test equipment may also be needed for compliance testing related to regulation. Where possible, these practical methods are identified and any limitations are described. Highly accurate time domain measurements are used to ensure that the COTS-based measurement methods are reliable.

Finally, an initial assessment of the effects of UWB signals on existing systems will indicate if, and how much, additional work is needed in this area. A limited effort to determine how much UWB signal power can pass through the front-end (antenna, amplifiers, and filters) of selected receivers provides a basis for more detailed investigations of the effects on victim system performance and allows the calculation of desired signal-to-noise and interference-to-noise ratios for the selected systems.

1.2 Specific Ultrawideband Systems Measured

The actual UWB emitters used in this work were borrowed from a number of sources, including UWB device manufacturers and owners of systems that contain UWB devices or that use UWB signals to perform their functions. These included prototype, experimental, and operational systems. Since the objectives of this work were to understand and characterize the radiated signals and not to evaluate the performance of the systems, the sources of UWB equipment are not identified. Of the dozen or so devices available, five were selected for the measurements described in subsequent sections of this report, and are labeled with letters, e.g. Device A. For comparison, the emissions of an electric drill were also characterized. It is identified simply as "electric drill." The devices selected are intended to provide a realistic sample of the various UWB signal structures being used today.

1.3 Organization of this Report

This investigation of UWB signal structure involved a number of aspects ranging from theoretical analyses to measurements, both in the laboratory and field, and computer simulations. As is often the case with broad investigations such as this, a number of workers with different

skills were involved. To give proper credit to the researchers in each area, the author (or authors) of each major section of the report is identified at the beginning of each section. The editor was responsible for assembling the full report.

The first two sections provide orientation and background for the reader. This section contains some essential background information and the objectives of the work. Section 2 provides the reader with a brief technical description of UWB technology and some of its salient applications; this same section also gives a brief history of UWB development and early applications. It also contains a brief overview of the regulatory issues.

Sections 3 and 4 examine the UWB signal from first principles. Using typical temporal characteristics of UWB waveforms, the associated spectral characteristics are derived in Section 3. Then in Section 4, the characteristics of a group of individual UWB signals, called the aggregate signal, is examined.

Sections 5 through 7 describe a variety of measurements of UWB signals and their effects on selected receivers. Section 5 describes the procedures and results for fundamental measurements in the time domain. Where possible, the waveform of individual pulses is obtained. Section 6 describes procedures for, and results of, making similar measurements using commercially-available test equipment. This section also describes procedures for, and results of, band limited spectral measurements. Section 7 describes the effects that were observed in the receivers of several Federal Government systems. These measurements do not include an assessment of the overall performance of those systems; only those effects that are observable in the radio-frequency (RF) or intermediate-frequency (IF) sections of those systems.

Section 8 summarizes the observations made throughout this investigation. These observations include: the general character of UWB signals (spectra) based on theoretical analyses (Sections 3 and 4); the nature of the actual UWB pulses, both conducted and radiated (Section 5); the nature of the UWB signal in both the time and frequency domains when received in a range of bandwidths (Section 6); and the effects on selected receivers (Section 7). Other observations include which procedures may be best suited for other laboratories that may have only commercial-off-the-shelf (COTS) test equipment; and the effects various detectors have on measurements.

Section 9 contains a comparison of results from measurement, theory, and simulation.

The Appendices to this report contain supporting information and detailed measurement results. Appendix A is a brief tutorial on the amplitude probability distribution (APD) which was chosen as a key measurand for this work. Appendix B describes simulations on the UWB signal temporal and spectral characteristics of a UWB signal when passed through a limited bandwidth (receiver or test instrument). Appendix C describes how to convert and/or correct certain measured values. Appendix D contains the measured data for the five UWB devices and an electric drill. Appendix E contains the measured data for an aggregate of two, independent UWB signals.

2. UWB TECHNOLOGY AND REGULATORY ISSUES

William A. Kissick and Robert J. Matheson[1]

The term "ultrawideband" refers to the spectral characteristics of this technology and originates in the work that led up to a Department of Defense (DoD) study [1]. Alternative terms for the same technology include impulse radar, impulse radio, carrierless, carrier-free, time-domain, and others. The fundamental principle is that a short (in time) pulse, also called an impulse, is generated, transmitted, received, and processed. A fundamental principle, true for any radio signal, is the relationship between pulse duration and the bandwidth occupied by that signal.

According to the theoretical Fourier transform, a pulse of duration T seconds (in the time domain) has an occupied bandwidth of 2/T Hertz (in the frequency domain). For example, a pulse on the order of a nanosecond in the time domain occupies about two gigahertz of bandwidth in the frequency domain. An example of time domain signal processing is pulse-position modulation (PPM). Consider the transmission of a train of pulses equally spaced in time. The receiver processing determines whether each received pulse is located where expected or arrives early or late. With PPM, a slightly retarded pulse could represent a "0" and a slightly advanced pulse could represent a "1" when transmitting digital information.

2.1 History of Ultrawideband Technology

One could say that the first wireless[2] system demonstrated by Gugliermo Marconi in 1897 [3], meets the description of UWB radio. Marconi's earliest spark-gap transmitters occupied a large portion of the spectrum, from very low frequencies up through the high-frequency (HF) band and beyond. And, these systems used manual time domain processing. Morse code was sent and received by human operators.

The foundations of modern UWB systems were laid down in work done at the Sperry Research Center in the 1980's by Ross [4]. The emphasis was on the use of UWB as an analytical tool to explore the properties of microwave networks and to determine the intrinsic properties of materials [4,5]. These techniques were then logically extended to support experimental analysis and synthesis of antenna elements [6,7]. These early successes led to the development of an indoor system to measure the impulse response properties of targets or obstacles [8]. This

---

[1]The authors are with the Institute for Telecommunication Sciences, National Telecommunications and Information Administration, U.S. Department of Commerce, Boulder, CO 80305.

[2]The term "radio" did not exist until 1912 [2]. It is a shortened form of "radioconductor" (a contraction of radiation conductor). "Wireless" was the common term before 1912.

approach of using "short-range radar" obviated the need for an expensive anechoic chamber to study radar targets, since unwanted reflections from walls and ceilings could be removed by time-gating techniques.

The use of UWB, with its time domain processing techniques, filled an important need in the early days of computer development. The appearance of high-speed, sub-nanosecond logic circuitry in the late 1960s and early 1970s made higher speed computation possible. However, it was necessary to deliver and distribute large amounts of digital data between the computer central processor and various input and output devices. This problem was solved by using multiplexing of multiple signals on a single transmission line using time-domain processing methods described in a patent by Ross, et al. [9]. This patent could be viewed as a key element in the foundation of UWB communications. It is a small step from this work to developing wireless UWB communications. Further developments during the 1970s led to a more thorough development of principles needed to fully describe and develop the field of time-domain electromagnetics [10, 11, 12].

In the 1980s and 1990s the principles of time domain electromagnetics were applied to wireless communications, in particular to short-range communications in dense multipath environments. Schotz [13] describes this application in detail and explores the advantages and disadvantages. He showed that a large number of such systems could operate in the same space and that such wide bandwidth signals are more immune to the deleterious effects of multipath than are narrow bandwidth signals. A potential application for UWB communications is the accommodation of many users in high-multipath environments, but the challenge is coexistence within the already highly-populated radio spectrum. The advantages may or may not outweigh the disadvantages, and other approaches to wireless operation in dense, high-multipath environments may perform as well as the UWB approach.

The other major application area of UWB technology is sensing, with the likely niche being short-range, high-resolution radar. This area requires much less signal processing and uses much simpler electronics, but has not received as much attention as the more complex communications applications. Ground penetrating radar was one of the first applications [14]. In 1974, Morey [15] patented a radar system that, due to the use of a very wide band of frequencies, was able to penetrate the ground to distances of one to several meters. This patent was later the basis of a commercial success.

2.2. Regulatory Issues

After receiving three requests by UWB developers, the Federal Communication Commission (FCC) issued a Notice of Inquiry (NOI)[3], to gather information on the possible uses of UWB devices. Many comments were received in response to that NOI. The FCC also issued the

[3]OET Docket 98-153, NOI issued Sept 21, 1998.

requested three waivers for a limited number of each of the three low power UWB devices after coordination on the technical limitations required by NTIA to approve the proposals[4]. Information gathered by that NOI led the FCC to release a Notice of Proposed Rule Making (NPRM) in May 2000. The major regulatory issues in that NPRM are centered on the question of how much interference UWB systems might cause to existing radio systems.

The FCC and NTIA jointly manage the radio spectrum in the United States. Part 15 of Volume 47 of the Code of Federal Regulations (47 CFR- Part 15) contains the FCC rules for authorizing non-licensed operation of low power radio devices that typically radiate signals in bands licensed for other types of devices. The current Part 15 rules define three classes of radiators: Incidental Radiators (which do not deliberately generate the RF signals they emit and are not regulated; e.g., an electric drill), Unintentional Radiators (which need to generate RF signals, but do not intend to radiate them, e.g., a computer), and Intentional Radiators (which deliberately radiate low-level radio signals, e.g., a garage door opener). The NPRM proposes that UWB devices be operated under a new section of the Part 15 rules, with approximately the same numerical limits for new UWB devices as for the existing intentional radiators.

Major regulatory issues include a determination of what numeric limits should apply to UWB emissions and what techniques should be used to measure those emissions. The NPRM proposes numerical limits and measurement techniques identical to those described in current Part 15 rules for Intentional Radiators, with the addition of a maximum total absolute peak limit or a possible peak limit measured in a 50-MHz bandwidth.

Important related questions include whether these limits should be lower in specific restricted frequency bands used by the Federal Government for particularly critical applications, including the Global Positioning System (GPS). These critical frequency bands have already been identified in the existing Part 15 rules, and Intentional Radiators are prohibited from deliberately radiating signals in any of these identified critical bands. Since UWB systems will typically radiate energy in frequency bands managed by NTIA, as well as frequency bands managed by the FCC, the two agencies must concur on the new rules.

2.3 References

[1] "Assessment of Ultra-Wideband (UWB) Technology," July 13, 1990. DTIC No. ADB146160. The Executive Summary of this report is published in the *IEEE Aerospace and Electronics Systems Magazine*, Nov. 1990. pp 45-49.

[2] W.F. Snyder and C.L. Bragaw, "Achievement in Radio," NBS Sp. Pub. 555, Oct. 1986.

[3] W.L. Weeks, *Antenna Engineering*, McGraw-Hill, 1968.

[4]Three waivers granted by Chief of OET, June 25, 1999, after coordination with NTIA.

[4] G.F. Ross, "The transient analysis of certain TEM mode four-post networks," IEEE Trans. on Microwave Theory and Tech., Vol. MTT-14, p. 528, Nov. 1986.

[5] A.M. Nicholson and G.F. Ross, "The measurement of the intrinsic properties of materials by time-domain techniques,"IEEE Trans. on Instrum. and Meas., Vol. IM-9, pp. 377-382, Nov. 1970.

[6] G.F. Ross, "A new wideband antenna receiving element," 1967 NREM Conference Symposium Record, Boston, MA, Nov. 1967.

[7] P. Fenster and G.F. Ross, "Members of the class of TEM-mode wire antennas with TLIR" presented at the IEEE International 1968 PGAP Symp., Boston, MA, Sept. 1968.

[8] A.M. Nicholson and G.F. Ross, "A new radar concept for short-range application." Proceedings of IEEE first Int. Radar Conf., pp. 146-151, Washington, D.C. Apr. 1975.

[9] G.F. Ross, L. Susman, and E. Eves, "Time-domain multiplexer-demultiplexer for digital transmission of GHz data," U.S. Patent No. 3,763,318, Oct. 1973.

[10] G.F. Ross, "A time-domain electromagnetics bibliography," Sperry Research Center, Report SCC-RR-75-1, Mar. 1975.

[11] C.L. Bennett and G.F. Ross, "Time-domain electromagnetics and its applications," Proceedings of IEEE, Vol. 66, No. 3, Mar. 1978.

[12] E.K. Miller (Ed), *Time domain measurements in electromagnetics*, Van Nostrand Reinhold, 1986.

[13] R.A. Scholtz, "Impulse Radio," IEEE PIMRC 97, Helsinki, Finland, 1997.

[14] D.L. Moffat and R.J. Puskar, "A subsurface electromagnetic pulse radar," Geophysics, Vol. 41, pp. 506-518, 1976.

[15] R.N. Morey, "Geophysical survey system employing electromagnetic impulses," U.S. Patent No. 3,806,795, Apr. 1974.

3. ANALYTICAL DESCRIPTION OF TIME AND SPECTRAL CHARACTERISTICS OF ULTRAWIDEBAND SIGNALS

Roger A. Dalke[1]

3.1 Introduction

A theoretical analysis of UWB signals can provide important insights into how UWB emissions affect various types of RF communications devices. In addition to allowing for direct calculation of interference effects, analytical results can be used to aid in the planning, design, and validation of measurements. This section details the results obtained from an analysis of proposed UWB pulse position modulation schemes.

The approach used in the analysis and the results are presented in this section. The mathematical details will be published elsewhere.

3.2 Power Spectrum of UWB Signals

The power spectral density is the average power in the signal per unit bandwidth and hence provides important information on the distribution of power over the RF spectrum. The power spectral density for a UWB pulse position modulation scheme using short duration pulses transmitted at some nominal pulse repetition rate (PRR) is given in this section. The pulse position is randomized or *dithered* with respect to the nominal pulse period. The randomization scheme analyzed in this section is referred to as *fixed time-base dither.*

3.2.1 UWB Signals Using Fixed Time-base Dither

In the fixed time-base dither scheme, each pulse occurs at the nominal pulse period, T, minus a time increment randomly distributed over a fraction of the nominal period as given in Equation 3.1. This expression also includes binary pulse modulation as proposed for communications applications.

$$x(t) = \sum_{n=-\infty}^{\infty} \sum_{k=0}^{1} \alpha_{kn} p_k(t - nT - \theta_n) \quad , \tag{3.1}$$

---

[1]The author is with the Institute for Telecommunication Sciences, National Telecommunications and Information Administration, U.S. Department of Commerce, Boulder, CO 80305.

where p_k represents the pulse shape that corresponds to an information bit (e.g., p_0 represents the value 0, p_1 represents the value 1). The coefficients α_{kn} are related to whether the n[th] information bit a_n has the value 0 or 1 as follows:

$$\alpha_{kn} = \begin{cases} 1 - a_n & k = 0 \\ a_n & k = 1 \end{cases} \quad , \qquad a_n = \begin{cases} 0 \text{ with prob } g_0 \\ 1 \text{ with prob } g_1 = 1 - g_0 \end{cases} \tag{3.2}$$

where g_k are the information bit probabilities (i.e., g_0 is the probability of a bit having the value 0, and $g_1 = 1 - g_0$ is the probability of a bit having the value 1). Finally, the random variables θ_n define the pulse randomization or *dithering* and are described by a density function $q(\theta)$, where

$$\Pr\{\theta \le \Theta \le \theta + d\theta\} = q(\theta)d\theta \quad . \tag{3.3}$$

For fixed time-base dither, the random variables θ_n and a_n are each assumed to be independent and identically distributed (iid).

It should be noted that the signal given in Equation 3.1 is quite general in terms of the pulse shape, binary modulation method, and pulse randomization statistics. Hence, the results presented in this section can be used to predict the power spectral density at various points in the radio link between an interfering UWB transmitter and a victim receiver (e.g., at the output of the UWB transmitter, the UWB signal radiated from a particular antenna, or in the IF section of a *narrowband* RF receiver). When dealing with linear systems, the various pulse shapes are simply related by convolutions with the appropriate transfer functions.

The power spectral density is the Fourier transform of the autocorrelation function. The autocorrelation function is obtained by taking the expected value of the signal at two different times which is expressed mathematically as

$$r_{xx}(t,s) = \mathcal{E}\{x(t)x(s)\} = \mathcal{E}\left\{\sum_n \sum_m \sum_k \sum_\ell \alpha_{kn}\alpha_{\ell m} p_k(t - nT - \theta_n) p_\ell(s - mT - \theta_m)\right\} \quad . \tag{3.4}$$

Taking the expectation in Equation 3.4 yields

$$r_{xx}(t,s) = \frac{1}{T^2}\left\{\sum_n \left|\sum_{k=0}^{1} g_k P_k(\frac{n}{T})\right|^2 \left|Q(\frac{n}{T})\right|^2 e^{i2\pi n\tau/T} + \right.$$

$$\left. \sum_{n\neq m} \left(\sum_{k=0}^{1} g_k P_k(\frac{n}{T})\right)\left(\sum_{k=0}^{1} g_k P_k(\frac{m}{T})\right) Q(\frac{n}{T})Q(\frac{m}{T}) e^{i2\pi(nt+ms)/T}\right\}$$

$$+ \qquad (3.5)$$

$$\frac{1}{T}\sum_n e^{i2\pi ns/T}\left\{ Q(\frac{n}{T}) \sum_{k=0}^{1} g_k p_k(\tau) \circledast p_k(-\tau) e^{i2\pi n\tau/T} - \right.$$

$$\left. \left(\sum_{k=0}^{1} g_k p_k(\tau) \circledast \sum_{\ell=0}^{1} g_\ell p_\ell(-\tau) e^{i2\pi n\tau/T}\right) \circledast \left(q(\tau) \circledast q(-\tau) e^{i2\pi n\tau/T}\right)\right\}$$

were the symbol $\circledast$ is the convolution operator and $\tau = s - t$ is the time lag. Functions given in upper case letters (P, Q) are the Fourier transforms of the pulse and dithering functions.

The statistics for this process are periodic with period T as is evidenced by Equation 3.5. Such processes are commonly referred to as *cyclostationary*. Essentially this means that the statistics depend upon when the process is observed during a period. The victim receiver may observe the process at an arbitrary time during a period and hence it is useful (and simplifying) to calculate the average over all possible observation times within a period. Taking the time average over one period and the Fourier transform of Equation 3.5 yields the average power spectral density of the fixed time-base dithered UWB signal

$$\bar{R}_{xx}(f) = L + C$$

$$L = \frac{1}{T^2}\left|\sum_{k=0}^{1} g_k P_k(f)\right|^2 \left|Q(f)\right|^2 \sum_n \delta(f - n/T) \qquad (3.6)$$

$$C = \frac{1}{T}\left[\sum_{k=0}^{1} g_k |P_k(f)|^2 - \left|\sum_{k=0}^{1} g_k P_k(f)\right|^2 \left|Q(f)\right|^2\right] \quad .$$

The power spectral density has both discrete L and continuous C components that depend on the pulse spectrum and the Fourier transform of the density function used to randomize the signal. Note that when $Q(f)$ is small at multiples of the PRR, the discrete components are small and the spectrum is predominantly continuous. When $Q(f)$ approaches one (negligible dithering) and

the bits do not change (e.g., $g_0 = 1$), the continuous spectrum disappears, and the line spectrum dominates. The quantity $g_0 P_0(f) + g_1 P_1(f)$ is the expected value of the pulses.

If bit values are equiprobable (i.e., $g_k = 1/2$) and the pulse representing a 1 is a time delayed version of the pulse representing a 0 (i.e., $p_1(t+\xi) = p_0(t) \equiv p(t)$), equation 3.6 reduces to

$$\bar{R}_{xx}(f) = L + C$$

$$L = \frac{1}{2T^2} |P(f)Q(f)|^2 [1 + \cos(2\pi\xi f)] \sum_n \delta(f - n/T) \qquad (3.7)$$

$$C = \frac{1}{T} |P(f)|^2 \left(1 - \frac{|Q(f)|^2 [1 + \cos(2\pi\xi f)]}{2} \right) \quad .$$

When the information bit time delay ξ is small relative to the to the dithering delay (i.e., $\cos(2\pi\xi f) \approx 1$ over the range of frequencies for which $Q(f)$ is significant), the effects of pulse position modulation on the power spectrum are inconsequential.

The results of an example calculation using Equation 3.7 are shown in the following figures. For this example, the signal consists of a short-duration pulse (Figure 3.1) transmitted at a 10 MHz PRR. The dithered pulse position is random and uniformly distributed over 50% of the pulse period. In this calculation, it is assumed that the effects of information bit modulation are negligible over the frequency range of interest. The power spectral density over a frequency range of 1-5000 MHz is shown in Figure 3.2. The magnitude of the spectrum is normalized to the peak of the continuous distribution (at about 250 MHz). The Fourier transform of the density function for this example is $Q(f) = sinc(\pi f T/2)$. This function has nulls at frequencies equal to $2k/T$ ($k = \pm 1, \pm 2, \pm 3, \ldots$), hence the interval between discrete spectral lines is 20 MHz as shown in the figures. For frequencies above 20 MHz, the continuous spectrum is approximately the same as the pulse spectrum (i.e., $P(f)$). Figure 3.3 shows the discrete spectrum over a more limited range (800-1600 MHz) to highlight the individual spectral lines.

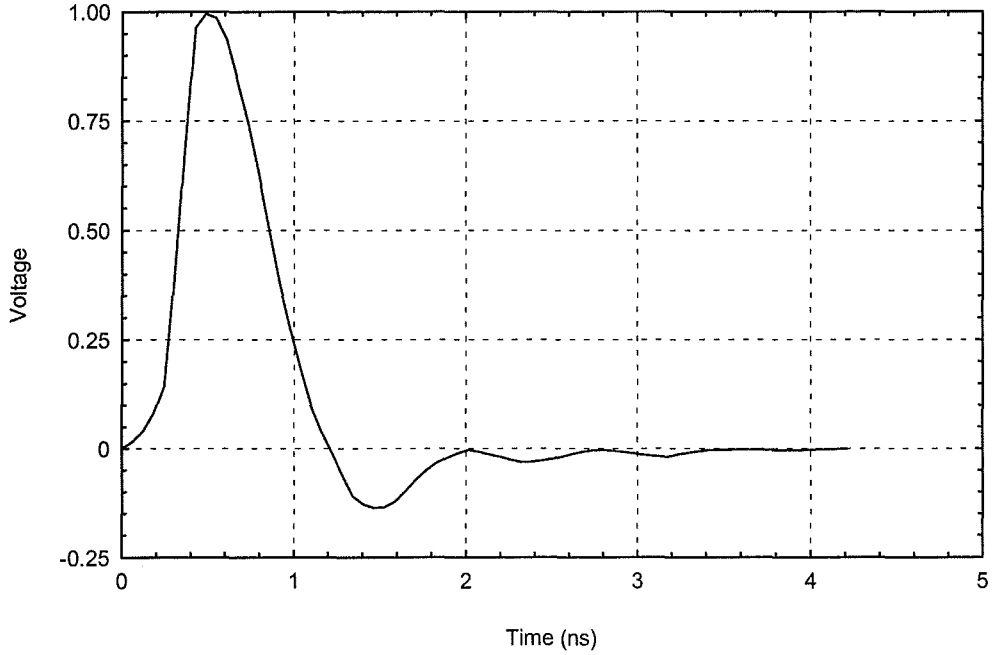

Figure 3.1. Time domain pulse shape.

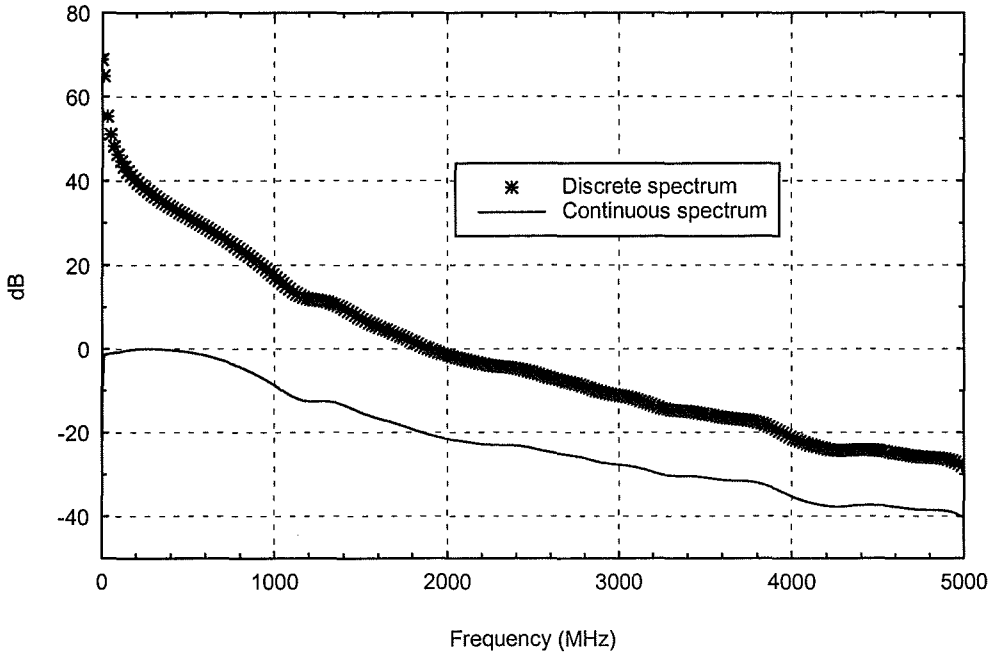

Figure 3.2. Power spectral density for a fixed time-base dithered 10 MHz UWB signal. The pulse positions are uniformly distributed over 50% of the pulse repetition period.

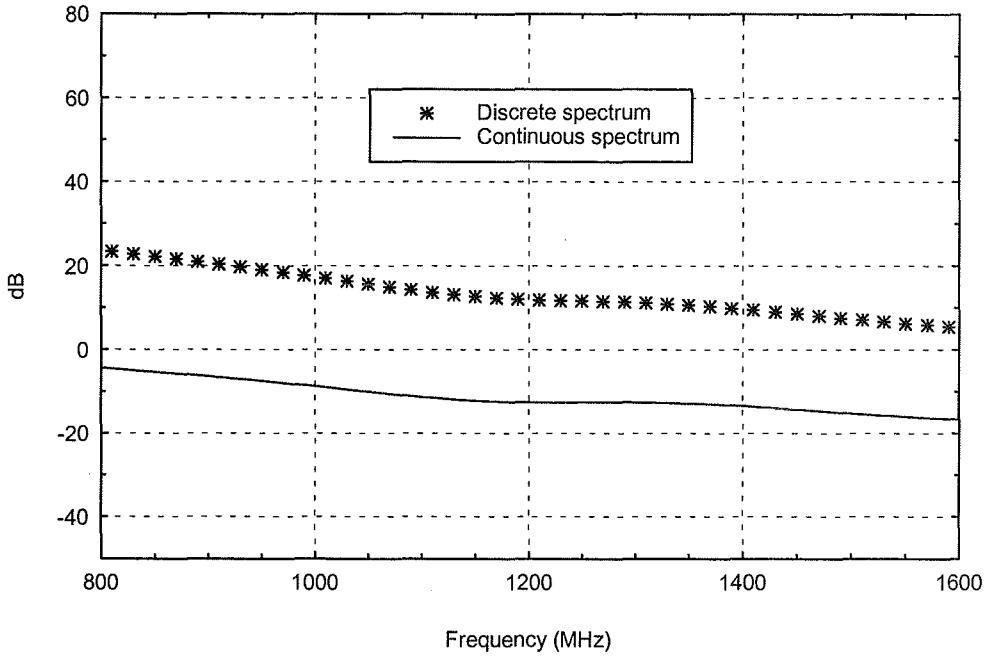

Figure 3.3. Power spectral density showing discrete and continuous spectrum from 800 to 1600 MHz.

The mean power in the bandwidth of a *narrowband* victim RF receiver as a function of frequency can easily be calculated from these results. For example, Figure 3.4 shows the power available to a receiver with a nominal 10 kHz bandwidth. As shown in the figure, the discrete spectrum is not a factor for RF frequencies above a few hundred MHz. For narrowband victim receivers where gains due to the UWB transmitter filters/antenna, propagation channel, and receiver are fairly constant over the receiver bandwidth, the received interference power can easily be calculated by applying the appropriate gain factors to the power in the receiver bandwidth at the center frequency of the receiver.

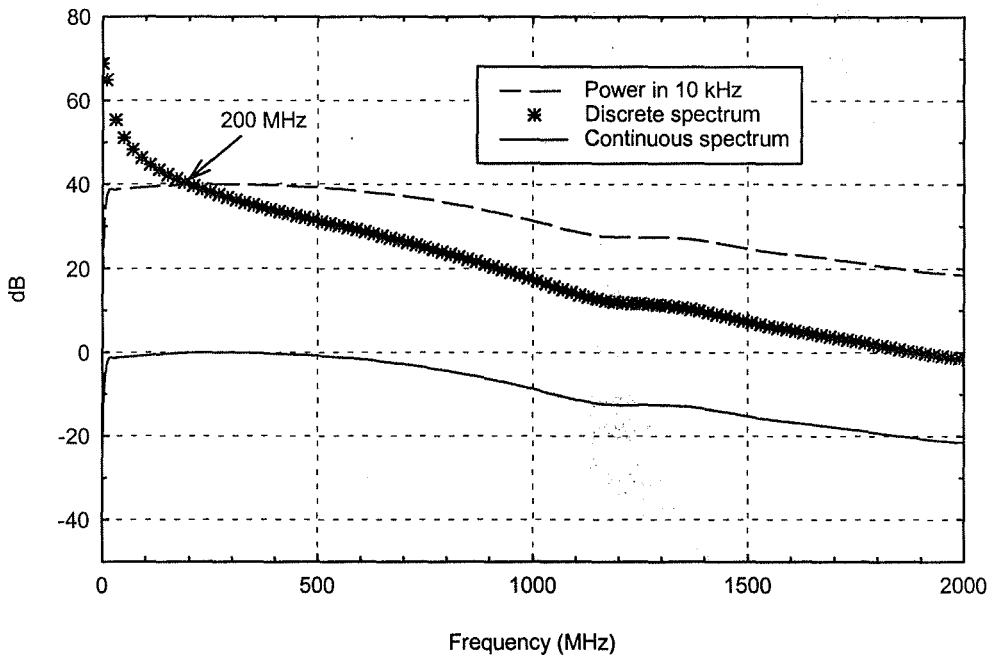

Figure 3.4 Power spectral density showing the continuous spectrum in a 10 kHz bandwidth compared to the discrete spectrum.

3.2.2 Power Spectrum for Finite Duration and Repeated Signals

The results based on Equation 3.1 assume that the signal is on continuously. Obviously, real signals are of finite duration. Also, for some proposed systems, the signal is transmitted for a length of time, say T', and then repeated. In this section, we extend the results presented above to finite duration and repeated signals.

To obtain the power spectrum for a finite duration signal, the following window function

$$w(t) = \begin{cases} 1 & -T' \le t \le T' \\ 0 & else \end{cases}$$
$$W(f) = 2T' sinc(2\pi T' f) \tag{3.8}$$

is multiplied by $x(t)$ (Equation 3.1). The result is that given in Equation 3.7 convolved with the spectrum of the window, i.e., $|W(f)|^2 \circledast \bar{R}_{xx}(f)$ as may be expected. As the window duration increases, the spectrum shape approaches $\bar{R}_{xx}(f)$.

When the series $x(t)$ is windowed and repeated, the autocorrelation function is obtained by taking the expectation of periodic extension of a windowed portion of the series or

$$\mathscr{E}\left\{\sum_{n=-\infty}^{\infty} w(t-nT')x(t-nT')\sum_{m=-\infty}^{\infty} w(s-mT')x(s-mT')\right\} \tag{3.9}$$

The resulting spectrum is

$$\frac{1}{T'^2}\sum_k \bar{R}_{xx}(\frac{k}{T'})\circledast|W(\frac{k}{T'})|^2 e^{i2\pi k\tau/T'} \quad , \tag{3.10}$$

which is now discrete with *spectral lines* at frequency intervals of $1/T'$.

3.3 Band Limited Signal Statistics for Fixed Time-base Dithered Systems

From the standpoint of a victim receiver, a fixed time-base dithered UWB signal is a random process. A knowledge of the statistics of such a process is important in predicting how interference affects the performance of a victim receiver. When the UWB PRR is larger than the receiver bandwidth, it may be expected that the received signal would appear to be indistinguishable from Gaussian noise. Since receiver performance in a Gaussian noise environment is well understood, quantifying conditions for which the received UWB interference resembles Gaussian noise is important in predicting receiver performance and developing emissions requirements. Also, when the received signal is Gaussian, only one parameter (mean power) is required to characterize the process. In this section we present the results of an analysis of the fixed time-base dither scheme that can be used to predict when the received UWB signal is approximately Gaussian.

For this analysis, we seek to determine the probability density function that describes the statistics of the UWB signal as seen by the victim receiver (e.g., the final IF stage of the receiver). The following relationship between the density function $a(y)$, its characteristic function $\phi(u)$, and the pulse randomization density function $q(\theta)$ is used to obtain an approximate expression for the received signal statistics

$$\phi(u) = \int e^{iuy} a(y)dy = \mathscr{E}\left\{e^{iux}\right\} = \int e^{iux(\theta)} q(\theta)d\theta \quad . \tag{3.11}$$

Formally, the desired density function is obtained by inserting the UWB signal $x(t)$ (Equation 3.1) into Equation 3.11 and taking the inverse Fourier transform of the characteristic function.

The characteristic function is periodic since the process is cyclostationary as discussed in Section 3.2.1. For purposes of this analysis, the time averaged statistics are obtained by averaging over a period as with the power spectral density function

$$\bar{\Phi}(u) = \int_0^T \prod_n \int e^{iup(t-nT-\theta)} q(\theta) d\theta \frac{dt}{T} \quad . \tag{3.12}$$

After some manipulations, the density function can be expanded into the well known Edgeworth [1] series. The first four terms of the series are

$$f(x) = \varphi^{(0)}(x) - \frac{\gamma_1}{3!}\varphi^{(3)}(x) + \frac{\gamma_2}{4!}\varphi^{(4)}(x) + \frac{10\gamma_1^2}{6!}\varphi^{(6)}(x) \quad , \tag{3.13}$$

where

$$\varphi^{(n)}(x) = \frac{d^n}{dx^n}\frac{1}{\sqrt{2\pi}}e^{-\frac{x^2}{2}} \quad . \tag{3.14}$$

The desired density function $a(y)$ is related to $f(x)$ by using the transformation $x = (y - m)/\sigma$ where m is the mean and σ is the standard deviation, hence $a(y) = f((y - m)/\sigma)/\sigma$. The first term in the series is the standard normal distribution. The following terms are scaled by coefficients known as the skewness γ_1 and excess γ_2 [1].

In general, the skewness and excess are rather complicated functionals of the pulse shape p and the pulse randomization statistics q. In the case of a narrowband receiver with a center frequency larger than twice the PRR, the expressions are greatly simplified. The following results assume that the power in the spectral lines (if present) is much smaller than that due to the power in the receiver bandwidth due to the continuous spectrum. In addition, if the UWB pulse $P(f)$ spectrum is approximately constant over the bandwidth of the receiver, the variance σ^2, skewness, and excess can be expressed in terms of the baseband impulse response of the receiver filter, $h(t)$, as follows:

$$
\begin{aligned}
m &\approx 0 \\
\sigma^2 &\approx \frac{1}{2T}\int_{-\infty}^{\infty} h^2(t)\,dt = \frac{1}{2T}\int_{-\infty}^{\infty} |H(f)|^2\,df \\
\gamma_1 &\approx 0 \\
\gamma_2 &\approx \frac{3}{4\sigma^4 T}\int_{-\infty}^{\infty}\left[\frac{h^4(t)}{2} - (h^2 \circledast q(t))^2\right]dt
\end{aligned}
\tag{3.15}
$$

These results show that the variance is proportional to the receiver bandwidth as expected. The mean and skewness are negligible due to the oscillatory characteristics of the bandpass filtered signal. The behavior of the excess as a function of receiver bandwidth was calculated for a receiver with a raised cosine lowpass characteristic and a UWB signal with a 10 MHz PRR. The signal is dithered uniformly over 50% of the pulse repetition period.

Figure 3.5 shows the excess as a funtion of receiver bandwidth. Note that the distribution is approximately Gaussian up to about a 1MHz bandwidth. The excess then decreases to a minimum at about 20 MHz, after which it increases. The normalized distribution for bandwidths below 1 MHz and at10 and 20 MHz are shown in Figure 3.6.

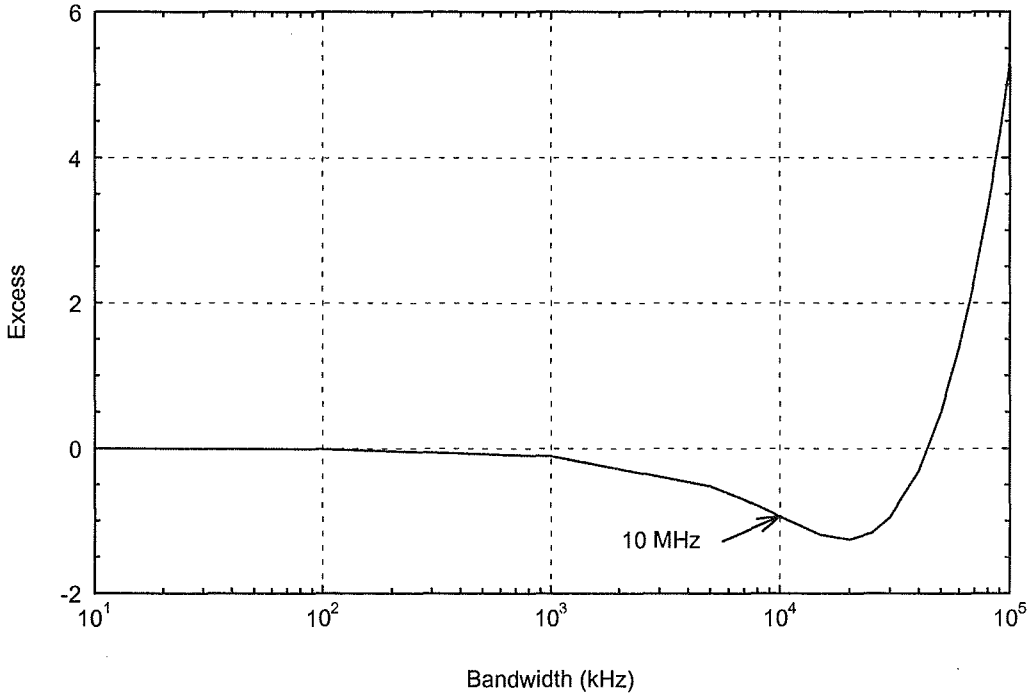

Figure 3.5. The excess as a function of receiver bandwidth.

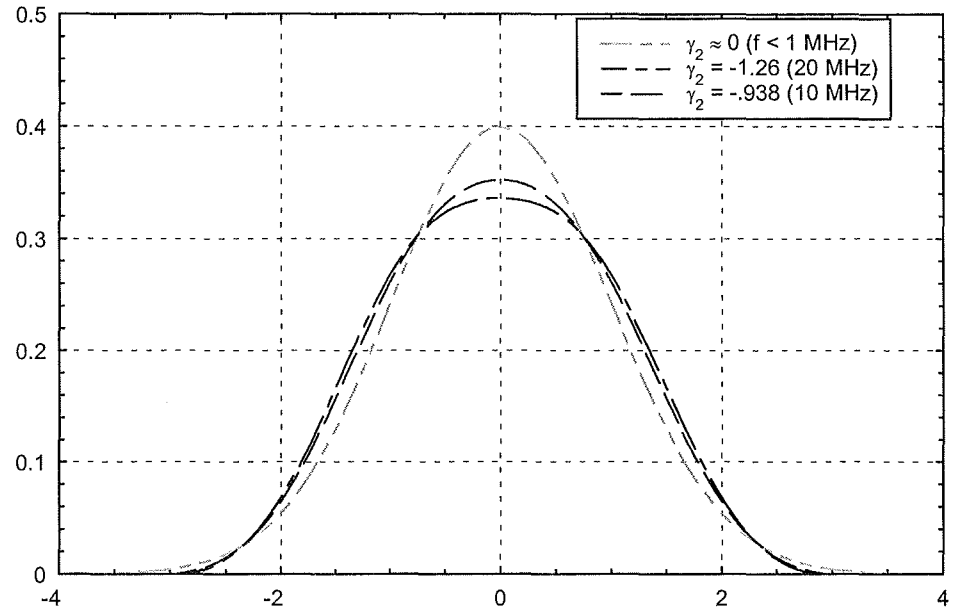

Figure 3.6. The distributions for various receiver bandwidths of less than 1 MHz, and bandwidths of 10 and 20 MHz.

The results presented in this section can be used to predict when an interfering fixed time-base dithered UWB signal is approximately Gaussian in nature, and hence, should be useful in providing guidance to system designers and regulators. Furthermore, as shown in the previous example, they can be used to estimate statistics for bandwidths comparable and exceeding the UWB PRR. In cases where the bandwidth is much larger than the PRR, so that the receiver actually resolves the individual pulses, the results presented above are no longer valid. In such cases, amplitude statistics can readily be estimated by calculating the fraction of time that a particular pulse (as seen by the receiver) amplitude is exceeded during the pulse repetition period.

3.4 References

[1] Harald Cramer, *Mathematical Methods of Statistics*, Princeton NJ: Princeton University Press, 1945.

4. CHARACTERISTICS OF AN AGGREGATE OF ULTRAWIDEBAND SIGNALS

Roger A. Dalke[1]

4.1 Introduction

The proliferation of UWB devices throughout the United States has been predicted by many industry sources. Hence, it is important that the effects of an aggregate of such devices on RF spectrum users be well understood by regulators, spectrum users, and UWB system designers. This section describes models that can be used to predict interference effects of many UWB devices on traditional narrowband RF receivers.

This model assumes that the *victim receiver* is *narrowband* and hence, it is sufficient to evaluate UWB parameters such as effective isotropically radiated average power (EIRP) and antenna gains at the center frequency of the receiver. The calculation of the power at the victim receiver requires an estimation of the basic transmission loss over the propagation path from the transmitters to the receiver. Single frequency propagation models used in traditional radio link calculations will be utilized in conjunction with the models described in this section. In the analysis which follows, it was convenient to use the basic transmission gain (denoted below as g_b) instead of loss. The basic transmission gain and loss are reciprocals and have the same absolute value but opposite signs when given in decibels.

In the first part of this section, the aggregate effects of a few similar devices in the immediate vicinity of a victim receiver are discussed. This is followed by the development of a statistical model that can be used to calculate the average received power from many UWB devices randomly distributed over the surface of the Earth. This model can be used to predict interference power for both terrestrial and airborne receivers.

4.2 Deterministic Interference Model for UWB Devices in the Vicinity of a Victim Receiver

The mean power in the receiver bandwidth due to UWB devices is simply the sum of the power received from each source or

$$w_r = \sum_{n=1}^{N} w_{t_n} g_{t_n} g_{b_n} g_{r_n} \quad , \tag{4.1}$$

---

[1]The author is with the Institute for Telecommunication Sciences, National Telecommunications and Information Administration, U.S. Department of Commerce, Boulder, CO 80305.

where w_r is the received power, w_t is the emitted EIRP in the receiver bandwidth, g_t is the transmitter gain, and g_r is the receiver gain in the direction of the n[th] transmitting device. When the locations of the devices are known and N is small, computing the received power is a relatively straightforward matter.

More realistically, one may have only a rough estimate of the ostensible number of such devices deployed in a particular geographic area (e.g., an average areal density) surrounding a particular RF receiver. In such cases, Equation 4.1 is not very useful since the parameters (perhaps the most important one being g_{b_n}) are not known. Hence statistical models and estimates are required to make any progress in predicting the potential for interference. The development of such a model is given in the next section.

Equation 4.1 is valid for commonly encountered random RF signals because the variance of the sum of zero mean random variables is the sum of the individual variances. When the received signals are normally distributed, the mean power is all that is needed to describe the statistics of the resulting interference. If there are many such devices with the same statistical properties (not necessarily normally distributed) then the statistics of the sum will approach a normal distribution [1]. In such cases, the models that predict the mean interference power provide the only statistic necessary to describe the process.

This leads directly to the question of how many signals must be added before the aggregate signal realistically appears to be normally distributed. Perhaps some insight can be gained by examining the results for a band limited fixed time-base dithered UWB signal as described in Section 3.3. In this example, the signal statistics are approximately normal for bandwidths well below the PRR. As the bandwidth increases, the absolute value of the excess increases and the statistics are no longer normal. The excess for an aggregate of such devices can be calculated as described below.

The aggregate excess for the sum of several random variables is related to the excess of each random variable γ_{2_n} as follows

$$\gamma_2 = \frac{\sum_n \gamma_{2_n} [\mu_{2_n}]^2}{\mu_2^2} \quad , \tag{4.2}$$

where μ_{2_n} is the second central moment of each variable and μ_2 is the sum of the moments. Since the processes are zero mean, the second central moment is just the signal power given in Equation 4.1.

The aggregate excess for band limited signals (e.g., as given in Section 3.3) is therefore

$$\gamma_2 = \frac{\sum_n \gamma_{2_n} \left| w_{t_n} g_{t_n} g_{r_n} g_{b_n} \right|^2}{\left[\sum_n w_{t_n} g_{t_n} g_{r_n} g_{b_n} \right]^2} \quad . \tag{4.3}$$

When the individual excesses, EIRP, and gains are the same, Equation 4.3 reduces to the *well known* result

$$\gamma_2 = \frac{\gamma_{2_n}}{N} \quad , \tag{4.4}$$

which indicates that the excess can decrease fairly rapidly as additional devices are added.

4.3 Statistical Aggregate Model

In this subsection, we develop a statistical model that can be used to estimate received interference power from many devices randomly distributed over the area surrounding a victim receiver. It is assumed that the devices are uniformly distributed over the surface of the Earth. The model requires an estimate of the path gain over the geographical area surrounding the receiver, the average receiver and transmitter antenna gains, and the average areal density of transmitters. The areal path gain can be calculated from traditional propagation models such as the Irregular Terrain Model [2]. A simple methodology that can be used to estimate average transmitter antenna gain is given in this subsection. Example calculations are given using simple receiving and transmitting antennas.

Let a UWB device with EIRP w_t and gain g_t be located at a point in space denoted by λ_i. The gain due to free space and terrestrial propagation from the point λ_i to the victim receiver, g_b, is a random variable that depends on location, terrain, climate, and other factors. Assuming a receiver gain g_r, the received power is

$$w_r = g_r w_t g_t g_b(\lambda_i, \omega_i) \quad , \tag{4.5}$$

where λ_i represents the dependence on the spatial location and ω_i are points in some probability space that characterizes, for example, random variations in devices, how, when and where they are deployed, propagation paths, etc. The average power at the victim receiver due to

many UWB devices is obtained by taking the expected value of the sum of the contribution from each device

$$\begin{aligned}\bar{w}_r &= \mathscr{E}\left\{\sum_i g_r w_t g_t g_b(\lambda_i, \omega_i)\right\} \\ &= \mathscr{E}\left\{\sum_{\Delta\lambda} n(\Delta\lambda) g_r w_t g_t g_b(\Delta\lambda, \omega_i)\right\}\end{aligned} \quad , \tag{4.6}$$

where $\Delta\lambda$ is an area increment at the point λ_i and $n(\Delta\lambda)$ is the number of devices in $\Delta\lambda$.

In this model, it will be assumed that the devices are randomly distributed in space according to *Poisson Postulates*. Essentially this means that the number of devices in non-overlapping regions of space are *independent*, the probability structure is both space and time invariant, and the probability of exactly one device being in a small increment of space $\Delta\lambda$ is approximately proportional to the increment

$$p(\Delta\lambda) = \rho\,\Delta\lambda + o(\Delta\lambda); \quad \Delta\lambda \to 0 \quad , \tag{4.7}$$

where ρ is the average density. The probability of more than one device being in a small interval is smaller than the order of magnitude of $\Delta\lambda$ (i.e., $o(\Delta\lambda)$). The average received power is then

$$\bar{w}_r = \rho \sum_{\Delta\lambda} \mathscr{E}\{w_t g_t g_r g_b(\lambda_i, \omega_i)\}\,\Delta\lambda \quad . \tag{4.8}$$

The expected values of the transmitted power $\bar{w}_t$ and gain $\bar{g}_t$ will depend, for example, on the range of possible devices and the antenna orientations with respect to the victim receiver. The mean path gain $\bar{g}_b$ is a function of the space coordinates. The mean receiver gain $\bar{g}_r$ will also in general be a function of the space coordinates. Assuming a distribution in 2-space corresponding to the surface of the earth, for small increments, the received power can be calculated via integration. Using polar coordinates with the victim receiver located at the origin, the average power (assuming $\bar{g}_r$ and $\bar{g}_b$ are independent) is

$$\bar{w}_r = \bar{w}_t \bar{g}_t \rho \int_0^{2\pi} \bar{g}_r(\phi)\,d\phi \int_0^{\infty} \bar{g}_b(r)\,r\,dr \quad . \tag{4.9}$$

In this expression, the basic path gain is the average over all possible radial paths and may be calculated, for example, by using the Irregular Terrain Model in the *area prediction mode.* The integral over ϕ includes the directive gain of a typical receiver. In this model, the parameter ρ is constant and is equal to the average number of devices per unit area.

4.3.1 Example Calculation Using the Irregular Terrain Model (ITM)

Converting Equation 4.9 to decibels, we have

$$\begin{aligned} \bar{W}_r &= \bar{W}_t + \bar{G}_t + \mathrm{P} + \Gamma_r + \Gamma_b \\ \Gamma_r &= 10\log_{10}\frac{1}{2\pi}\int_0^{2\pi} \bar{g}_r(\phi)\,d\phi \\ \Gamma_b &= 10\log_{10} 2\pi \int_0^{\infty} \bar{g}_b(r)\,r\,dr \end{aligned} \qquad (4.10)$$

As is customary, upper case letters are used to denote decibel equivalents . The mean transmitter power can be estimated from specifications or measurements of typical UWB devices.

A Method for Estimating $\bar{G}_t$

In this model, it is assumed that the transmitting antennas are randomly oriented. The average is obtained by assuming a probability distribution for the orientations and applying a typical UWB transmitter gain function which can be defined in terms of the usual spherical coordinate system angles θ and α. In what follows, θ is the angle from the pole of the sphere located, for example, at the top of the transmitter antenna (e.g., the top of a vertical dipole) and α is the azimuth.

In the case of a victim receiver near the ground, it is reasonable to assume that the direction of propagation to the receiver is uniformly distributed over a solid angle Ω_0 defined by a *band* on the unit sphere bounded by spherical angles θ_0 and $\pi - \theta_0$ ($0 \le \alpha \le 2\pi$). The expected value of the gain in the direction of the victim receiver in terms of the directive gain function $g_t = f(\Omega)$ is

$$\mathscr{E}\{f(\Omega)\} = \int_{\Omega_0} f(\Omega)\frac{d\Omega}{\Omega_0} \quad , \qquad (4.11)$$

where

$$\Omega_0 = 2\int_0^{2\pi}\int_{\theta_0}^{\pi/2} \sin\theta \, d\theta \, d\alpha = 4\pi\cos\theta_0 \quad . \tag{4.12}$$

The expected value of g_t is then

$$\mathscr{E}\{f(\theta,\alpha)\} = \frac{1}{4\pi\cos\theta_0}\int_0^{2\pi}\int_{\theta_0}^{\pi-\theta_0} f(\theta,\alpha)\sin\theta \, d\theta \, d\alpha \quad . \tag{4.13}$$

As an example, consider a short dipole where $f(\theta,\alpha) = 1.5\sin^2\theta$. The expected value of the gain is

$$\mathscr{E}\{g_t\} = 1.5\left(1 - \frac{\cos^2\theta_0}{3}\right) \quad . \tag{4.14}$$

When the transmitters are oriented so that $\theta_0 \approx \pi/2$, $\bar{G}_t \approx 1.76$ dB and when $\theta_0 = 0, \bar{G}_t = 0$ dB.

Calculation of Areal Gain Γ_b Using ITM

The ITM in area prediction mode was used to obtain the average path gain $\bar{g}_p$ relative to free space g_{fs} as function of distance from the victim receiver. The basic path gain $\bar{g}_b = \bar{g}_p g_{fs}$ was then integrated to obtain Γ_b. Table 4.1 gives typical ITM parameter settings used for examples given below unless otherwise specified.

Referring to Equation 4.10, the basic path gain is integrated over the interval $[0,\infty]$. The usual free space gain formula is only valid in the far field and has a singularity at $r = 0$. In the near field (less than a few wavelengths), power is transferred between the antennas via *mutual* coupling. For the purposes of this analysis, close proximity free space coupling was approximated by fitting a function to data obtained from a numerical analysis of the maximum coupling between two half-wave dipoles in the near field [3]. The resulting function used to calculate free space gain is

$$G_{fs} \approx -20\log_{10}\left(\frac{4\pi r}{\lambda} + 1.64\right) \quad , \tag{4.15}$$

which closely approximates near-field results and gives the usual far-field behavior when the antennas are separated by more than a few wavelengths. The numerical results for near-field coupling and G_{fs} (maximum coupling less the gain of the half-wave dipoles) as a function of antenna separation are shown in Figure 4.1.

For large distances, the integration is truncated well into the diffraction region (beyond the smooth earth radio horizon) where contributions are negligible. Figure 4.2 shows the basic transmission gain $\bar{G}_b$ and path gain $\bar{G}_p$, obtained from ITM for the parameters given in Table 4.1.

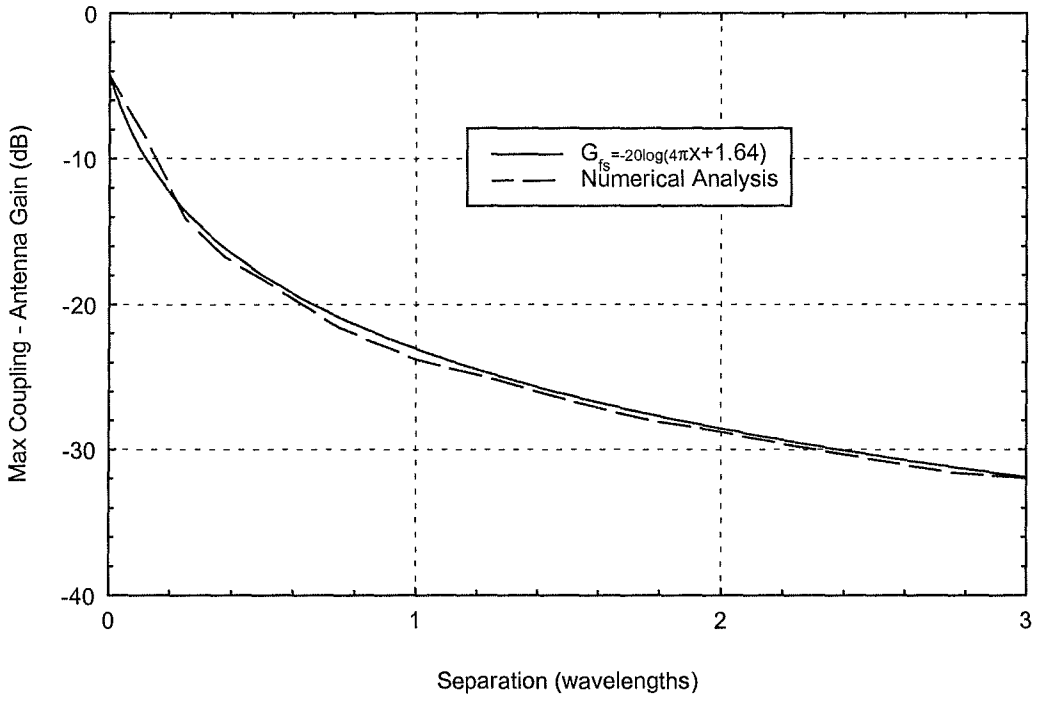

Figure 4.1 Approximation for near field antenna coupling.

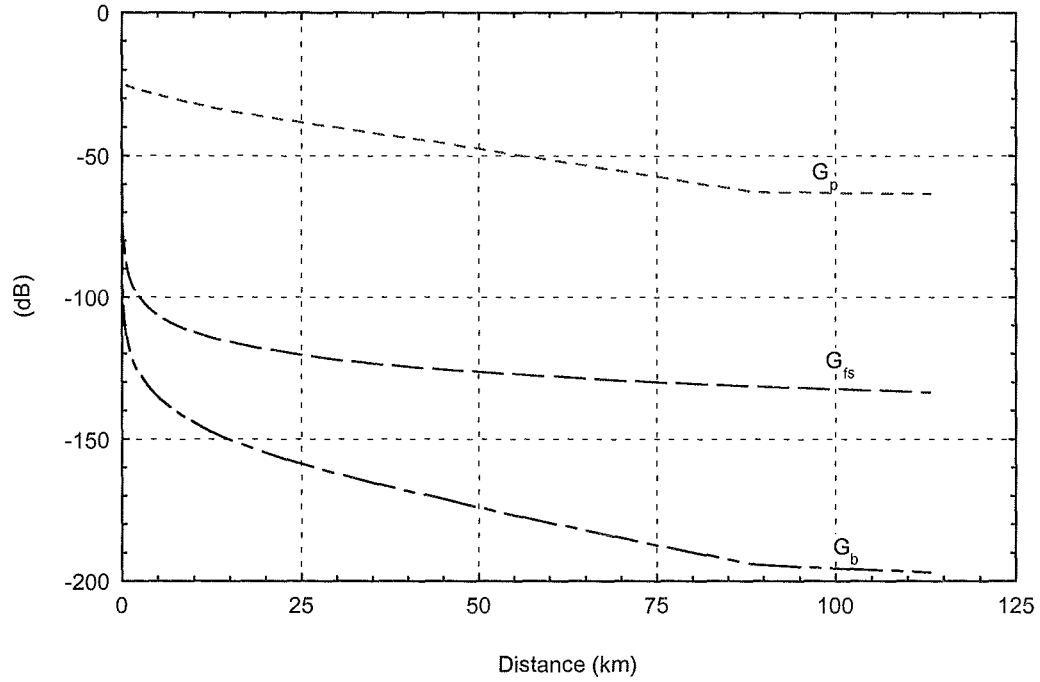

Figure 4.2. Example calculation of basic transmission gain G_b using ITM. G_p is the path gain and G_{fs} is the free-space gain. (1000 MHz, Δh=90 m, T_x = 2 m, R_x = 3 m).

Effects of Δh and Receiver Height

In area prediction mode, the statistical parameter Δh is used to characterize terrain in the geographical region of interest. The dependence of the parameter Γ_b on Δh is shown in Figure 4.3. Of note is the fact that in *flat* terrain Γ_b is more than 20 dB greater than for *hilly* terrain (Δh = 90 m).

In Figure 4.4, the parameter Γ_b is plotted as a function of receiver height. Basically, the path gain increases with increasing antenna height since terrestrial attenuation is not a factor at increasing distances from the receiver (as the receiver height increases). With increasing height, the path gain from the entire region within line-of-sight of the receiver is essentially due to free space propagation.

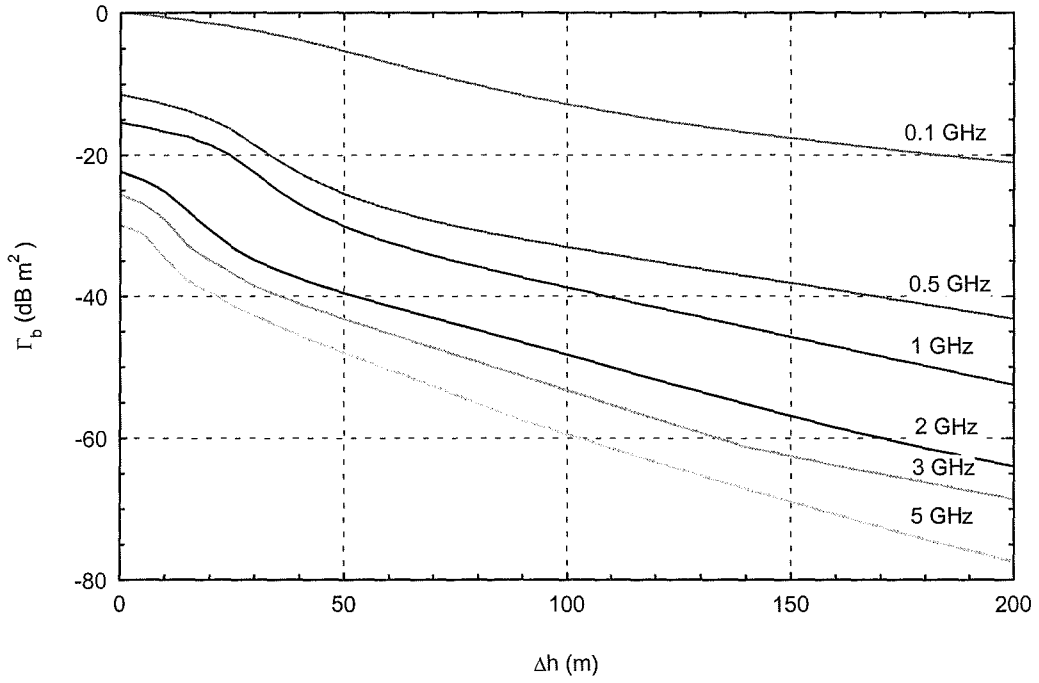

Figure 4.3. Basic areal gain Γ_b as a function of Δh and frequency. (T_x = 2 m, R_x = 3 m).

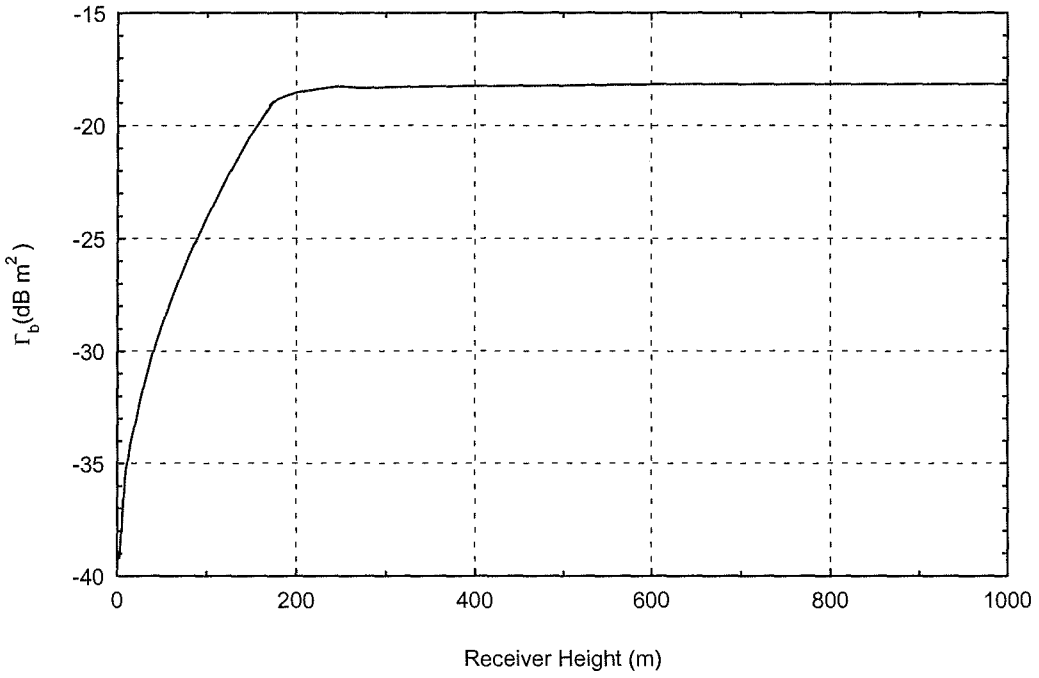

Figure 4.4. Basic areal gain Γ_b as a function of receiver height. (1000 MHz, Δh=90 m).

Table 4.1 Parameters for ITM Calculations

ITM Parameter	Value
Frequency	Various
Receiver Antenna Height	3 m
Transmitter Antenna Height	2 m
Polarization	Vertical
Terrain Irregularity Parameter Δh	90 m, 30 m, 0
Ground Electrical Constants	.005 S/m, $\epsilon_r = 15$
Surface Refractivity	301 N-units
Climate	Continental Temperate
Siting Criteria	Random
Time and Location Variability	50%
Confidence	50%

Estimated Interference Power Levels for a Half-wave Dipole Receiver

Referring to Equation 4.9, azimuthal dependence of the receiver gain in the direction of the UWB transmitters can be explicitly included in the analysis. The quantity Γ_r defined in Equation 4.10 is just the *average* gain in the azimuthal direction. To give a simple example, a half-wave dipole has a constant azimuthal gain of 2.15 dBi, hence $\Gamma_r = 2.15\ dBi$.

Assuming that the UWB transmitters are short dipoles and $\bar{G}_t = 1.76$, the power at the receiver per watt of transmitted power is

$$W_r = 3.91 + \mathrm{P} + \Gamma_b \ dBW \quad , \tag{4.16}$$

where P is the average density in dB per unit area, and Γ_b is *area average of path gain*. Calculated values for various frequencies and terrain parameters associated with so called *flat* ($\Delta h = 0$), *plains* ($\Delta h = 30\ m$), and *hills* ($\Delta h = 90\ m$) environments are given in Table 4.2 below.

Table 4.2 Γ_b as a Function of Δh and Frequency (Based on Parameters Given in Table 4.1)

	$\Gamma_b\ dB\,m^2$		
Frequency (MHz)	$\Delta h = 0$	$\Delta h = 30m$	$\Delta h = 90m$
100	0.14	-2.51	-11.61
500	-11.46	-18.56	-31.97
1000	-16.84	-27.48	-39.11
1500	-20.03	-32.02	-43.35
2000	-22.32	-34.88	-46.53
2500	-24.10	-36.93	-49.13
3000	-25.56	-38.53	-51.26
3500	-26.81	-39.84	-53.11
4000	-27.89	-40.97	-54.74
4500	-28.83	-41.96	-56.24
5000	-29.69	-42.77	-57.51

4.3.2 Example Calculation Assuming Free Space Propagation to the Radio Horizon

When the victim receiver is located high above the earth, as with an aircraft receiver, the transmission path to the radio horizon is largely unaffected by the earth (see Figure 4.4). In such cases, the interfering signal power can be estimated by assuming free space propagation to all devices located within the radio horizon. It should be noted that the methodology described below neglects the effects of line-of-sight propagation in the troposphere and that due to diffraction and tropospheric scatter from beyond the radio horizon. The over-the-horizon diffracted and scattered signals will be minimal in most cases of interest.

The areal gain Γ_b is calculated from

$$\Gamma_b = 10\log_{10}\frac{\lambda^2}{8\pi}\int_0^{r_{horiz}}\frac{r\,dr}{(h_r-h_t)^2+r^2} \quad , \tag{4.17}$$

where h_r is the height of the receiver, h_t is the height of the transmitter, and r_{horiz} is the distance to the radio horizon which can be calculated using the following approximate expression [2]

$$r_{horiz} = \sqrt{2h_r/\gamma_e} + \sqrt{2h_t/\gamma_e} = \sqrt{2a_e h_r} + \sqrt{2a_e h_t} \quad . \tag{4.18}$$

The earth's effective curvature γ_e is the reciprocal of the earth's effective radius a_e and is normally determined from the surface refractivity using the empirical formula [2]

$$\begin{aligned} \gamma_e &= \gamma_a/K \\ a_e &= Ka \\ K &= \left(1 - 0.04665\,e^{N_s/N_1}\right)^{-1} \quad , \end{aligned} \tag{4.19}$$

where K is the *effective earth radius factor*, N_s is the surface refractivity, $N_1 = 179.3$ N-units, and $\gamma_a = 1/a = 157 \times 10^{-9}\ \mathrm{m}^{-1} = 157$ N-units/km [2].

Evaluating the integral in Equation 4.17 gives

$$\Gamma_b = 10\log_{10}\left(\frac{\lambda^2}{16\pi}\log_e\left(\frac{(h_r-h_t)^2 + r_{horiz}^2}{(h_r-h_t)^2}\right)\right) \quad . \tag{4.20}$$

When the receiver height is much greater than the transmitter height the result can be reduced to

$$\Gamma_b = 32.52 - 20\log_{10}f_{MHz} + 10\log_{10}\log_e\left(1 + \frac{2Ka}{h_r}\right) \quad dB\,m^2 \quad . \tag{4.21}$$

Assuming a standard four thirds earth ($K = 4/3$), Figure 4.5 shows the areal gain as a function of frequency and receiver antenna height as compared with Γ_b calculated using the ITM up to its recommended limit of 1 km. Note that at 1 km, the results are within about 0.5 dB. Using Equation 4.21, Figure 4.6 shows Γ_b for various frequencies as a function of receiver height up to 10 km.

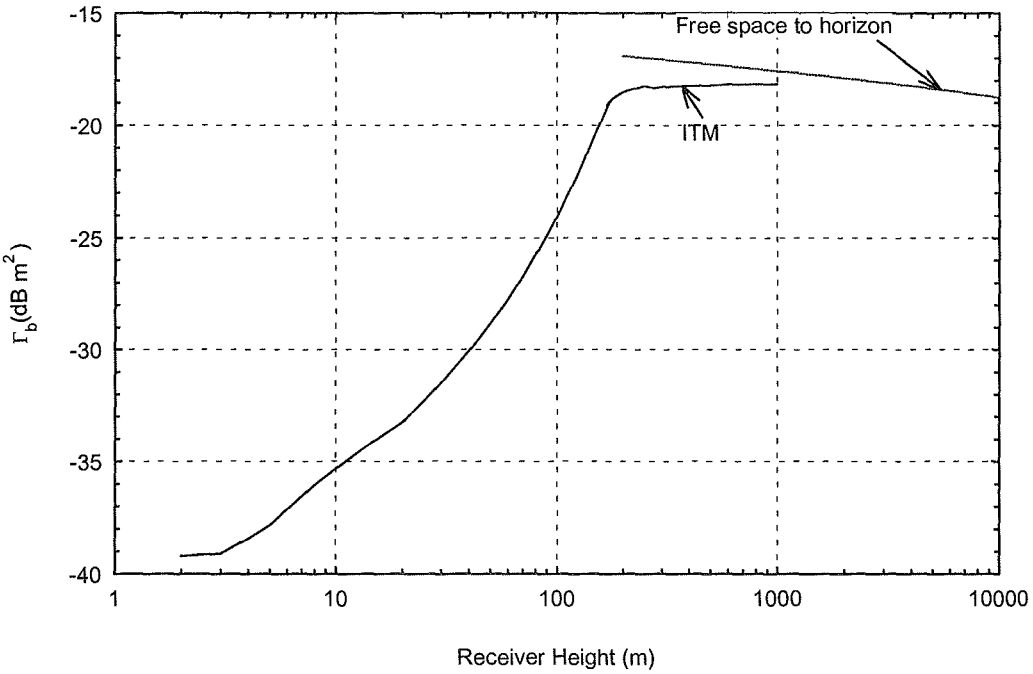

Figure 4.5. Basic areal gain Γ_b as a function of receiver height using ITM compared with a direct calculation assuming free-space propagation. (1000 MHz, Δh=90 m).

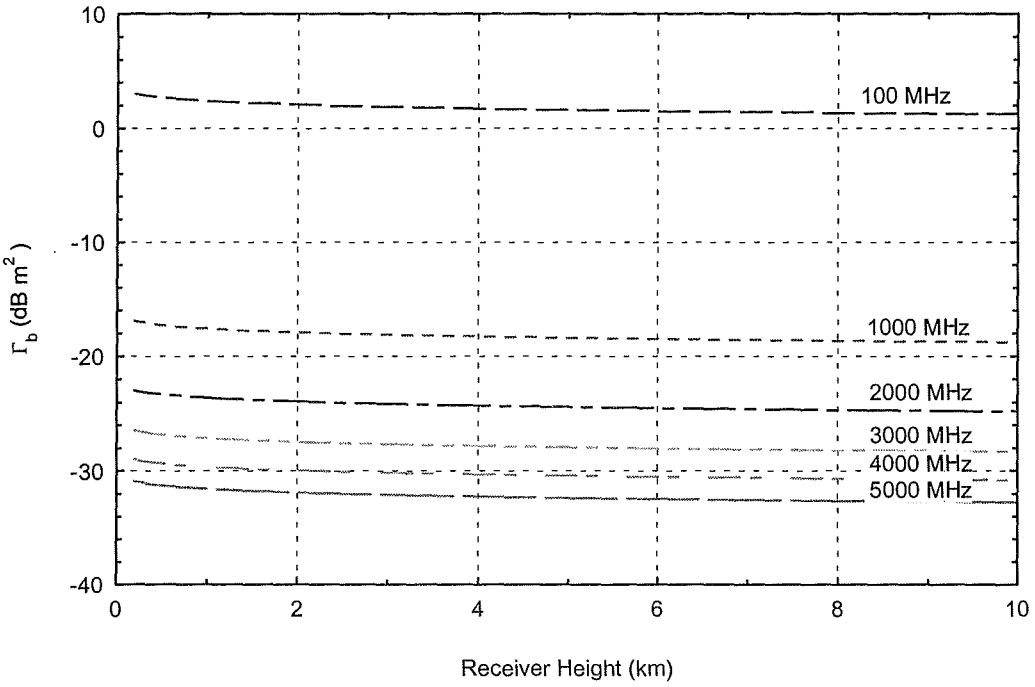

Figure 4.6. Basic areal gain Γ_b as a function of receiver height assuming free-space gain to the radio horizon.

4.4 References

[1] Harald Cramer, *Mathematical Methods of Statistics,* Princeton NJ: Princeton University Press, 1945.

[2] G.A. Hufford, A.G. Longely, and W. Kissick "A guide to the use of the ITS irregular terrain model in the area prediction mode," NTIA Report 82-100, April 1982.

[3] Constantine A. Balains, *Antenna Theory Analysis and Design*, 2nd Edition, New York: John Wiley and Sons, 1997, p 442.

5. FULL-BANDWIDTH REFERENCE MEASUREMENTS OF ULTRAWIDEBAND EMISSIONS

Brent Bedford,[1] Robert T. Johnk,[2] and David R. Novotny[2]

5.1 Introduction

Ultrawideband (UWB) signals, by definition, contain energy over a larger range of the frequency spectrum than do conventional radio signals which are relatively narrow-banded. The majority of conventional radio test equipment, however, are designed to measure the signals from the majority of radio systems in use, which constitute mostly narrowband and a few wideband signaling systems. UWB is a new class of signals that places new demands on measurement equipment.

There exists a need to characterize this new class of signals across their full emission bandwidth. This section describes measurements that address that need by capturing the pulse shapes and inner pulse structure from a selection of UWB devices. The UWB signals in this study are very narrow pulses of RF energy that are modulated or envelope-shaped in various ways. This study provides a view of the UWB pulses that cannot be directly measured with common narrower bandwidth equipment. From this full-bandwidth view of the pulses, comparisons can be made with measurement results performed with conventional equipment. The measurement results in this section provide a reference to which other measurement results can be compared, to see how well the reference set of signal parameters can be predicted from measurements using bandwidth-limited equipment.

5.2 Measuring Instruments and Calculation Methods

The signals emitted from a selection of UWB devices (see section 1.2) were measured by the National Institute of Standards and Technology (NIST) Radio-Frequency Technology Division to obtain data that represents the radiated time-domain waveform. The goal of these measurements was to capture a detailed view of a single pulse. The pulses were measured in two different environments. The first environment was called "conducted measurements." The second environment was called "radiated measurements."

---

[1]The author is with the Institute for Telecommunication Sciences, National Telecommunications and Information Administration, U.S. Department of Commerce, Boulder, CO 80305.

[2]The authors are with the Radio-Frequency Technology Division, National Institute for Standards and Technology, U.S. Department of Commerce, Boulder, CO 80305.

Two different measuring instruments were used in making the full-bandwidth measurements. The first instrument was a sampling oscilloscope. This instrument was capable of achieving very high equivalent sample rates when digitizing the input signal. The instrument used in this study possessed a bandwidth of 20 GHz with the ability to acquire 4,096 samples in a single time-domain record. Due to the nature of how this instrument performs its sampling, it had two limitations. The repetition rate of the pulses to be measured must be constant and the pulse shape invariant. While some UWB devices satisfy this requirement, there are devices that do not and were measured by a second measuring instrument.

The second measuring instrument was a single-event transient digitizer. This instrument had the advantage of placing fewer restrictions on the pulse parameters that it can measure. The digitizer possessed a bandwidth of 4.5 GHz with a maximum of 1,024 samples in a single shot. The instrument was designed to perform high fidelity measurements on a single pulse.

Two quantities were calculated from each measured waveform. The first quantity was "Total Peak Power." Given that there are i sample points in the time-domain waveform and x is the ith sample point, total peak power was calculated using equation 5.1 and was the maximum ith value of the power vector.

$$power_i = \frac{x_i^2}{50} \tag{5.1}$$

The second quantity was "Total Average Power." It was calculated as shown in equation 5.2.

$$Average\ Power = \frac{1}{pri} * \sum_i \left(\frac{x_i^2}{50} \right) * \Delta t \tag{5.2}$$

where x_i is the ith time-domain sample
Δt is the sample interval
pri is the pulse repetition interval

The PRI that was used in the calculation is the shortest time interval between any two pulses. Effects which could lengthen the PRI such as On-Off-Keying or the quiet time between bursts of pulses were not considered since measuring these parameters was beyond the scope of this investigation. Some devices could operate with more than one mode setting. For these devices, the maximum and minimum PRIs were used in the calculation.

5.3 Conducted Measurements

Two different test setups were implemented for the conducted measurements. The first is shown in Figure 5.1. The RF output of the UWB device-under-test was connected using a coaxial transmission line to an attenuator. The attenuator was used to prevent overloading and damage to the measurement instrument from too strong a signal level. The signal was then split into two equal amplitude levels and fed into a trigger port and a signal port on a sampling oscilloscope. Several pulses were measured to check for pulse shape variations that might induce measurement errors. This setup was used to perform conducted measurements on device A, which has a constant pulse repetition frequency.

The second test setup is shown in Figure 5.2. The only difference from Figure 5.1 is the use of a single-event transient digitizer. This setup was used to perform conducted measurements on devices B and D due to a non-constant pulse repetition rate in the emissions.

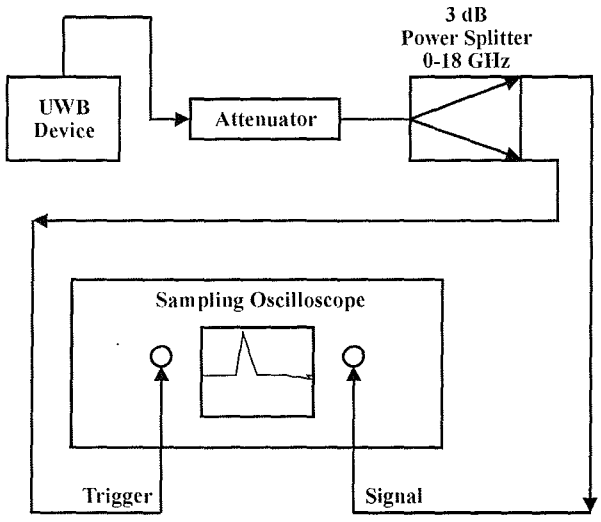

Figure 5.1. Device A, conducted measurement test setup.

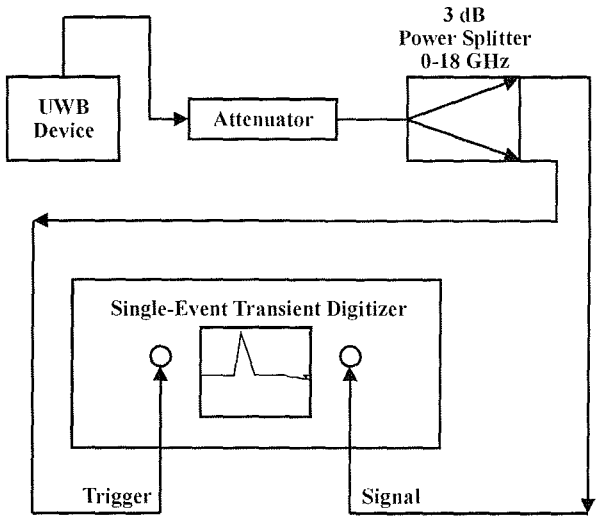

Figure 5.2. Device B and D, conducted measurement test setup.

The measured time-domain waveform for device A is shown in Figure 5.3. It exhibits a large main pulse followed by some damped ringing. The vertical axis represents voltage at the RF output connector of the UWB device. The corresponding frequency-domain power spectrum, which was calculated from the time-domain waveform, is shown in Figure 5.4. The vertical axis represents decibels relative to a milliwatt at the RF output connector of the UWB device. The caption presents a Δf number which is the frequency spacing between the graphed points.

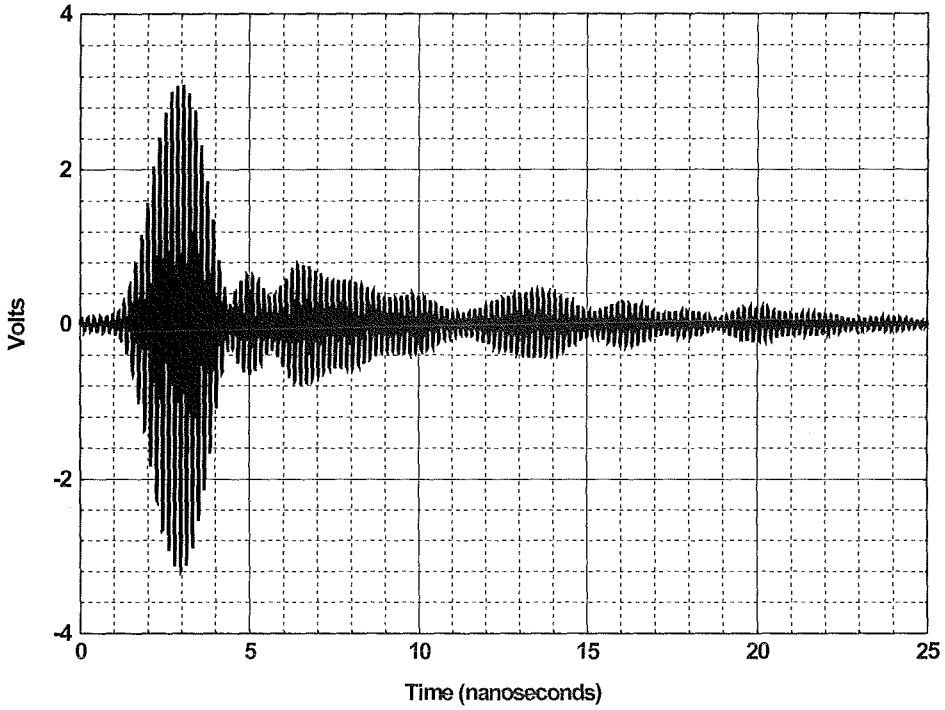

Figure 5.3. Device A, conducted time-domain waveform.

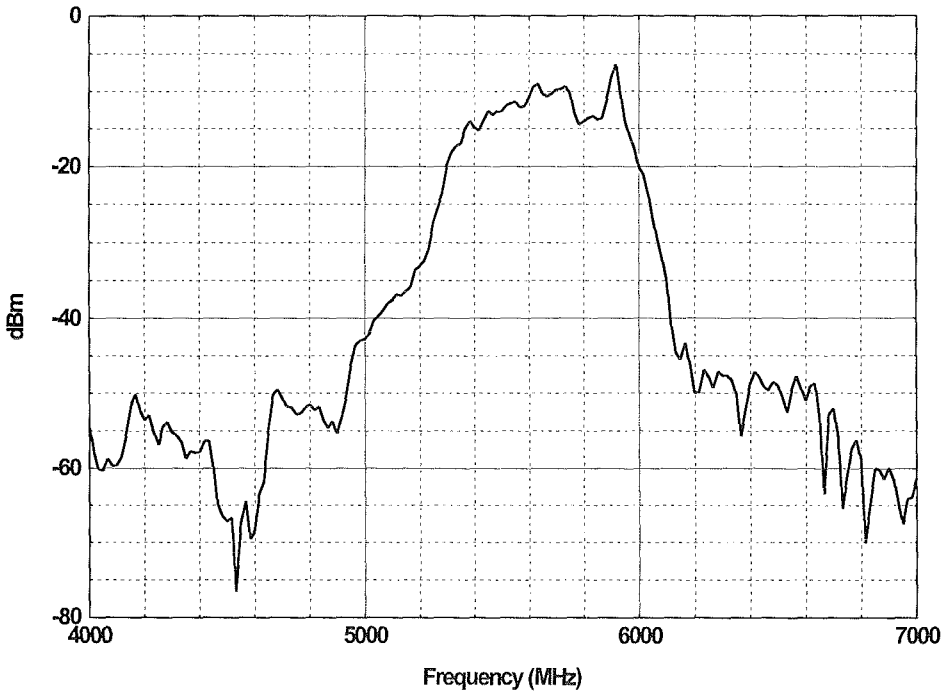

Figure 5.4. Device A, conducted power spectrum, $\Delta f = 16.67$ MHz.

The following table summarizes the Total Peak Power and the Total Average Power calculated for the devices for which conducted measurements were performed.

Table 5.1. Total Peak and Total Average Powers from the Conducted Measurements.

Device Letter	Total Peak Power (dBm)	Total Average Power (dBm)
A	23.1	-27.8
B	32.0	-4.5
D	17.4	-16.0

The -10 and -20 dB bandwidths were extracted from the frequency-domain power spectrum graphs. These bandwidths, from the conducted measurements, are summarized below.

Table 5.2. Emission Bandwidth from the Conducted Measurements.

Device Letter	-10 dB Bandwidth (MHz)	-20 dB Bandwidth (MHz)
A	616.6	799.9
B	479.9	539.9
D	1349	2597

Appendix D contains the complete set of conducted measurement graphs for devices A, B, and D.

5.4 Radiated Measurements

Four different test setups were implemented for the radiated measurements. All of the test setups were performed in the NIST anechoic chamber. The first test setup is shown in Figure 5.5. The UWB device-under-test radiates using its manufacturer supplied antenna into the chamber. A ridged horn antenna was used in this configuration. The measurement frequency range using this antenna was 1 GHz to 4 GHz. Two stages of amplification were needed in this configuration to provide enough signal to drive the measuring instrument. A calibration was performed on the amplifiers to provide a frequency response correction. The signal was then split into two equal amplitude levels and fed into a trigger port and a signal port on a single-event transient digitizer. This setup was used to perform radiated measurements on device C. Figure 5.6 shows the second test setup that was used. The only difference from the previous test setup is a single stage of amplification since this UWB device produced a stronger signal. This setup was used to perform radiated measurements on device D. Figure 5.7 shows the third setup. The only difference from the previous test setup is the use of a different receiving antenna. The receiving antenna was a NIST 30 cm TEM horn, which produces minimal waveform distortion. The measurement

frequency range using this antenna was 200 MHz to 4000 MHz. This setup was used to perform radiated measurements on device E (1500 MHz and 900 MHz modes). Figure 5.8 shows the fourth test setup. The only difference from the previous test setup is the addition of an attenuator to trim the measurement system gain down to an optimum level for the measurement. The NIST 30 cm TEM horn was used in this measurement as the receiving antenna. This setup was used to perform radiated measurements on device E (300 MHz mode) and B.

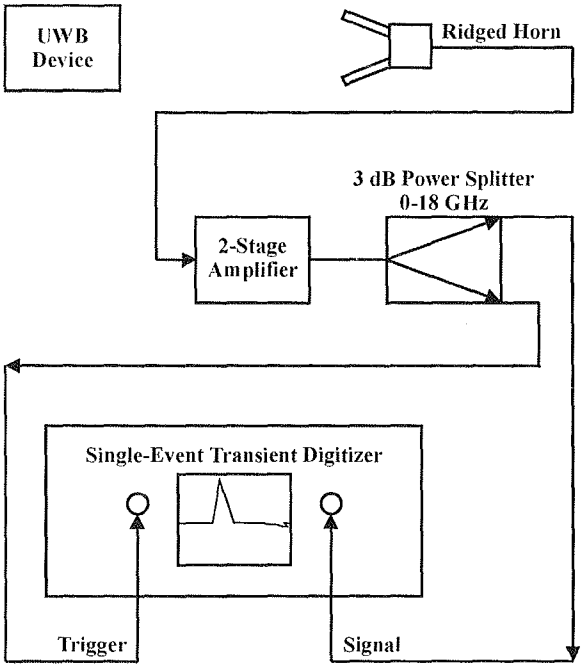

Figure 5.5. Device C, radiated measurement test setup.

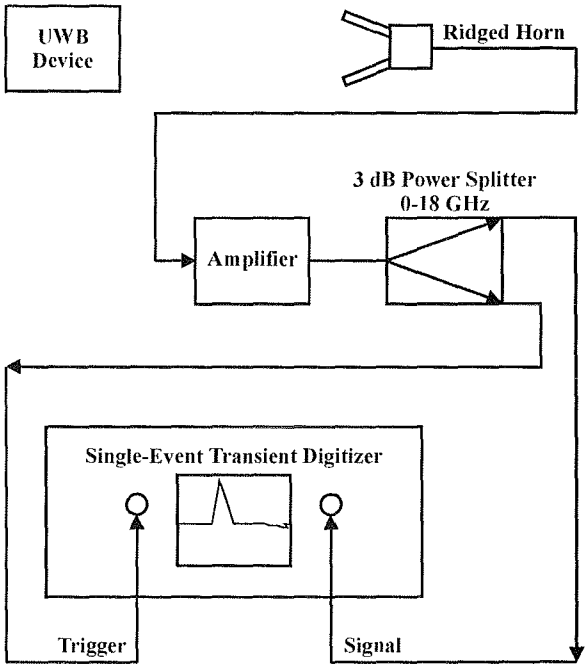

Figure 5.6. Device D, radiated measurement test setup.

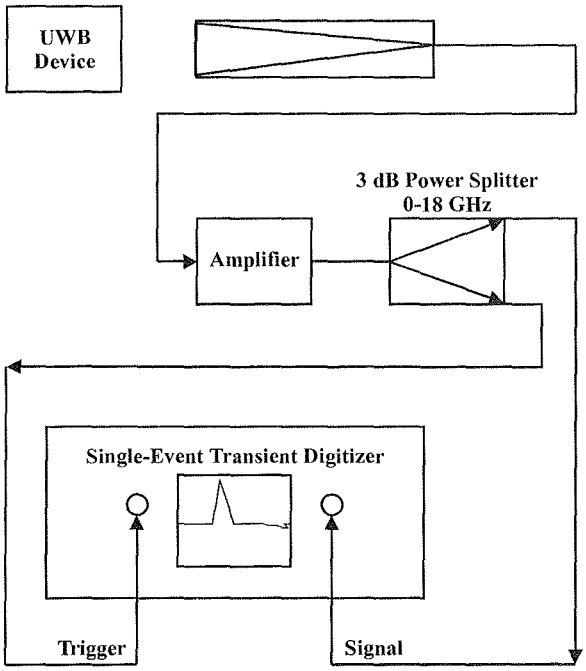

Figure 5.7. Device E (1500 MHz and 900 MHz), radiated measurement test setup.

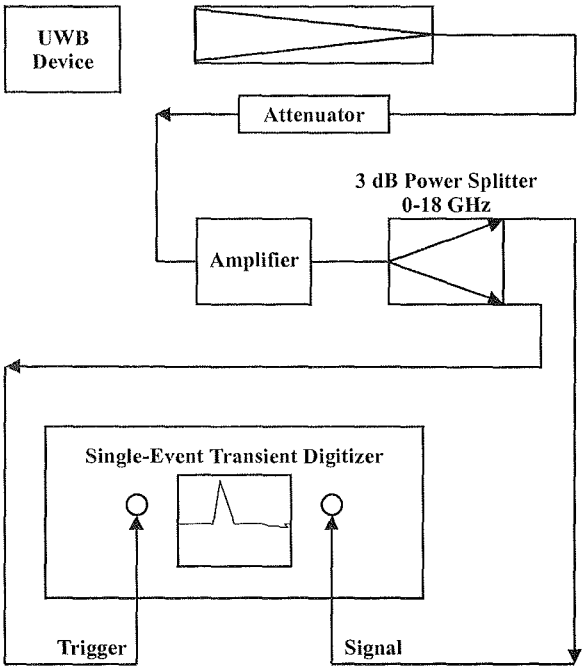

Figure 5.8. Device E (300 MHz) and B, radiated measurement test setup.

The measured time-domain waveform for device C is shown in Figure 5.9. The vertical axis represents voltage at the receiving antenna terminals. The separation distance between the receiving antenna and the transmitting antenna was one meter. The corresponding frequency-domain spectrum is shown in Figure 5.10. The vertical axis represents field strength (decibels relative to a microvolt per meter), calculated from the time-domain waveform, at the receiving antenna's location. The caption presents a Δf number, which is the frequency spacing between the graphed points.

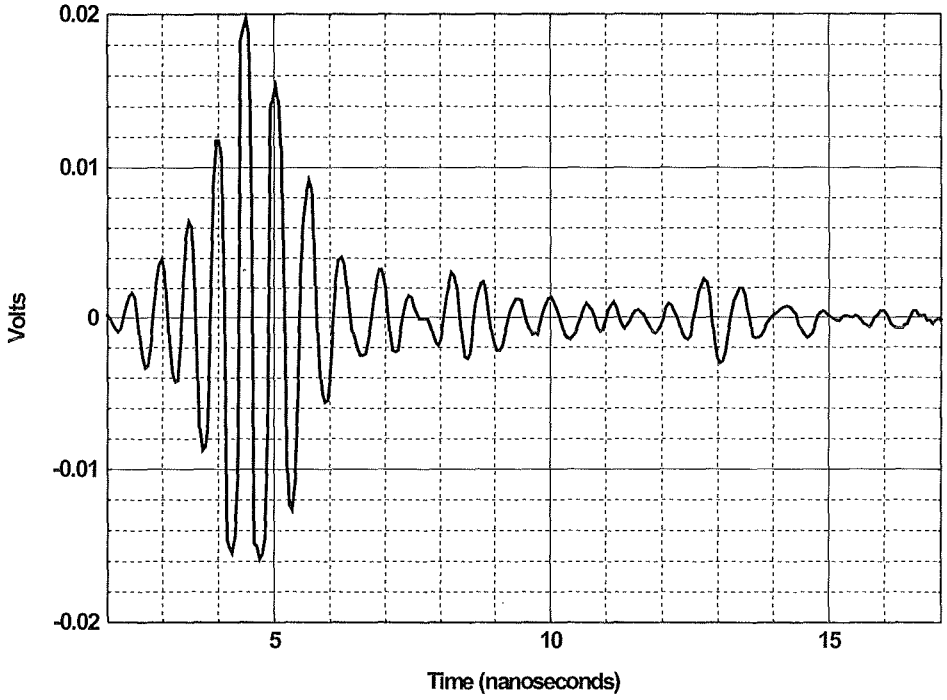

Figure 5.9. Device C, radiated time-domain waveform.

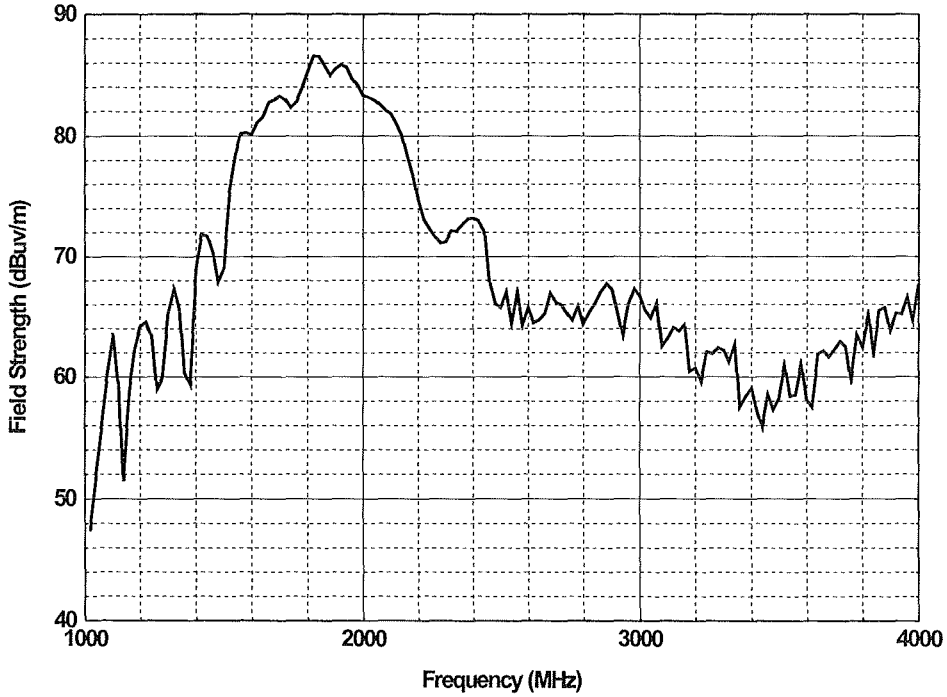

Figure 5.10. Device C, radiated peak field strength at 1 m, $\Delta f = 20$ MHz.

The following table summarizes the Total Peak Power and the Total Average Power calculated for the devices for which radiated measurements were performed.

Table 5.3. Total Peak and Total Average Powers from the Radiated Measurements.

Device Letter	Total Peak Power (dBm)	Total Average Power (dBm)
B (maximum PRI)	-3.2	-39.8
B (minimum PRI)	-3.2	-33.7
C	-21.1	-48.6
D (maximum PRI)	-20.5	-51.8
D (minimum PRI)	-20.5	-41.8
E (1500 MHz)	-7.9	-55.6
E (900 MHz)	-3.7	PRI unknown
E (300 MHz)	12.5	PRI unknown

.

The -10 and -20 dB bandwidths were extracted from the frequency-domain radiated spectrum graphs. Some of the devices had combinations of center frequency and bandwidth such that the portion of the spectrum of interest exceeded the valid frequency range of the radiated measurements. The bandwidth could not be determined so these cases are marked with "NA". The bandwidths, from the radiated measurements, are summarized below.

Table 5.4. Emission Bandwidths from the Radiated Measurements .

Device Letter	-10 dB Bandwidth (MHz)	-20 dB Bandwidth (MHz)
B	319.9	539.9
C	659.8	1080
D	NA	NA
E (1500 MHz)	2799	NA
E (900 MHz)	1650	NA
E (300 MHz)	NA	NA

Appendix D contains the complete set of radiated measurement graphs for devices B, C, D, and E. It is interesting to compare the conducted and radiated results for devices B and D. For both devices, the radiated and conducted waveforms are significantly different. While device B's conducted and radiated spectrums look similar, device D's conducted and radiated spectrums are significantly different over the 1 GHz to 2 GHz regions.

6. BANDWIDTH LIMITED MEASUREMENTS OF ULTRAWIDEBAND DEVICE EMISSIONS

Frank Sanders[1]

6.1 Introduction

In many cases, the characteristics of UWB signals must be measured using equipment that is bandwidth limited. I.e., the measurement bandwidth is less than the UWB emission bandwidth. Bandwidth limited measurements are necessary for at least three reasons:

- Coupling between UWB emissions and various types of radio receiver equipment will generally be bandwidth limited (by either the receiver RF front-end or the receiver IF section). Bandwidth limited measurements closely match the case of bandwidth limited coupling into receivers.

- Regulatory standards may be specified in particular bandwidths. Compliance measurements must be performed in (or extrapolated to) the required bandwidths.

- Adequate full-bandwidth measurement systems are not likely to be available to all measurement facilities. Even if such equipment is available, the outputs generated may not be satisfactory for all measurement purposes.

In this section, measurement techniques are described that may be generally applied with commercial, off-the-shelf (COTS) equipment.[2] COTS-compatible methods are included for measuring the following UWB emission parameters:

- emission spectra as a function of IF measurement bandwidth,
- pulse width estimation,
- pulse shape as a function of IF measurement bandwidth,
- pulse repetition rates, sequences, and gating,
- amplitude probability distributions as a function of IF measurement bandwidth,
- peak power,
- average power.

---

[1]The author is with the Institute for Telecommunication Sciences, National Telecommunications and Information Administration, U.S. Department of Commerce, Boulder, CO 80305.

[2]COTS equipment is defined as measurement devices that are commercially available.

This section provides guidance for other laboratories in the implementation of UWB emission measurement techniques. Each technique is described both generically and as performed specifically at ITS using COTS equipment.[3] Based upon experience gained at the ITS laboratory, the technical strengths and weaknesses of each approach are described. Particular problems that other laboratories may encounter with these techniques are noted, along with any practicable solutions developed by ITS measurement personnel.

6.2 Bandwidth Limited Measurement Theory

A measurement result is the convolution of an input signal with the impulse response of the measurement device in the appropriate domain (e.g., time or frequency). The convolution width of a measurement device's impulse response may be wider than, equal to, or narrower than the input signal function. For UWB device emissions, the measurement convolution width is generally narrower than the device emission.[4] However, there may exist within the UWB emission some features that are individually narrower than the measurement convolution. These and other characteristics of UWB emissions must be taken into account in emission measurements, as described below.

6.2.1 Bandwidth Limited Time Domain Measurement Theory[5]

The convolution bandwidth of a time domain measurement may be limited by either the RF front-end or the time domain digitizer. If the RF front-end is an instrument such as a spectrum analyzer, then it will be the limiting factor. If the front-end is a wideband detector diode (typically a discrete component with 18 GHz bandwidth), then the digitizer will limit. In either case, the measurement system response will show time domain features that are limited by the fastest response of the slowest component. That is, a 500-MHz single-shot digitizer (with a wideband detector) will produce pulse widths that are no shorter than 2 ns. Given the emission characteristics of UWB devices examined in this study, this may be inadequate for accurate

---

[3]Unless otherwise noted, all measurement techniques described in this section have been implemented by ITS and have been used to generate the data that appear in Section 8 and Appendix D.

[4]Emission width may be defined at the 3 dB, 6 dB, 10 dB, 20 dB points, etc., in the appropriate domain.

[5]This discussion of time domain measurements assumes that the UWB RF emission is rectified by a diode or equivalent detector, either as a discrete component or as part of a system such as a spectrum analyzer. For other types of time domain measurements, including those that preserve phase information, see Section 5 of this report.

measurements of UWB pulse widths. But it will probably be more than adequate for measurements of pulse repetition rate, pulse sequences, and gating behavior. It will also be adequate for measurements of pulse-to-pulse dither intervals.

It is possible to utilize a wideband time domain measurement system to digitize a pulse (preserving the phase information) and then transform the waveform into a wideband spectrum, using the Fourier transform, as described in Section 5. Such a spectrum may in turn be convolved with narrower IF bandwidths to replicate the spectrum envelope that would be measured in any arbitrarily chosen receiver IF. While this approach may be feasible for some UWB systems, pulse to pulse waveform variation may require repetitive sampling measurements to form a spectrum, and dithering may make repetitive sampling difficult or impossible. Dynamic range may also be limited for some pulse measurements.

6.2.2 Bandwidth Limited Frequency Domain Measurement Theory

The convolution of a frequency domain measurement may be limited by either the RF front-end or the IF bandwidth of the measurement device, assumed to be a spectrum analyzer. The IF bandwidth is normally the limiting factor.[6] For this discussion, the spectrum analyzer convolution function is assumed to be essentially the IF filter shape.

If the IF bandwidth curve is substantially narrower than the spectrum being measured, then the convolution of the two functions is nearly identical to the input spectrum function. In this case, the spectrum measurement is nearly identical to the spectrum function that was applied to the analyzer input.

The features visible in the measured spectrum will only be resolvable down to the IF filter width. Features narrower than the filter will convolve to yield merely the IF filter shape. To further resolve those features, narrower IF filtering must be used.

While narrower IF filtering provides better resolution on spectrum features, two drawbacks result. The first is true for all spectrum measurements, while the second will occur in particular cases. The first problem is that the measurement takes proportionally longer to complete as the IF is narrowed. A trade-off results between measurement time and amount of detail in the resulting spectrum measurement. Measurement efforts must balance these factors. In practice, the width of the IF filtering will often be determined by the need to resolve the spectrum with the same bandwidth as a particular type of potential victim receiver. For example, a 30 kHz bandwidth

---

[6]In exceptional cases, the RF front-end is narrower than the IF section; those analyzers can usually be retrofitted with wider bandwidth (essentially wide-open) front-ends. The result is that the spectrum analyzer bandwidth is still ultimately limited by the IF section.

may be selected in the spectrum analyzer to match as nearly as possible the 25 kHz bandwidth of some types of land mobile radio receivers.

The second problem is that the signal-to-noise ratio (SNR) of the measured signal can decrease in narrower IF bandwidths. This will occur if the noise power in the measurement system decreases more slowly in the IF bandwidth than the power coupled from the spectrum being measured. The result is decreased dynamic range in the measurement. For example, in a narrow IF bandwidth the spectrum might only be measured 20 dB down from the highest point, as compared to perhaps 35 dB down in a wider bandwidth.

To determine when dynamic range will decrease with narrow IF bandwidth, consider first the manner in which measurement system inherent thermal noise varies as a function of IF bandwidth. The noise power present is directly proportional to the IF bandwidth. Measured in decibels, the inherent noise power therefore varies as 10 log (IF bandwidth).

Likewise, if the measured spectrum is noise, or approximates noise characteristics, then the spectrum power convolved in the IF varies as $10\log_{10}$ (IF bandwidth). In this case, the SNR of the spectrum is constant with IF bandwidth, and the dynamic range of the measurement is unaffected by the choice of IF bandwidth. A drawback to a narrower IF bandwidth is the longer time required to complete the measurement.

If the measured spectrum is not noise-like, the convolved measured power may change at a rate that is faster than $10\log_{10}$ (IF bandwidth). This case occurs for spectra generated by pulsed transmitters. Consider the case in which pulse width is t, pulse repetition interval is T, and normalized voltage measured in a spectrum analyzer peak detector at the fundamental frequency is A. For such transmitters, the spectrum that contains most of the transmitted power consists of lines spaced (1/T) apart. The line power envelope is classically sinc^2, with the first two nulls occurring at $\pm(1/t)$ relative to the fundamental frequency and subsequent nulls occurring at intervals of (1/t).[7]

The power measured in a line at the fundamental frequency is

$$p_{line} = A^2 \tag{6.1}$$

and the line power in decibels is

$$P_{line} = 10\log_{10}(A^2) \tag{6.2}$$

[7]The sinc^2 spectrum is only dominant through the first few lobes; more extended portions of the spectrum are dominated by transient effects in the rising and falling edges of the pulses.

The average power is

$$p_{ave} = A^2\left(\frac{t}{T}\right) \tag{6.3}$$

or, in decibels

$$P_{ave} = \left[10\log_{10}(A^2) - 10\log_{10}\left(\frac{t}{T}\right)\right] = \left[P_{line} - 10\log_{10}(duty\ cycle)\right] \quad , \tag{6.4}$$

where duty cycle = (t/T) .

For pulsed emissions, peak power is the rate at which energy is transmitted during each pulse. This is therefore a linear function of the ratio of the pulse width to the pulse repetition interval. Therefore, the peak power is related to the average power and the line power by the following relationship:

$$P_{peak} = \left[P_{ave} - 10\log_{10}(duty\ cycle)\right] = \left[P_{line} - 20\log_{10}(duty\ cycle)\right] \quad . \tag{6.5}$$

For n lines convolved within a measurement bandwidth, the measured peak power varies with n as

$$P_{peak} = 10\log_{10}(n\cdot A)^2 = 20\log_{10}(n) + P_{line} \quad . \tag{6.6}$$

Since the number of lines within the convolution bandwidth is proportional to the bandwidth, the peak power varies as $20\log_{10}$ of the measurement bandwidth for line spectra. Figures 6.1 and 6.2 illustrate the behavior of a line spectrum convolved with bandwidths that range from significantly less than the line spacing to significantly wider than the pulse width. For typical analogous UWB device emissions, note that the width of the central lobe corresponding to that in Figure 6.2 will be on the order of a gigahertz or more.

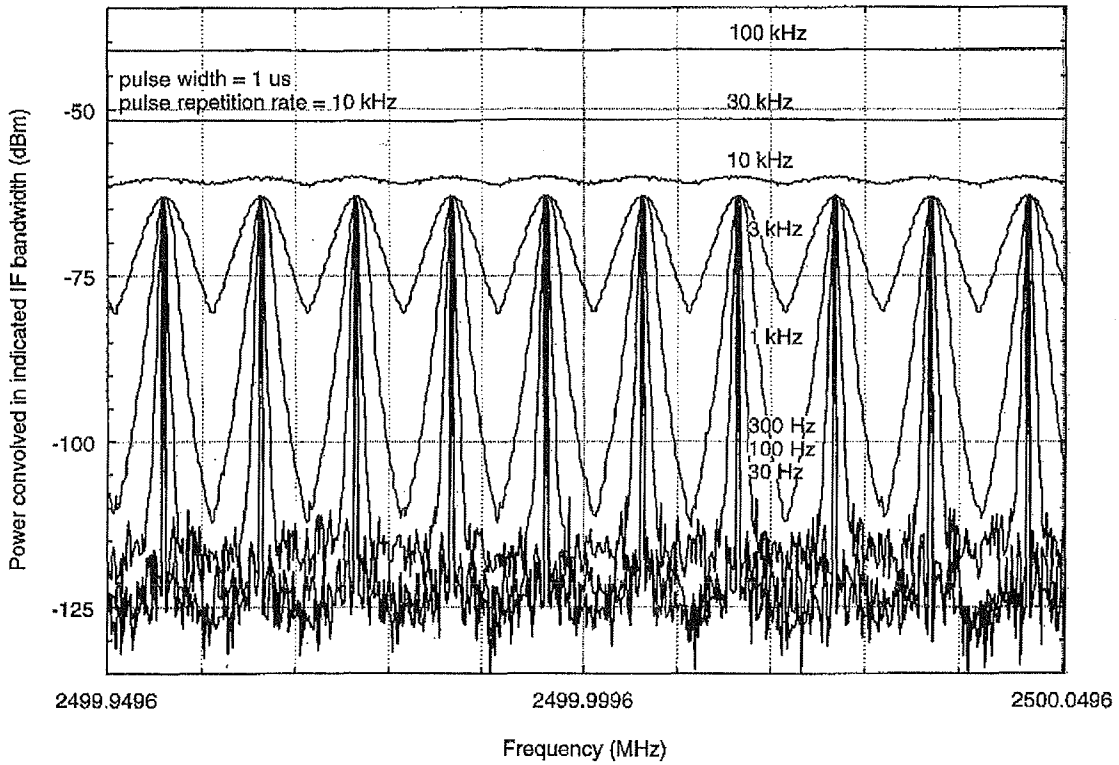

Figure 6.1. Detailed line spectrum measurement for a fixed-pulse-repetition rate transmitter. Pulse width is 1 μs and pulse repetition rate is 10 kHz (pulse repetition interval is 100 μs). Duty cycle is 10log(1/100) = -20 dB. Peak power from the transmitter is -20 dBm and RMS average power is -40 dBm. Measured line power is -60 dBm. Multiplying the power per line by the number of lines in the central lobe of the spectrum at the 3-dB points gives [(-60 dBm + 20 dB) = -40 dBm] for the computed average power, in agreement with the known average power. Note 20log(bandwidth) progression for measured power when convolution bandwidth exceeds the line spacing.

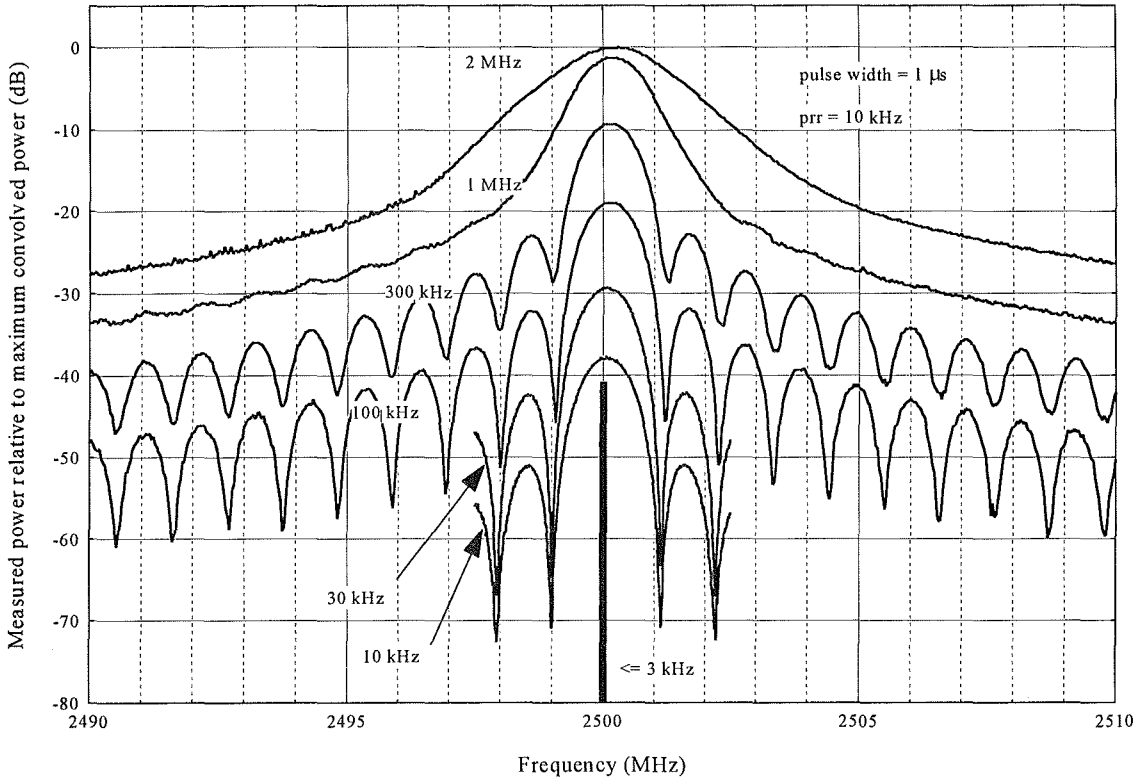

Figure 6.2. The spectrum of Fig. 6.1 is shown for wider measurement bandwidths. 20log(bandwidth) progression holds up to bandwidth of (1/pulse width)= 1 MHz. When bandwidth exceeds (1/pulse width), only a small additional percentage of power is convolved.

As long as measurement bandwidths are narrower than the convolved spectrum features, the measured emission envelopes of all peak-detected emission spectra will vary as a function of measurement bandwidth at a rate between $10\log_{10}$(bandwidth), as for noise, and $20\log_{10}$ (bandwidth), as for pulsed signals. Other signal modulations may produce rates intermediate between $10\log_{10}$ and $20\log_{10}$. UWB device emission levels may vary with bandwidth at such intermediate rates.

Measurements of UWB emissions will show the functional bandwidth dependence empirically. If the dependence is $10\log_{10}$ (the same as thermal noise in the measurement system), then the SNR and dynamic range of the measurement will be constant as a function of measurement bandwidth. If the UWB emission dependence is between $10\log_{10}$ and $20\log_{10}$ of measurement bandwidth, then SNR and dynamic range of a UWB spectrum will increase with increasing measurement bandwidth, until the measurement bandwidth equals the emission bandwidth of the UWB emitter. If measurement bandwidth exceeds the UWB emission bandwidth, the SNR and

dynamic range will decrease, as the convolved power in the UWB spectrum will remain constant but the thermal noise convolved by the measurement system will increase at a $10\log_{10}$ rate.[8]

6.3 Measurement Approaches

The application of hardware and software to the task of characterizing UWB emissions is described below. Unless otherwise noted, the descriptions are taken directly from operational measurements performed on UWB devices at the ITS laboratory.[9]

6.3.1 COTS Hardware Requirements

The following types of equipment are generally required for UWB measurements:[10]

- spectrum analyzer with general purpose interface bus (GPIB) capability,
- digital oscilloscope with GPIB capability,
- RF front-end hardware such as low noise amplifiers, bandpass filters, and attenuators, packaged either as discrete components or within COTS RF front-end preselectors,[11]
- broadband antennas designed for electromagnetic interference (EMI) and electromagnetic compatibility (EMC) measurements, and

---

[8]As the emission bandwidths of UWB devices are often in excess of a gigahertz, it may be assumed that a bandwidth limited measurement system will not have an IF bandwidth wide enough to completely convolve the UWB emission.

[9]The results of measurements performed with these procedures are reproduced in detail in Appendices A-E, and are summarized in Section 8 of this report.

[10]A vector signal analyzer (VSA) may be substituted for the spectrum analyzer and oscilloscope specified in this list. However, ITS has not yet performed UWB emissions with a VSA, and the ultimate feasibility of these measurements with a VSA has therefore not been determined by this laboratory.

[11]For example, this capability may be provided by an Agilent (formerly Hewlett-Packard) 85685A preselector. Other COTS RF front-ends are available from other manufacturers; the equipment described here is specified only for the purpose of explaining the type of capability that the RF front-end is expected to contain.

- laptop PC-compatible computer or equivalent that can be connected to a GPIB or equivalent interface for instrument control and data acquisition.[12]

6.3.2 Software Requirements

Some measurements that characterize UWB emissions, such as amplitude-probability distributions (APDs, described below), require the acquisition of thousands or millions of data points.[13] Such measurements are difficult or impossible to perform adequately[14] with systems that are manually controlled and operated. Raw measurement data may be so voluminous as to make analog recording techniques (e.g., pen-plotter outputs) impractical; some types of data analysis (e.g., APD generation from raw data) operate on data quantities that can only be reduced by computers. For these reasons, measurement laboratories engaged in UWB emission characterization should be equipped with a computer that can be used to control measurement instrumentation, acquire data through a widely available bus interface (e.g., GPIB), and analyze the resulting data.

Software to perform limited instrument control, data retrieval, and analysis will be necessary to complete the measurements and produce analyzed data sets. The software should perform the following functions:

- Set spectrum analyzer parameters, including center frequency and frequency span, IF bandwidth, video bandwidth, detector type, sweep time, attenuation, reference level, and number of points per data trace (if necessary);

- Set digital oscilloscope measurement parameters, including time base, voltage scale, coupling mode, and trigger mode;

- Command a specified number of data traces (e.g., 1000 traces) to be triggered on a spectrum analyzer; and

---

[12]An example of this type of interface is the National Instruments GPIB-to-parallel interface adapter. Other types of GPIB adapters are available from other manufacturers; this device is specified only for the purpose of describing the type of capability required.

[13]Some spectrum analyzers with integrated APD capabilities are becoming available as of the release date of this report. These machines were not available for use by ITS when the report was written.

[14]An adequate measurement is defined to be efficient (requiring a minimum of operator time and knowledge to perform), repeatable, and automatically documented by the measurement system.

- Command a specified number of data traces to be taken on a digital oscilloscope;

- Record to selected media (hard disk, magneto-optical disk, etc.) all triggered data traces from a spectrum analyzer and a digital oscilloscope to the controlling computer. Each trace from the measurement instrument should be recorded as an individual data record; and

- Record critical supporting information with each data record. Such documentation might consist of instrument settings, date, time, and logistics information such as the name of the device being measured and the measurement engineer.

The software must support the following functions on recorded data:

- Add calibration factors to measured data values, if such corrections were not included in raw data (necessary corrections are described in detail below);

- Correct measured spectra for variable effective aperture of the measurement antenna, as described in Part 4 of Appendix C and (also below in this section);

- Retrieve individual data records (with corrections described above) for CRT screen display and printing (these should include spectrum measurements and time waveforms);

- Process hundreds or thousands of individual spectrum analyzer or oscilloscope data records into APDs, as described below (software should store generated APDs for later retrieval and printing). (Alternatively, some newly available spectrum analyzers incorporate integrated APD capabilities. See footnote 13.)

Commercially available measurement and data analysis software packages that perform every function described above probably are not available; however, some combination of commercially available packages may be adequate to perform the necessary functions.[15]

---

[15]At the ITS, the software used for these measurements was originally written to control a custom-designed NTIA measurement facility, the Radio Spectrum Measurement System (RSMS). As such, the RSMS software package is much more complex than is required for UWB device emission measurements.

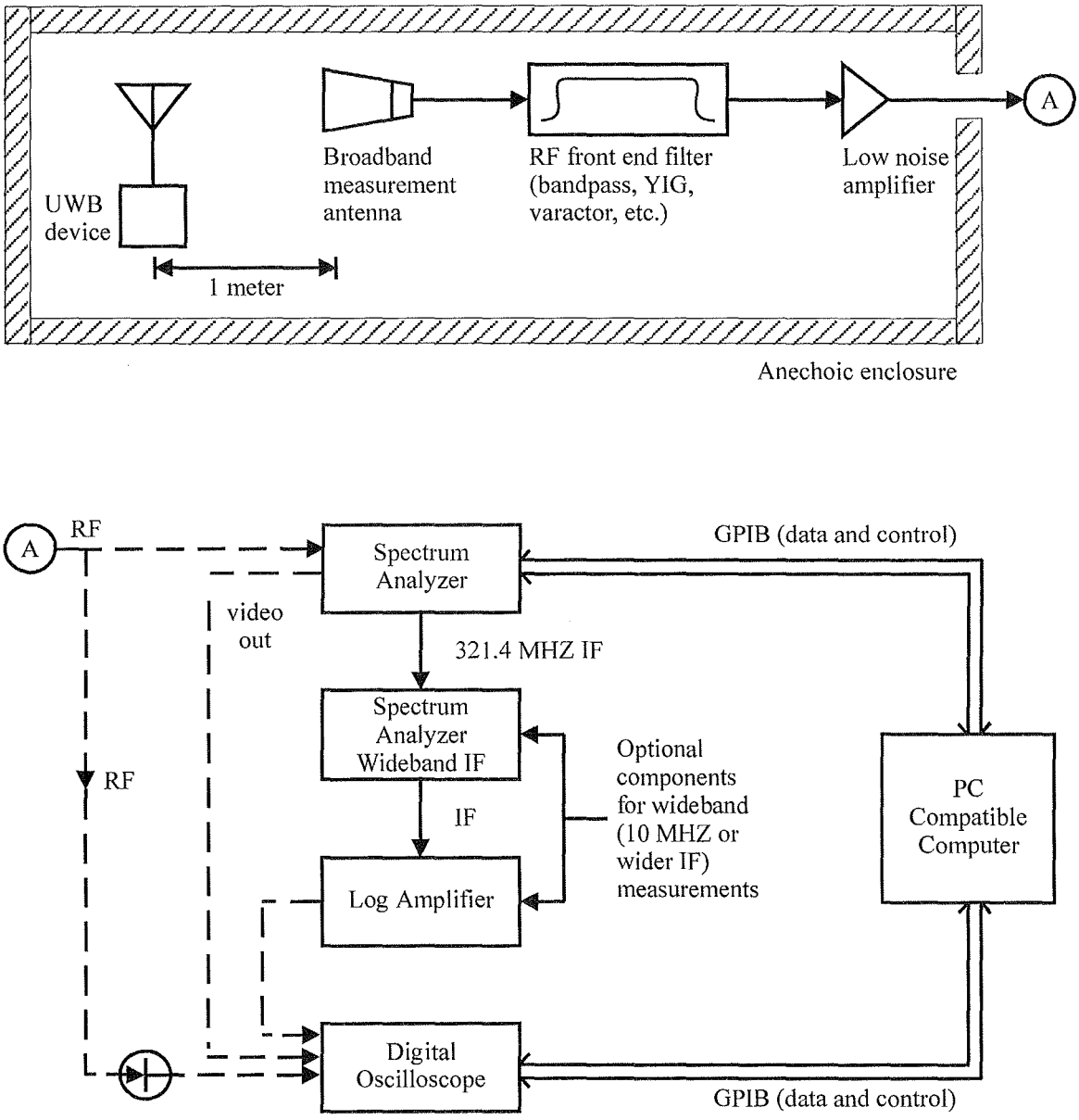

Figure 6.3. UWB emission measurement block diagram.

6.3.3 Generalized Measurement System

A generalized measurement system for characterization of UWB device emissions is shown in Figure 6.3. The components shown in the figure are described in detail below.

Measurement Environment. The UWB device should be placed in an environment where measurement system multipath and external radio signals are eliminated or minimized. The best

possible choice is a high-performance anechoic chamber. For ITS measurements, no such facility could be scheduled for use within the time constraints of this project. Two alternative environments that were utilized during ITS measurements were a large room (measuring about 15 m by 15 m by 10 m high) with a metal ground plane, and a smaller laboratory room with a temporary enclosure built of stacked anechoic foam blocks. In the large room, UWB devices were mounted on Styrofoam blocks about 2.5 m above the ground plane; in the anechoic enclosure, UWB devices were mounted at a height of about 1 m above the floor.

Background signals may present a problem for UWB measurements not performed in an anechoic chamber. This problem is exacerbated by the emission bandwidths of UWB signals, which may in some cases occur in portions of the spectrum occupied by prominent background signals including UHF television (512-806 MHz); analog cellular and trunked mobile communications (806-902 MHz); pagers (928-932 MHz); PCS cellular communications (1.9 GHz); air route surveillance radars (1215-1400 MHz); and tactical air surveillance radars (2.7-3.7 GHz, and especially 2.7-2.9 GHz for airport surveillance radars). Signals from these sources may be attenuated somewhat by the walls of the laboratory, and may be further reduced within an anechoic foam enclosure. But measurements of background levels should be performed prior to UWB device emission measurements, and can subsequently be subtracted from the measured UWB spectra to yield the UWB spectra alone.

Measurement Antenna. Measurement antennas must have a sufficiently wide frequency response. This may be a non-trivial problem for UWB device emissions. UWB measurements by ITS have typically spanned such frequency ranges as 600 MHz to 6 GHz, a full octave. Multiple antennas may be required if the frequency range to be measured is not completely included by a single antenna.[16] Commercially available wideband horn antennas have performed well for all ITS and some National Institute of Standards & Technology (NIST) measurements described in this report. If the measurement antenna polarization is linear, the antenna orientation needs to be matched to the polarization orientation of the device being measured. This is accomplished by rotating the measurement antenna until the received power level is maximized.

Because UWB device emissions may be relatively low-amplitude, the measurement antenna will usually be placed as close as practicable to the device. The ITS measurements performed in the course of this project utilized an antenna at a distance of 1 m from the devices being measured.[17]

The measurement antenna must be calibrated for the distance at which measurements are performed. Again, wideband horn antennas have proven to be workable in this respect, as they

---

[16]Some commercially available antennas may perform adequately at frequencies beyond their nominal specifications. Such performance extensions can be determined at a qualified antenna test facility.

[17]The antenna must be located in the far field of the device being measured.

typically can be acquired with calibration curves made at 1 m. If the measurement antenna does not have a constant effective aperture (i.e., if the antenna gain does not increase as $20\log_{10}$ [measurement frequency]), the resulting spectra must be corrected to the constant effective aperture case. Section C.4 of Appendix C describes the necessary spectrum corrections for non-constant effective aperture measurement antennas.

RF Front-end. Because UWB device emissions are often too weak to overdrive the noise figure of spectrum analyzers, a low-noise amplifier may be required at the output of the measurement receiver antenna. All devices measured by ITS for this report required such front-end preamplification. In an optimized measurement system, the sum of the preamplifier gain and preamplifier noise figure should be nearly equal to the noise figure of the spectrum analyzer across the frequency range to be measured.[18]

Although UWB device emissions may have low amplitude within the convolution bandwidth of the measurement system, the total power convolved by the front-end preamplifier may be high enough to cause overload of that component. The preamplifier may also experience overload due to ambient signals if the measurements are not being performed in an anechoic chamber. Overload conditions must be checked by measurement personnel.[19] If overload is experienced, then appropriate RF filtering will be required between the antenna and the preamplifier.

Spectrum Analyzer. A spectrum analyzer may be used to measure both the bandwidth limited spectra and time domain information (when operated in zero hertz span). Spectrum analyzers typically have noise figures of 25 dB or more at frequencies below 2.5 GHz, and noise figures increase with frequency due to mixer noise, typically at a rate of about 5 dB per mixing stage.[20] As noted above, the preamplifier noise figure and gain should be optimized to work with this noise figure.

---

[18]Higher noise figure results in loss of sensitivity; gain that is too low will fail to overdrive measurement system noise, while gain that is too high will reduce available dynamic range. But since UWB emission measurements typically observe low-amplitude signals, dynamic range is not likely to be an important problem for these measurements.

[19]Overload may be checked by inserting attenuation between the antenna and the preamplifier and observing a corresponding drop in signal level at the spectrum analyzer output. If the drop is less than the attenuator value, then feed-through directly into the preamplifier or the spectrum analyzer may be occurring, or the preamplifier may be in an overload condition.

[20]Spectrum analyzer noise figure at a given frequency may be checked by terminating the input, setting RF attenuation to zero, IF bandwidth to 1 MHz, video bandwidth to 1 kHz, and detector to sample. The difference between the measured noise level and -114 dBm is the analyzer noise figure at that frequency.

Detector and Oscilloscope. Time domain measurements at bandwidths wider than those available in the spectrum analyzer are performed with a diode detector and an oscilloscope, as shown in Figure 6.3. For these measurements, the RF line is disconnected from the spectrum analyzer and is routed through the diode to the oscilloscope. Note that the bandwidth limited video output from a spectrum analyzer can also be routed to the oscilloscope, omitting the detector.

Optional Measurement Hardware for Bandwidths Wider than Nominal Spectrum Analyzer IF. For the ITS measurements, a commercially available wideband IF module was procured for one of the spectrum analyzers. This module was specified with performance to 100 MHz bandwidth, but the spectrum analyzer RF front-end was only 22 MHz wide, thus limiting the overall performance to a maximum of 22 MHz.[21] Because the wideband IF section did not include a detector, ITS measurements utilized a wideband log amplifier/detector at that module's output. The log detector output was connected to the oscilloscope input. Calibration was performed manually for this project, although software will be required in the long term.

6.3.4 Calibration

Measurement devices must be individually calibrated by certified facilities. But additional calibrations and corresponding corrections may be expected to be necessary for the complete UWB measurement system. These include:

Corrections for Non-constant Effective Aperture Measurement Antenna, and Conversion to Incident Field Strength. As described in Section C.4 of Appendix C, the measured spectra must be corrected for non-constant aperture of the measurement antenna. This correction is also required if the measured spectra are to be easily converted to incident field strength. Conversions between measured power in a circuit and incident field strength are derived in Section C.1 - C.3 of Appendix C.

RF Front-end. The frequency-dependent gain of the RF front-end (including the loss through the front-end filtering, if any, and the RF line from the preamplifier to the spectrum analyzer) must be subtracted from the power values measured at the spectrum analyzer. ITS generally uses a Y-factor noise diode calibration procedure for this purpose. Signal generators may also be used.

Special Wideband IF Unit and Discrete Wideband Log Amplifier/Detector, if Used. The wideband IF unit used by ITS for some measurements required provision for an IF gain factor within that unit. The response of the discrete log amplifier/detector between the wideband IF and the oscilloscope must also be calibrated, if these devices are used in the measurement system (Figure 6.3).

---

[21]The IF was used at 10 MHz and 20 MHz for the ITS measurements.

6.4 Types of UWB Measurements

6.4.1 Spectrum Measurements

Spectrum analyzer RF front-ends are sometimes on the order of two to three gigahertz wide for tuned RF frequencies below about three gigahertz.[22] At higher frequencies, such analyzers may incorporate a tunable RF bandpass filter which may be approximately 20 MHz wide. Some spectrum analyzers may be used in combination with external preselectors. These preselectors typically utilize varactor filters at frequencies below 500 MHz and yttrium-iron-garnet (YIG) filters at higher frequencies. The bandwidths of these preselector stages may be expected to be between 15 MHz and 35 MHz. If the ultimate bandwidth limit is in the IF section, then the widest bandwidths available will most often be between 3 MHz and 10 MHz. In exceptional cases, spectrum analyzer IF sections may be procured that are as wide as 100 MHz (as in Figure 6.3).

Spectrum Envelope Measurements. ITS spectrum analyzer measurements of UWB emissions were found to be most efficiently performed with the following spectrum analyzer settings: Swept-frequency mode, zero front-end RF attenuation, reference level chosen as appropriate for the UWB emission levels, positive peak detection, maximum-hold trace mode, video bandwidth at maximum, and IF bandwidth selected progressively from the widest available bandwidth (3 MHz) to a much narrower setting (10 kHz, for approximation of land mobile radio bandwidths).

Swept-frequency measurements have been found to be fast and practical for UWB device emissions in this project. Only at bandwidths narrower than about 30 kHz does the sweep time exceed a few seconds across the requisite several gigahertz of spectrum. For some spectrum analyzers, it may be impossible to perform a single sweep across the entire range of interest (e.g., 800 MHz to 6 GHz). In those cases, the spectrum is swept in two or more measurements (e.g., 800 MHz to 2.5 GHz, and then 2.5 GHz to 6 GHz). Automation of these measurements by ITS has increased the speed and reliability of the UWB measurement project and its results.

For spectrum measurements in IF bandwidths greater than the widest available in a conventional spectrum analyzer (e.g., wider than 3 MHz or 10 MHz, depending upon spectrum analyzer model), an optional wideband IF module and log amplifier/detector (or other circuitry with equivalent operational capability) will be required, as shown in Figure 6.3. The wide-bandwidth measurement is performed as follows: The spectrum analyzer is tuned to the first frequency to be measured in the spectrum, in a zero hertz span. A single oscilloscope trace is acquired through the wideband IF and the log amplifier, as shown in Figure 6.3. The oscilloscope sweep time must be long enough to ensure that a maximum-power pulse from the UWB device is recorded

[22]This is the case, for example, for some spectrum analyzers which couple input signals at frequencies below two or three gigahertz directly into a mixer downconverter.

somewhere on the trace. After the oscilloscope trace is recorded, the spectrum analyzer is tuned (still in a zero hertz span) to a second frequency. The second frequency should be as close as practicable to the first frequency plus the IF bandwidth. For example, if the first frequency is 800 MHz and the IF bandwidth is 20 MHz, then the second frequency is 820 MHz. The measurement is repeated, with a data trace recorded as before. This process continues until the entire spectrum has been measured. For the example given here, if the spectrum to be measured is 800 MHz to 6 GHz, then the set of frequency steps at which measurements will be recorded from the oscilloscope will be 800 MHz, 820 MHz, 840 MHz, etc., to 6 GHz. For the hypothetical case described here, the measurement would require the acquisition of 260 oscilloscope traces; therefore, this process is most efficiently and reliably performed with an automated (software-controlled) data collection system.

To generate the spectrum in the wide IF bandwidth, each oscilloscope trace must be retrieved from storage, the maximum (peak-voltage) point on each trace must be determined, and those voltages must be converted to power values in the measurement circuit. This is done by making use of the log amplifier/detector calibration that was performed earlier. The final spectrum for the example considered here would consist of 260 data points. The process of retrieving thousands of raw data points, selecting the 260 maximum amplitude points from each trace, converting those points to power in the measurement circuit, and plotting the points as a spectrum requires software.

Bandwidth-dependence Measurements. As noted in 6.2.2 (above), measured emission amplitudes from UWB devices vary as a function of measurement bandwidth. This variation represents the relative levels that are coupled into receivers that are bandwidth limited. For purposes of EMC/EMI characterization, and possibly also for regulatory and statutory purposes, it is therefore necessary to understand the rate of the progression for extrapolation to arbitrarily specified receiver bandwidths. Determination of this bandwidth dependence may be performed in two ways. The first is to measure the entire spectrum (as above) in at least several bandwidths, and note the progression between one spectrum and the next. The second method, which can be performed at specific frequencies of particular interest (e.g., a global positioning system satellite frequency at 1575 MHz) may be performed as follows:

Place the spectrum analyzer in a zero hertz span mode at the frequency of interest. Set the detector to positive peak and the attenuation to zero. Set the video and IF bandwidths to their widest possible values. Set the sweep mode to "single" (i.e., so that only one sweep will be acquired when the proper trigger button on the analyzer is pushed). Set the sweep time to 60 seconds. With the UWB device emissions in progress, start the single sweep. At intervals of 6 seconds, reduce the IF bandwidth in a 1, 3, 10 progression or some approximate equivalent. The result will be a stair-step trace as shown in Figure 6.4. This progression is a direct indication of the relative peak-detected coupling at IF bandwidths of 3 MHz, 1 MHz, 300 kHz, etc., down to 100 Hz.

Depending upon the transmitter characteristics, it has been observed that the bandwidth progression is not necessarily constant from one step to the next, as seen in Figure 6.4. Such non-uniformity is documented by this measurement technique. At wider bandwidths, the

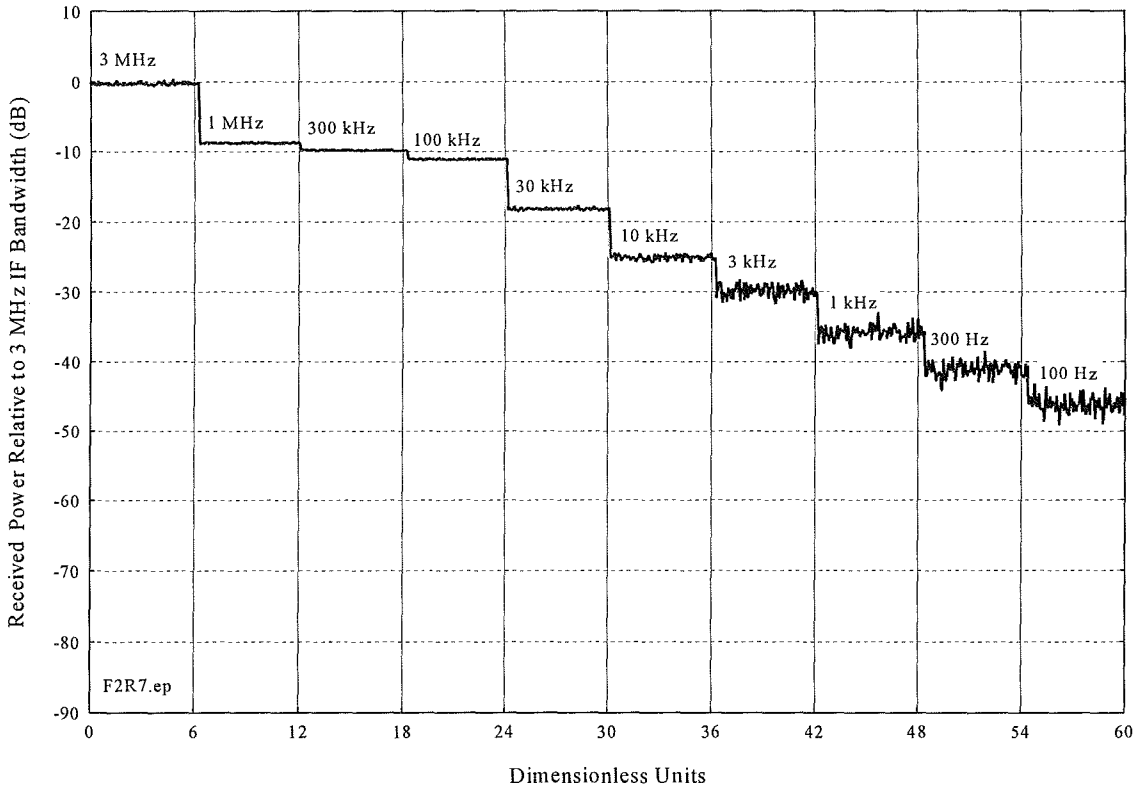

Figure 6.4. Bandwidth progression measurement example for a UWB signal. The emission is a pulse sequence (2 MHz pulse repetition rate) that dithers about 1% of the nominal pulse repetition interval on a relative (pulse-to-pulse) time base. The variable-rate progression demonstrates the usefulness of empirical data for determination of coupled UWB peak power as a function of receiver bandwidth.

progression indicates extrapolated levels for bandwidths wider than those that can be directly measured (e.g., 50 MHz). The method of extrapolation is described in Section 8 of this report.

6.4.2 Amplitude Probability Distribution Measurements

Amplitude probability distribution (APD) measurements show the percentage of time[23] that emissions from a device exceed a given power threshold. APD plots are typically produced on Rayleigh scales, as shown in Figure 6.5. APDs have been a critically important tool for the ITS characterization of UWB emissions. An APD curve will show the entire time-occupancy distribution at a frequency and in a selected bandwidth. It may be processed to show peak level in the bandwidth and several averages, including root-mean-square (RMS) (that is, linear average power), average voltage, and log average. APDs are discussed in more detail in Appendix A.

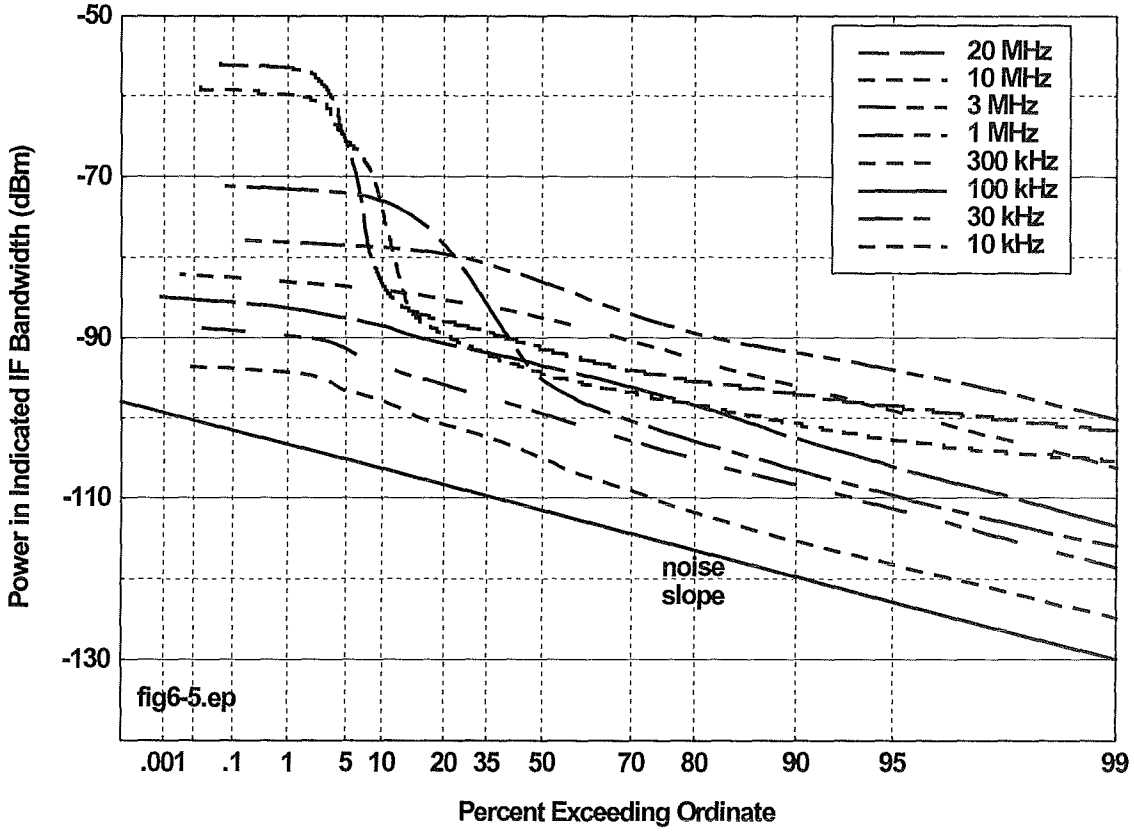

Figure 6.5. APD measurement example. The data for bandwidths of 10 kHz to 3 MHz were acquired with a spectrum analyzer. The data in 10 MHz and 20 MHz bandwidths were acquired with a commercially available wideband IF spectrum analyzer, detected with an external log amplifier, and recorded from a digital oscilloscope. Refer to Figure 6.3 for measurement system block diagram.

[23]Actually, percentage of samples, but if the sampling is not correlated with the device emissions, this becomes equivalent to percentage of time.

APD measurements require that power level in the UWB device emission be sampled as a function of time at the desired frequency and bandwidth. The time sampling may be performed with either a spectrum analyzer or a digital oscilloscope.[24] For either approach, the APD measurement will require automation of at least some portions of the measurement system.

APD Sampling with a Spectrum Analyzer. Unless a spectrum analyzer incorporates an integrated APD capability (see footnote 13), APD sampling is performed as follows: The spectrum analyzer is tuned in a zero hertz span to the desired frequency. Attenuation is set to zero, and reference level is set to a value that is about 10 dB above the maximum UWB emission amplitude. The spectrum analyzer video bandwidth is set to the widest possible value. Sample detection is selected.[25] The IF bandwidth is selected as required for the APD curve (in these measurements, values between 10 kHz to 20 MHz were used). Sweep time is unimportant, with the caveat that it must not be synchronized with the UWB device operation in any way.

With the UWB device in operation, a sweep is taken, and the data trace that results is stored electronically for future retrieval. This process is repeated until an adequate number of samples have been collected. If 1,000 points are generated within each spectrum analyzer sweep, then 100 sweeps will collect 100,000 points. It has been determined that between 100,000 and 1,000,000 points are required for adequate APD data on a variety of UWB transmitters. In the experience of ITS on this project, the measurement system needs to be automated for the generation and acquisition of the corresponding number of sweeps (between 100 to 1,000) if the measurements are to be performed efficiently and reliably.

Because APD measurements do not reconstruct waveforms, APD sampling rates are not constrained by the classical Nyquist rate of (2 x sampling bandwidth). Slower sampling is permitted under the condition that the samples are statistically uncorrelated with UWB device

---

[24]APD sampling may also be performed directly with some newly available spectrum analyzers. Vector signal analyzers may also be feasible, but ITS has not tried a VSA to date.

[25]In the course of this project, it was observed that the sample detector bandwidths of some spectrum analyzer models are narrower than the widest IF bandwidths in the same analyzers. This problem can be checked as follows: Terminate the spectrum analyzer input, set the frequency span to zero Hz, and set the tuned frequency to any value (e.g., 1 GHz). Select the widest IF bandwidth with positive peak detection and maximum-hold trace mode. Allow the trace to build to a maximum. Retain the resulting trace on the analyzer display. Select a second trace, and change to sample detector mode. Select maximum-hold trace mode and allow the resulting trace to build to a maximum. If the maximum-hold sample detector trace does not eventually build to the same level as the maximum-hold positive peak detector trace, contact the spectrum analyzer manufacturer.

operations (e.g., the UWB pulse gating interval should not be synchronized with measurement equipment sampling).

APD Sampling with an Oscilloscope. An oscilloscope may be required for the collection of data samples at IF bandwidths exceeding the maximum available in conventional spectrum analyzer IFs. The ITS system, for example, utilized a specially procured (but commercially available) wideband IF unit that is housed in a spectrum analyzer chassis but that does not incorporate the spectrum analyzer detector functions (Figure 6.3). An external, discrete wideband log amplifier/detector was used to send 10 MHz and 20 MHz IF data to a digital oscilloscope. The oscilloscope was used to collect APD data in the same manner as the spectrum analyzer. The oscilloscope must not be set in an envelope-detection or peak-detection mode or some other mode that biases the samples toward higher values. Oscilloscope data traces are recorded electronically for later retrieval and analysis. As for the spectrum analyzer, this is best accomplished with software-automated data collection routines.

APD Data Analysis. APD raw data must be converted into finished APD curves. Unless a spectrum analyzer contains an integrated APD capability (see footnote 13), there is no practicable way to do this without software. APDs may be generated by separating the points into predetermined bin sizes (thus reducing the size of the finished file), or by accumulating all of the 100,000 or 1,000,000 points into a statistically indexed array (resulting in a larger final APD file size). The APD curve is conventionally graphed on a Rayleigh plot,[26] as shown in Figure 6.5.

APD curves may be further analyzed to determine the following critical emission parameters at the measured frequency in the measured bandwidth: peak power, RMS average, average voltage, and log average. ITS engineers have found APD curves to be useful in part because of the amount of information that can be directly determined from them.

6.4.3 Pulse Width and Shape Measurements

Pulse Width. Detailed pulse width measurements require the use of a measurement systems such as those described in Section 5. But COTS equipment may be used to estimate pulse width. Two methods are available. The first is to measure the width of the UWB spectrum at 10 dB or 20 dB points.[27] The inverse is approximately equal to pulse width. This is only an approximate measure

---

[26]The Rayleigh plot shows decibel power on the ordinate vs. $10\log_{10}[-\ln(\%\ \text{samples}/100)]$ for samples exceeding the ordinate power.

[27]UWB spectrum measurements performed in this project did not generally result in clearly defined 3-dB bandwidths. Sometimes 10 dB was difficult to define; 20-dB points were generally definable.

of emitted pulse width, and includes the effects of final-stage UWB RF components such as output bandpass filters and the radiating antenna.

The second pulse width measurement method is to send the output of the measurement system to a discrete-component wideband diode detector, and connect the detector output to an oscilloscope. The oscilloscope may be used to estimate pulse width down to at least the inverse of the maximum oscilloscope bandwidth in single-shot (as opposed to repetitive sampling) mode. For a 50 MHz bandwidth, for example, pulse width may be estimated down to 20 ns. A scope that operates at 1 GHz bandwidth without repetitive sampling may be adequate to measure pulse widths down to about 1 ns. If scope bandwidth in single-shot mode is inadequate for measurement of a UWB pulse width, then the first method (estimating pulse width from spectrum width) may be the only available alternative.

Pulse Shape as a Function of Receiver Bandwidth. For purposes of EMI/EMC evaluation with various receiver types, the shape of the pulse should be measured through a spectrum analyzer in a variety of IF bandwidths. The pulse shapes are recorded in a range of bandwidths (e.g., 10 kHz to 20 MHz) for future reference in studies of compatibility with receivers having corresponding IF bandwidths. (This assumes that the pulse shapes so measured are determined by the impulse response of the receiver IF section.)

6.4.4 Pulse Repetition Rate, Dither Sequence, and Gating Measurements

In order to measure nominal repetition rates, dither sequences, and gating, pulse sequences must be measured. These have been found to be most easily measurable with the RF from the UWB transmitter connected to a wideband discrete-component diode detector. The diode output is connected to an oscilloscope and the pulse sequences are measured and recorded at time intervals ranging from several seconds to as little as (1/oscilloscope bandwidth).

Nominal Pulse Repetition Rate (PRR). The nominal PRR, if any is present, is easily read from an oscilloscope display.

Dither Measurement. Two types of dithering have been observed in UWB devices measured by ITS during this project. One is absolute time-base dither, in which pulses are triggered relative to an absolute time base. The other is relative time-base dither, in which each pulse is triggered at an interval that is measured relative to the preceding pulse, with no reference to a fixed time base. Absolute dither systems may have 50% dither on a pulse-to-pulse basis. Relative time-base systems may have only a 1% dither from pulse to pulse, but the variance in pulse occurrence grows with time. Both types of dither act to suppress lines in resulting emission spectra.

Dither may be observed and documented by triggering a storage oscilloscope on a pulse and then observing the intervals at which subsequent pulses occur. If absolute time-base dithering is occurring, only a few pulses need be measured to document this behavior. If relative time-base

dithering is occurring, then a storage oscilloscope is used to trigger on a pulse, and then the display is scrolled for an appropriate length of time (possibly many tens of milliseconds) to observe long-term growth in the dither variance. That is, if the relative time-base dither is 1%, hundreds of pulses must be observed after the trigger pulse to observe the total growth in the variance of pulse-occurrence time.

Gating. Pulse gating is a higher-level modulation of the UWB output, in which the transmitter is quiescent for intervals that are long compared to the nominal pulse repetition interval. Gating is easily observed on an oscilloscope output. It can also usually be measured on a spectrum analyzer in a zero hertz span mode, since the gating intervals are usually on the order of a few milliseconds to tens of milliseconds in duration.

6.4.5 Peak Power Measurements

Peak power may be measured in a bandwidth as described in Section 6.4.3 above. A spectrum analyzer is used to determine peak power in either a spectrum trace or at a single frequency in a zero hertz span mode. Peak power may also be read from an APD curve, as described above.

A significant problem is to measure total peak power in the emission bandwidth of the UWB device. This is not generally feasible in a direct measurement with COTS equipment. ITS equipment is currently capable of measuring peak power in 20 MHz bandwidth at the widest. Although an upgrade to 50 MHz and ultimately 100 MHz is planned for ITS systems, the COTS systems that will accomplish this are known to be expensive, and will require additional calibration routines (requiring dual implementation in software and hardware).

In short, for many laboratories engaged in UWB emission measurements, IF bandwidths between 3 MHz to 10 MHz may be the widest available for the immediate future. And in no case will peak power likely be measured at bandwidths equaling UWB emission bandwidths. Extrapolation to wider bandwidths will be a necessity if wider-bandwidth peak power measurements are required. Extrapolation will require the measurement of the emission in a succession of bandwidths (as the stair-step measurement in Figure 6.4), so that the rate of progression can be measured.

6.4.6 Average Power Measurements

Two averages that are widely used for various purposes are root mean square (RMS) average and logarithmic average. RMS average is the equivalent constant-rate of flow of energy from the transmitter over a time interval that is long compared to the nominal pulse repetition interval. Logarithmic average (average decibels) is required by such regulatory standards as Part 15 of CFR 47.209. While the logarithmic average is sometimes used vernacularly in an interchangeable sense with the term "average power," it must be stressed that the average decibel

level emitted by a transmitter is not equivalent to the RMS (arithmetic mean) average output power level.

Measurement of RMS Average. At least five alternative techniques for using COTS equipment to measure RMS emissions from UWB transmitters have been found to be feasible, as detailed below.

RMS Detector Integrated into a Spectrum Analyzer. As of 2000, most commercially available spectrum analyzers do not incorporate RMS detectors. But as of late 2000 and early 2001, some analyzers with integrated RMS detectors are becoming available on the commercial market. One such analyzer became available to ITS engineers for evaluation purposes just prior to this report's release, too late to be used in the UWB measurements contained in this report. But ITS engineers were able to evaluate the detector's performance characteristics on some UWB signals. The outcome of that preliminary evaluation indicated that this integrated detector appeared to offer a technically feasible solution to the problem of measuring RMS values of UWB emissions. It is anticipated that similar RMS detectors in other newly available spectrum analyzers will be similarly feasible for measurement of UWB average emissions.

Power Meter RMS Measurement.[28] RMS power may be measured directly with a power meter, under some conditions. The power meter must utilize a bolometer-type sensing head. The UWB signal must be at least 10 dB above the thermal noise in the measurement head, so that the power being averaged is primarily an indication of the UWB device emission and not of the thermal noise in the power meter. The limited experience that ITS has in this particular measurement on UWB-like signals has indicated that it is difficult to realize a sufficiently high SNR on UWB signals if measurements are performed on radiated (as opposed to hardline-coupled) signals. Diode-type power meters may have insufficient dynamic range for the required UWB measurements.

Spectral Line Power Measurement. If the UWB device produces a line spectrum (i.e., the signal is not a dithered pulse sequence or other noise emission), then average power may be derived from measured power in a maximum-amplitude spectrum line. The functional relationship is given by Equation 6.5, above.

---

[28]The measurement of RMS power from UWB devices with power meters was not part of this project.

APD Curve Calculation. RMS may be directly computed from the APD curve for the frequency and bandwidth in question. It may also be computed as the APD is generated.

Computation from Spectral Line Measurement or from Duty Cycle and Peak Power Measurement. The peak power is related to the average power and the power in a maximum-amplitude line by the relationship in Equation 6.5. However, many UWB devices do not generate line spectra.[29] For these devices, average RMS power may be calculated by multiplying the peak power in a bandwidth by the duty cycle. Duty cycle may be measured directly (if pulse width can be measured directly or at least estimated (see above)). Less desirably, from the standpoint of measuring quantities directly, duty cycle may be taken from a specification sheet for the device.

Measurement of Logarithmic Average. A logarithmic average may be measured directly from a spectrum analyzer as follows: With the analyzer in a zero-hertz span mode, set IF bandwidth to a desired value (e.g., 1 MHz, if log average power in 1 MHz is required). Video bandwidth is narrowed to a value on the order of a few hertz. (10 Hz to 10 kHz video bandwidth is specified by some regulatory measurement procedures.) The resulting log (decibel) average is read from the spectrum analyzer display, with some caveats.

The caveats are critical, from a technical standpoint. First, ITS has discovered that some UWB emissions generate log averages that are below measurement system noise, as shown in Figure 6.6. In such a case, the attempted log average measurement converges on the measurement system noise floor rather than the log average emission of the UWB device. Given that the measurement system noise in the widely used COTS preselector was eleven decibels above ambient thermal noise in this case, and that the broadband horn measurement antenna was placed 1 m from the UWB device, it is difficult to design a COTS measurement system that will achieve better SNR on the UWB signal than that shown in Figure 6.6. The failure of the log average technique to indicate only the measurement system noise in this case means that the technique is not generally applicable to UWB devices as a class.

Log average may also be computed from an APD curve, just as for RMS average. But if the log average is below the measurement system noise, the log average will not be computable from the APD curve.

---

[29]This includes devices that generate line spectra; for example, absolute time-based dither signals generate lines at the interval of a PN code sequence, on the order of 1 kHz or 10 kHz.

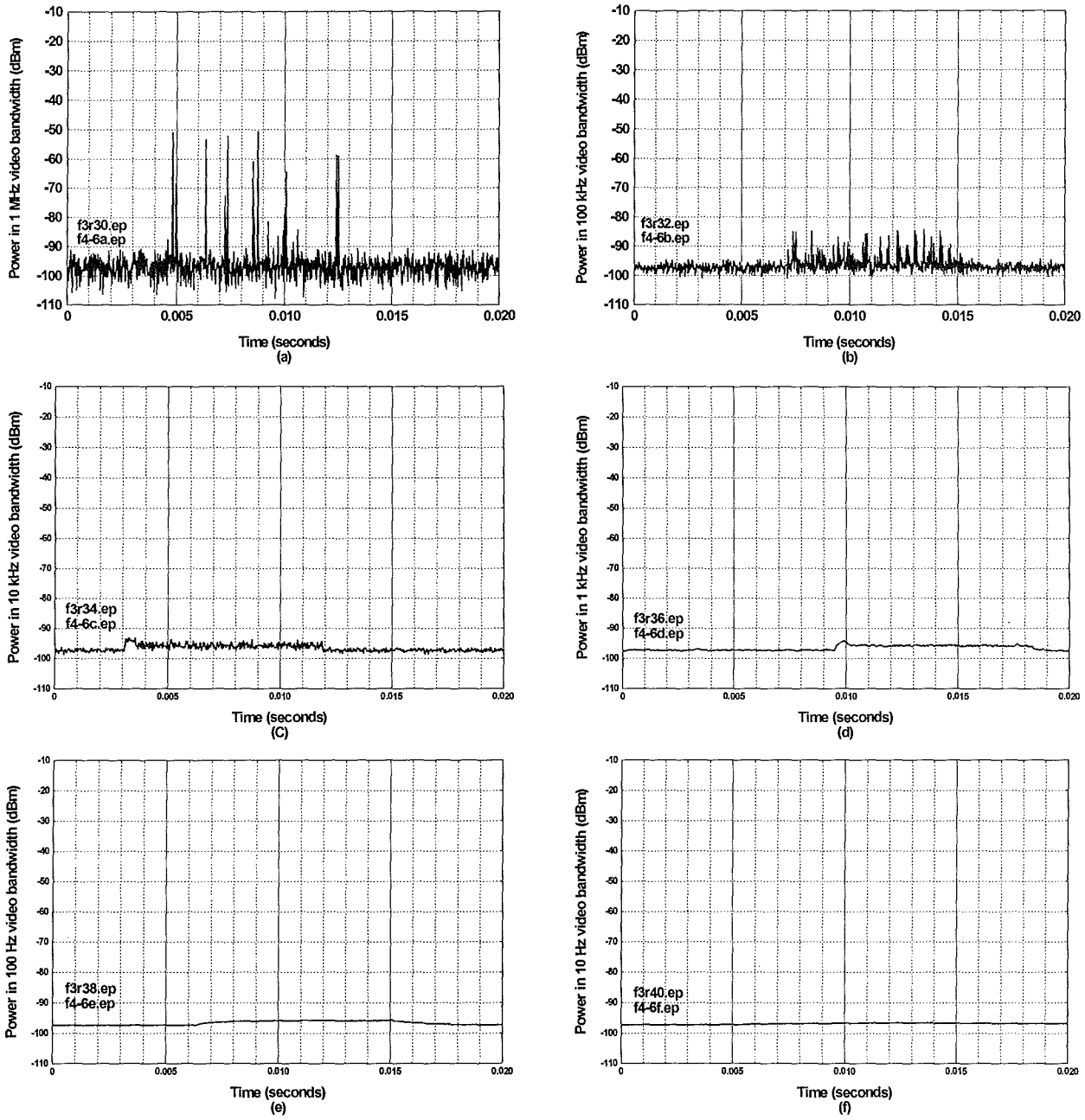

Figure 6.6. Log average measurement for a gated UWB transmitter with a low duty cycle. IF bandwidth = 3 MHz and video bandwidth is narrowed from 1 MHz to 10 Hz ((a) through (f)). This measurement converges on the measurement system noise floor, and thus fails to indicate the device's true log average. Measurement antenna was 1 m from transmitter, and measurement system noise figure was 11 dB. Given that little improvement in signal to noise ratio would be achievable for this measurement with COTS equipment, this serves as an example of the difficulty in assessing average power from all types of UWB transmitters using this technique.

6.5 Summary of Bandwidth Limited Measurement Techniques for UWB Devices

In summary, a UWB measurement system utilizing COTS equipment for bandwidth limited measurements can be achieved with commonly available laboratory hardware. The general measurement configuration may be as shown in Figure 6.3. Low-noise preamplification will often be required. Calibration of measurement equipment is critical, and should include corrections for non-constant aperture measurement antennas.

The primary measurement equipment required includes a spectrum analyzer, an oscilloscope, a discrete-component diode detector, a laptop computer that can perform simple commands and data acquisition on the analyzer and the oscilloscope, and software that can perform limited commands, data retrieval, and data processing as described above.

Emission spectra, bandwidth dependence of emission amplitudes, amplitude probability distributions, pulse repetition rates, pulse dither sequences, and emission gating may be measured. Pulse shapes may be measured as a function of receiver IF bandwidth. Pulse width may be estimated but probably not measured precisely. Peak power in a bandwidth may be measured, and may be estimated for any bandwidth. Average power measurements are more problematic; RMS may be measured directly with an appropriately equipped spectrum analyzer or a power meter (if important conditions are met). Average power may alternatively be estimated with alternative methods. Log average may be directly measured for some UWB devices, but cannot be measured for UWB emitters as a general class.

SECTION 7: EFFECTS OF TWO UWB SIGNALS ON THREE FEDERAL RADARS

Brent Bedford[1]

7.1 Introduction

Some UWB signals appear to occupy a relatively large portion of the spectrum when compared to the spectral occupancy of the signals of conventional systems. This leads to the notion that UWB systems may need to share the same spectrum with conventional incumbents. As in the case where two conventional systems share spectrum, questions are raised about the effects of a new system sharing spectrum with an incumbent. NTIA conducted the following study to determine the levels at which a UWB signal could be present within a radar receiver.

The study involved two types of UWB signals. Both types of UWB signals consisted of pulses at a 10 MHz pulse repetition rate (PRR). Both types had the same pulse shape and amplitudes. The first signal type was dithered using pulse position modulation over 50% of its basic repetition rate. In other words, there was a basic repetition interval of 100 ns. Each pulse was delayed from 0 ns to 50 ns within each interval. The position for each pulse was determined by a uniformly distributed random number generator. The second signal type was not dithered; the pulses were generated at a constant rate. The non-dithered signal produces spectral lines which have a frequency spacing equal to the reciprocal of the pulse rate. Since the pulse rate used in this study was greater than the receiver's bandwidth, for the case of the non-dithered signal, only a single spectral line was present within the receiver's passband.

Three Federal Aviation Administration (FAA) radio receivers were involved in the testing: the Air Route Surveillance Radar (ARSR-4), the Airport Surveillance Radar (ASR-8) and the Air Traffic Control Beacon Interrogator (ATCBI-5). The ARSR-4 is a long range radar that detects targets up to 518 kilometers away. The ASR-8 assists with traffic control at airports and detects targets up to 124 kilometers away. The ATCBI-5 transmitter interrogates transponders that are located on aircraft, while its receiver detects and processes the responses from the aircraft transponders. All three of these receivers are located at the FAA Mike Monroney Aeronautical Center (MMAC) in Oklahoma City, Oklahoma.

7.2 Radiated Measurements

The radiated measurements involved radiating a signal over a line-of-sight path from the UWB source to the receiver under test. The levels, relative to the receiver's noise floor, were measured

---

[1]The author is with the Institute for Telecommunication Sciences, National Telecommunications and Information Administration, U.S. Department of Commerce, Boulder, CO 80305.

and recorded. The results of this study will assist with determining any effects on these receivers if their spectrum is shared with UWB devices. The radars at the MMAC are good representations of radars that are operating in the field. These radars are fully functional but they are not being used to generate the critical information needed by air traffic controllers. The receivers are connected to rotating antennas that are the same as the field units. The FAA uses these radars to test new concepts before implementing the concepts on all their units and to train new personnel.

To conduct this study, the following approach was implemented. A measurement vehicle was outfitted to record the received signal level from an operating radar while the vehicle was in motion. A GPS unit was installed in the vehicle. The measurement started on the road next to the radar. The starting location was stored as a way point in the GPS receiver. The GPS receiver was set to display the distance and bearing from the vehicle to the radar. The vehicle was driven along roads that approximated radials from the transmitter. When a peak in the signal level occurred, the distance and bearing to the radar were recorded.

The results from the various runs were examined to identify the locations in which the maximum signal level was received. By reciprocity, these locations would offer the best chances for seeing any effects that the UWB transmitter would have on the receivers. The results showed that the signal level right under the radar was not the maximum level. Radar antennas typically concentrate their radiated energy into narrow beams. This is necessary for them to determine bearing and range to a target. These beams are directed into the sky to detect airborne craft. The lowest angle of interest for the beam is usually slightly above the horizon. The area under and close to the antenna is not directly illuminated by the beam, so only a moderate signal level exists. An example of this is shown in Figure 7.1. For approximately the first 1.75 horizontal divisions, the signal is relatively undefined with rapid variations. After 1.75 horizontal divisions, the spikes are well defined and vary smoothly.

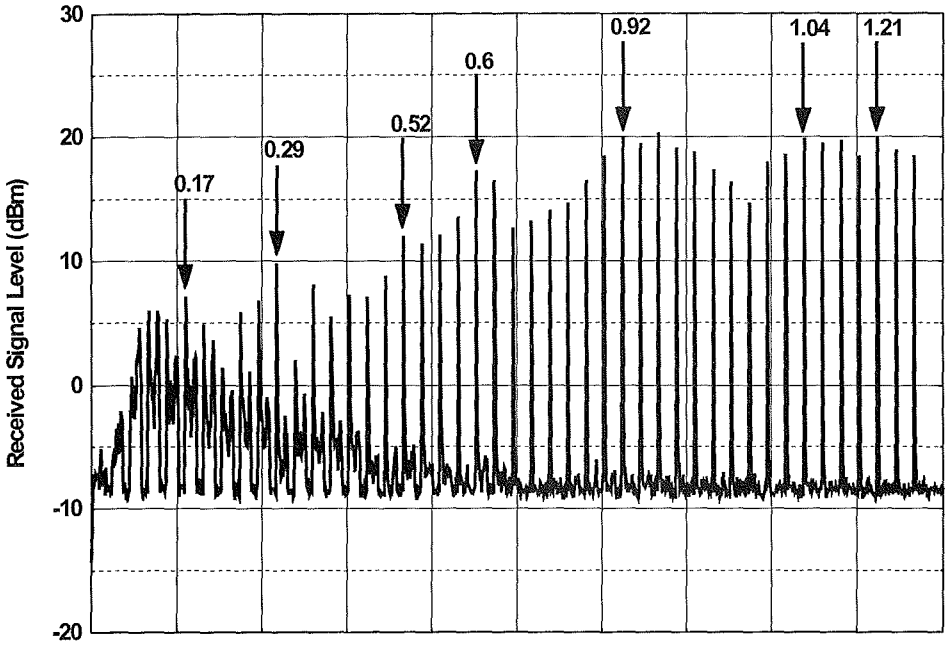

Figure 7.1. ARSR-4 signal level along a southern radial.

Foliage and buildings are other factors that influence the received signal level. When either of these obstructions enter the line-of-sight path between the vehicle and the radar, the received signal level drops rapidly and a good sample at that distance is lost. The measurements were conducted over several approximately radial paths in an attempt to get samples over a large number of distances.

Once the locations of highest signal level were known, the next part of the study took place. The Intermediate Frequency (IF) output of the radar receiver under test was connected to the spectrum analyzer. The noise level on the spectrum analyzer was noted at the expected IF frequency before connection to the IF output. All the levels were measured with the spectrum analyzer resolution bandwidth set to 1 MHz and the video bandwidth set to 10 Hz. This is the same spectrum analyzer settings that are used in a FCC Part 15 compliance measurement for frequencies above 1 GHz. The spectrum analyzer was connected to the receiver's IF output and the noise level was noted again. It was necessary for the noise coming from the IF receiver to raise the noise floor of the spectrum analyzer a perceptible amount in order for the measurements to be valid. This was the case for all of the receivers in this study.

The measurement vehicle was configured to house the UWB transmitter. A ridged horn antenna was mounted on a telescoping mast on the vehicle. While measurements were being conducted, the horn antenna was elevated above the vehicle roof to prevent reflections. For each measurement, the UWB transmitter was adjusted, by a variable attenuator, to produce an effective isotropic radiated power of -41 dBm. This level corresponds to the radiated emission limits found in FCC Part 15.209 for frequencies above 1 GHz.

The measurement vehicle was parked near some of the locations of highest signal level as well as a few others. It usually was not possible to pull off the road right where a peak occurred. The horn antenna was raised and pointed at the radar under test and the UWB transmitter was activated. The radar transmitter was then turned off and its antenna was manually pointed in the azimuth of the vehicle. The antenna was swung through many degrees to find the peak delta marker value, which was recorded. The delta marker value consists of setting a reference level with the UWB transmitter off, then measuring the decibel increase in the level with the UWB transmitter on. Various attenuator settings were tried. The attenuator settings and the resulting delta marker values were recorded.

In addition to the UWB transmitter measurements, a few incidental radiators were activated, with line-of-sight paths to the radars, at the above sites. The delta marker values due to these devices were recorded. This shows a comparison between UWB sources and incidental radiators.

7.2.1 ARSR-4 Radiated Measurements

The ARSR-4 receiver frequency was 1241.47 MHz. The PRR for the non-dithered UWB signal had to be adjusted to put a spectral line within the passband of the receiver. It was calculated that if the PRR was increased by 10.01 kHz, this would put a spectral line at 1241.241 MHz. This new PRR was used for this radar.

The vehicle was driven along two paths. One path was along a southern radial that started at the radar. The received signal level along this path is shown in Figure 7.1. The graph is labeled with the distances from the radar in kilometers where the peaks occurred. The second path was on a southern path that started 0.64 kilometers west of the radar. The received signal level along this path is shown in Figure 7.2. On this graph, there is a gap in time, because the vehicle was stopped and some time passed before the recording resumed. Although the vehicle was driven at a constant speed and in most cases distances can be interpolated between the marks on the graph, one should not interpolate across the gap in time.

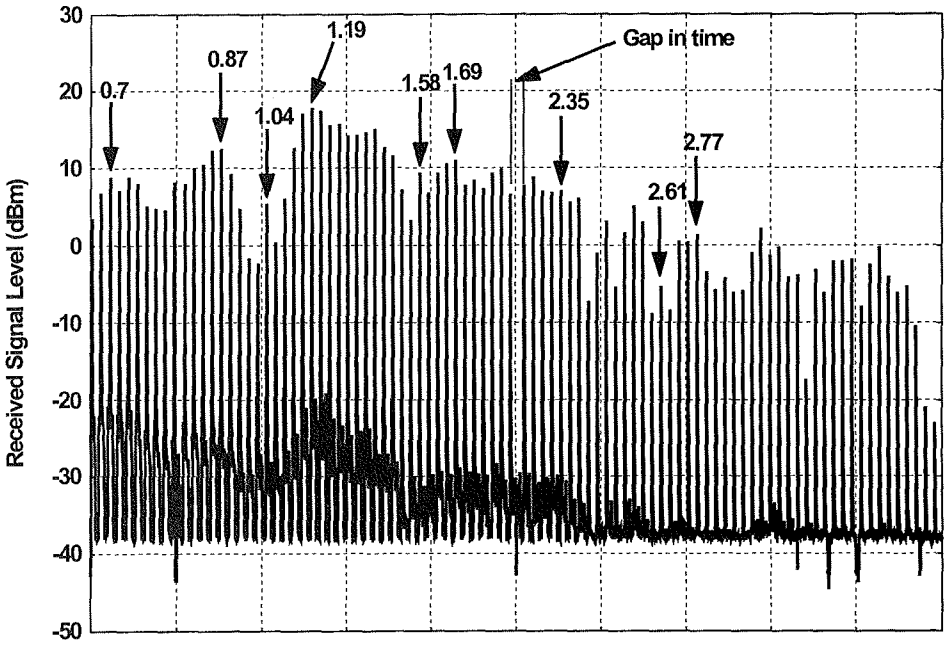

Figure 7.2 ARSR-4 signal level along a southern path.

Next, the vehicle was driven to three sites where measurements were performed. The first site was 1.26 kilometers from the radar at a bearing of 178 degrees. For a 10 MHz PRR dithered signal, radiated at the FCC Part 15.209 radiated emission limit, the delta marker value was 9 dB. Attenuating the UWB transmitter output by 6 dB brought the delta marker value down to 6 dB. Attenuating the UWB transmitter output by 12 dB brought the delta marker value down to 2 dB. Attenuating the UWB transmitter output by 15 dB brought the delta marker value down to 1 dB. For the non-dithered signal, radiated at the FCC Part 15.209 radiated emission limit, the delta marker value was 0 dB. In this case, the UWB signal did not affect the noise floor. An electric drill and an electric shaver were turned on to see if their radiation could be observed at the receiver's IF. The electric shaver produced asynchronous spikes 10 to 15 dB above the noise floor but this did not affect the noise floor. This is shown in Figure 7.3. The electric drill did not affect the noise floor.

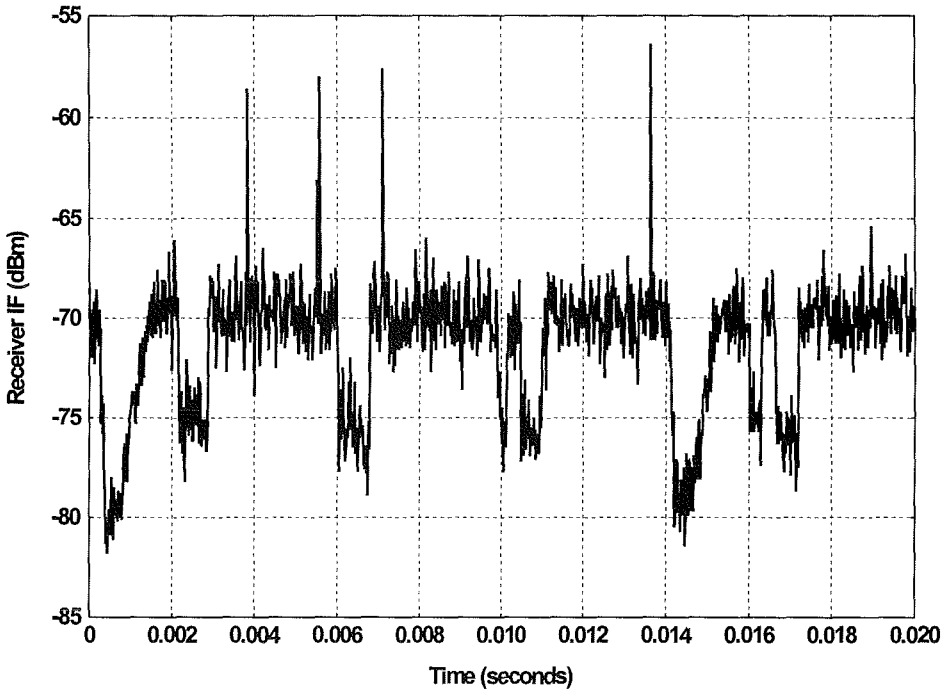

Figure 7.3. Asynchronous spikes produced by the electric shaver.

The second site was 2.08 kilometers from the radar at a bearing of 199 degrees. For a 10 MHz PRR dithered signal, radiated at the FCC Part 15.209 radiated emission limit, the delta marker value was 11 dB. Attenuating the UWB transmitter output by 6 dB brought the delta marker value down to 8 dB. Attenuating the UWB transmitter output by 12 dB brought the delta marker value down to 4 dB. Attenuating the UWB transmitter output by 18 dB brought the delta marker value down to 2 dB. For the non-dithered signal, radiated at the FCC Part 15.209 radiated emission limit, the delta marker value was 0 dB. In this case, the UWB signal did not affect the noise floor. An electric drill and an electric shaver were turned on to see if their radiation could be observed at the receiver's IF. Neither item affected the noise floor.

The third site was 3.17 kilometers from the radar at a bearing of 53 degrees. For a 10 MHz PRR dithered signal, radiated at the FCC Part 15.209 radiated emission limit, the delta marker value was 8 dB. Attenuating the UWB transmitter output by 6 dB brought the delta marker value down to 5 dB. Attenuating the UWB transmitter output by 12 dB brought the delta marker value down to 2 dB. Attenuating the UWB transmitter output by 15 dB brought the delta marker value down to 1 dB. For the non-dithered signal, radiated at the FCC Part 15.209 radiated emission limit, the delta marker value was 0 dB. In this case, the UWB signal did not affect the noise floor. An electric drill and an electric shaver were turned on to see if their radiation could be observed at the receiver's IF. Neither item affected the noise floor.

For a dithered UWB signal, radiated at the FCC Part 15.209 radiated emission limit, the maximum delta marker value was 11 dB. For a non-dithered UWB signal, radiated at the FCC

Part 15.209 radiated emission limit, the maximum delta marker value was 0 dB.

7.2.2 ASR-8 Radiated Measurements

To find the locations of highest signal level, the vehicle was driven along three paths. One path started at the radar, went west for 0.22 kilometers, then went north. The received signal level along this path is shown in Figure 7.4. The second path was on a northern radial that started approximately 0.48 kilometers northeast of the radar. The received signal level along this path is shown in Figure 7.5. The third path was a northward extension of the first path. This path started 0.78 kilometers northwest of the radar and went north. The received signal level along this path is shown in Figure 7.6. On this graph, there is a gap in time, because the vehicle was stopped and some time passed before the recording resumed. Although the vehicle was driven at a constant speed and in most cases, distances can be interpolated between the marks on the graph, one should not interpolate across the gap in time.

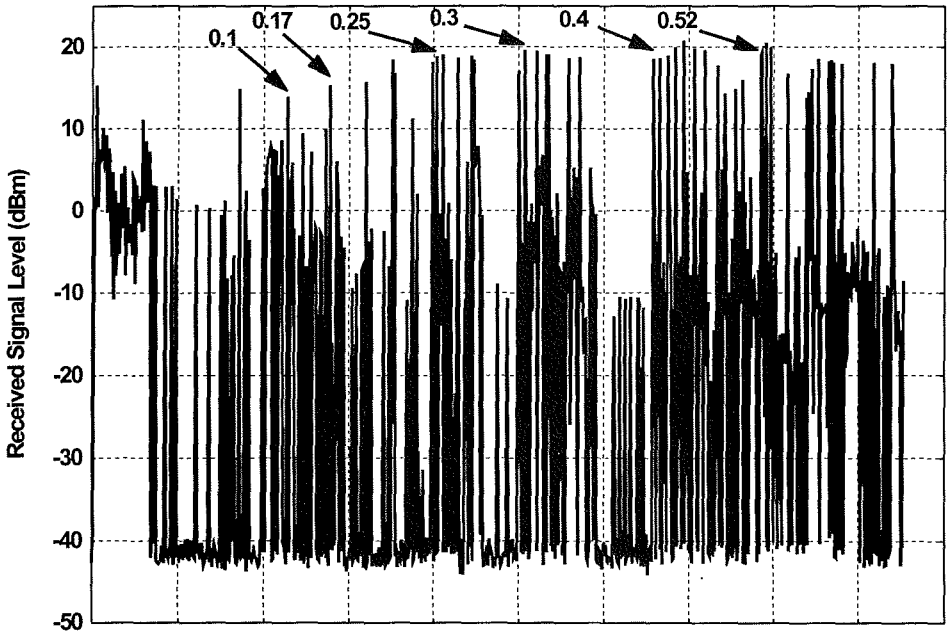

Figure 7.4. ASR-8 signal level along a mostly northern path.

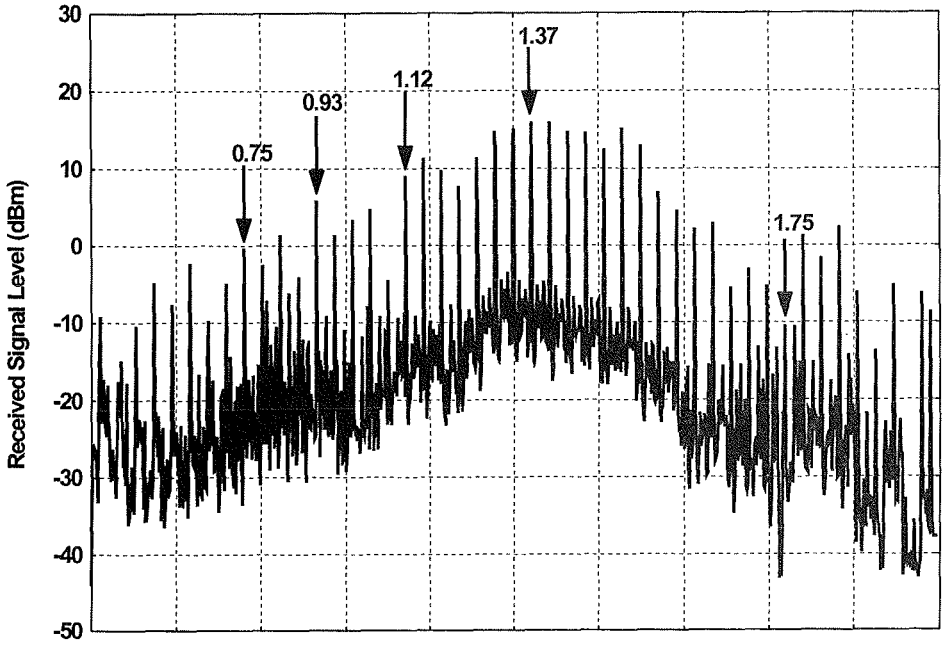

Figure 7.5. ASR-8 signal level along a northern radial.

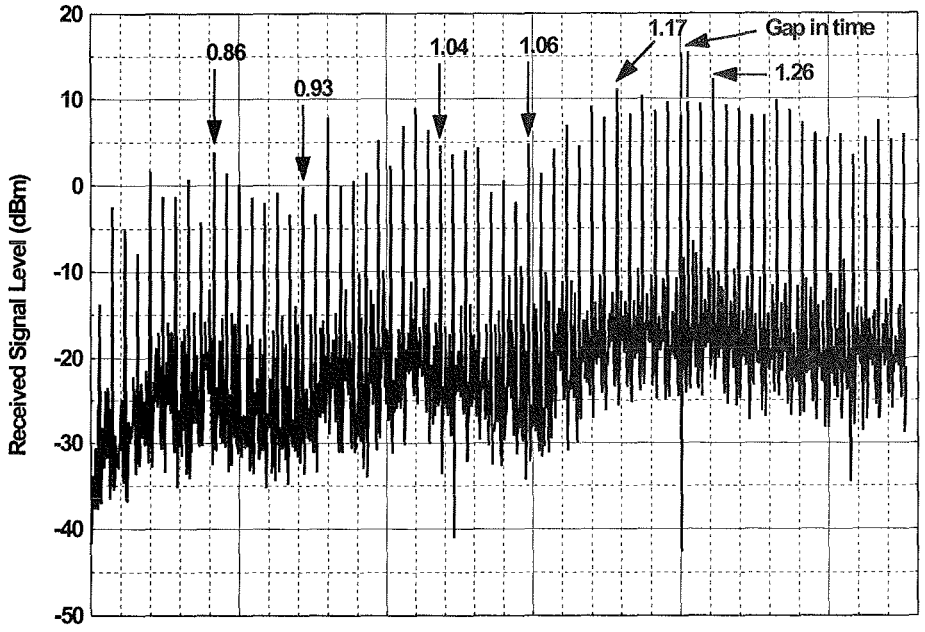

Figure 7.6. ASR-8 signal level along a northern extension of figure 7.4.

Next, the vehicle was driven to two sites where measurements were performed. The two sites were located as close to a recorded signal peak as possible. The first site was 0.4 kilometers from the radar at a bearing of 326 degrees. For a 10 MHz PRR dithered signal, radiated at the FCC Part 15.209 radiated emission limit, the delta marker value was 6 dB. Attenuating the UWB transmitter output by 3 dB brought the delta marker value down to 3 dB. For the non-dithered signal, radiated at the FCC Part 15.209 radiated emission limit, the delta marker value was 5 dB. Attenuating the UWB transmitter output by 3 dB brought the delta marker value down to 2 dB. An electric drill, electric hair dryer and an electric shaver were turned on to see if their radiation could be observed at the receiver's IF. These items did not affect the noise floor.

The second site was 1.41 kilometers from the radar at a bearing of 11 degrees. For a 10 MHz PRR dithered signal, radiated at the FCC Part 15.209 radiated emission limit, the delta marker value was 1 dB. For the non-dithered signal, radiated at the FCC Part 15.209 radiated emission limit, the delta marker value was 3 dB. Attenuating the UWB transmitter output by 2 dB brought the delta marker value down to 2 dB. An electric drill, electric hair dryer and an electric shaver were turned on to see if their radiation could be observed at the receiver's IF. These items did not affect the noise floor.

For a dithered UWB signal, radiated at the FCC Part 15.209 radiated emission limit, the maximum delta marker value was 6 dB. For a non-dithered UWB signal, radiated at the FCC Part 15.209 radiated emission limit, the maximum delta marker value was 5 dB.

7.2.3 ATCBI-5 Radiated Measurements

This radar at this location is mounted on top of a 30.5 meter tower. Because the typical ASR beacon installation is not this high, these measurements may give rather optimistic results. If the UWB signal was seen by this configuration, then the typical configuration would probably see the signal at a higher level.

The vehicle was driven to two sites where measurements were performed. The first site was 1.26 kilometers from the radar at a bearing of 178 degrees. For a 10 MHz PRR dithered signal, radiated at the FCC Part 15.209 radiated emission limit, the delta marker value was 0 dB. For the non-dithered signal, radiated at the FCC Part 15.209 radiated emission limit, the delta marker value was 0 dB. An electric drill and an electric shaver were turned on to see if their radiation could be observed at the receiver's IF. These items did not affect the noise floor.

The second site was 0.5 kilometers from the radar at a bearing of 178 degrees. For a 10 MHz PRR dithered signal, radiated at the FCC Part 15.209 radiated emission limit, the delta marker value was 1 dB. For the non-dithered signal, radiated at the FCC Part 15.209 radiated emission limit, the delta marker value was 0.6 dB. An electric drill and an electric shaver were turned on to see if their radiation could be observed at the receiver's IF. These items did not affect the noise floor.

For a dithered UWB signal, radiated at the FCC Part 15.209 radiated emission limit, the maximum delta marker value was 1 dB. For a non-dithered UWB signal, radiated at the FCC Part 15.209 radiated emission limit, the maximum delta marker value was 0.6 dB.

While the vehicle was parked 15.2 meters from this radar, an electric drill and an electric shaver were turned on to see if their radiation could be observed at the receiver's IF. These items did not affect the noise floor.

7.3 Summary

It is instructive to gather the results into tables for examination. Table 7.1 contains the delta marker values for the dithered UWB signal. Table 7.2 contains the delta marker values for the dithered UWB signal. All of the values correspond to the cases where the UWB signal is radiated at the FCC Part 15.209 radiated emission limit. The results indicate that all three radars experience a noticeable effect for at least one and in some cases, both types of UWB signals that were generated in this study. The ARSR-4 presented an interesting case in two ways. Within the constraints of three site testing, Table 7.1 shows a relatively large effect with a dithered signal and Table 7.2 shows no effect with a non-dithered signal.

Table 7.1. Delta Marker Values in Decibels for the Dithered UWB Signal.

Radar	First Site	Second Site	Third Site
ARSR-4	9	11	8
ASR-8	6	1	
ATCBI-5	0	1	

Table 7.2. Delta Marker Values in Decibels for the Non-Dithered UWB Signal.

Radar	First Site	Second Site	Third Site
ARSR-4	0	0	0
ASR-8	5	3	
ATCBI-5	0	.6	

8. MEASUREMENT SUMMARY AND CONCLUSIONS

Robert .J. Matheson[1]

8.1 Introduction

This section contains a summary of the measurements made on various UWB devices using the measurement techniques described in Sections 5 and 6. The data presented in this section have been selected from the total measurement set made on each UWB device; additional measurement data for each device is included in Appendix D.

Measurements from six devices are included.

8.2 Examples for Detailed Analysis

This section describes the selected measured data in detail, using examples from Devices A, B, and D. It is expected that the reader will apply the explanations to corresponding data from the remainder of the UWB devices, as appropriate. Data for each device will be presented in the same order to facilitate locating data and comparing results between different devices

8.2.1. Device Description

This is a short description of the UWB technology employed. ITS is making no claims that the UWB device works as intended or as described. In most cases, ITS did not functionally test the UWB device performance in any way (except to ascertain that the UWB transmitter was apparently functioning), and consequently ITS is unaware of whether a specific UWB device achieves any of its intended or claimed functional performance objectives.

---

[1]The author is with the Institute for Telecommunication Sciences, National Telecommunications and Information Administration, U.S. Department of Commerce, Boulder, Colorado 80305

Device A uses a 10-kHz pulse repetition rate (PRR), apparently not gated, dithered, or modulated. ITS had no information on the operational aspects of this device (e.g., whether there was any adaptive modification of transmitter modes depending on device location), and testing proceeded on the assumption that the on-off switch was the only significant test variable.

8.2.2. Full-Bandwidth Pulse Shape

Figure 8.1 is an example of a full-bandwidth pulse shape measurement, as described in Section 5. Major objectives of this measurement include understanding full bandwidth pulse shapes, evaluating the possible utility of various pulse-width models for engineering and regulatory purposes (especially to relate pulse shape to the emission spectrum), and furnishing raw data for fast Fourier transform (FFT) computations of emission spectra.

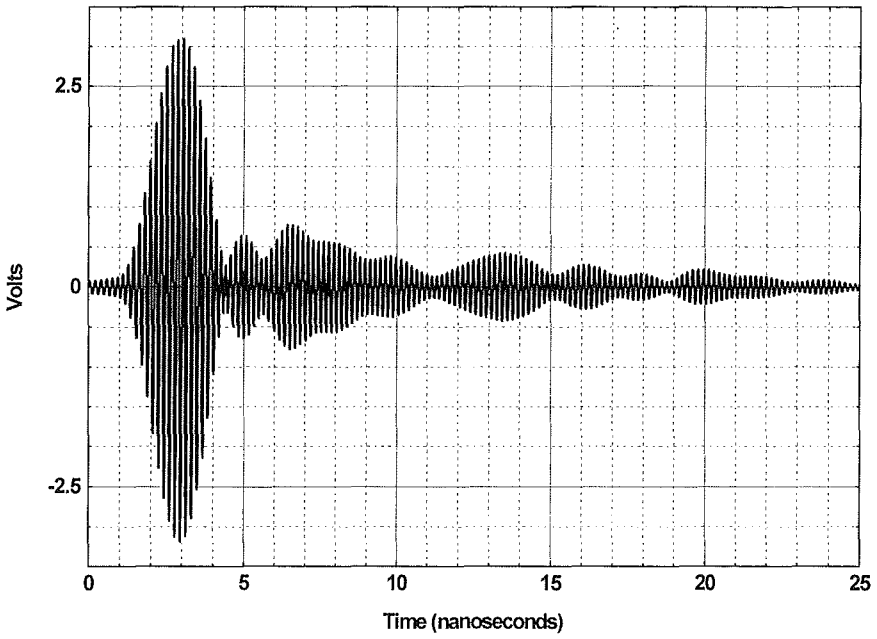

Figure 8.1. Device A full bandwidth pulse shape.

Depending on the UWB device, the full bandwidth pulse shape measurements were made on a conducted basis and/or a radiated basis at a distance of 1 meter. Conducted measurements were calibrated in dBm; radiated measurements were calibrated in voltage available at the terminals of a ridged horn or TEM horn antenna at a distance of 1 m. For the radiated measurements, the effects of the measurement antenna frequency-dependent gain and delay on the pulse shape have not been corrected, though techniques to provide a calibration in absolute field-strength are still being investigated. This process would involve performing an FFT of the uncorrected pulse, correcting the resulting spectrum with frequency-dependent antenna delay and gain factors, and performing a inverse FFT on the corrected spectrum to obtain a corrected pulse shape.

The Device A full bandwidth pulse shape in Figure 8.1 is relatively complex, involving multiple lobes and many crossings of the zero-axis. A complex waveform like this is typical of UWB signals that have been filtered with relatively high-Q resonant circuits to provide a signal limited to a well-controlled RF bandpass. Other UWB devices (e.g., Device E) may have a much simpler pulse shape with only a few zero-crossings.

8.2.3. FFT Emission Spectrum

Figure 8.2 is an example of an emission spectrum calculated via FFTs from the full-bandwidth pulse shape in the previous figure. Device A's full bandwidth pulse shape was measured in the conducted mode, so the spectrum calculated via FFTs was calibrated in peak dBm in a specific bandwidth = Δf. In this case, a Δf bandwidth of 16.7 MHz was used. For large bandwidths, the calculated peak dBm will change according to a 20 $\log_{10}$ B rule.

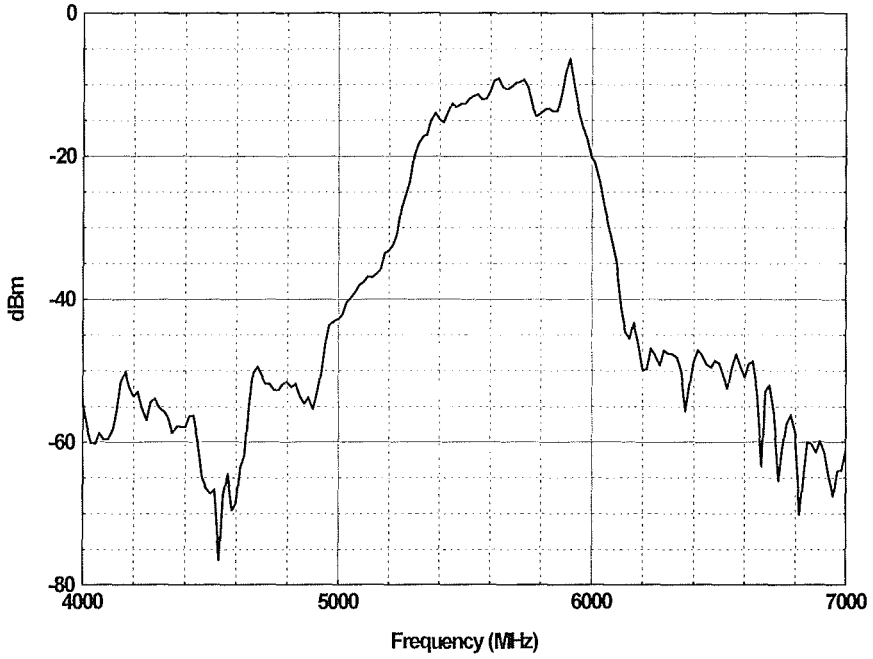

Figure 8.2. Device A conducted FFT spectrum, Δf = 16.7MHz.

Most of the UWB devices were measured in the radiated mode at a distance of 1 meter. In the radiated pulse shape measurements, the pulse shape was not corrected for the effects of the frequency-dependent receiving antenna gain. However, the spectrum calculated from the pulse shape via FFTs is corrected for antenna gain and plotted as field strength at 1 meter. The field strength values are based on peak power in a given computational bandwidth, Δf, and plotted in dBμV/m. The peak field strength can be directly compared to the spectrum analyzer measurements by using an appropriate bandwidth conversion factor (e.g., 20 $\log_{10}$ B for wider bandwidths where the UWB pulses are independently resolved). The FFT is based on the

emission from a single pulse. Therefore, it contains none of the spectrum fine structure caused by a train of impulses and the associated pulse train modulation techniques.

Major objectives for FFT calculation of emission spectra include a comparison with spectrum analyzer measurements. Close agreement between FFT and measured spectra ensures confidence in the accuracy of the full-bandwidth pulse shape measurements and the adequacy of narrowband spectrum analyzer measurements in determining the RF envelope of UWB emissions. Since the Device A full bandwidth pulse shape (and the corresponding FFT spectra) was measured in the conducted mode, while the spectrum analyzer measurements in the following sections were made in the radiated mode, no direct quantitative comparison of the full bandwidth measurements and the spectrum analyzer measurements is possible. A full set of radiated measurements were made with many of the other UWB devices, however, and these show good quantitative comparison between the full bandwidth data and the spectrum analyzer data. On a qualitative basis, the Device A conducted FFT spectrum shows the same concentration of energy in the 5300-6100 MHz region shown in the radiated spectrum analyzer measurements described next.

8.2.4. Narrowband Peak Emission Spectra

Figure 8.3 contains a series of emission spectra measured at a distance of 1 m with a spectrum analyzer using a peak detector and bandwidths of 10 kHz to 3 MHz, as described in Section 6.4.2. This data is calibrated using two scales: The left-hand scale is in dBm, referenced to the antenna terminals of an imaginary antenna having a constant aperture equivalent to what a 5.9 dBi antenna would have at 1 GHz. This calibration removes the effects of a frequency-dependent receiving antenna aperture (unlike the full-bandwidth pulse measurements), leaving the dBm value unchanged at 1 GHz. The right-hand scale is in dBμV/m at a distance of 1 m. The details of these calibrations can be found in Appendix C.

Major objectives for these measurements include development of techniques for UWB spectrum measurements using commercial off-the-shelf (COTS) equipment, investigation of the relative utility of -10-dB and -20-dB and mid-band frequency points on the UWB spectra, peak detector bandwidth correction factors, investigation of preferred spectrum measurement bandwidths for various regulatory and modeling purposes, and comparison with spectra derived by FFT processing of full bandwidth pulse shapes. Successful comparison between the FFT-derived emission spectra and spectrum analyzer measurements would strongly suggest that spectrum analyzer measurements in a narrower bandwidth are accurate and adequate for purposes of describing the overall UWB emission spectrum, along with the -10-dB and -20-dB frequency points.

If the measurement system bandwidth is sufficiently greater than the UWB device PRR, the UWB impulses are resolved in the measurement system IF as independent, non-overlapping pulses – also called "impulsive" behavior. The peak value of these pulses is expected to depend on the measurement bandwidth, B, according to a 20 $\log_{10}$ B rule. This would result in approximate 10-dB differences between successively larger measurement bandwidths, when

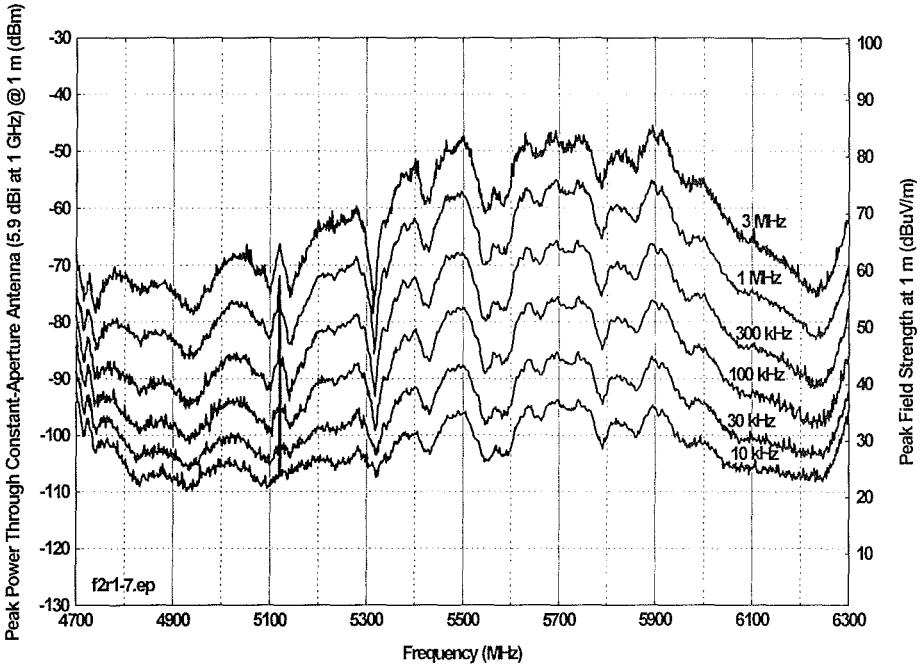

Figure 8.3. Device A measured spectra as a function of bandwidth.

those bandwidths increase in a 1, 3, 10 progression. In this example, the 10-kHz PRR of Device A causes the peak signal to appear impulsive for all measurement bandwidths greater than 10 kHz (i.e. all of the bandwidths measured in Figure 8.3).

If the measurement bandwidth is less than the UWB PRR, the UWB energy is stretched out in time in the receiver IF such that successive UWB pulses overlap, causing the appearance of a more-or-less continuous signal. Depending on the timing between successive UWB impulses, the IF signal can appear like a continuous wave (CW) signal, or Gaussian noise, or other modulations. Signals that appear noise-like are expected to follow a 10 $\log_{10}$ B rule. This would result in approximate 5-dB increases between successively larger measurement bandwidths, when the bandwidths follow a 1, 3, 10 progression. Signals that have a CW appearance do not change in amplitude as the measurement bandwidth is increased. In this example, since no emission spectrum measurements were made with bandwidths less than 10 kHz, there was no opportunity to observe the behavior of signals from Device A in the noise-like or CW region.

Most of the energy in this spectrum is contained in the 5300-6100 MHz range. These spectra have numerous irregular lobes that were about 250 MHz wide, with 10-20 dB nulls between them. Detailed measurements showing UWB signal behavior as a function of higher spectrum resolution, bandwidth, and/or time, as described in the remainder of this section, were made near 5700 MHz. The measurements near 5700 MHz show an impulsive behavior (10 dB between successive measurement bandwidths). Measurements made near 4800 MHz or 6200 MHz tend to show 5-dB differences between successive bandwidths. This was probably because the UWB peak signals were not sufficiently above the measurement system noise levels near these

frequencies, and the measurements were substantially affected by system noise (5-dB difference between successive detector bandwidths).

8.2.5. Spectrum Fine Structure

The details of the spectrum fine structure are a result of the techniques used for dithering or modulating the pulse train. In general, various measurements of the detailed spectrum fine-structure were attempted for all UWB devices, but these measurements sometimes provided inconclusive results that were not included in this collection of significant measurement results. The purpose of these measurements was to gain information on PRR and modulation details so that later measurements of APDs and detector values could be understood more completely.

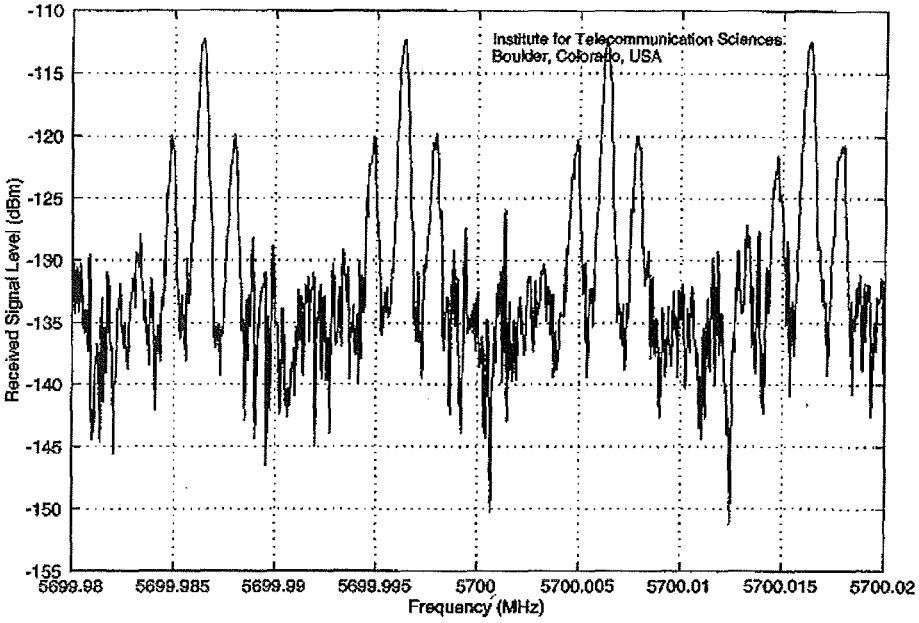

Figure 8.4. Device A spectrum fine structure (5700 MHz).

Measurements of spectrum fine-structure may reveal unexpected details like the repetition frequency of the sequence used to dither the impulse train, etc. Specifically, non-dithered pulse trains will show discrete spectral lines at harmonics of the PRR. When the basic PRR is dithered with a sequence that repeats at a certain rate, discrete spectral lines will appear separated by that rate (frequency). The relative amounts of energy in the spectral lines caused by the dither sequence, the spectral lines caused by the PRR, and the continuous spectral background are determined by the modulation and dithering details.

Device A (Figure 8.4) showed major spectral lines at a 10-kHz spacing, as expected from the 10-kHz PRR that was measured in the time domain. A closer examination showed the additional fine structure of distinct spectral lines on either side of the main lines about 1700 Hz away. The cause of these sidebands is not known.

8.2.6. Bandwidth Progression Stairstep Measurements

This measurement shows the values of peak detector readings made with a range of measurement bandwidths (100 Hz - 3 MHz). Specifically, it shows that the UWB device PRR causes impulsive behavior (10-dB steps between successive measurement bandwidths) for bandwidths greater than the PRR. For bandwidths less than the PRR this graph will show noise-like (5-dB steps between successive bandwidths), CW-like (constant values independent of bandwidth), and various other behaviors.

Figure 8.5 shows the peak signal level bandwidth progression measurements for Device A (PRR = 10 kHz), showing 10-dB spacing for bandwidths greater than 10 kHz. The apparent departure from 5-dB spacing for some of the narrower measurement bandwidths is caused by: 1) the details of the dithering technique, 2) the measurement frequency, and 3) the lower number of independent samples (which limits the ability of the peak detector to reach statistically valid peak

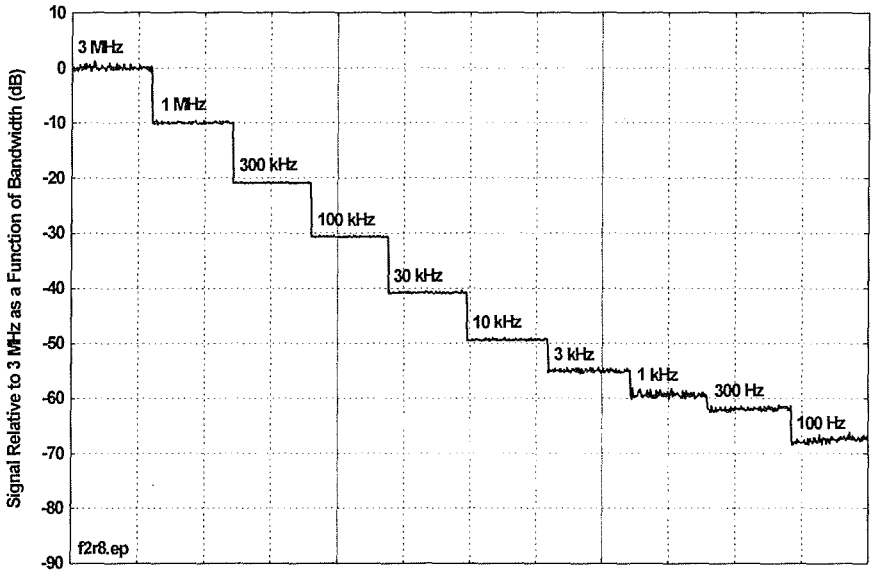

Figure 8.5. Device A, peak signal bandwidth progression stairstep .

values). This last factor is apparently not present in the Device A measurements, but it can be seen clearly in the measurements of some of the other devices (e.g. Device B, Figures 8.20 and 8.21). It is present in those cases because the rate at which independent samples occur is proportional to the measurement bandwidth, and the decreased bandwidth results in fewer independent samples during the fixed time period of these samples. This accounts for the jagged appearance of the narrowest bandwidths, where many of the time samples failed to contain any of the statistically rarer peaks that are 8-10 dB above the average values. For these cases, the 5-dB rule appears to be maintained more closely if one considers the peak value seen within the whole stair "step." Using the whole "step" has the effect of increasing the number of independent samples for the lowest bandwidths, partially correcting the problem of too few samples.

8.2.7. Gating, PRR, and Modulation

These observations are intended to show the occurrence of patterns of pulses, as measured in the time domain at a single frequency. The purpose of these measurements was to help gain detailed information on PRR and modulation so that later measurements of APDs and detector values could be understood more completely. Depending on the features employed in a specific UWB device, these measurements could show the basic PRR (Figure 8.6), the pattern of gated pulse bursts (Figure 8.23), or the modulation method used to add dithering or data to the pulse trains (Figure 8.26). Such modulation methods could include on-off modulation of individual pulses, fixed or variable pulse delays referenced to an absolute time base, or fixed or variable pulse delays referenced to the preceding pulse. These measurements can be gathered under a wide range of bandwidths, time scales, and detector types, as needed to best show the details of the significant features.

Figure 8.6 shows the appearance of the Device B as a function of time, as seen using a wideband RF detector with logarithmic compression. This figure shows a 100-kHz PRR gated pulse train, without apparent dithering or other modulation.

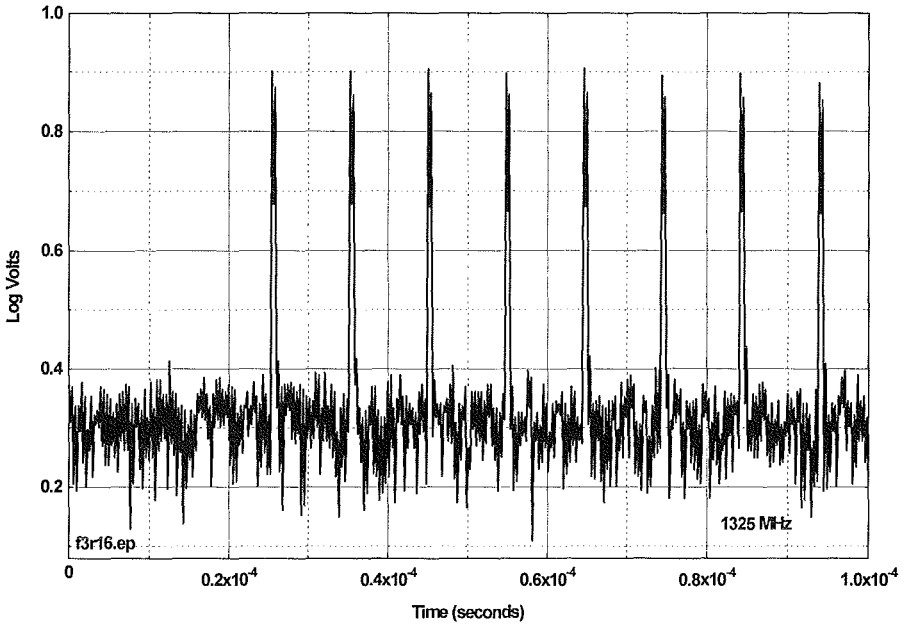

Figure 8.6. Device B, pulse train PRR,16 kBit/second mode, external detector.

In addition to dithering (used to make UWB emission spectra look more noise-like) and modulation (employed to provide for transmission of data), some UWB systems also employ gating. A gated system employs a programmed set of periods where the UWB transmitter is turned off or on for a period of many UWB pulses. For example, a UWB system might transmit a gated burst of data lasting 10 ms, followed by a 40-ms period where no pulses are transmitted.

These so-called "gated" modes are different from data encoding techniques, where individual pulses are turned off or on to encode a digital message.

8.2.8. Amplitude Probability Distribution (APD)

The APD contains information on the percentage of time the envelope of UWB signals in a specific IF bandwidth exceeds various amplitudes. A more complete description of APDs is included in Appendix A. Figure 8.7 contains APDs from Device D, 1-MHz PRR, 100% gating (i.e., transmitting continuously). These APDs were measured in bandwidths between 10 kHz and 20 MHz at a single center frequency near the frequency of maximum UWB spectral power. With some devices, two sets of APDs were measured to distinguish between different signal fine structures seen at different frequencies. Some UWB devices measured earlier in the measurement program did not include the 10-MHz and 20-MHz bandwidth measurements, as this capability was not yet available to us.

Since the APD will change substantially as a function of measurement bandwidth (or in victim receivers having various bandwidths), the graph contains a family of APDs measured in bandwidths between 10 kHz and 3 MHz, and sometimes including10-MHz and 20-MHz bandwidths. The APD provides a conceptual technique for understanding how various UWB signals will appear within victim receivers of various bandwidths. In particular, since the raw bit error rate of a victim receiver is closely related to the probability that the interfering UWB signal will exceed the amplitude of the desired signal, the APD provides a tool to relate UWB characteristics to the interference caused to various victim systems. (Note that many modern systems employ a variety of error correction techniques that are intended to correct most raw bit errors, so the number of errors presented to the system user may be related to the APD in more complex ways.)

The APD graph is plotted in power (dBm) versus the percentage of time (or probability) that the signal envelope will exceed a specified level. The percentage-of-time scale is weighted as 0.5 $\log_{10}(-\ln P(A>a))$, as described in Appendix A. This particular weighting function has two important consequences. First, the envelope of Gaussian noise (including receiver noise) plots as a straight line, making it easy to recognize when UWB signals act in a non-Gaussian manner. Second, these APD graphs never reach 0% or 100%, but only approach these percentages. This reflects the real world circumstance that the maximum and minimum peak amplitudes of many phenomena (including Gaussian noise) are dependent on the total number of independent measurements included in the sample.

In the APD graph, the individual APDs are labeled by IF measurement bandwidth. The amplitude (power) scale is in dBm, referred to the output terminals of the measurement antenna, which was located 1 m from the UWB source. The gain of the ridged-horn measurement antenna was between 5 dBi and 10 dBi, depending on the measurement frequency. Although the APD calibration could have been converted to field strength, the primary object of the APD

measurements and analysis was to show the relative behavior of UWB signals as a function of measurement bandwidth (where absolute field strength calibration was less important).

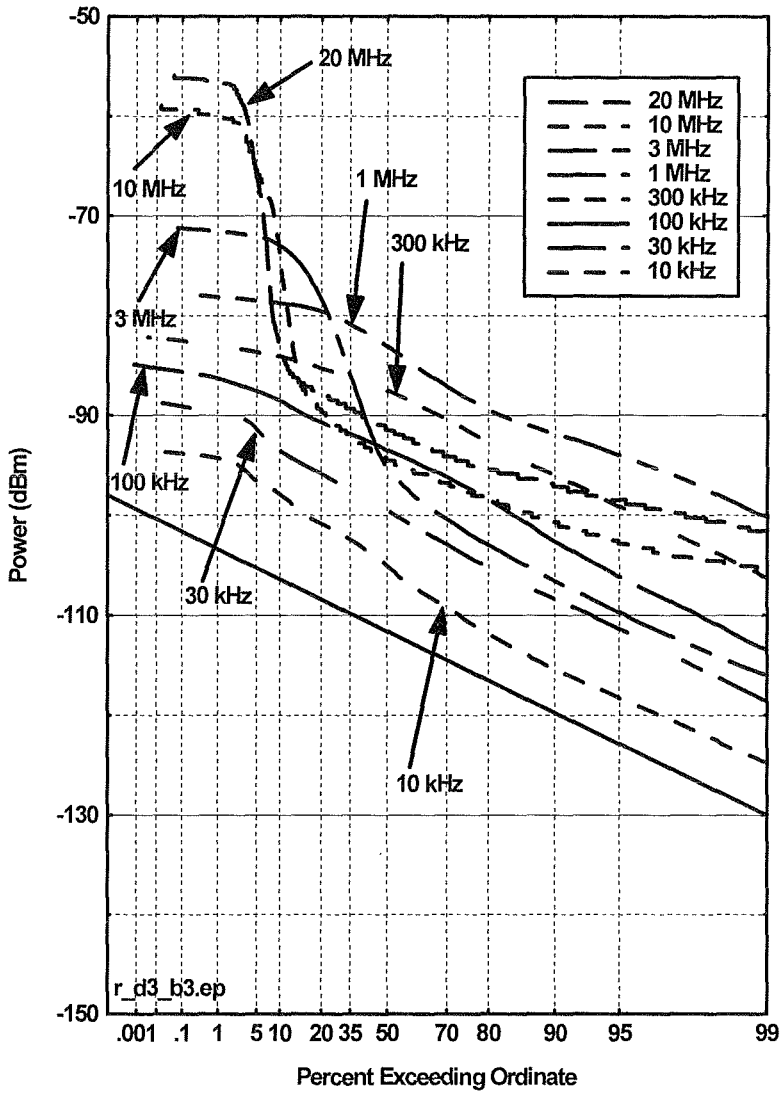

Figure 8.7 Device D APDs, 1-MHz PRR, 100% gating.

Most APDs show two distinct patterns, depending on the relationship of the measurement bandwidth to the PRR. For measurement bandwidths greater than the PRR (bandwidths of 3 MHz and above for Device D, PRR = 1 MHz), the UWB signals look impulsive. This means that the individual UWB RF impulses are converted to independent pulses within the receiver IF bandwidth. The peak amplitude of these IF pulses varies as 20 $\log_{10}$ B, and the duration of these pulses is approximately 1/B. For example, in the 10-MHz bandwidth, each pulse will last approximately 0.1 μs. With a PRR of 1 MHz, the total duration of these pulses adds up to a total of 0.1 s each second. This is a total pulse duration equal to about 10% of the total time, matching the approximate 10% "plateau" on the 10-MHz APD in Figure 8.7.

The peak amplitude of the plateau is expected to vary according to a 20 $\log_{10}$ B rule for independent pulses. Thus, the 20-MHz APD should have a peak value 16.5 dB greater than the 3-MHz APD – very close to the difference in Figure 8.7.

As shown in the graph, the Device D pulse was present in the 20-MHz bandwidth about 5% of the total time. During the 95% of the time that the Device D pulse was not present in the measurement receiver, the only "signal" present in the measurement receiver was receiver system Gaussian noise. Thus, the remainder of the APD (after the impulsive signals have been subtracted) is only system noise. In the example, the 20-MHz APD tends to match a straight line drawn on the graph corresponding to Gaussian noise over the percentage ranges between about 20% and 80%. This straight line corresponds to a 20-MHz receiver bandwidth with a noise figure of 10 dB. The APD of system noise corresponding to other bandwidths and noise figures would be represented by a straight line with an identical slope, but offset vertically and intercepting the 37% value at Noise (dBm) = NF + 10 $\log_{10}$ B(Hz) -174, where NF is the measurement system noise figure in dB.

The departure of the measured APDs from the expected Gaussian noise straight line (the 80-99% range on the 20-MHz APD, and various amounts on other curves) is not completely resolved, but it is probably due to insufficient video bandwidth in the measurement system that was assembled to make the 10-MHz and 20-MHz bandwidth measurements. As expected, the departure-from-ideal-response was greater for the wider bandwidths.

Within measurement bandwidths equal to or less than the UWB PRR (1-MHz and less, in this example), the UWB energy does not appear as independent pulses. In this "non-impulsive" mode, the energy from successive UWB pulses is sufficiently stretched out in time by the IF bandwidth filter that the "pulses" overlap. Depending on the timing between pulses, the overlapping pulses can constructively or destructively interfere in the receiver IF bandwidth. This process can produce various results, including a series of discrete spectral lines at the harmonics of a uniform undithered PRR, or a continuum of energy resembling Gaussian noise for modulated or dithered UWB pulse trains. The use of a repeated binary sequence to dither the pulse train can produce discrete close-spaced spectral lines at frequencies related to the repetition rate for the whole sequence.

Although some dithering or modulation techniques may produce signals that appear like Gaussian noise in narrow bandwidths, this apparent Gaussian noise is different in origin from the Gaussian noise that is present in the wider bandwidth impulsive modes and in gated modes. In the narrowband mode (bandwidths less than the PRR) the energy from ungated UWB impulses is continually present in a narrow IF bandwidth, and the measured signal (often a signal with Gaussian characteristics) comes from the UWB energy. In wideband and gated modes, there are time intervals where no UWB energy is present, and measurement system (Gaussian) noise appears whenever the UWB energy is absent. Therefore, although the APDs measured in these two cases may both appear like Gaussian noise, it is important to note that for gated signals or wide measurement bandwidths the low amplitude Gaussian portion of the APD is not caused by

the UWB signal. In the case of the Device D example, the amplitude of the Gaussian noise in the 30-kHz APD is about 17 dB higher than would have been calculated on the basis of system noise figure and bandwidth.

8.2.9. Detector Summary

While the complete APD data set may give good insights on how specific UWB devices will interact with specific victim receivers, a specification for computing a single numerical value from any APD may be desirable for comparing UWB emissions with regulatory limits. APDs can be processed to give numerical values for detector functions (called "statistics" in Appendix A) like peak, RMS, average voltage, average logarithm, median, etc. The specific intent of this section is to explain the numeric values produced by various detectors and measurement bandwidths, based on the particular characteristics of UWB signals. These results are intended to give information on which detector functions and bandwidths are most suited for specifying Part 15 limits, rather than to suggest specific numerical values for these limits.

Since the APD contains only first-order statistics, presumably any detector function that can be derived from first-order statistics can be computed from the APD. The detector summary analysis computes the following detector values from APDs measured in various bandwidths: peak, RMS, average voltage, and average logarithm. In some EMI receivers and newer spectrum analyzers these statistics are made available by hardware detectors or real-time digitizer/signal processors designed to process the IF signal in comparable ways. The quasi-peak detectors specified by the FCC for most Part 15 measurements below 1 GHz cannot be computed from the APD, because quasi-peak measurements are a function of second-order statistics, as well as first-order statistics.

8.2.10. FCC Proposed Part 15 Measurement Procedures

The FCC suggested in the UWB NPRM that UWB devices be measured according to the existing Part 15.35 (b) measurement techniques referred to in Part 15.209. These measurement techniques include quasi-peak detectors for frequencies below 1 GHz and a pair of measurements (average and peak) for frequencies above 1 GHz. For frequencies above 1 GHz, the FCC specifies in 15.35 (b) that measurements shall be made using an "average detector function." It also states that a maximum peak UWB value should be no more than 20 dB above the average limits, and that (unless otherwise specified) measurements should be made with a minimum bandwidth of 1 MHz. Based on this text, we believe that the FCC has described a Part 15 average detector function corresponding to the average voltage value computed from the 1-MHz APD.

However, the FCC has proposed in their NPRM (Question #50) that Part 15 average measurements be made with a spectrum analyzer using 1-MHz bandwidth, video filtering (between 10-kHz and 10-Hz bandwidth) and a peak detector. No guidance is given in the NPRM

concerning whether logarithmic or linear IF compression is to be used.[2] It is likely that the use of a logarithmic IF amplifier would give a result very similar to the average logarithm value computed from the 1-MHz APD. If a linear IF were used instead of a logarithmic IF, the result should be very similar to the average voltage value computed from the 1-MHz APD. To confirm this possibility, we also performed an independent measurement that followed the FCC procedures exactly, using a 1-MHz bandwidth, logarithmic IF mode, video filtering, and sample detector. The function of the FCC peak detector is duplicated by manually reading the highest value from the resulting graph. This modified procedure makes it possible to understand the role of sufficient lowpass video filtering in the suggested FCC measurement. This result is labeled "FCC Part 15" and represented by a hollow square in the detector summary graphs.

Detector functions corresponding to peak, RMS, average voltage, and average logarithm have been computed from the APDs measured in each bandwidth and plotted at the corresponding bandwidth for Device D in Figure 8.8. Details on this computation are included in the discussion of APDs in Appendix A. These four detector functions tend to emphasize particular parts of the APD. The peak detector looks only at the single highest measurement value, ignoring all other measurement values. The RMS detector performs an integration of average power. Because power is related to "voltage-squared," the effect of the higher amplitudes in the APD is enhanced. The average voltage detector tends to be affected more equally by the whole range of values. The average logarithm detector gives greatest weight to the lower values. The detectors are normalized to give the same value for a CW signal.

Some common "rules-of-thumb" for these detectors (which should be tested against the detector values actually obtained) include:

1. For Gaussian noise, the peak detector value is typically 8-11 dB greater than the RMS value (depending on the number of samples), the average voltage is 1 dB less than the RMS value, and the average logarithm is 2.5 dB less than the RMS value. The RMS value is exceeded 37% of the time.

2. For non-overlapping pulses, the peak value varies as $20 \log_{10} B$.

3. The RMS value varies as $10 \log_{10} B$

4. Peak $\geq$ RMS $\geq$ average voltage $\geq$ average logarithm.

Figure 8.8 shows the detector summary graph for Device D, 1-MHz PRR, 100% gating. Dashed lines have been drawn on the graph, corresponding to $10 \log_{10} B$ and $20 \log_{10} B$ slopes. These lines are intended as graphical aids, not as suggested conclusions.

---

[2]In a separate communique related to the NTIA UWB test plan, the FCC indicated that the intention was to employ the spectrum analyzer in the logarithmic IF mode.

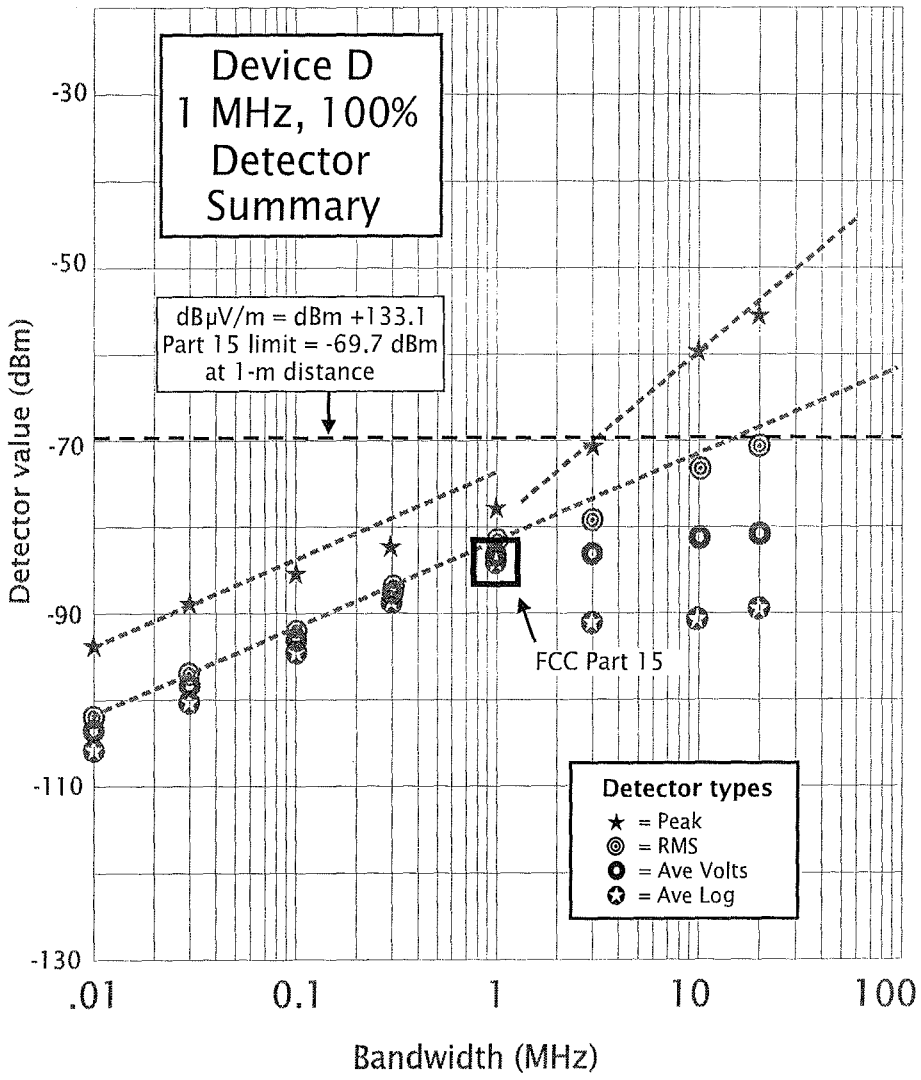

Figure 8.8. Device D detector summary,1-MHz PRR, 100% gating.

The detector summary shows two major regions: the impulsive region (B >> PRR) and the noise-like region (B >> PRR). In the noise-like region, the values for the RMS, average voltage, and average log detectors are closely spaced (2.5 dB theoretical difference between average log and RMS for Gaussian noise). The peak reading is about 8 dB above the RMS (the peak value is theoretically 8-11 dB above the RMS value for Gaussian noise). The values for all detectors change according to a 10 $\log_{10}$ B trend. The similarity between the Device D detector readings and the corresponding readings that would have been theoretically produced by Gaussian noise suggest that the Device D signal dithering was selected to make it look similar to Gaussian noise.

A completely different pattern of detector function values is found in the impulsive region (B >> PRR). There is a much wider divergence between various detector values at any single bandwidth, and this divergence becomes greater as the bandwidth increases. The peak values follow a 20 $\log_{10}$ B trend line, and the RMS values follow a 10 $\log_{10}$ B trend line. The value of the average voltage and average log detectors drop substantially when the wider bandwidths allow low amplitudes associated with measurement system noise to be seen between the duration of UWB impulses. Since the average log value emphasizes the lowest amplitude signals, the average logarithm value is most dramatically affected when the IF output drops to the measurement system noise level between impulses. The difference between peak values and average logarithm values is as much as 35 dB for the 20-MHz bandwidth. These relatively large differences between detector values suggest that the detector functions used in measuring Part 15 regulatory limits must be specified unambiguously.

The smallest differences between the various detector functions is often seen when B = PRR. In this example, there is only a 6-dB difference between average logarithm and peak values for the 1-MHz values.

The FCC-proposed Part 15 measurement procedure using a spectrum analyzer with 1-MHz bandwidth, logarithmic IF, video filtering, and peak detection was used to make a direct measurement of the Device D signal. This measurement produced a value of about -84 dBm, which was essentially identical to the average logarithm detector value computed from the 1-MHz bandwidth APD.

In addition to the dBm scale on the detector summary graphs, a level has been marked with a horizontal dashed line. This level corresponds to the FCC Part 15 limits from 15.209, which is specified as 500 μV/m at a distance of 3 meters. Since all of the measurements in this section of the report were measured at a distance of 1 meter, the FCC limit has been adjusted for a 1-m distance and the gain of the antenna used for the measurement. More details on this conversion can be found in Appendix C.

8.3 Measured Data Summaries for Devices

The following sections contain compilations of measured data from UWB devices A-E and an electric drill. Additional measured data on each device is contained in a corresponding separate section in Appendix D.

8.3.1 Summary of Device A Measurements

Device description. Device A uses a 10-kHz PRR, apparently not gated, dithered, or modulated. ITS had no information on the operational aspects of this device, and testing proceeded on the assumption that the on-off switch was the only significant test variable.

Full bandwidth pulse shape. Figure 8.9 shows a complex pulse shape with multiple lobes, probably caused by a multipole sharp-cutoff RF filter giving a tightly-defined UWB spectrum.

FFT emission spectrum. Figure 8.10 shows most UWB energy is in the 5100-6100 MHz band.

Narrowband peak emission spectra. Spectrum analyzer measurements (Figure 8.11) show most energy in the 5100-6100 MHz range. This spectra had 5-6 irregular lobes about 250 MHz wide, with 10-20 dB nulls between them.

Spectrum fine-structure. Figure 8-12 shows details near 5700 MHz reflecting the 10-kHz PRR of Device A .

Bandwidth progression stairstep. Figure 8-13 clearly shows 10-dB steps for bandwidths greater than the 10-kHz PRR (impulsive behavior) and 5-dB steps (noise-like behavior) for bandwidths less than 10 KHz .

APDs. Figure 8-14 shows impulsive behavior for all measurement bandwidths greater than 10 kHz. However, although the peak values followed a 20 $\log_{10}$ B trend line for the narrower bandwidths, the 1-MHz and 3-MHz peak values (Figure 8.15) were appreciably lower than the trend line (8 dB lower at the 3-MHz bandwidth). This 8-dB difference was traced to a deficient component in the spectrum analyzer, which was found to provide insufficient spectrum analyzer video bandwidth and was replaced by the manufacturer. Unfortunately, Device A had already been returned to its owner when the repaired spectrum analyzer became available. It should probably be assumed that a re-measurement of Device A would have placed the 1-MHz and 3-MHz readings on the proper trend lines.

Detector summary. We note in Figure 8-15 that the detector values are within 8 dB of each other in the 10-kHz measurement bandwidth, and they diverge rapidly as the bandwidth is increased. The difference between peak and average logarithm is as much 40 dB for the 3-MHz bandwidth (presumably, this difference would have been 8 dB greater – a 48-dB difference – if the spectrum analyzer had been working properly during these measurements).

FCC Part 15 measurement. The FCC-recommended Part 15 measurement procedure (1-MHz bandwidth, logarithmic IF, video filtering, and peak detection) produced a value of -112 dBm with a 300 Hz video bandwidth (300 Hz was the minimum video bandwidth for the spectrum analyzer when used with 1-MHz resolution bandwidth). This matches the -112 dBm average logarithm detector value in Figure 8-15 computed from the 1-MHz bandwidth APD.

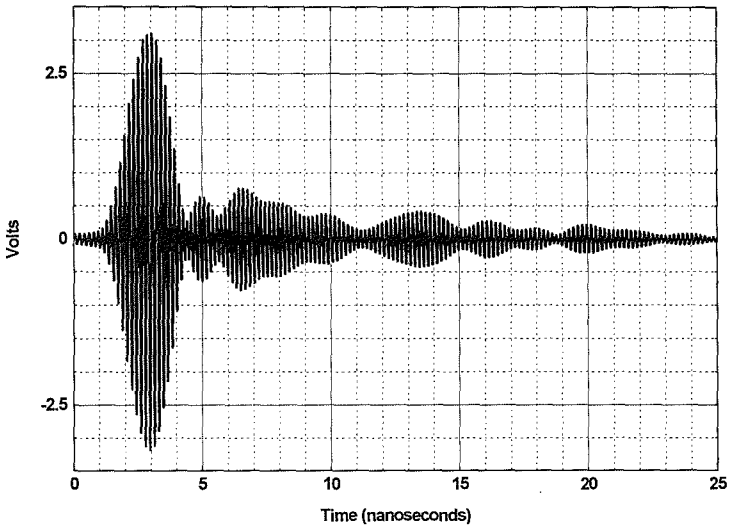

Figure 8.9. Device A full bandwidth pulse shape.

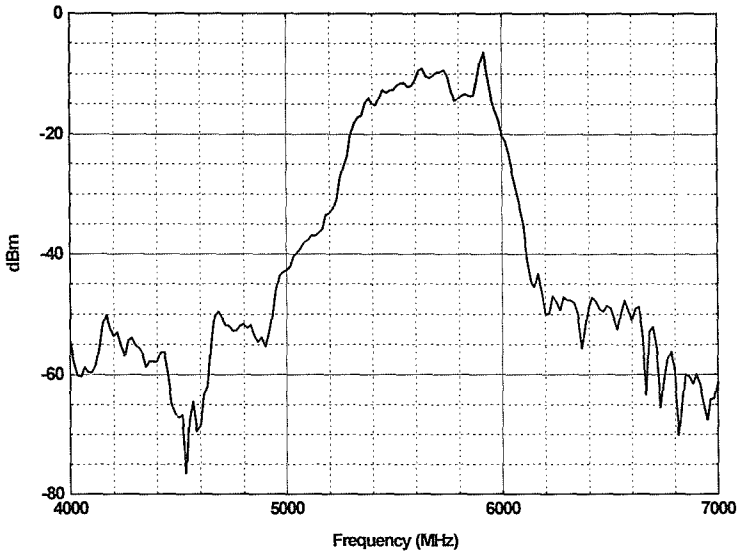

Figure 8.10. Device A, conducted power spectrum, $\Delta f = 16.67$ MHz.

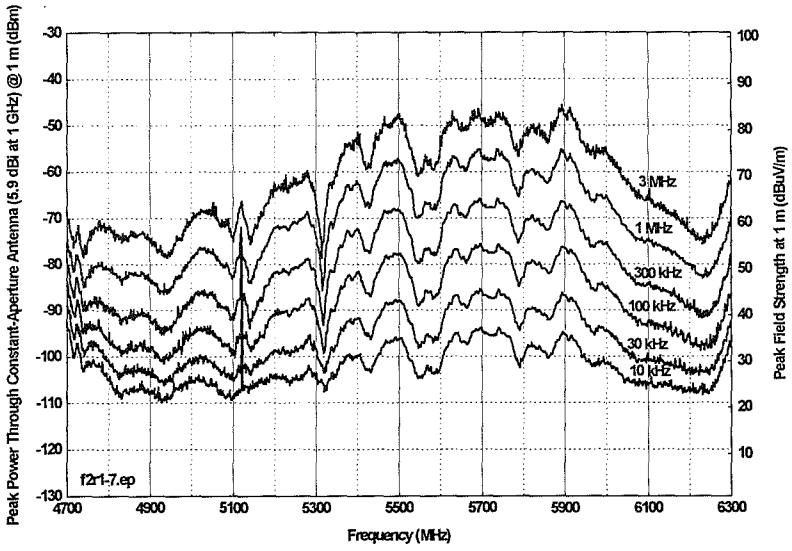

Figure 8.11. Device A spectra as a function of measurement bandwidth.

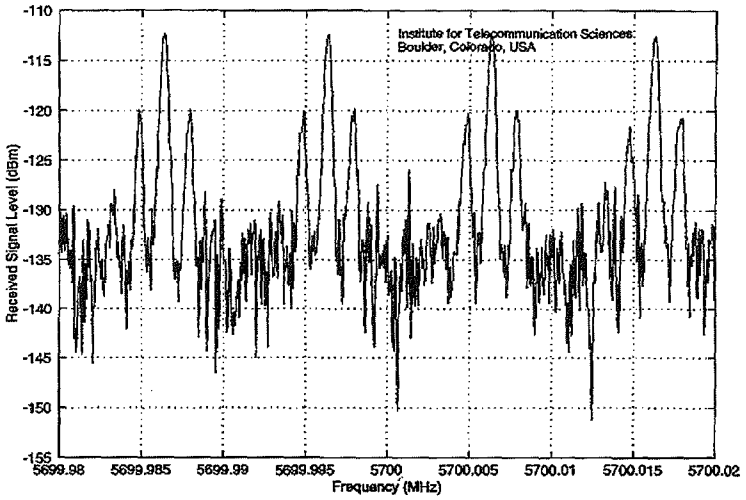

Figure 8.12. Device A spectrum fine structure.

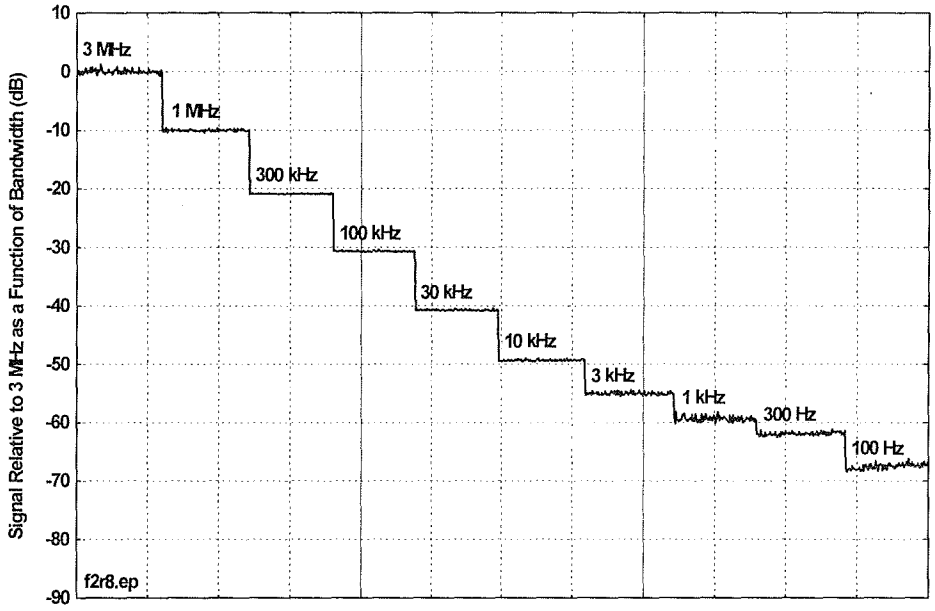

Figure 8.13. Device A peak amplitude as a function of bandwidth.

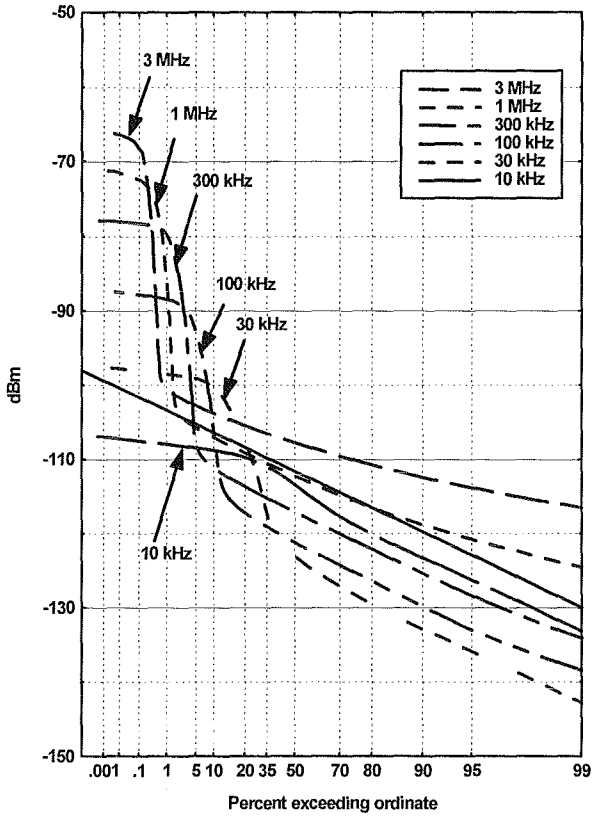

Figure 8.14. Device A APDs.

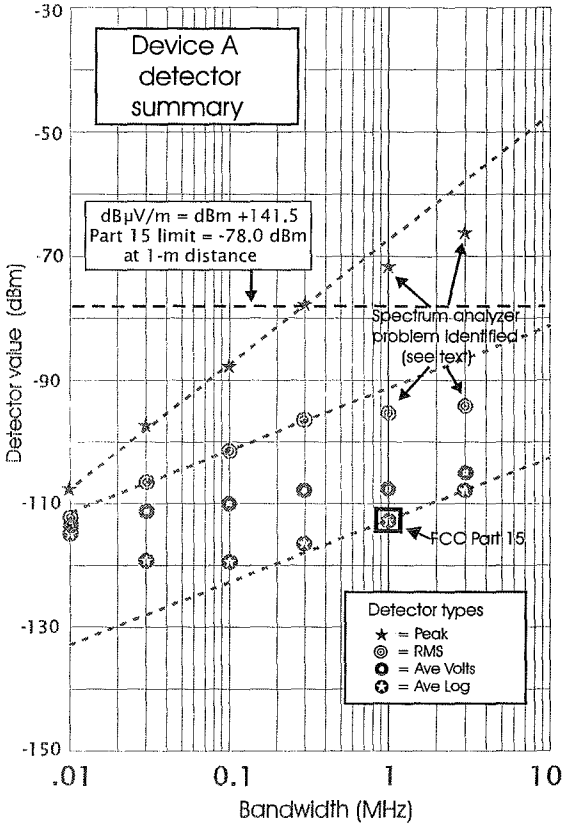

Figure 8.15. Device A detector summary.

8.3.2 Summary of Device B Measurements

Device description. Device B operates in four data rate modes, ranging between 16 kb/s and 128 kb/s. Any of these data rates can be used to support a two-way voice circuit or a two-way data circuit. ITS measured the device in its 16-kb/s and 128-kb/s voice modes, but did not measure the intermediate 32-kb/s and 64-kb/s modes.

The 16-kb/s mode provides an average user data rate of 16 kb/s, using a transmitted signal of about 100 K impulses per second, which is gated on for 8.8 ms and gated off for 35.2 ms (44 ms total cycle time). During the 8.8 ms when the signal is gated on, the data stream is modulated on the train of impulses by deleting selected pulses (on-off keying). Corresponding gating and PRR values for the other modes can be found in Table 8.1.

Table 8.1. Burst and PRR Timing for Various Data Rates

Data Rate (kb/s)	Burst length (on time, ms)	Burst Repetition time (ms)	Burst duty cycle (gating)	Pulse repetition rate (PRR)
16	8.8	44	20%	100 kHz
32	4.4	22	20%	200 kHz
64	2.2	11	20%	400 kHz
128	2.2	5.5	40%	400 kHz

Full bandwidth pulse shape. Device B emission spectrum is tightly filtered to limit it to a 500 MHz-wide bandwidth This filtering produces relatively complex and extended pulse shapes, lasting up to 30-40 ns (Figure 8.16).

FFT emission spectrum. The FFT-derived spectrum (Figure 8.17) shows a sharply-defined 500-MHz RF bandwidth. The peak signal in the FFT-derived spectrum is 116 dBμV/m in a bandwidth, Δf, equal to 20 MHz.

Narrowband peak emission spectra. Figures 8.18 and 8.19 show a sharply-defined bandwidth between 1250 and 1800 MHz, with 5-6 ripples of 5-10 dB depth across the passband. The peak signal measured with a spectrum analyzer in a 3-MHz bandwidth (Figures 8.1 or 8.19) is approximately 100 dBμV/m. Since the UWB signal for Device B is impulsive at bandwidths greater than the PRR (maximum PRR = 400 kHz) a 20 $\log_{10} B_1/B_2$ correction factor is needed to convert the 3-MHz bandwidth data to 20-MHz data. This correction factor equals16.5 dB. This converts the 3-MHz bandwidth value measured by the spectrum analyzer to the corresponding 20-MHz bandwidth value of 116.5 dBμV/m, which compares closely with the FFT-computed value of 116 dBμV/m.

Bandwidth progression stairstep. The stair step bandwidth progression figures (Figures 8.20 and 8.21) suggest that Device B produces signals that appear noise-like for measurement bandwidths less than the 100-kHz or 400-kHz PRR's associated with the respective 16-kb/s and 128-kb/s modes, made at 1325 MHz and 1500 MHz respectively.

Gating, PRR, and modulation. Figures 8.22 and 8.23 show the 20% and 40% gating duty cycles for the 16-kb/s and 128-kbs/s modes, respectively. Figures 8.24 and 8.25 show the basic PRRs for the 16-kb/s and 128-kb/s modes, respectively. Figure 8.26 shows an example of a missing pulse, caused by the on-off pulse modulation of the Device B data stream.

APDs. Both APDs (Figures 8.28 and 8.29) were measured at 1545 MHz. These APDs were inadvertently measured using video filtering equal to the resolution bandwidth, which prevented the low-amplitude portion of the APD from reaching minimum values. This effect is believed to have prevented this portion of the APDs from following the expected straight line. This problem was recognized and corrected in subsequent APD measurements for other devices. The very steep sides on the "plateau" at 20% and 40% respectively for the 16-kb/s and 128-kb/s modes reflect the respective 20% and 40% gating modes.

Detector summaries. The detector summaries (Figures 8.30 and 8.31) show approximately a 30-dB difference between peak and average logarithm and a 20-dB difference between average logarithm and RMS values for the narrower bandwidths, caused mainly by the gating modes. During the gated-off period, system noise is the only signal contributing to the APD. Since the average logarithm value is affected most by low amplitude, high-percentage signals, measurement system noise has a strong effect on the average logarithm value of gated signals.

The peak value follows a 10 $\log_{10}$ B trend line (like Gaussian noise) for bandwidths less than the PRR and a 20 $\log_{10}$ B trend (like an impulse) for bandwidths greater than the PRR. Peak measurements are identical for both 3-MHz bandwidth APDs, where impulses are non-overlapping. For the lower bandwidths where the signal acts like Gaussian noise, peak measurements for each PRR differ by about 6 dB, which would be expected from the 4:1 ratio in the number of pulses/s (not counting the percentage gating ratio).

The RMS values follow a 10 $\log_{10}$ B line for all bandwidths. The best-fit trend lines for the two modes are about 8 dB apart. A difference of 9 dB would have been expected, based on the 8:1 ratio in the total number of impulses (including the effect of the 2:1 change in gating ratio).

FCC Part 15 measurement. A measurement similar to the Part 15 measurement (except using a 3-MHz bandwidth) was done at 1650 MHz, 128 kb/s mode with logarithmic IF, 10-Hz video bandwidth, and sample detection (Figure 8.27). This gave an maximum measurement of about -74.5 dBm, with less than 1-dB time ripple caused by the 5.5 ms gating cycle. Compensating for the gain of the 19 dB preamplifier, the "Part 15-like" value was -93.5 dBm, which is within 2 dB of the average logarithm computed from the 3-MHz APD. No Part 15 measurements were made at 1-MHz bandwidth or using the 16-kb/s mode.

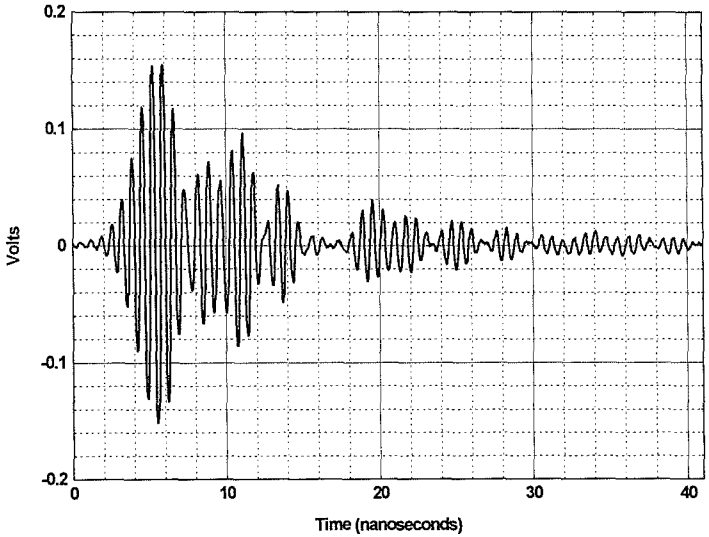

Figure 8.16. Device B full bandwidth pulse shape.

Figure 8.17. Device B, radiated peak field strength at 1 m, $\Delta f = 20$ MHz.

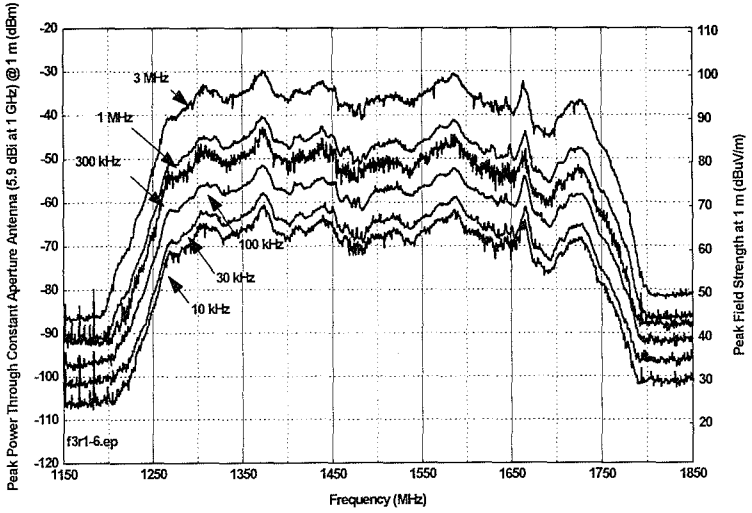

Figure 8.18. Device B, spectra as a function of bandwidth, 16-kb/s voice mode.

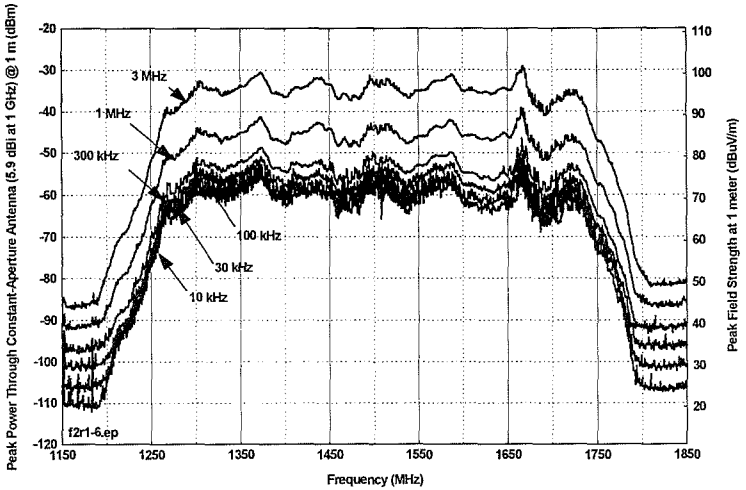

Figure 8-19. Device B, spectra as a function of bandwidth, 128-kb/s voice mode.

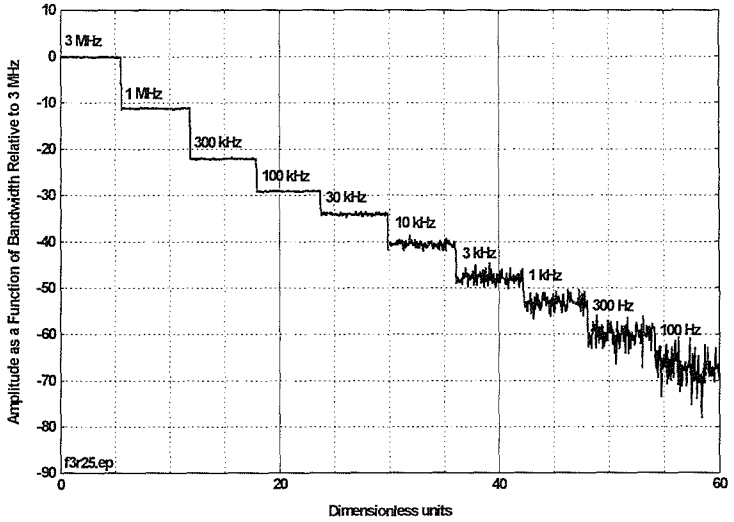

Figure 8.20. Device B, 16-kb/s voice mode, bandwidth progression stairstep.

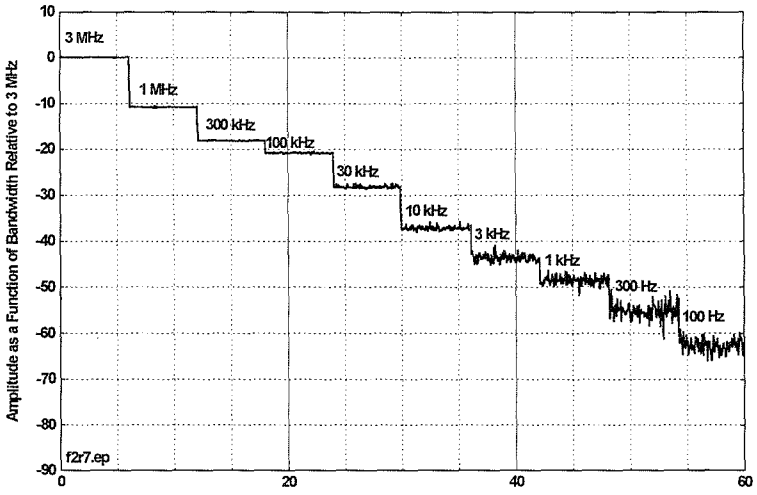

Figure 8.21. Device B, 128-kb/s voice mode, bandwidth progression stairstep.

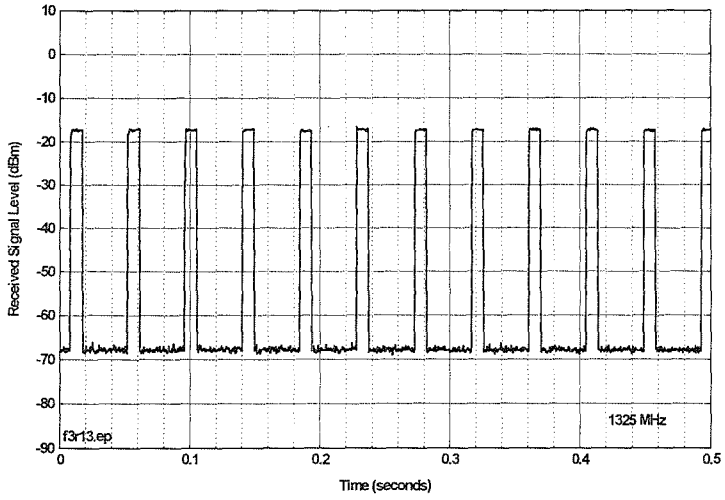

Figure 8.22. Device B, 16-kb/s mode, 3-MHz IF bandwidth, positive peak detector.

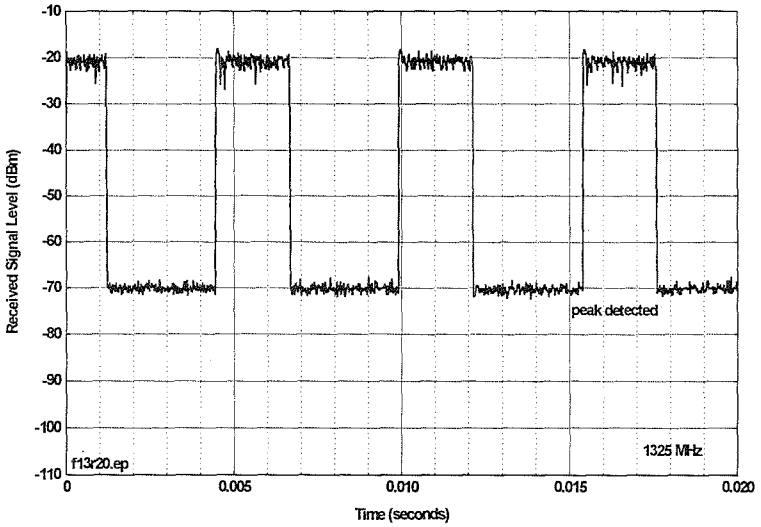

Figure 8.23. Device B, 128-kb/s mode, 3-MHz IF bandwidth.

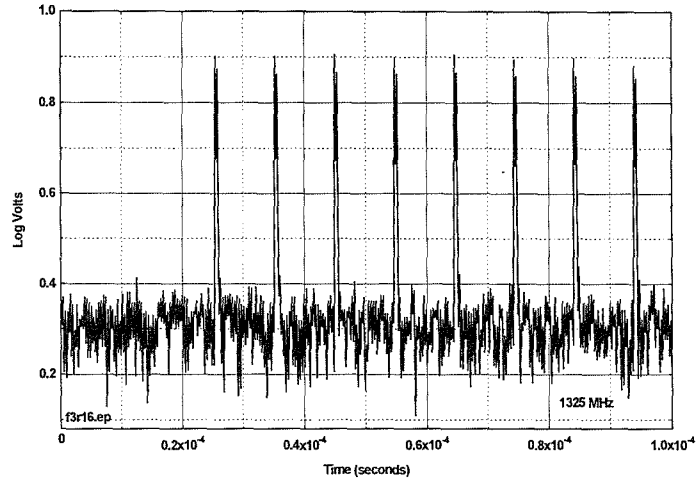

Figure 8.24. Device B PRR waveform, 16-kb/s mode, external detector.

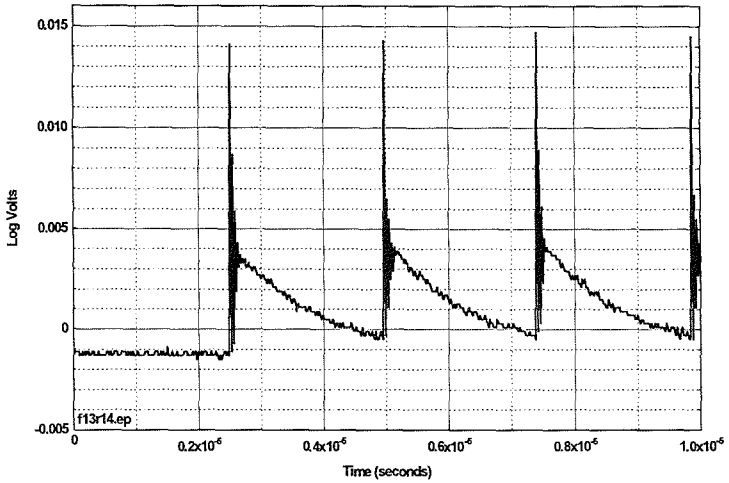

Figure 8.25. Device B PRR waveform, 128-kb/s mode, external detector.

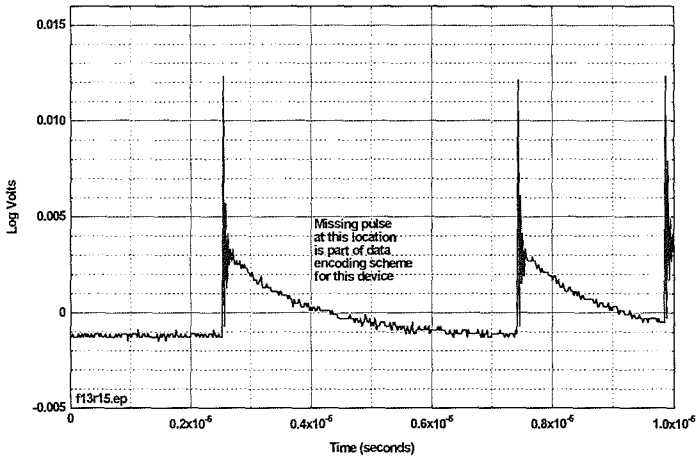

Figure 8.26. Device B, waveform showing on-off modulation, 128-kb/s mode.

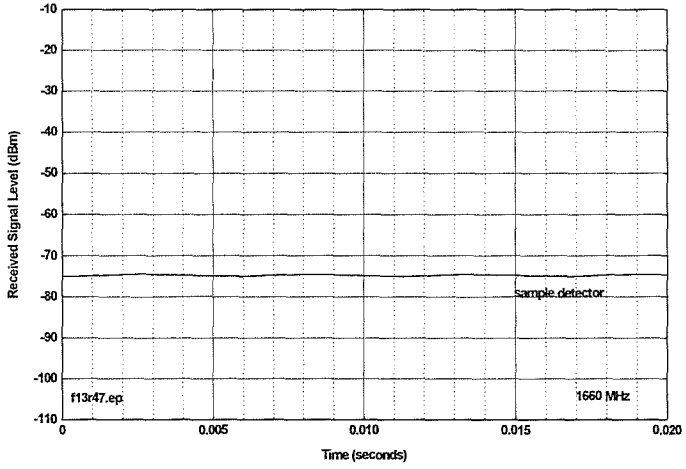

Figure 8.27. Device B, 128-kBit/second mode, 3 MHz BW, 10-Hz video (Part 15-like).

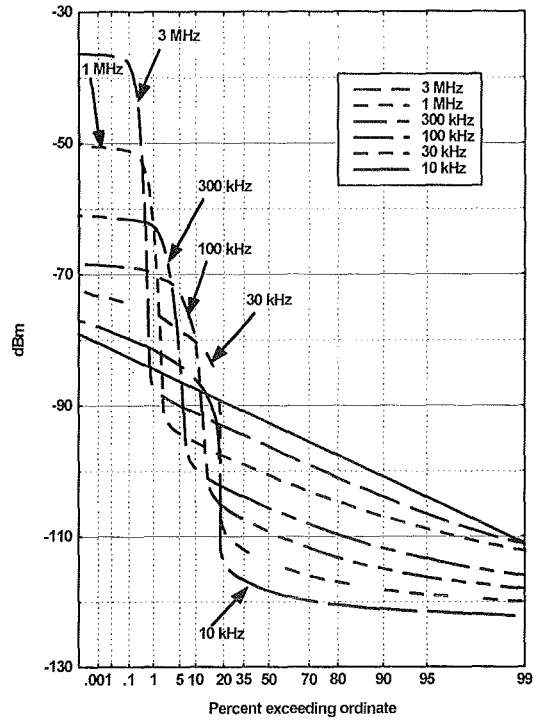

Figure 8.28. Device B APDs, 16 kb/s.

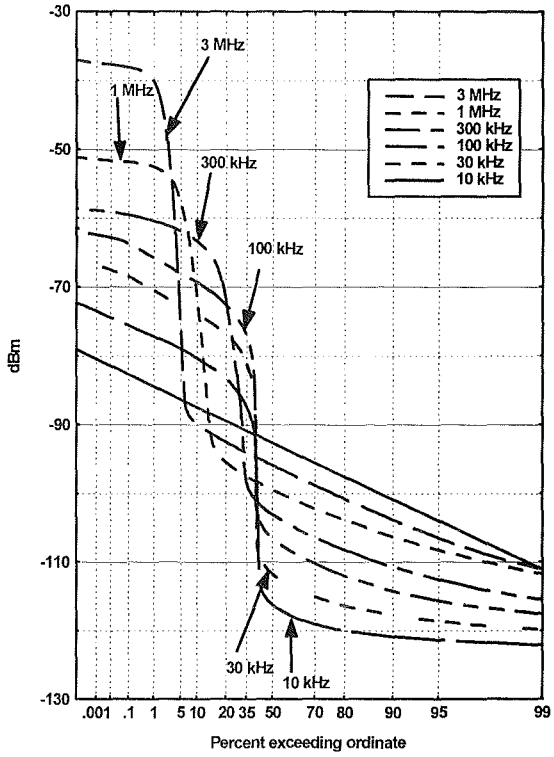

Figure 8.29. Device B APDs, 128 kb/s.

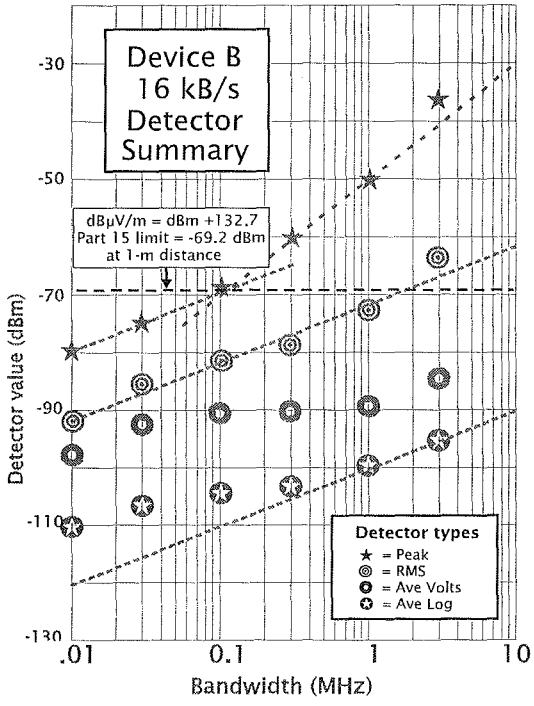

Figure 8.30. Device B detector summary, 16kb/s.

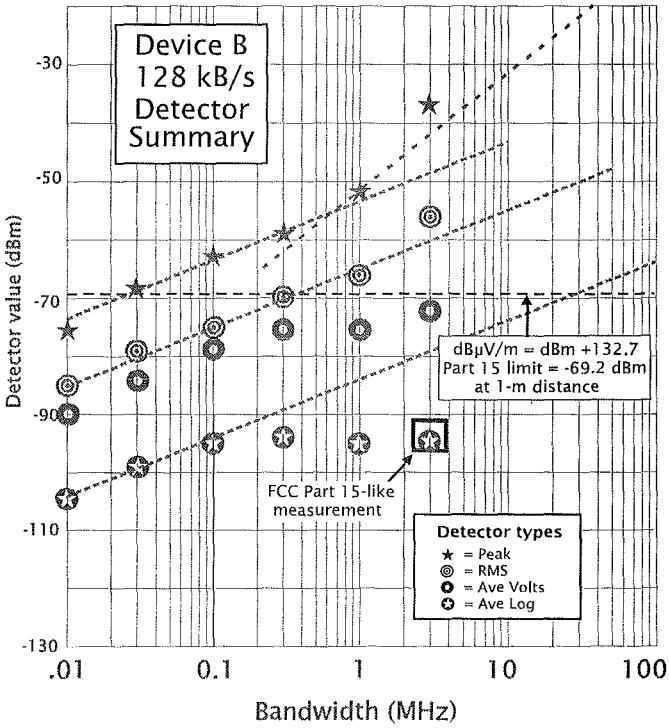

Figure 8.31. Device B detector summary, 128 kb/s.

8.3.3 Summary of Device C Measurements

Device description. Device C transmits an ungated 2-MHz PRR pulse train over the 1-5 GHz range. Device C uses a "relative" dithering technique. This dithering technique uses only a small amount of pulse delay (in this case, 1.25% delay out of 500 ns average pulse spacing), but timing is referred to the preceding pulse instead of being referred to a fixed time base. Figures 8.32 to 8.35 show how a continually larger timing variation builds up over elapsed time, until the 1.25% delay (494-500 ns) for individual pulse-to-pulse spacing covers the entire pulse-to-pulse interval.

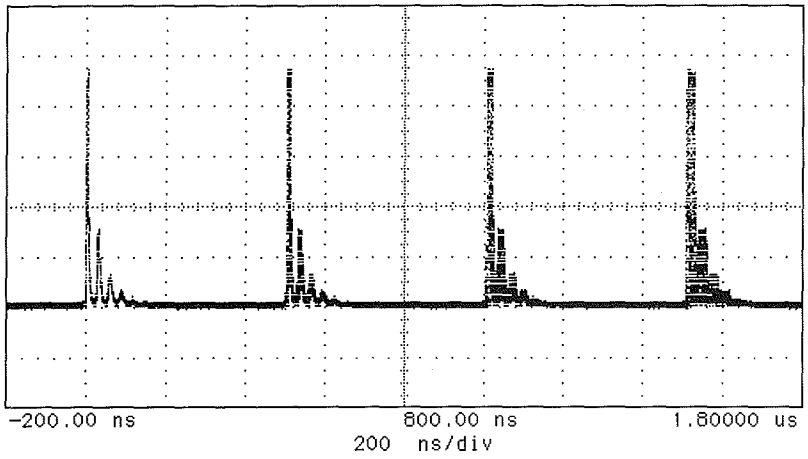

Figure 8.32. Device C dither at starting point.

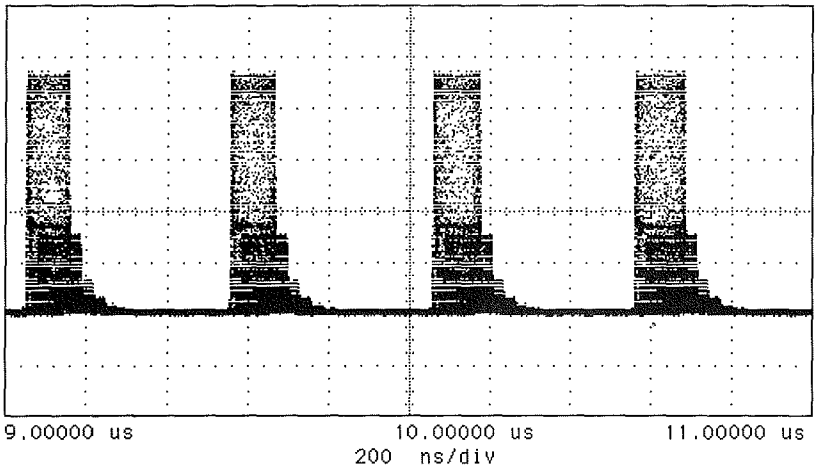

Figure 8.33. Device C dither 20 pulses after zero point.

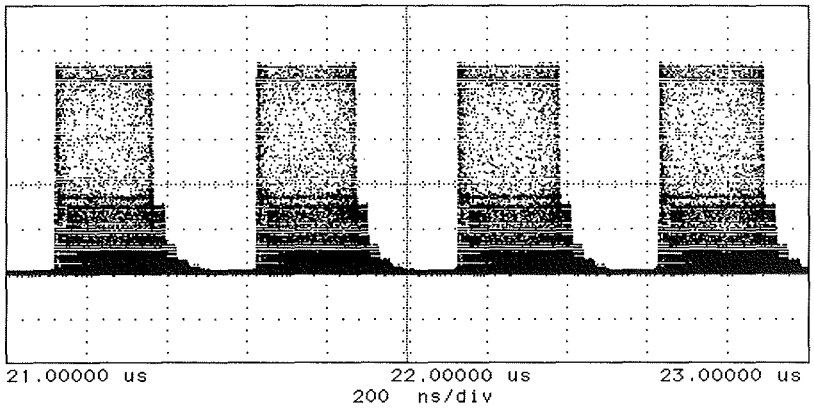

Figure 8.34. Device C dither 44 pulses after zero point

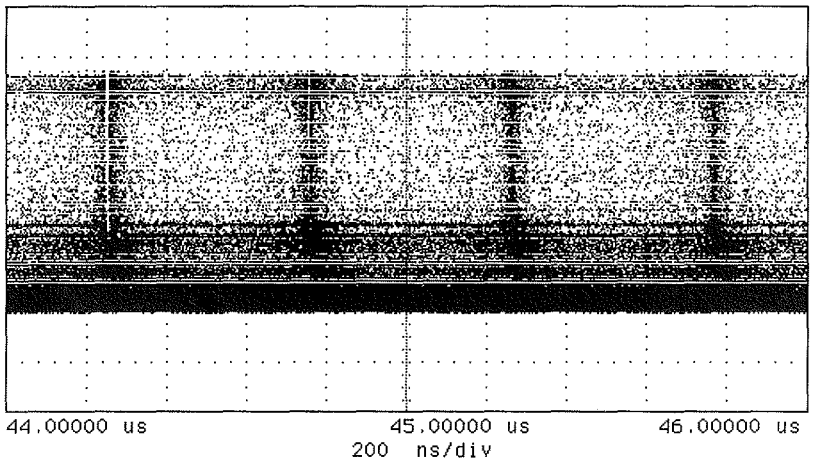

Figure 8.35. Device C dither 90 pulses after zero point

Full-bandwidth pulse shape. Figure 8.36 shows a complex pulse with extended ringing.

FFT emission spectra. Figure 8.37 shows a well-defined emission about 600 MHz wide and centered at about 1800 MHz. The calculated peak radiated field strength is approximately 86 dBμV/m in a 20-MHz bandwidth..

Narrowband peak emission spectra. Figure 8.38 shows emission spectra with a peak about 700 MHz wide, centered at about 1800 MHz, though the details appear somewhat different from the FFT spectrum. The 20-MHz bandwidth measurements show a measured peak field strength of 87 dBμV/m, closely matching the FFT spectrum.

Spectrum fine structure. Figure 8.39 shows a subtle set of fine structures related to the 2-MHz average PRR. The relative dithering technique appears to be effective in eliminating 2-MHz discrete spectral lines that extend above the surrounding spectrum. The signals at all frequencies

appear to have about the same maximum power, with a mix of amplitudes that are distributed across a range between the maximum and as much as 30 dB below the maximum. However, there is a pattern of higher-than-average-power frequencies repeated every 2 MHz, where the average signal power is maximized by spending less time at the lower amplitudes. These higher-than-average-power frequencies were designated "on-spectral-lines" frequencies, and intermediate frequencies with less average power were designated "between-spectral-lines" frequencies.

Bandwidth progression stairsteps. Figure 8.40 shows a bandwidth progression measurement made at an "on-spectral-lines" frequency. This measurement shows impulsive behavior at 3-MHz bandwidth, CW-like results for bandwidths between 100 kHz and 1 MHz, and noise-like behavior for narrower bandwidths.

Gating, PRR, and modulation. Figure 8-41 shows a measurement of the Device C pulse train, which exhibits no obvious pulse position modulation. Figures 8-42 and 8-43 show the modulated IF waveforms at 1-MHz and 100-kHz bandwidths. Surprisingly, the 100-kHz waveform contains much more amplitude modulation than the 1-MHz waveform.

APDs. APDs were measured at between-spectral-lines and on-spectral-lines frequencies – Figures 8-44 and 8-45, respectively. Measurements for the between-spectral-lines case were also made using 10-MHz and 20-MHz bandwidths.

Detector summaries. The two APDs and the corresponding detector summaries (Figures 8-46 and 8-47) show some interesting results. The two dashed lines on each detector summary are drawn as best-fit trend lines for the RMS detectors for the on-spectral-lines and between-spectral-lines measurements, showing about 2.5-dB difference between the two cases. The 3-MHz on-spectral-lines RMS value drops to the between-spectral-lines trend line, showing that the effect of the relatively narrow bandwidth concentration of on-spectral-lines energy disappears when the measurement bandwidth is widened beyond the 2-MHz fine structure.

The between-spectral-lines detector summary shows a large divergence between different detector values at 100-kHz bandwidth, including a 15-dB difference between average logarithm and RMS and a 27-dB difference between average logarithm and peak. The minimum difference between detector values occurs at 1-MHz bandwidth, where there is only a 6-dB difference between average logarithm and peak values. These results are particularly interesting (and somewhat counterintuitive) because they illustrate a UWB modulation technique that produces impulse-like results (i.e., wide divergence between detector values) at lower bandwidths and CW-like results at higher bandwidths. The proposed FCC Part 15 limits, however, assume that a UWB signal will appear more CW-like at lower bandwidths (average limit specified in 1-MHz bandwidth), and more impulsive at higher bandwidths (peak limit specified in B = 50 MHz).

FCC Part 15 measurements. Part 15 measurements were made at the "on-line" frequency using a 300-Hz video filter, which produced a signal with about 0.5 dB peak-to-peak ripple and a peak amplitude of -74 dBm. This compares with a computed average logarithm of -74.2 dBm.

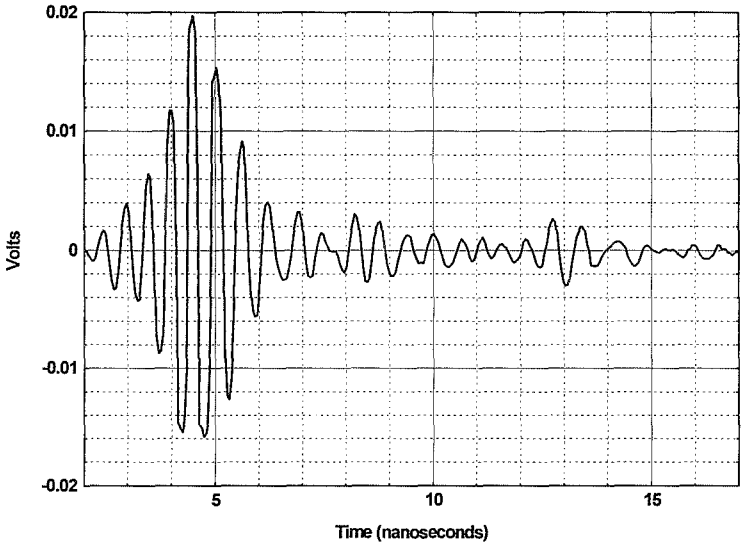

Figure 8.36. Device C full bandwidth pulse shape.

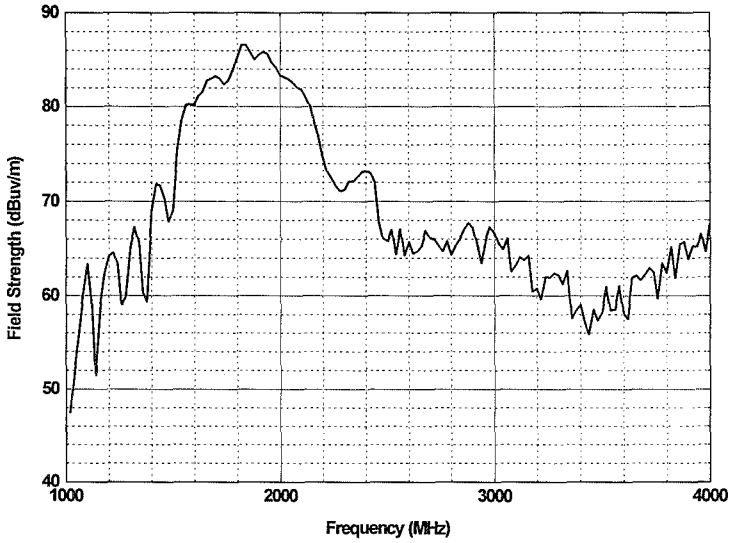

Figure 8.37. Device C, radiated peak field strength at 1 m, $\Delta f = 20$ MHz.

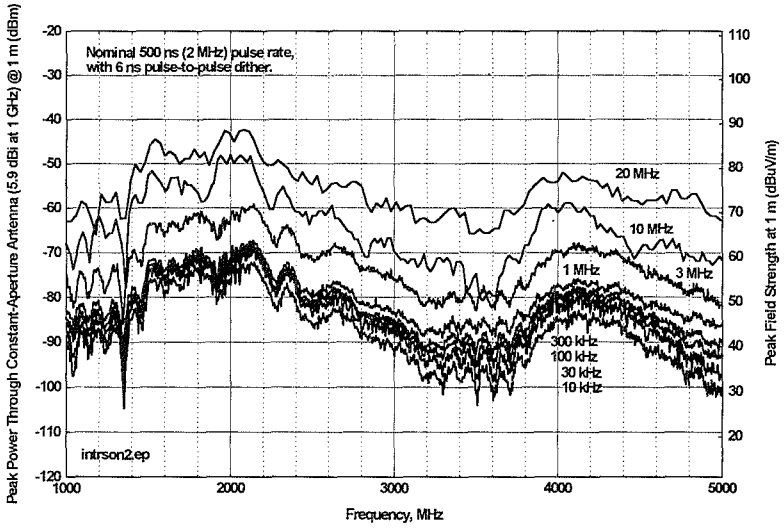

Figure 8.38. Device C spectra in multiple bandwidths.

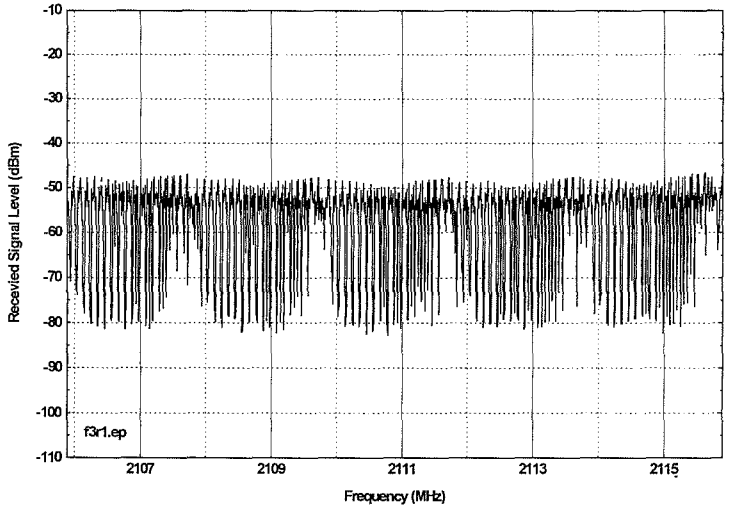

Figure 8.39. Device C, peak-detected to show spectral line patterns in noise.

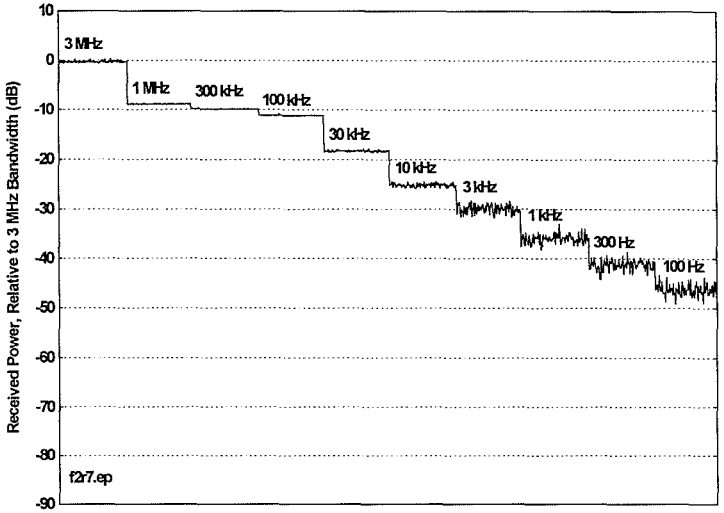

Figure 8.40. Device C, peak bandwidth progression stairstep.

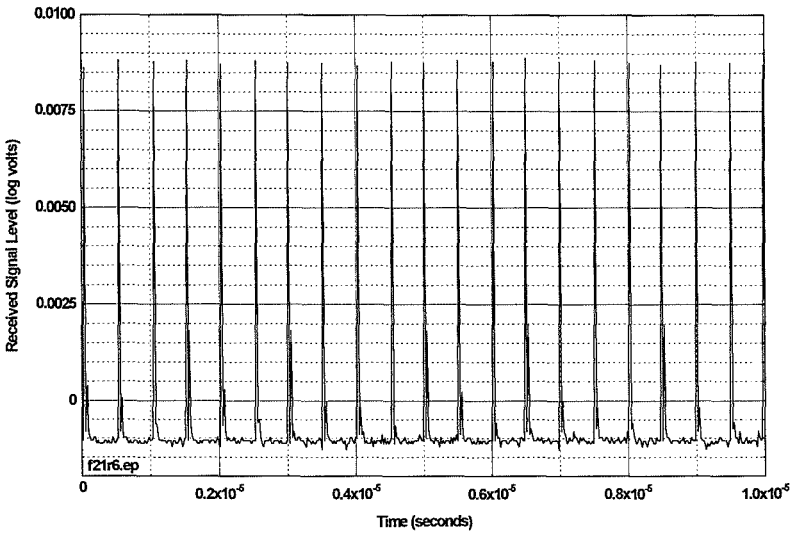

Figure 8.41. Device C, pulse train waveform for 10 microseconds, external detector.

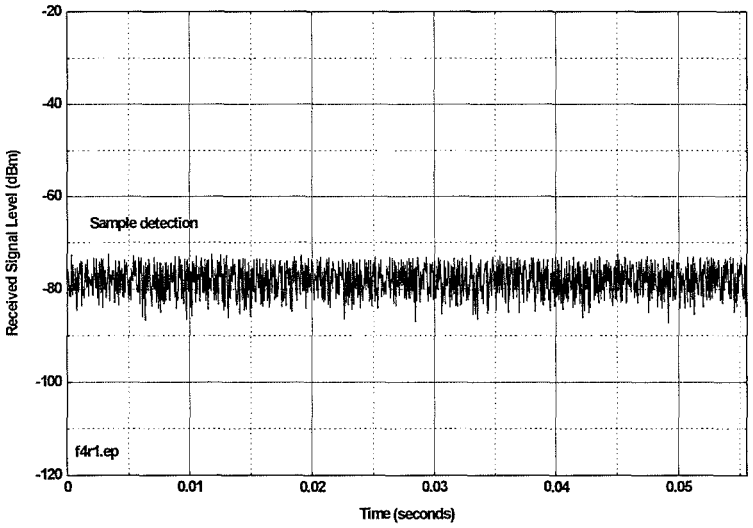

Figure 8-42. Device C, time waveform in 55 ms, 3-MHz IF bandwidth.

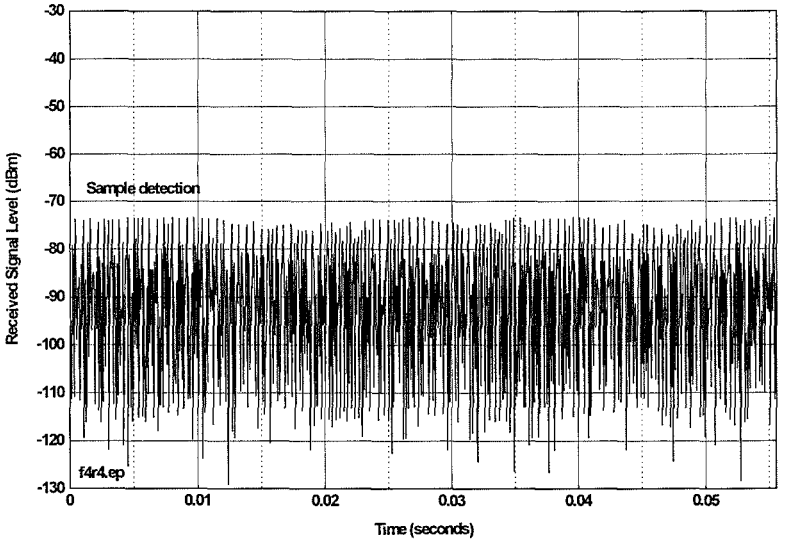

Figure 8.43. Device C, time waveform in 55 ms, 100-kHz IF bandwidth.

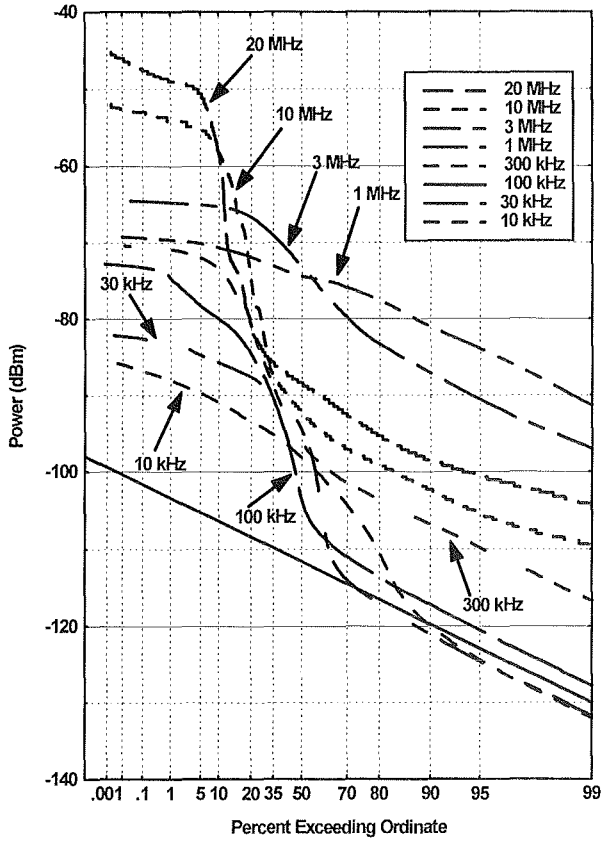

Figure 8.44. Device C APDs, between spectral lines.

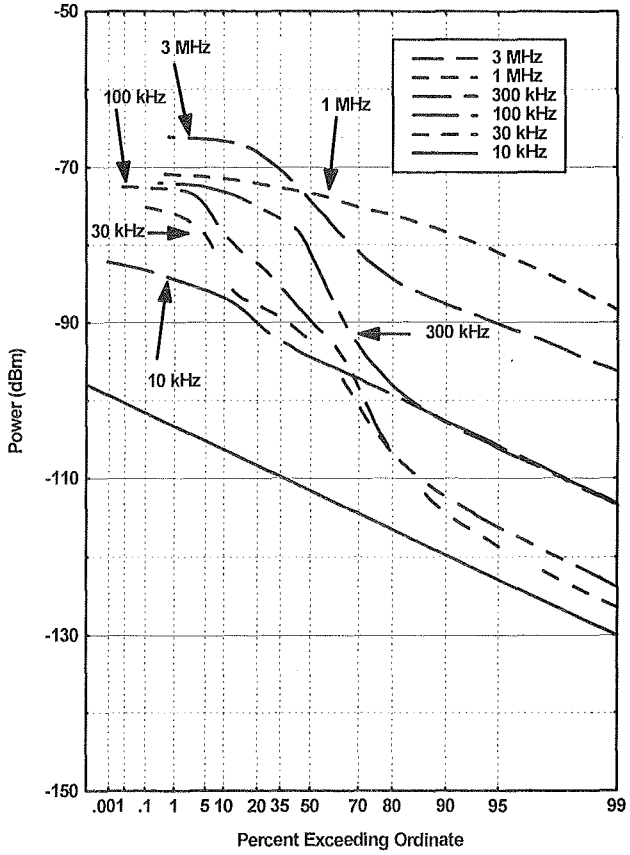

Figure 8.45. Device C APDs, on spectral lines.

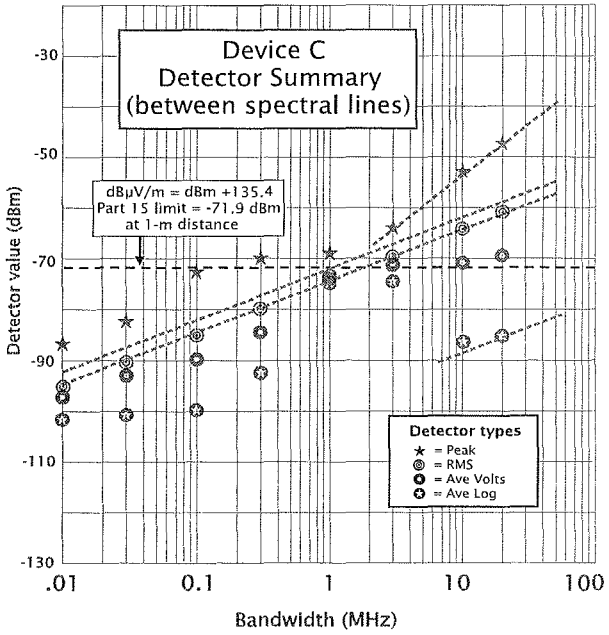

Figure 8.46. Device C, detector summary (between spectral lines).

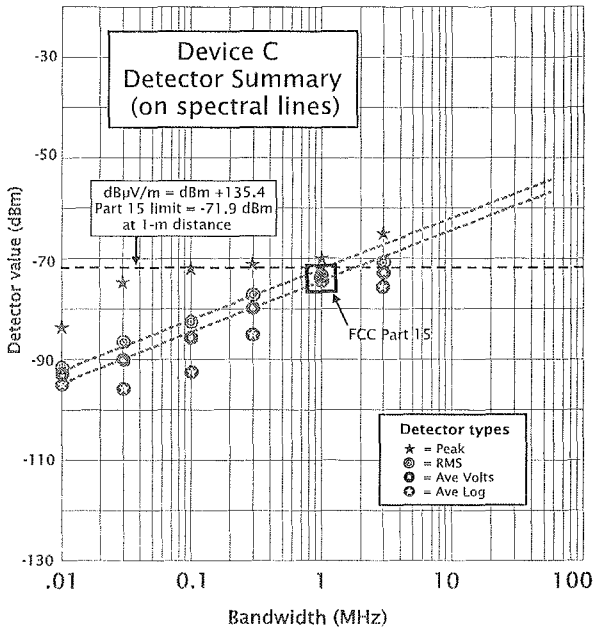

Figure 8.47. Device C, detector summary (on spectral lines)

8.3.4 Summary of Device D Measurements

Device Description: Device D operates with basic PRRs of 1 MHz, 5 MHz, and 10 MHz, with gating duty cycles available between 25% and 100% (continuously on). A fixed 25% dither is applied, using an absolute time base in all modes. The device was measured in four modes: 1-MHz PRR, 25% gated duty cycle; 1-MHz PRR, 100% gated duty cycle; 10-MHz PRR, 25% gated duty cycle; and 10-MHz PRR, 100% gated duty cycle. The gating cycle for both PRRs utilized a 2-ms "on" period and a 6-ms "off" period. This data transmission device was measured without transmitting any actual data.

Full-bandwidth pulse shape and FFT spectrum. The Device D radiated full-bandwidth pulse shape (Figure 8.48) was used to compute an FFT peak spectrum over the 1-4 GHz range (Figure 8.49).

Narrowband peak emission spectra. Figures 8.50-8.53 contain spectrum measured for each of four Device D operating modes. These spectra compared closely in shape and amplitude with the FFT spectrum. Figure 8.53 included measurements made in a 20-MHz bandwidth, which show close agreement (within 1-2 dB) with the FFT values computed in a 20-MHz bandwidth.

Bandwidth progression stairstep. The stair-step bandwidth progression graphs (Figures 8.54-8.57) were measured at a frequency near 1560 MHz and show substantial differences between the 1-MHz PRR and the 10-MHz PRR modes. These differences are likely caused by the higher power and greater frequency separation of the discrete spectral lines in the 10-MHz PRR modes.

Spectrum fine structure. Details of the spectrum fine structure showed strong lines with1-kHz spacing in the 1-MHz PRR mode (Figure 8.58) and 10-kHz spacing in the 10-MHz PRR mode (Figure 8.59). It is not known whether these lines would be present with transmission of actual data. Figure 8-60 shows pulse-position modulation, measured in a 10-MHz bandwidth.

APDs. The APDs are shown in Figures 8.62 to 8.65. The non-gated modes (100% gating) appear like Gaussian noise for bandwidths less than the PRR and appear impulse-like for bandwidths larger than the PRR. The gated modes show clear break-points at the 25% point, with measurement system noise present for the remaining 75% of the duration.

Detector summary. The detector summaries (Figures 8.66 to 8.69) show that the ungated modes appeared similar to Gaussian noise for bandwidths less than the PRR. For all narrower bandwidths, peak values were about 10-dB greater than the RMS, and the average voltage and average logarithm were tightly clustered within a few dB less than the RMS. All of the detector functions followed a 10 $\log_{10}$ B trend line. The corresponding trend lines were 8-10 dB higher for the 10-MHz PRR than for the 1-MHz PRR mode. Only when the bandwidth was greater than the PRR, did the detector values at a bandwidth begin to diverge. The peak values then followed a 20 $\log_{10}$ B trend. The average logarithm and average voltage decreased substantially at larger bandwidths, when pulses did not overlap and system noise was momentarily the only signal.

The gated modes provided peak values identical to the corresponding ungated (i.e.,100%) modes. The gated RMS values were approximately 6 dB lower than those of the corresponding ungated modes, as expected when the total number of impulses was decreased by 75%. The gated mode average logarithm dropped to within a few dB of system noise (present 75% of the time), with the 10-MHz PRR average logarithm being 1-2 dB higher than the 1-MHz logarithm.

FCC Part 15 Measurements. Part 15 measurements for the ungated 1-MHz PRR and 10-MHz PRR modes matched the average logarithms at -84 dBm and -74 dBm, respectively. Part 15 measurements for the gated modes were -100 dBm and -97 dBm for the 1-MHz PRR mode and 10-MHz PRR mode (Figure 8.61), respectively. The 1-2 dB discrepancy between Part 15 and average logarithm for gated modes was caused by insufficient video filtering of the 8 ms gating cycle, which allowed 2-3 dB of ripple on the video filter output.

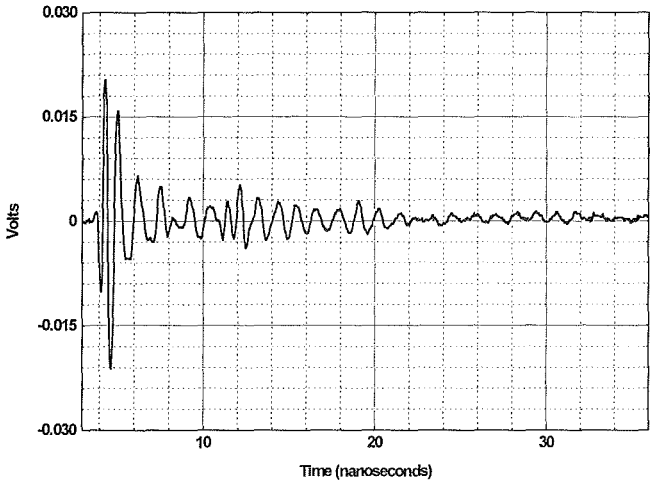

Figure 8.48. Device D radiated full-bandwidth pulse shape

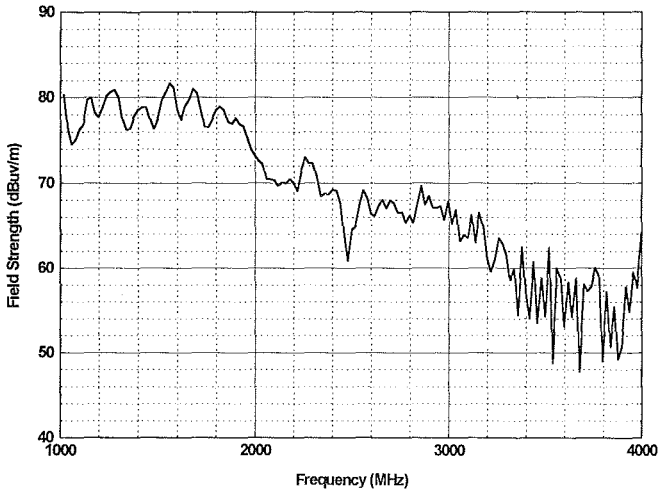

Figure 8.49. Device D, radiated peak field strength at 1 m, $\Delta f = 20$ MHz.

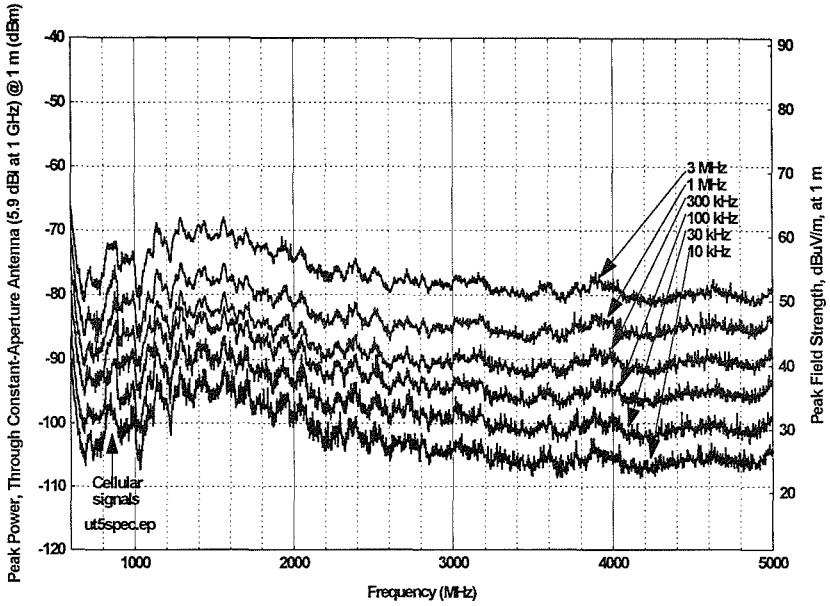

Figure 8.50. Device D spectra,1-MHz PRR, 25% gating.

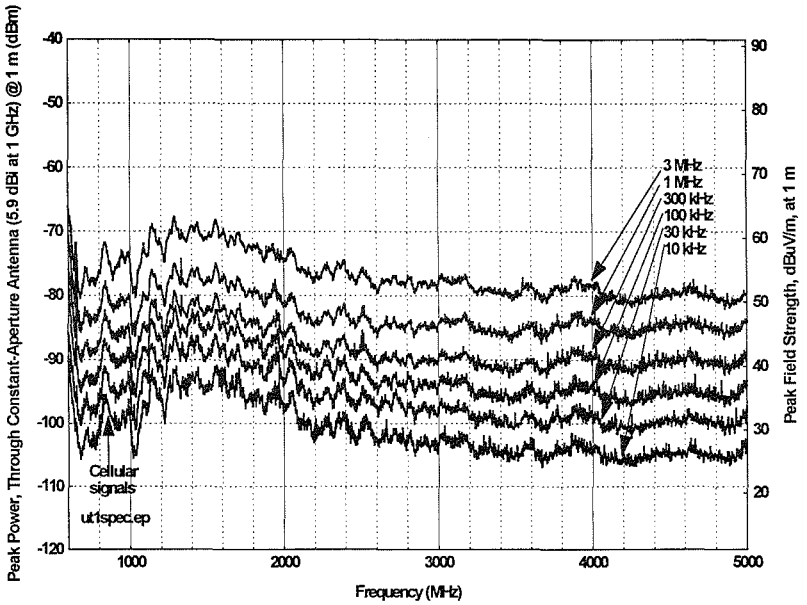

Figure 8.51. Device D spectra, 1-MHz PRR, 100% gating.

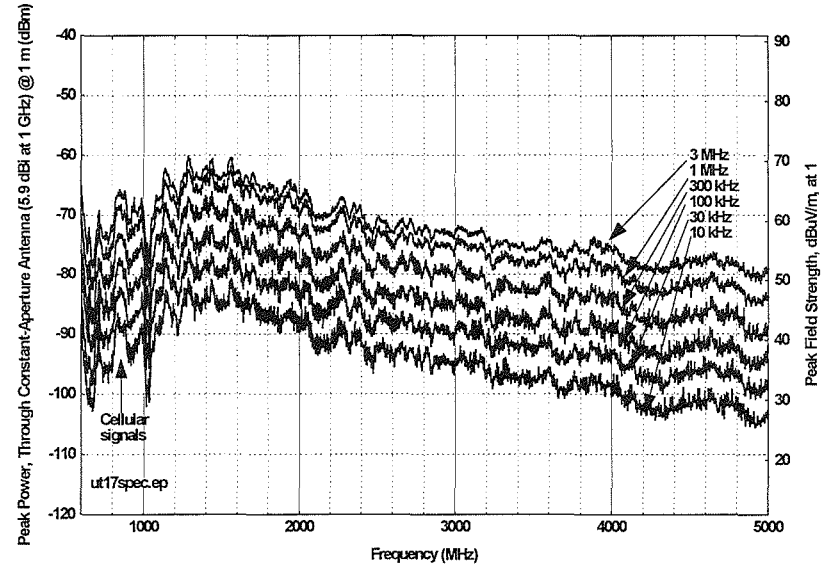

Figure 8.52. Device D spectra, 10-MHz PRR, 25% gating.

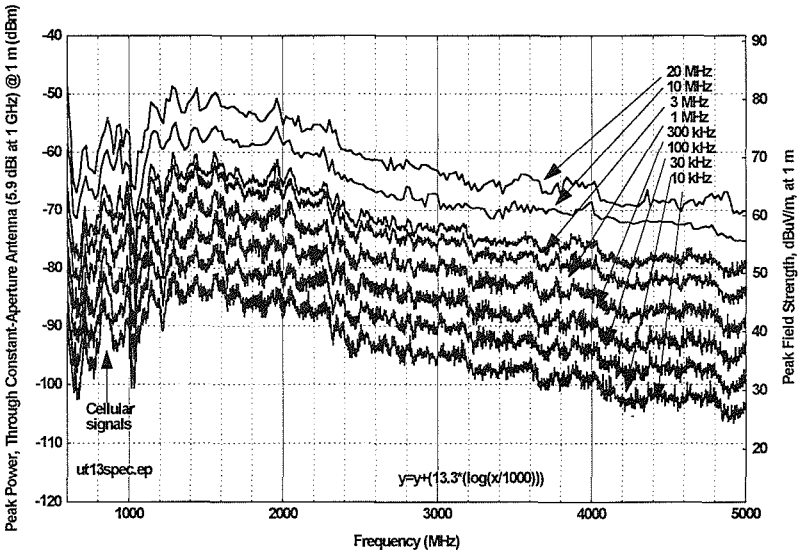

Figure 8.53. Device D spectra, 10-MHz PRR, 100% gating.

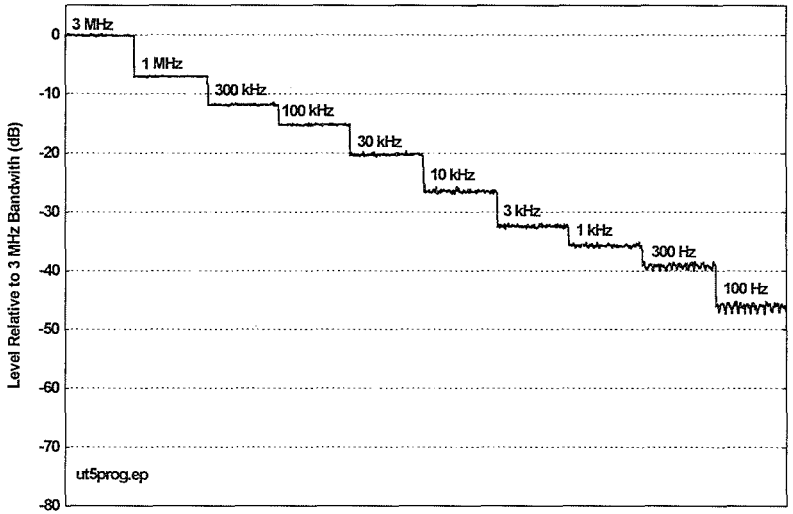

Figure 8.54. Device D bandwidth progression stairstep, 1-MHz PRR, 25% gating.

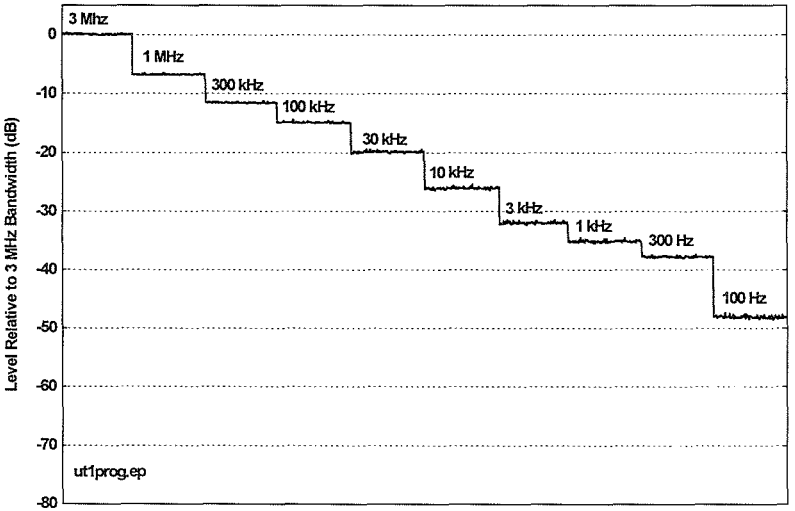

Figure 8.55. Device D bandwidth progression stairstep, 1-MHz PRR, 100% gating.

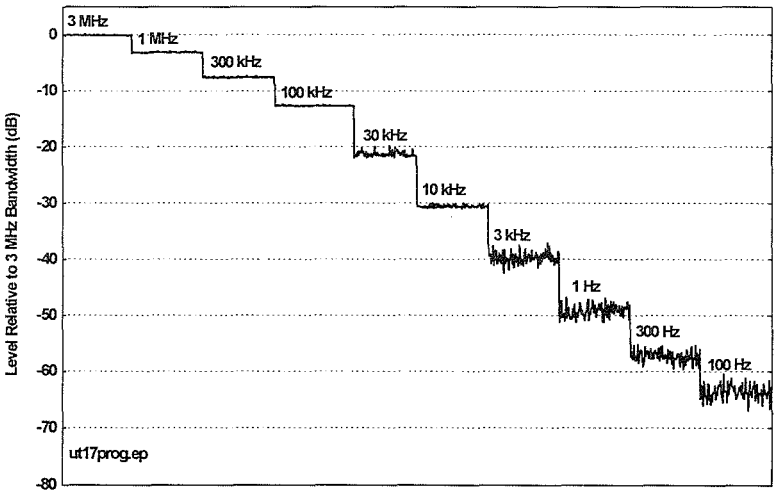

Figure 8.56. Device D bandwidth progression stairstep, 10-MHz PRR, 25% gating.

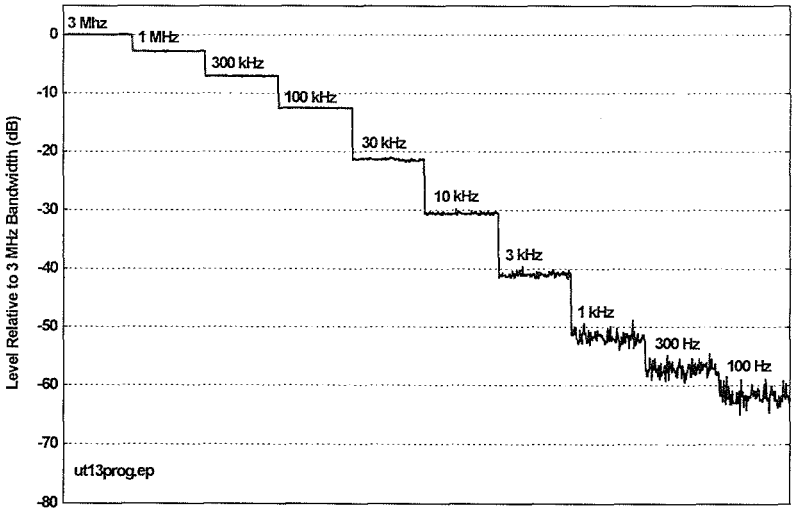

Figure 8.57. Device D bandwidth progression stairstep, 10-MHz PRR, 100% gating.

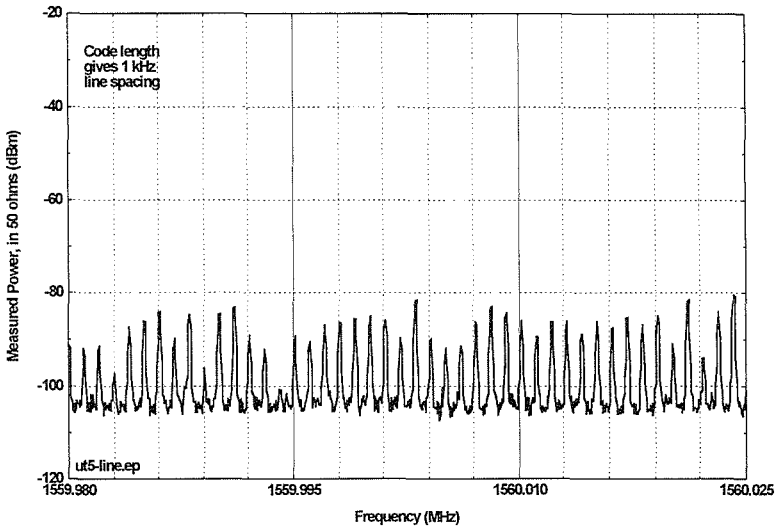

Figure 8.58. Device D 1-kHz emission lines, 1-MHz PRR, 25% gating.

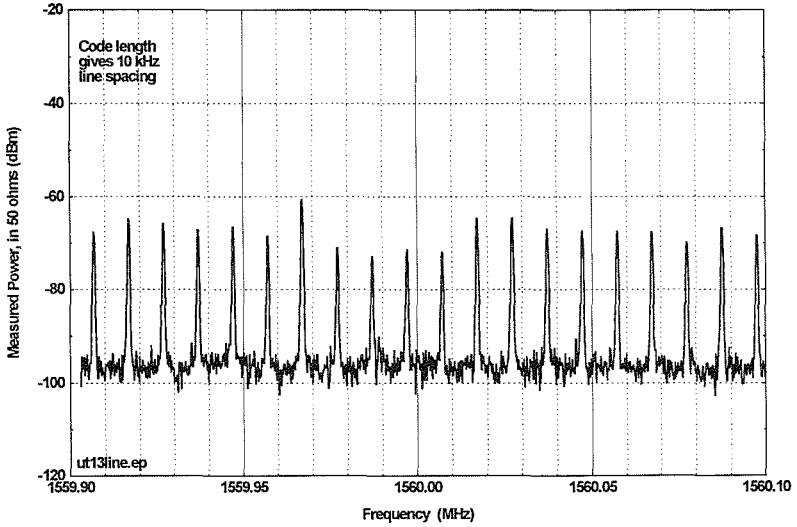

Figure 8.59. Device D 10-kHz emission lines, 10-MHz PRR, 100% gating.

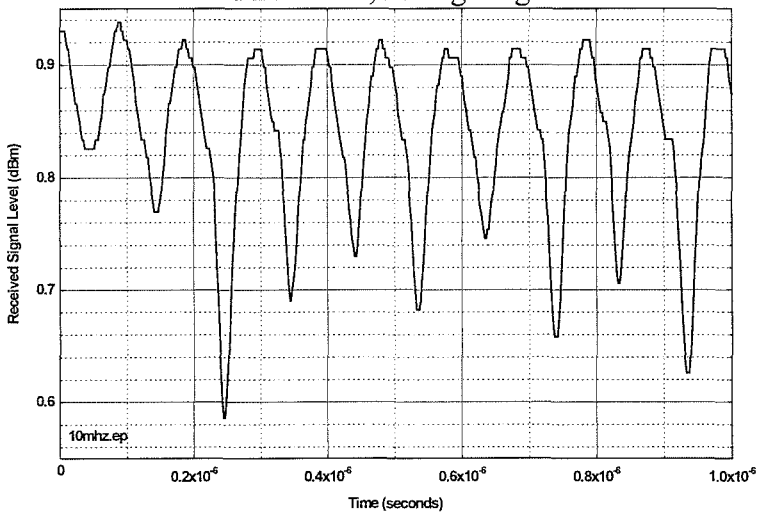

Figure 8.60. Device D waveforms, 10-MHz IF, 10-MHz PRR, 100% gating, 25% dither, showing pulse position modulation.

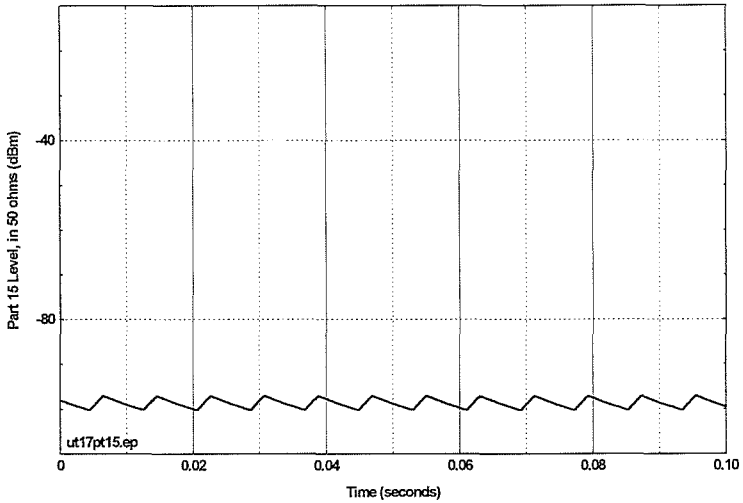

Figure 8.61. Device D, 10-MHz PRR, 25% gating, Part 15 measurement showing ripple in 10-Hz video BW.

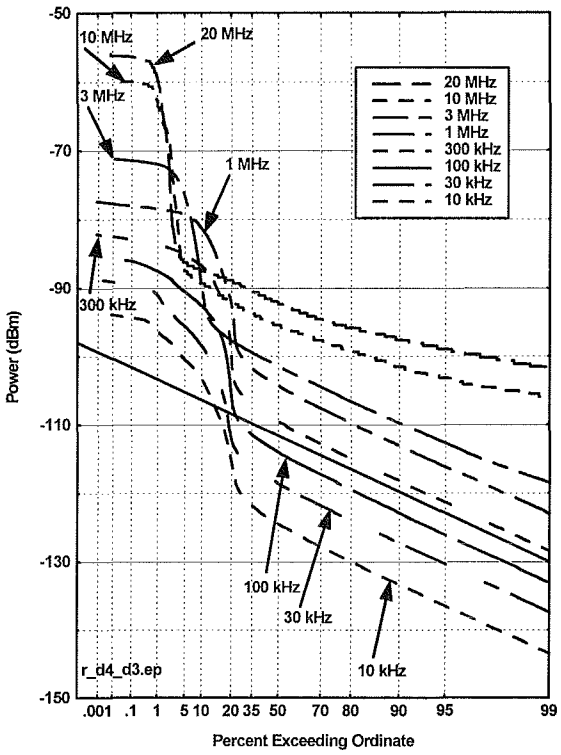

Figure 8-62. Device D APDs, 1-MHz PRR, 25% gating.

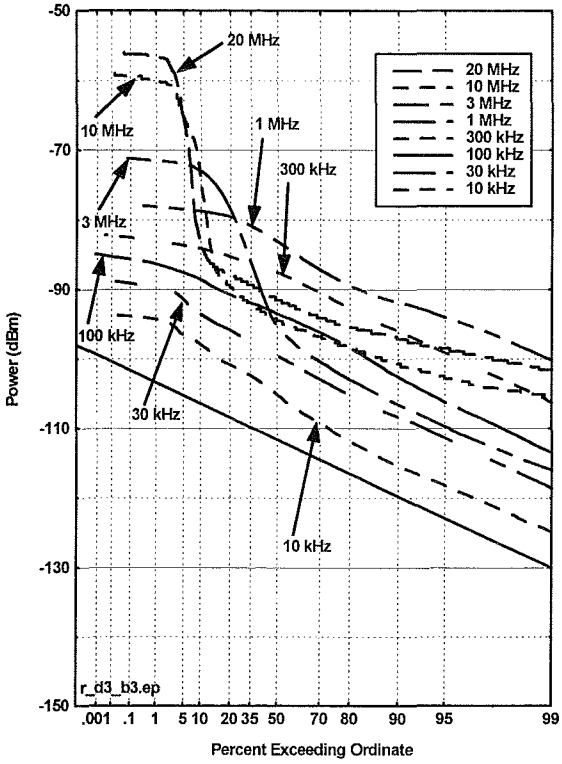

Figure 8.63. Device D APDs, 1-MHz PRR, 100% gating.

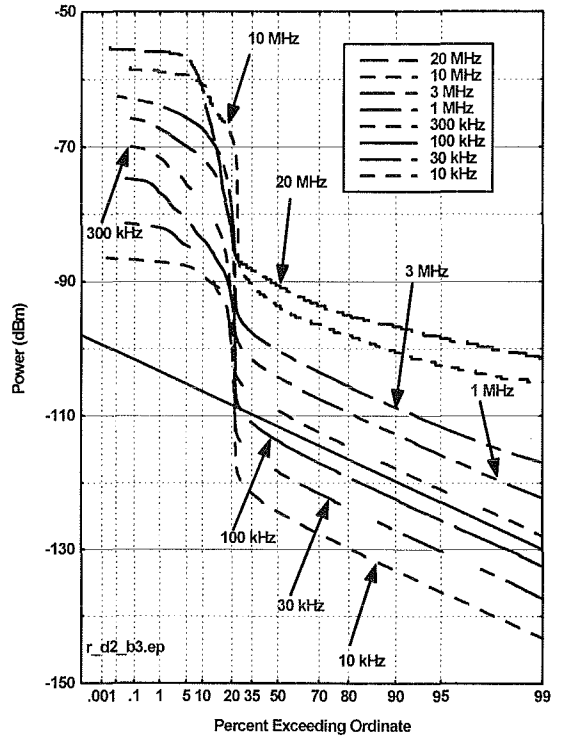

Figure 8.64. Device D APDs, 10-MHz PRR, 25% gating.

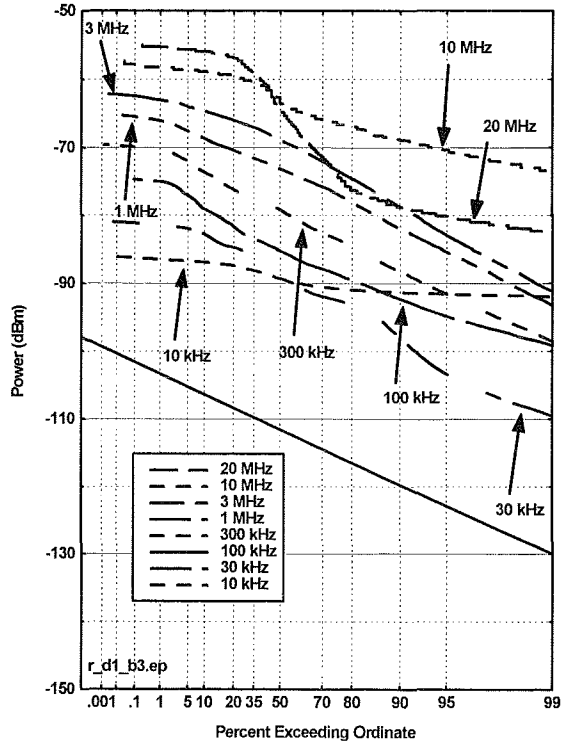

Figure 8.65. Device D APDs, 10-MHz PRR, 100% gating.

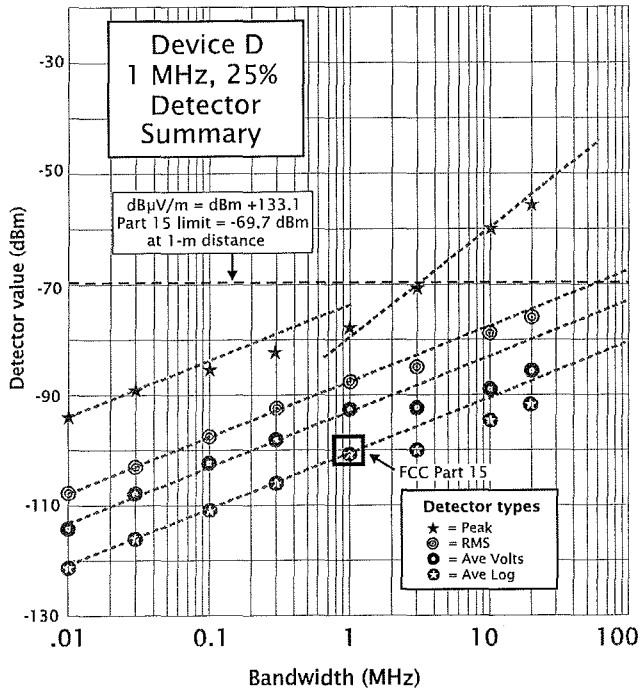

Figure 8.66. Device D detector summary, 1-MHz PRR, 25% gating.

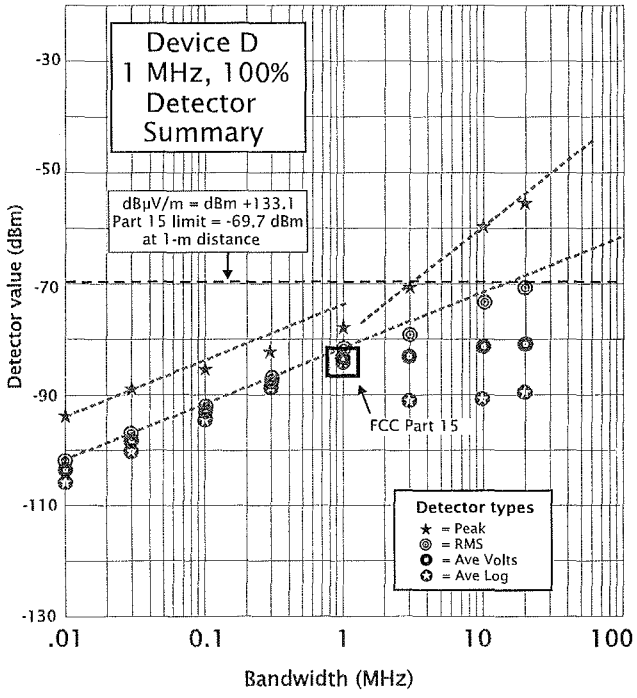

Figure 8.67. Device D detector summary, 1-MHz PRR, 100% gating.

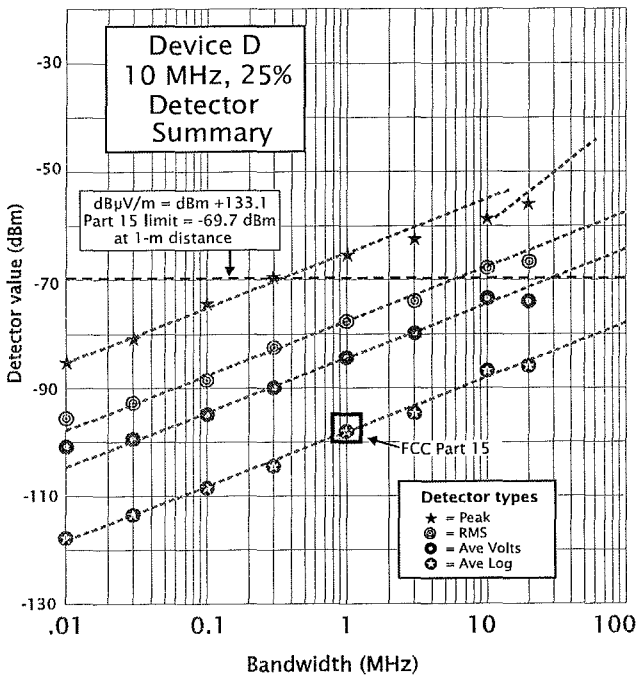

Figure 8.68. Device D detector summary, 10-MHz PRR, 25% gating.

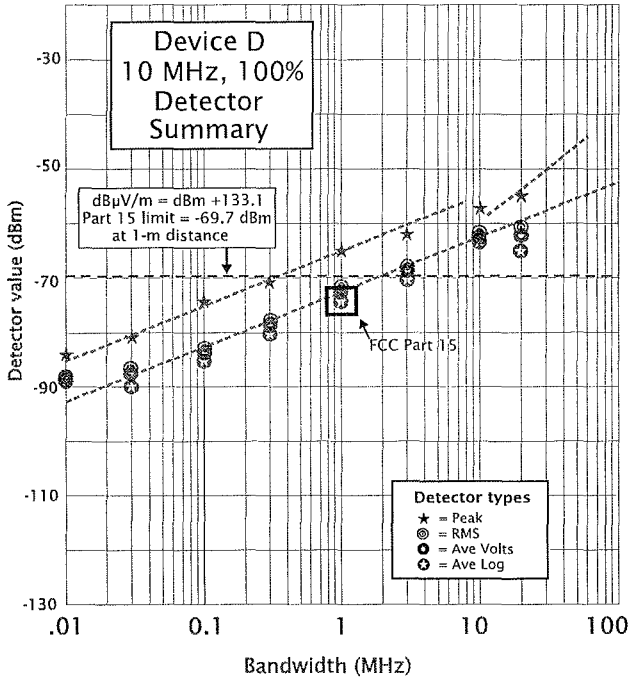

Figure 8.69. Device D detector summary, 10-MHz PRR, 100% gating.

8.3.5 Summary of Device E Measurements

Device description: Device E is designed to radiate mainly towards the ground. Interchangeable RF heads permitted operation at nominal frequencies of 300 MHz, 900 MHz, and 1500 MHz.. Device E is capable of operating with multiple PRRs.

Full-bandwidth pulse shapes. Full-bandwidth pulse shape measurements were made with all three RF heads (Figures 8.69, 8.71, and 8.73), with the Device E antennas aimed directly at the measurement antenna 1 m away. These pulse shapes are very simple, with no additional lobes or extended ringing.

FFT emission spectra. FFT spectra were computed from each of the measured pulse shapes (Figures 8.70, 8.72, and 8.74, respectively).

Narrowband peak emission spectra. Spectrum analyzer measurements were made only with the 1500-MHz head, with Device E resting on a concrete floor, aiming downwards, with the measurement antenna 1 meter away from the edge of Device E and slightly above the floor. The spectrum analyzer measurements signal amplitudes cannot be compared with the FFT spectra because of different measurement conditions.

Bandwidth progression stairstep. Figure 8.76 shows the Device E emission spectrum, using the 1500- MHz RF head..

Gating, PRR, and modulation. The mode that was measured included a PRR near 85 kHz and a gating duty cycle of approximately 25 ms on, 6 ms off (Figures 8-78 and 8-79).A distinguishing feature of the Device E spectrum analyzer measurements was relatively low received power, which prevented Part 15 measurements from being made, and which also made it difficult to see some details of the modulation.

APDs. Figure 8.80 show APD measurements for the Device E 1500-MHz RF head.

Detector summary. Figure 8.81 shows a detector summary for Device E. Detector values for bandwidths less than 1 MHz seem to be mostly measurement system noise.

FCC Part 15 measurements. The signal from Device E was apparently below measurement system noise and Part 15 measurements could not be performed.

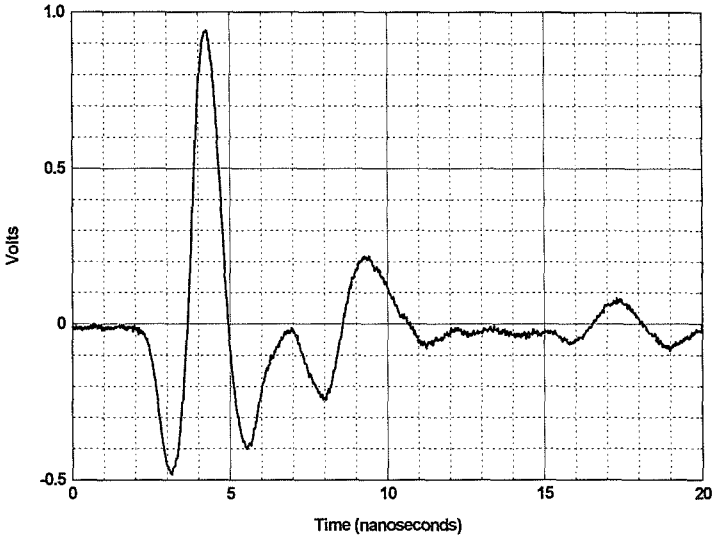

Figure 8.70. Device E full bandwidth pulse shape, 300-MHz RF head, main beam.

Figure 8.72. Device E full bandwidth pulse shape, 900-MHz RF head, main beam.

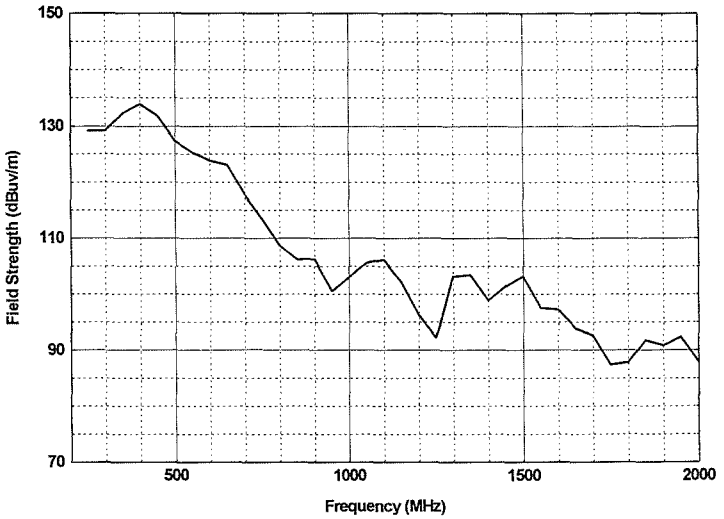

Figure 8.71. Device E, (300-MHz head), peak field strength at 1 m, main beam, $\Delta f = 50$ MHz.

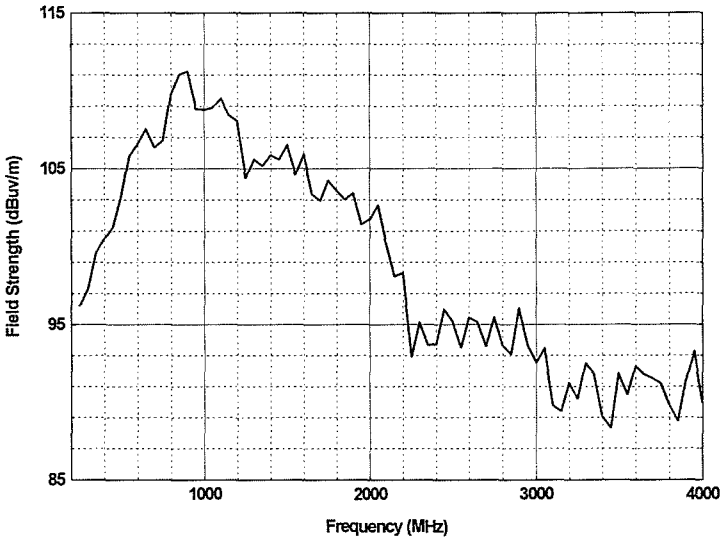

Figure 8.73. Device E (900-MHz head) peak field strength at 1 m, main beam, $\Delta f = 50$ MHz.

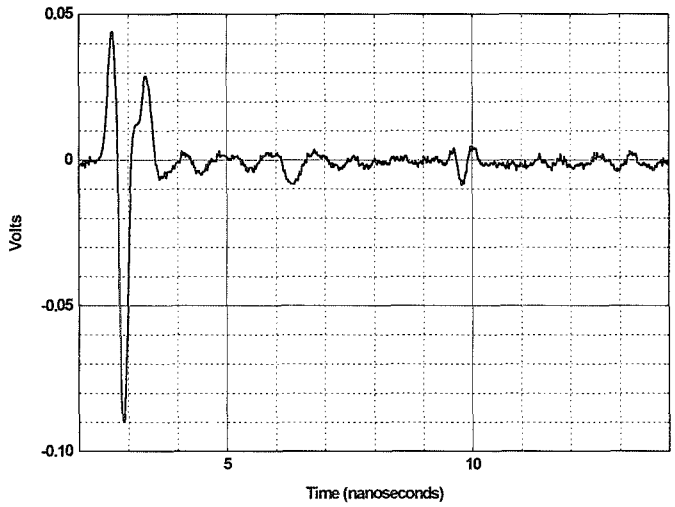

Figure 8.74. Device E full bandwidth pulse shape, 1500-MHz RF head, main beam.

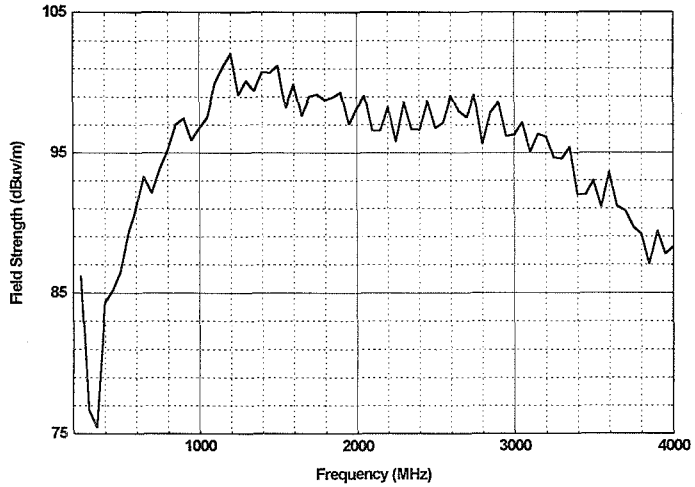

Figure 8.75. Device E (1500-MHz head) peak field strength at 1 m, main beam, $\Delta f = 50$ MHz.

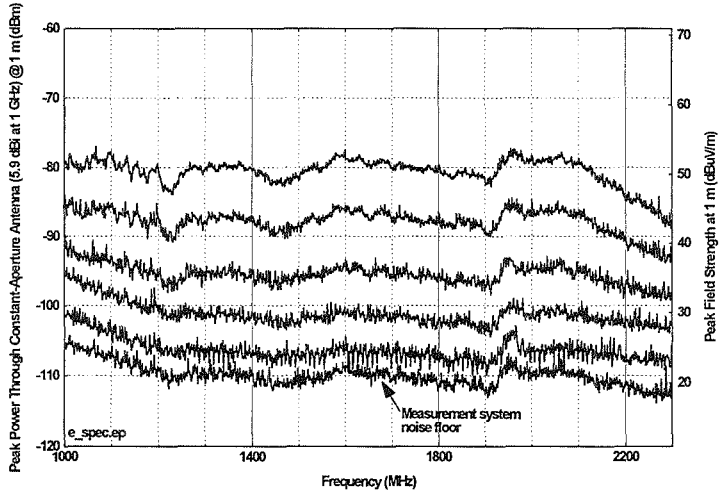

Figure 8.76. Device E 1500-MHz RF head, spectra as a function of measurement bandwidth.

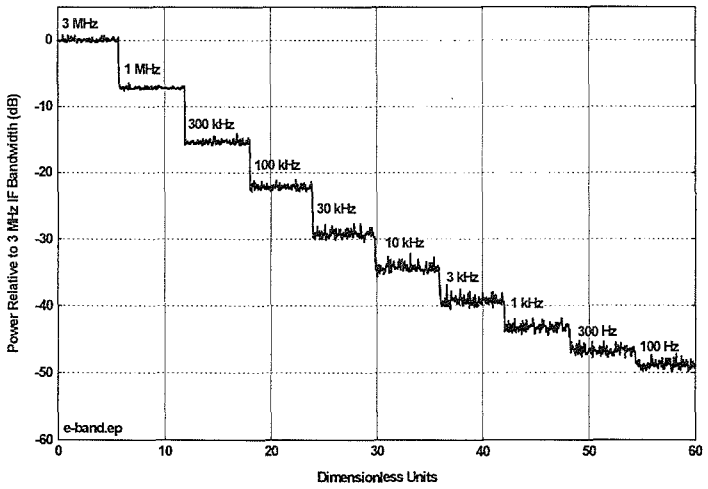

Figure 8.77. Device E 1500-MHz RF head, peak bandwidth progression stairstep.

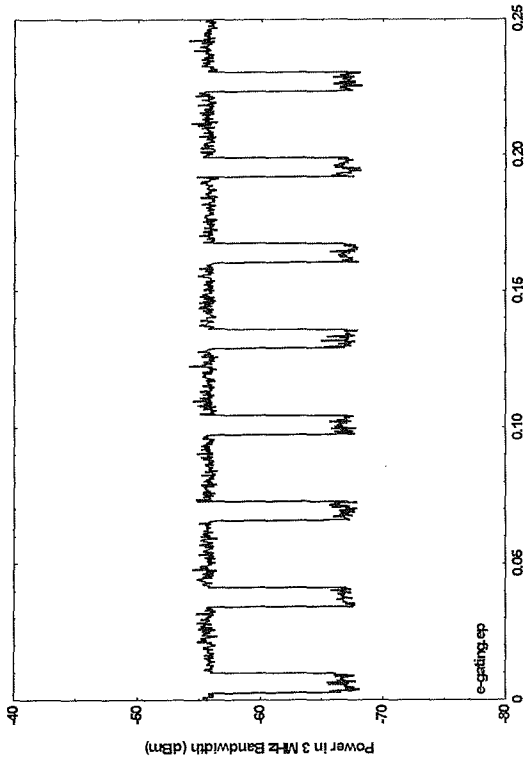

Figure 8.78. Device E pulse train.

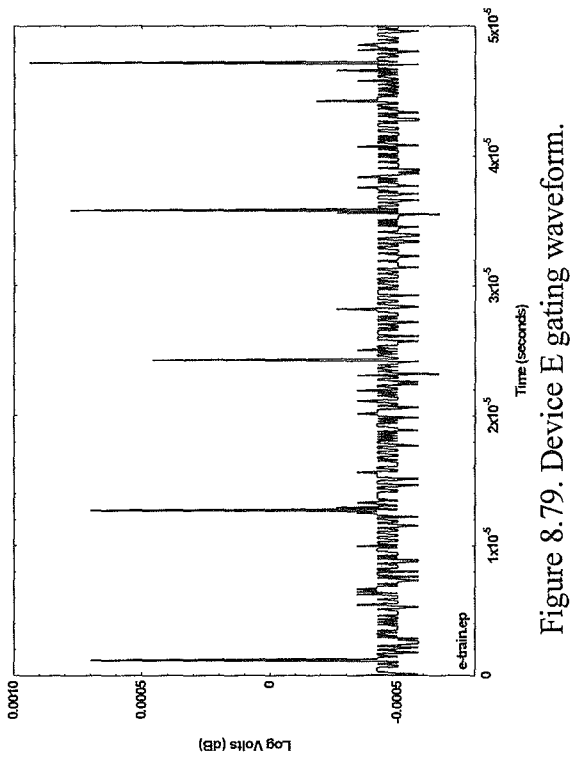

Figure 8.79. Device E gating waveform.

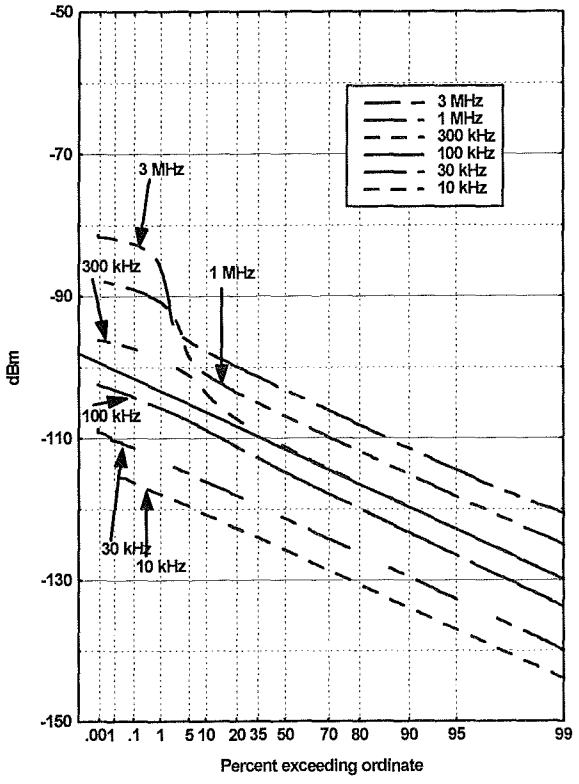

Figure 8.80. Device E APDs.

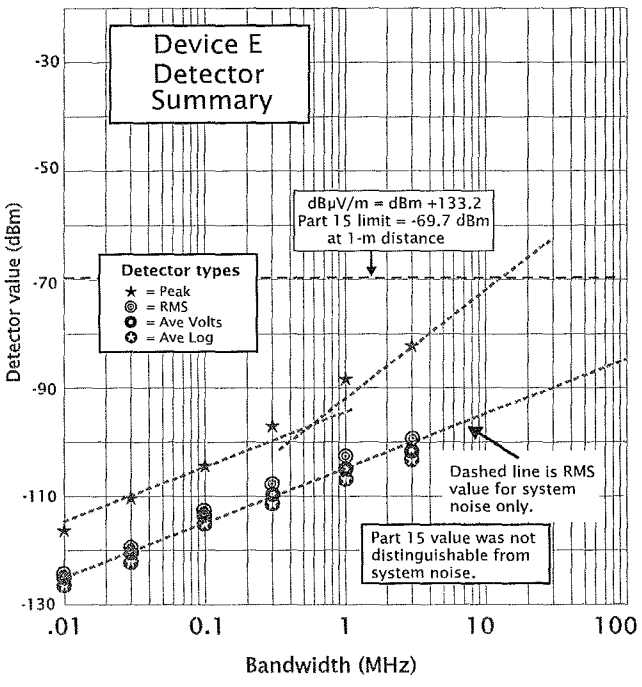

Figure 8.81. Device E, detector summary.

8.3.6 Summary of Electric Drill Measurements

An electric drill is included in the category of Part 15 Incidental Radiators, since it radiates radio frequency energy, although its function does not require the generation of radio frequency signals. The electric drill controls included only an on/off switch (i.e., no electronic speed control), and it was measured without any mechanical loading on the drill shaft.

Full-bandwidth pulse shapes. The random nature of the timing and amplitude of the electrical impulses from the drill made it impossible to use a sampling oscilloscope to measure the emitted impulses. Therefore, no full-bandwidth pulse shape measurements were made, and no FFT spectrum could be derived from the pulse.

Narrowband peak emission spectra. The energy radiated from the electric drill was measured by the spectrum analyzer over the 0.6-5.0 GHz range (Figure 8.82), including a noticeable "bulge" in the 3.1-4.2 GHz range. The highest frequency of measurable signal is not known. The apparent change of amplitudes measured with various bandwidths using the peak detector seems to be about 42 dB for a 2.5-decade change in bandwidth, i.e., a 17 $\log_{10}$ B trend line.

Gating, PRR, and modulation. Figure 8.83 shows the gradually building and declining burst of noise that occurs about every 17 ms and is related to the 60 Hz power line frequency.

APDs. Each drill APD in Figure 8.84 appears to be divided into impulsive and noise-like parts, with the noise-like portion determined by measurement system noise and following a 10 $\log_{10}$ B rule. The impulsive portion, unlike typical UWB devices, assumes a steep, straight-line slope without any hint of a plateau. The 1-MHz and 3-MHz APDs seem to develop an even steeper slope at the low-probability end, beginning at the 0.1% point. The APDs were only measured to .001% (100 k samples); it is likely that the peak values for the wider bandwidths might have been considerably higher (perhaps 10 dB higher?) had they been extended to the left-hand edge of the graph. The drill APDs are somewhat problematic, since the peak amplitudes of apparently independent pulses do not increase as rapidly as 20 $\log_{10}$ B. In addition, the very steep slope of the low-probability end makes the measured peak very dependent on the sample size.

Detector summary. The drill detector summary (Figure 8.85) shows that the relative values of the various detectors remain almost the same for all bandwidths; all detectors follow a 10 $\log_{10}$ B rule. This behavior fails to match the RF spectrum graphs, which show the peak dB values increasing with a 17 $\log_{10}$ B trend line. This discrepancy can be partly explained because the peak measurements for the wider bandwidth spectrum measurements contained a much larger number of independent samples than the narrower bandwidths, which substantially increased the wider bandwidth peak values. It is also likely that the number of "pulses" seen in the drill emission increases proportionately with measurement bandwidth–a much different statistical process than a typical UWB signal (which has a constant number of pulses for wider bandwidths). The Part 15 measurements were too close to system noise to be useful.

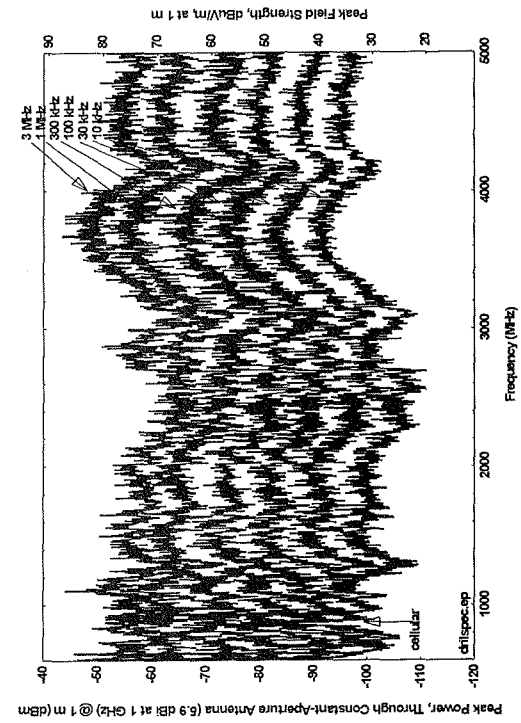

Figure 8.82. Electric drill spectrum as function of measurement bandwidth.

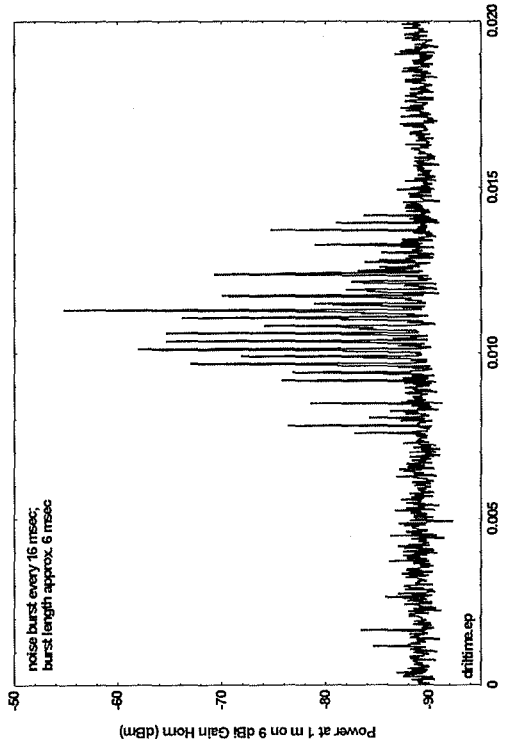

Figure 8.83. Typical electrical drill pulse train.

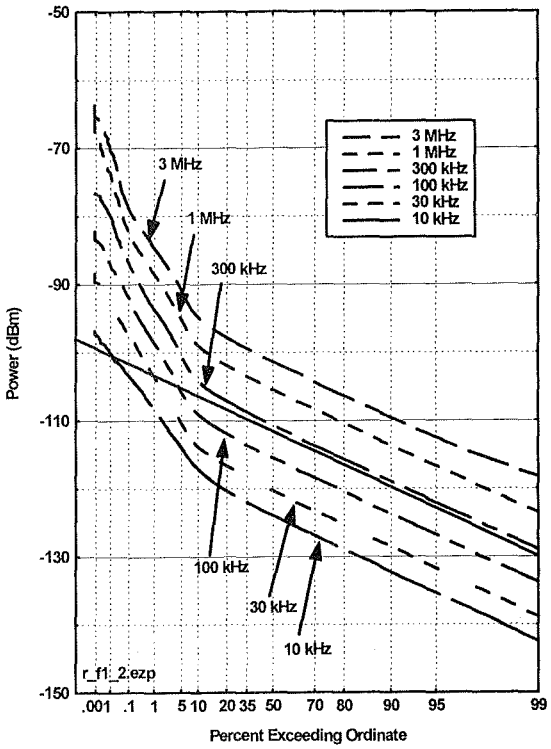

Figure 8.84. Electric drill APDs.

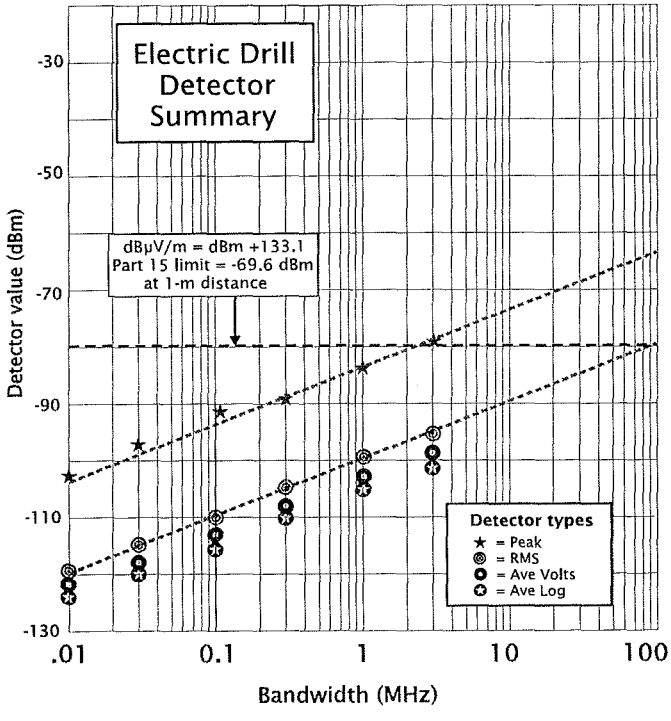

Figure 8.85. Electric drill detector summary.

8.4 Measurement Conclusions

1. The field strength in a bandwidth derived from an FFT of a full bandwidth pulse shape measurement matches the field strength shape measured in a narrower bandwidth by a spectrum analyzer in general shape and absolute amplitude at the peak emission frequency. This confirms that narrowband spectral measurements with a spectrum analyzer or other measurement receiver can be expected to provide accurate information to characterize the overall shape and absolute amplitude of the RF spectrum of UWB signals.

2. Specialized facilities and expertise are needed to obtain accurate measurements of full bandwidth pulse shape. Some of the possible errors associated with this technique are subtle, and many test labs may find that a comparison between FFT-derived spectra and band-limited spectrum analyzer measurements is the only way to verify the accuracy of the full bandwidth pulse shape measurements.

3. There appears to be no simple and accurate technique for relating full bandwidth pulse width data to the 10-dB or 20-dB emission spectra. This is especially true when the UWB pulse is used to excite multiple resonant elements, producing an RF pulse with a multi-lobed ringing response.

4. Amplitude probability distributions (APDs) made with multiple bandwidths provide a useful and theoretically consistent description of UWB signals and how they would affect receivers having various bandwidths. Various detector functions (peak, RMS, average voltage, and average logarithm) can be computed from the APDs or measured directly (if the measurement instrument has the appropriate capabilities).

5. For most UWB devices, the recommended FCC Part 15 non-quasi-peak measurement procedure produces results identical to the average logarithm derived from the 1-MHz bandwidth APD. In situations where the previous statement is not true, the discrepancy is due to insufficient video filtering allowing amplitude variations caused by long-duration duty-cycle events (e.g., gating) to get through to the peak detector.

6. The value measured with an average logarithm detector is substantially affected by measurement system noise for gated or impulsive signals. The average logarithm value is mostly insensitive to energy contained in low-duty-cycle, high-amplitude signals. This results in Part 15 measurement values that can be substantially lower (10-15 dB) than the RMS value (average power) in the UWB signal.

7. The RMS value produces results that are proportional to measurement bandwidth and spectral power density, irrespective of PRR or modulation. Depending on the integration time selected for an RMS measurement, the RMS value can be properly associated with average power when a gated signal is gated on, average power across an entire gating cycle, or average power during other operational periods.

8. Based on measurements of Device C, it seems possible to develop modulation techniques that could cause a UWB signal to look impulsive/gated in a 1-MHz bandwidth and like a CW signal in a 50-MHz bandwidth. Such signals could pass the 1-MHz Part 15 average limit (slipping high-power impulsive signals through the Part 15 average logarithm detector) and the 50-MHz 20-dB peak-to-average limit, while containing average power 15-20 dB above the Part 15 numerical limits. In fact, a signal could probably be designed so that its average power would be within a few dB of the peak level permitted in a 50-MHz bandwidth, while still passing the 1-MHz Part 15 average logarithm limit.

9. A Part 15 average limit based on RMS values would not have the problems described in #6, #7, and #8.

10. Many UWB devices employ dithering, which make their emissions appear more like Gaussian noise (for bandwidths less than the PRR). While this technique is at least partially successful, the specific modulation and dithering techniques may leave a spectrum fine structure that contains many low-level discrete spectral lines and/or other time or frequency distributions that are significantly different from Gaussian behavior. Some of these non-Gaussian characteristics may tend to disappear when actual data are transmitted by UWB devices used for communications, but this effort did not test UWB devices under these conditions.

11. For UWB signals measured with a spectrum analyzer using bandwidths larger than the average PRR, the peak measured values varied according to a 20 $\log_{10}$ B rule.

12. Spectrum analyzers having a 50-MHz bandwidth are not yet readily available at test laboratories. A 20-MHz measurement bandwidth was the largest spectrum analyzer bandwidth used in these tests to make peak measurements. Based on #11, a useful alternative to making peak measurements in a 50-MHz bandwidth may be to make measurements in a smaller bandwidth (but large enough that the UWB signal looks impulsive) and to extrapolate to a 50-MHz bandwidth using a 20 $\log_{10}$ B rule.

13. We encountered a wide variation of center frequencies (300 MHz to 5 GHz), spectral shapes (very broad to quite narrow), PRR (10 kHz to 10 MHz), modulation techniques (none, absolute dither, relative dither, on-off), gating structures (none, 20%-90%), power levels, and operational functions (short-range to long-range sensing, one-way and two-way communications).

14. Based on measurements of a small sample of existing UWB devices, we are unable to easily or confidently assign UWB devices to a limited number of operational categories having certain distinctive technical characteristics. Therefore, it seems unwise to base any proposed regulations on the assumption that future UWB devices will limit themselves to a few applications and techniques that have been currently developed and demonstrated. Instead, it should be assumed that designers of future UWB devices will creatively explore many additional extensions and combinations of these technologies, and that any UWB device permitted by the regulations will eventually be developed -- possibly in large quantities.

15. Based on measurements of multiple UWB devices, as well as theoretical considerations, the following model (Figure 8.86) describes idealized detector response rules for peak and RMS detectors. This is an idealized treatment, which may or may not apply exactly to specific real systems. One assumption is that the UWB dithering or modulation produces a signal whose narrowband statistics are indistinguishable from Gaussian noise. Actual real-world dithering techniques may or may not approach this ideal, and some UWB devices (e.g., Device C) use dithering techniques whose narrow bandwidth results are quite non-Gaussian. The model assumes that the total number of pulses/s remains equal to the PRR; i.e., that neither gating, on-off keying (OOK), or other dithering/modulation techniques significantly changes the total number of pulses emitted.

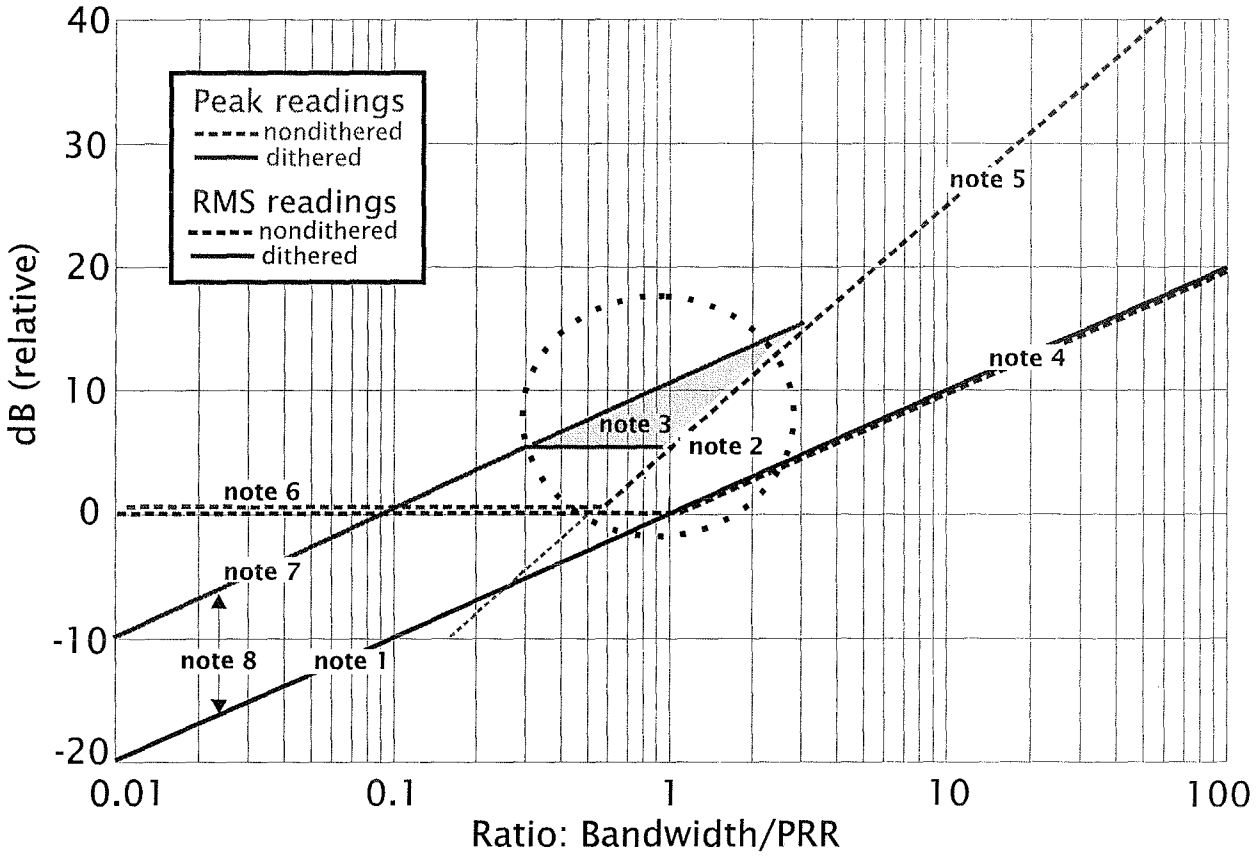

Figure 8.86. Idealized peak and RMS detector values model.

Figure 8.86 describes how a UWB signal measured with peak or RMS detectors in a given a bandwidth can be converted to corresponding readings in another bandwidth. This graph is referenced to the ratio of receiver bandwidth, B, to pulse repetition rate, PRR. This ratio (rather than any particular bandwidth or PRR) is what is critical in determining the rules that govern detector readings. Values of B/PRR >> 1 give non-overlapping impulse responses (the impulsive region). Values of B/PRR << 1 give overlapping responses that look like Gaussian

noise (dithered case) or discrete CW lines (non-dithered case). Values of B/PRR = 1 represent transitional cases, whose behavior varies depending on the details of the modulation on the PRR. The figure shows readings for peak and RMS detectors, for dithered and non-dithered UWB signals. The figure assumes that no gating is present. If gating is present, the figure should be modified by reducing all RMS readings by 10 log D, where D is the gating duty cycle, and leaving all peak readings unchanged. The following notes expand on several of the details of the figure.

Note 1. The dithered RMS detector response strictly follows a 10 $\log_{10}$ B line, since it is assumed that the total power intercepted by the measurement receiver is strictly proportional to receiver bandwidth. This will be the case for dithered UWB signals for all B/PRR ratios, as well as for B/PRR substantially greater than 1 for the non-dithered case, where the number of discrete CW lines within a bandwidth is proportional to the value of B.

Note 2. The detailed shape of all of these curves near the transition value B/PRR = 1 is not well known. It will depend substantially on the details of the UWB device modulation and receiver bandwidth filter response. Filter shapes with sharp suppression of adjacent channel responses will typically have an extended time response and a smaller peak value (i.e., will appear like a smaller bandwidth with respect to the peak value and the duration of the pulse). In general, the slope of the various response curves is trustworthy for bandwidth values far away from the transition point, but neither the exact shape of the transition curves nor the straight-line intercepts between the noise-like and impulse-like regions have been precisely determined for a variety of bandpass characteristics and UWB modulations..

Note 3. The behavior near the transition region where B/PRR = 1 for "dithered peak" is particularly obscure. This is partly because there is a transition between a Gaussian probabilistic region and a deterministic impulsive environment. The area in the shaded triangle represents a range of responses that has been observed in this set of measurements, but this region should be examined more carefully. Some measured systems show a very tight grouping of detector readings (4-5 dB difference between average log and peak) when B/PRR = 1, while other systems do not.

Note 4. Since impulses have no time overlap in the impulsive region (B/PRR >> 1), there is no difference in responses between dithered and non-dithered pulses. Therefore, the dithered and non-dithered RMS curves will overlay exactly in the B/PRR >>1 region, and both will follow a 10 $\log_{10}$ B slope.

Note 5. For the same reasons described in note 3, the dithered and non-dithered peak curves will overlay exactly in the B/PRR >>1 region, and both will follow a 20 $\log_{10}$ B slope.

Note 6. The response for non-dithered UWB pulses produces evenly-spaced discrete CW lines when B/PRR<< 1. The graph assumes that measurements are made centered on one of the discrete CW lines. Since the envelope response for a single CW line is a constant voltage, the peak and RMS detectors give the same response. Moreover, since the voltage remains constant

for all bandwidths (assuming that the measurement bandpass remains centered on the CW signal), the common response for peak and RMS detectors follows a single horizontal line for B/PRR << 1.

Note 7. The value of the dithered peak reading will be about 10 dB above the value of the dithered RMS reading. This is based on the assumption that dithering produces statistics identical to Gaussian noise for B/PRR << 1. Also, see Note 8.

Note 8. It should be noted that the ratio between peak and RMS for detected Gaussian noise is not a constant; instead, it is a statistical quantity that depends on the number of independent observations. For example, there is a 1% chance that the peak will exceed the RMS by about 7 dB, a 0.1% chance of exceeding the RMS by about 8.5 dB, a 0.01% chance of exceeding the RMS by about 10 dB, etc. Therefore, the 10-dB peak-to-RMS ratio is based on collecting the peak reading from 10,000 independent observations. The peak-to-RMS ratio may need to be adjusted to use other probabilities, depending on the exact circumstances of how the model is to be applied.

9. COMPARISON OF THEORY AND MEASUREMENTS

Robert J. Achatz and Roger A. Dalke[1]

It is important to compare theoretical calculations with measurements whenever possible to validate results. Such validation is usually based on comparing salient features of measured results with corresponding features based on theoretical predictions.

Theoretical results given in Section 3 predict that 1) fixed time-base dithering will attenuate spectral lines (relative to the non-dithered periodic signal) and also introduce a continuous spectrum with a shape similar to the pulse spectrum, 2) periodically repeating the dithered signal will introduce spectral lines at the dither signal repetition frequency, and 3) statistics obtained from filtered UWB signals will be approximately Gaussian when the bandwidth is less than the PRR. Note that baseband Gaussian signal statistics yield Rayleigh amplitude statistics.

Device D measurements, summarized in Section 8.3.4, are for a 25% fixed dithered UWB device. Measurements include a 10 MHz PRR mode with 100% gating. These measurement results were compared with theoretical predictions given in Section 3. A synopsis of the comparison is given in this section.

Fixed time-base dithering features

Theoretical results for the 50% fixed time-base dithered, 10 MHz PRR PSD are presented in Section 3.2.1. These results predict that at frequencies of several hundred MHz and higher, spectral lines are only 10-20 dB above the continuous spectrum and hence should not be observable when the receiver bandwidth significantly exceeds 20 dB Hz. In addition, the continuous spectrum should have a shape corresponding to the pulse spectrum.

The pulse shape of Device D was measured with the full bandwidth test described in Section 5.2. The emission spectra was measured with the spectrum analyzer test described in Section 6. The spectrum analyzer test for a 25% fixed dithered, 10 MHz PRR UWB signal is summarized in Figure 8.53. These emission spectra measurements have the same shape as the pulse spectrum measured by the full bandwidth test in Figure 8.49 as predicted. Also, spectral lines at the PRR intervals were not evident in the emission spectra measurements as predicted by theory.

---

[1]The authors are with the Institute for Telecommunication Sciences, National Telecommunications and Information Administration, U.S. Department of Commerce, Boulder, CO 80305.

Dither signal repetition features

Theoretical results presented in Section 3.2.2 show that for repeated fixed dithered signals, spectral lines should be observed at frequencies corresponding to the signal repetition period. Figure 8.59 shows an emission spectrum measurement of a 25 % fixed dither, 10 MHz PRR UWB signal with a dither repetition frequency of 10 kHz. The measurement shows the spectral lines due to the repeating dither signal at 10 kHz intervals as predicted.

Band Limited UWB signal APD features

Theoretical results for the band limited 50% fixed dithered, 10 MHz PRR, UWB signal PSD were presented in Section 3.3. These results show that when the UWB signal passes through a receiver filter that is well below the PRR, the signal statistics are approximately Gaussian. As the filter bandwidth increases, the shape of the density function deviates from Gaussian. This deviation is measured by a statistic called excess which is a function of filter bandwidth as shown in Figure 3.5. Excesses near zero are indicative of an underlying Gaussian process. The excess factor deviates from zero at approximately 3 MHz bandwidth. This trend continues and at 10 MHz the value of the excess is significantly greater than zero.

The APD of for a 25 % fixed dithered, 10 MHz PRR APD shows the same non-Gaussian trend for bandwidths greater than 3 MHz where the statistics become increasingly impulsive. When the UWB signal is passed through filters with bandwidths of 1 MHz or less measurements show that the signal statistics are approximately Gaussian as predicted by theory.

APPENDIX A. TUTORIAL ON USING AMPLITUDE PROBABILITY DISTRIBUTIONS TO CHARACTERIZE THE INTERFERENCE OF ULTRAWIDEBAND TRANSMITTERS TO NARROWBAND RECEIVERS

Robert J. Achatz[1]

A.1 Introduction

The *amplitude probability distribution function* (APD) is used in radio engineering to describe signal amplitude *statistics*. The APD and its corresponding graph, shown in Figure A.1, succinctly express the probability that a signal amplitude exceeds a threshold. For example, the APD in Figure A.1 shows that the signal amplitude rarely exceeds high voltages. Statistics such as percentiles, deciles, and the median can be read directly from the APD. Other statistics such as average power can be computed with the APD.

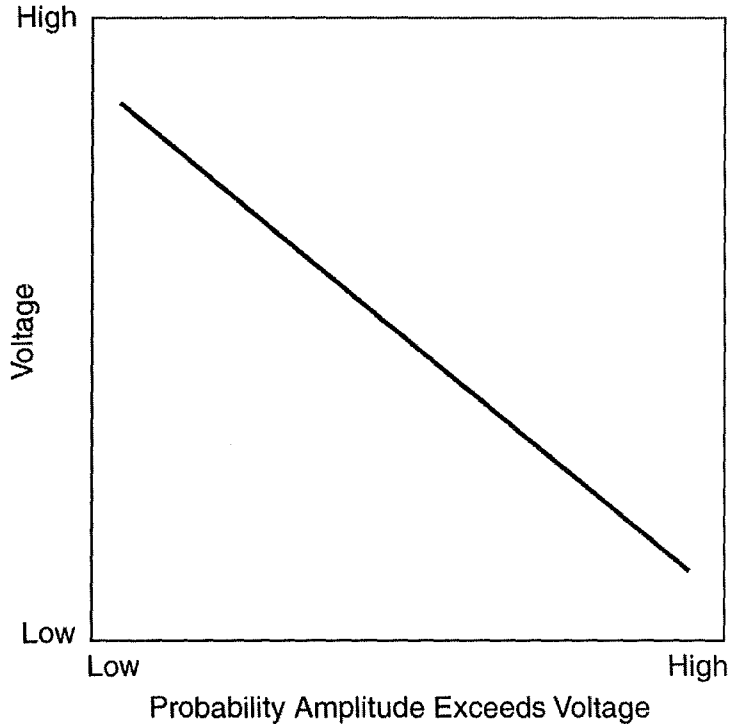

Figure A.1. Amplitude probability distribution.

The "signal" the APD characterizes is often noise or interference. For example, APDs are commonly used to characterize the amplitude statistics of *non-Gaussian* noise produced by

---

[1]The author is with the Institute for Telecommunication Sciences, National Telecommunications and Information Administration, U.S. Department of Commerce, Boulder, CO 80305.

lightning or unintentional emissions from man-made electrical or electronic devices. Numerous studies have shown that average noise power alone cannot predict the performance of receivers operating in non-Gaussian noise. APD statistics are needed for accurate predictions.

Today, many radio engineers are unfamiliar with the APD and its applications. This is because most modern receivers are designed to operate in bands with (zero-mean) *Gaussian* noise which is completely characterized by the average noise power statistic alone. Consequently, APD statistics are not needed for more accurate predictions.

Recently, federal spectrum regulators have been asked to allow emissions from *ultrawideband* (UWB) transmitters to overlay bands licensed to services that use *narrowband* receivers. Critics have charged that UWB transmitters may cause interference to 'victim' narrowband receivers. The amplitude statistics of this potential interference are dependent upon the specifications of the UWB signal and the band limiting filter in the narrowband receiver. The APD can be used to characterize this interference and correlate UWB signal and band limiting filter specifications to narrowband receiver performance.

The purpose of this tutorial is to introduce basic APD concepts to radio engineers and spectrum regulators who have not previously used the APD. It is hoped that these concepts will provide a firm basis for discussions on regulation of UWB transmitters. Emphasis is placed on understanding features likely to be found in band limited UWB signal APDs. These features are demonstrated with "tutorial" APDs of Gaussian noise, sinusoid (continuous wave) signals, and periodically pulsed sinusoid signals. Although the audience is intended to be broad, a limited number of mathematic expressions are used to avoid the ambiguity found in everyday language.

A.2 Signal Amplitude Characterization

A.2.1 APD Fundamentals

A *bandpass signal* is a signal whose bandwidth is much less than the *center frequency*. Bandpass signals are expressed mathematically as

$$s(t) = A(t)\cos(2\pi f_c + \theta(t)) ,$$

where A(t) is the baseband amplitude, $\theta(t)$ is the baseband phase, and f_c is the center frequency. The amplitude and phase define the *complex baseband signal*, $A(t)e^{j\theta(t)}$, whose spectrum is centered about 0 Hz.

The amplitude is always positive and is considered to be a *random variable*, A, when characterized by an APD. Formally, a new random variable, $\underline{A}_n$, is present at each sampling instant. The set $\{A_1, A_2, \ldots A_N\}$ is called the *random sample* of the random variable A if each

random variable is independent and identically distributed. Realizations or values of the random sample are denoted by the set $\{a_1, a_2, \ldots a_N\}$.

Associated with every random variable is a *probability density function* (PDF). The discrete PDF expresses the *probability* that a random variable "A" will have a realization equal to "a_i":

$$p(a_i) = P(A=a_i) ,$$

where $P()$ is the probability of its argument. PDF values are positive and the area under a PDF is equal to 1.0.

The *cumulative distribution function* CDF expresses the probability that a random variable "A" will have a realization less than or equal to "a":

$$c(a) = P(A \leq a) .$$

The discrete CDF is obtained by integrating the discrete PDF

$$c(a) = \sum_i p(a_i) ,$$

for all a_i less than or equal to a. CDF values range from 0.0 to 1.0.

Radio engineers are generally more concerned about how often a noise or interference amplitude exceeds a threshold. Thus they often prefer to use the complement of the CDF (CCDF) or APD. The APD function expresses the probability that a random variable "A" will have a realization greater than "a":

$$cc(a) = P(A>a) .$$

The discrete APD is obtained by subtracting the discrete CDF from 1.0.

$$cc(a) = 1.0\text{-}c(a) .$$

For clarification, Figure A.2 shows graphs of the discrete PDF, CDF, and APD for the random sample realizations:

$$\{a_1, a_2, \ldots a_{10}\} = \{1,2,3,3,1,4,4,3,4,3\} \text{ volts.}$$

The discrete PDF is estimated from the histogram. By convention, the axes of the APD are oriented differently from the axes of the CDF and PDF.

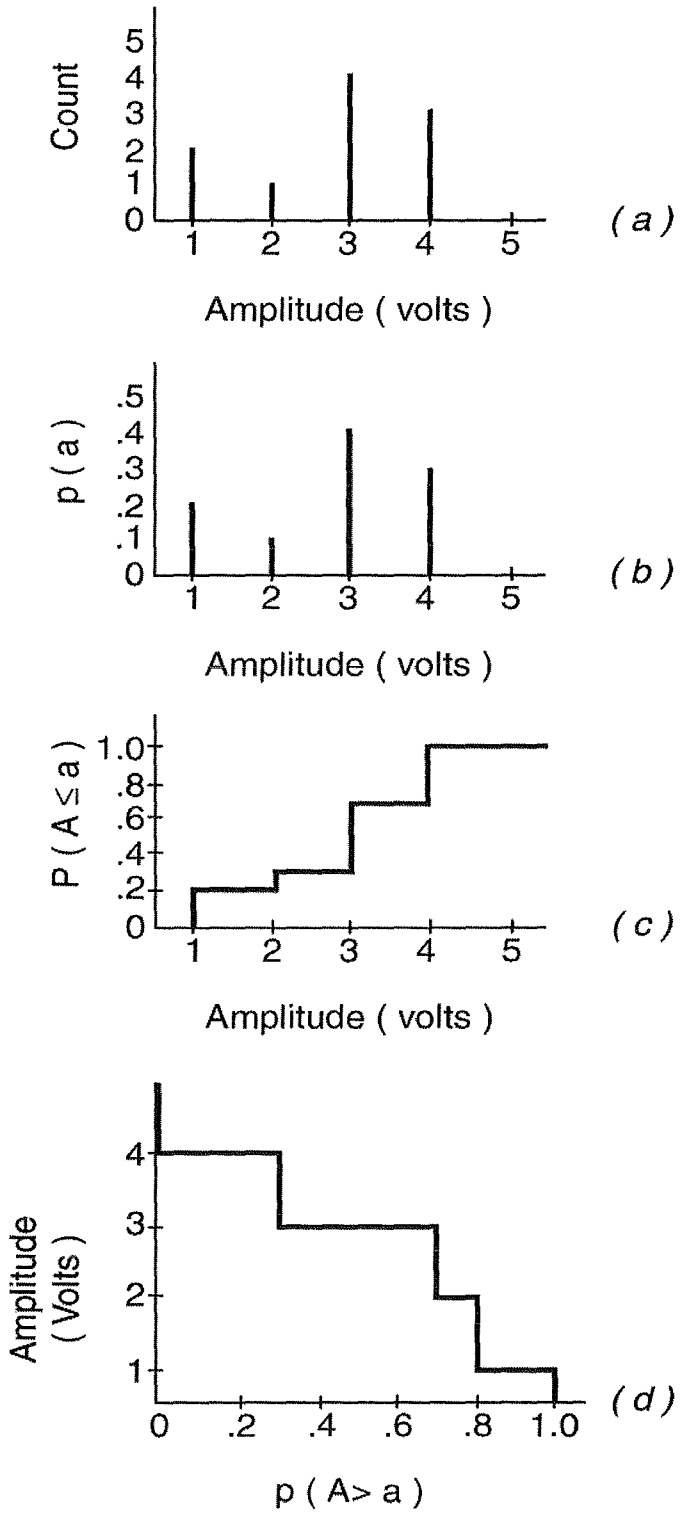

Figure A.2. Example histogram (a), probability density function (b), cumulative distribution function (c), and amplitude probability distribution function (d).

A.2.2 Statistic fundamentals

Statistics are functions that operate on the random sample. The *statistic value* is the result of a statistic operating on *random sample values*. Figure A.3 illustrates these relationships. Common statistical functions are percentile, mean or average, and root mean square (RMS). *First-order* statistics, addressed in this tutorial, assume the random variables are independent and identically distributed. *Second-order* statistics, not addressed in this tutorial, measure the correlation between these random variables. *Stationary* statistics are independent of time whereas *non-stationary* statistics are functions of time. Noise and interference amplitude statistics are non-stationary in many cases. Thus radio engineers sometimes measure the statistics of the amplitude statistics such as the median average noise power.

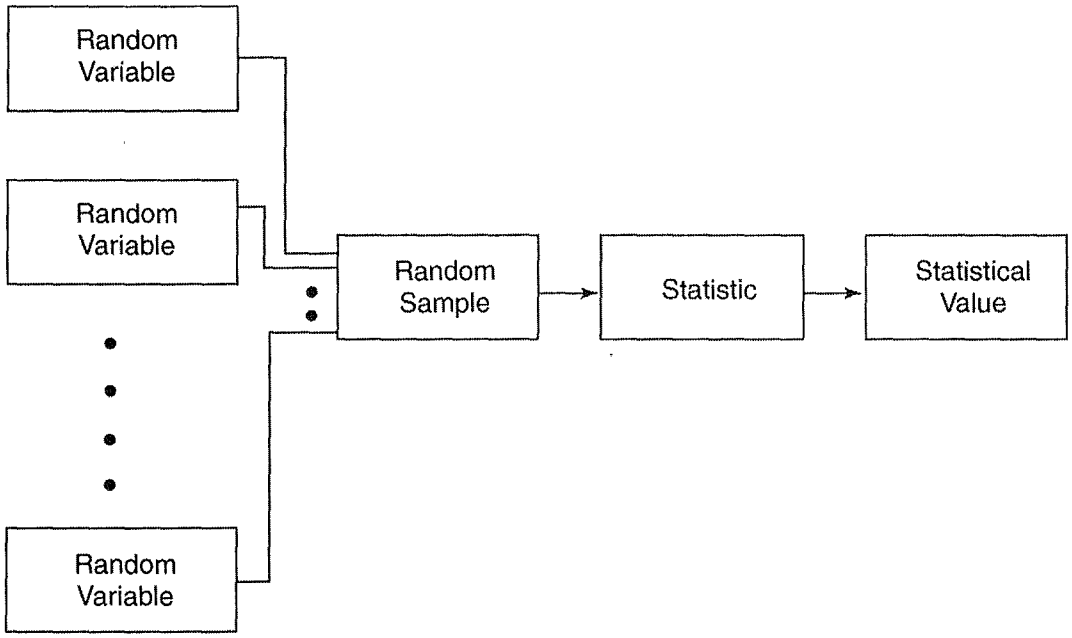

Figure A.3. Language of statistics.

Percentile amplitude statistics can be read directly from the APD. Peak and median amplitude statistics are the most widely used percentile statistics. The peak statistic is sometimes arbitrarily defined by the amplitude that is exceeded 0.0001% of the time:

$$V_p = cc^{-1}(0.000001) ,$$

where $a = cc^{-1}(P(A>a))$. The median statistic is defined by the amplitude that is exceeded 50% of the time:

$$V_{median} = cc^{-1}(0.5) .$$

The mean and RMS statistics are determined directly from the random sample values. The mean statistic is defined by:

$$V_{mean} = \frac{1}{N}\sum_{n} a_n ,$$

where N is the number of samples. The mean-logarithm statistic is defined by:

$$V_{mean-\log} = \frac{1}{N}\sum_{n} \log_{10}(a_n) ,$$

and the RMS statistic is defined by:

$$V_{RMS} = \sqrt{\frac{1}{N}\sum_{n} a_n{}^2} .$$

The discrete APD and its corresponding discrete PDF can be used to calculate the mean and RMS statistics if the random sample values are no longer available. The choice of histogram bin size may affect the accuracy of these statistics. In this case the mean statistic is defined by:

$$V_{mean} = \sum_{i} a_i p(a_i) ,$$

where a_i represents a discrete PDF value. The mean logarithm statistic is defined by:

$$V_{mean-\log} = \sum_{i} \log_{10}(a_i) p(a_i) ,$$

and the RMS statistic is defined by:

$$V_{RMS} = \sqrt{\sum_{i} a_i{}^2 p(a_i)} .$$

As a reference, statistical values for the tutorial PDF presented in section 2.1 are 4.0, 3.0, 2.8, 0.4, and 3.0 for the peak, median, mean, mean logarithm, and RMS statistics.

A.2.3 Graphing the APD

The APD of Gaussian noise is of particular interest to radio engineers because it is encountered in many practical applications. The amplitude of Gaussian noise is *Rayleigh distributed.* A Rayleigh distributed random variable is represented by a straight, negatively-sloped line on a *Rayleigh graph.* Figure A.4 shows the APDs of Gaussian and non-Gaussian noise on a Rayleigh graph.

The Rayleigh graph displays probability on the x-axis and amplitude on the y-axis. The probability is scaled by the function

$$x = 0.5\log_{10}(-\ln(P(A>a))) ,$$

and converted to percent to represent the "*percent (of samples or time) exceeding ordinate.*" The amplitude in volts is converted to units of power such as dBW, i.e. scaled by the function

$$y = 20log_{10}(A)\ ,$$

or alternatively it is displayed in dB relative to a standard noise power density or noise power.

Figure A.4 shows the statistics of Gaussian noise on a Rayleigh graph. Gaussian noise average power or RMS voltage corresponds to the power or voltage that is exceeded 37% of the time. Gaussian noise peak voltage is approximately 10 dB above RMS voltage. Gaussian noise average voltage, median voltage, and average-logarithm voltage are approximately 1dB, 2 dB, and 2.5 dB below RMS voltage respectively.

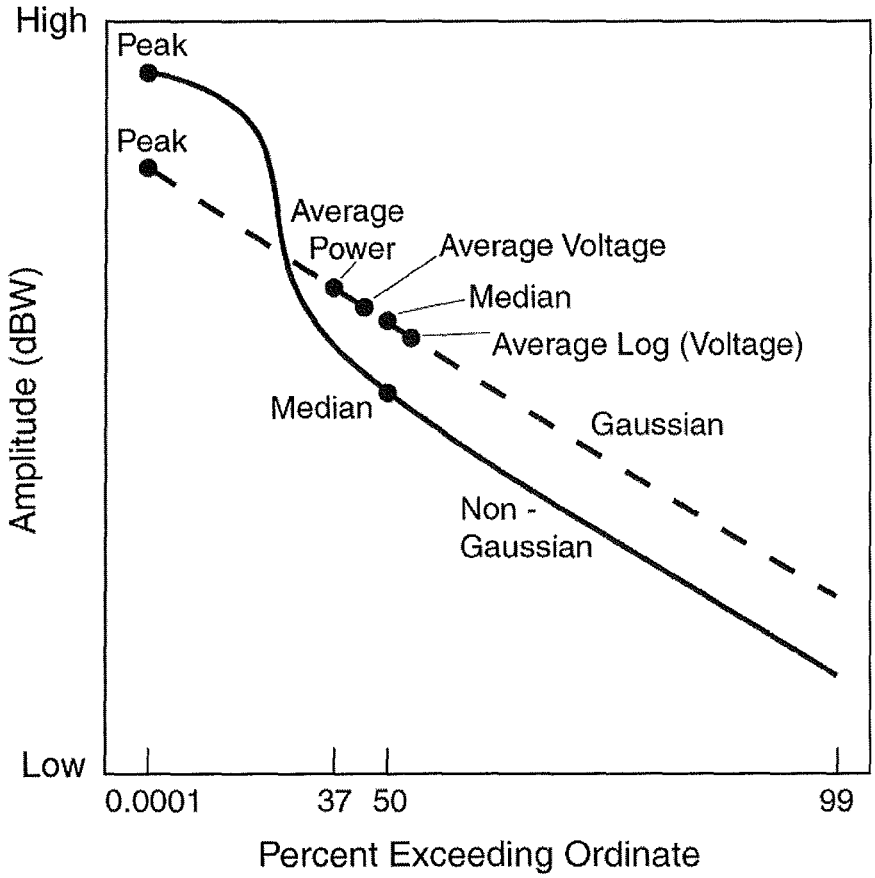

Figure A.4. Gaussian noise and non-Gaussian noise APDs plotted on a Rayleigh graph.

A.3 Tutorial APDs

A.3.1 Random Noise

Band limited random noise, i.e. the random noise present after a band limiting filter, is a random-amplitude and random-phase bandpass "signal" defined by

$$n(t) = A(t)\cos(2\pi f_c + \theta(t)) \ .$$

Band limited random noise is represented in the frequency domain by a *power spectral density* (PSD) in units of watts/Hz. The random noise "signal," amplitude, and PSD are shown in Figure A.5.

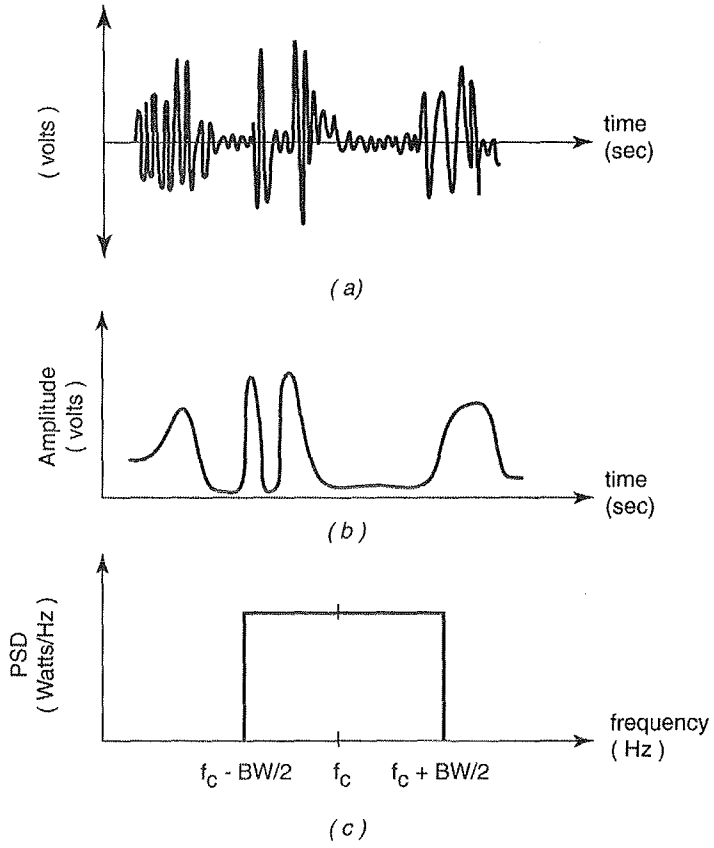

Figure A.5. Random noise (a), amplitude (b), and power spectral density (c).

Band limited noise average power is computed from the noise PSD

$$P = \int_{f_c - BW/2}^{f_c + BW/2} N(f)df \quad ,$$

where N(f) is the noise PSD in units of watts/Hz. Band limited *white* noise power density is constant over the band limiting filter bandwidth. As a result, the average noise power is directly proportional to the filter bandwidth and the RMS amplitude is directly proportional to the square root of bandwidth. This is sometimes referred to as the "$10\log_{10}$ bandwidth" rule. The amplitude of band limited Gaussian noise is Rayleigh distributed. Figure A.6 shows the APD of band limited white-Gaussian noise (WGN) for two different bandwidths on a Rayleigh graph.

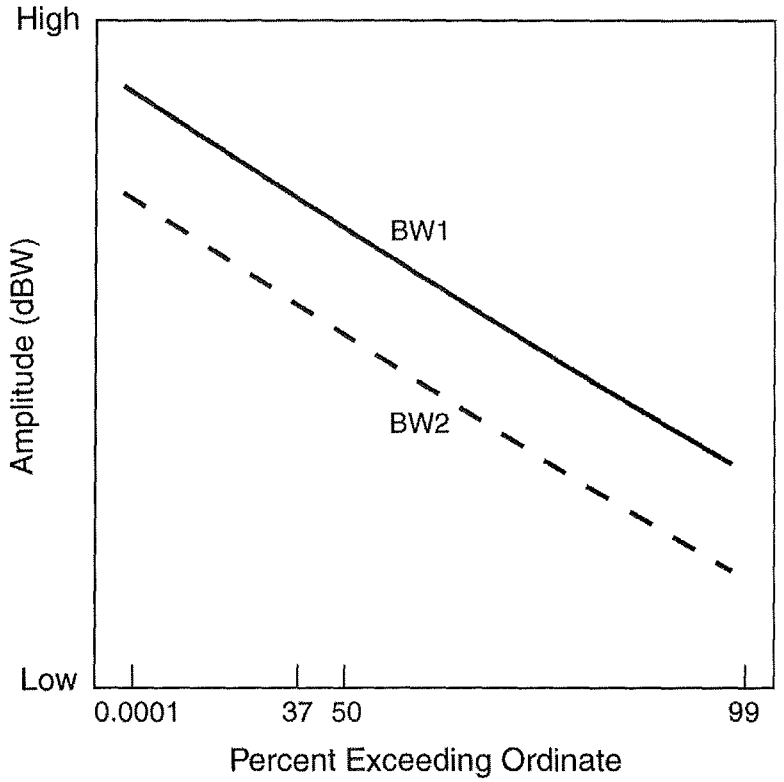

Figure A.6. Bandlimited Gaussian noise APDs with two different bandwidths. BW1 is greater than BW2.

A.3.2 Sinusoid Signal

The sinusoid (continuous wave) signal is a narrowband, constant amplitude and constant phase signal. It is defined by

$$s(t) = A\cos(2\pi f_c + \theta) .$$

The signal, signal amplitude, and amplitude spectrum are shown in Figure A.7. The APD of the sinusoid signal is a flat line from the lowest to the highest percentile on a Rayleigh graph. Changing the receiver center frequency can change the amplitude of the sinusoid signal.

Widening the bandwidth of a receiver filter in the presence of noise causes the statistics to be *Rician*. Rician statistics are dependent on the ratio of the sinusoid power to the noise power. The Rician APD corresponds to the sinusoid signal APD when noise is absent and the Rayleigh APD when the signal is absent. Sinusoid, Rician, and Rayleigh APDs are depicted in Figure A.8.

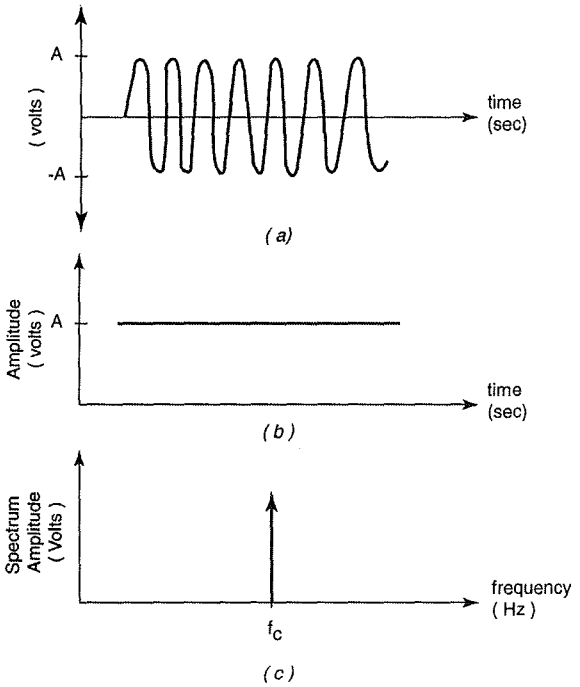

Figure A.7. Sinusoid signal (a), signal amplitude (b), and amplitude of the signal spectrum (c).

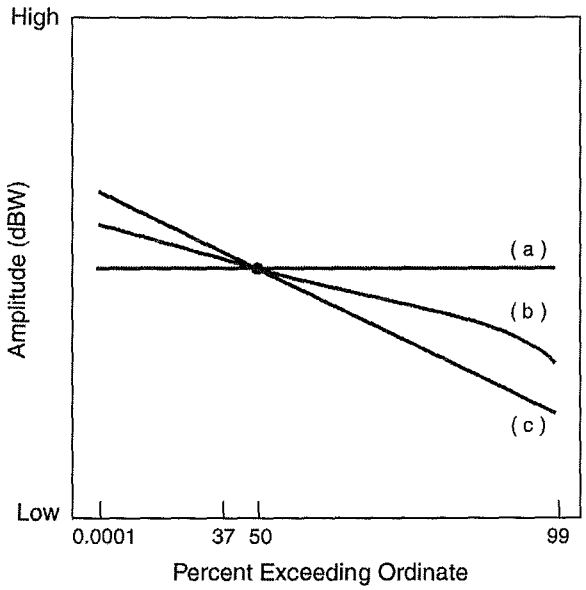

Figure A.8. Sinusoid signal APD without (a) and with (b) random noise. Sinusoid signal with random noise has Rician amplitude statistics. The Gaussian noise APD (c) is included for reference.

A.3.3 Periodically Pulsed Sinusoid

The periodically pulsed sinusoid is a deterministic, time-varying amplitude and constant phase signal defined by

$$s(t) = A(t)\cos(2\pi f_c + \theta) .$$

The amplitude varies between 'on' and 'off' pulse states. The 'on' duration is the *pulse width* (PW) and the repetition rate of pulses is the *pulse repetition rate* (PRR) or the pulse repetition frequency (PRF). Amplitude spectrum *lines* are spaced at the PRR. Amplitude spectrum *nulls* are spaced by the reciprocal of the PW. The signal, signal amplitude, and amplitude of the signal spectrum are shown in Figure A.9.

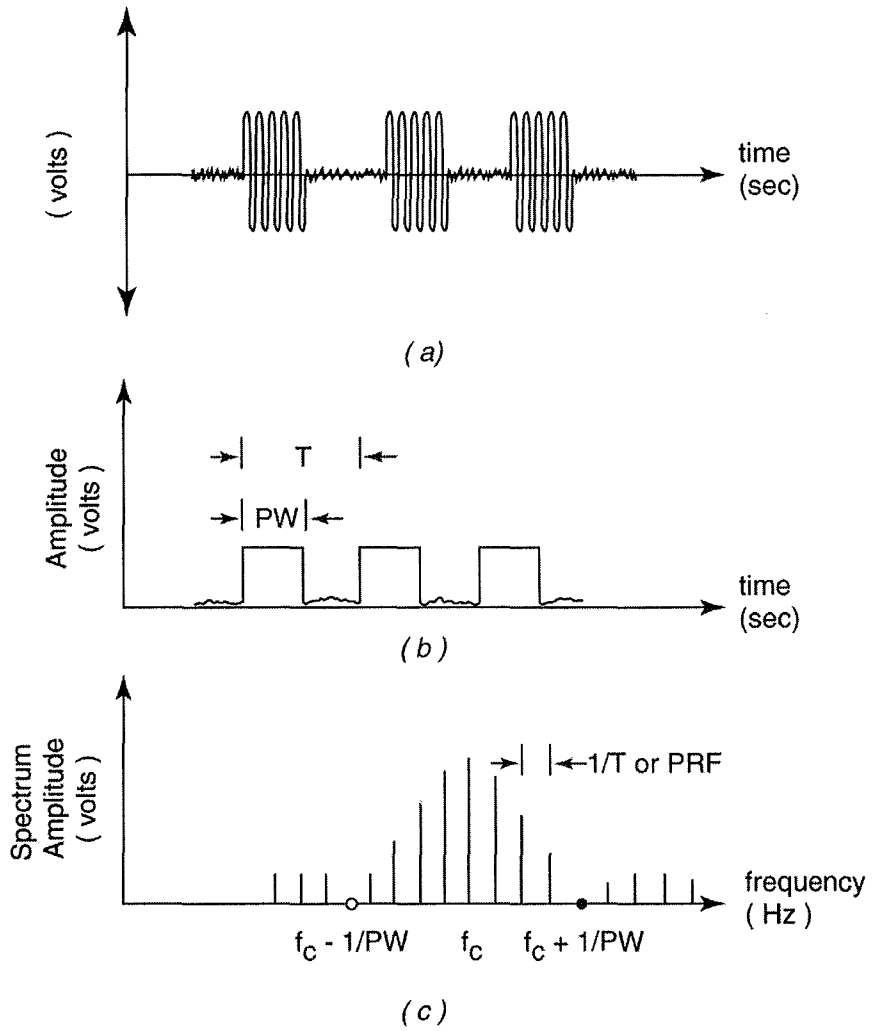

Figure A.9. Periodically pulsed sinusoid signal (a), signal amplitude (b), and amplitude of signal spectrum (c).

The APD of a periodically pulsed sinusoid is dependent on the receiver center frequency, band limiting filter parameters, and pulse parameters. *Pulse overlap distortion* is significant until the *band limited pulse* bandwidth (BW) exceeds the PRR. The band limited pulse is the pulse present at the output of the receiver filter. Analytically the band limited pulse is obtained by convolving the pulse shape with the receiver filter impulse response. Band limited pulses with minimal overlap are considered *independent* or *resolved*. The transmitted pulse shape is fairly well preserved when the filter BW is greater than 2/PW. The two graphs in Figure A.10 show a succession of APDs with the different receiver center frequency and BW combinations listed in Table A.1. The first graph has filter BWs less than the PRR while the second graph has filter BWs greater than the PRR.

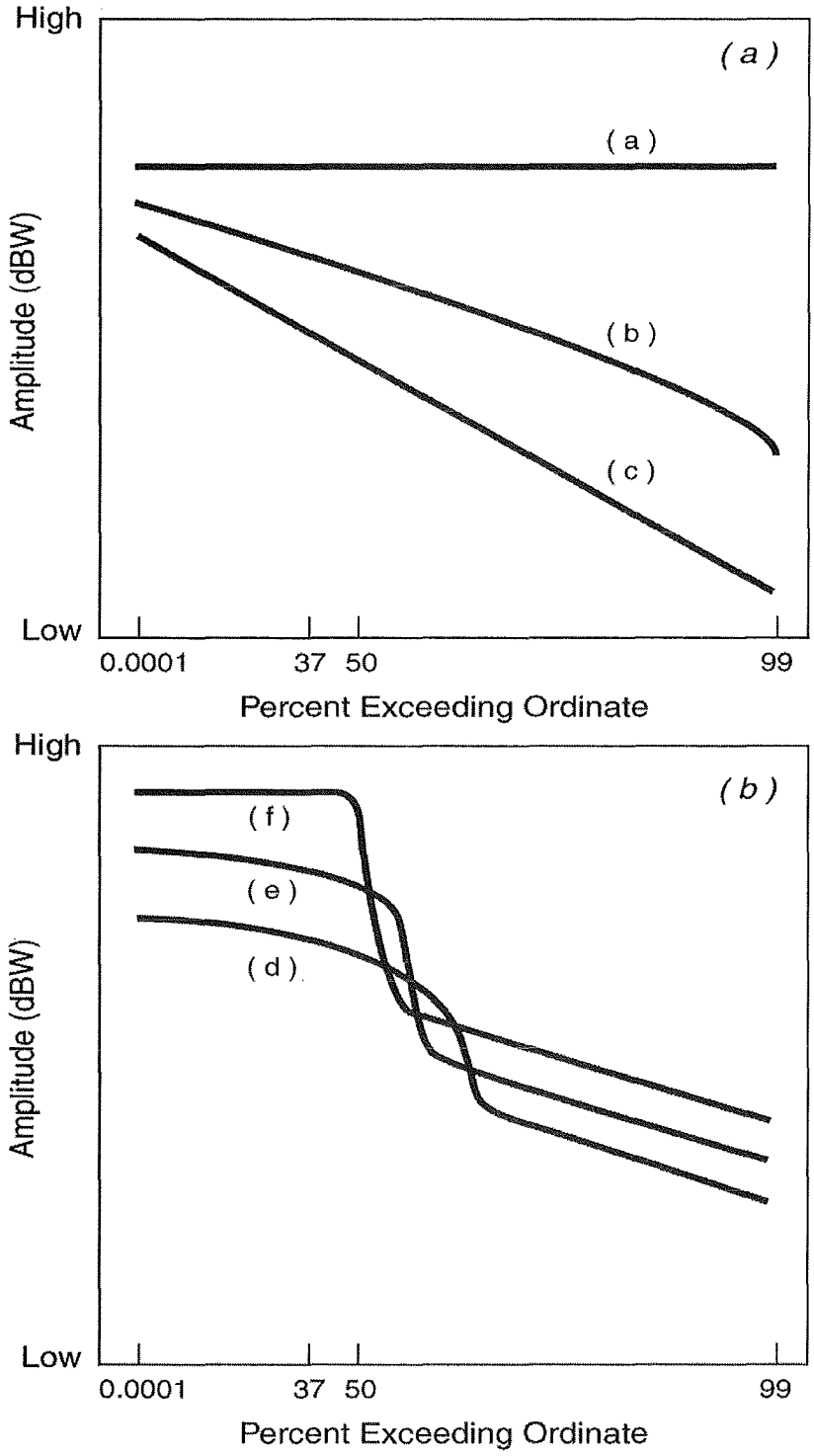

Figure A.10. Periodically pulsed sinusoid APD with pulse repetition frequencies less than (a) and greater than (b) the receiver filter bandwidth. See Table A.1 for receiver center frequency and filter bandwidth conditions for curves a-f.

Table A.1. Figure A.10 APD Conditions

Figure, Curve	**Receiver Center Frequency**	**Bandwidth**
A.10a, a	Tuned to spectral line	Filter BW<< PRR
A.10a, b	Tuned to spectral line	Filter BW< PRR
A.10a, c	Tuned off spectral line	Filter BW< PRR
A.10b, d	Tuned to pulse center frequency	Band limited pulse BW>PRR
A.10b, e	Tuned to pulse center frequency	Band limited pulse BW>>PRR
A.10b, f	Tuned to pulse center frequency	Band limited pulse BW > 2/PW

The APD takes on three characteristics when the filter bandwidth is less than the PRR, as shown in Figure A.10a. If the center frequency is tuned to a spectral line frequency and the filter bandwidth is able to *resolve* the line, it has a sinusoid APD (a). If the center frequency is tuned to a spectral line frequency, but the filter bandwidth is wider than necessary to resolve the line, it can have a Rician APD (b). If the center frequency is tuned to avoid a spectral line frequency, it has a Rayleigh APD (c).

Pulse overlap distortion decreases as the band limited pulse BW increases beyond the PRR as shown in Figure A.10b. The APDs are clearly non-Gaussian. The APD is somewhat curved at the lower probabilities for narrow filter bandwidths where there is pulse overlap (d). The APD flattens at low probabilities for wider filter bandwidths where the pulse overlap is minimal (f).

The low probability amplitudes correspond to the band limited pulse amplitudes. The high probability amplitudes correspond to the receiver noise amplitudes. The amplitudes at low probabilities are proportional to filter BW corresponding to a '$20\log_{10}$ bandwidth rule'. The amplitudes at high probabilities are proportional to the square root of filter BW corresponding to the '$10\log_{10}$ bandwidth rule'. The transition probability between these two domains is related to the band limited pulse duty cycle.

A.3.4 Summary Table

Table A.2. summarizes the APD dependencies for the three tutorial signals.

Table A.2. Tutorial Signal APD Dependencies

Signal	Receiver Center Frequency	Receiver Filter	Other Parameters
WGN	No	BW	
Sinusoid with WGN	Yes	BW	
Periodically-pulsed sinusoid with WGN	Yes	BW	PW, PRR

A.4 Band Limited UWB APDs

A.4.1 UWB Signals

The UWB signal is a train of pulses whose widths (in time) are "ultrashort" and bandwidths (in frequency) are "ultrawide". Like the periodically pulsed sinusoid, the pulses are defined by a PW and PRR. Unlike the periodically pulsed sinusoid, the impulses do not modulate a carrier frequency prior to being transmitted.

For some applications the pulse train may be pulse position modulated by a *time-dither sequence.* Time-dithering attenuates the discrete spectral line PSD component caused by periodic pulse transmission and introduces a continuous, random noise PSD component. The effectiveness of dithering is dependent on time-dither characteristics such as the distribution of dithering times, the reference time of the time-dithered pulse (absolute or relative to the last pulse), and the length of the time-dither sequence.

UWB signals are used in radar and communication devices. These devices reduce power requirements and alleviate spectral congestion by "gating" the pulse train off when continuous transmissions are not needed. They also use uncorrelated dither sequences to minimize interference to other UWB devices operating in the same room or building.

Figure A.11 shows a UWB undithered pulse train, a dithered pulse train, and a gated and dithered pulse train. Figure A.11 also shows an example UWB signal PSD with continuous and discrete components.

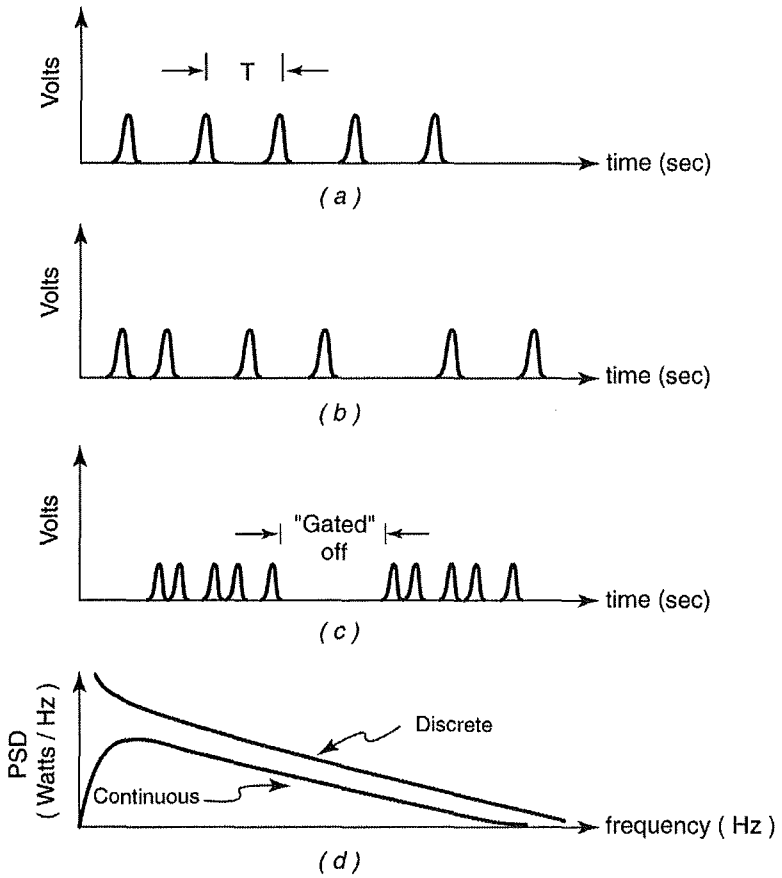

Figure A.11. Undithered (a), dithered (b), and dithered and gated (c) ultawideband signal. Dithered ultrawideband signal power spectral density (d) showing discrete and continuous components. The discrete components are represented as a curve because the lines cannot be resolved graphically.

A.4.2 Band Limited UWB Signals

The bandwidth of the interfering UWB signal is typically several orders of magnitude wider than that of the band limiting filters in the victim narrowband receiver. Thus the pulse shape and BW of the band limited pulse corresponds to the impulse response and BW of the receiver filter. Pulses are independent or resolved when the filter BW is greater than the PRR. Pulses that were independent or resolved before dithering may not be when dithering is introduced. To remain resolved, the pulse repetition period must be greater than the sum of the pulse duration and the maximum dither time.

Band limiting can occur in several of the narrowband receiver functions including demodulation, detection, and signal parameter estimation. Signal parameter estimation is necessary to provide frequency, phase, amplitude, and timing information to the demodulation and detection functions. The bandwidths associated with each of these functions may differ by several orders of magnitude. The relationships among these functions are shown in Figure A.12.

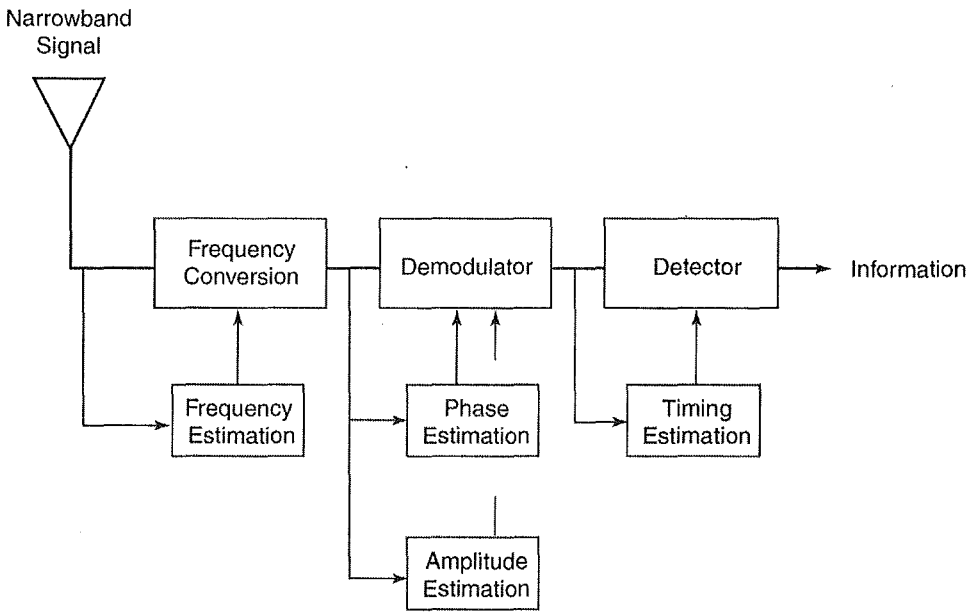

Figure A.12. Locations of band limiting filters in narrowband receivers.

A.4.3 Band Limited UWB Signal APDs

The undithered UWB signal APD will behave similarly to the periodically pulsed sinusoid APD as the filter bandwidth is varied from less than the PRR towards filter bandwidths much greater than the PRR. The dithered UWB signal APD will also behave similarly to the periodically pulsed sinusoid APD as long as the dithered pulses remain resolved. Figure A.13 shows an example of the changes that might happen to an unresolved dithered UWB signal APD when dithering is varied and BW is constant. These effects of dithering are only one possibility among many which are dependent on frequency, dithering distribution, dither reference time, length of dither sequence, gating, modulation, and filtering. In filter bandwidths less than the PRR increased dithering caused this APD to progress from the sinusoid APD to the Rician APD and finally to the Rayleigh APD. The receiver center frequency in this case was tuned to a spectral line. This progression is illustrated in Figure A.13a. In filter bandwidths comparable to the PRR, increased dithering caused this APD to progress from the non-Gaussian noise APD towards the Gaussian noise APD with Rayleigh distributed amplitudes. This progression is illustrated in Figure A.13b.

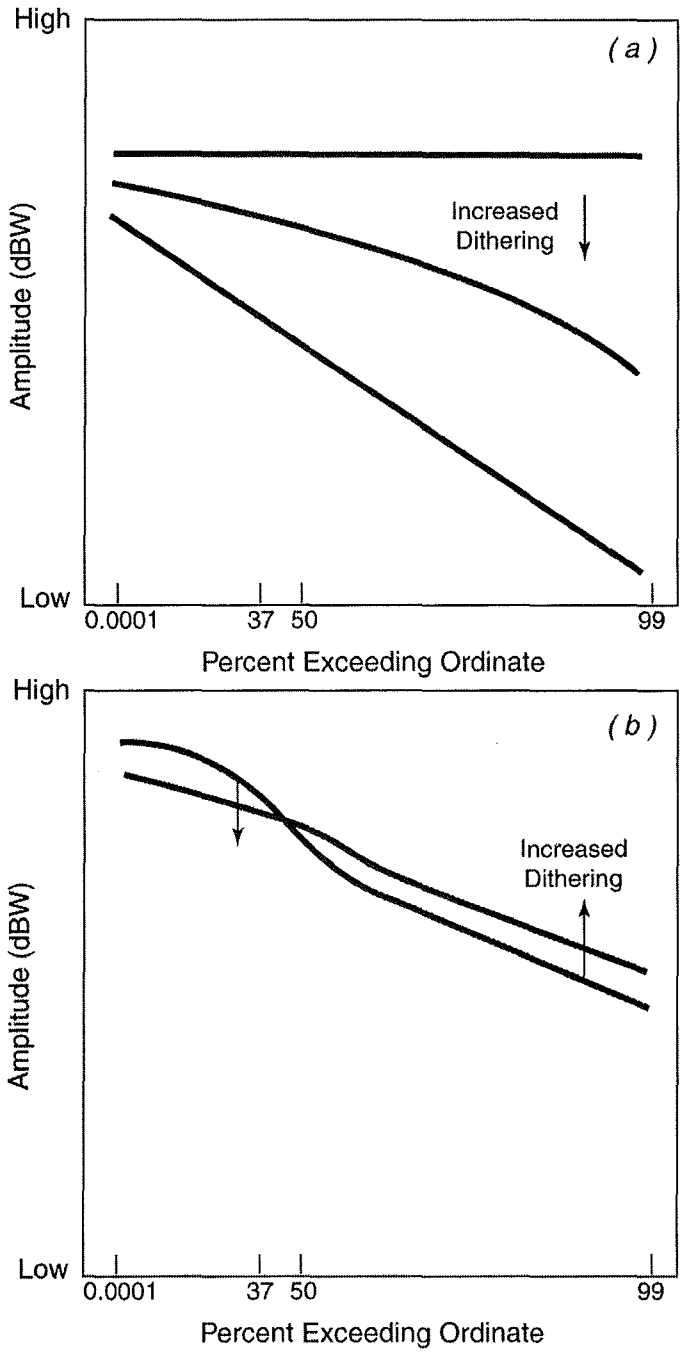

Figure A.13. Effects of increased dithering when band limiting filter bandwidth is less than (a) and comparable to (b) the pulse repetition frequency.

A.5 APD Special Topics

A.5.1 APD Measurement

Spectrum analyzer measurements can be used to estimate the APD or an amplitude statistic such as peak voltage. A block diagram of a spectrum analyzer is shown in Figure A.14. The received signal is converted to an intermediate frequency, band limited by the variable resolution bandwidth filter, and compressed by the log amplifier. Compression by the log amplifier extends the dynamic range of the measurement. The envelope detector extracts the amplitude from the band limited and compressed signal. The video bandwidth filter is used to (video) average the amplitude. The peak detector holds the highest amplitude since it was last reset.

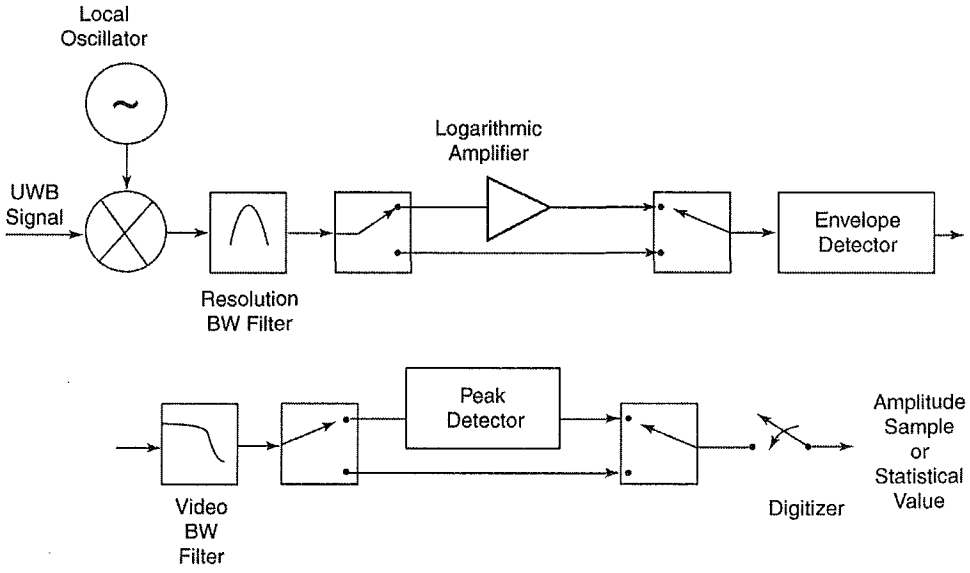

Figure A.14. Spectrum analyzer block diagram.

The statistics of the APD are derived from independent amplitude measurements. The amplitude measurements are considered independent if the sample time is 5 to 10 times the resolution bandwidth. The peak detector is bypassed and video averaging is disabled during an APD measurement. A histogram of the amplitude measurements is used to estimate the APD as shown in Section 2.1.

The peak voltage statistic is measured with the peak detector. Video averaging is disabled during peak detection. Average voltage statistics are measured with the video bandwidth filter. The log amplifier is bypassed and the peak detector is disabled for this measurement. The integration-time of the video bandwidth filter is long enough to suppress variation but surely more than the reciprocal of the resolution bandwidth. Average logarithm voltage statistics are measured in the same manner as the average voltage; however, the signal is log amplified.

A.5.2 APD of the Sum of Band Limited UWB Signals

APDs of band limited UWB signals are often collected individually in a laboratory setting. These APDs are useful for studying the interference of one UWB signal. However, in everyday life, more than one UWB device may be transmitting at a time. The statistics of the aggregate signal are conditional on the distributions of the individual band limited UWB signals and the number of signals that are to be added. Assuming the phases of the band limited UWB signals are uniformly distributed, four cases of interest emerge as shown in Table A.3.

Table A.3. Distributions of Four Aggregate APD Cases

	Distributions of band limited UWB signals	
Number of UWB signals	**Rayleigh**	**Any Distribution**
Few	(1) Rayleigh	(3) Non-Rayleigh
Many	(2) Rayleigh	(4) Rayleigh

In case 1 and 2 all the band limited UWB signals have Rayleigh distributions and the aggregate is also Rayleigh distributed. Case 4 is Rayleigh distributed by virtue of the central limit theorem of statistics. In cases 1,2, and 4 the aggregate power is simply the sum of the individual UWB signal powers. Measurement system average noise power can be removed from individual APDs before summing. In addition the average power of the individual APD may have to be reduced by attenuation due to the propagation channel to compensate for differences in location.

Case number 3 is more difficult for two reasons. First measurement system noise statistics cannot be removed from the measured statistics. Second, the computation of the aggregate APD requires using the joint statistics of a band limited UWB signal amplitude and phase distributions. For these reasons it is best to measure these statistics as an aggregate.

A.5.3 Performance Prediction

Characterizing the band limited UWB signal with an APD is not enough. Ultimately the effect that the amplitude statistics have on victim receiver performance has to be determined. The band limited UWB interference takes three guises: sinusoidal interference, Gaussian noise with Rayleigh distributed amplitudes, and non-Gaussian noise. The APD is particularly useful for predicting the performance of non-Gaussian noise.

For example, Figure A.15 shows how the non-Gaussian noise APD can be used to predict bit error rate (BER) for non-coherent binary frequency-shift keying. The straight, sloped APD is the result of band limited Gaussian noise produced in the receiver. The stepped APD is the result of band limited non-Gaussian interference. The average receiver noise power is represented by a

horizontal line on the graph. The signal-to-noise ratio (SNR) is represented as another horizontal line SNR dB above the noise power line. The BER is approximately one-half the probability where the SNR line intersects the APD curve.

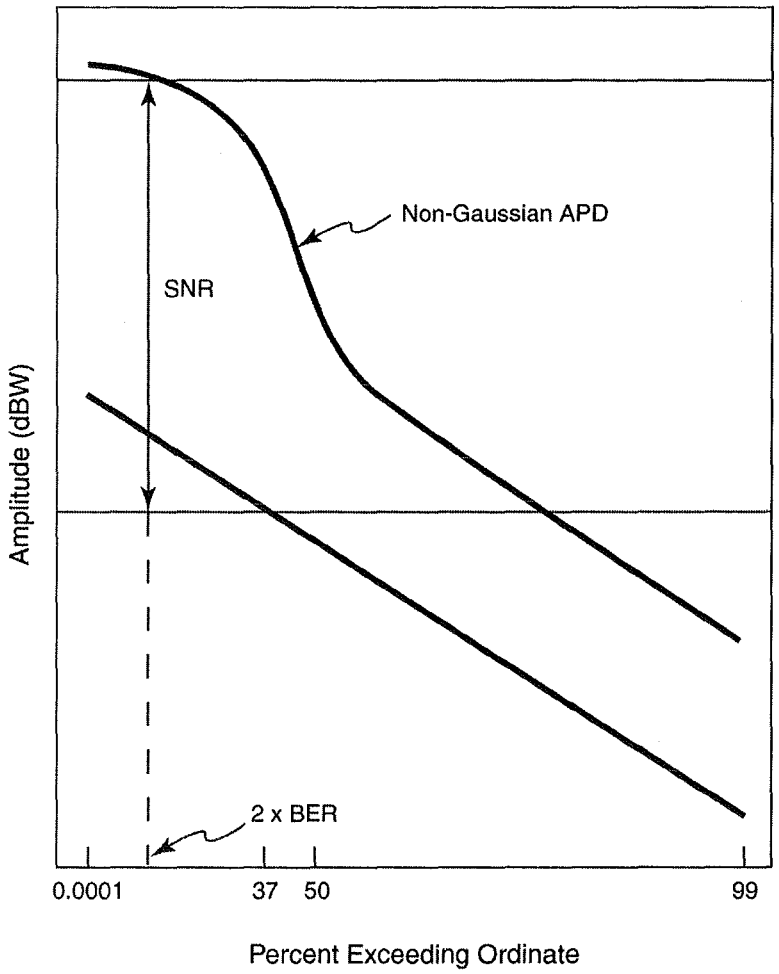

Figure A.15. Estimation of bit error rate from a non-Gaussian noise APD.

Many modern digital receivers use elaborate error correction and time-interleaving techniques to correct errors in the received bit sequence. In such receivers, the corrected BER delivered to the user will be substantially different from the received BER. Computation of BERs in these receivers will require much more detailed interference information than is contained in the APDs. For example, second-order statistics of noise amplitudes describing the time of arrival of noise amplitudes may be needed.

A.6 Concluding Remarks

This tutorial has shown that the APD is a useful tool for describing the UWB signal and analyzing UWB signal interference to victim narrowband receivers. It is useful because it 1) is measurable, 2) provides a variety of statistical values, and 3) can be used to aid in receiver performance prediction.

The APD gives insight to the potential interference from UWB signals in a wide variety of receiver bandwidths and UWB characteristics, especially when the combination of interferer and victim produces non-Gaussian interference in the victim receiver. If the interference is Gaussian, victim receiver performance degradation is correlated to the interfering signal average power alone and there is no need for further analysis using the APD. If the interference is non-Gaussian or sinusoidal, information in the APD may be critical to quantifying its effect on victim receiver performance degradation. Band limited UWB interference becomes increasingly non-Gaussian as the victim narrowband receiver bandwidth increases beyond the UWB signal PRR. Band limited UWB interference becomes increasingly sinusoidal as the victim narrowband receiver bandwidth decreases below the UWB signal PRR and a spectral line is present within the receiver bandwidth.

Spectrum regulators frequently use amplitude statistics such as peak, RMS, or average logarithm voltage to regulate transmitters. Further work is needed to determine if these statistics are strongly correlated to narrowband receiver performance. If these statistics are not correlated to receiver performance, it may be necessary to set regulatory limits in terms of the APD itself.

A.7 Bibliography

[1] A.D. Spaulding and R.T. Disney, "Man-made radio noise, part 1:Estimates for business, residential, and rural areas," OT Report 74-38, Jun. 1974.

[2] A.D. Spaulding, "Digital system performance software utilizing noise measurement data," NTIA Report 82-95, Feb. 1982.

[3] A.D. Spaulding,"The natural and man-made noise environment in personal communication services bands," NTIA Report 96-330, May 1996.

[4] R.J. Achatz, Y. Lo, P.B. Papazian, R.A. Dalke, and G.A. Hufford, "Man-made noise in the 136-138-MHz VHF meteorological satellite band," NTIA Report 98-355, Sep. 1998.

[5] R.A. Dalke, "Radio Noise," in the *Wiley Encyclopedia of Electrical and Electronics Engineering*, Vol. 18., J.G. Webster, Ed.,John Wiley & Sons, Inc., New York: N.Y., 1998, pp. 128-140.

[6] R.J. Matheson, "Instrumentation problems encountered making man-made electromagnetic noise measurements for predicting communication system performance," *IEEE Transactions on Electromagnetic Compatibility*, Volume EMC-12, Number 4, Nov. 1970.

[7] J.S. Bendat and A.G. Piersol, *Measurement and Analysis of Random Data*, New York, NY: John Wiley & Sons, Inc, 1966.

[8] P.L. Meyer, *Introductory Probability and Statistical Applications*, Second Edition, Reading, Mass: Addison-Wesley Publishing Company, 1970.

APPENDIX B. SIMULATIONS OF TIME AND SPECTRAL CHARACTERISTICS OF ULTRAWIDEBAND SIGNALS AND THEIR EFFECTS ON RECEIVERS

Edmund A. Quincy[1]

B.1 Introduction

In this appendix a class of time-dithered, time-hopped UWB systems is modeled and simulated from an analytic description of the system. These simulated time waveforms and Fourier spectrum results are analyzed to show the effect of a receiver's intermediate frequency (IF) bandwidth (BW) on peak and average power. These peak and average power curves provide the basis for establishing a normalized bandwidth correction factor (BWCF) curve and equation. The BWCF is used to estimate peak power over a range of bandwidths from average power measurements made in a 1 MHz BW as prescribed by the FCC for Part 15 devices. Simulation of the UWB devices complements measurements and other analytic model results for these devices.

B.2 UWB Model

The simulated time-dithered ultrawideband system block diagram is shown in Figure B.1. The system transmits a quasi-periodic, very low duty cycle, dithered pulse train *s(t)* where delta functions (narrow pulses in hardware) are pulse position modulated (PPM) and shaped with a Gaussian 2nd derivative filter *w(t)*. The analytic expression for *s(t)* and *w(t)* are provided in (1) and (1a) where d_k is the total dither in time units and N_p is the number of pulses in the pulse train. In the simulation results the number of pulses was set at 100 (10,000 ns). This was estimated to be similar to the observation window of a spectrum analyzer measurement. The model employed here is similar to that used by Win and Scholtz [1] except that their pulse trains were infinite in length, which led to smoothed spectral lines corresponding to this infinite observation window.

$$s(t) = w(t) * \sum_{k=1}^{N_p} \delta \left[t - d_k - (k-1)T \right] \qquad (1)$$

$$w(t) = \left[1 - 2(\pi\ t f_c)^2 \right] e^{-(\pi\ t f_c)^2} \qquad (1a)$$

---

[1]The author is with the Institute for Telecommunication Sciences, National Telecommunications and Information Administration, U.S. Department of Commerce, Boulder, CO 80305.

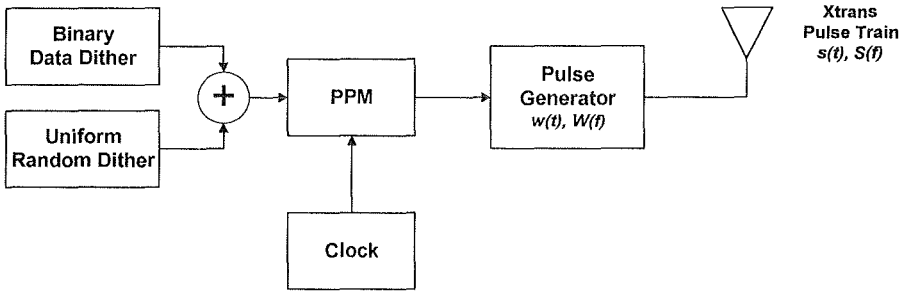

Figure B.1. Time-dithered ultrawideband system model.

The shaping filter for a specific hardware configuration depends on the transmit and receive antennas and may deviate some from this model. The specific pulse shape is probably not as important a factor in determining a receiver's narrow IF BW response as the pulse width and corresponding BW. The receiver IF filtering will remove pulse shape details if the pulse is sufficiently narrow and the corresponding BW sufficiently wide, compared to the receiver IF bandwidth. Shape details are filtered out in these simulations, as will be seen in the IF output pulses. In this system the dither consists of two components: a pseudo-random time-hopping dither and a data dither. Usually the time-hopping dither is large compared to the data dither. In our case the time-hopping dither was uniformly distributed between 0 and 0.5T (50% dither); whereas the data dither represented binary 0s and 1s with 0 or 0.045T (4.5% dither). The time-hopping dither values are commonly generated from a pseudo-noise sequence. An undithered pulse repetition rate (PRR) of 10 MHz was used, which made the nominal pulse train period T= 100 ns. Simulation results were also obtained for the 0 or the non-dithered case where the waveforms are periodic with a period T=100 ns resulting in a line spectra with a fundamental frequency equal to the PRR .

B.3 UWB Simulation

The simulation and power calculation processes are shown in the flow diagram of Figure B.2. A periodic impulse train is dithered by the combined amount of dither and then Fourier transformed using the FFT (Fast Fourier Transform). Then the spectrum is shaped using the Gaussian 2nd derivative filter transfer function *W(f)* described by the analytic expression in (2a). Alternatively, the complex Fourier spectrum, *S(f)*, can be calculated using the analytic expression in (2).

$$S(f) = W(f)\sum_{k=1}^{N_p} e^{-j2\pi f\left[d_k+(k-1)T\right]} \tag{2}$$

$$W(f) = \left(\frac{f}{f_c}\right)^2 e^{\left[1-\left(\frac{f}{f_c}\right)^2\right]} \tag{2a}$$

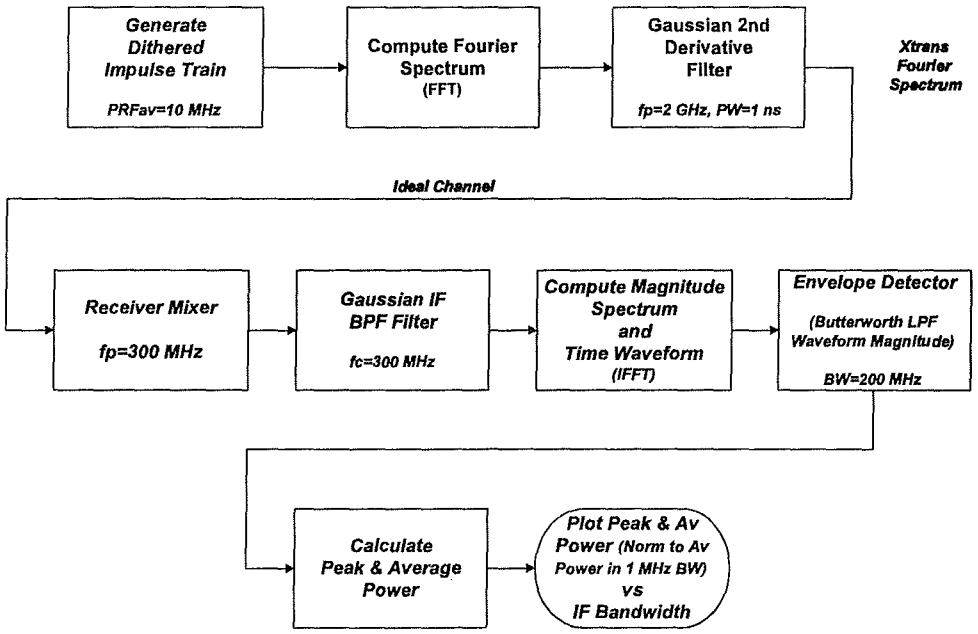

Figure B.2. Simulation and power calculation process.

The transmitted 50% dithered pulse train is shown in the top Figure B.3 plot and an individual pulse is shown in the bottom plot. The transmitted pulse width was approximately 1 ns and the corresponding wideband spectrum peaked at 2 GHz with 40 dB down from the peak occurring at frequencies of 0.25 GHz and 5 GHz. The transmitter spectra are shown in Figure B.4 with dithered pulse train spectrum (before shaping) shown in the top and the shaped transmitter output spectrum shown in the bottom. Note that the spectrum before shaping appears quite noise-like with 50% dither. This random appearance can change significantly with less dither, particularly below 25% dither. With dithers greater than 50% the random appearance does not change significantly. With BWs of 100 MHz or less centered about the peak at 2 GHz, the spectrum still appears quite flat even after shaping.

The transmitter output in Figure B.2 is fed through an ideal channel to a receiver (victim or spectrum analyzer) where the signal is mixed down to a center frequency of 300 MHz. This frequency f_c now is also the peak frequency of the spectrum. That is, the original peak frequency f_p=2 GHz was mixed down to 300 MHz. Next the mixer output is filtered by a Gaussian-shaped filter with an adjustable bandwidth. A Gaussian shape was chosen for three reasons: (1) the spectrum analyzer response, used to make measurements at an IF frequency, resembles a non-symmetric Gaussian; (2) as more stages of IF filtering are employed, their composite response usually tends towards a Gaussian; and (3) simplicity. Bandwidths were employed from 100 MHz down to 0.3 MHz. The IF filter was followed by an envelope detector implemented by computing the waveform magnitude and lowpass filtering it with a 6-pole Butterworth filter using a BW of 200 MHz. Higher bandwidths allowed some ripple through at the IF frequency.

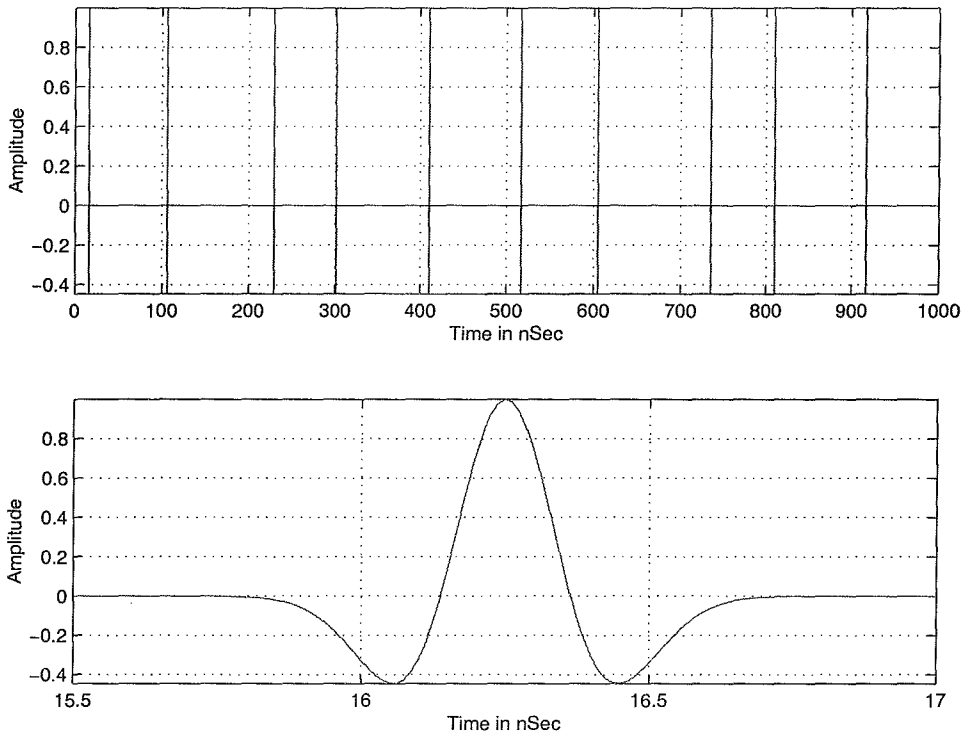

Figure B.3. Normalized 2nd derivative Gaussian dithered pulse train (50% dither); Top: full record, Bottom: exploded view.

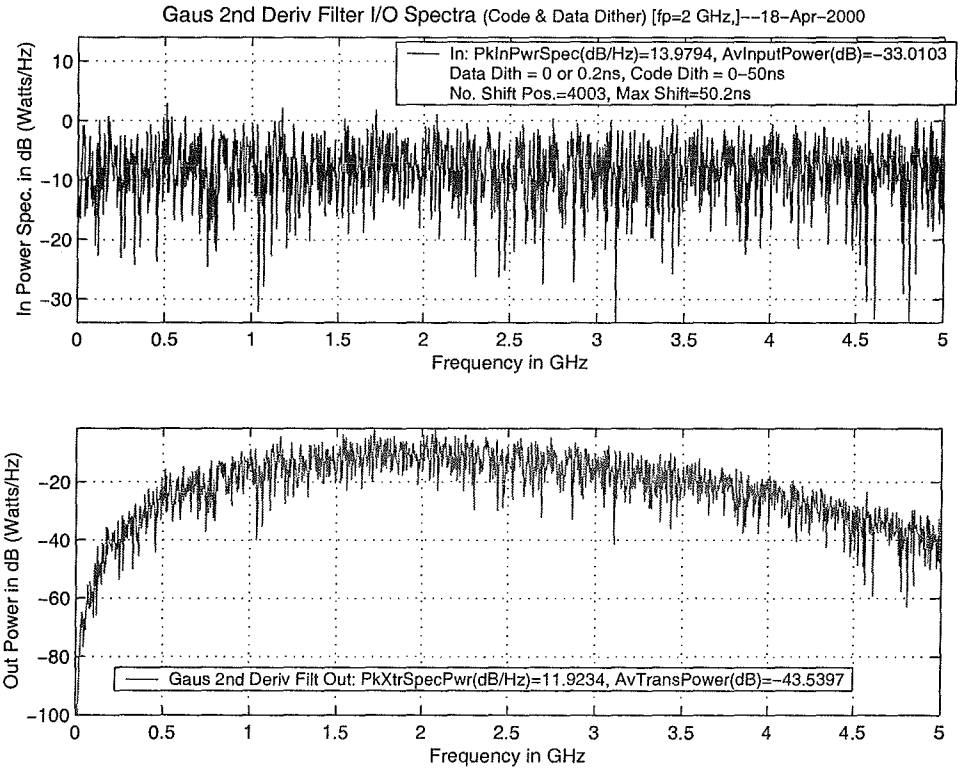

Figure B.4. Transmitter spectra (50% dither); Top: before Gaussian filter, Bottom: after Gaussian filter.

An example output is shown in Figure B.5 employing an IF BW of 30 MHz. The top plot shows the filtered received spectrum centered at 300 MHz, the center plot contains the pulse train out of the IF showing the pulsed RF oscillating at approximately the 300 MHz IF frequency. The bottom plot displays the envelope waveform out of the IF filter. Note the variable spacing of the pulses corresponding to the 50% dither. At a BW of 30 MHz the pulses out of the IF just touch each other. For wider BWs they are completely separated and for narrower BWs they are overlapped, causing peaking in the envelope as observed in Figures B.6 and B.7 for 10 MHz and 3 MHz IF bandwidths respectively. Figures B.8 compare this peaking effect of the detected envelope for these same 3 BWs over a record length of 100 pulses (10,000 ns). It is particularly interesting to compare the 50% and 0 dither cases. With the periodic (no dither) pulse train, the IF filter gets pinged by pulses at a regular interval and just provides periodic pulses out of the detector without peaking. At a BW of 3 MHz the 50% randomly dithered pulse train creates significant peaks and valleys (1 down to 0), whereas the periodic pulse train has a constant envelope coming out of the IF filter.

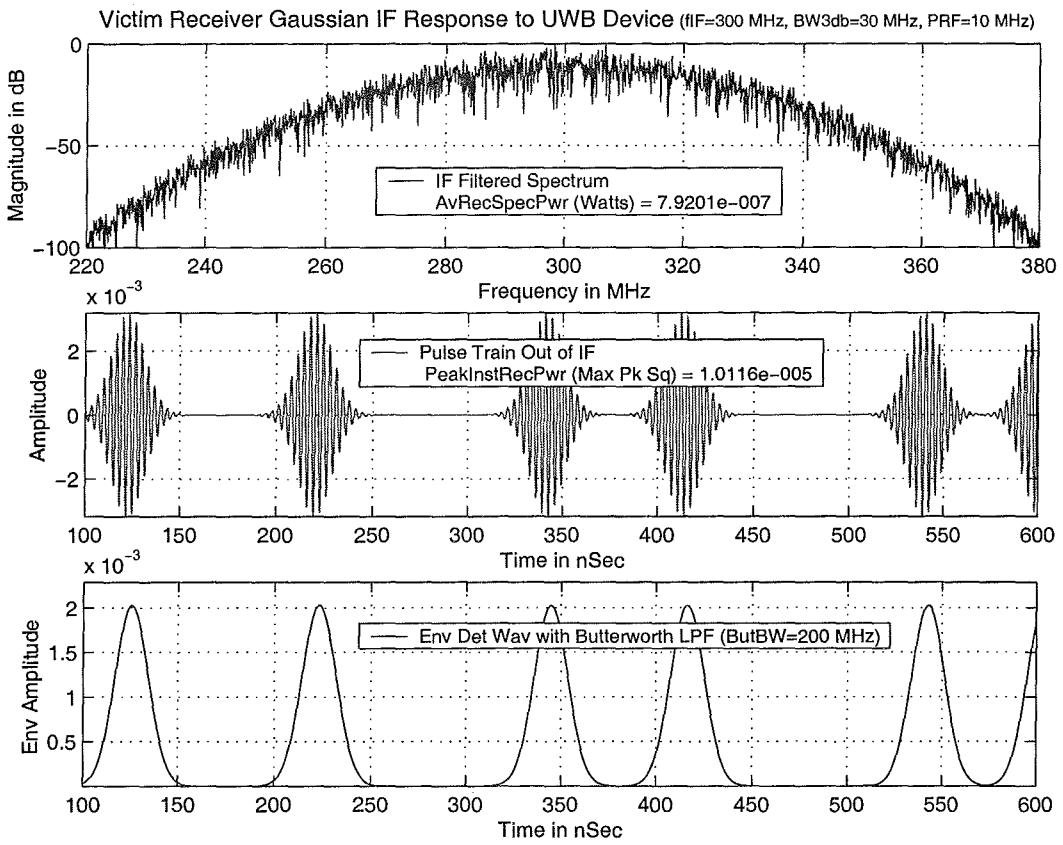

Figure B.5. Receiver 30 MHz IF bandwidth (50% dither); Top: output spectrum, Middle: pulsetrain, and Bottom: envelope detected pulse train.

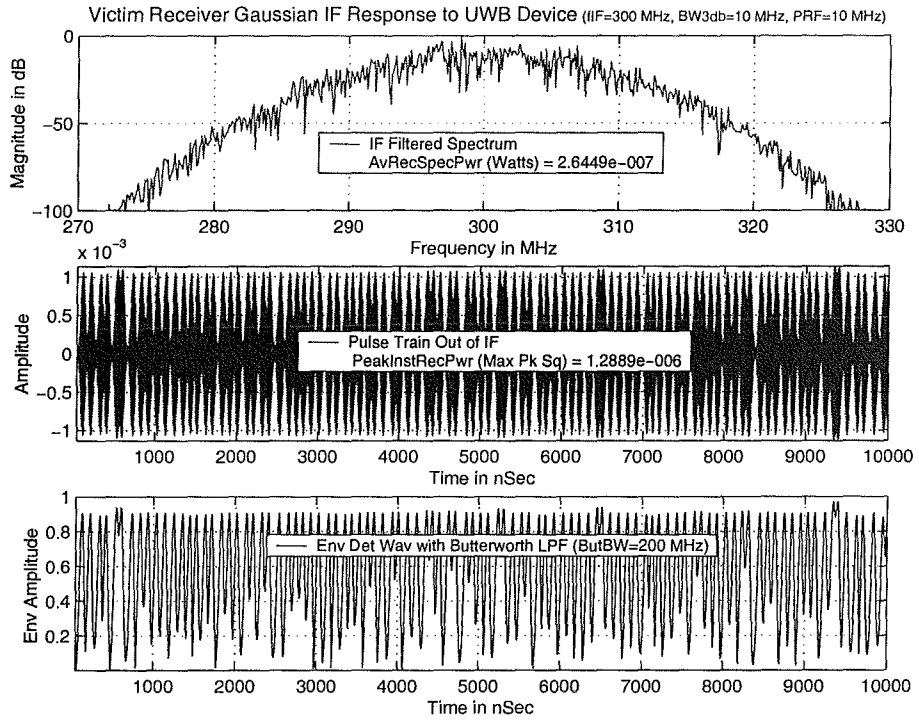

Figure B.6. Receiver 10 MHz IF bandwidth (50% dither); Top: output spectrum, Middle: pulse train, and Bottom: envelope detected pulse train.

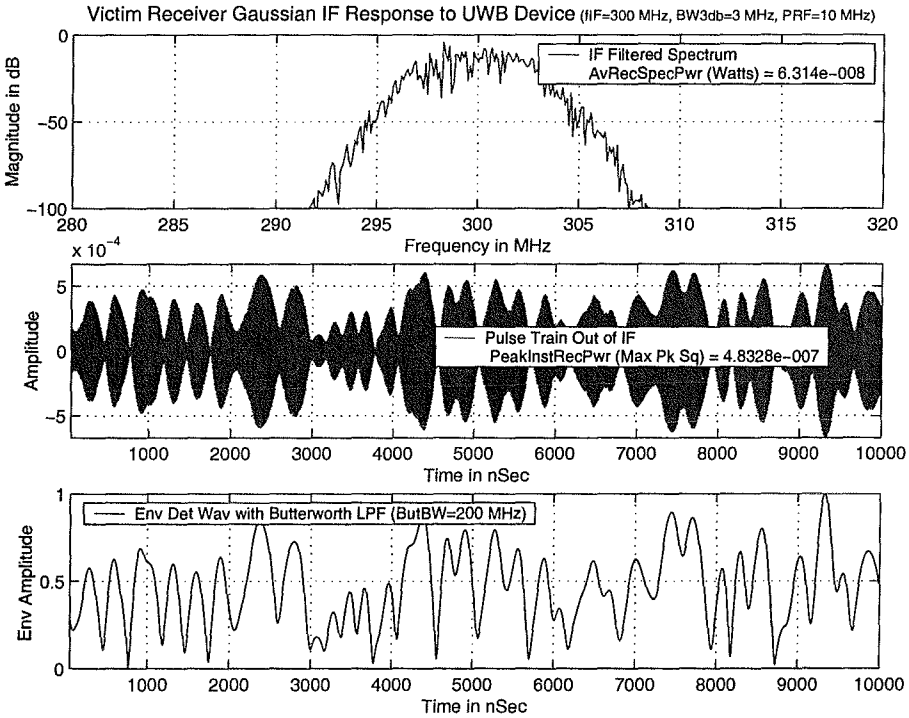

Figure B.7. Receiver 3 MHz IF bandwidth (50% dither); Top: output spectrum, Middle: pulse train, and Bottom: envelope detected pulse train.

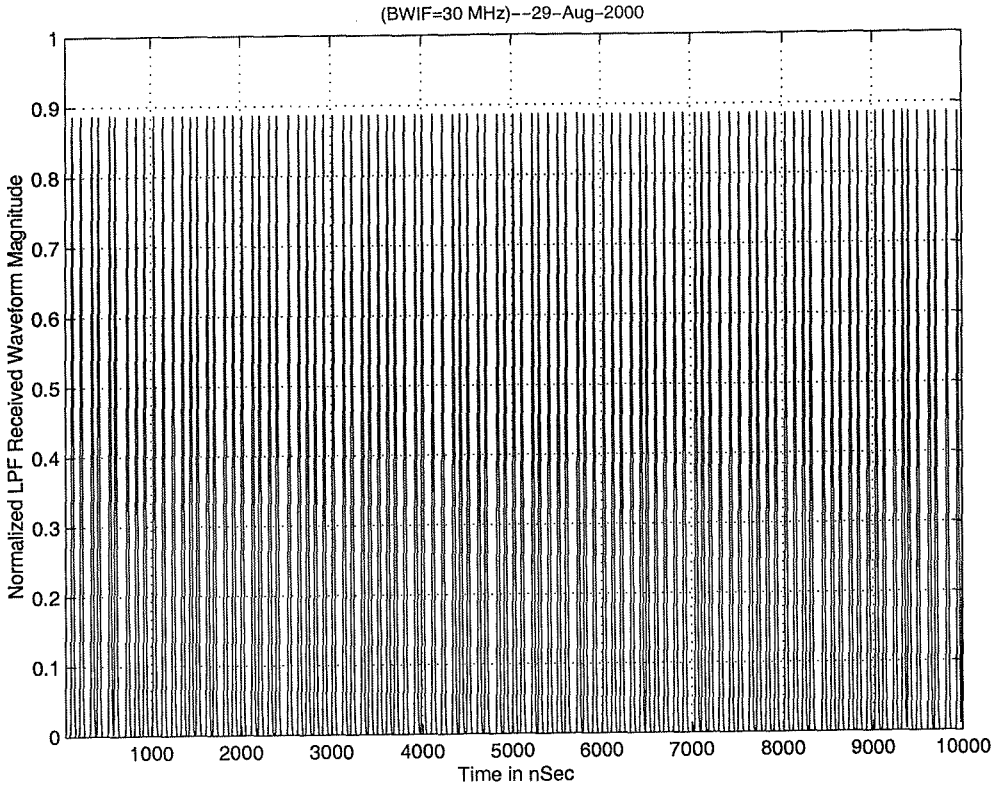

Figure B.8.A. Receiver IF envelope for 30 MHz bandwidth with 50% dither.

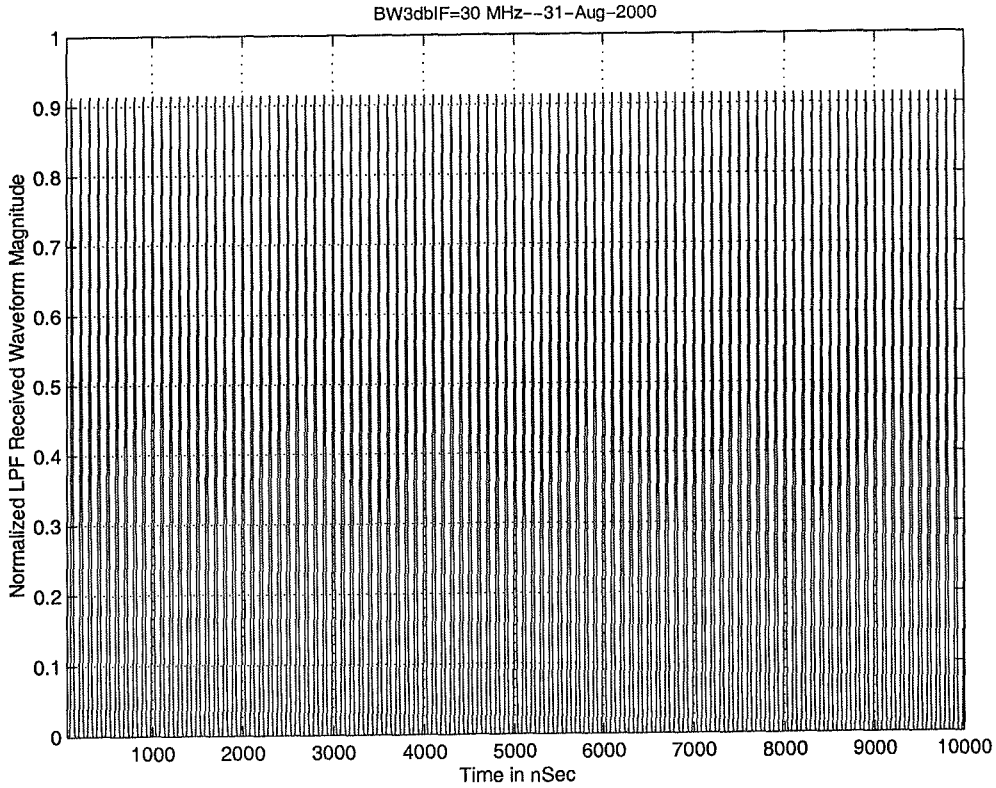

Figure B.8.B. Receiver IF envelope for 30 MHz bandwidth with 0% dither.

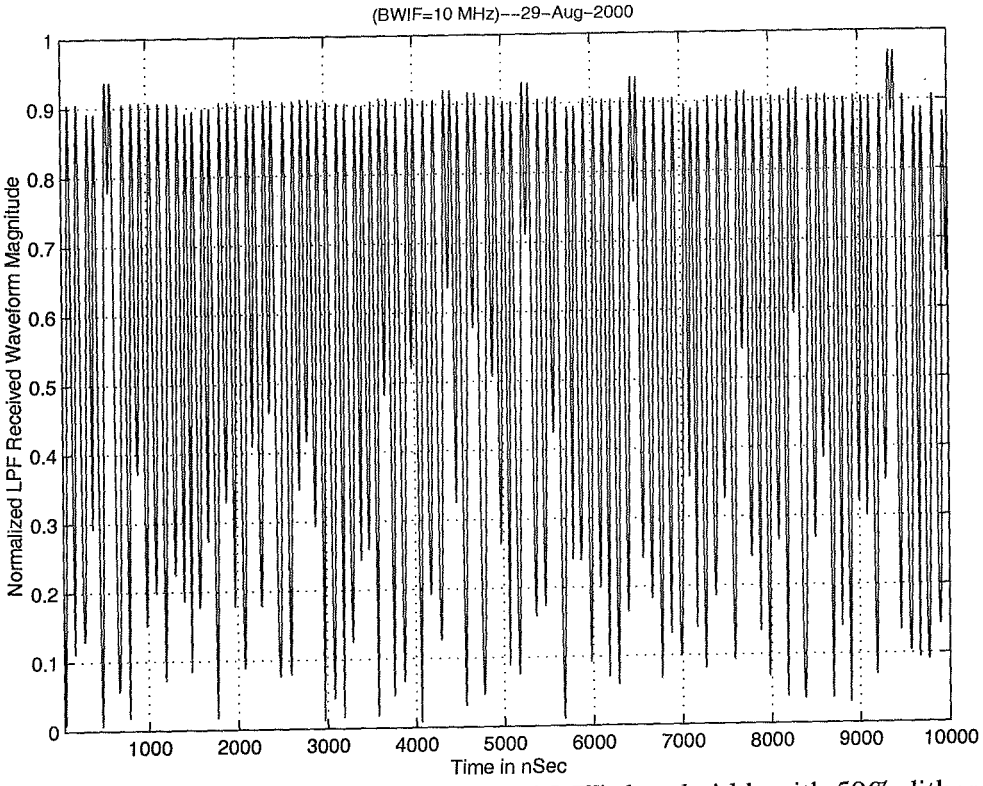

Figure B.8.C. Receiver IF envelope for 10 MHz bandwidth with 50% dither.

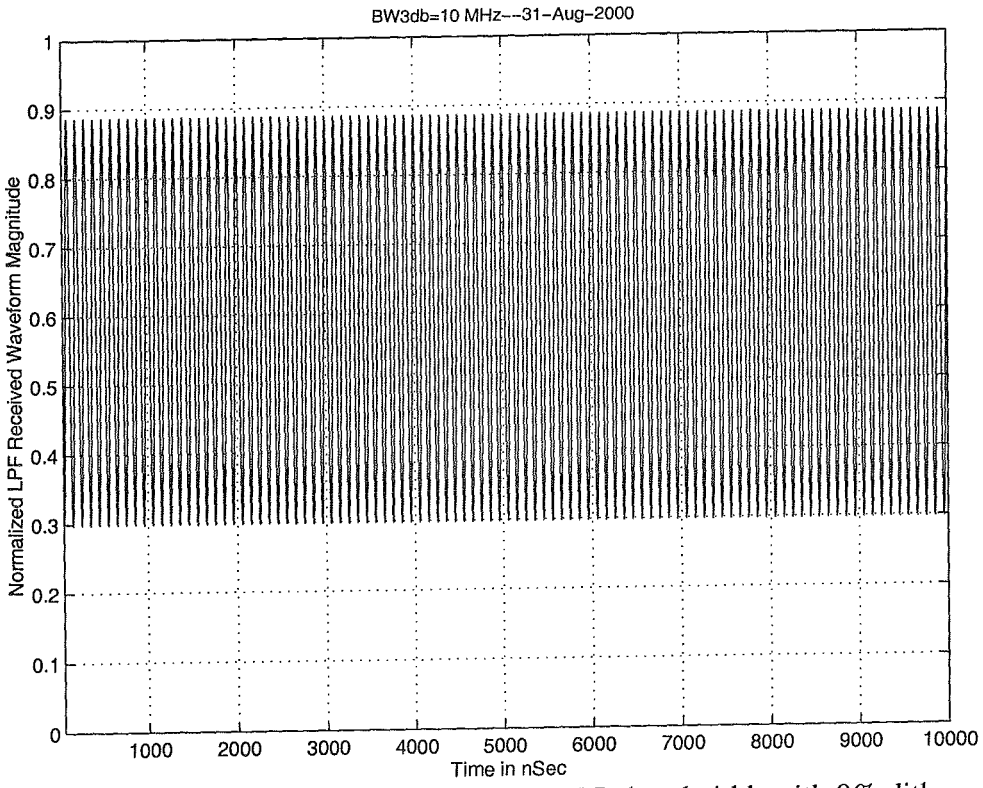

Figure B.8.D. Receiver IF envelope for 10 MHz bandwidth with 0% dither.

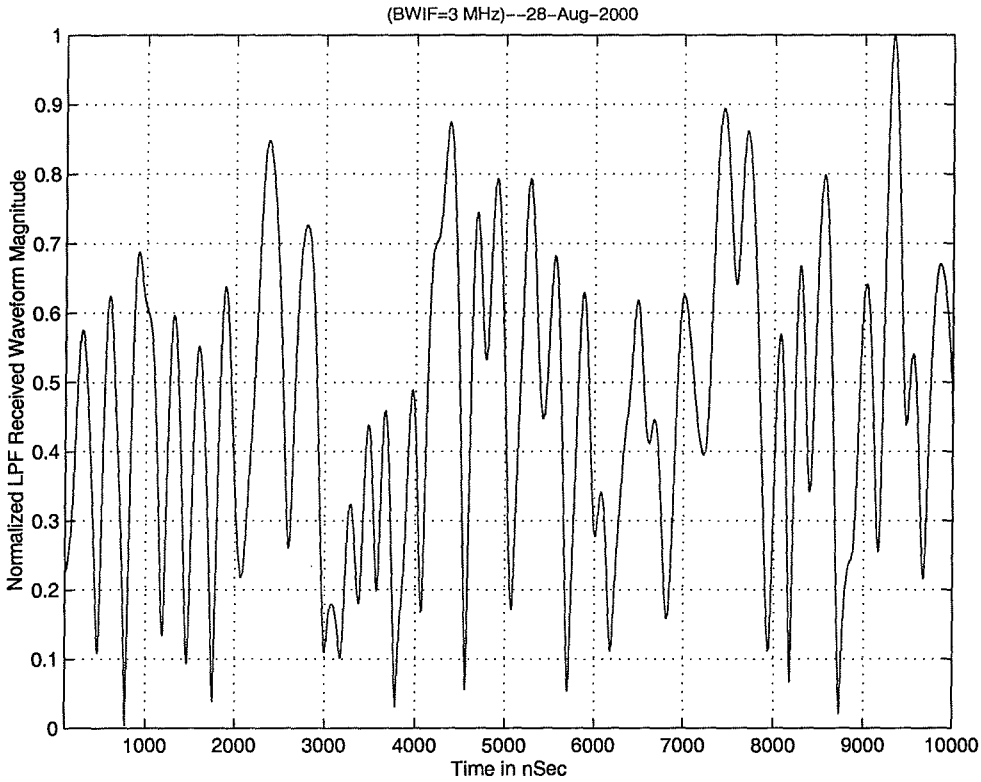

Figure B.8.E. Receiver IF envelope for 3 MHz bandwidth with 50% dither.

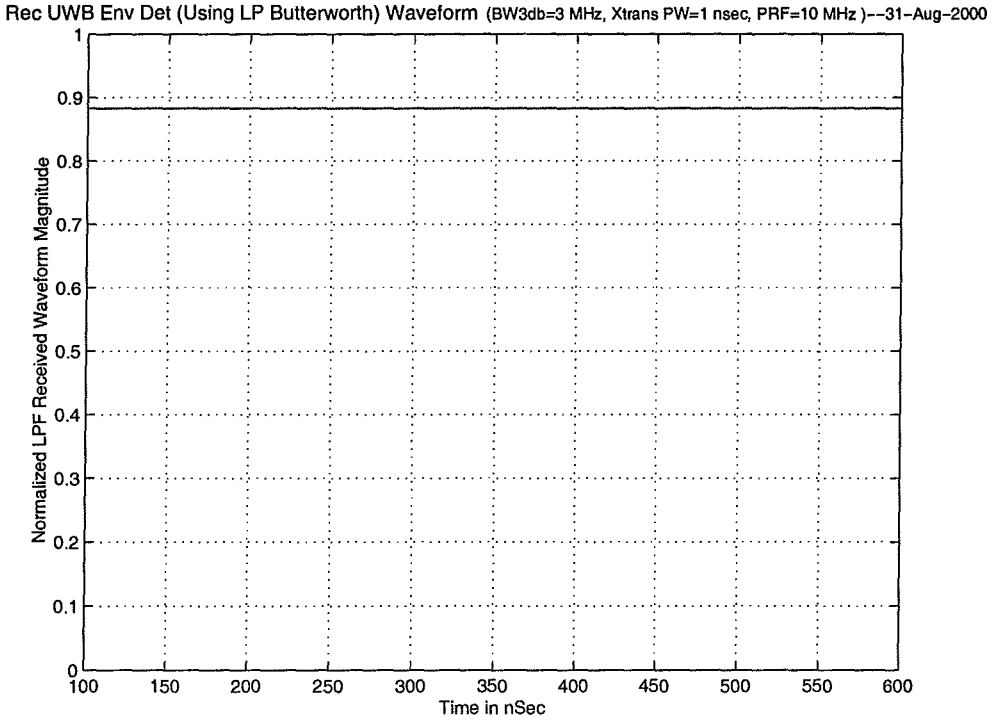

Figure B.8.F. Receiver IF envelope for 3 MHz bandwidth with 0% dither.

B.4 Power Calculations in Receiver IF Bandwidths

Figures B.9 show the received instantaneous peak and average power computed from the simulated time waveforms for receiver IF bandwidths ranging from 0.3 MHz to 100 MHz. These powers were normalized to the average power in a BW of 1 MHz (a 1-MHz BW is specified by the FCC for Part 15 average measurements). Consequently, the average power curves all go through 0 dB at 1 MHz. These curves provide the basis to develop bandwidth correction factors (BWCF). The BWCFs are used to estimate the amount of peak power at a given BW, starting with measuring the average power in this 1-MHz BW.

In addition to peak and average power curves, another guideline is provided. This straight line on a log-log plot is the 10 $\log_{10}$(BW) average power trend line. It follows the average power quite well for 50% dither (both pre-detection and post-detection); however, for the non-dithered case it follows the average power only for BWs greater than or equal to 10 MHz where the pulses are separated. As pulses overlap for narrower BWs of this non-dithered case, the envelope is constant and the peak and average power are constant as expected. Consequently the power does not change as a function of BW. Another way to look at this is in the frequency domain. An undithered PRR of 10 MHz results in a spectral line at 10 MHz and its harmonics. There is therefore a line at 2 GHz which is down converted to 300 MHz, the center frequency of the IF filter. As the BW increases above 10 MHz, more lines are included in the passband and the power increases linearly with BW. At 10 MHz and below there is a single line in the passband so that the power remains constant. This is in contrast to the 50% dithered case for narrow BWs where the peak and average powers change according to a 10 $\log_{10}$BW rule.

For both the 50% dithered and non-dithered cases, the peak power for BWs greater than or equal to 10 MHz (also the PRR) increases as 20 $\log_{10}$(BW). This is the BW where pulses become distinct in the pulsetrain at the output of the IF, as can be seen in the envelopes shown in Figure B.8.C through Figure B.8.F.

B.5 Reference

[1] M.Z. Win and R.B. Scholtz, "Impulse radio: How it works," *IEEE Communications Letters,* pp. 10-12, Jan. 1998.

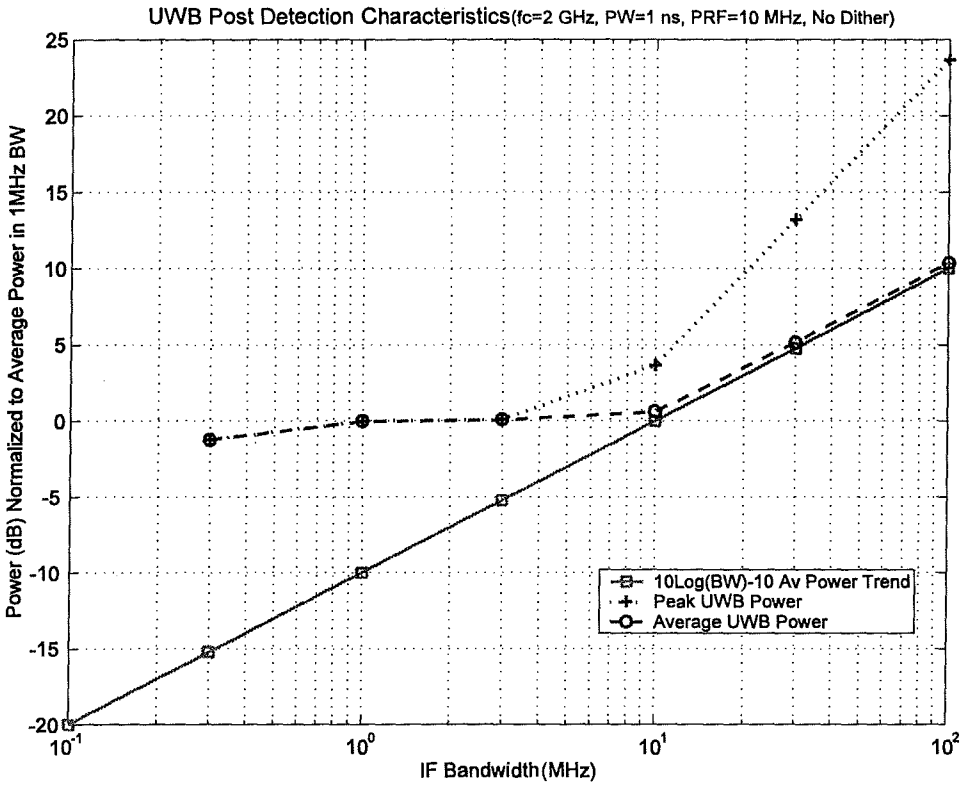

Figure B.9.A. Receiver peak and average power dependence on IF bandwidth (post detection, no dither).

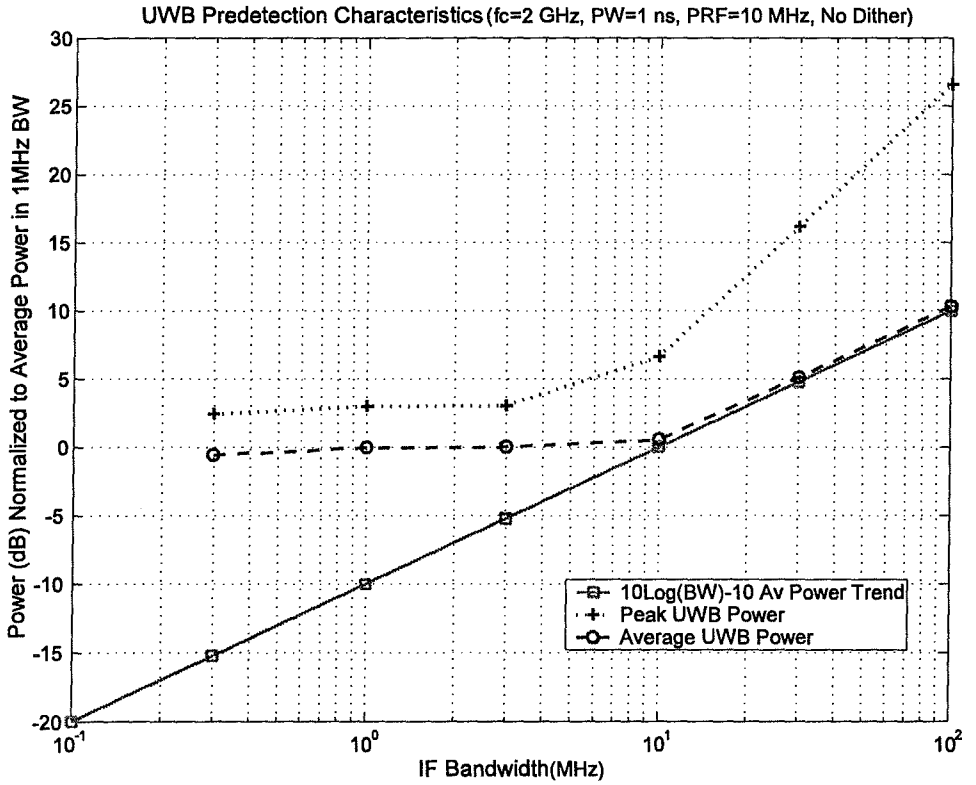

Figure B.9.B. Receiver peak and average power dependence on IF bandwidth (predetection, no dither).

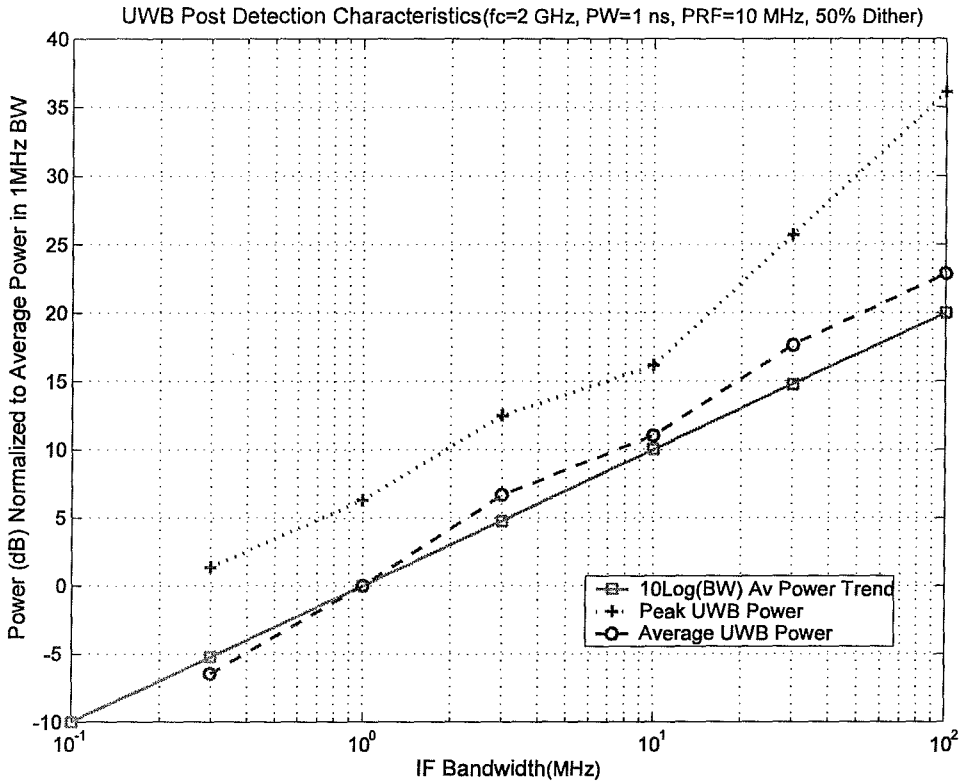

Figure B.9.C. Receiver peak and average power dependence on IF bandwidth (post-detection, 50% dither).

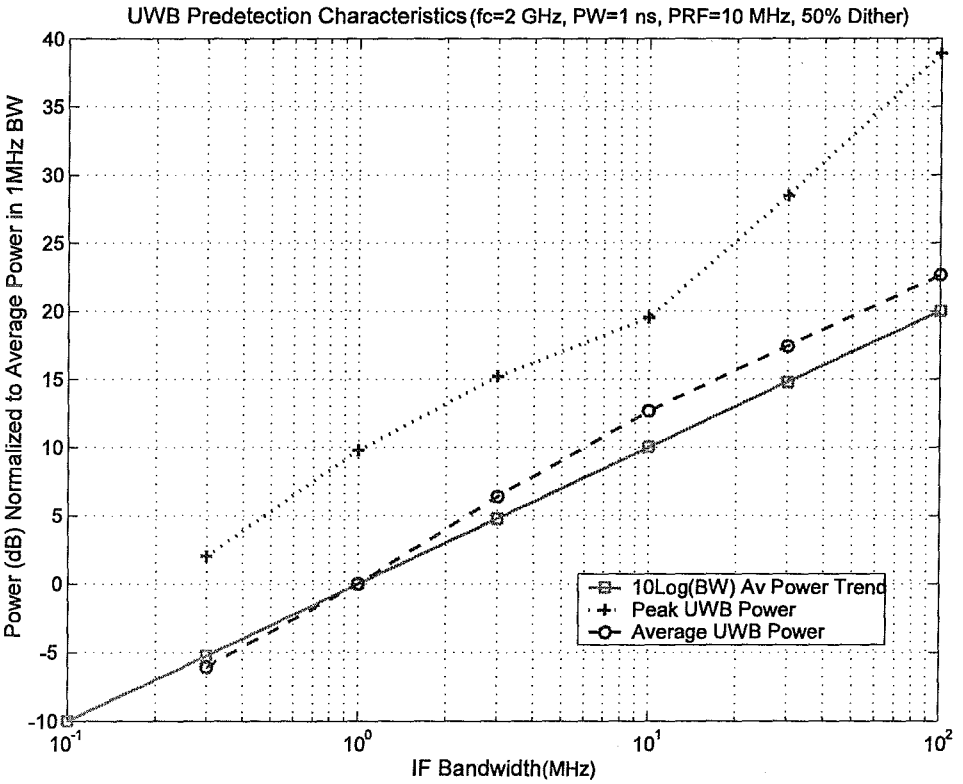

Figure B.9.D. Receiver peak and average power dependence on IF bandwidth (pre-detection, 50% dither).

APPENDIX C. CONVERSION OF POWER MEASURED IN A CIRCUIT TO INCIDENT FIELD STRENGTH AND INCIDENT POWER DENSITY, AND CORRECTIONS TO MEASURED EMISSION SPECTRA FOR NON-CONSTANT EFFECTIVE APERTURE MEASUREMENT ANTENNAS

Frank Sanders[1]

This appendix derives conversions between power measured in a circuit and incident field strength and effective radiated power from a transmitter.[2] Necessary corrections to measured emission spectra for non-constant effective aperture measurement antennas are also derived and explained.

C.1 Directivity, Gain, Effective Antenna Aperture, and Antenna Correction Factor

The starting point is *directivity* and *gain*, which are both measures of how well energy is concentrated in a given direction. *Directivity*, *d*, is the ratio of power density, p_{den} in that direction, to the power density that would be produced if the power were radiated isotropically, $p_{den\text{-}iso}$:

$$d = \frac{p_{den}}{p_{den-iso}} \quad . \tag{C.1}$$

The reference can be linearly or circularly polarized. By geometry, directivity is:

$$d = \frac{4\pi p_{den}}{\frac{\sqrt{E}}{\mu}\int\int E^2 d\Omega} \tag{C.2}$$

where E is the field strength [1]. Directivity makes reference only to power in space around the antenna; it is unrelated to power at the antenna terminals. There is loss between the terminals and free space. *Gain*, *g*, includes these antenna losses; gain is the field intensity produced in the given direction by a fixed input power, p_{in}, to the antenna. Gain and directivity are related by efficiency, ϵ:

---

[1]The author is with the Institute for Telecommunication Sciences, National Telecommunications and Information Administration, U.S. Department of Commerce, Boulder, Colorado 80305.

[2] In this appendix, quantities in linear units (e.g., milliwatts) are written in lower case; decibel quantities [10 log (linear power ratio)] are written in upper case.

$$g = d\epsilon \tag{C.3}$$

or,

$$g = \frac{(4\pi\ p_{den})}{p_{in}} \quad . \tag{C.4}$$

Through reciprocity, directivity is independent of transmission or reception, as is gain. *Effective antenna aperture*, a_e is unrelated to the physical aperture of an antenna. a_e is defined as:

$$a_e = \frac{\lambda^2 g}{4\pi} \tag{C.5}$$

where λ is the free-space wavelength. Note that a_e has the units of area. For an antenna matched to a load, the power in the load, p_{load}, is related to the free-space power density by a_e:

$$p_{load} = p_{den} \cdot a_e \quad . \tag{C.6}$$

If p_{load} is in a 50-ohm circuit and p_{den} is in a free-space impedance of 377 ohms, then the following relations apply:

$$p_{load} = \frac{V_{load}^2}{50} \tag{C.7a}$$

and

$$p_{den} = \frac{V_{space}^2}{377} \quad . \tag{C.7b}$$

Rewriting Eq. C.6 gives:

$$\frac{V_{load}^2}{50} = a_e \cdot \left(\frac{V_{space}^2}{377} \right) \tag{C.8}$$

Note that the voltage in the circuit, V^2_{load}, is in units of volts, but that the free-space field strength, V^2_{space} is in units of volts/m. The effective aperture, in units of m^2, converts the free-space power density on the right to the power in a circuit on the left.

At this point, we introduce the *antenna correction factor, acf,* which is defined as follows:

$$acf = \frac{V_{space}^2}{V_{load}^2} \quad . \tag{C.9}$$

Note that acf has the units of m^{-2}. Rewriting Eq. C.8 with this substitution for acf gives:

$$acf = \frac{377}{50} \cdot \left(\frac{1}{a_e} \right) \quad . \tag{C.10}$$

Because a_e is dependent upon both gain and frequency, so is acf. Substituting Eq. C.5 into Eq. C.6 gives:

$$acf = \left(\frac{377}{50} \right) \left(\frac{4\pi}{\lambda^2 g} \right) \quad . \tag{C.11}$$

If the frequency, f, is in megahertz, then the substitution [$\lambda = c/(f \cdot 10^6) = 3 \cdot 10^8/(f \cdot 10^6)$] gives:

$$acf = \left(\frac{377}{50} \right) (4\pi) \left[\left(\frac{10^{12}}{(3 \cdot 10^8)^2} \right) \cdot (f,\ MHz)^2 \cdot \left(\frac{1}{g} \right) \right] \tag{C.12}$$

which, calculating the constant term values, gives:

$$acf = \left(1.03 \cdot 10^{-3}\right) \cdot (f,\ MHz)^2 \cdot \left(\frac{1}{g} \right) \quad . \tag{C.13}$$

Taking 10log(*acf*) gives *ACF* in dB:

$$(ACF,\ dB) = (-29.78\ dB) + 20\log(f,\ MHz) - 10\log(g) \quad . \tag{C.14}$$

C.2 Free Space Field Strength Conversion

Signals are commonly measured in circuits as either voltages or log-detected voltages proportional to power. In either case, the signal measurement within a circuit is usually converted to equivalent power in the circuit impedance. This conversion is usually accomplished automatically within the measurement device (e.g., a spectrum analyzer). This measured power within a circuit, p_{load}, is converted to incident field strength using either the antenna correction

factor or antenna gain relative to isotropic, as follows. Writing Eq. C.6 with a substitution for a_e from Eq. C.5 gives:

$$p_{load} = \left(\frac{\lambda^2 \cdot g \cdot (V_{space})^2}{4\pi \cdot 377} \right) \quad , \tag{C.15}$$

and substituting for (λ= c/f), $f = 10^6 \cdot f$(MHz), and c = $3 \cdot 10^8$ m/s gives:

$$p_{load} = \left[\frac{(3 \cdot 10^8)^2 \cdot g \cdot (V_{space})^2}{(f,\ MHz)^2 \cdot (10^6)^2 \cdot 4\pi \cdot 377} \right] \quad . \tag{C.16}$$

For power in milliwatts and field strength in microvolts/meter, the conversions (power, mW) = 1000·(power, W) and (field strength, v/m) = 10^{-6}·(field strength, μV/m) are used:

$$(p_{load},\ mW) = \left[\frac{1000 \cdot (3 \cdot 10^8)^2 \cdot g \cdot (10^{-6})^2 \cdot (V_{space},\ \mu V/m)^2}{(f,\ MHz)^2 \cdot (10^6)^2 \cdot 4\pi \cdot 377} \right] \tag{C.17}$$

which, upon computing the constant terms, becomes:

$$(p_{load},\ mW) = \left[\frac{1.90 \cdot 10^{-8} \cdot g \cdot (V_{space},\ \mu V/m)^2}{(f,\ MHz)^2} \right] \quad . \tag{C.18}$$

Taking 10log of both sides gives:

$$10\log(p_{load},\ mW) = (-77.2\ dB) + 10\log(g) + 20\log(V_{space},\ \mu V/m) - 20\log(f,\ MHz) \quad . \tag{C.19}$$

Rearrangement of terms yields:

$$(field\ strength,\ dB\mu V/m) = (P_{load},\ dBm) + (77.2\ dB) + 20\log(f,\ MHz) - G \quad . \tag{C.20}$$

Note that P_{load} is related to the power measured within a circuit (e.g., a spectrum analyzer) by the correction for path gain between the antenna and the analyzer: $P_{load} = P_{meas}$ - (path gain to antenna). This changes Eq. C.20 to:

$$(fieldstrength,\ dB\mu V/m) = (P_{meas},\ dBm) - (path\ gain) + (77.2\ dB) + 20\log(f,\ MHz) - G. \tag{C.21}$$

Eq. C.21 is key for the conversion of measured power in a circuit into incident field strength in dBμV/m. For example, suppose that an antenna has gain G = 17 dB, at a frequency of 2300

MHz, with 28 dB path gain between the antenna and the spectrum analyzer. The measured power is -12 dBm on the spectrum analyzer display. Then field strength is +87 dBμV/m.

If an equation is required to relate field strength in dBμV/m to the *ACF,* then Eq. C.8 is used to relate acf to voltage in a circuit and free-space field strength:

$$\frac{V_{load}^2}{50} = \left(p_{load}\right) = \frac{V_{space}^2}{(50 \cdot\ acf)} \quad . \tag{C.22}$$

Converting power in watts into power in milliwatts, and converting voltage in volts/meter into microvolts/meter, gives

$$\left(p_{load,\ mW}\right) = \left[\frac{1000 \cdot \left(10^{-6}\right)^2 \cdot \left(V_{space,\ \mu V/m}\right)^2}{50acf}\right] \tag{C.23}$$

which, upon computing the group of constant terms, gives:

$$\left(p_{load,\ mW}\right) = \frac{\left(2 \cdot 10^{-11}\right)\left(V_{space,\ \mu V/m}\right)^2}{acf} \tag{C.24}$$

and which, taking 10log of both sides, means that

$$\left(P_{load,\ dBm}\right) = \left(-107\ dB\right) + \left(V_{space,\ dB\mu V/m}\right) - ACF \quad . \tag{C.25}$$

Rearranging terms and substituting [P_{meas} - (path gain)] for P_{load}:

$$V\left(dB\mu V/m\right) = P_{meas} - \left(path\ gain\right) + \left(107\ dB\right) + ACF \quad . \tag{C.26}$$

For example, suppose a measurement of -12 dBm is taken on a spectrum analyzer, with 28 dB net gain in the path between the antenna and the analyzer, and measurement antenna acf of 111 (corresponding to G = 17 dBi at 2300 MHz, as in the example above). Then *ACF* = 20.5 dB, and the corresponding free-space field strength is computed using Eq. C.26 to be +87 dBμV/m.

C.3 Effective Isotropic Radiated Power Conversion

It may be necessary to know the effective isotropic radiated power (EIRP) that a device transmits. The conversion from measured power in a circuit to EIRP is described in this section.

Free space loss must be determined: For transmit power (watts) p_t; transmit antenna gain relative to isotropic g_t; receive antenna gain relative to isotropic g_r; receive power (watts) p_r; and receive antenna effective aperture a_e; the effective isotropic radiated power is

$$(eirp) = (p_t \cdot g_t) \tag{C.27}$$

and

$$p_r = a_e \cdot \left(\frac{eirp}{4\pi r^2} \right) \tag{C.28}$$

with r being the distance between the transmit and receive antennas.

The effective aperture of the antenna is the effective aperture of an isotropic antenna multiplied by the antenna's gain over isotropic, or

$$a_e = \left(\frac{\lambda^2}{4\pi} \right) \cdot g_r \quad . \tag{C.29}$$

A change to decibel units makes Eq. C.28:

$$P_r = EIRP + G_r + 20\log(\lambda) - 20\log(4\pi) - 20\log(r) \quad . \tag{C.30}$$

Substituting c/f for λ,

$$P_r = EIRP + G_r + 20\log(c) - 20\log(f) - 20\log(4\pi) - 20\log(r) \quad . \tag{C.31}$$

If frequency is in megahertz and distance is in meters, then Eq. C.31 becomes

$$P_r = EIRP + G_r + 20\log(c) - 20\log(f, MHz \cdot 10^6) - 20\log(4\pi) - 20\log(r) \quad , \tag{C.32}$$

which yields

$$P_r = EIRP + G_r + 169.5 - 20\log(f, MHz) - 120 - 22 - 20\log(r, meters) \tag{C.33}$$

or

$$P_r = EIRP + G_r + 27.5 - 20\log(f,MHz) - 20\log(r, meters) \quad , \tag{C.34}$$

Similarly, for r in kilometers, Eq. C.31 becomes

$$P_r = EIRP + G_r - 32.5 - 20\log(f, MHz) - 20\log(r, km) \quad \text{(C.35)}$$

and Eq. C.31 for r in miles is

$$P_r = EIRP + G_r - 36.5 - 20\log(f, MHz) - 20\log(r, miles) \quad . \quad \text{(C.36)}$$

For measurements of Part 15, Part 18, and ultrawideband transmitters, Eq. C.34 is convenient. If the gain of the receive antenna is known and the received power has been measured at a known distance from the emitter, then Eq. C.34 can be rearranged to yield *EIRP:*

$$(EIRP, dBW) = (P_r, dBW) - G_r - 27.5 + 20\log(f, MHz) + 20\log(r, meters) \quad . \quad \text{(C.37)}$$

If the received power is measured in dBm rather than dBW, Eq. C.37 becomes

$$(EIRP, dBW) = (P_r, dBm) - G_r - 57.5 + 20\log(f, MHz) + 20\log(r, meters) \quad . \quad \text{(C.38)}$$

If EIRP in decibels relative to a picowatt (dBpW) is required, then Eq. C.38 becomes:

$$(EIRP, dBpW) = (P_r, dBm) - G_r + 62.5 + 20\log(f, MHz) + 20\log(r, meters) \quad . \quad \text{(C.39)}$$

For example, if a value of -10 dBm is measured at a frequency of 2450 MHz, with an antenna gain +16.9 dBi, at a distance of 3 meters, then the EIRP value is +113 dBpW.

Effective radiated power relative to a dipole (ERP_{dipole}) is sometimes required. EIRP is 2.1 dB higher than ERP_{dipole}.

Finally, the conversion to incident power density is considered. The incident power density, P_{den}, in W/m^2, is equal to the incident field strength squared (units of $(V/m)^2$), divided by the ohmic impedance of free space:

$$(P_{den}, W/m^2) = \left(\frac{(field\ strength, V/m)^2}{377} \right) \quad . \quad \text{(C.40)}$$

Using more common units for field strength of ($dB\mu V/m$), and more common units for incident power of ($\mu W/cm^2$):

$$(1\ W/m^2) = \frac{100\ \mu W}{cm^2} = \frac{10^{12}}{377}(\mu V/m)^2 \quad \text{(C.41)}$$

gives

$$1\ (\mu W/cm^2) = \frac{10^{10}\ (\mu V/m)^2}{377} \quad . \tag{C.42}$$

The incident power density is thus

$$(P_\rho,\ \mu W/cm^2) = \frac{377}{10^{10}} \cdot (field\ strength,\ \mu V/m)^2 \tag{C.43}$$

or

$$(P_\rho,\ \mu W/cm^2) = 3.77 \cdot 10^{-8} \cdot (field\ strength,\ \mu V/m)^2 \quad . \tag{C.44}$$

C.4 Correction of Measured Emission Spectra for Non-Constant Effective Aperture Measurement Antennas

With reference to Eq. C.5, the effective aperture of an isotropic antenna as a function of frequency, f, is:

$$a_e = \frac{g}{4\pi f^2} \tag{C.45}$$

or

$$A_e = G - 10\log(4\pi) - 20\log(f) \quad . \tag{C.46}$$

If gain relative to isotropic, g, is arbitrarily normalized to 4π, then the functional dependence of effective aperture on frequency is clear:

$$A_e \propto -20\log(f) \quad . \tag{C.47}$$

The effective aperture of a constant-gain isotropic antenna decreases as the square (i.e., 20 log) of the frequency. If an isotropic antenna were realized physically, and were then used to measure an emission spectrum, it would be necessary to correct the measured spectrum for this drop in aperture with increasing frequency.

For an isotropic antenna, the measured spectrum amplitudes would have to be increased as (20log(frequency)) to represent the energy that would be coupled into a constant effective aperture. Parabolic reflector antennas in principle have constant apertures; their gain nominally

increases at the rate of (20 log(frequency)). Consequently emission spectra measured with high-performance parabolic antennas do not require antenna aperture corrections.

Wideband horn antennas represent an intermediate case between the (-20 log) decrease in effective aperture of theoretical isotropic antennas and the constant-aperture condition of nominal parabolic reflector antennas. For example, the gain curve of a widely used double-ridged waveguide horn (Figure C.1) increases with frequency, but at the rate of approximately (6.7 log(frequency)). Since this is [(20-6.7)log] = 13.3 log below a constant-aperture condition, the spectra measured with such an antenna must be corrected at the rate of (13.3 log(frequency)).

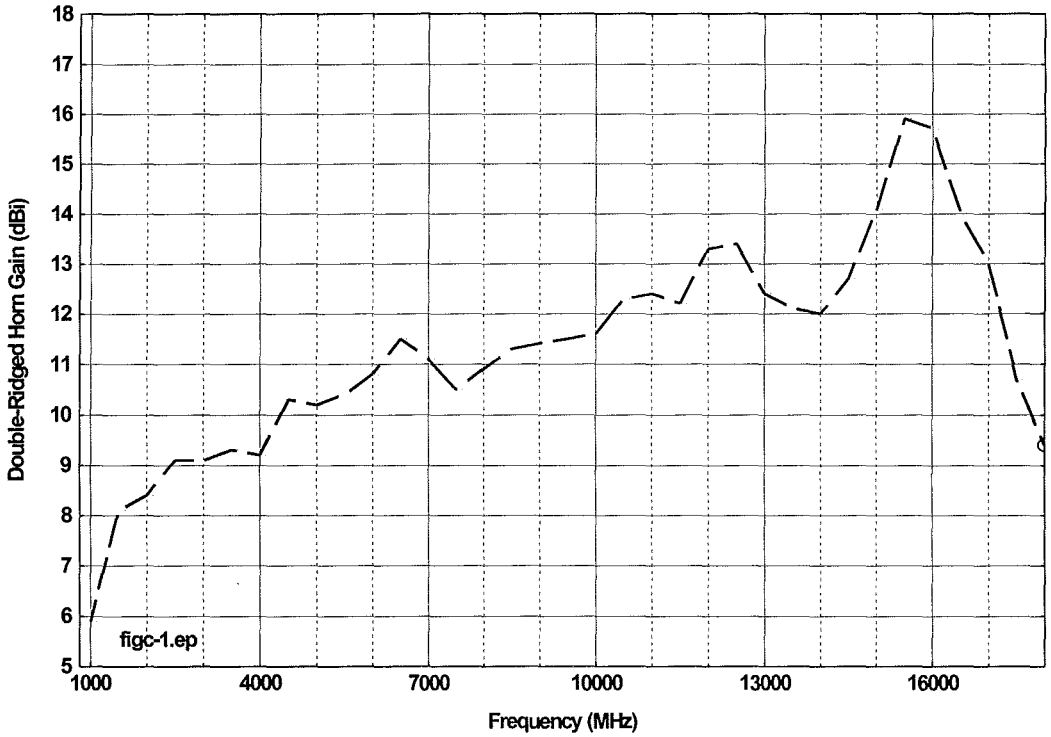

Figure C.1. Broadband double-ridged waveguide antenna gain as a function of frequency. The effective aperture would be constant if the gain curve varied as 20log frequency).

Operationally, this correction is performed by ITS engineers as follows: The spectrum is measured across a given frequency range and the uncorrected curve is stored. During the data analysis phase, the original spectrum is corrected relative to an arbitrarily chosen frequency, according to the following equation:

$$\left(P_{corrected}\right) = \left(P_{measured}\right) + 13.3\left[\log\left(\frac{f_{measured}}{f_{reference}}\right)\right] \quad . \tag{C.48}$$

For example, if a spectrum is measured between 1 GHz and 5 GHz, a convenient reference frequency might be 1 GHz, since the corrected spectrum will then have a zero correction at the left-hand side of the graph. The correction will increase from zero at 1 GHz to a maximum of 9.3 dB at 5 GHz on the right-hand side of the graph, as in Figure C.2.

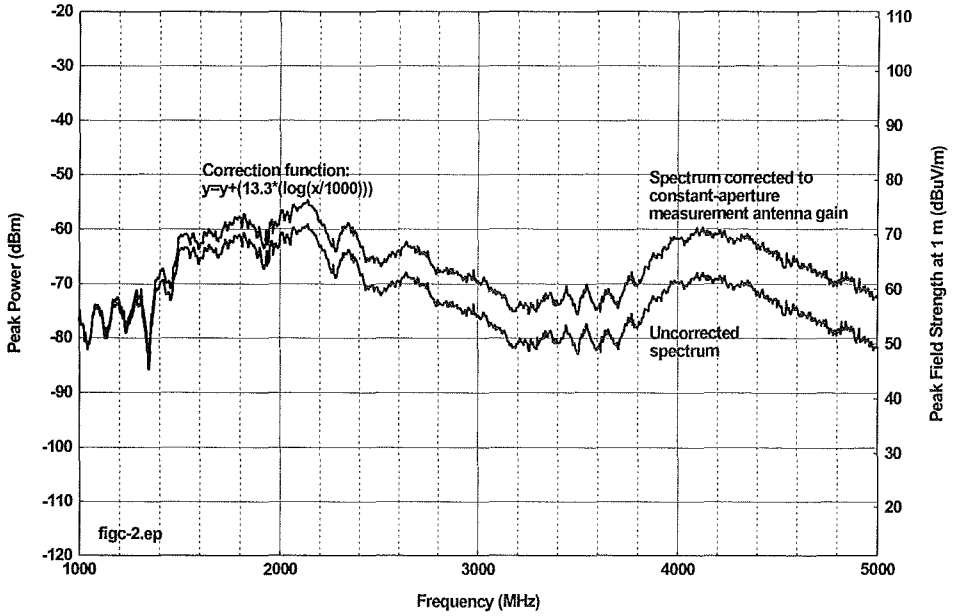

Figure C.2. Demonstration of emission spectrum measurement corrected to a constant effective aperture measurement antenna. With this correction it becomes possible to add a second axis for incident field strength.

The graph's power-axis label needs to reflect the fact that the spectrum has been rendered as measured with a constant-effective-aperture antenna. This can be done in two ways. The first is to reference the antenna's gain relative to isotropic at the reference frequency. If the antenna in question had 5.9 dBi gain at the reference frequency of 1 GHz, then the axis label could read: "Power measured with constant-aperture antenna, 5.9 dBi gain at 1 GHz (dBm)."

The label above might as easily refer to the antenna correction factor (acf) of the antenna at the reference frequency. The second method is to compute the effective aperture of the antenna and quote that in the label. In this example, the gain of 5.9 dBi at 1 GHz yields an effective aperture in Eq. C.45 of $3.1 \cdot 10^{-7}$ m^2. The corresponding axis label could read:

"Power measured with antenna of constant effective aperture $3.1 \cdot 10^{-7}$ m^2 (dBm)"

While accurate, this expression's reference to an effective aperture is unconventional.

An advantage of correcting a measured emission spectrum to constant measurement antenna effective aperture is that a second axis can be added to the right-hand side of the graph showing

field strength. With the effective aperture correction having been made, the field strength becomes an additive factor to the power measured in a circuit. In this example (5.9 dBi gain at 1 GHz, constant aperture correction made to the rest of the spectrum), Eq. C.21 is used to arrive at the following conversion to field strength:

$$(Field\ strength,\ dB\mu V/m) = P_{meas} - (path\ gain) + 77.2 + (60 - 5.9) \qquad (C.49)$$

or

$$(Field\ strength,\ dB\mu V/m) = P_{meas} - (path\ gain) + (131\ dB) \quad . \qquad (C.50)$$

Figure C.2 shows an example of a corrected spectrum with the field strength axis added in accordance with Eq. C.48 and Eq. C.50.

C.5 References

[1] E. C. Jordan, Ed., *Reference Data for Engineers: Radio, Electronics, Computer, and Communications*, Seventh ed., Macmillan, 1989, pg. 32-33.

APPENDIX D. EMISSION DATA FOR ULTRAWIDEBAND TRANSMITTERS

Frank Sanders,[1] Brent Bedford,[1] Robert T. Johnk,[2] and Robert Matheson[1], David R. Novotny[2]

This appendix contains measured emission spectra and time waveforms for five ultrawideband transmitters, and also for a Part 15 device (specifically, an electric drill). Measurement techniques are described in Sections 5 and 6. Analysis and commentary are provided in Section 8.

[1]The authors are with the Institute for Telecommunication Sciences, National Telecommunications and Information Administration, U.S. Department of Commerce, Boulder, CO 80305.

[2]The authors are with the Radio-Frequency Technology Division, National Institute for Standards and Technology, U. S. Department of Commerce, Boulder, CO 80305.

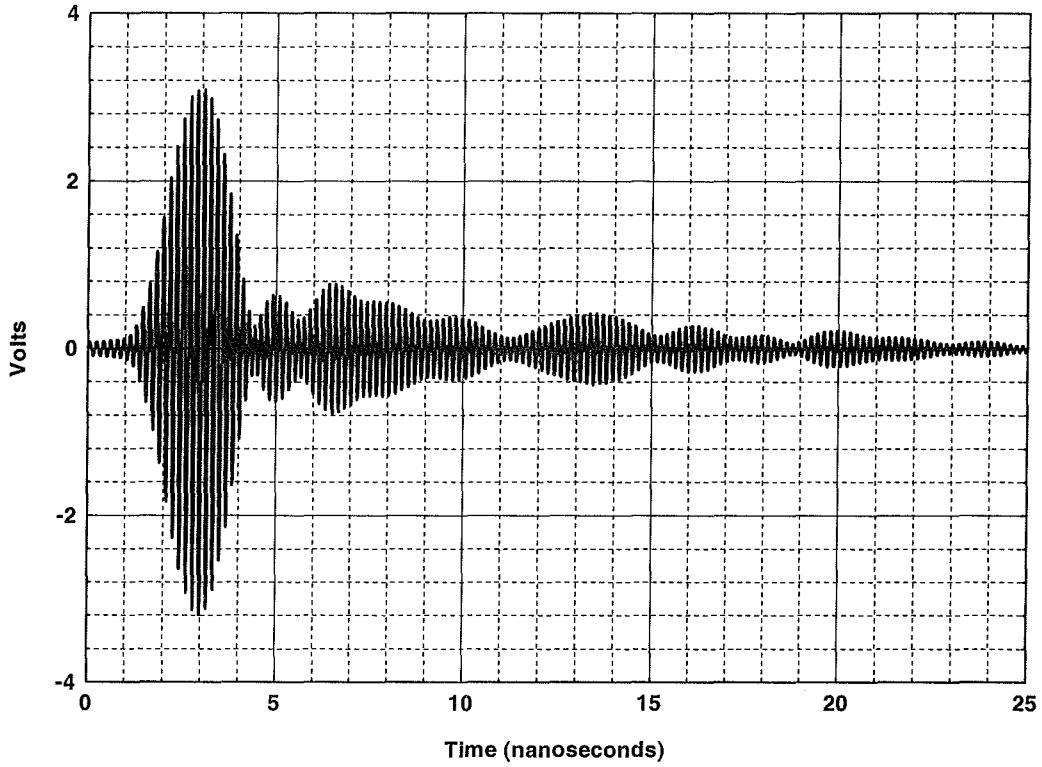

Figure D.A.1. Device A, conducted time-domain waveform.

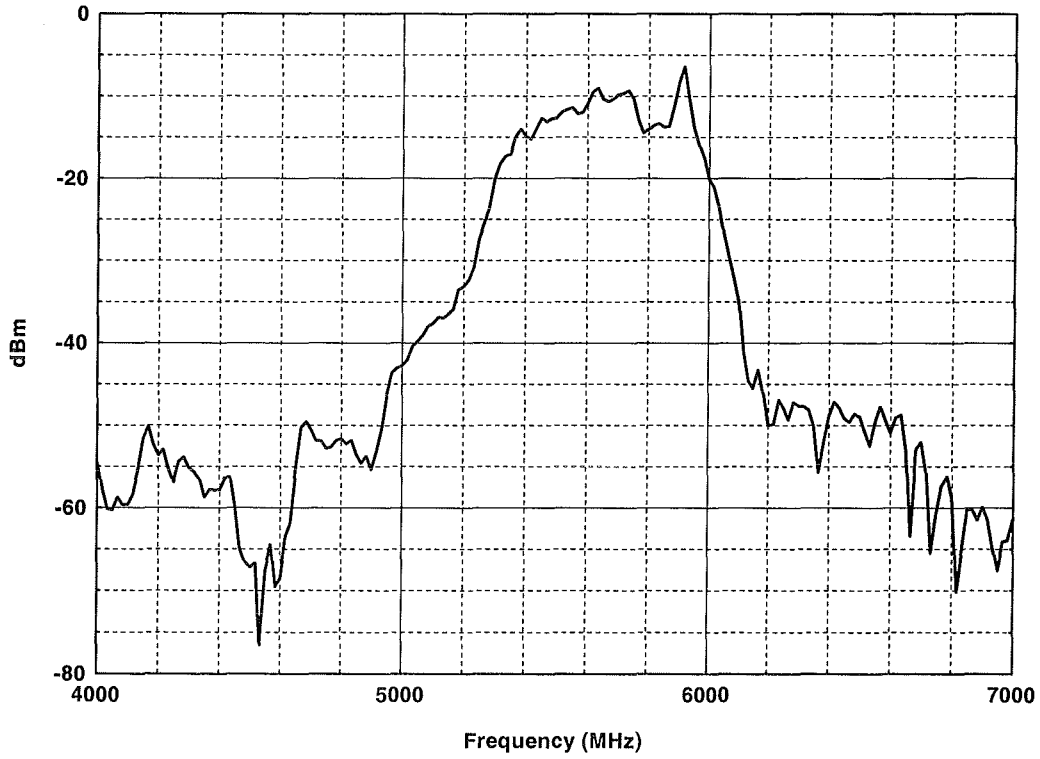

Figure D.A.2. Device A, conducted power spectrum, Δf = 16.67 MHz.

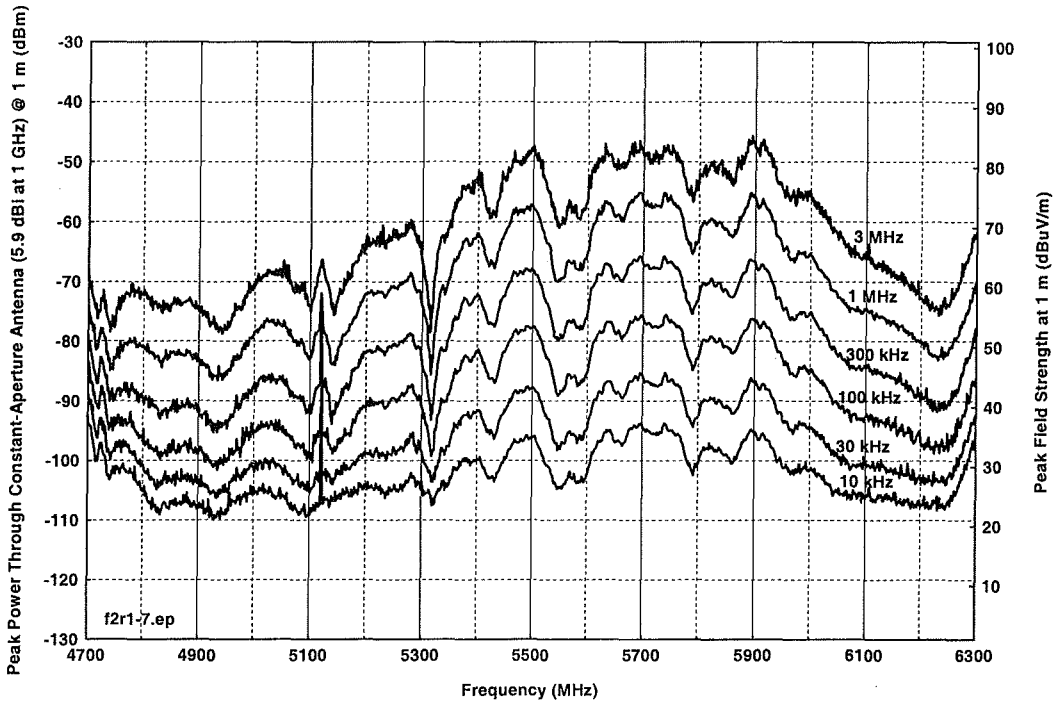

Figure D.A.3. Device A, spectra as a function of measurement bandwidth.

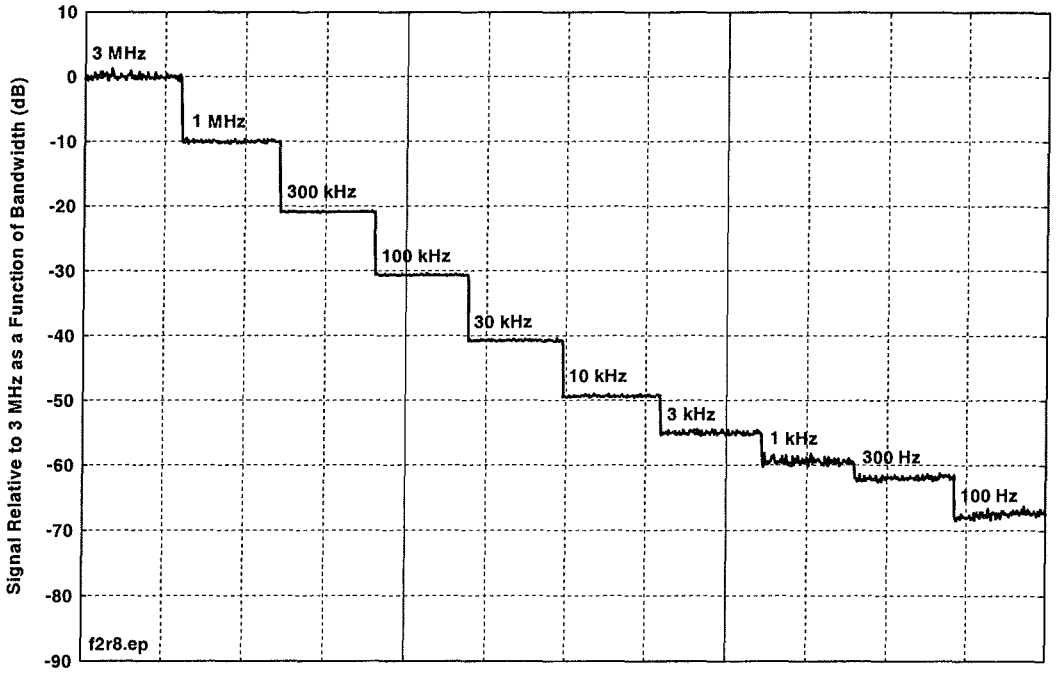

Figure D.A.4. Device A, peak signal level as a function of bandwidth.

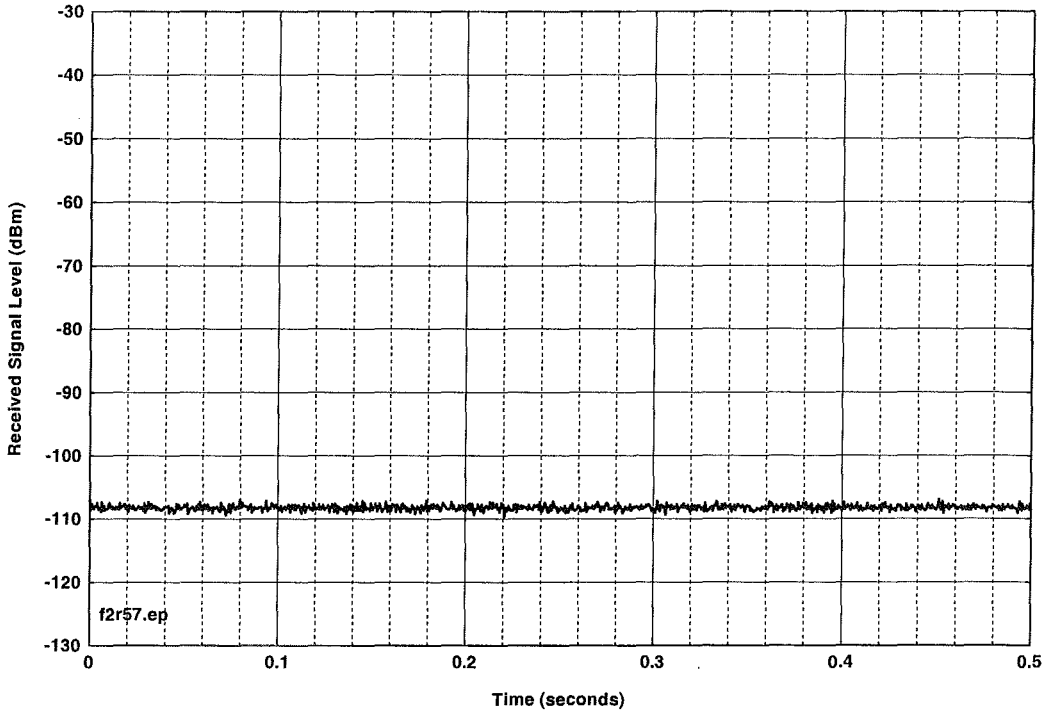

Figure D.A.5. Device A, emission in 10-kHz video bandwidth.

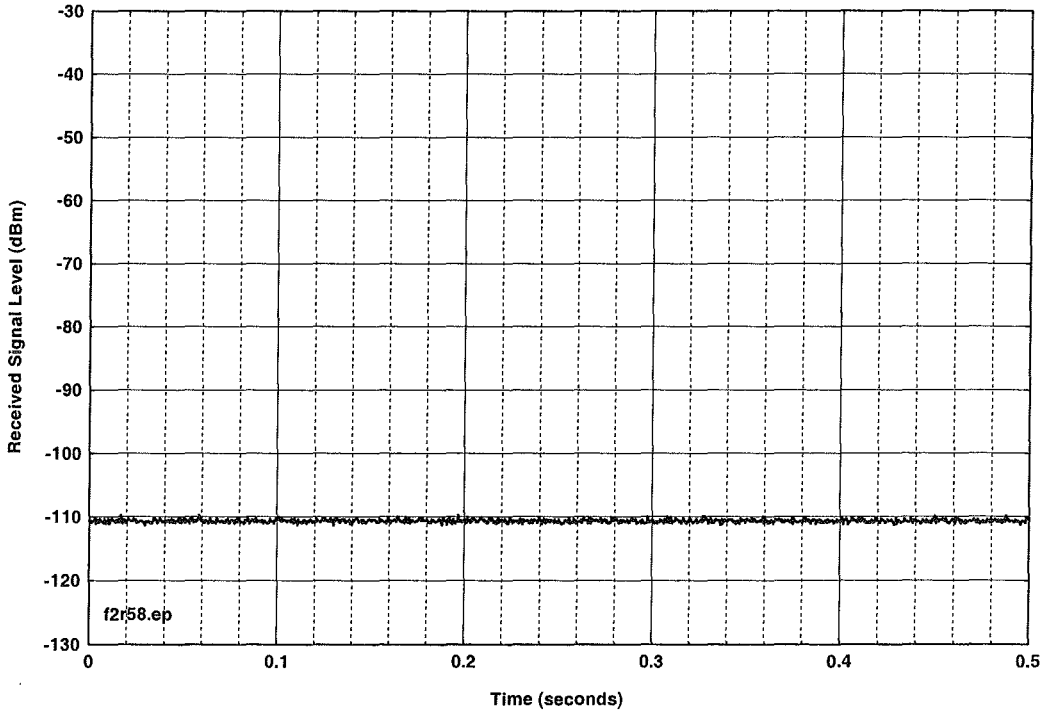

Figure D.A.6. Device A, emission in 3-kHz video bandwidth.

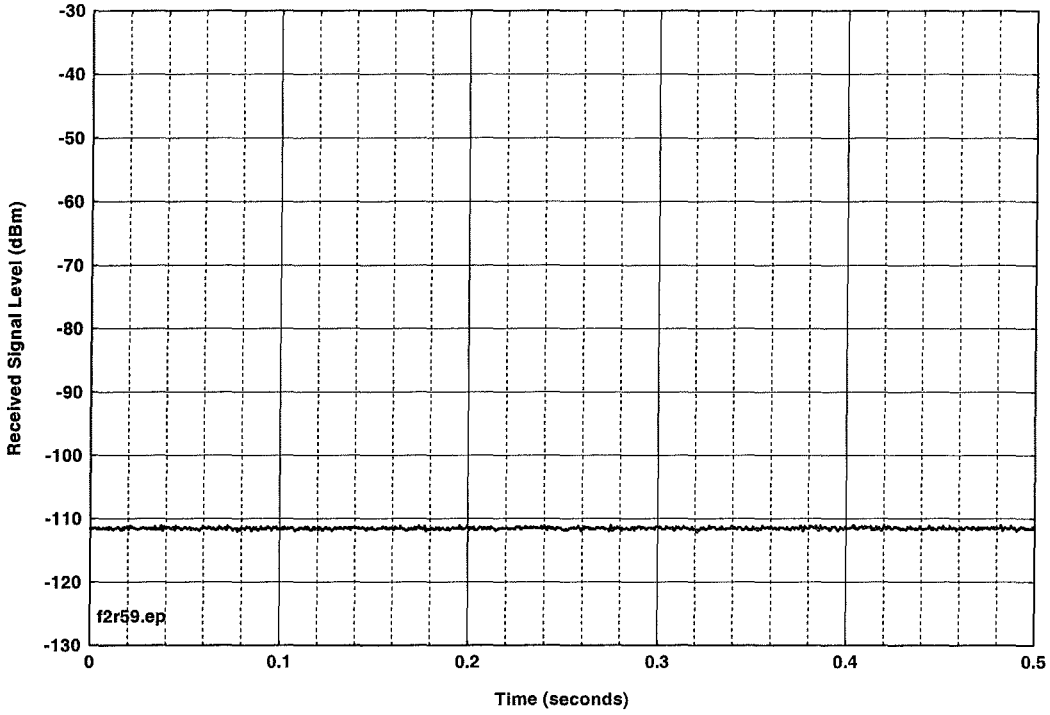

Figure D.A.7. Device A, emission in 1-kHz video bandwidth.

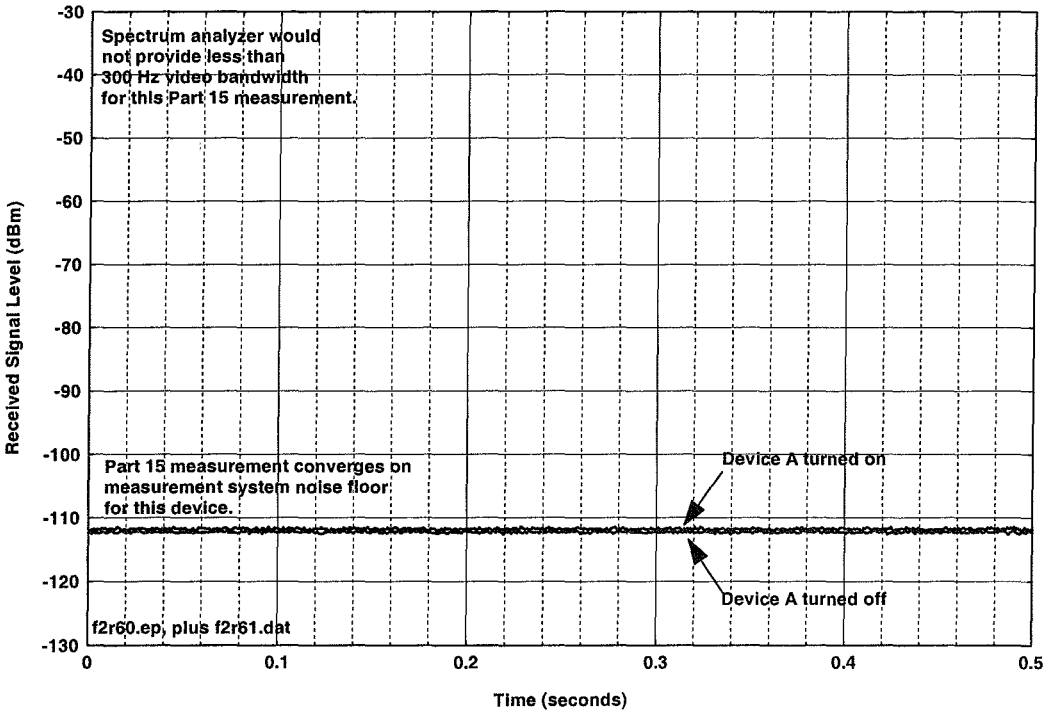

Figure D.A.8. Device A, emission in 300-Hz video bandwidth: converges on measurement system noise floor.

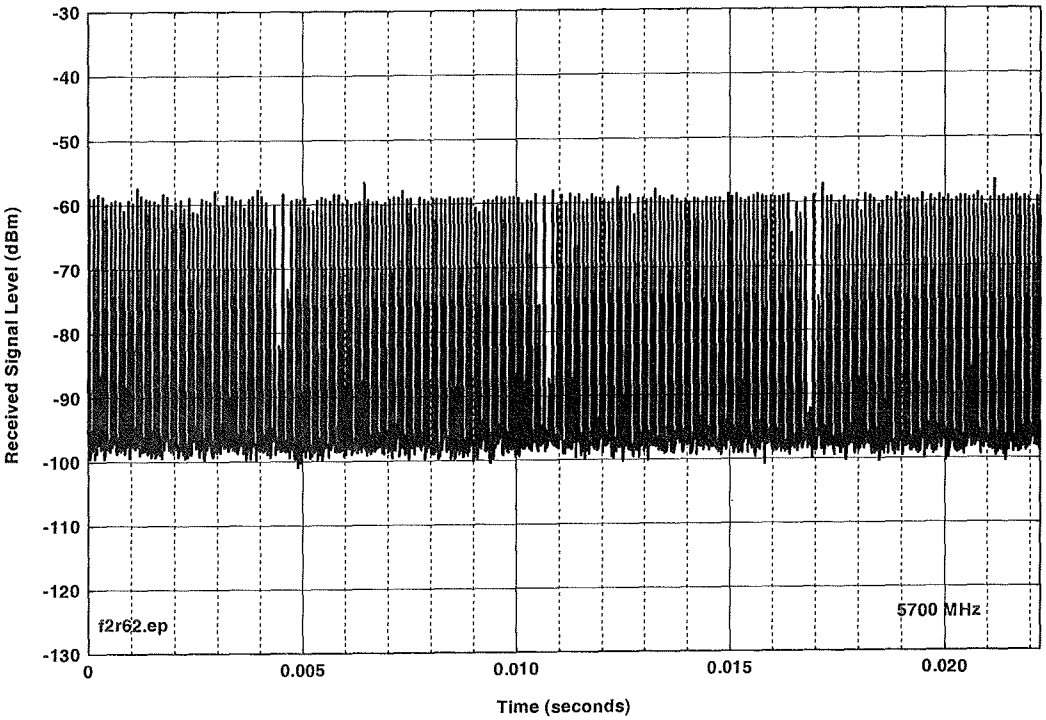

Figure D.A.9. Device A, peak emission in 3-MHz IF bandwidth.

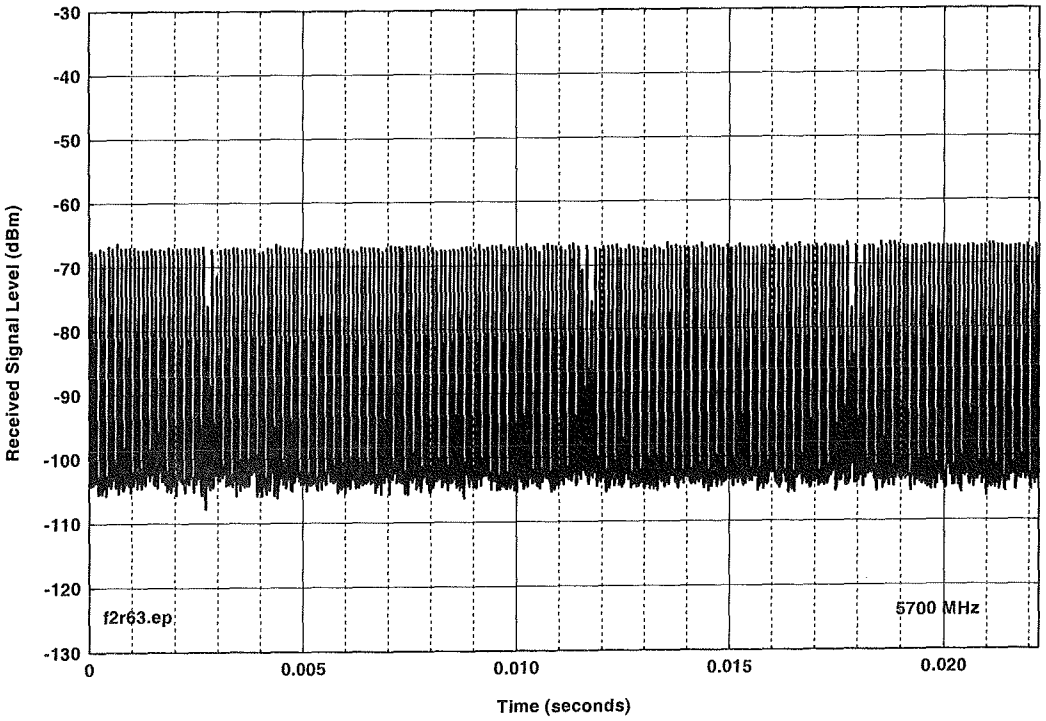

Figure D.A.10 Device A, peak emission in 1-MHz IF bandwidth.

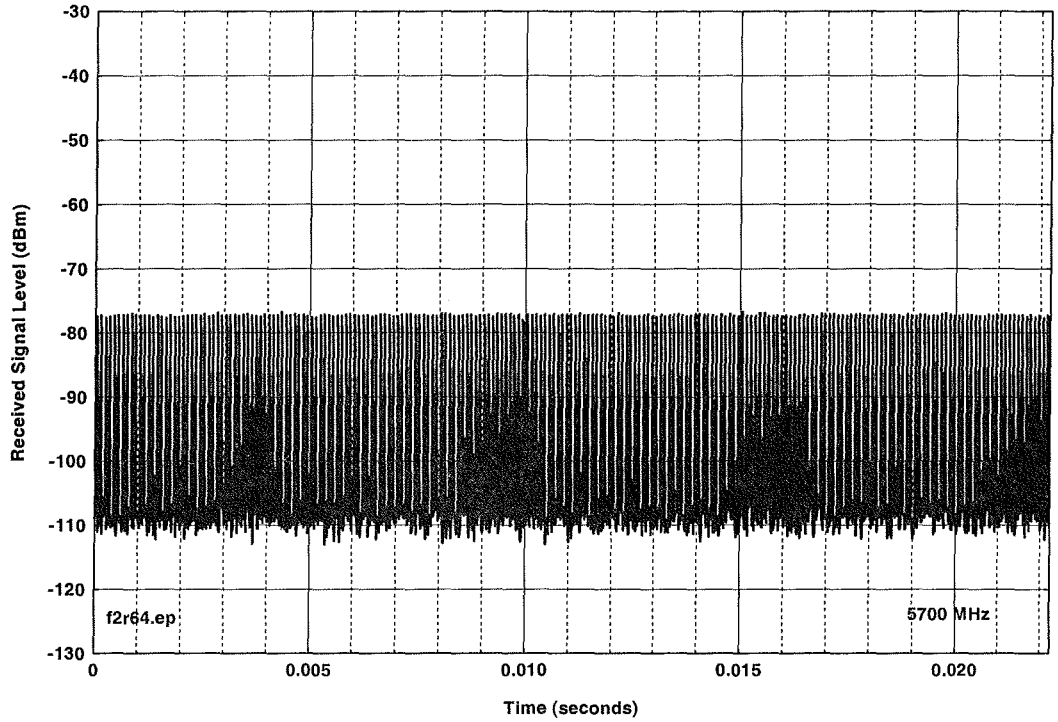

Figure D.A.11. Device A, peak emission in 300-kHz IF bandwidth.

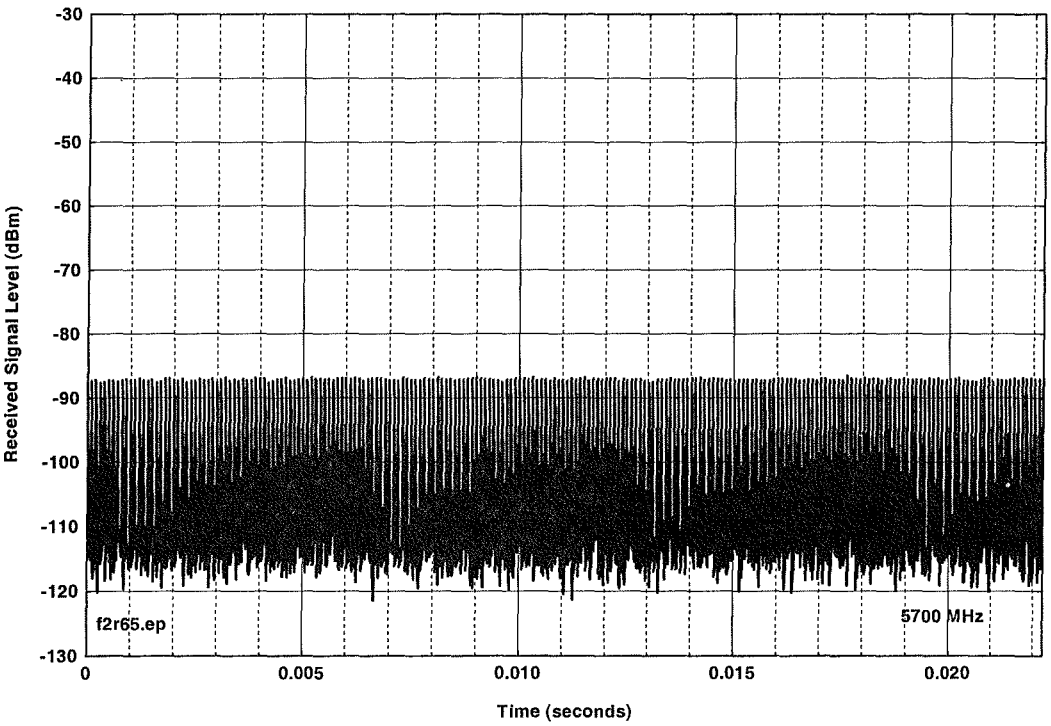

Figure D.A.12. Device A, peak emission in 100-kHz IF bandwidth.

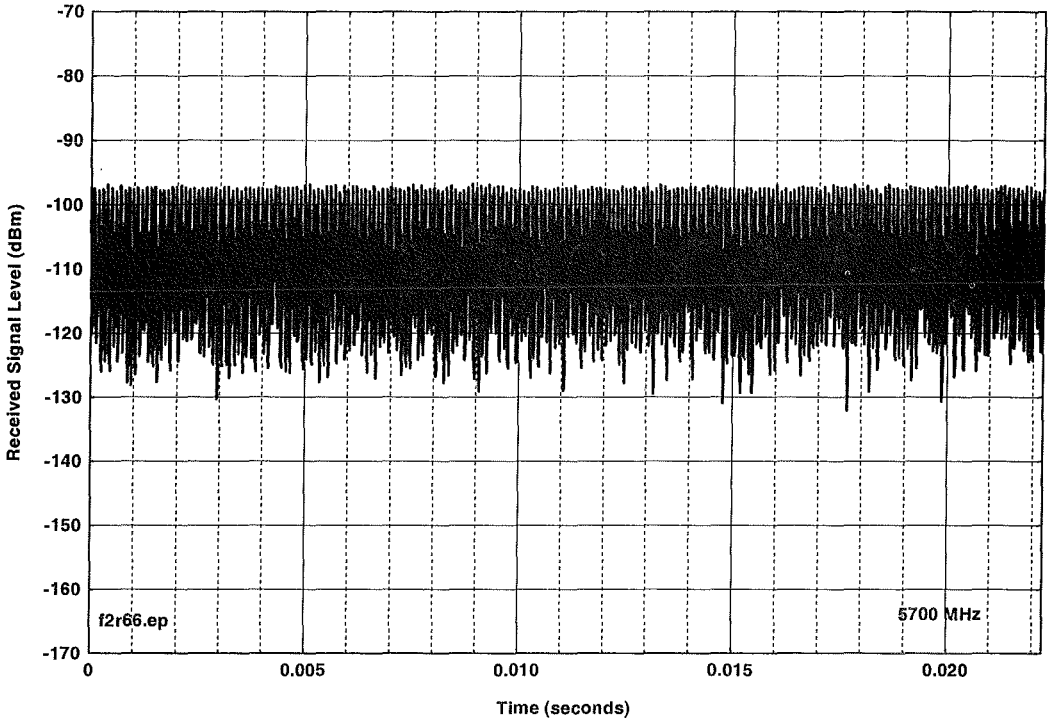

Figure D.A.13. Device A, peak emission in 30-kHz IF bandwidth.

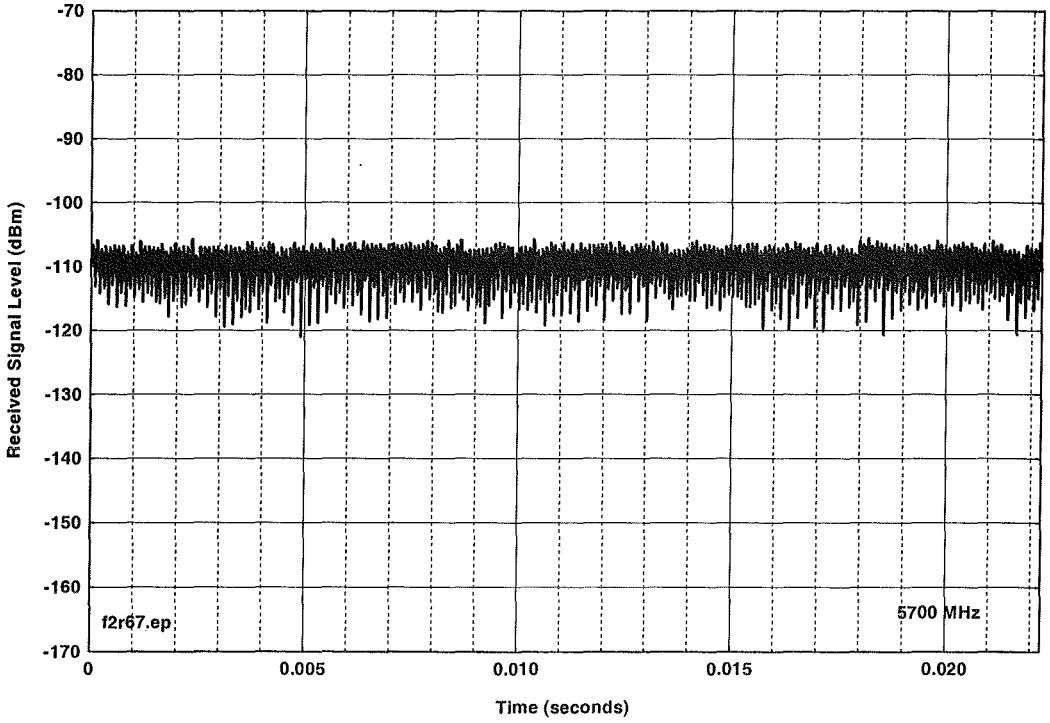

Figure D.A.14. Device A, peak emission in 10-kHz IF bandwidth.

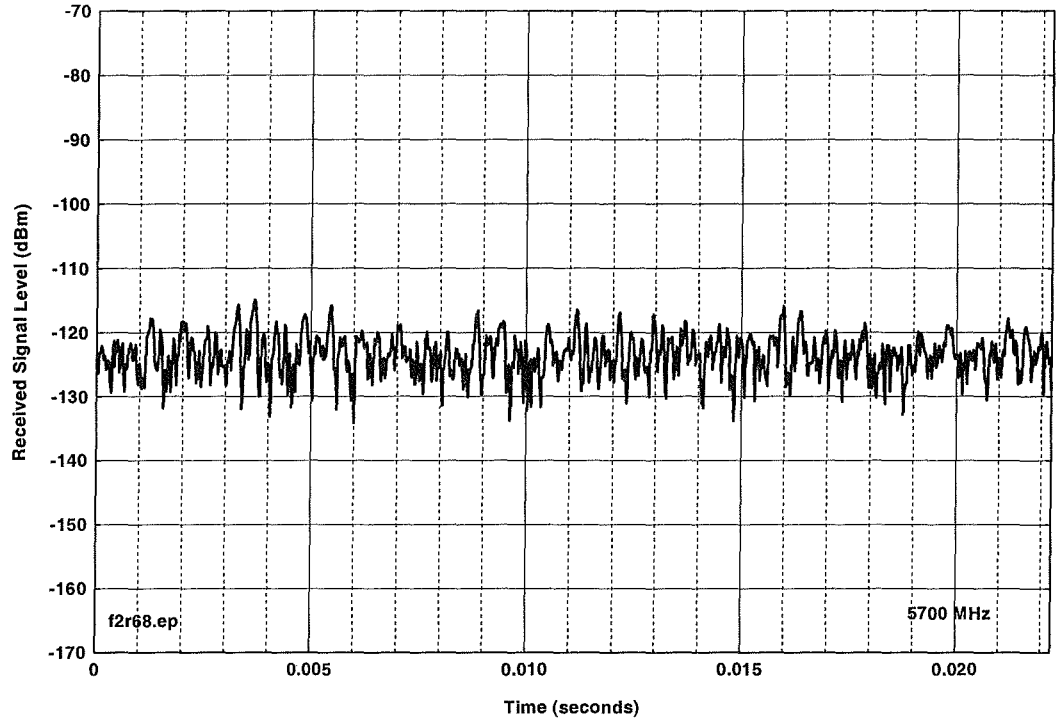

Figure D.A.15. Device A, peak emission in 3-kHz IF bandwidth.

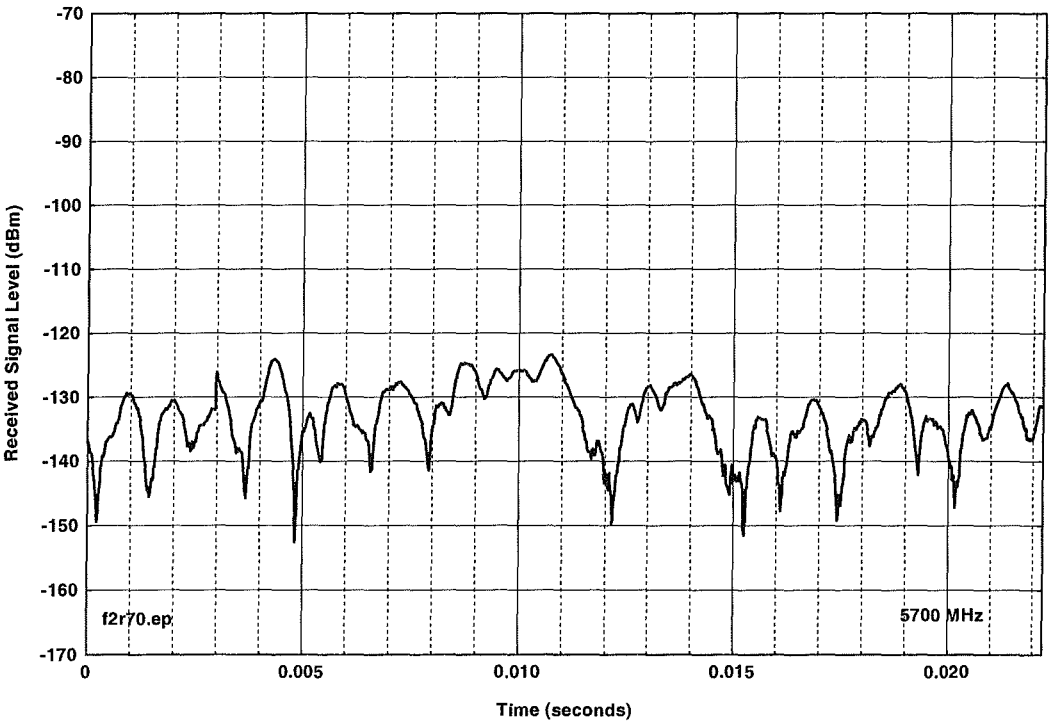

Figure D.A.16. Device A, peak emission in 1-kHz IF bandwidth.

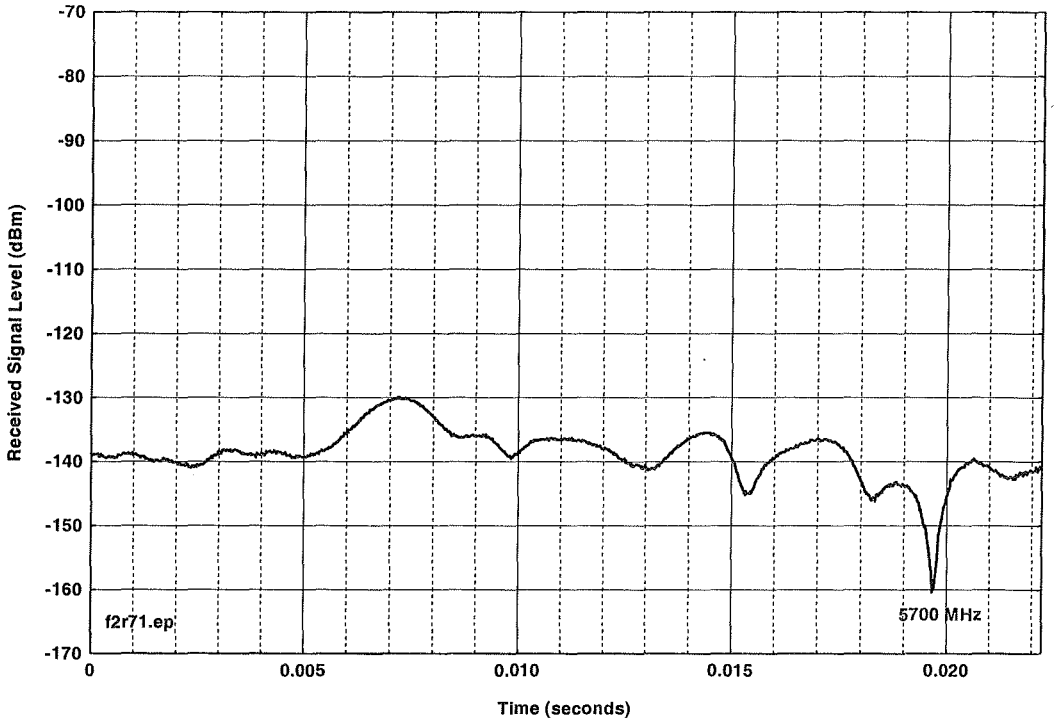

Figure D.A.17. Device A, peak emission in 300-Hz IF bandwidth.

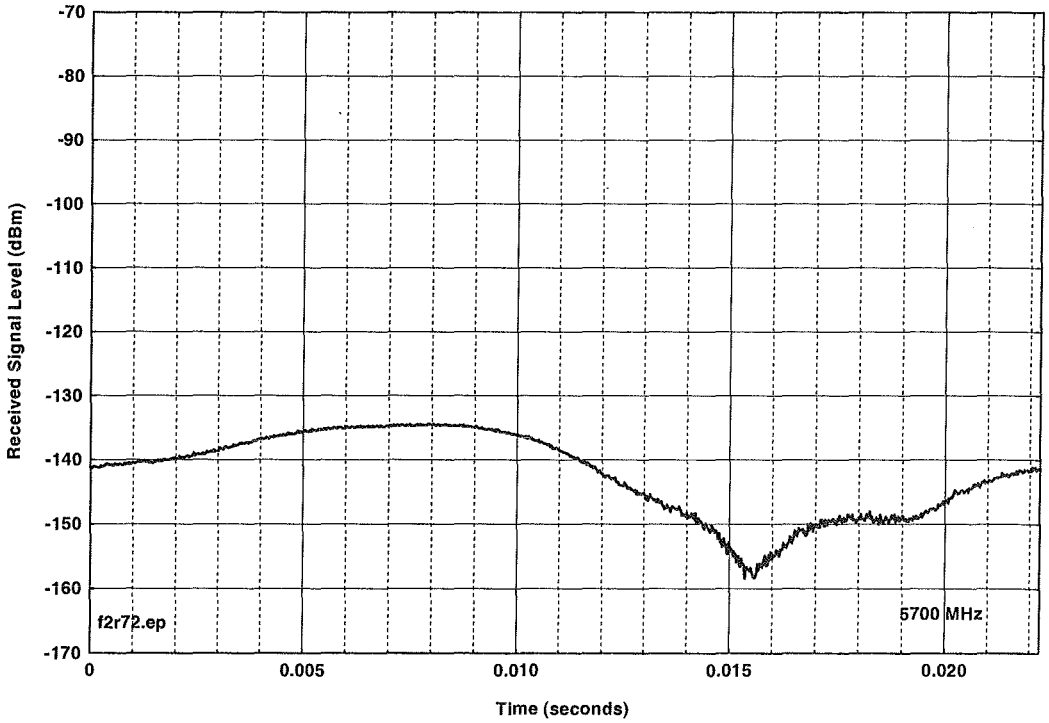

Figure D.A.18. Device A, peak emission in 100-Hz IF bandwidth.

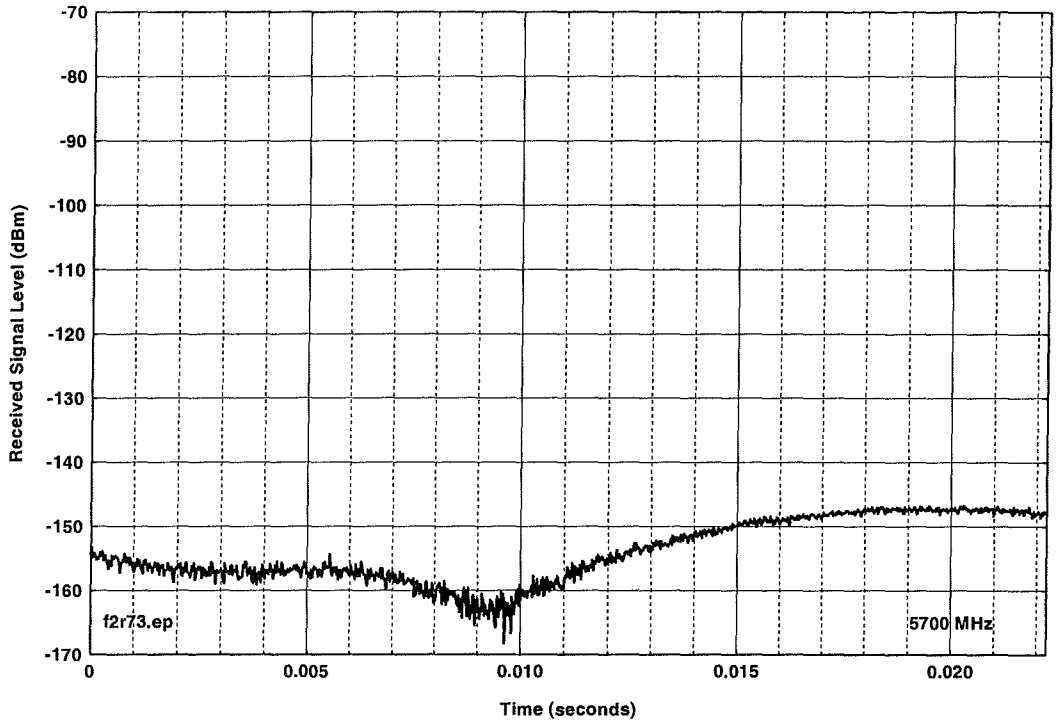

Figure D.A.19. Device A, peak emission in 30-Hz IF bandwidth.

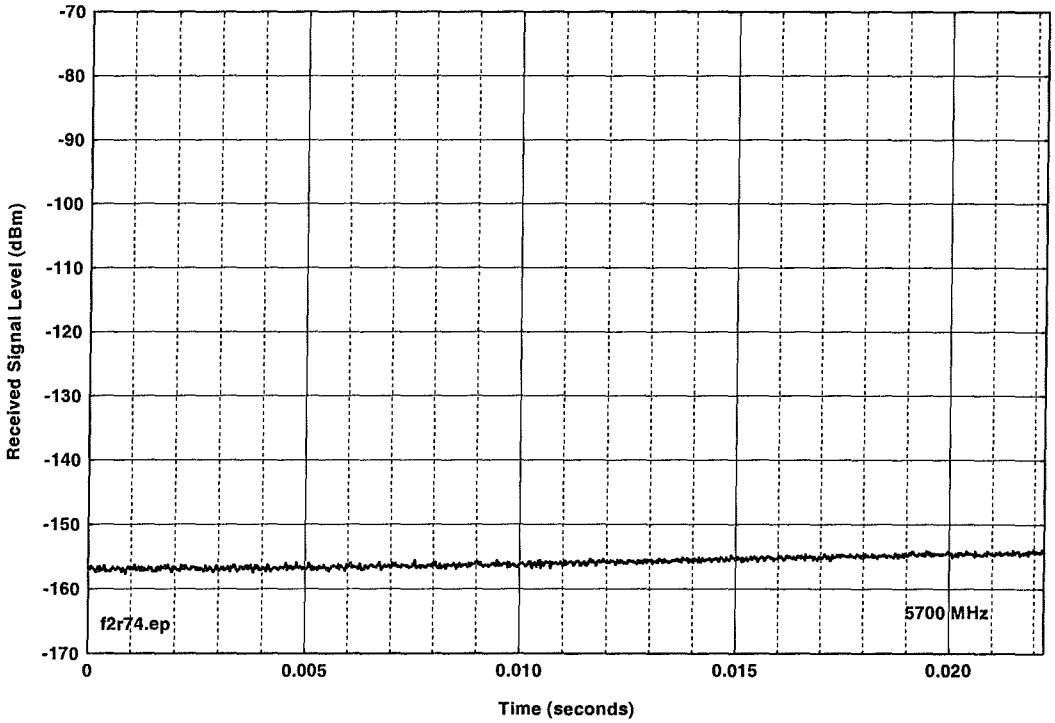

Figure D.A.20. Device A, peak emission in 10-Hz IF bandwidth.

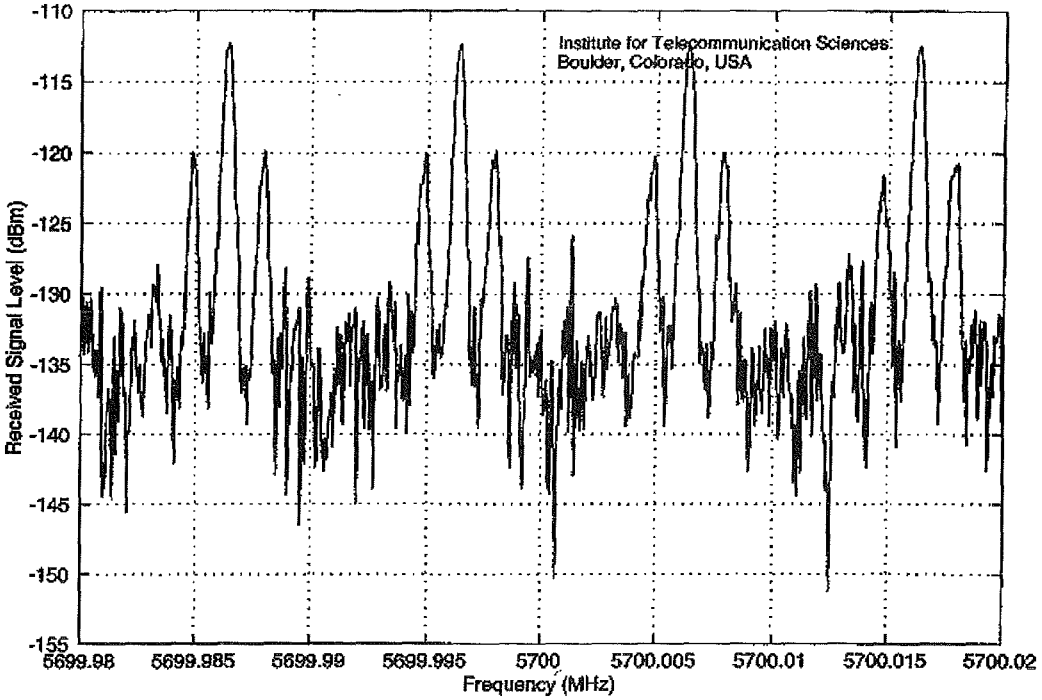

Figure D.A.21. Device A, spectrum fine structure.

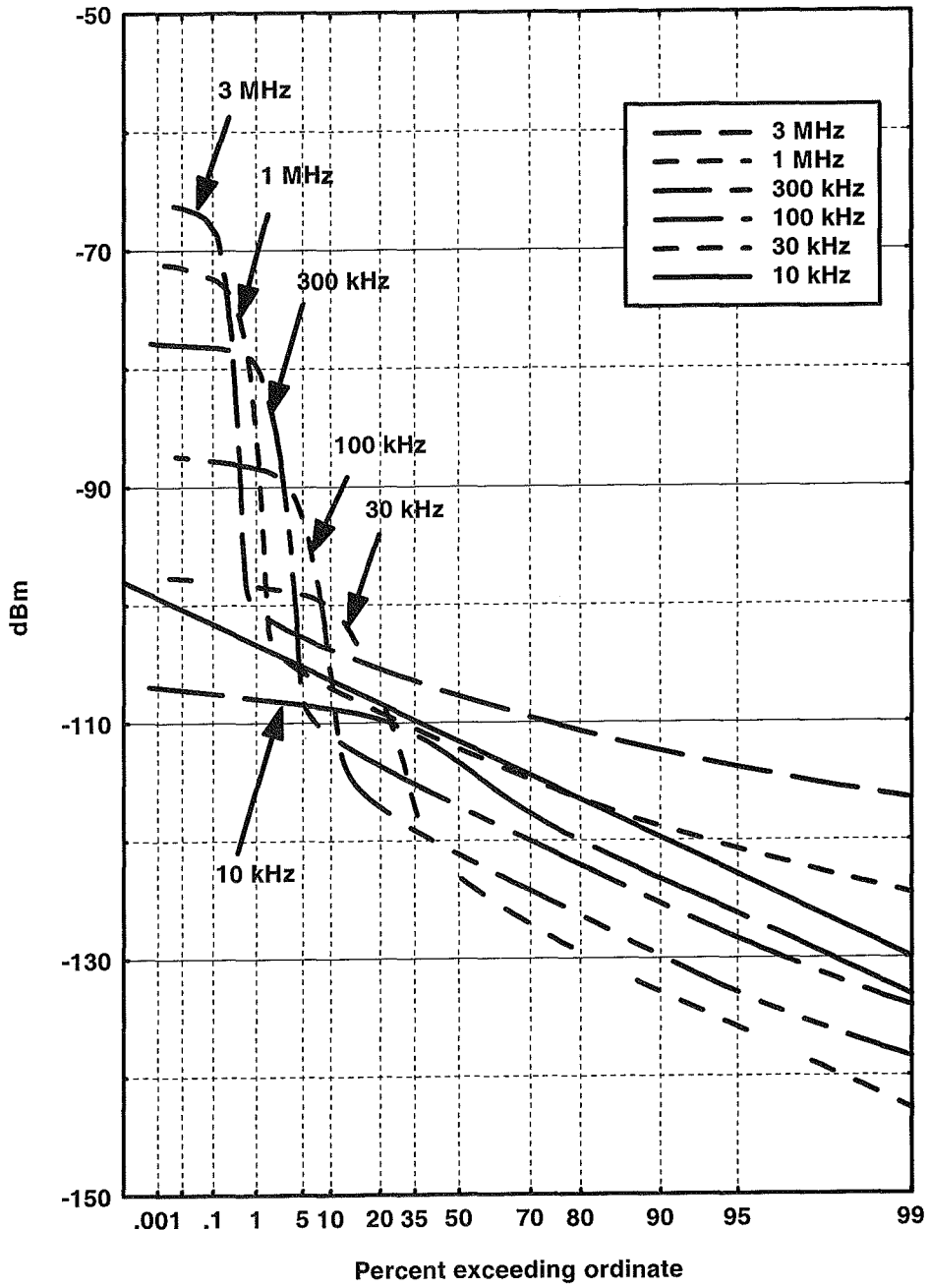

Figure D.A.22. Device A, APDs.

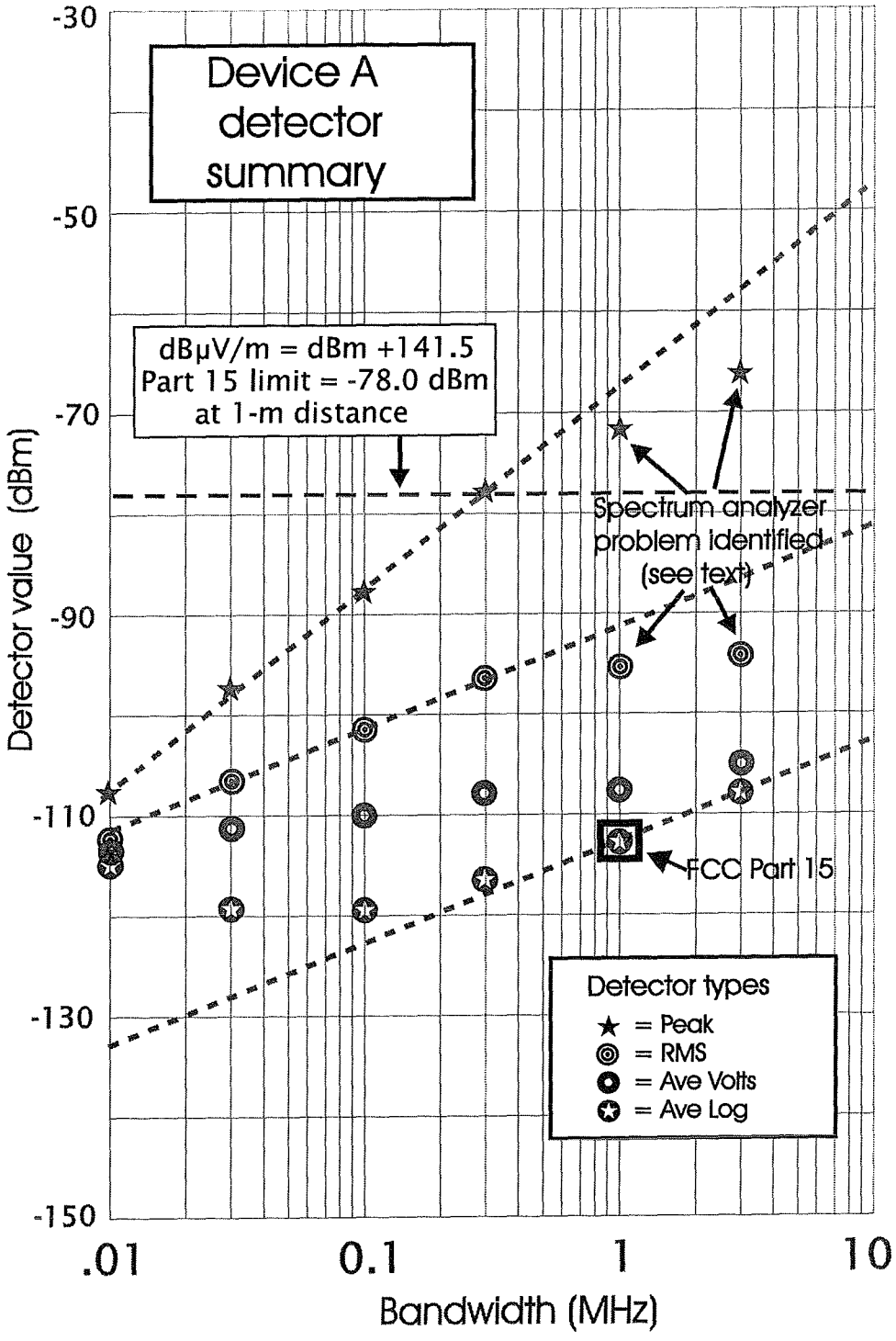

Figure D.A.23. Device A, detector summary.

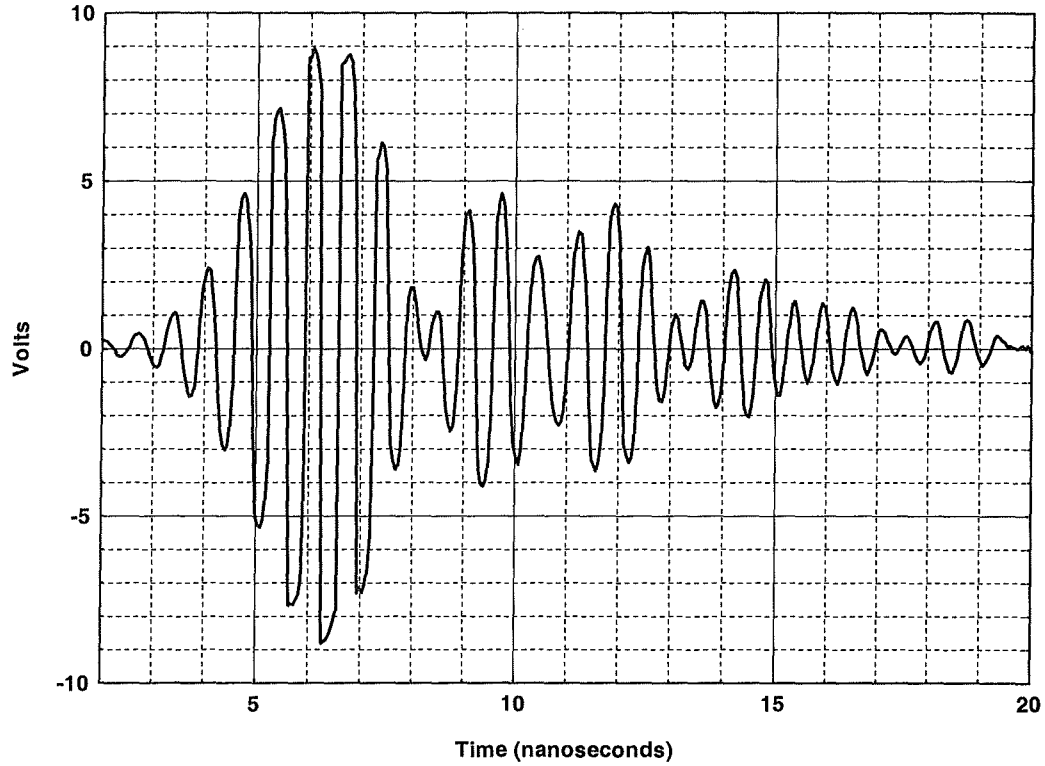

Figure D.B.1. Device B, conducted time-domain waveform.

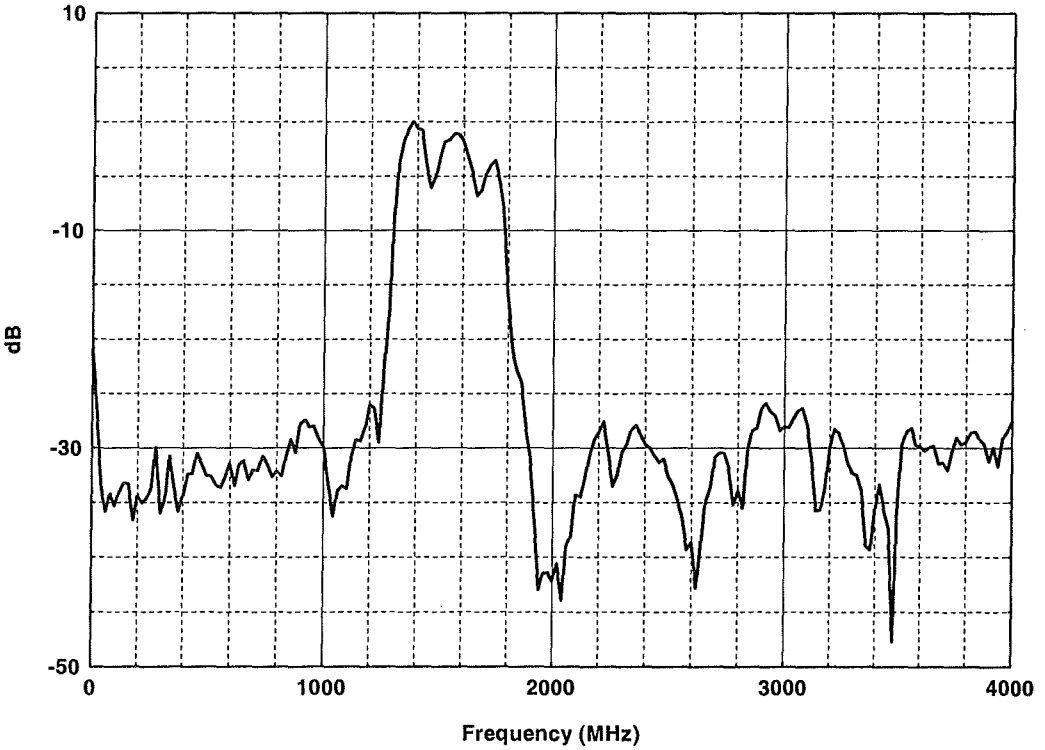

Figure D.B.2. Device B, conducted power spectrum, $\Delta f = 20$ MHz.

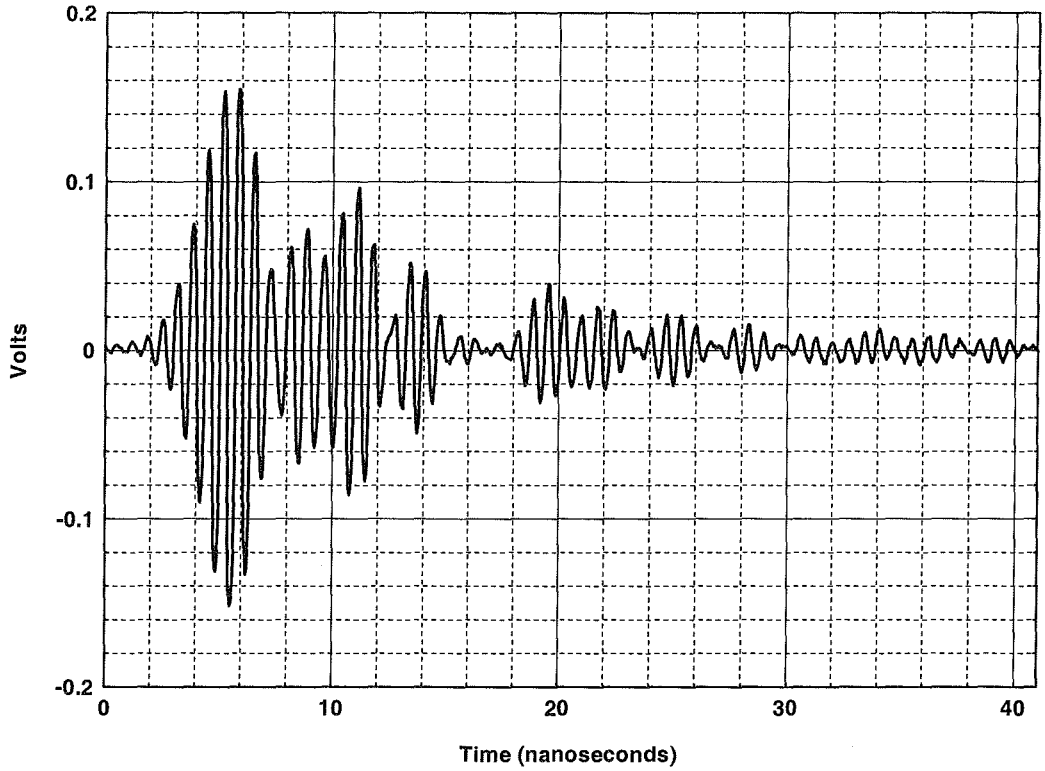

Figure D.B.3. Device B, radiated time-domain waveform.

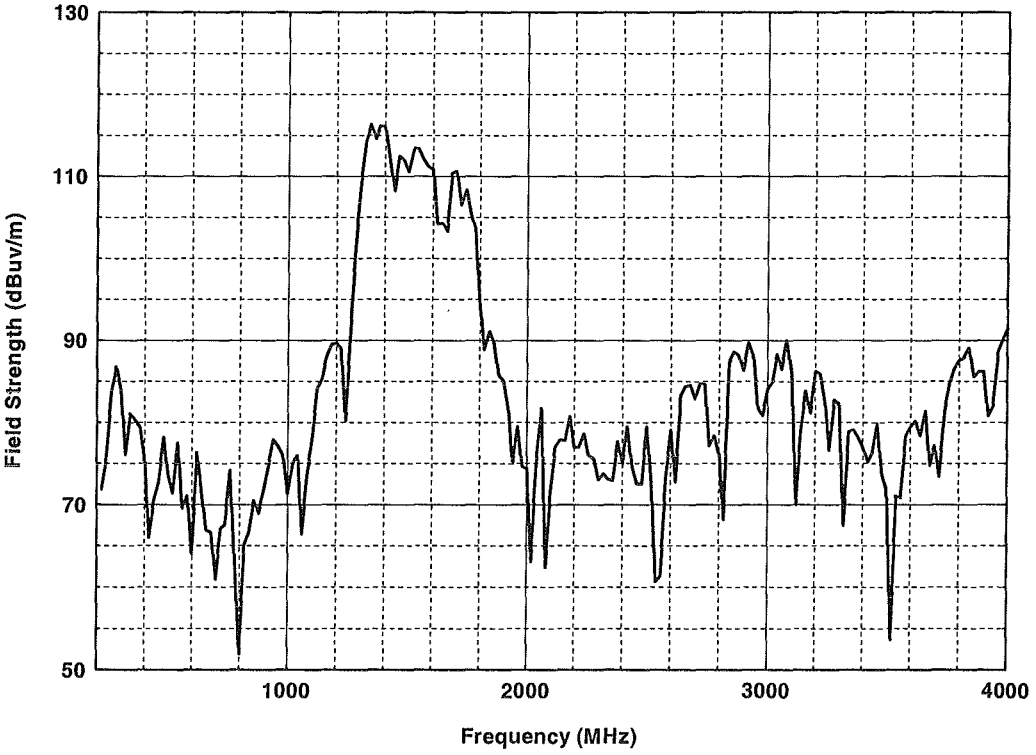

Figure D.B.4. Device B, radiated peak field strength at 1 m, $\Delta f = 20$ MHz.

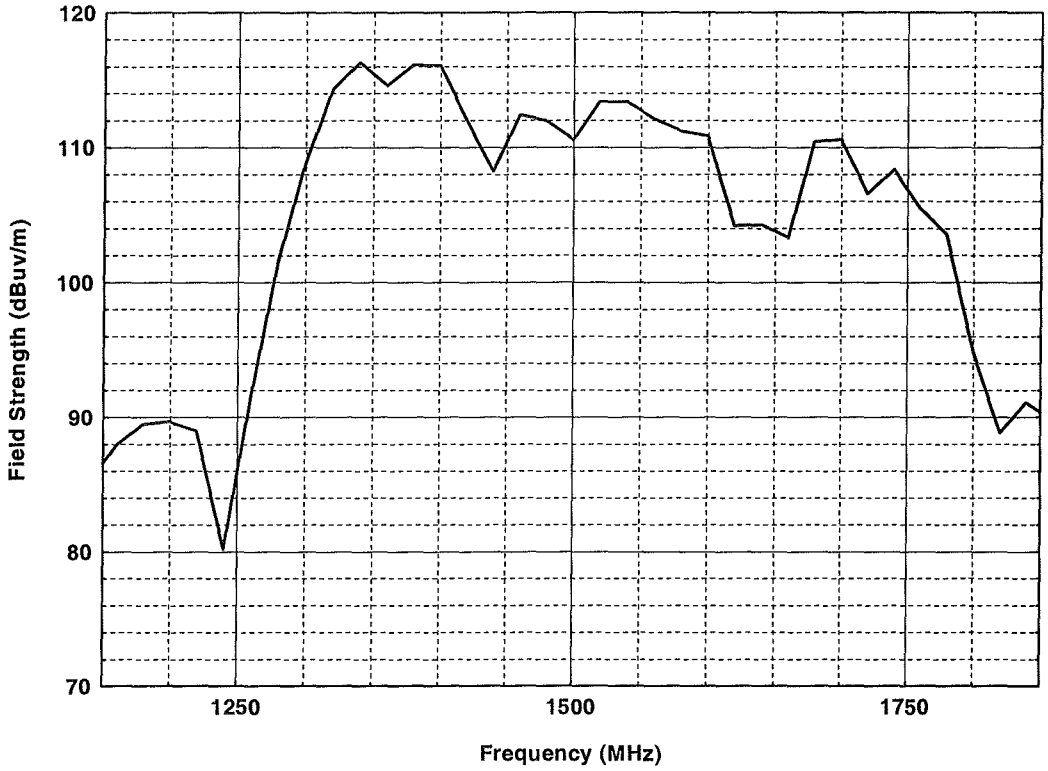

Figure D.B.5. Device B, radiated peak field strength at 1 m, $\Delta f = 20$ MHz.

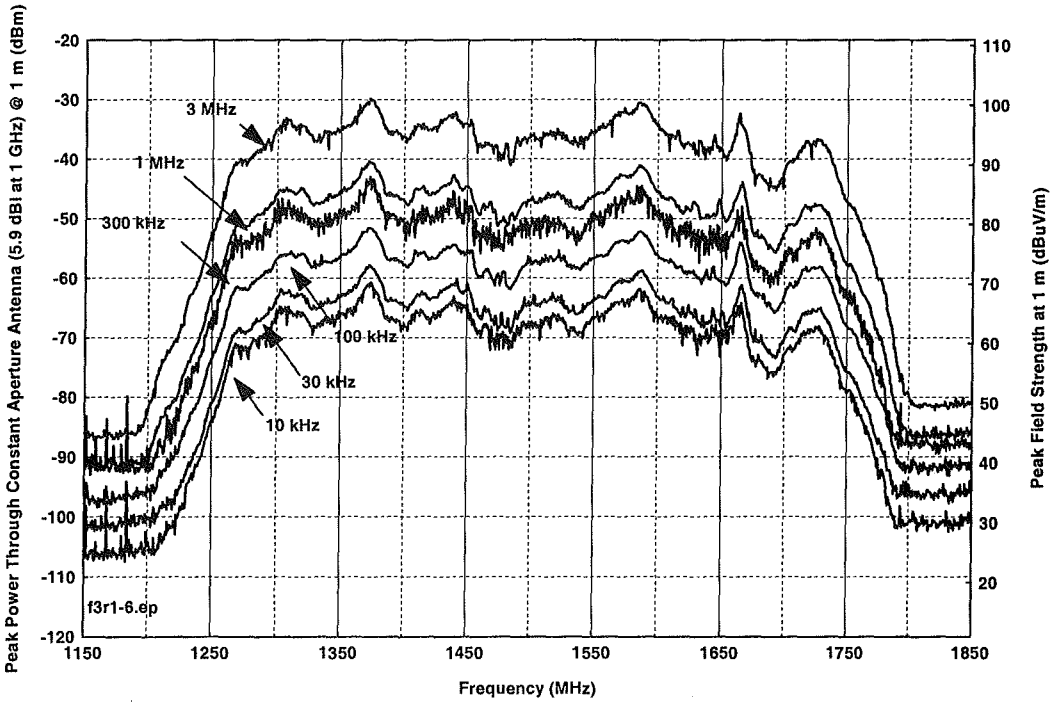

Figure D.B.6. Device B, spectra as a function of bandwidth, 16-kB/s voice mode.

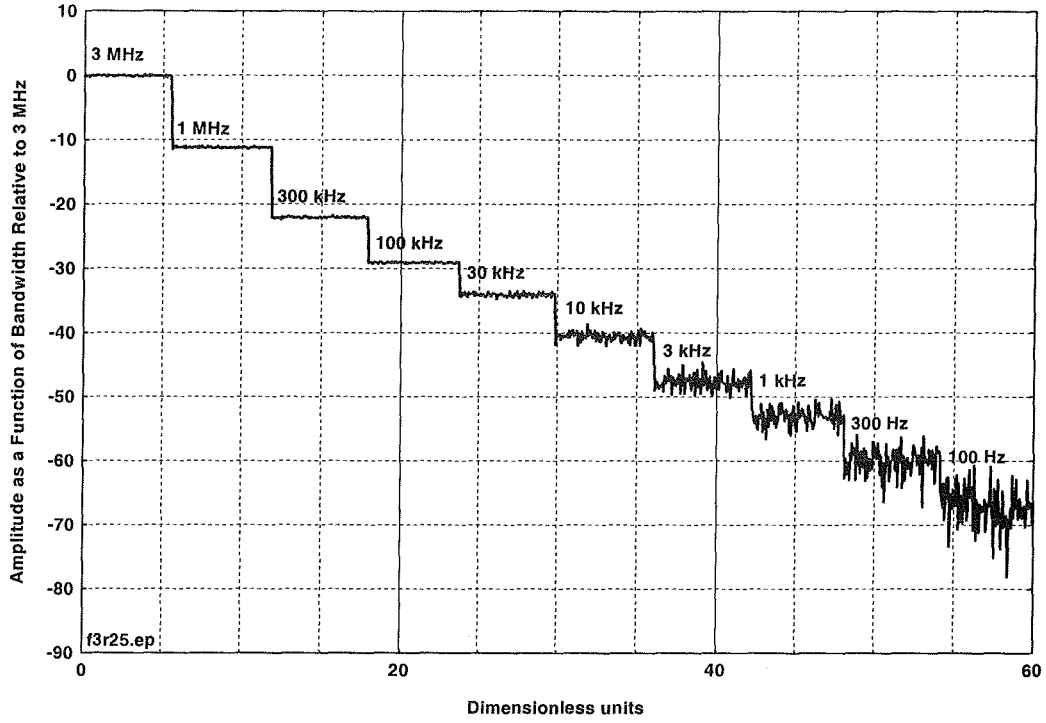

Figure D.B.7. Device B, in 16-kB/sec voice mode, bandwidth progression stairstep.

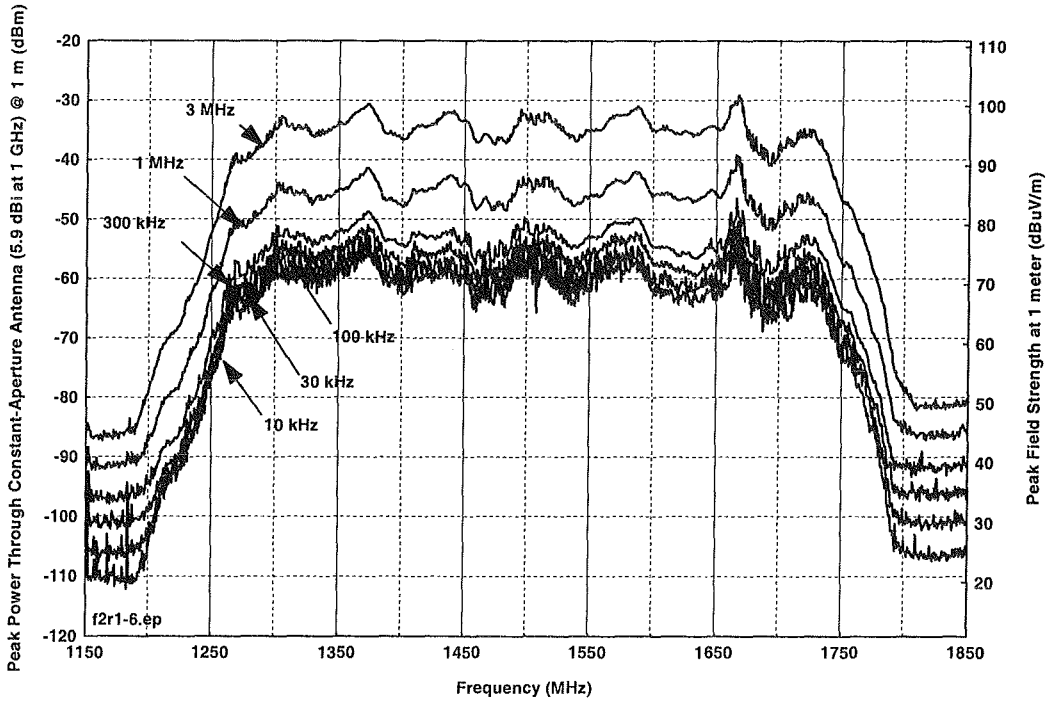

Figure D.B.8. Device B, spectra as a function of bandwidth, 128-kB/sec voice mode.

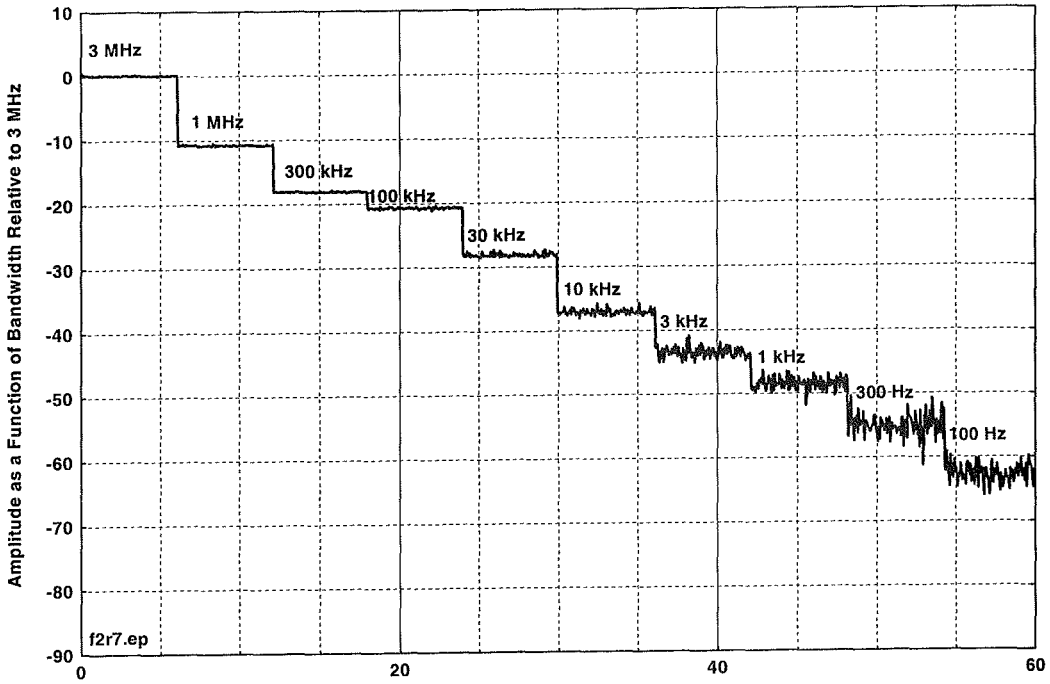

Figure D.B.9. Device B, in 128-kB/sec voice mode, bandwidth progression stairstep.

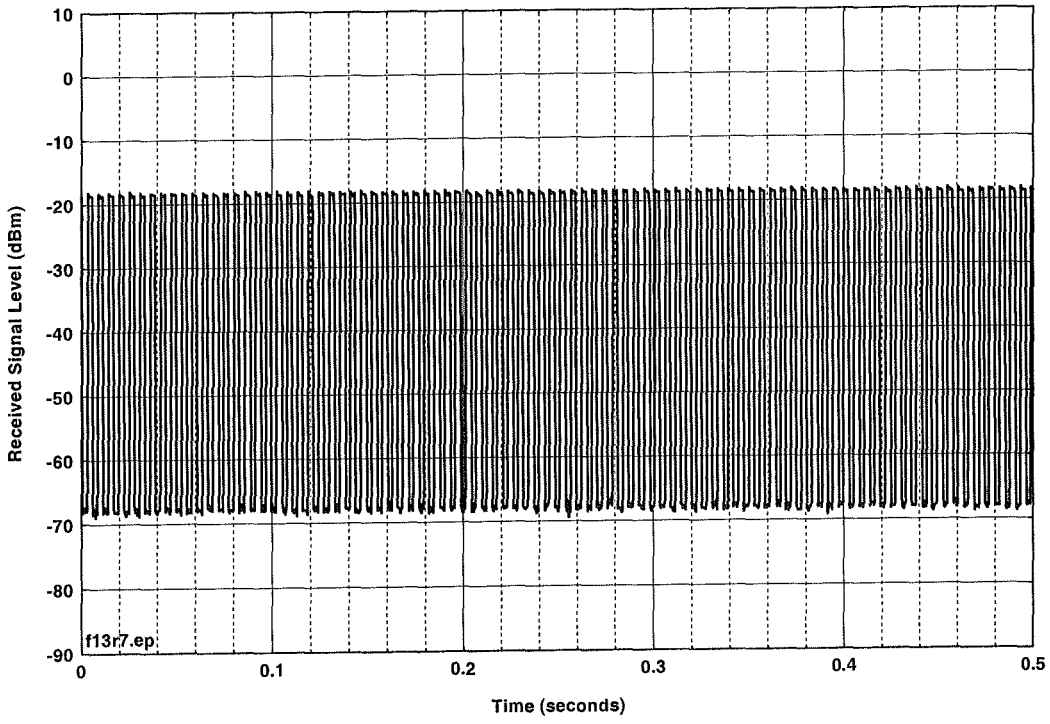

Figure D.B.10. Device B, 0.5 seconds, 128-kBit/sec mode.

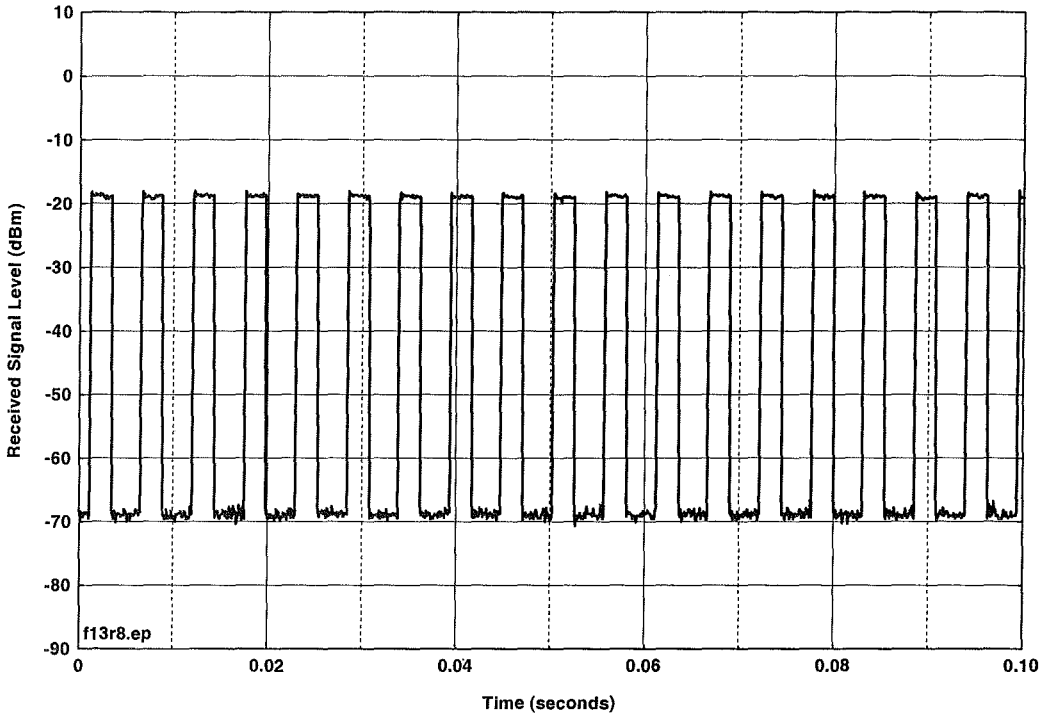

Figure D.B.11. Device B, 128-kBit/sec mode, 0.1 seconds.

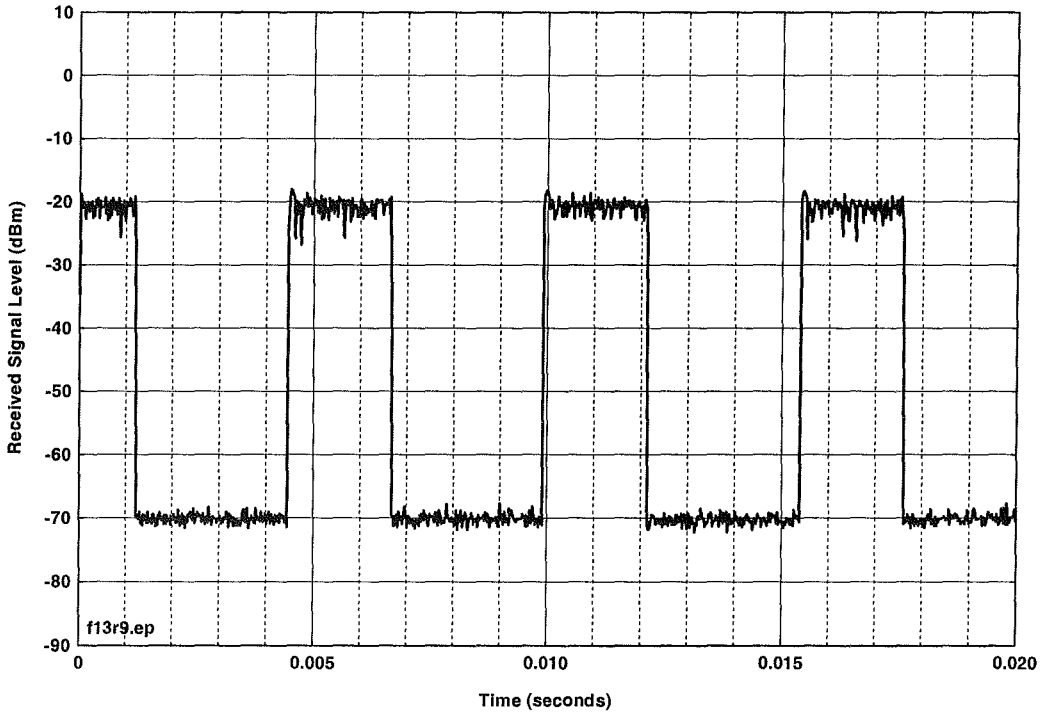

Figure D.B.12. Device B, 128-kBit/second mode, 0.02 seconds.

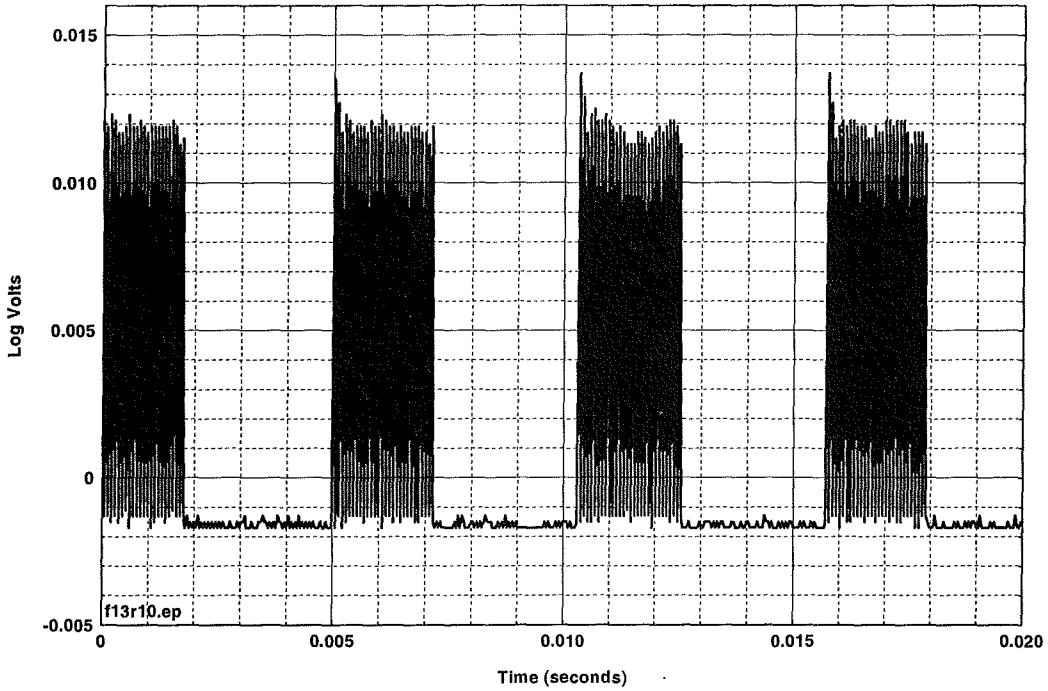

Figure D.B.13. Device B, 128-kBit/second mode, 0.02 seconds, external log detector.

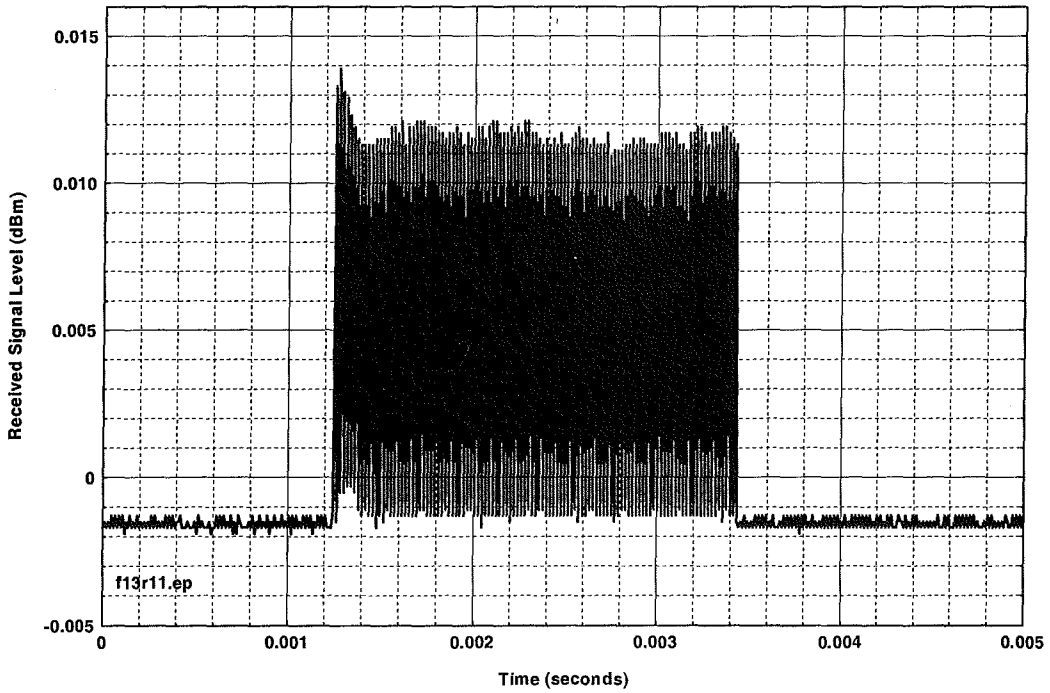

Figure D.B.14. Device B, 128-kBit/second mode, 0.005 seconds, external detector.

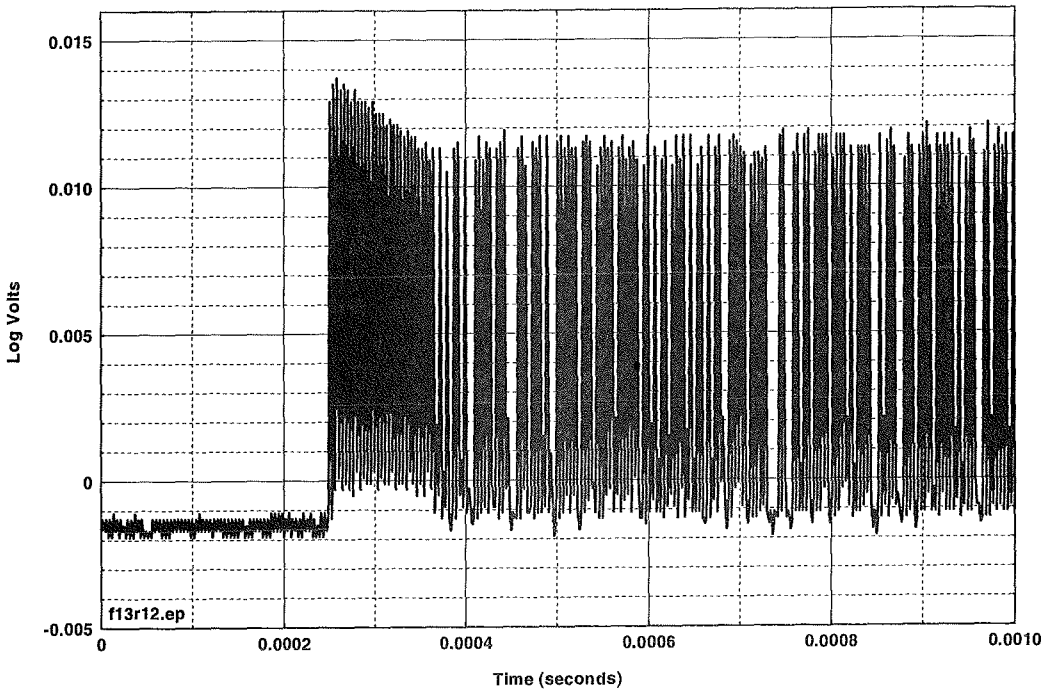

Figure D.B.15. Device B, 128-kBit/second mode, 0.001 seconds, external log detector.

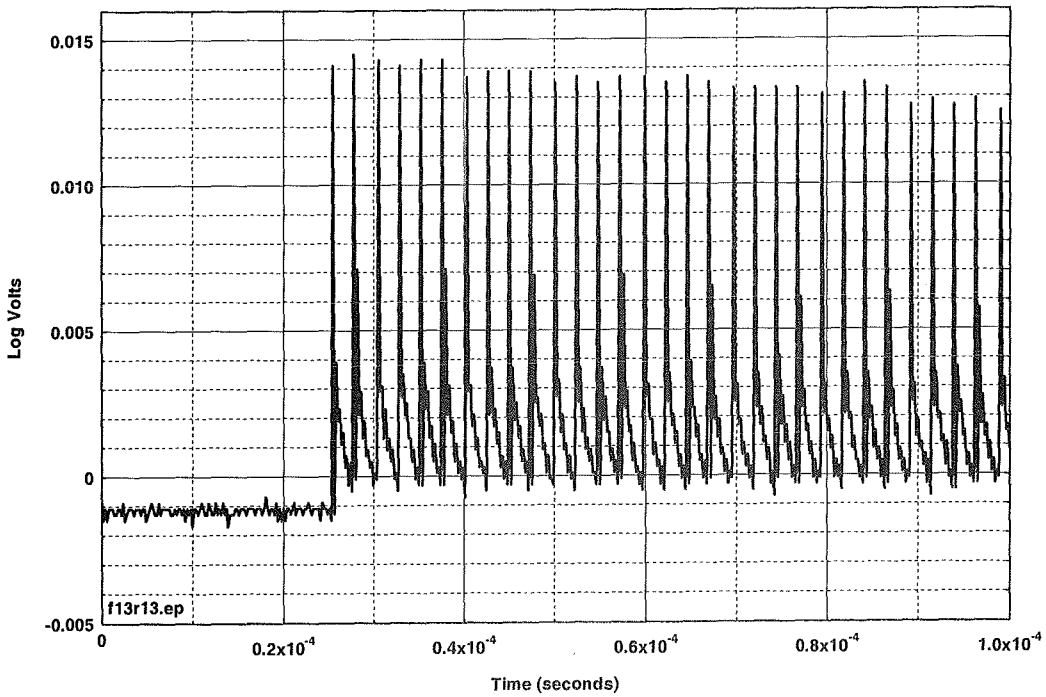

Figure D.B.16. Device B, 128-kBit/second mode, 0.1 msec, external log detector.

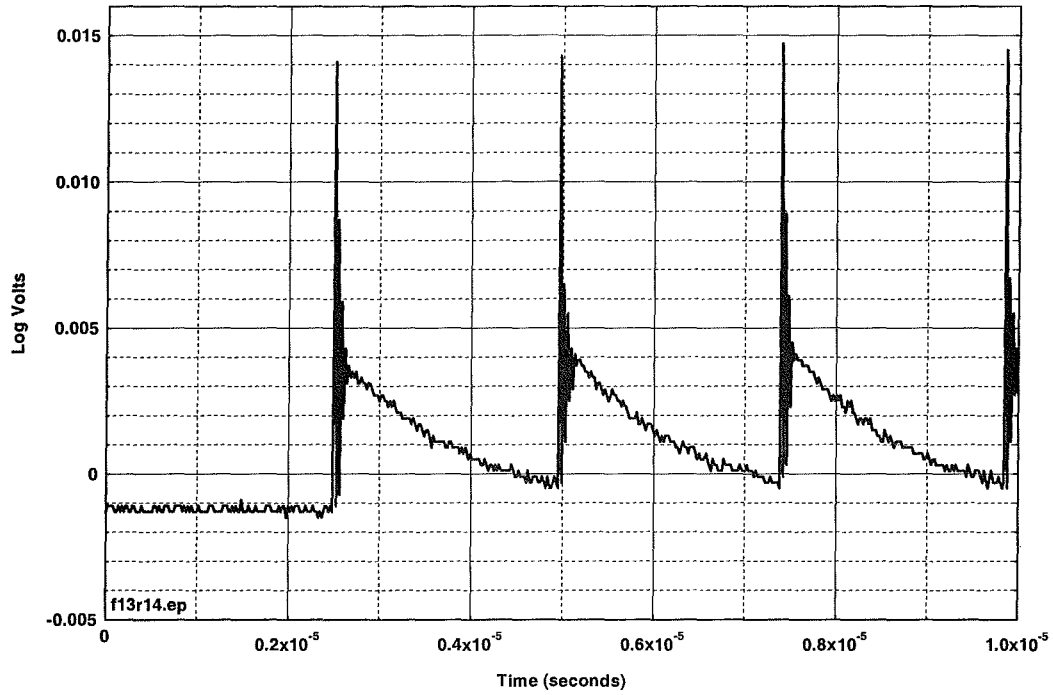

Figure D.B.17. Device B, 128-kBit/second mode, 10 us, external log detector.

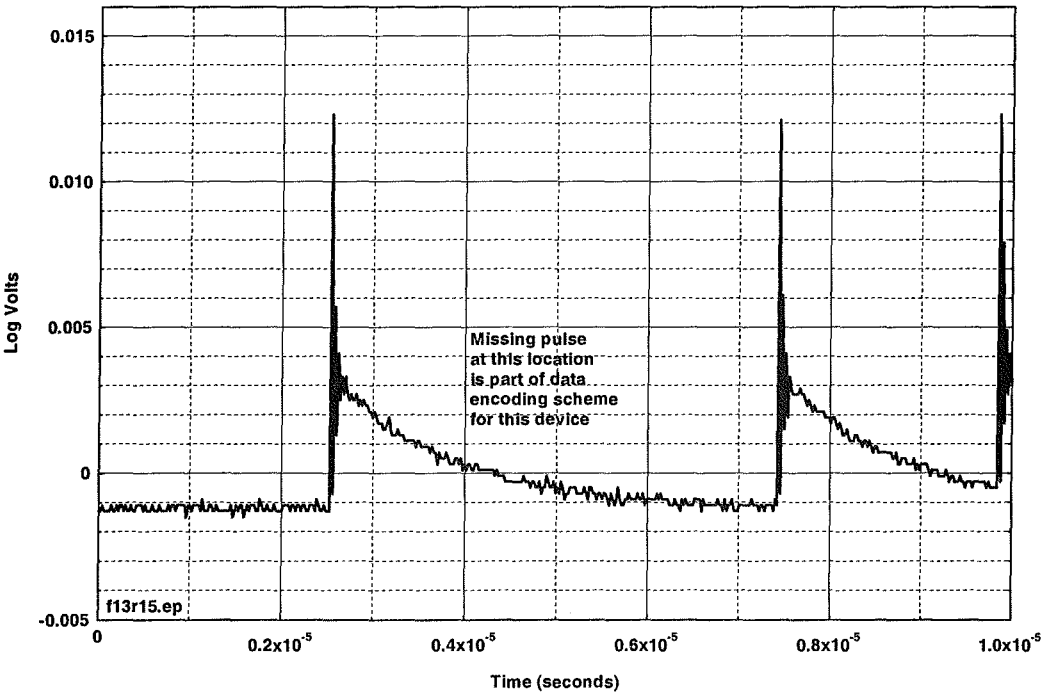

Figure D.B.18. Device B, 128-kBit/second mode, 10 us, external log detector.

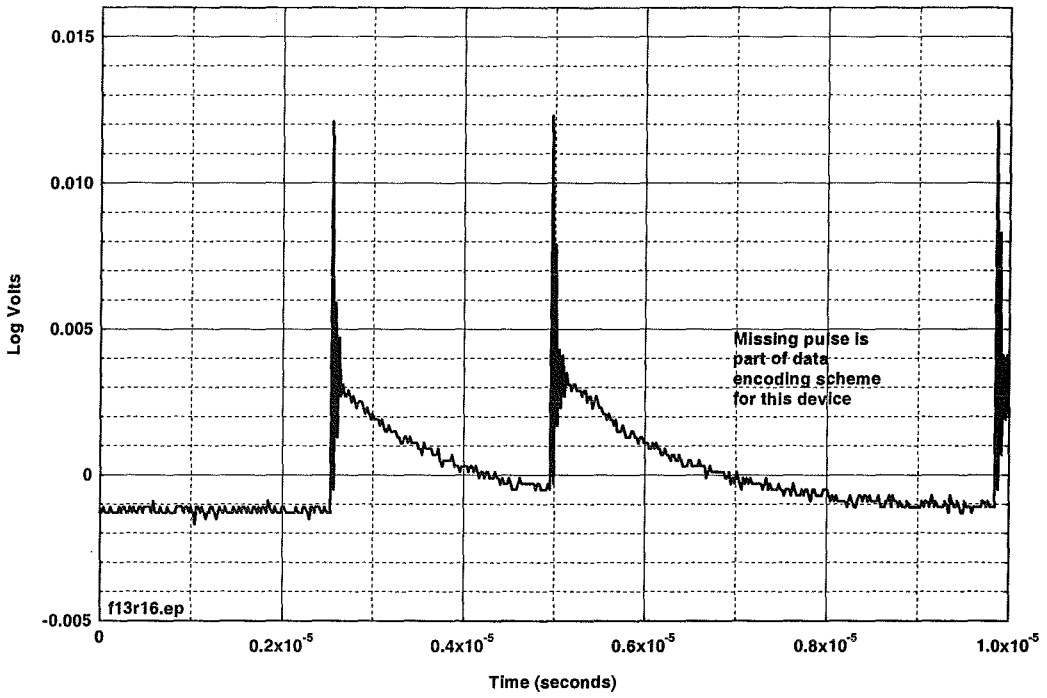

Figure D.B.19. Device B, 128-kBit/second mode, 10 us, external log detector.

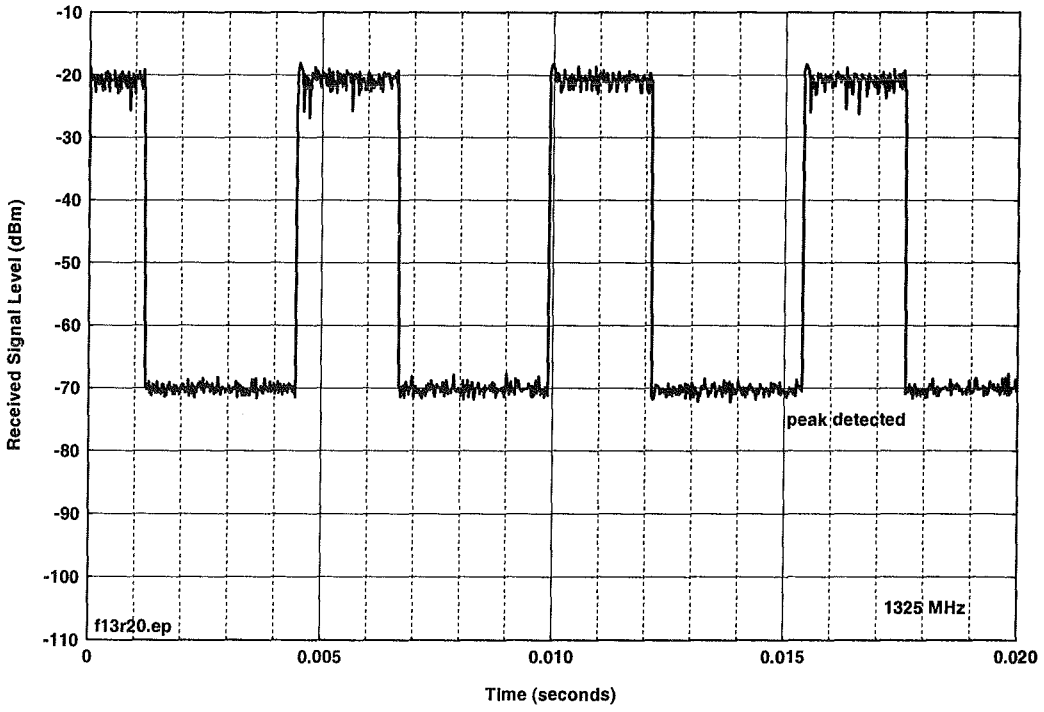

Figure D.B.20. Device B, 128-kBit/second mode, 3-MHz IF bandwidth.

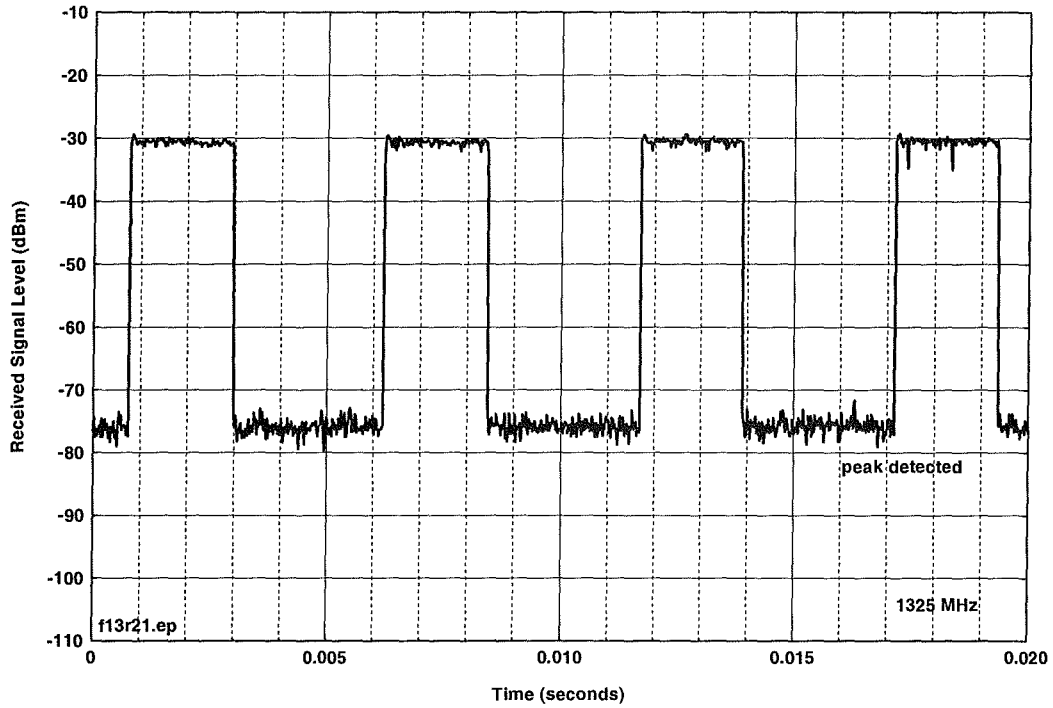

Figure D.B.21. Device B, 128-kBit/second mode, 1-MHz IF bandwidth.

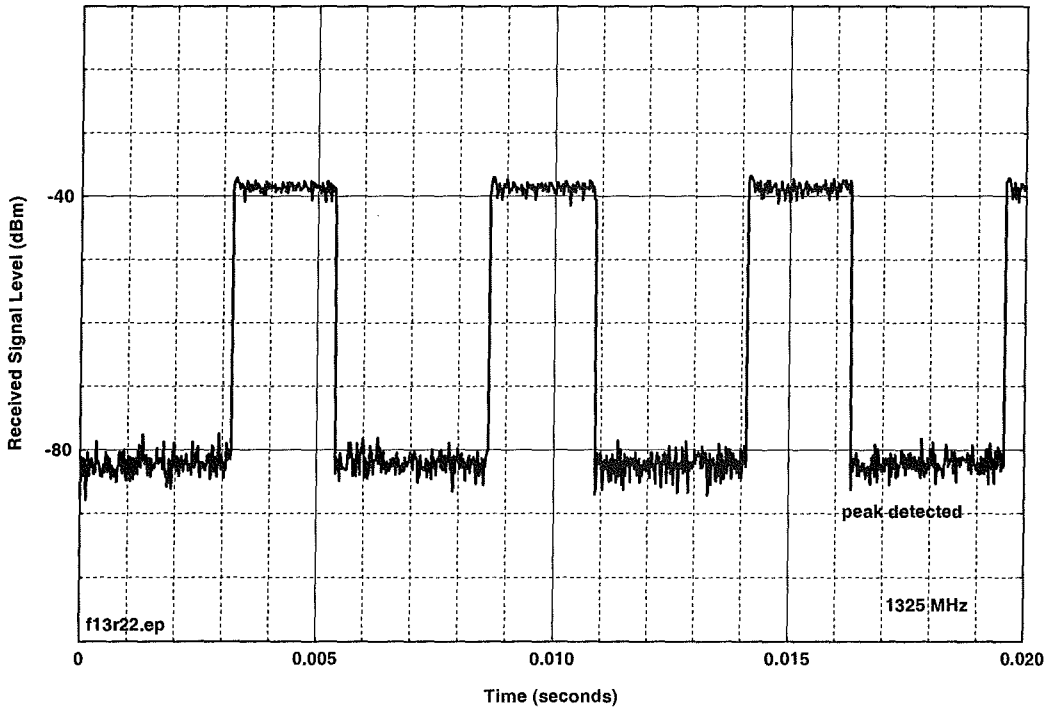

Figure D.B.22. Device B, 128-kBit/second mode, 300-kHz IF bandwidth.

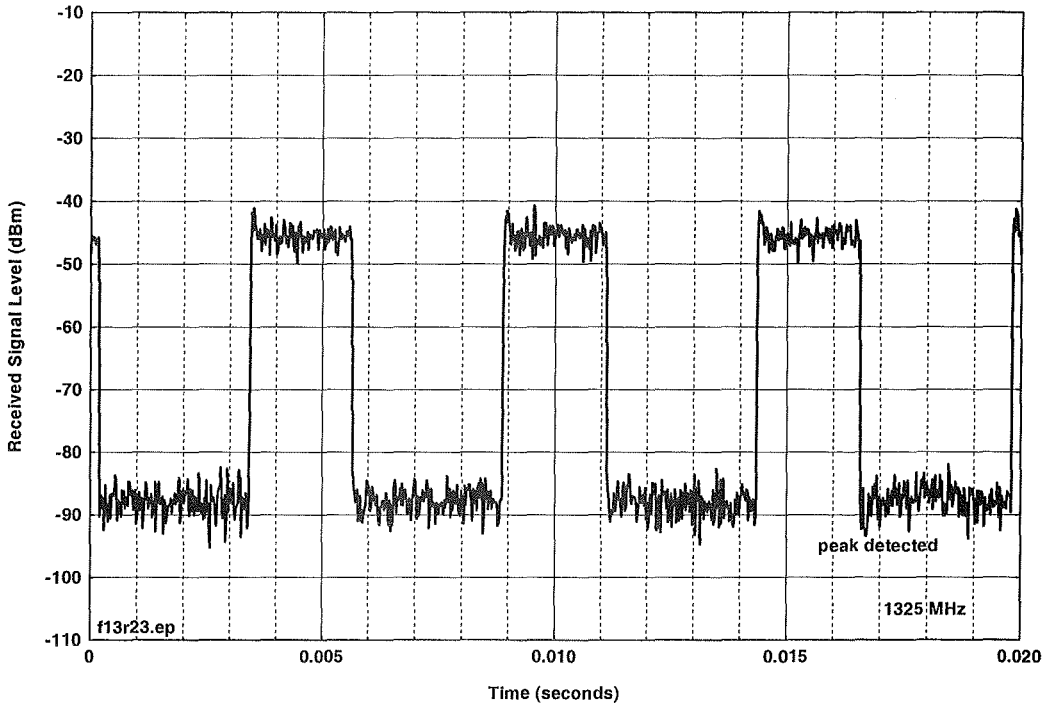

Figure D.B.23. Device B, 128-kBit/second mode, 100-kHz IF bandwidth.

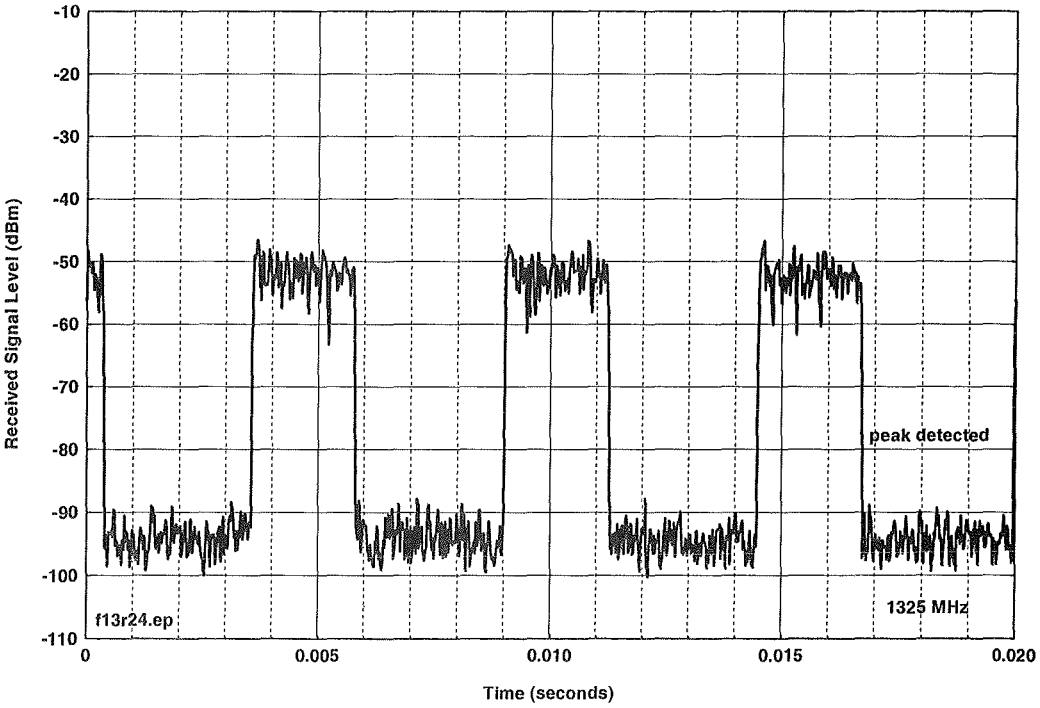

Figure D.B.24. Device B, 128-kBit/second mode, 30-kHz IF bandwidth.

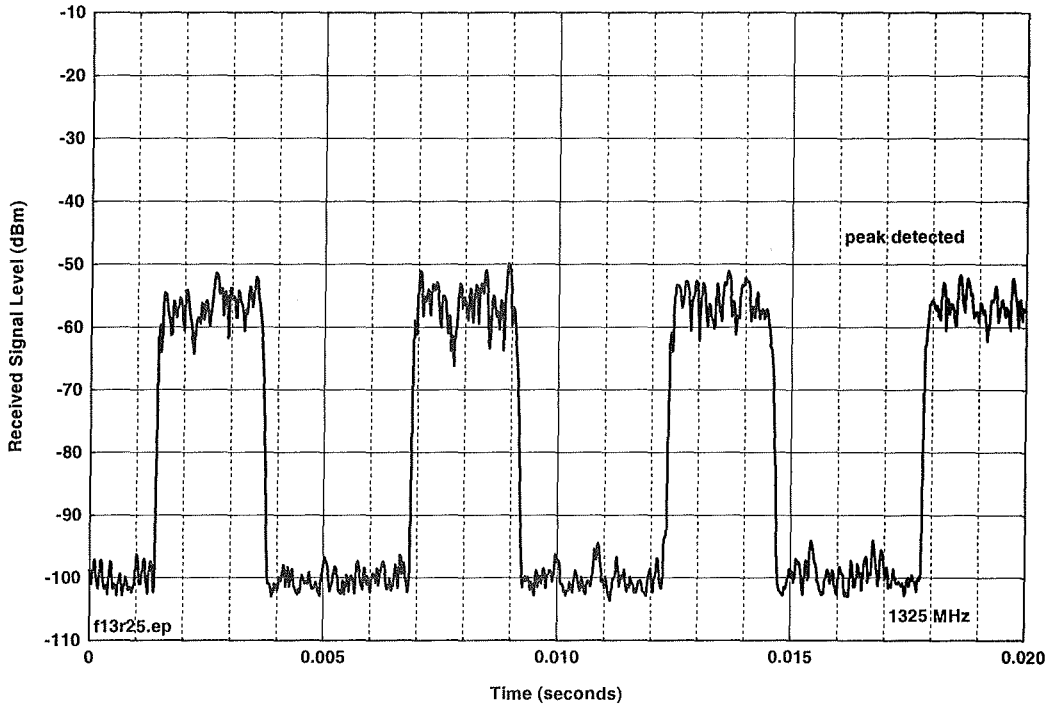

Figure D.B.25. Device B, 128-kBit/second mode, 10-kHz IF bandwidth.

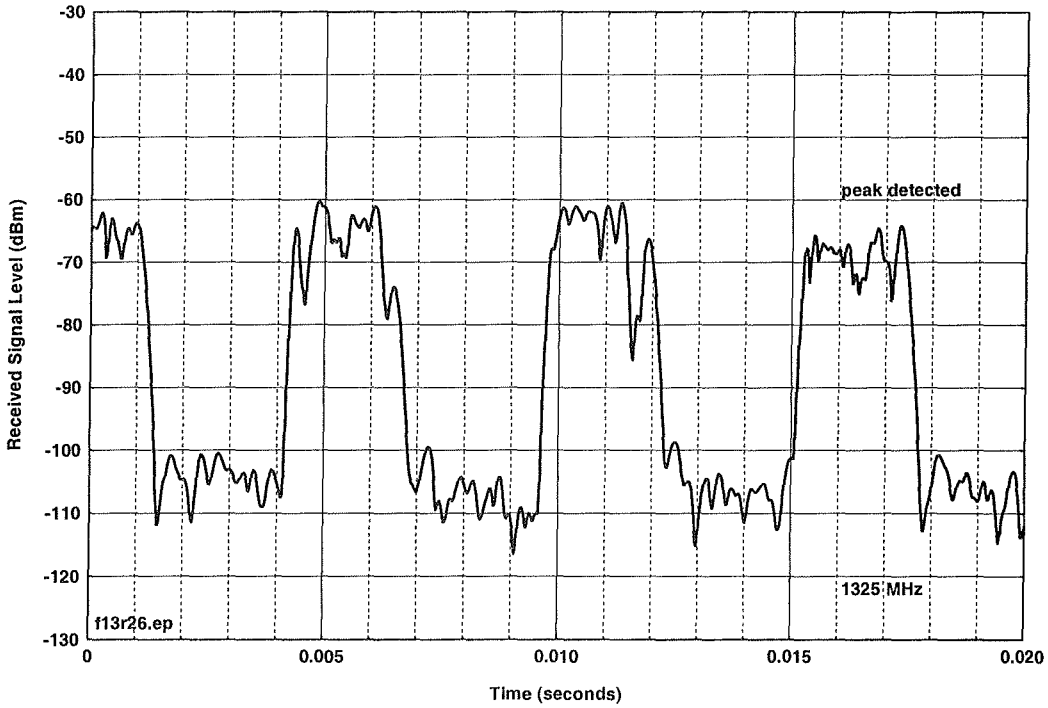

Figure D.B.26. Device B, 128-kBit/second mode, 3-kHz IF bandwidth.

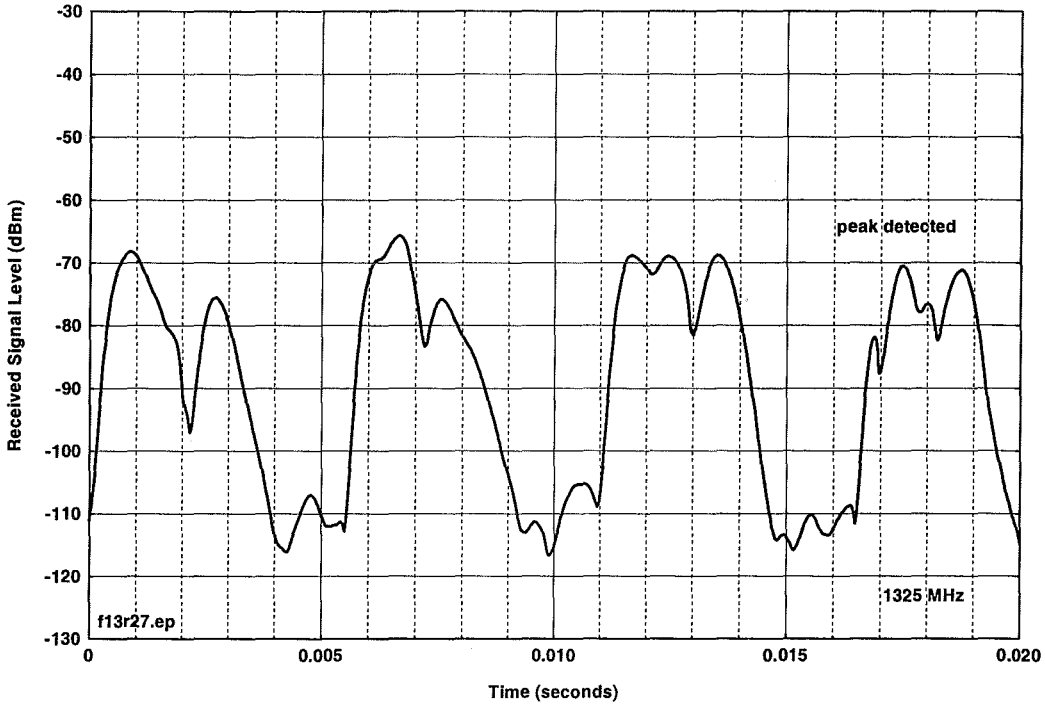

Figure D.B.27. Device B, 128-kBit/second mode, 1-kHz IF bandwidth.

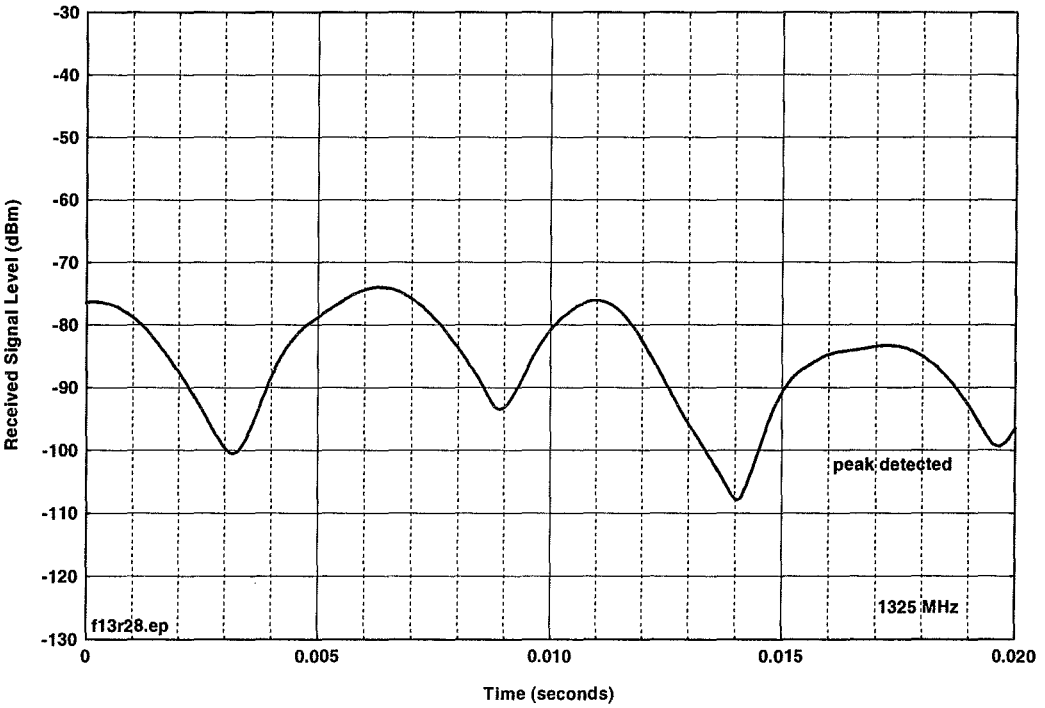

Figure D.B.28. Device B, 128-kBit/second mode, 300-Hz IF bandwidth.

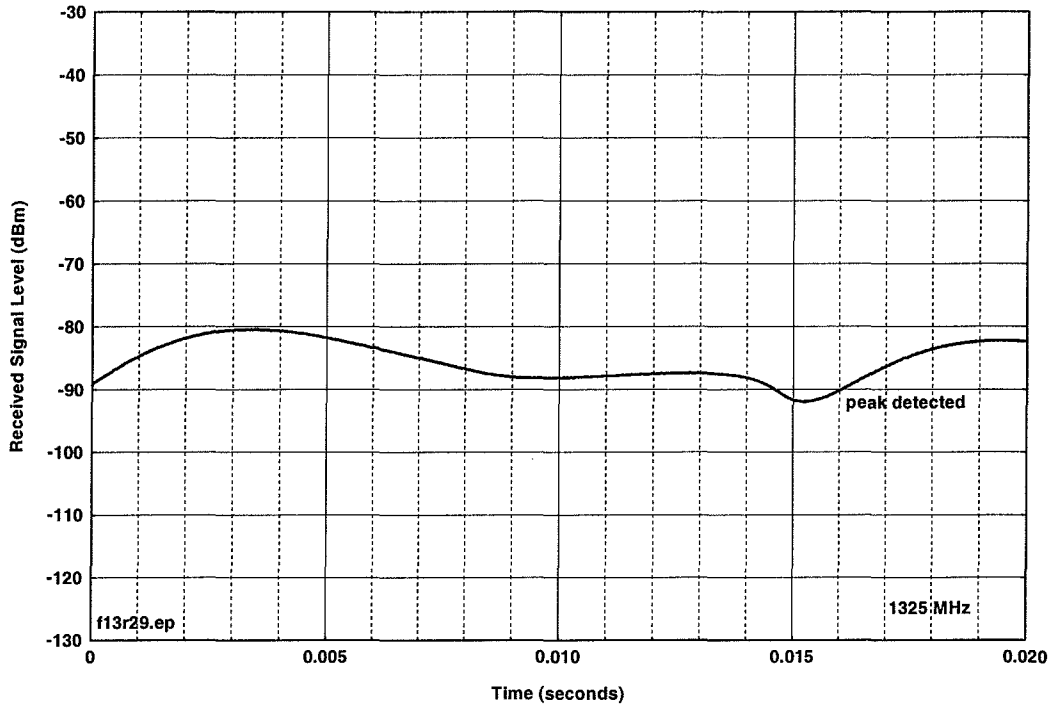

Figure D.B.29. Device B, 128-kBit/second mode, 100-Hz IF bandwidth.

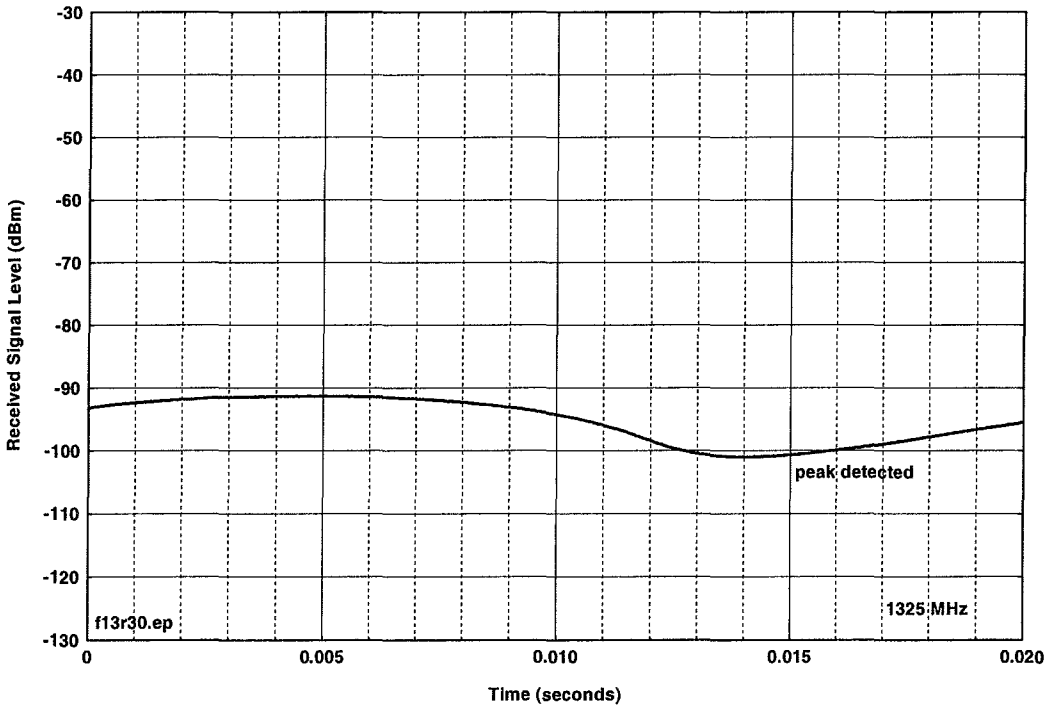

Figure D.B.30. Device B, 128-kBit/second mode, 30-Hz IF bandwidth.

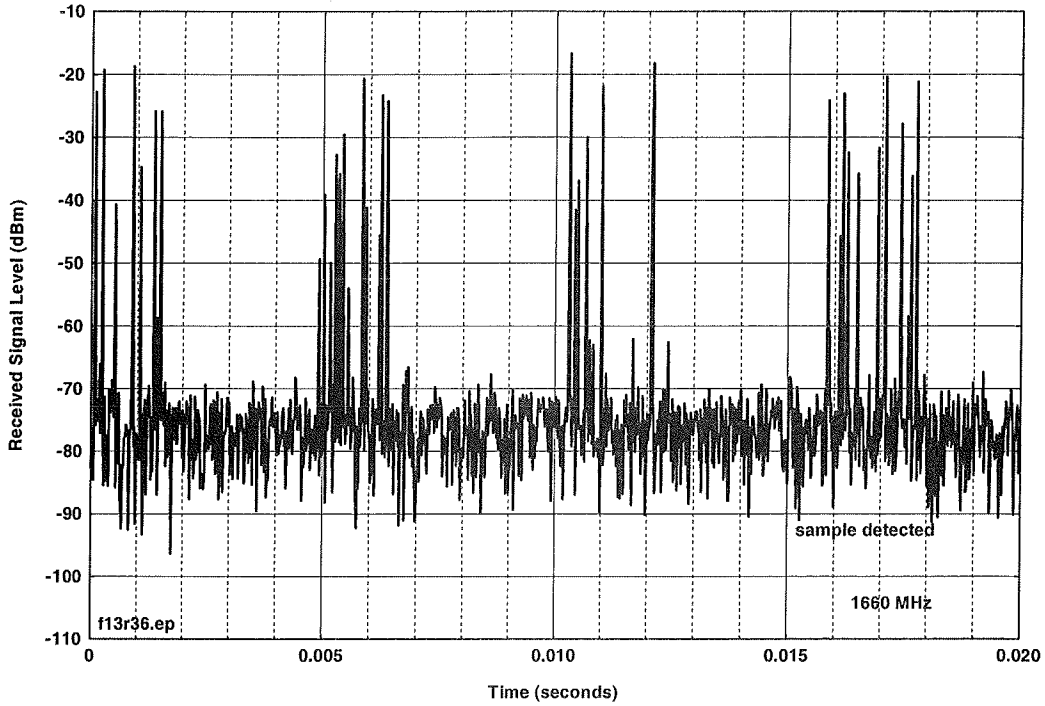

Figure D.B.31. Device B, 128-kBit/second mode, 3-MHz video bandwidth.

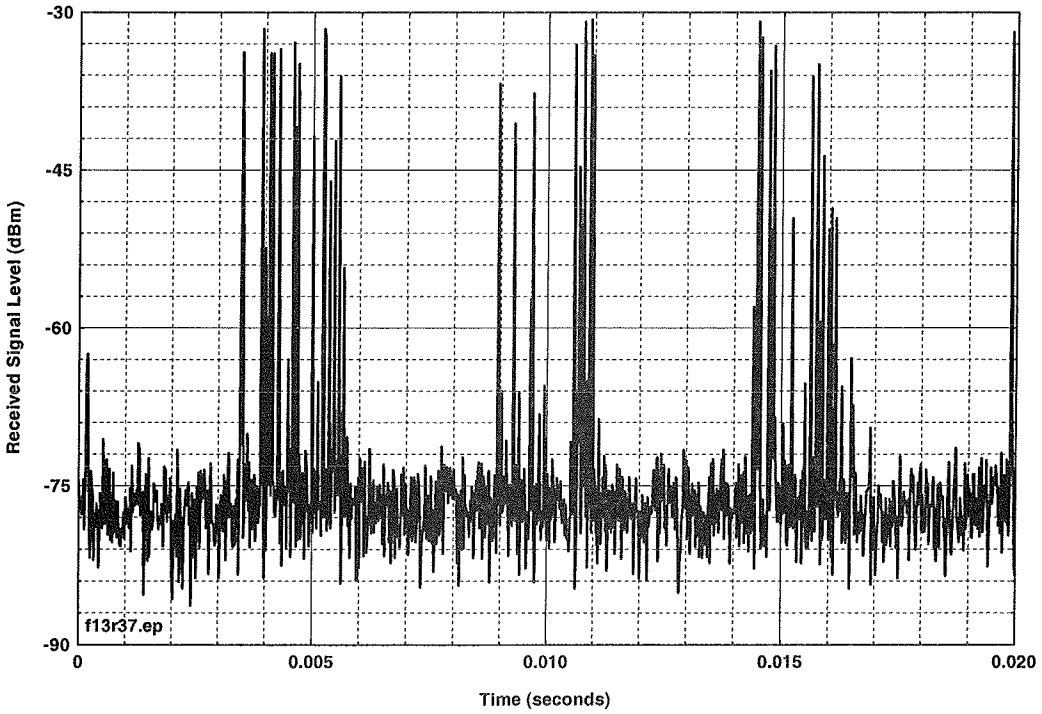

Figure D.B.32. Device B, 128-kBit/second mode, 1-MHz video bandwidth.

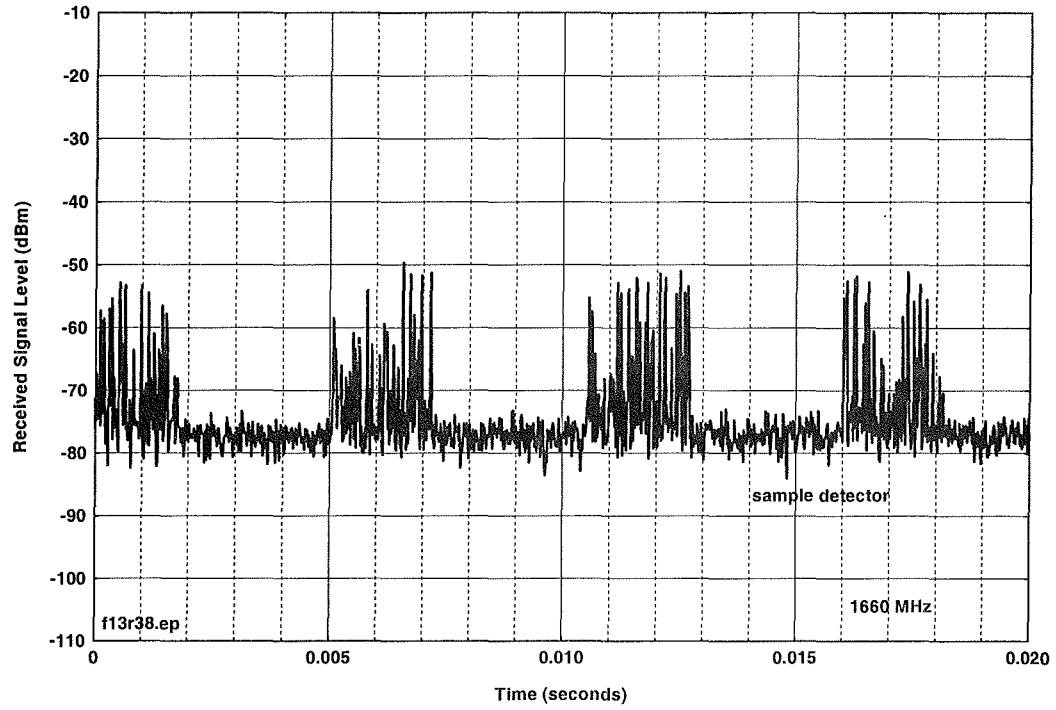

Figure D.B.33. Device B, 128-kBit/second mode, 300-kHz video bandwidth.

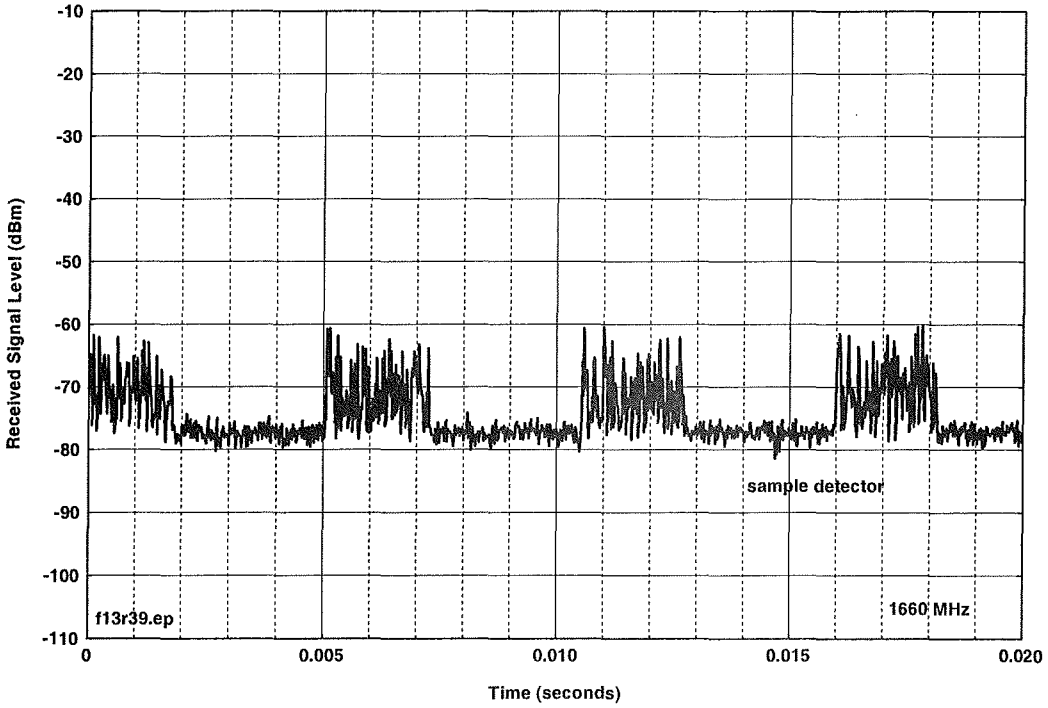

Figure D.B.34. Device B, 128-kBit/second mode, 100-kHz video bandwidth.

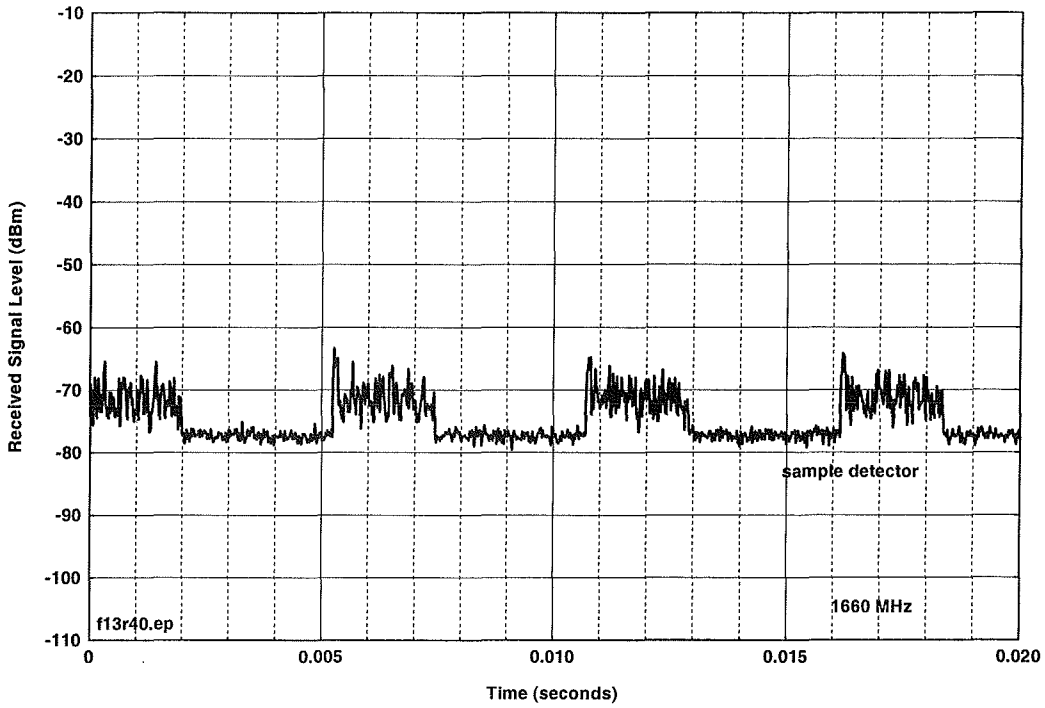

Figure D.B.35. Device B, 128-kBit/second mode, 30-kHz video bandwidth.

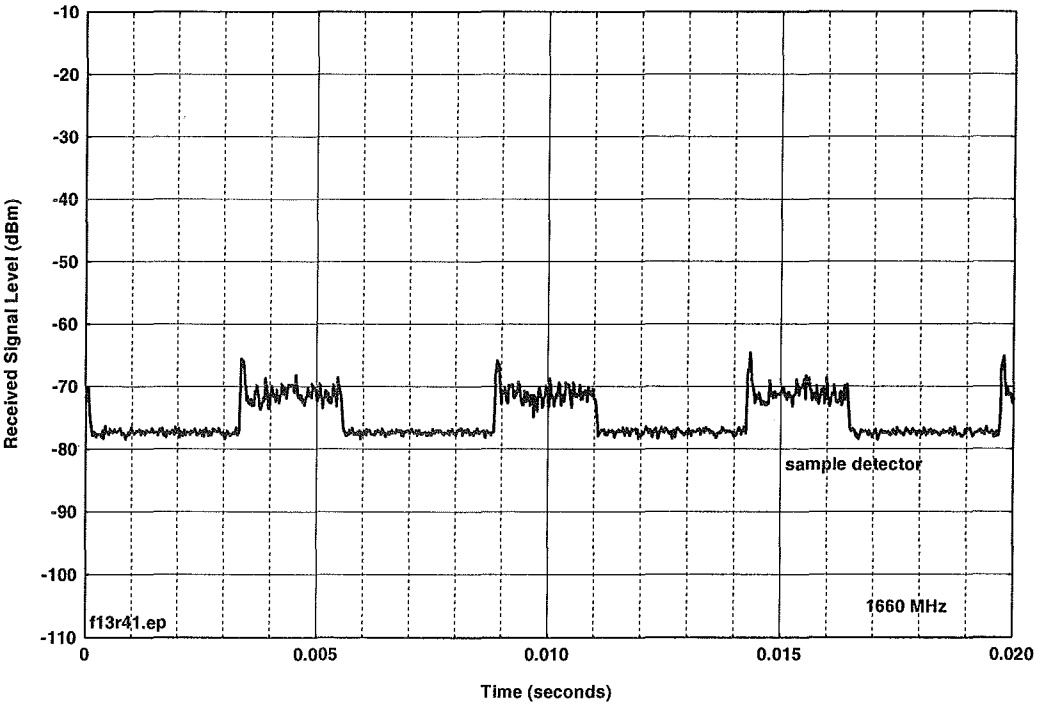

Figure D.B.36. Device B, 128-kBit/second mode, 10-kHz video bandwidth.

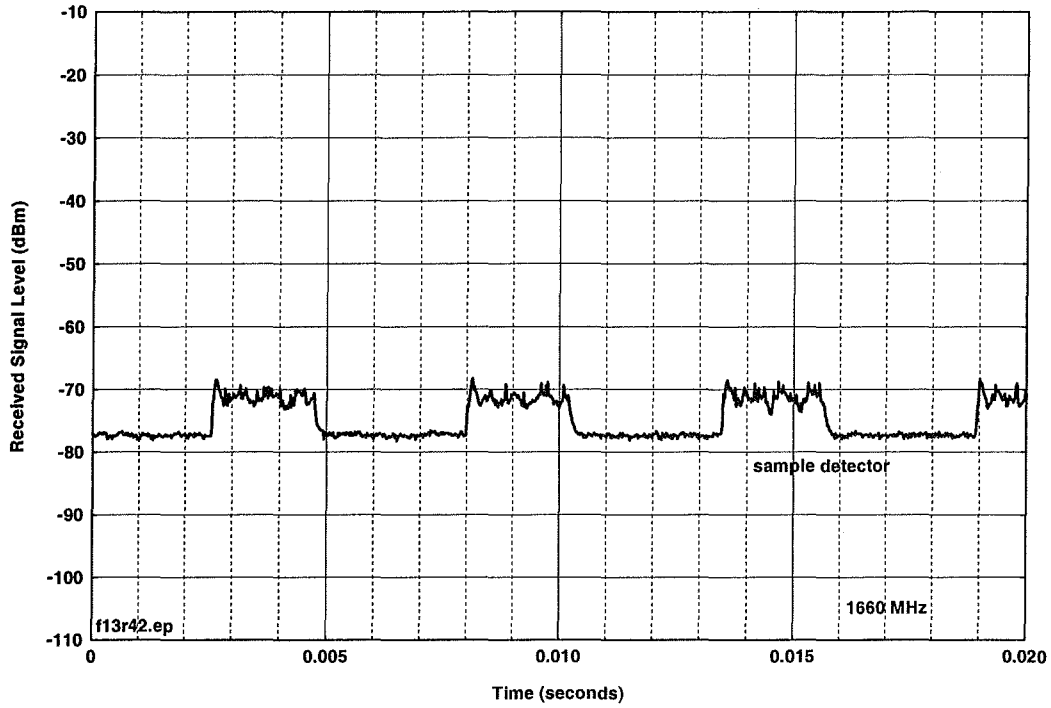

Figure D.B.37. Device B, 128-kBit/second mode, 3-kHz video bandwidth.

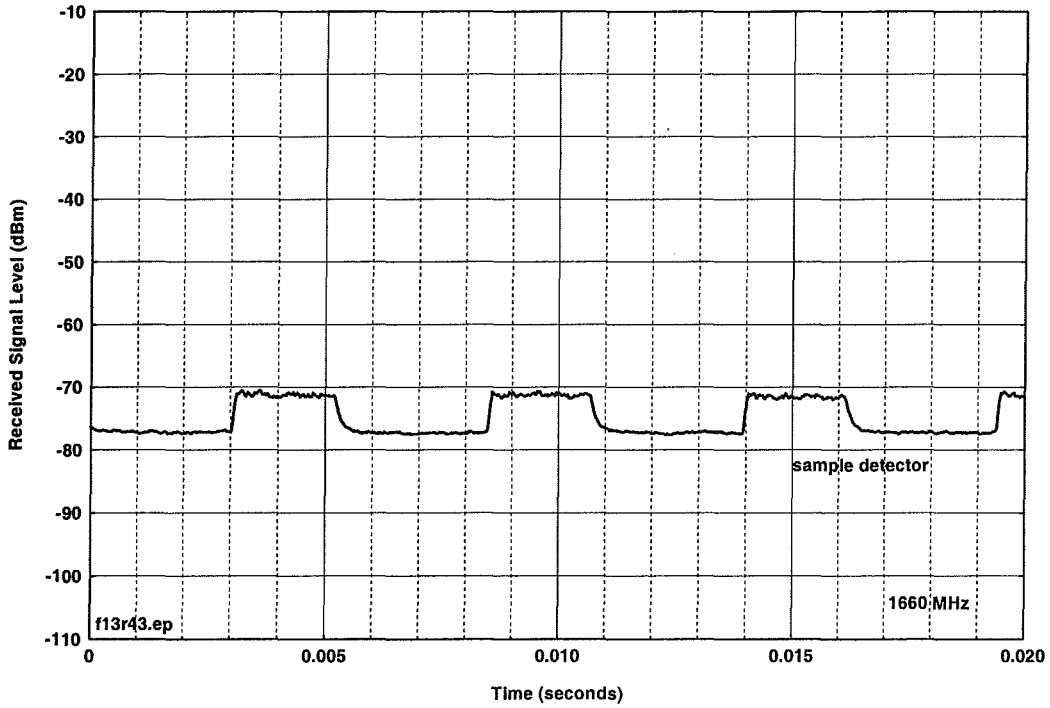

Figure D.B.38. Device B, 128-kBit/sec mode, 1-kHz video bandwidth.

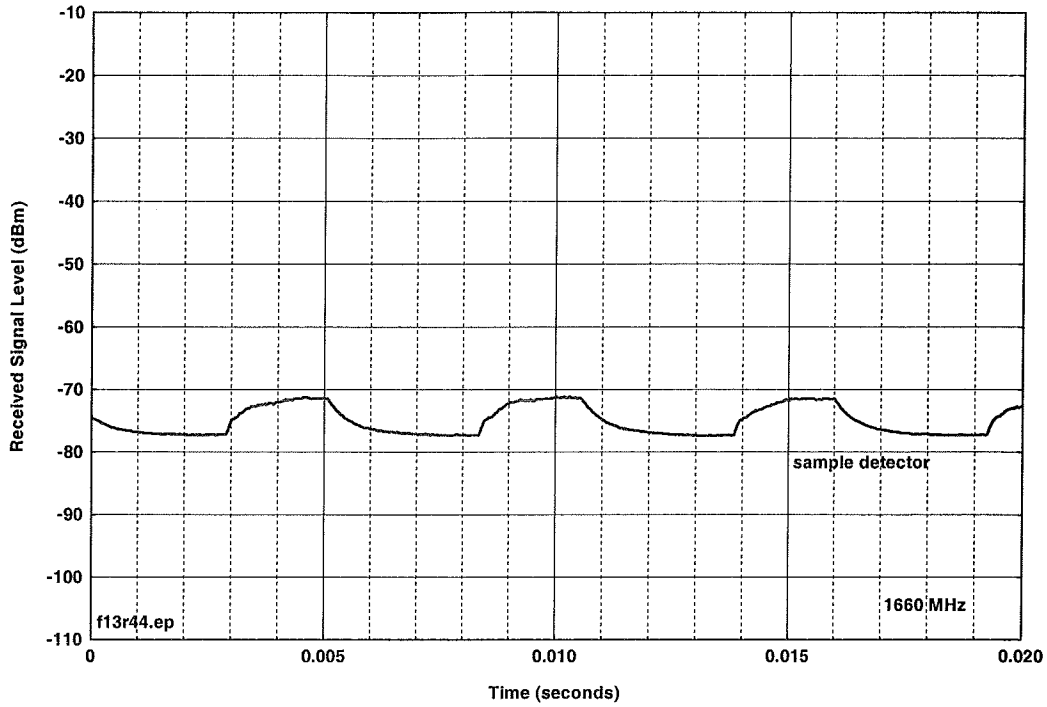

Figure D.B.39. Device B, 128-kBit/second mode, 300-Hz video bandwidth.

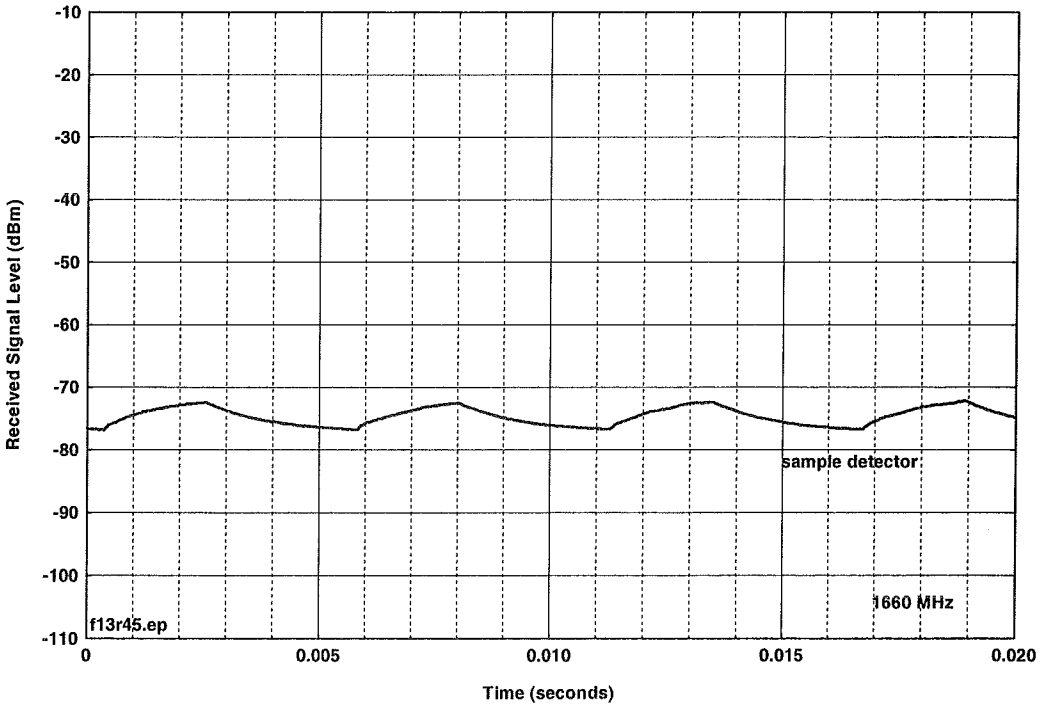

Figure D.B.40. Device B, 128-kBit/second mode, 100-Hz video bandwidth.

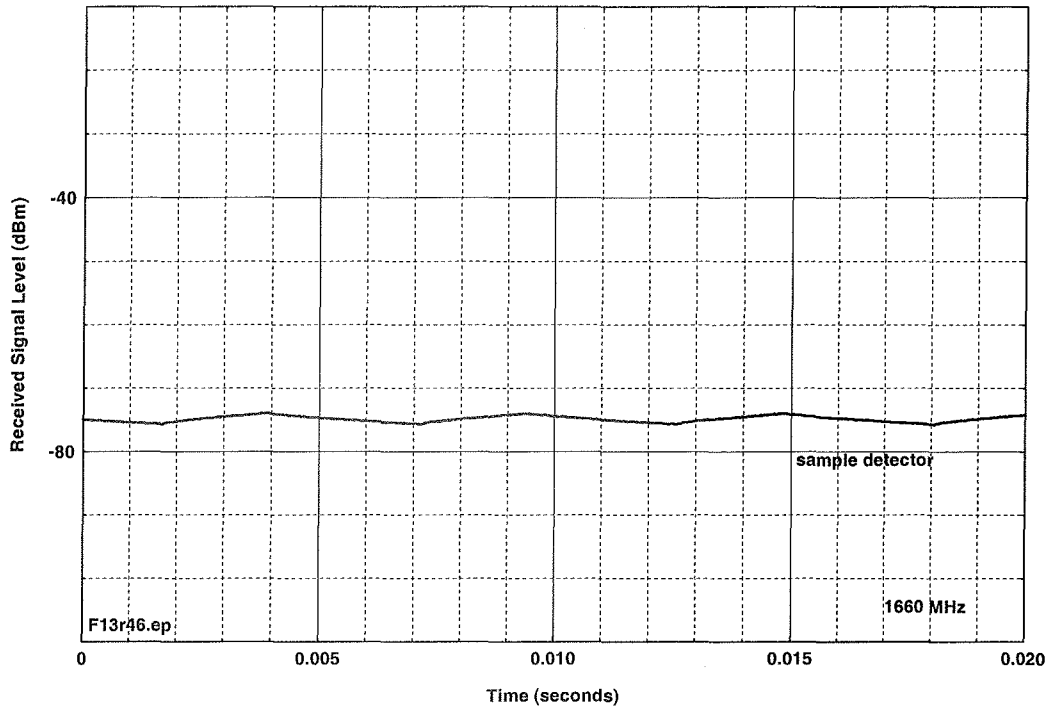

Figure D.B.41. Device B, 128-kBit/second mode, 30-Hz video bandwidth.

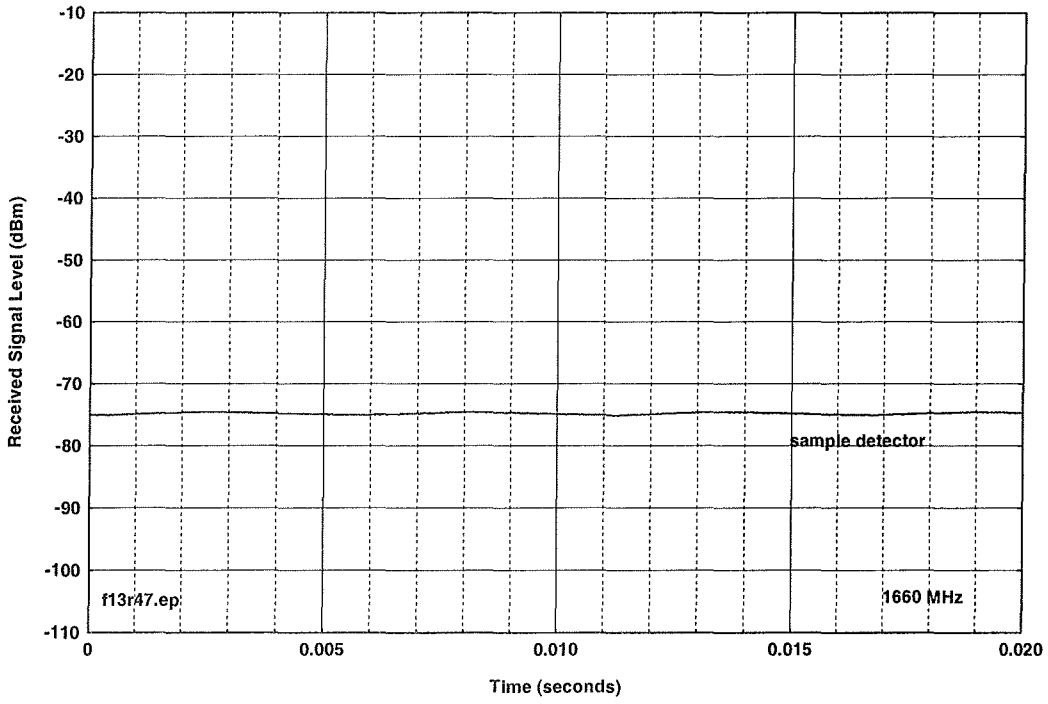

Figure D.B.42. Device B, 128-kBit/second mode, 10-Hz video bandwidth.

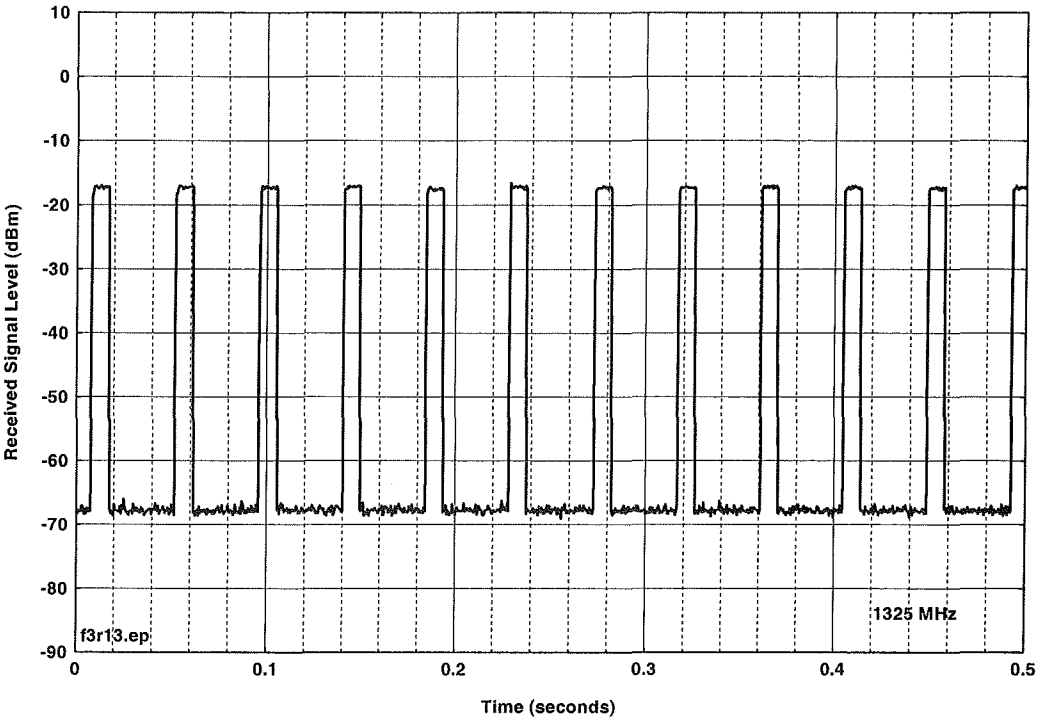

Figure D.B.43. Device B, 16-kBit/second mode, 3-MHz IF bandwidth, positive peak detector.

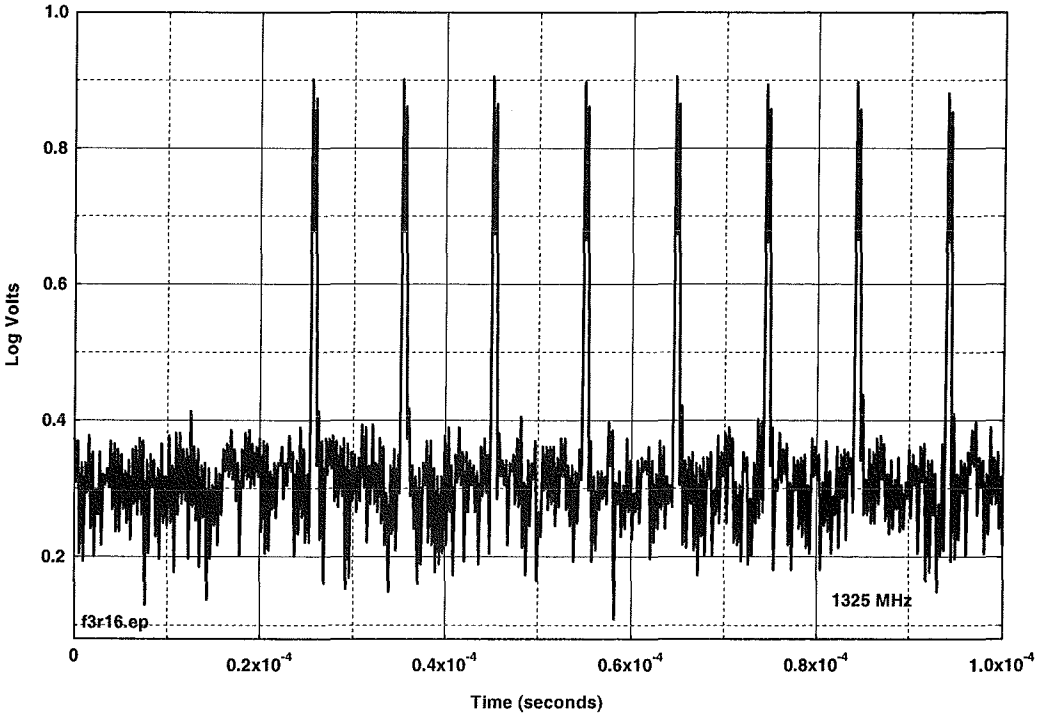

Figure D.B.44. Device B, 16-kBit/second mode, external log detector.

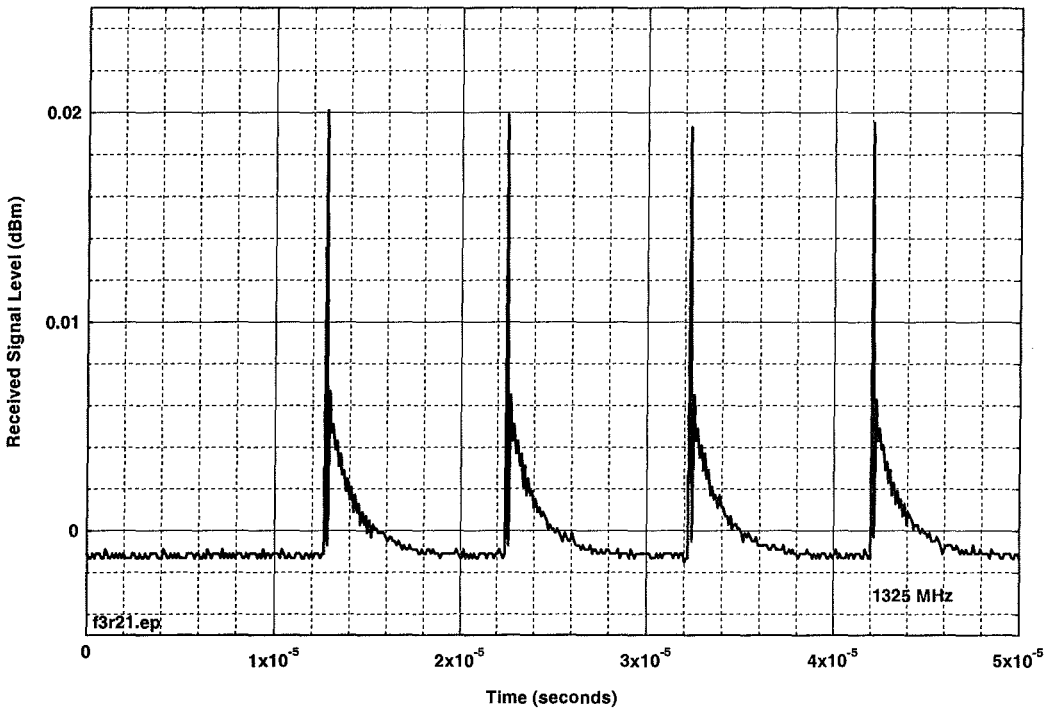

Figure D.B.45. Device B, 16-kBit/second mode, external detector.

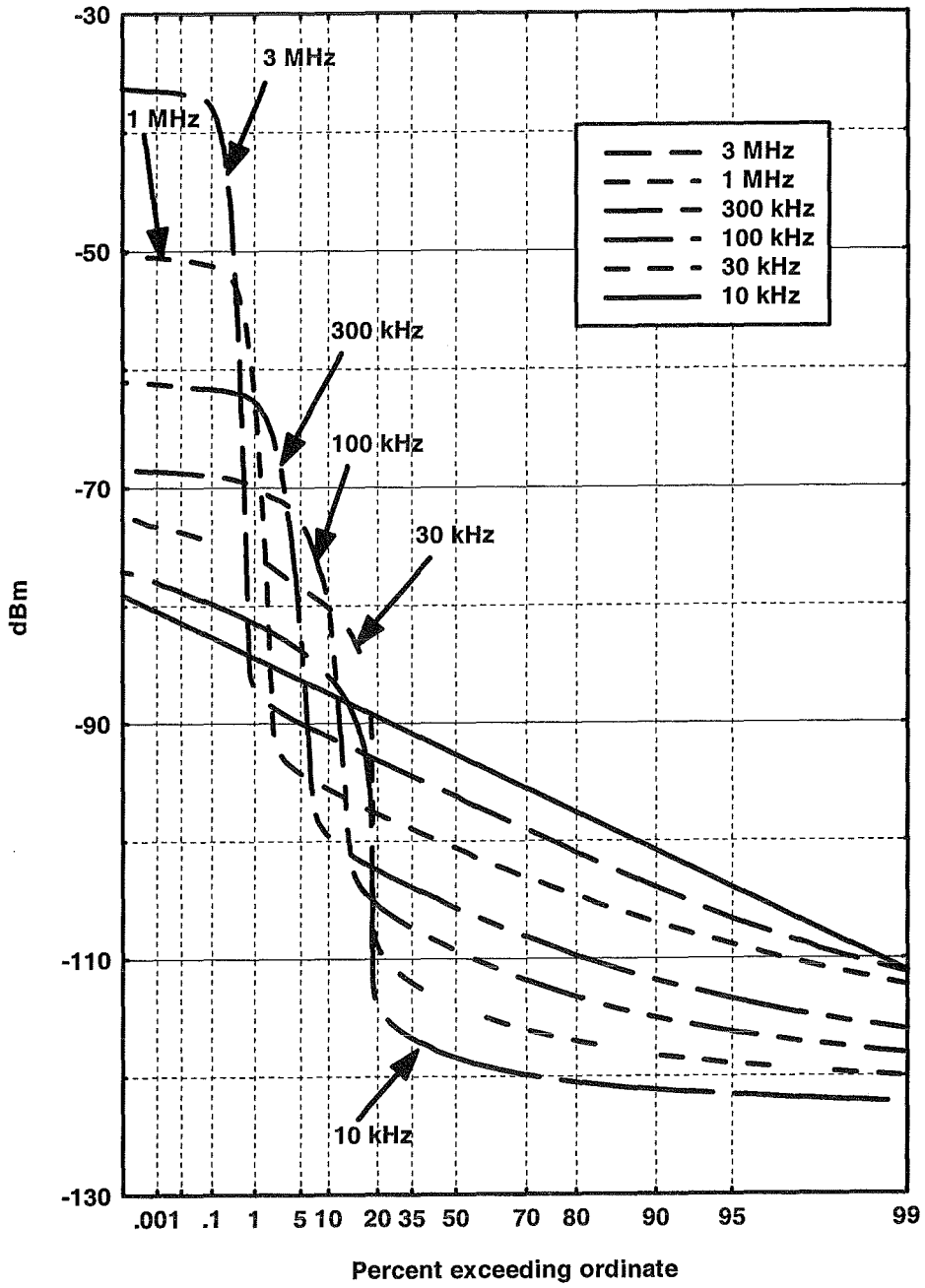

Figure D.B.46. Device B, 16 kb/s APDs.

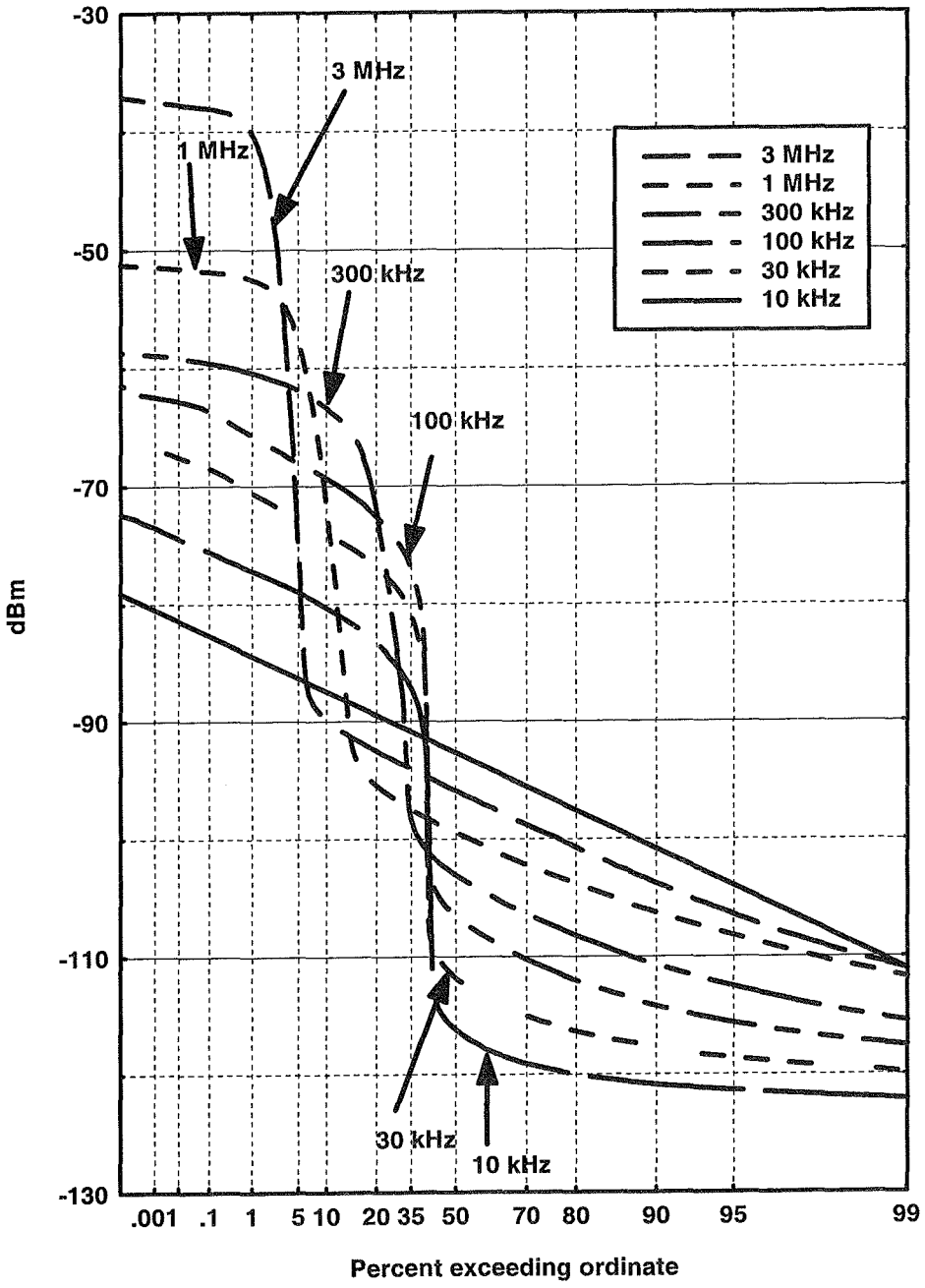

Figure D.B.47. Device B, 128 kb/s APDs.

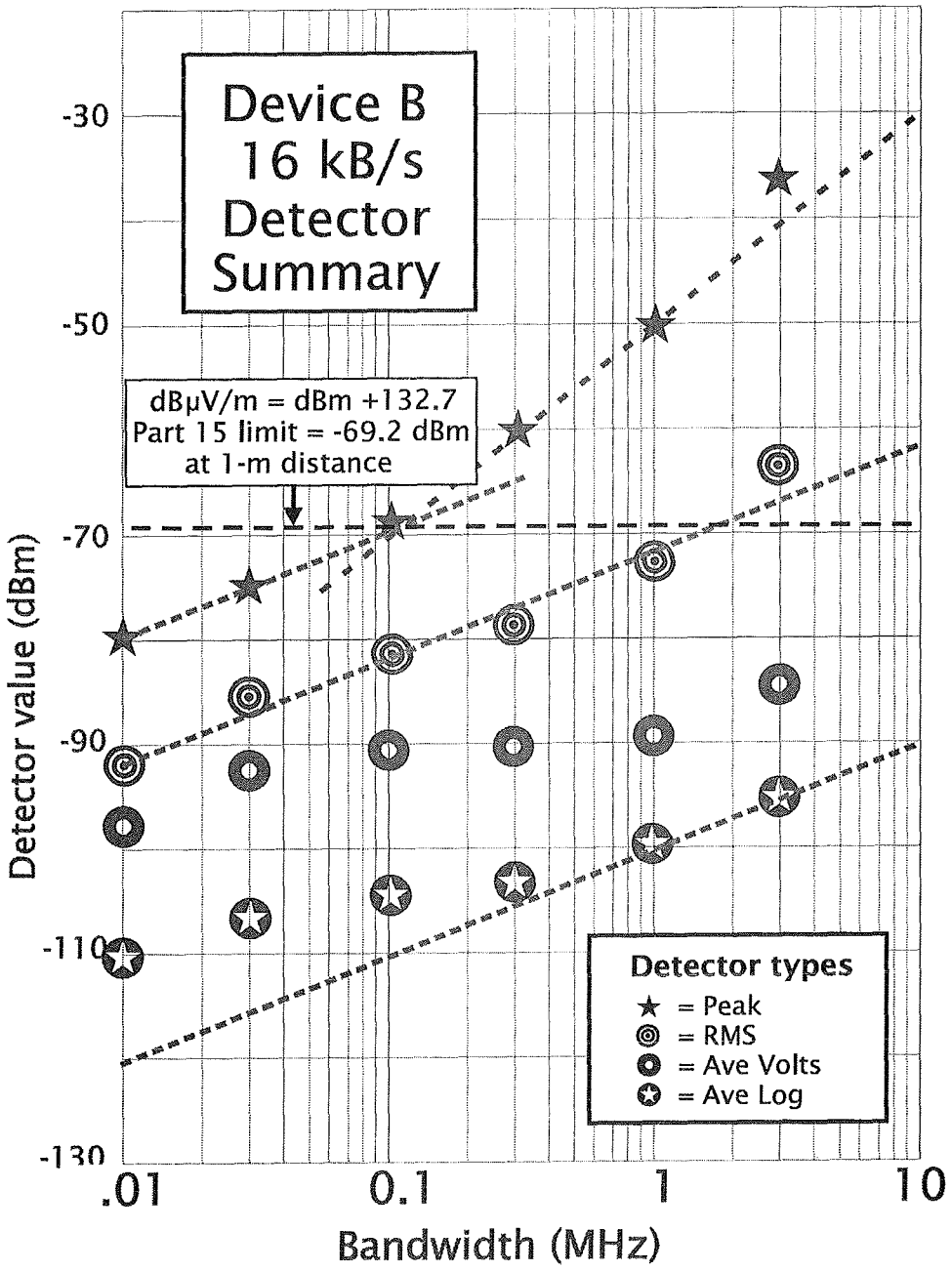

Figure D.B.48. Device B, detector summary.

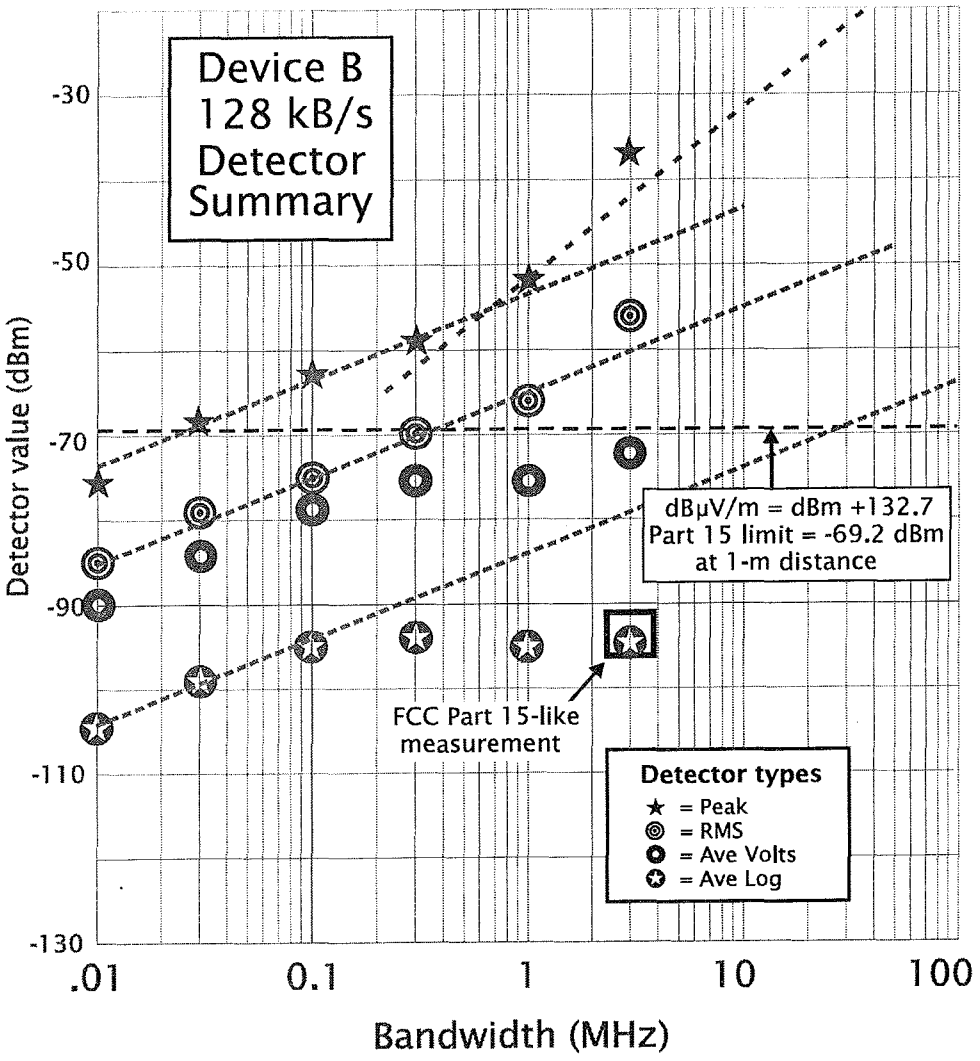

Figure D.B.49. Device B, detector summary

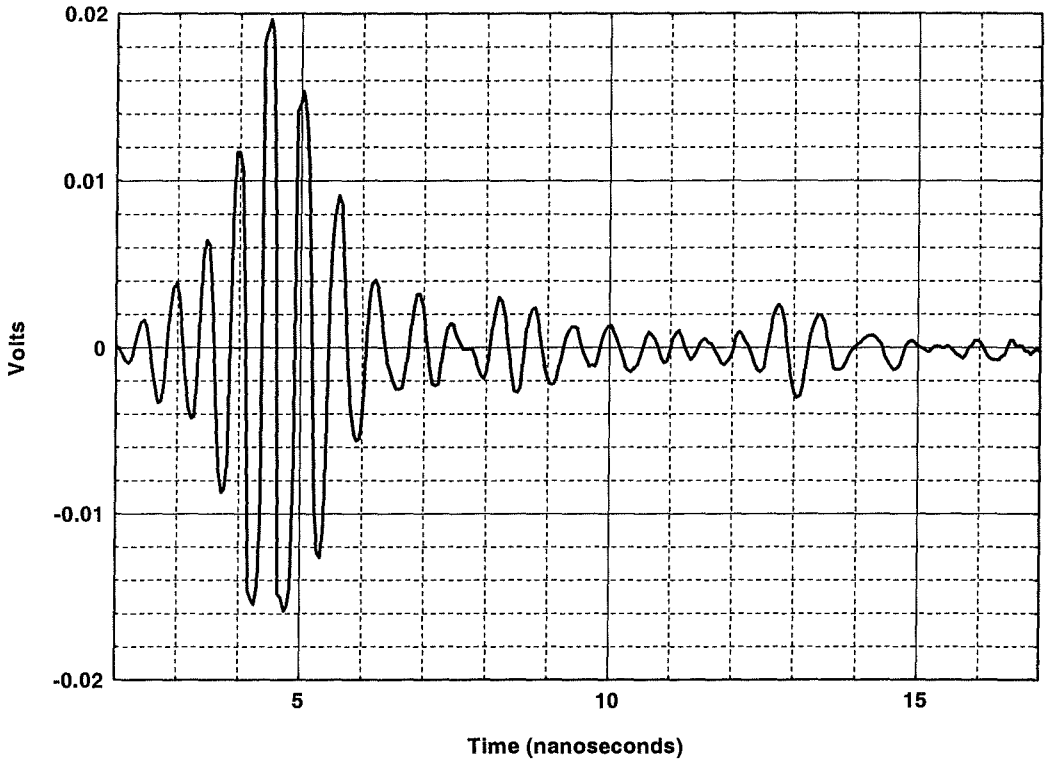

Figure D.C.1. Device C, radiated time-domain waveform.

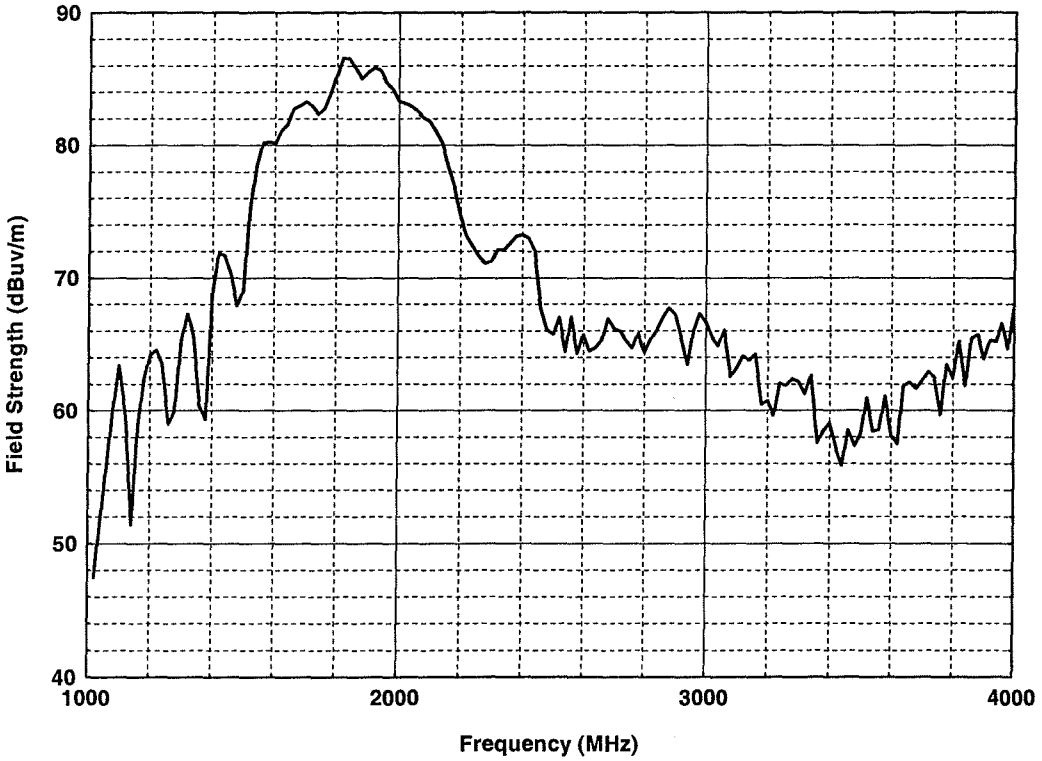

Figure D.C.2. Device C, radiated peak field strength at 1 m, $\Delta f = 20$ MHz.

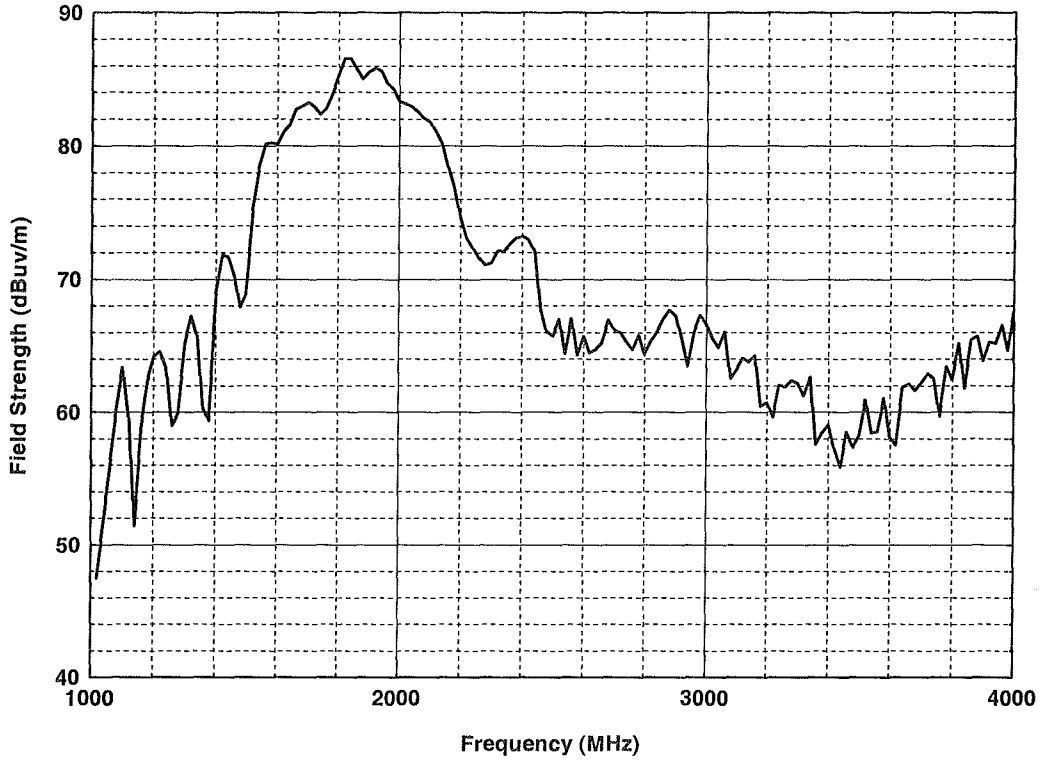

Figure D.C.3. Device C, radiated peak field strength at 1 m, $\Delta f = 20$ MHz.

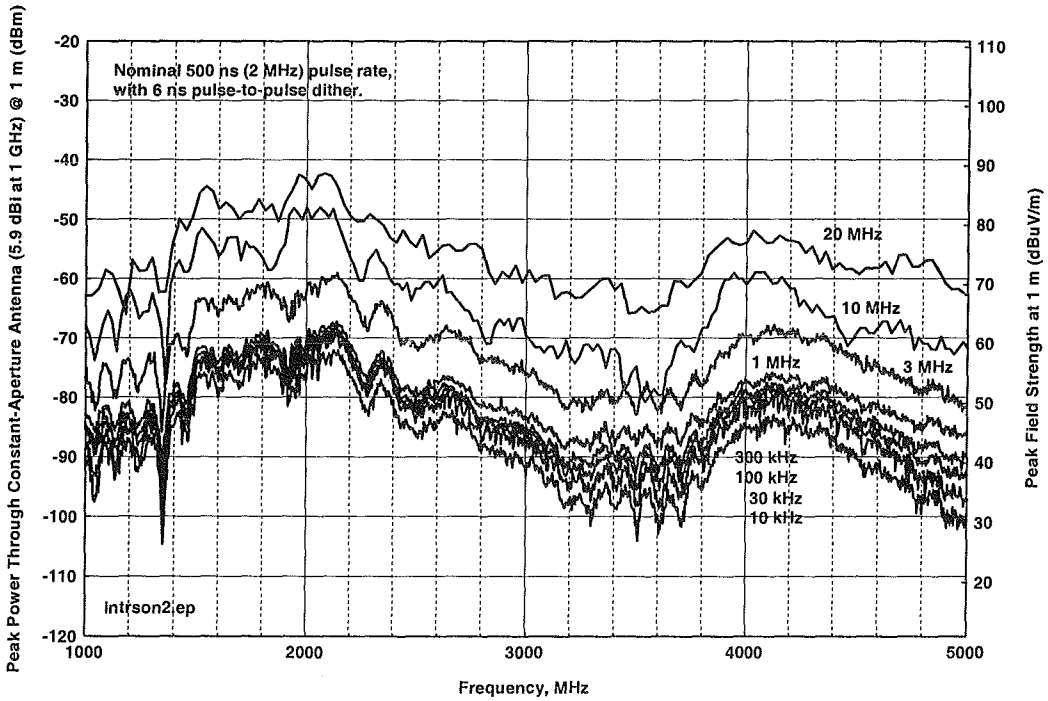

Figure D.C.4. Device C, 1.25% pulse-to-pulse dithered.

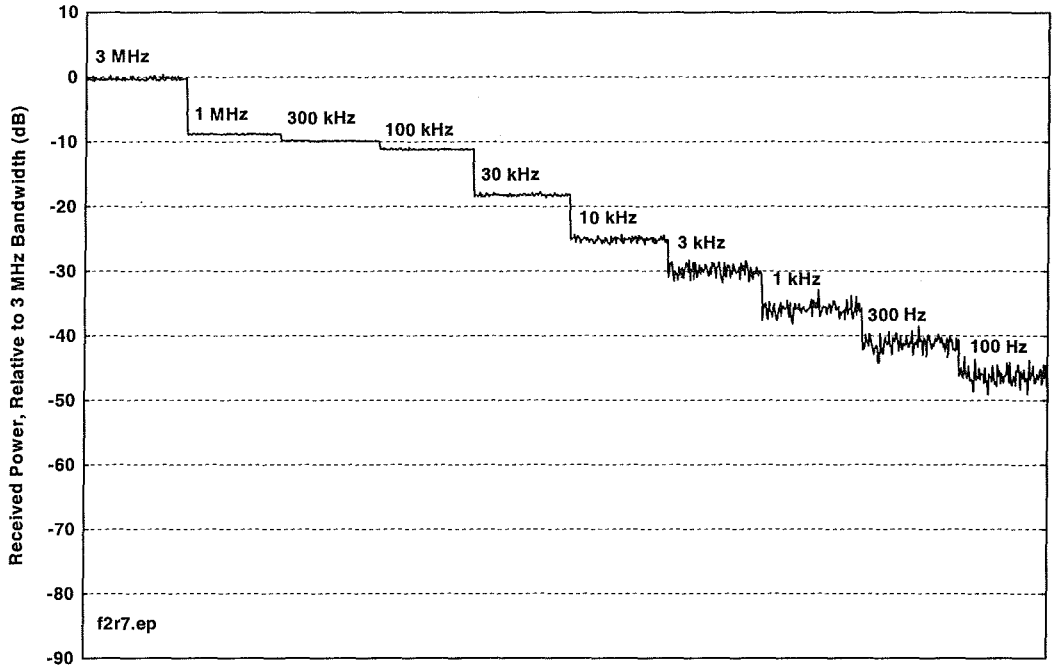

Figure D.C.5. Device C, bandwidth progression stairstep.

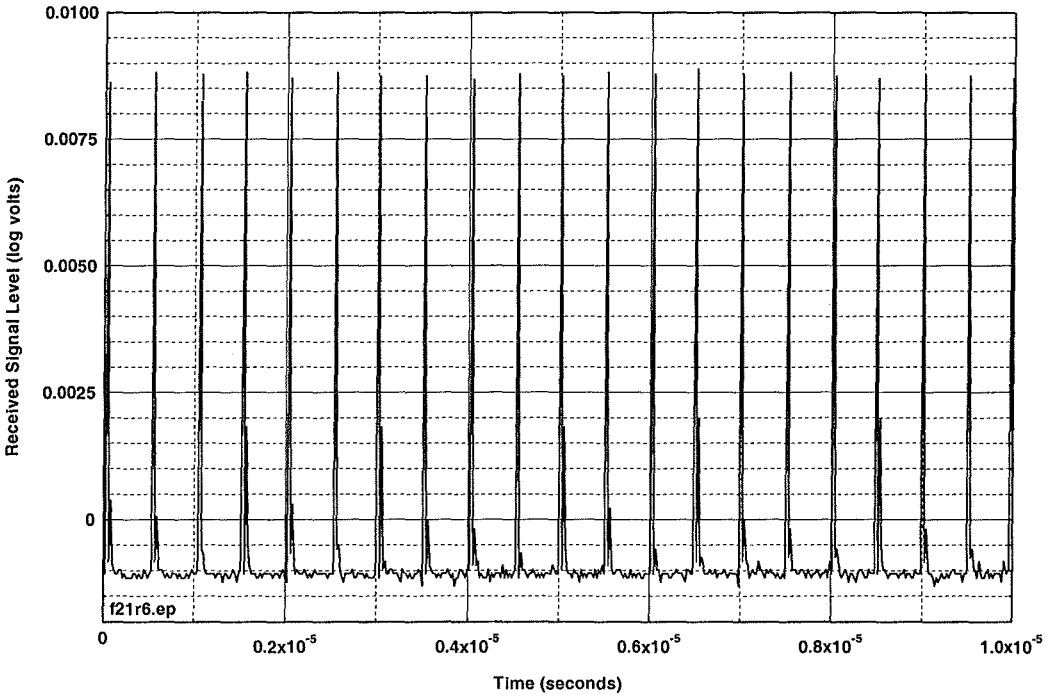

Figure D.C.6. Device C, time waveform for 10 microseconds, 18-Ghz envelope detector.

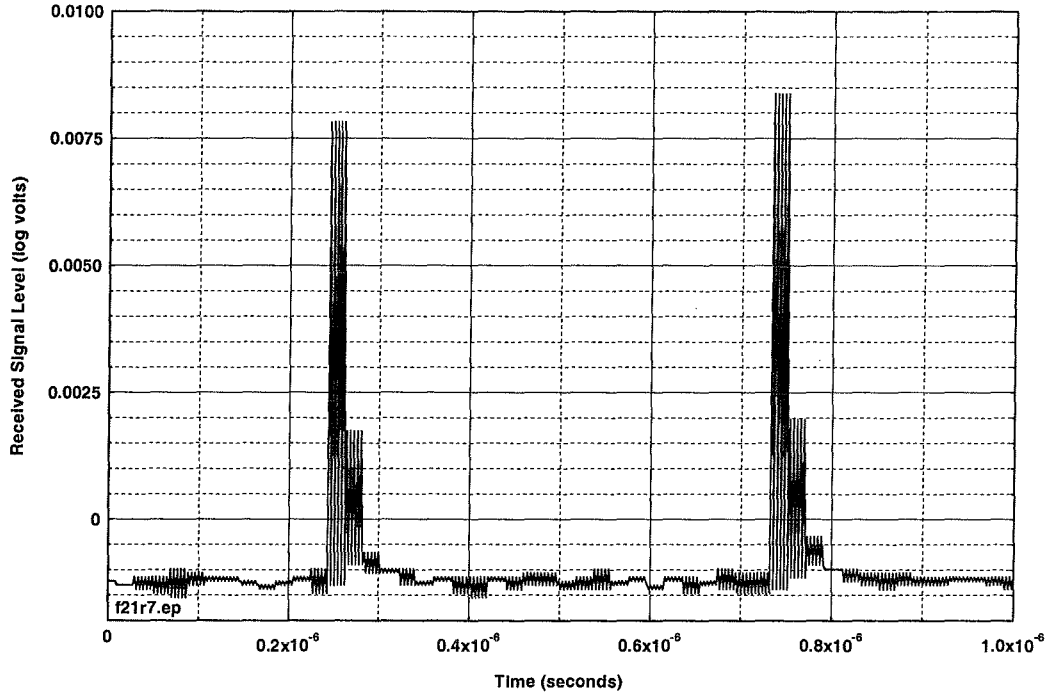

Figure D.C.7. Device C, time waveform, 1 microsecond, 18-GHz envelope detector.

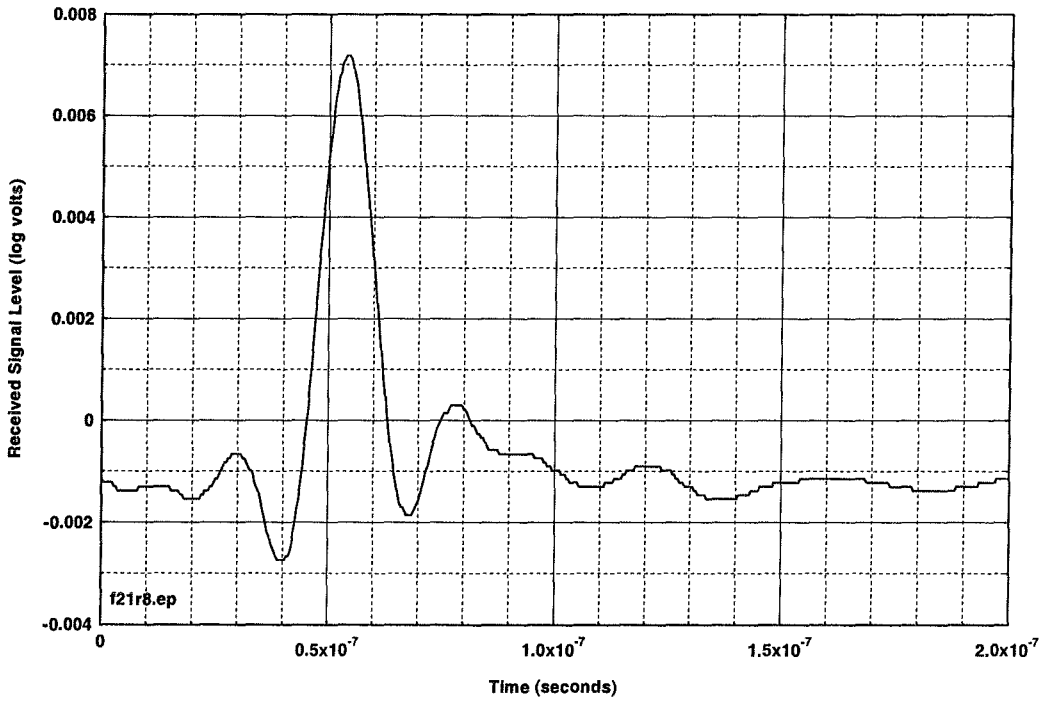

Figure D.C.8. Device C, time waveform, 200 nsec, bandwidth-limited by oscilloscope.

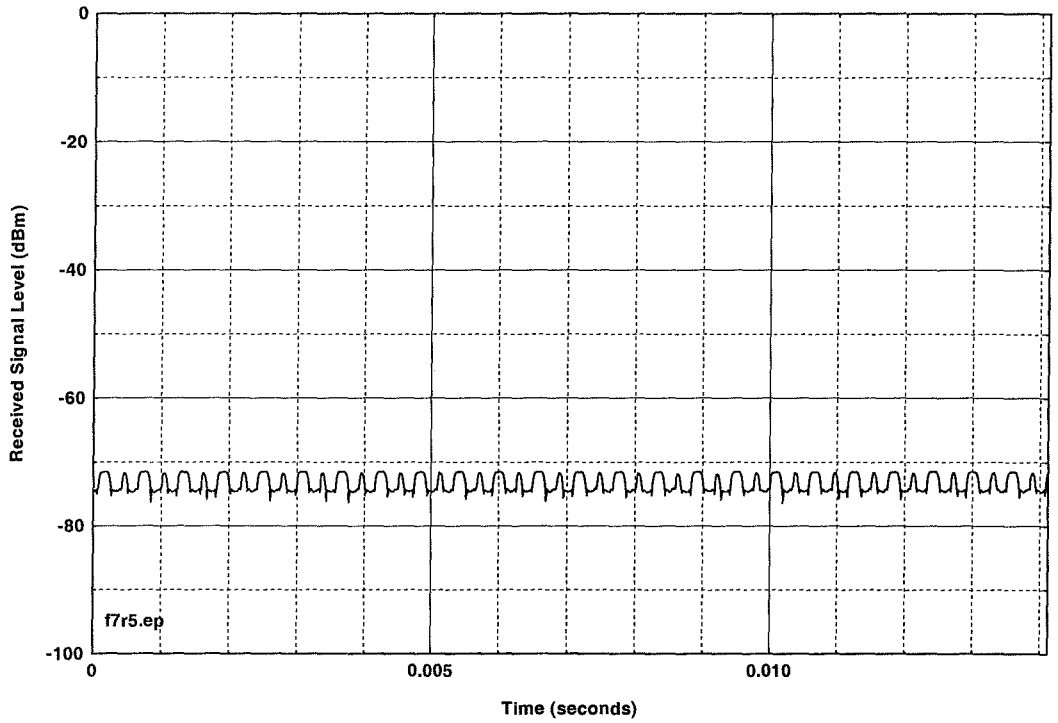

Figure D.C.9. Device C, Part 15 measurement in 10-kHz video bandwidth.

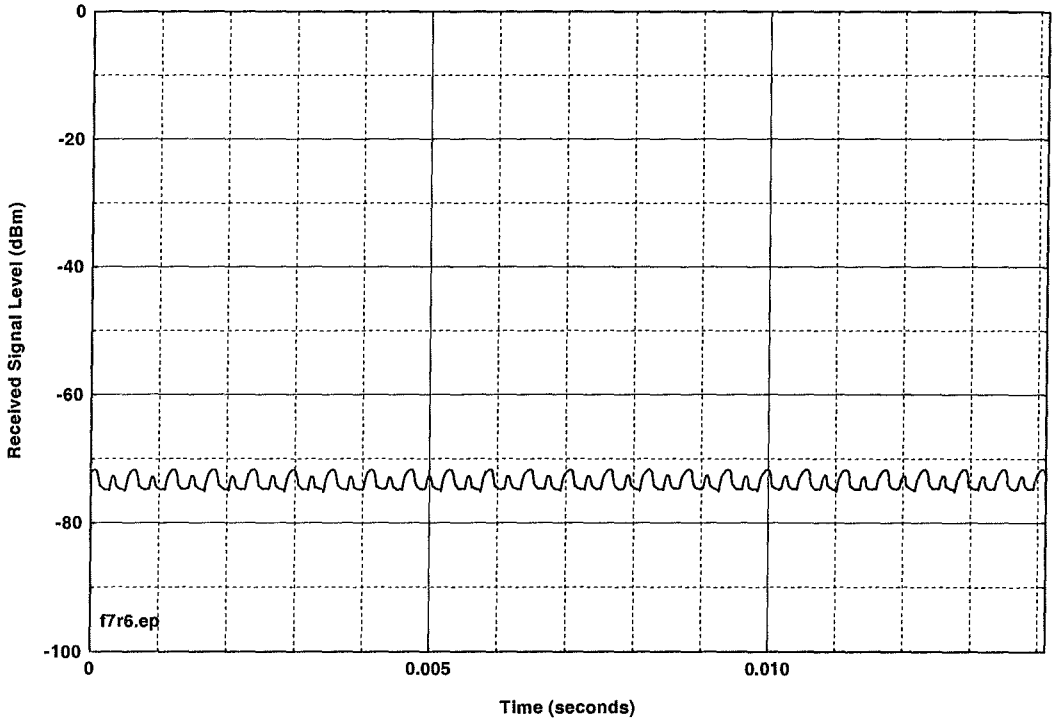

Figure D.C.10. Device C, Part 15 measurement in 3-kHz video bandwidth.

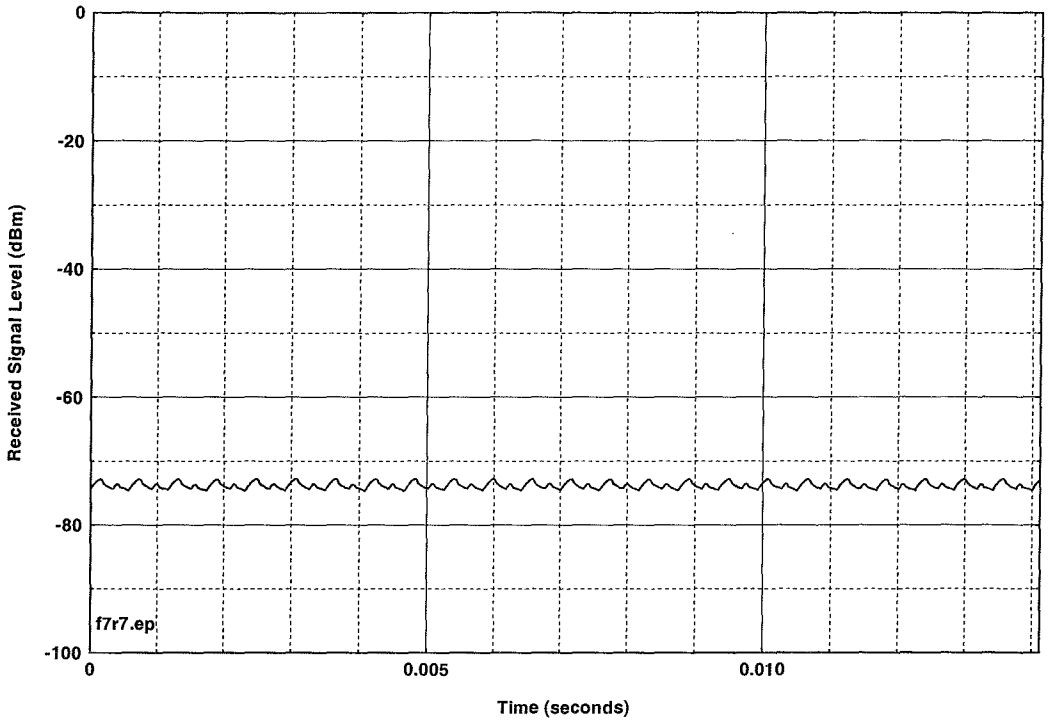

Figure D.C.11. Device C, Part 15 measurement in 1-kHz video bandwidth.

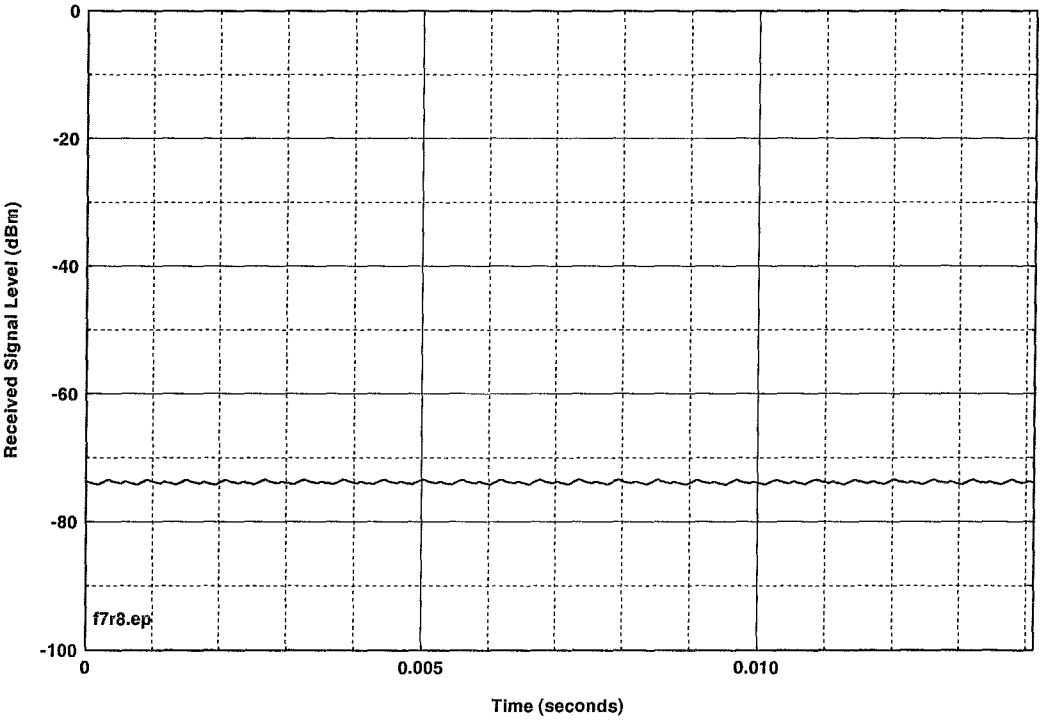

Figure D.C.12. Device C, Part 15 measurement in 300-Hz video bandwidth.

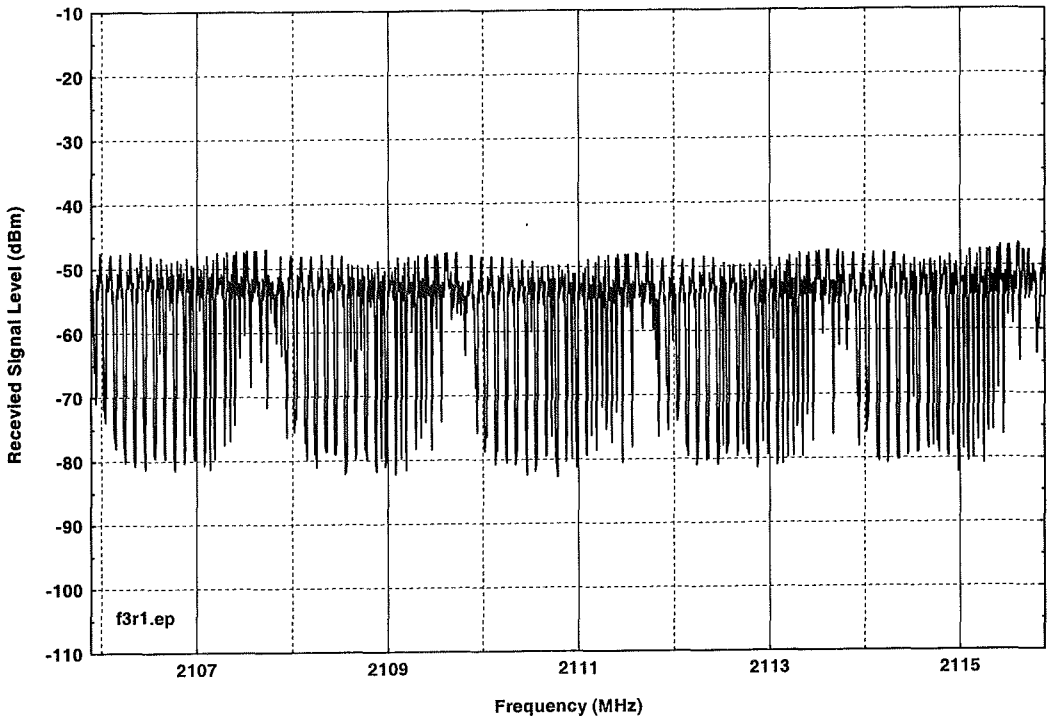

Figure D.C.13. Device C, peak-detected to show lines in noise.

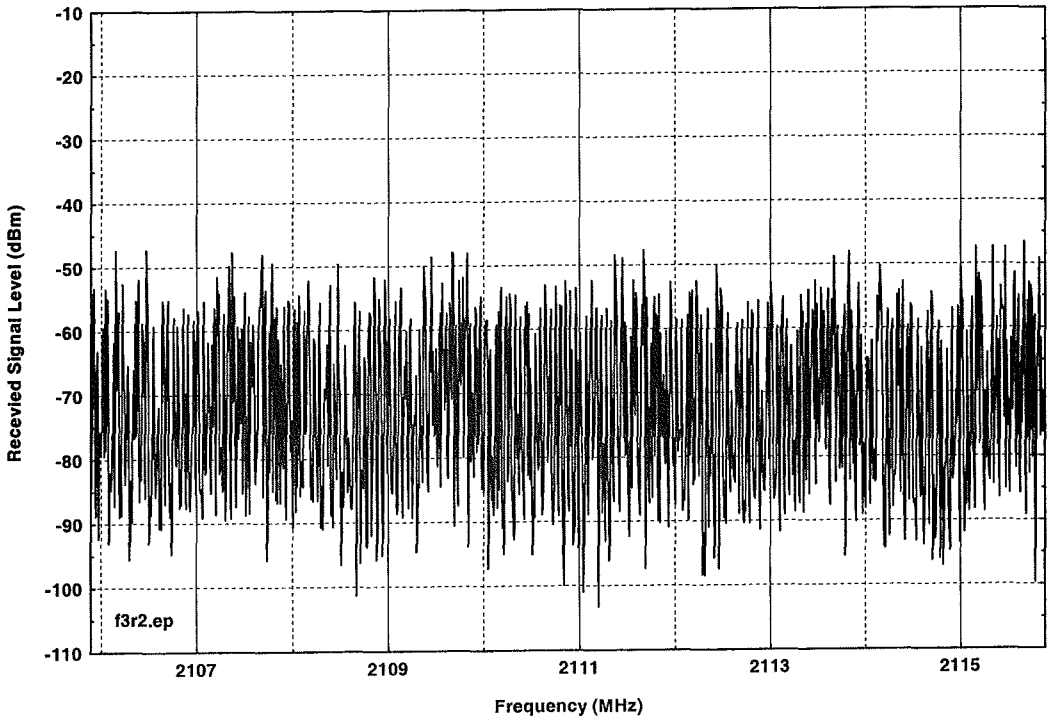

Figure D.C.14. Device C, sample-detected to show how lines are not normally visible.

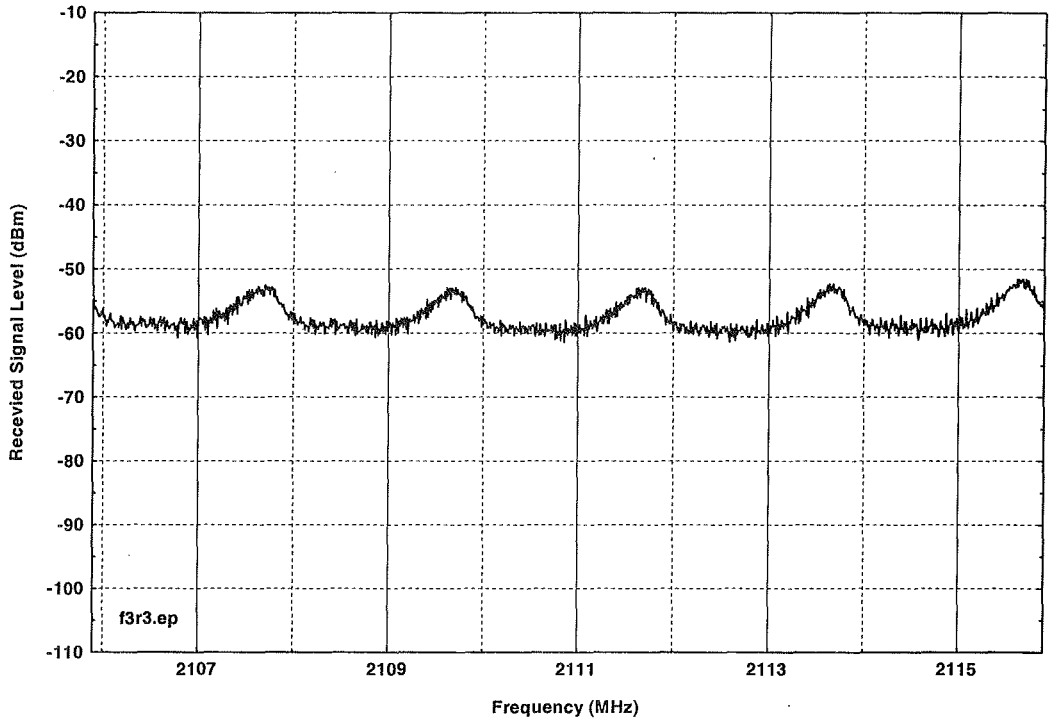

Figure D.C.15. Device C, video-averaged with peak detector to force lines to show.

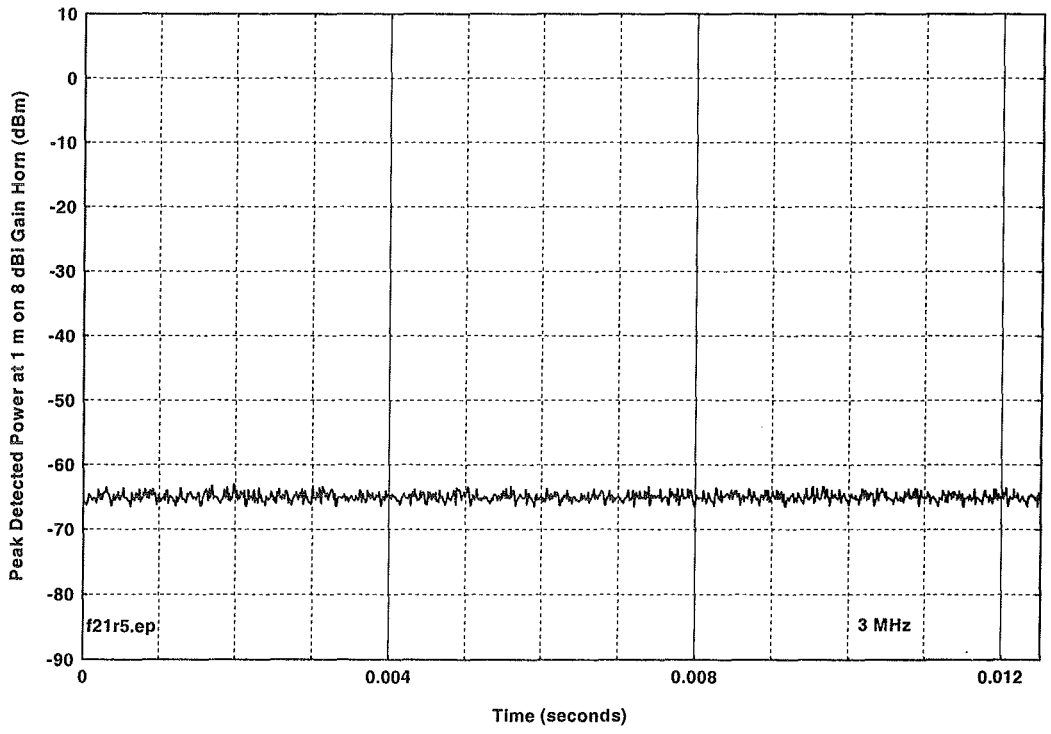

Figure D.C.16. Device C, output in 12 milliseconds.

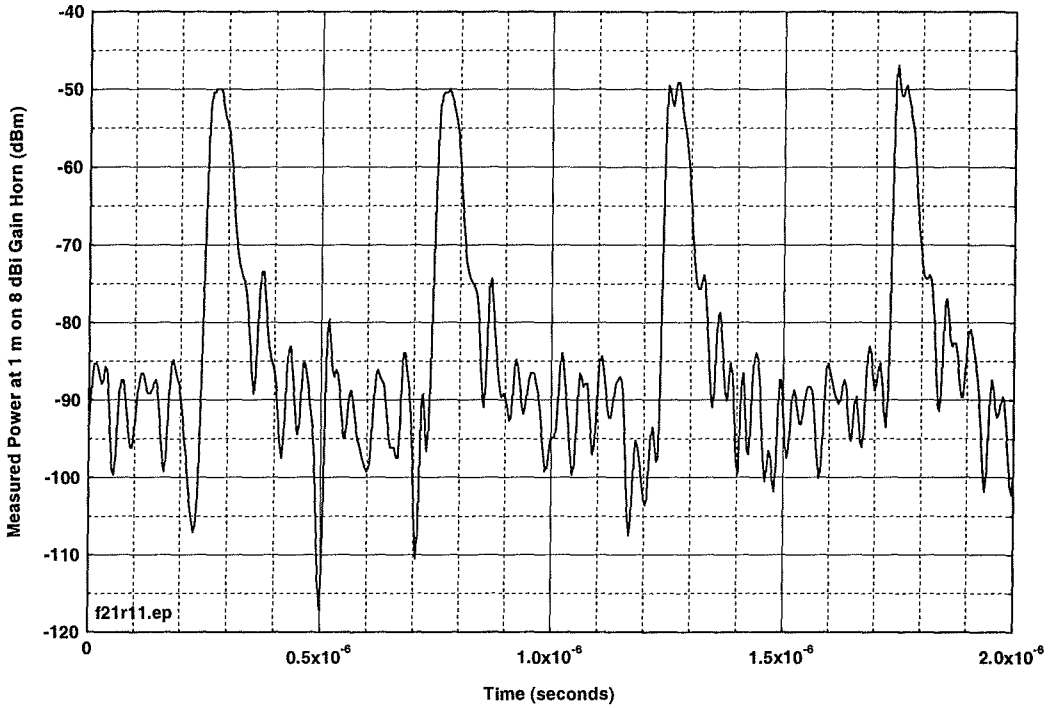

Figure D.C.17. Device C, time waveform in 20-MHz bandwidth.

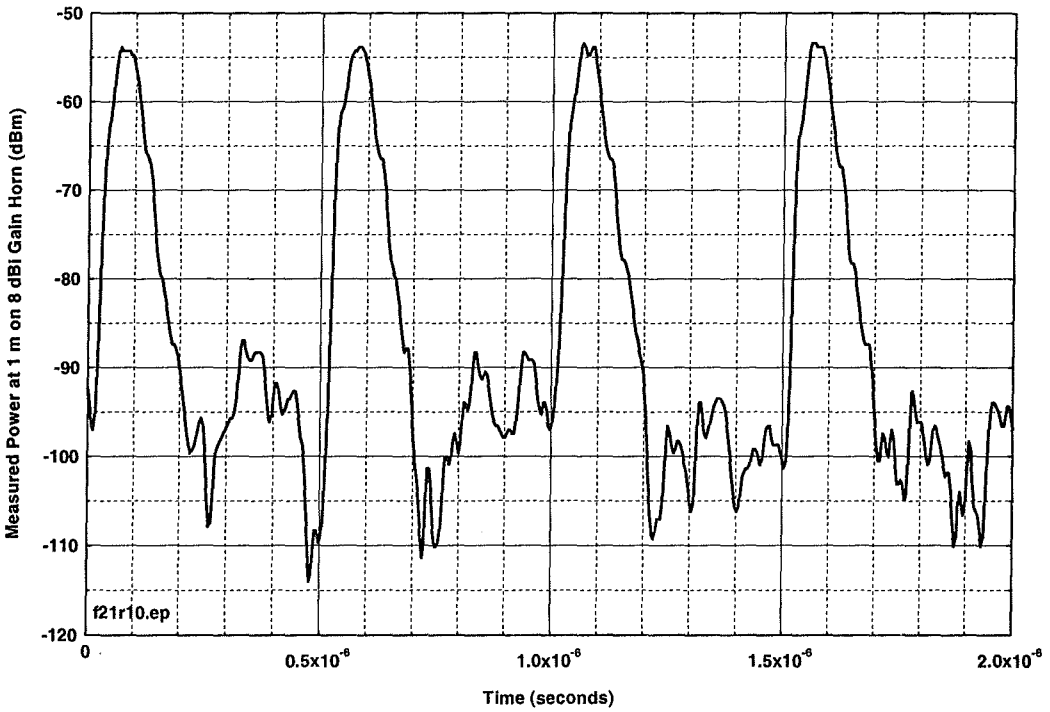

Figure D.C.18. Device C, time waveform in 10-MHz bandwidth.

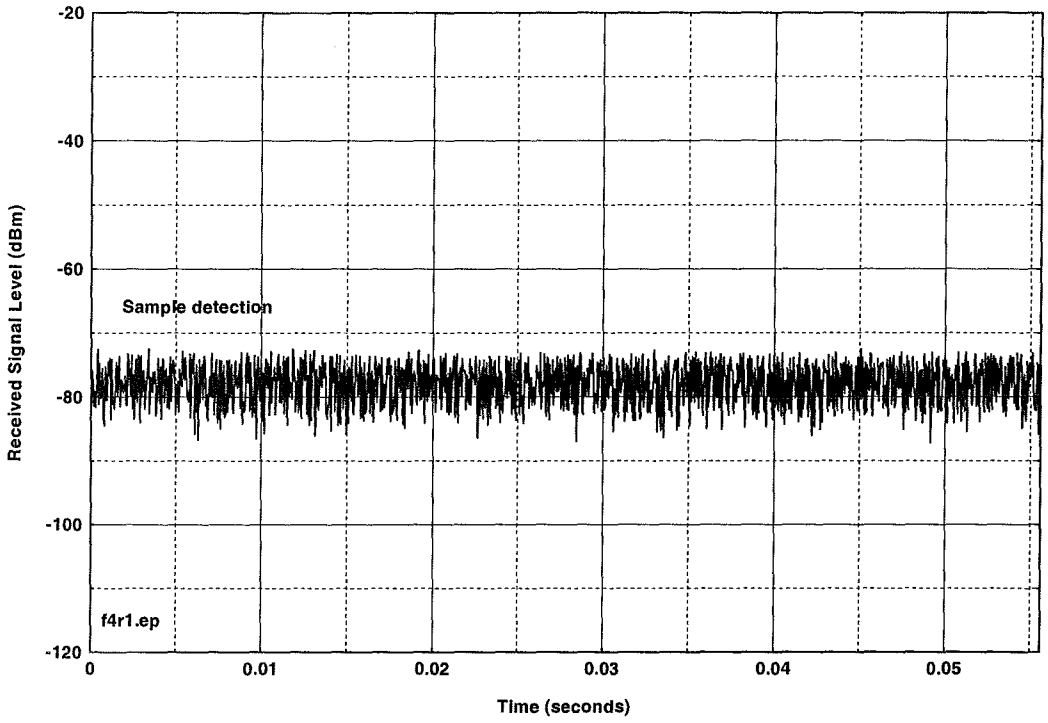

Figure D.C.19. Device C, time waveform in 55 ms, 3-MHz IF bandwidth.

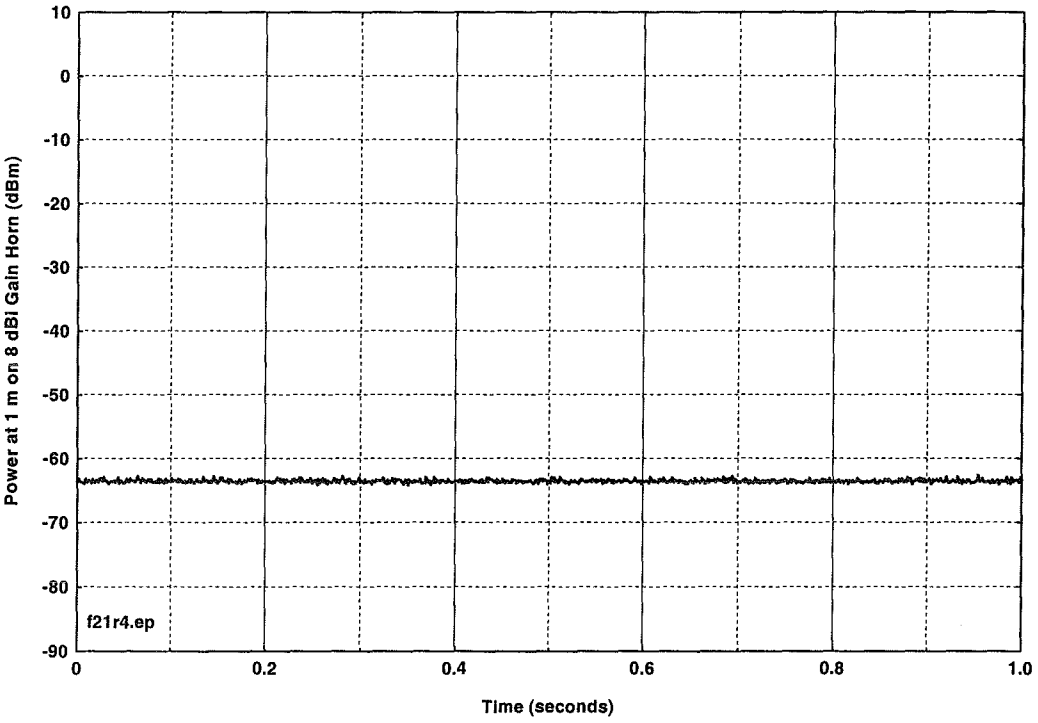

Figure D.C.20. Device C, output in one second.

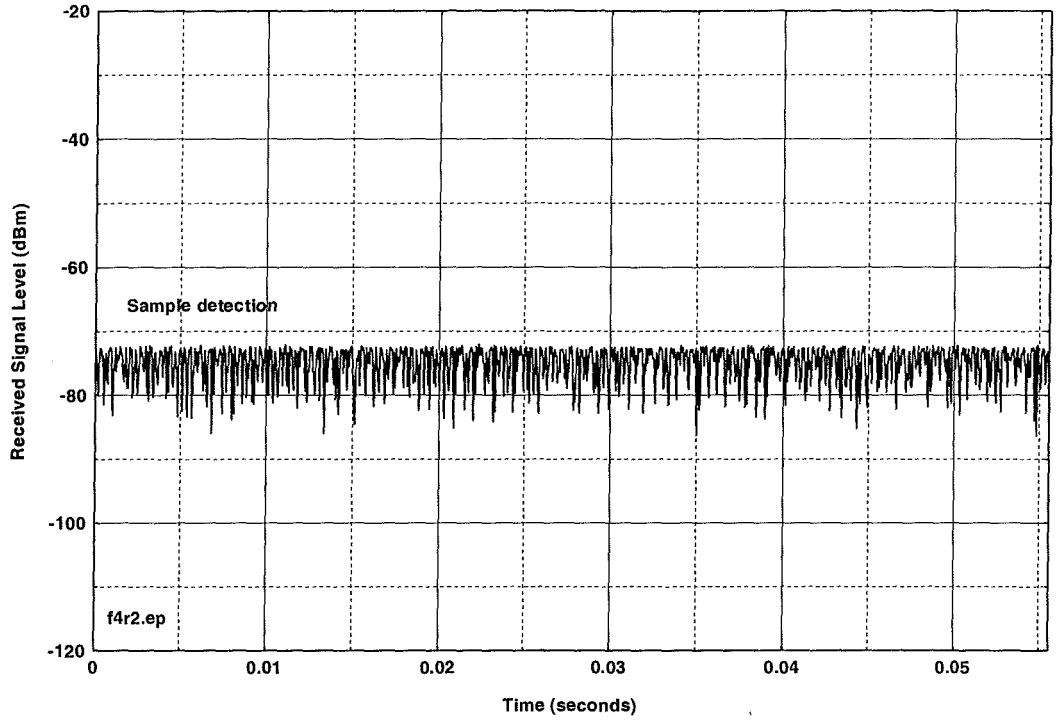

Figure D.C.21. Device C, time waveform, 55 ms, 1-MHz IF bandwidth.

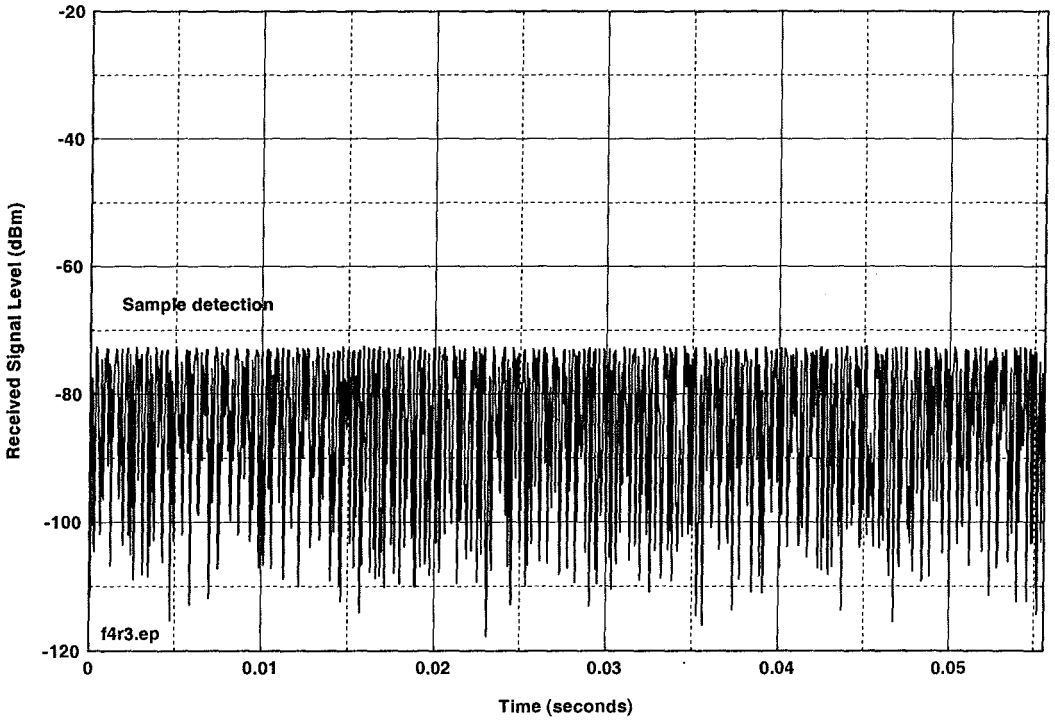

Figure D.C.22. Device C, time waveform, 55 ms, 300-kHz IF bandwidth.

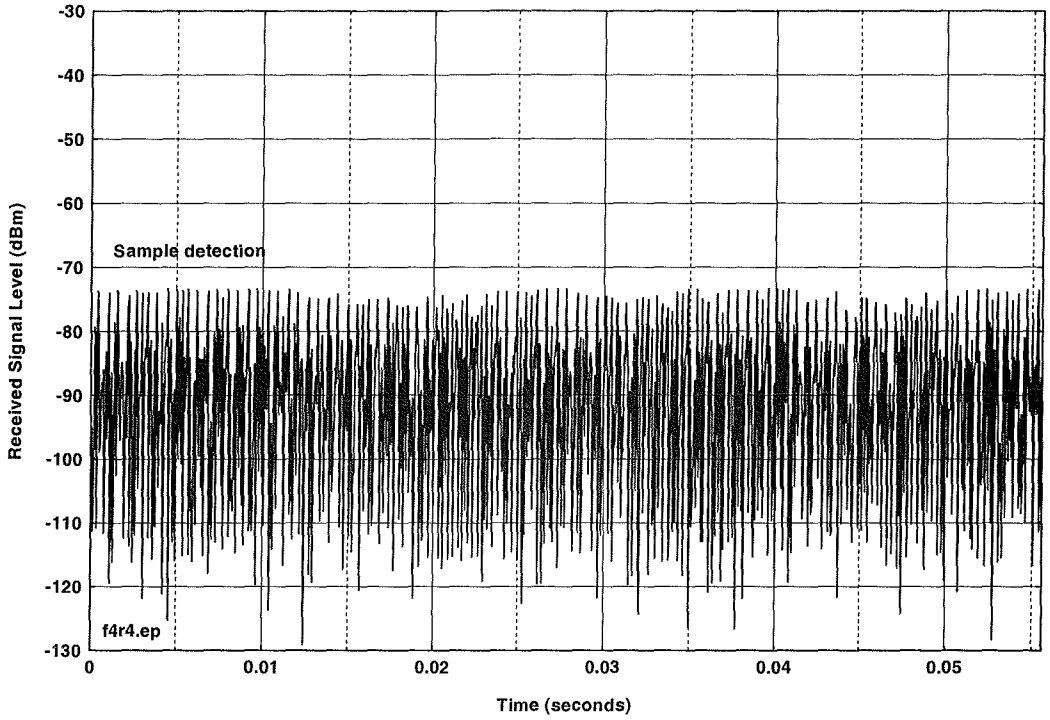

Figure D.C.23. Device C, time waveform, 55 ms, 100-kHz IF bandwidth.

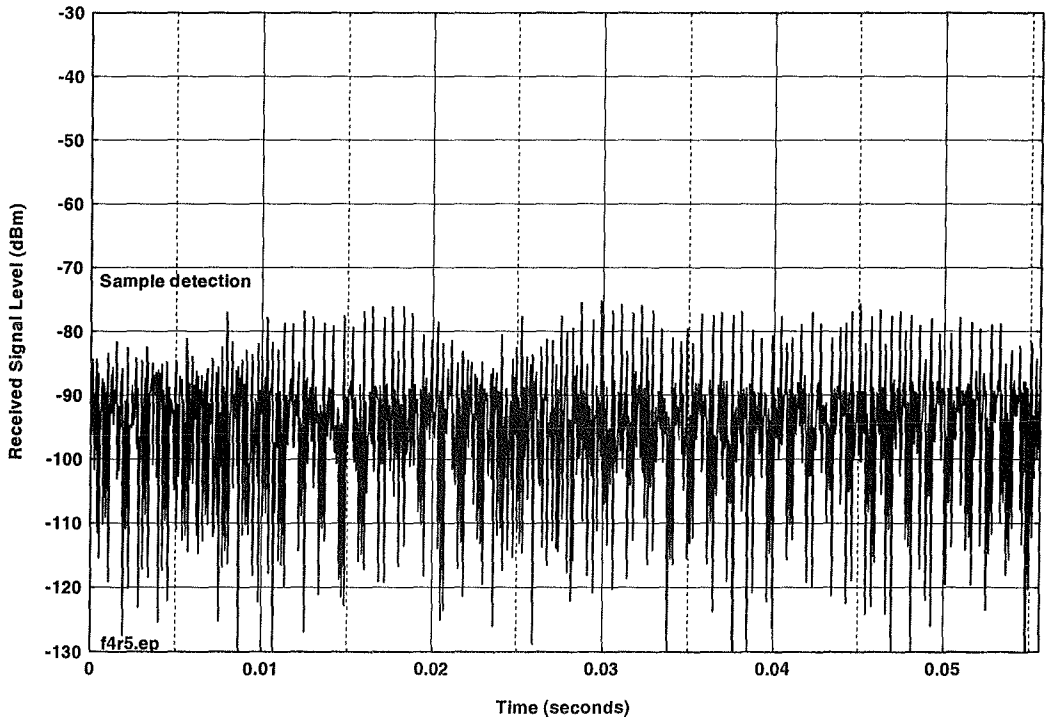

Figure D.C.24. Device C, time waveform, 55 ms, 30-kHz IF bandwidth.

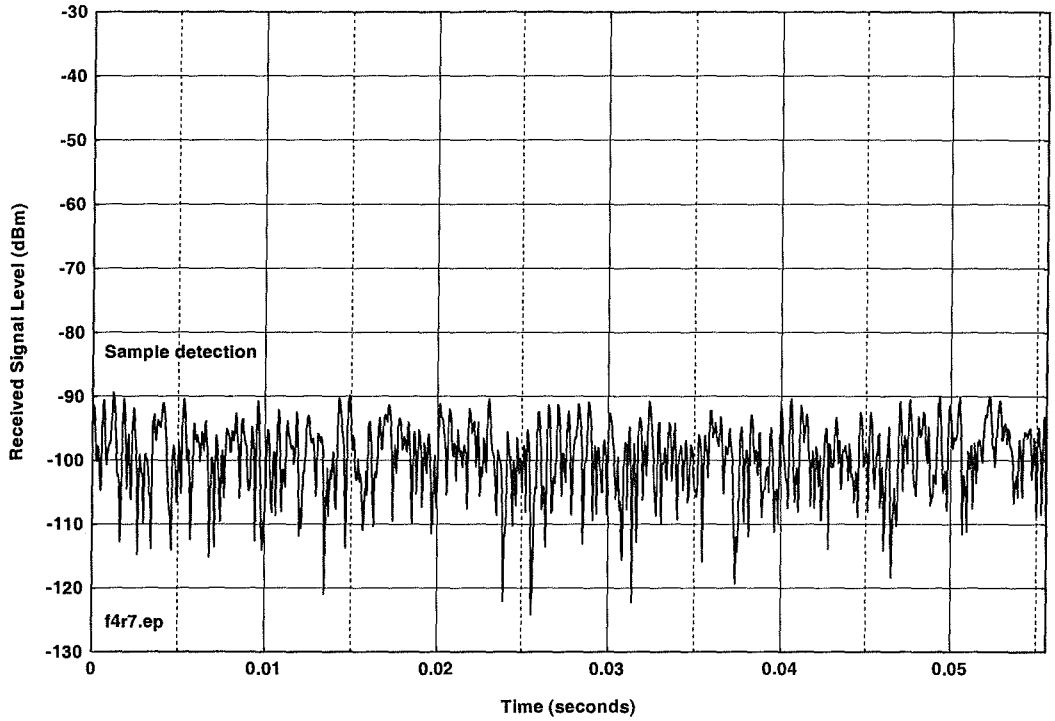

Figure D.C.25. Device C, time waveform, 55 ms, 3-kHz IF bandwidth.

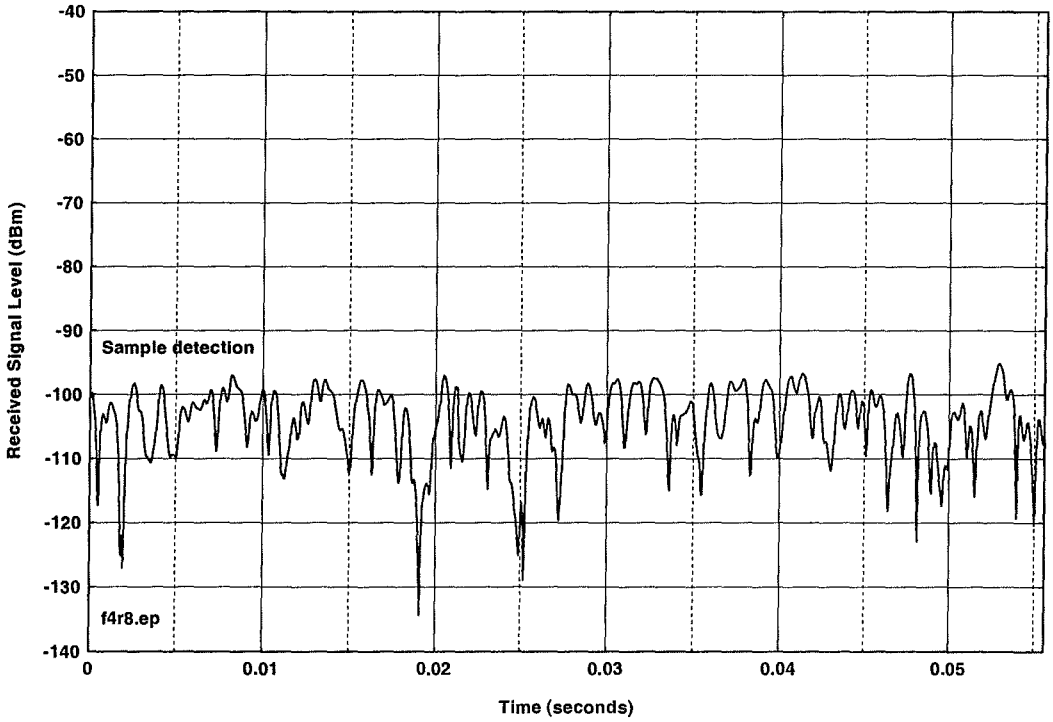

Figure D.C.26. Device C, time waveform, 55 ms, 1-kHz IF bandwidth.

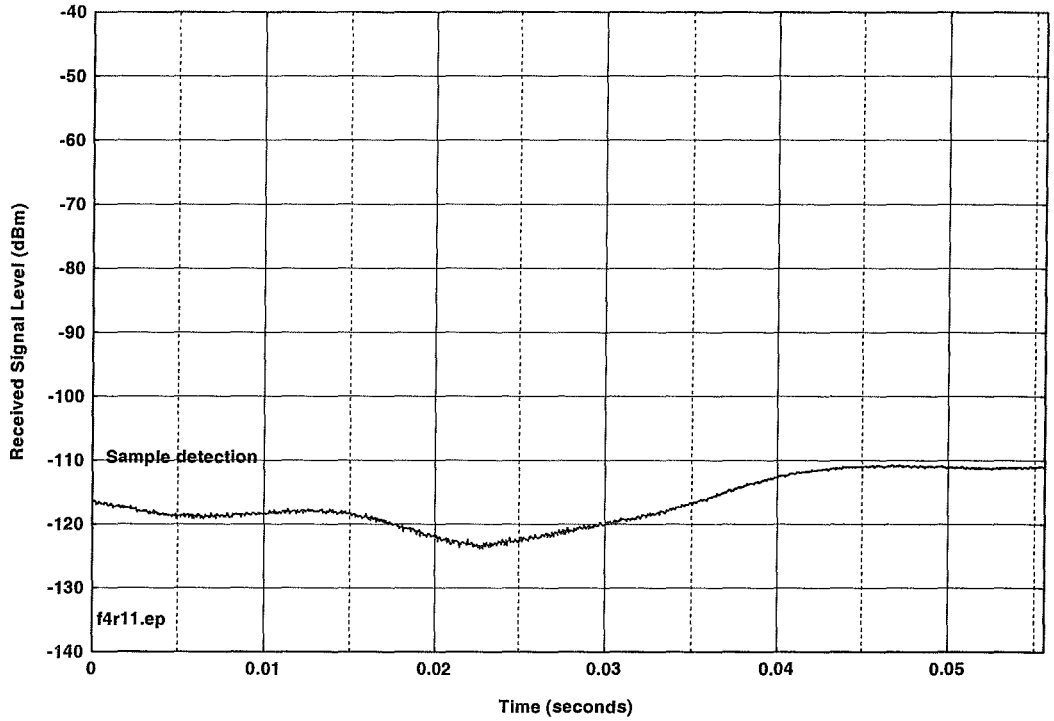

Figure D.C.27. Device C, time waveform, 55 ms, 30-Hz IF bandwidth.

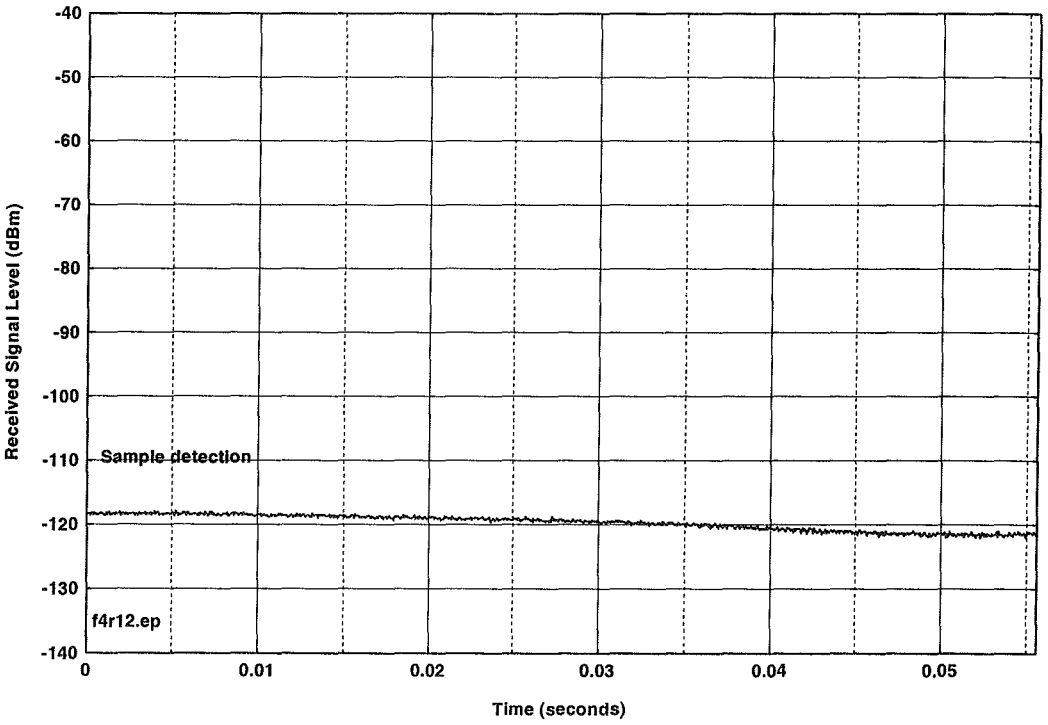

Figure D.C.28. Device C, time waveform, 55 ms, 10-Hz IF bandwidth.

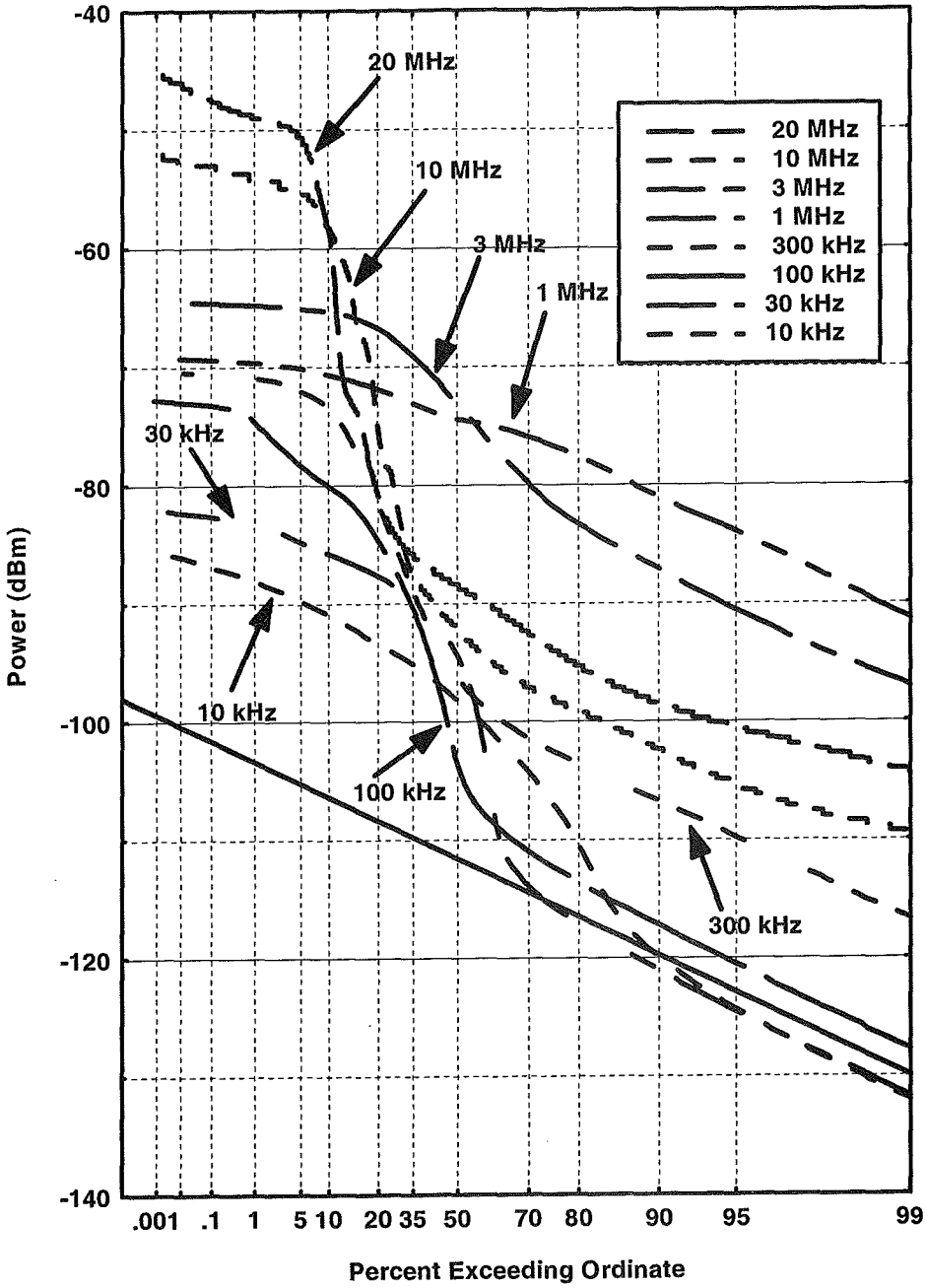

Figure D.C.29. Device C, APDs, between lines.

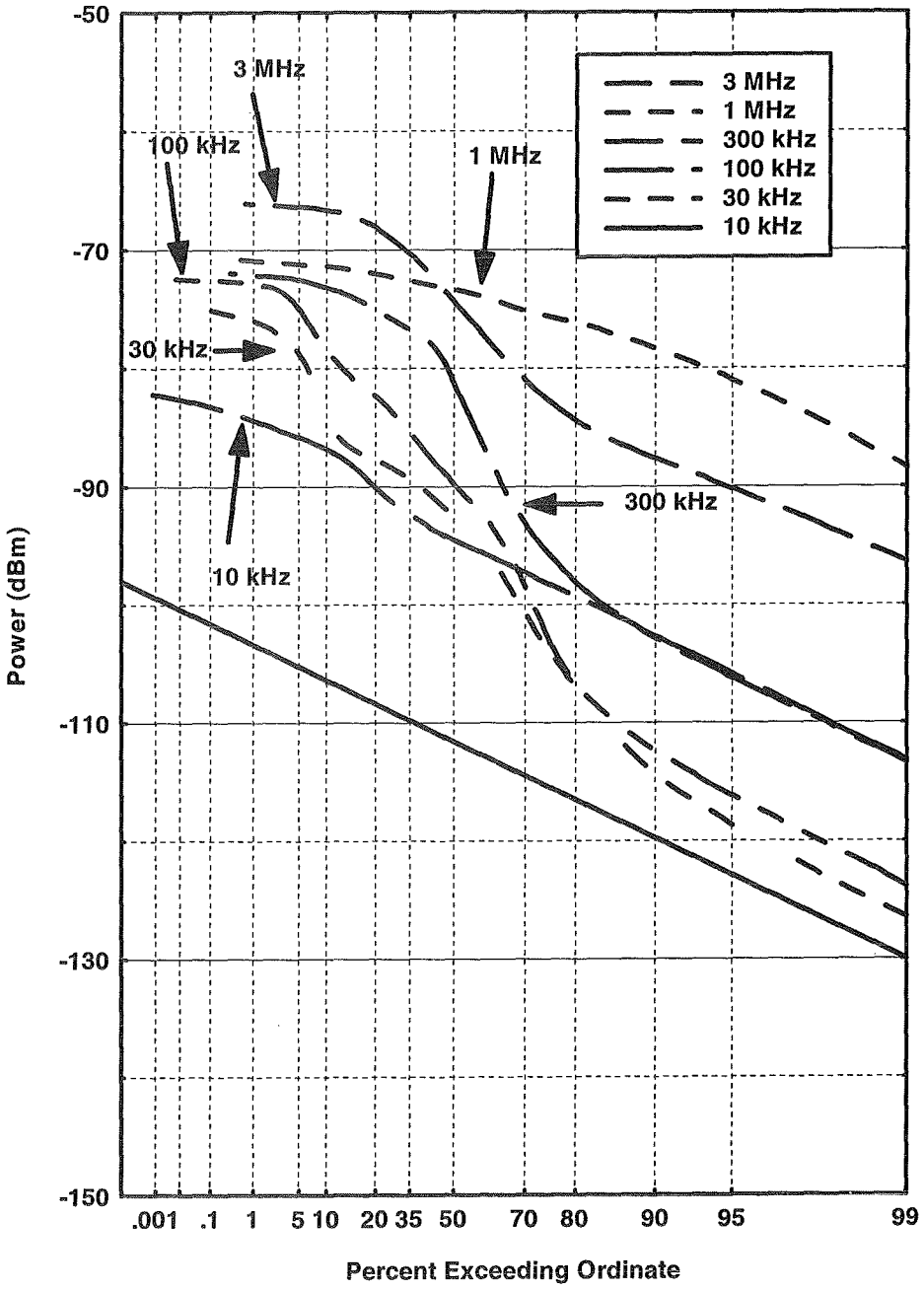

Figure D.C.30. Device C, APDs, on lines.

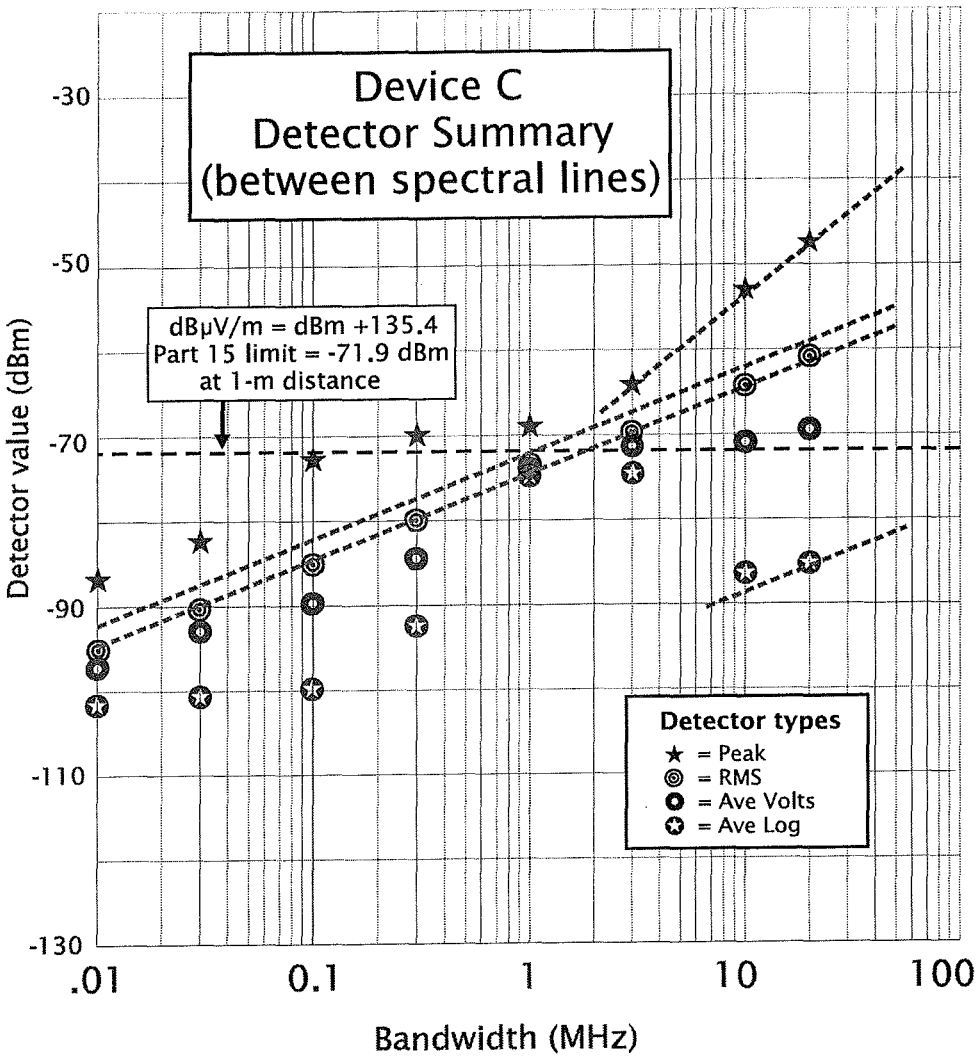

Figure D.C.31. Device C, detector summary (between spectral lines).

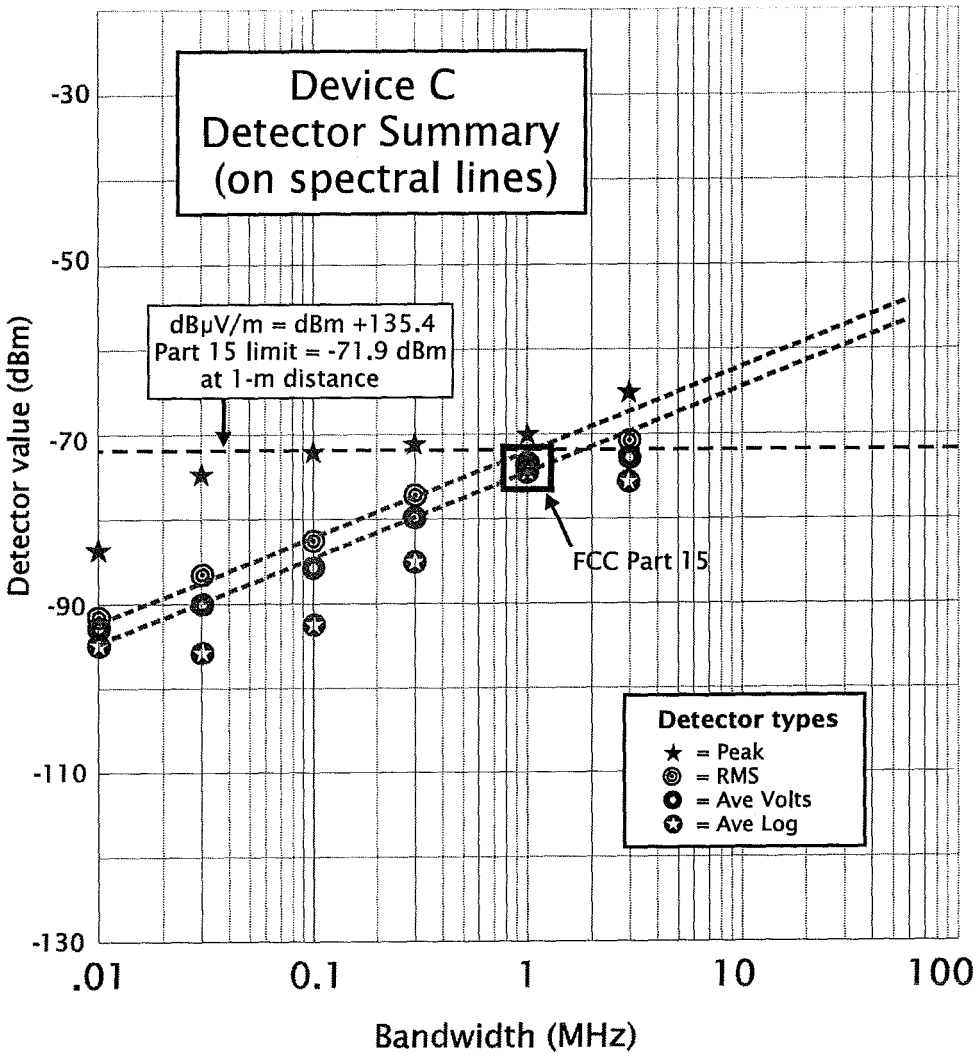

Figure D.C.32. Device C, detector summary (on spectral lines).

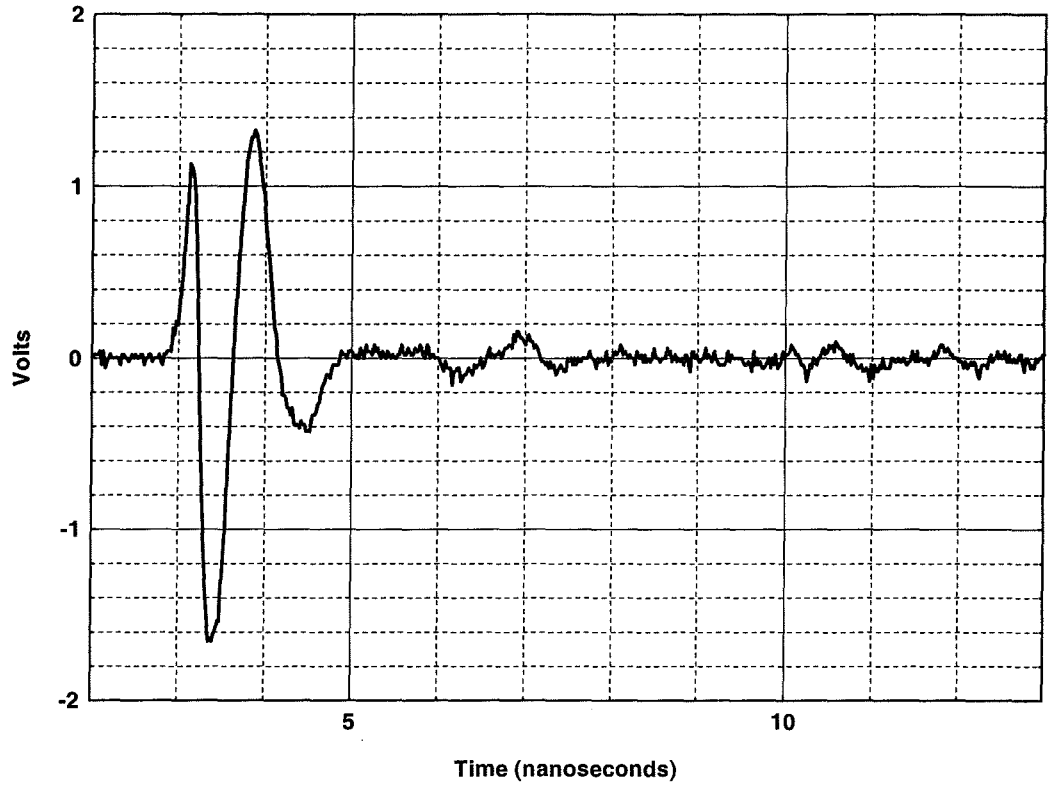

Figure D.D.1. Device D, conducted time-domain waveform.

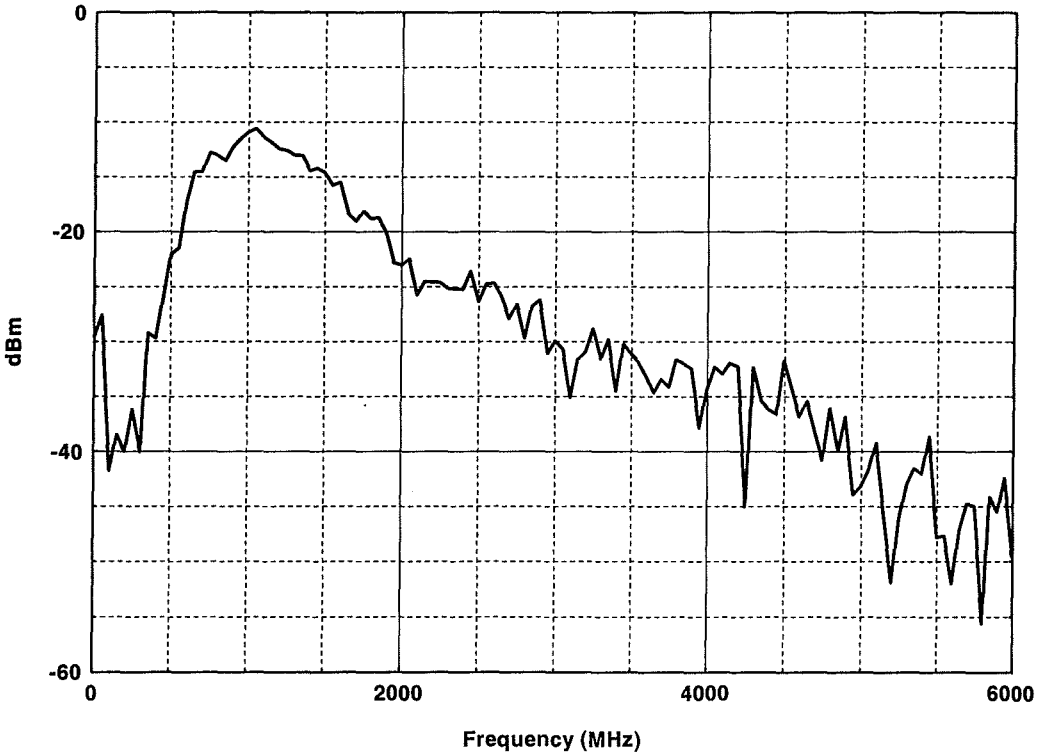

Figure D.D.2. Device D, conducted power spectrum, $\Delta f = 49.95$ MHz.

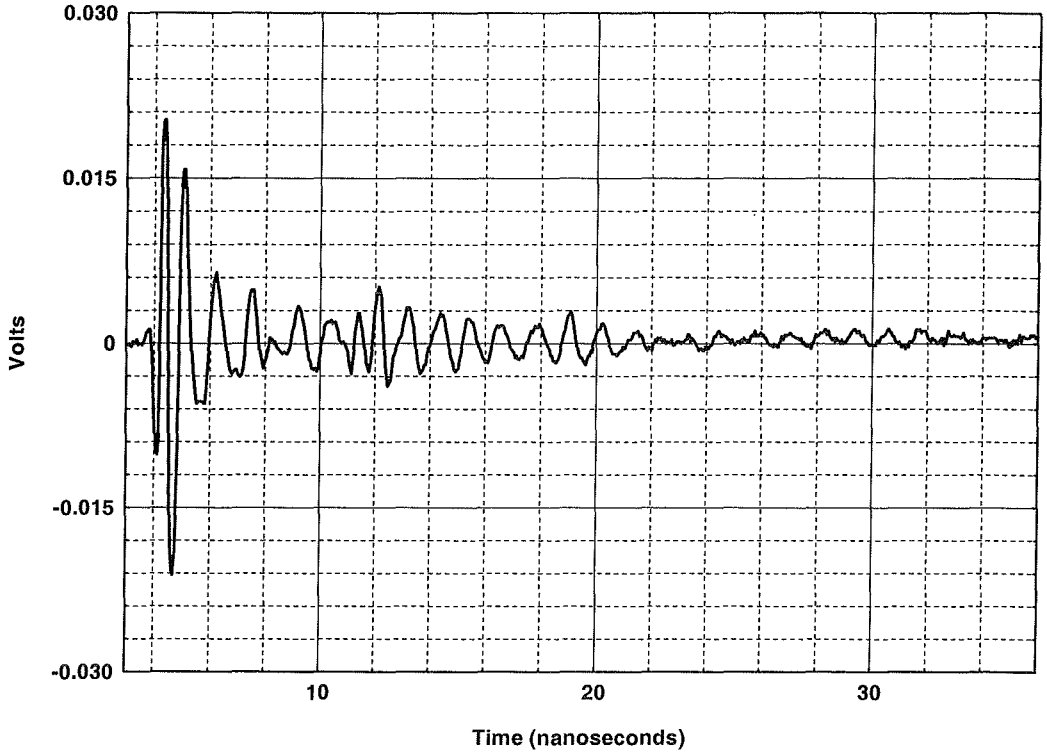

Figure D.D.3. Device D, radiated time-domain waveform.

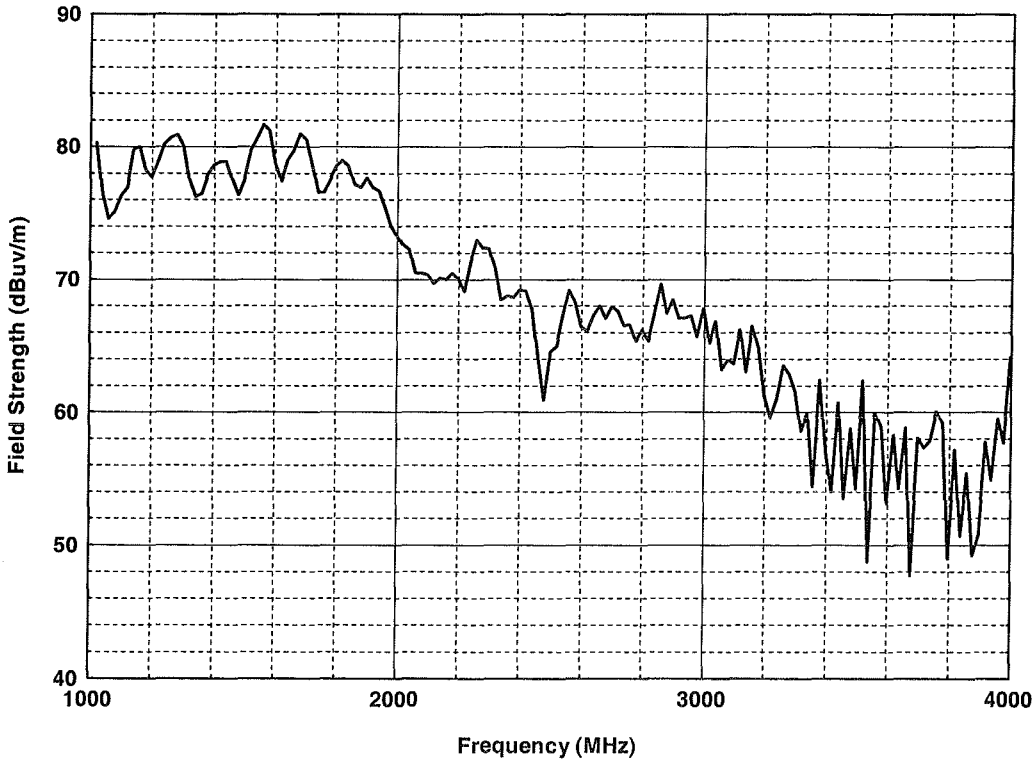

Figure D.D.4. Device D, radiated peak field strength at 1 m, Δf = 19.98 MHz.

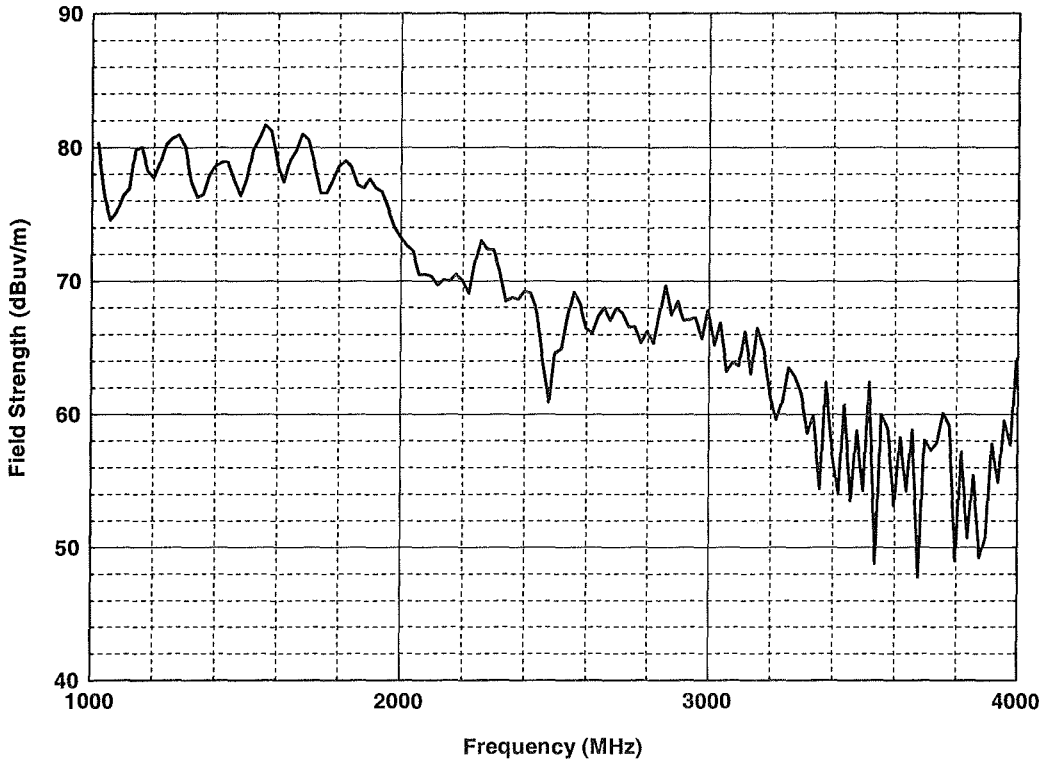

Figure D.D.5. Device D, radiated peak field strength at 1 m, Δf = 19.98 MHz.

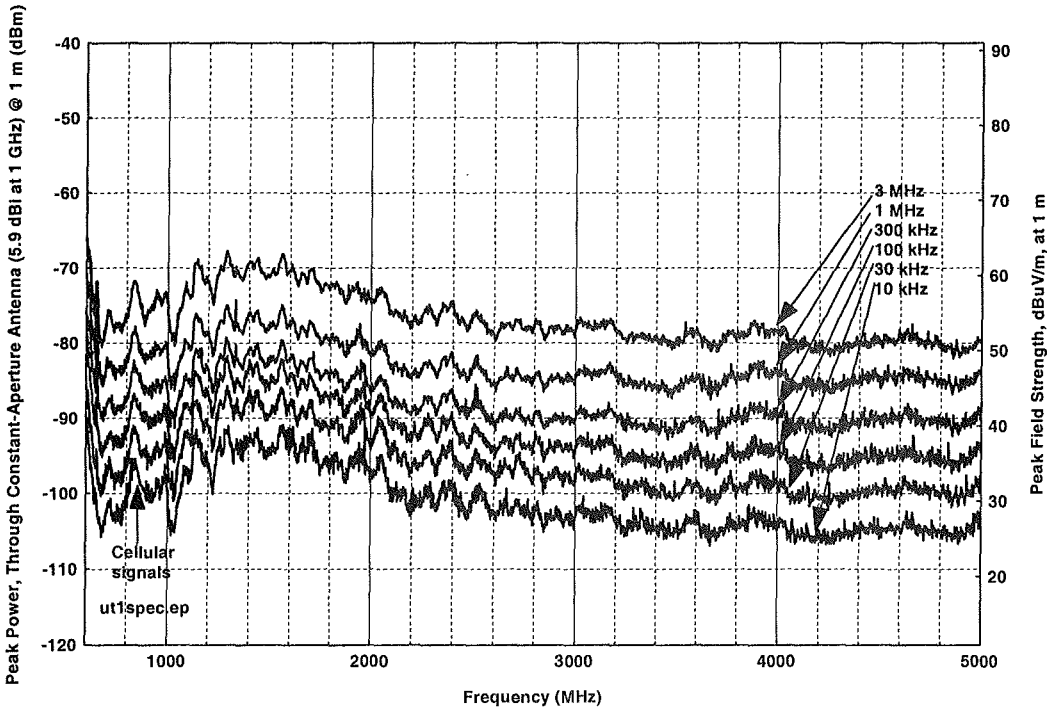

Figure D.D.6. Device D, absolute dither, 1-MHz nominal PRR, no gating.

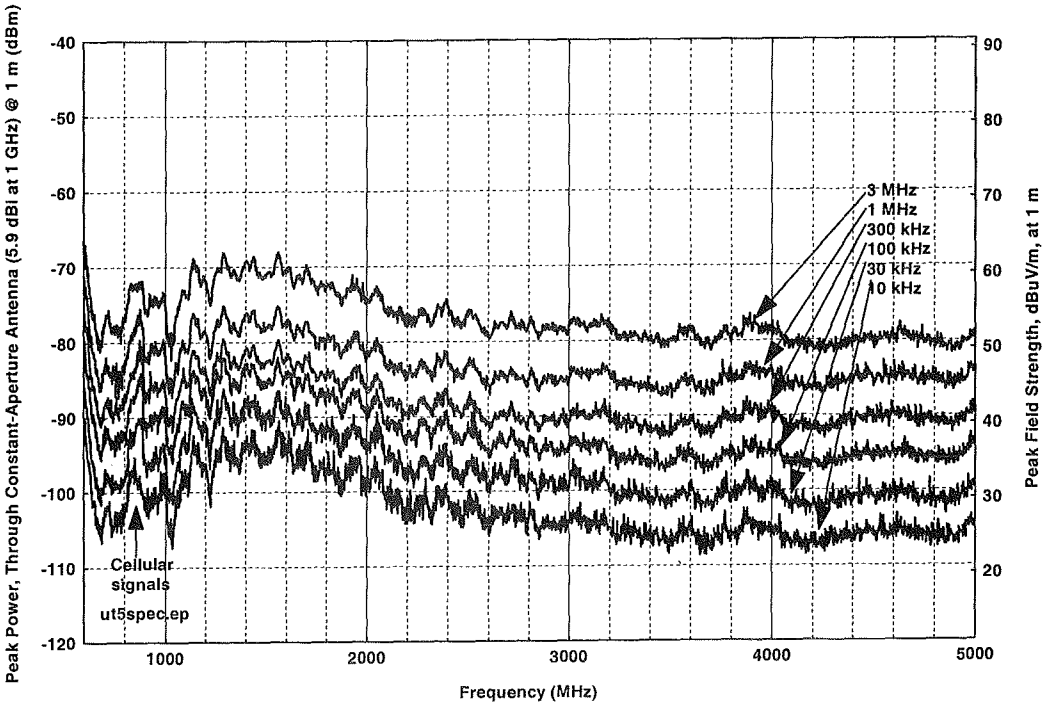

Figure D.D.7. Device D, absolute dither, 1-MHz nominal PRR, 25% gating.

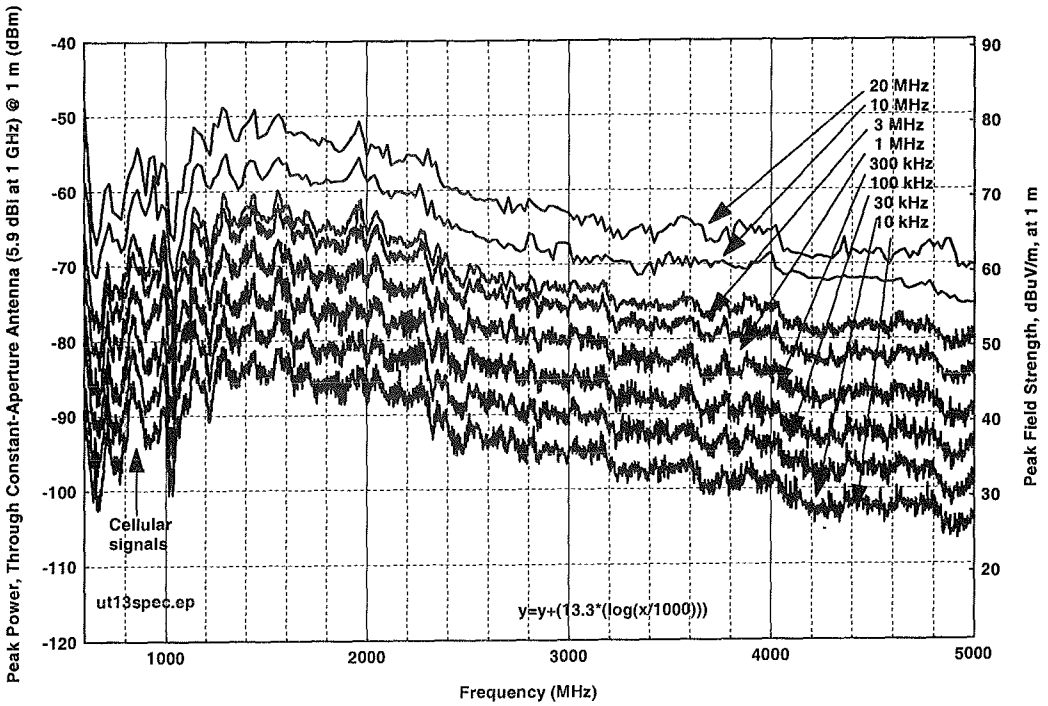

Figure D.D.8. Device D, absolute dither, 10-MHz nominal PRR, no gating.

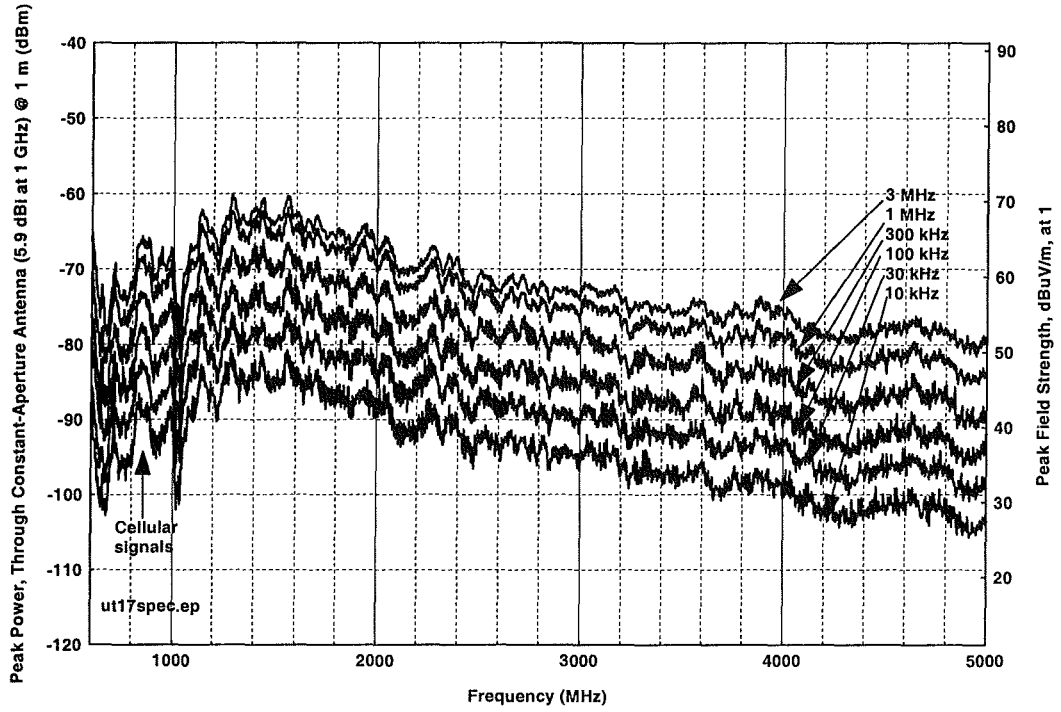

Figure D.D.9. Device D, absolute dither, 10-MHz nominal PRR, 25% gating.

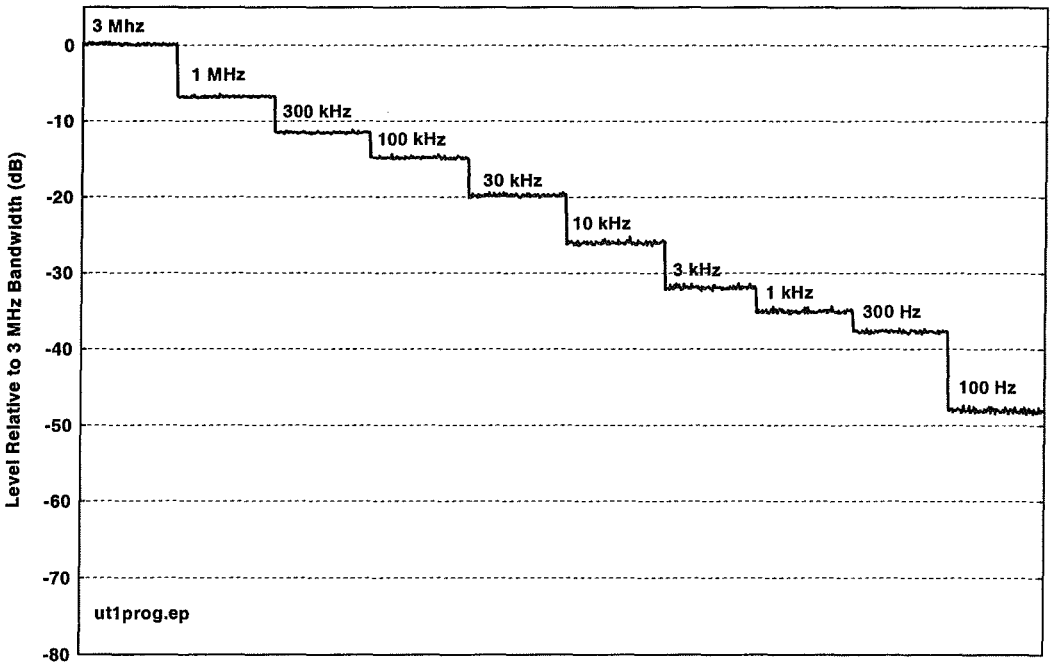

Figure D.D.10. Device D, 1-MHz nominal PRR, no gating, 25% dither (absolute time base).

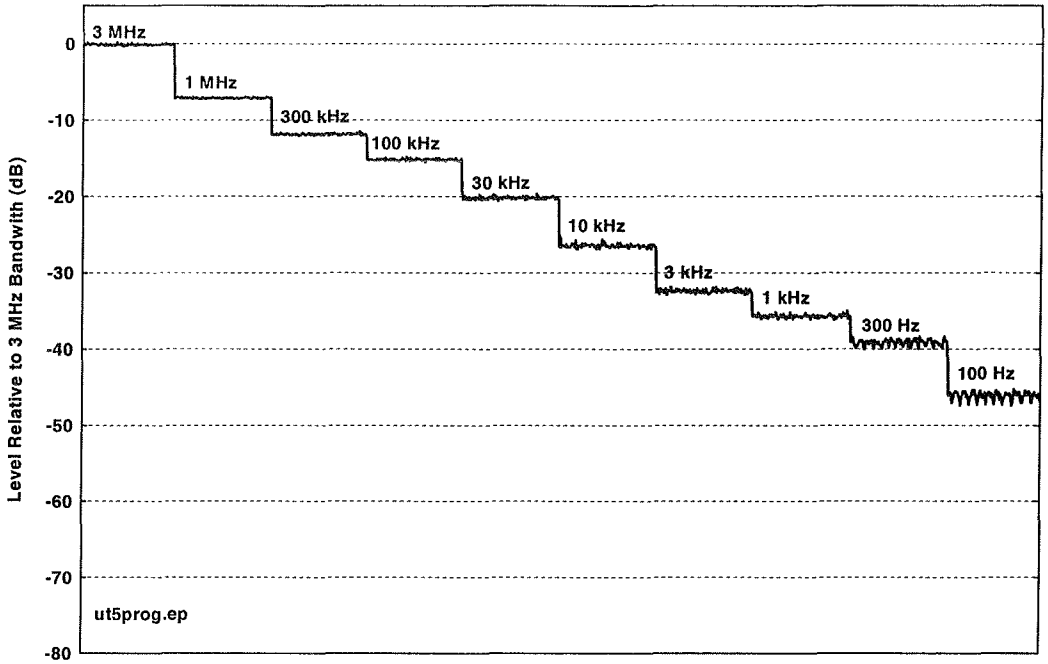

Figure D.D.11. Device D, 1-MHz nominal PRR, 25% gating, 25% dither (absolute time base) stairstep.

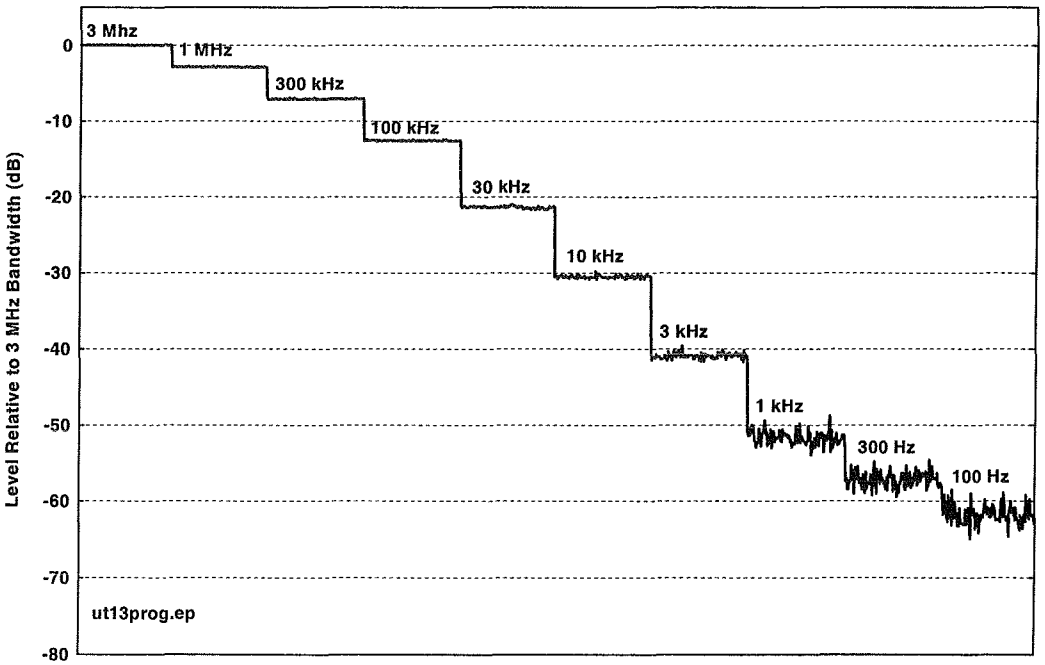

Figure D.D.12. Device D, 10-MHz nominal PRR, no gating, 25% dither (absolute time base) stairstep.

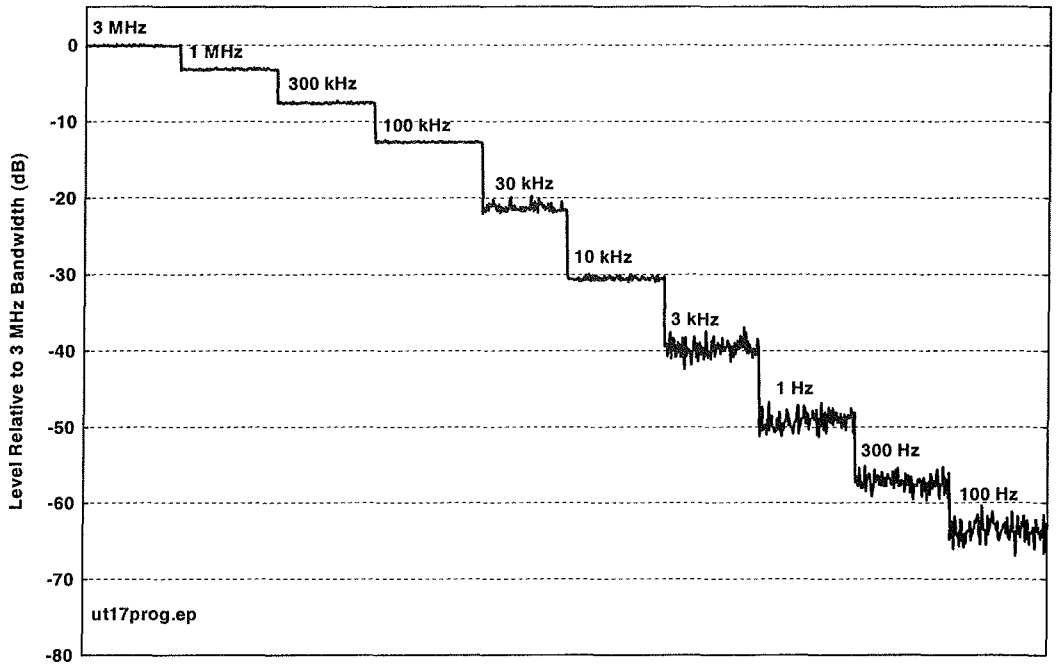

Figure D.D.13. Device D, 10-MHz nominal PRR, 25% gating, 25% dither (absolute time base) stairstep.

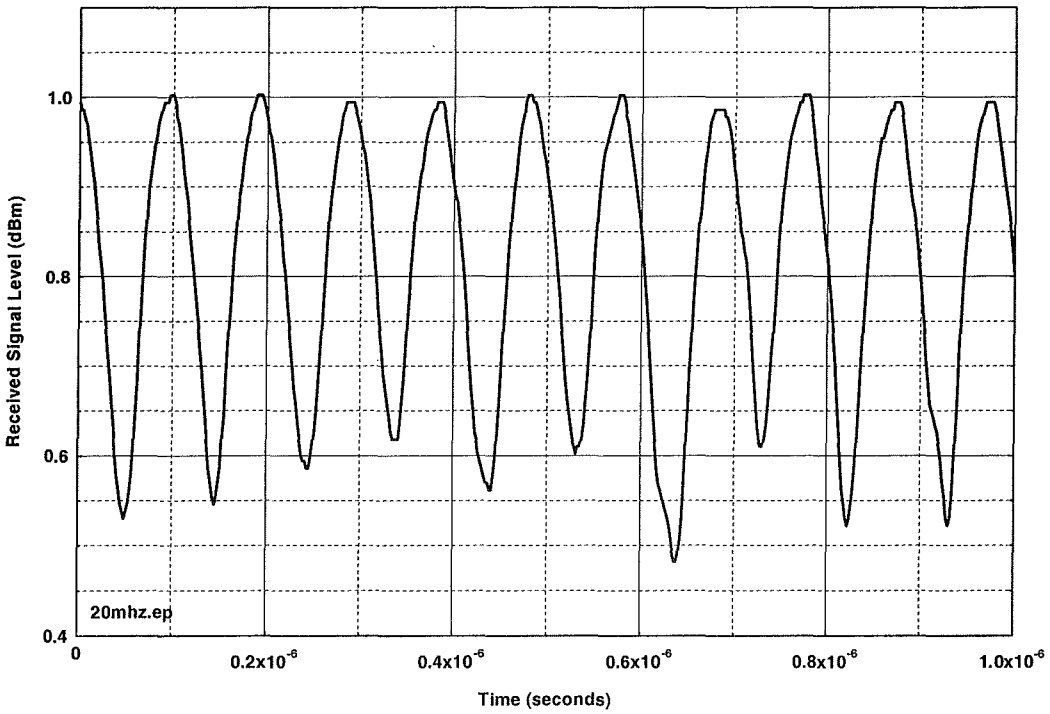

Figure D.D.14. Device D, 10-MHz nominal PRR, no gating, 25% dither, 20-MHz measurement bandwidth.

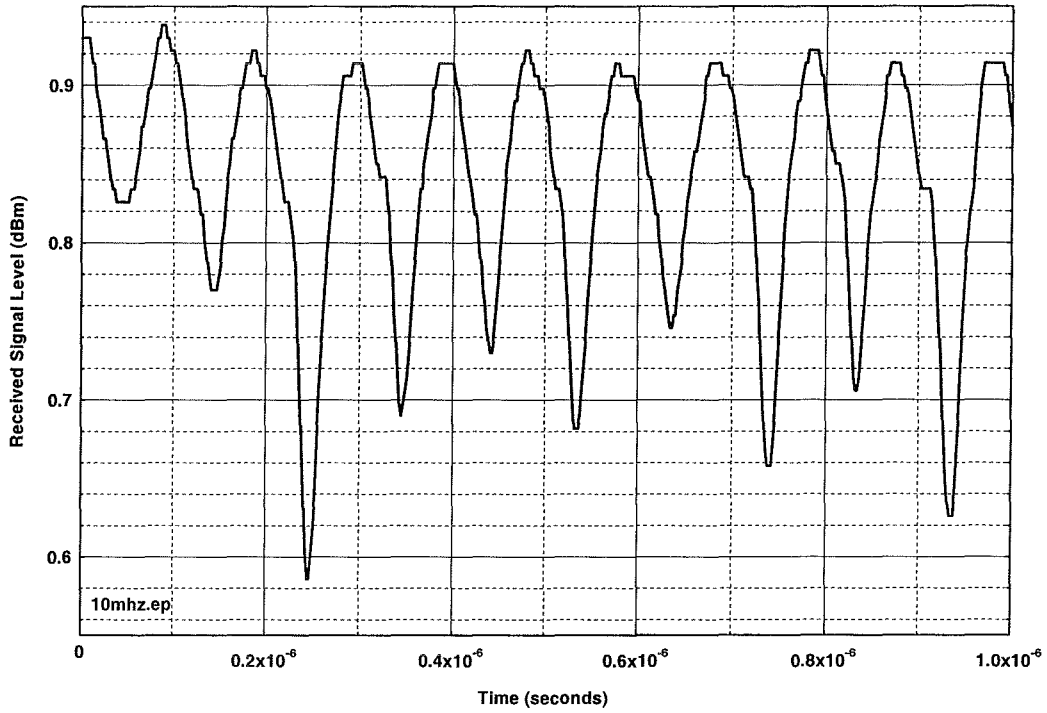

Figure D.D.15. Device D, 10-MHz nominal PRR, no gating, 25% dither, 10-MHz measurement bandwidth.

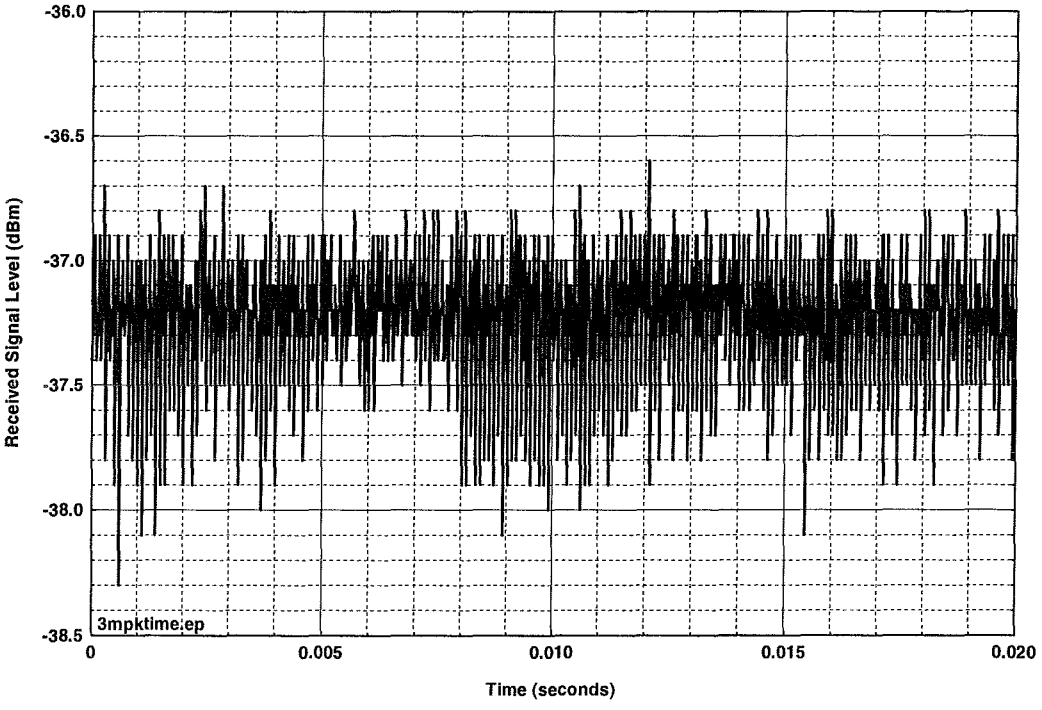

Figure D.D.16. Device D, 10-MHz nominal PRR, no gating, 25% dither, 3-MHz measurement bandwidth.

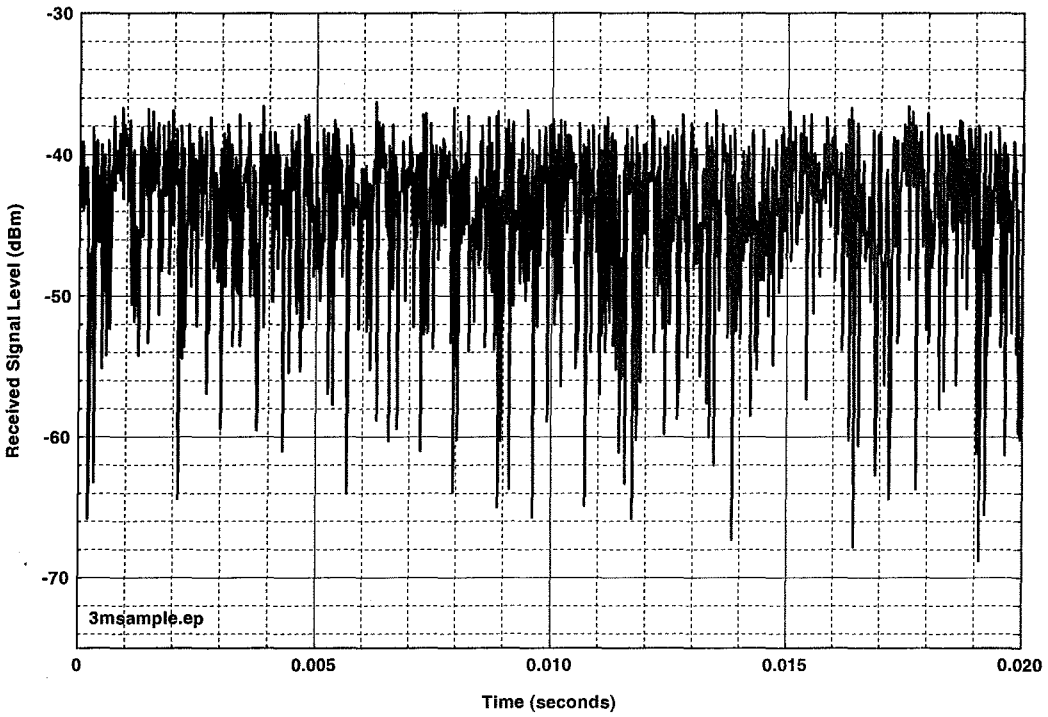

Figure D.D.17. Device D, 10-MHz nominal PRR, no gating, 25% dither, 3-MHz bandwidth, sample detector.

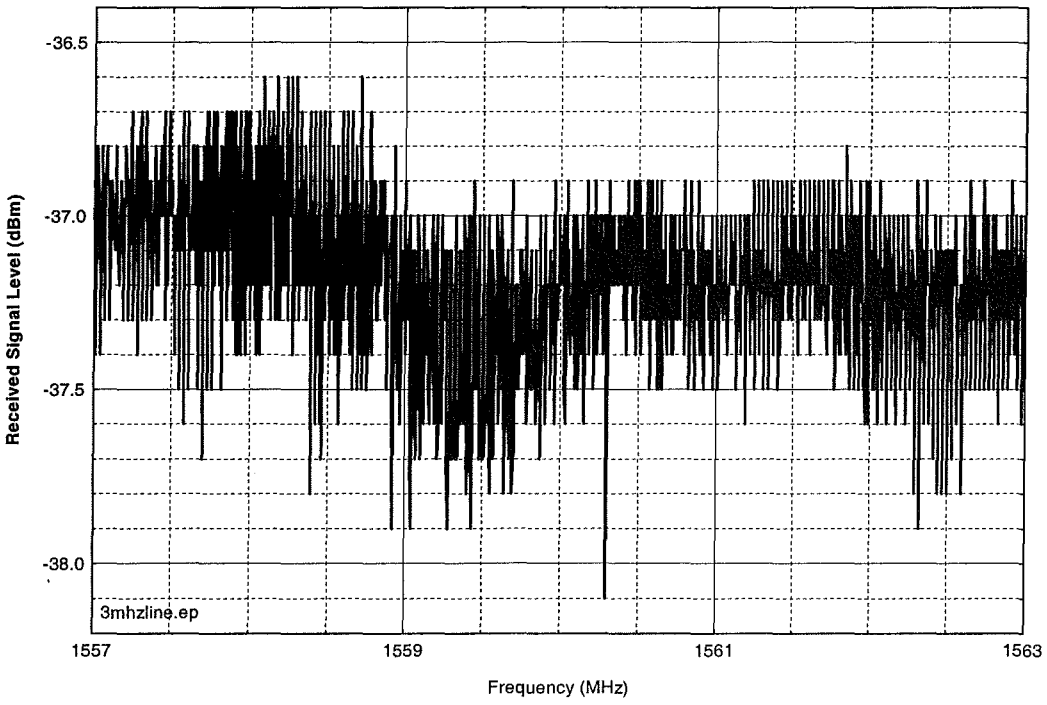

Figure D.D.18. Device D, 10-MHz nominal PRR, no gating, 25% dither, 3-MHz bandwidth.

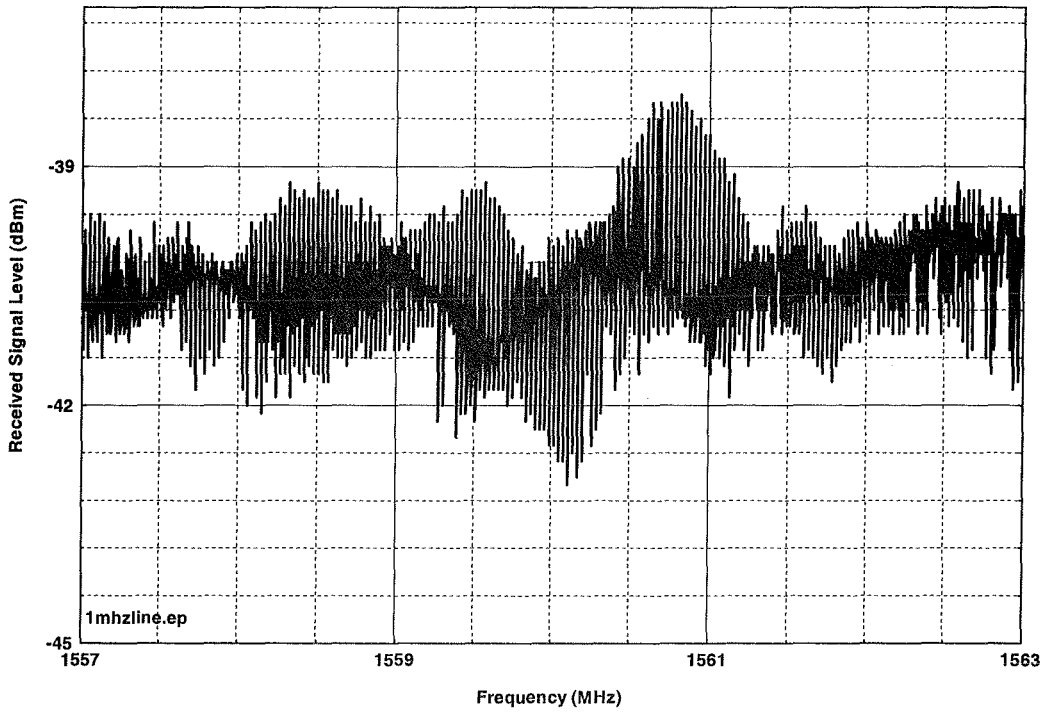

Figure D.D.19. Device D, 10-MHz nominal PRR, no gating, 25% dither, 1-MHz measurement bandwidth..

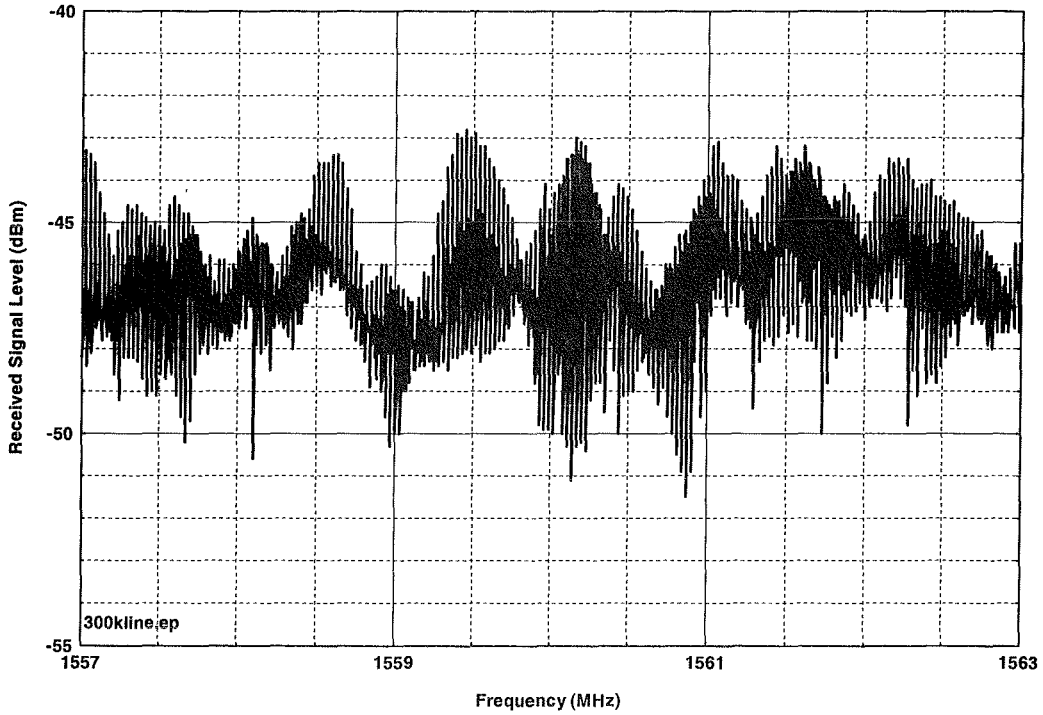

Figure D.D.20. Device D, 10-MHz nominal PRR, no gating, 25% dither, 300-kHz measurement bandwidth.

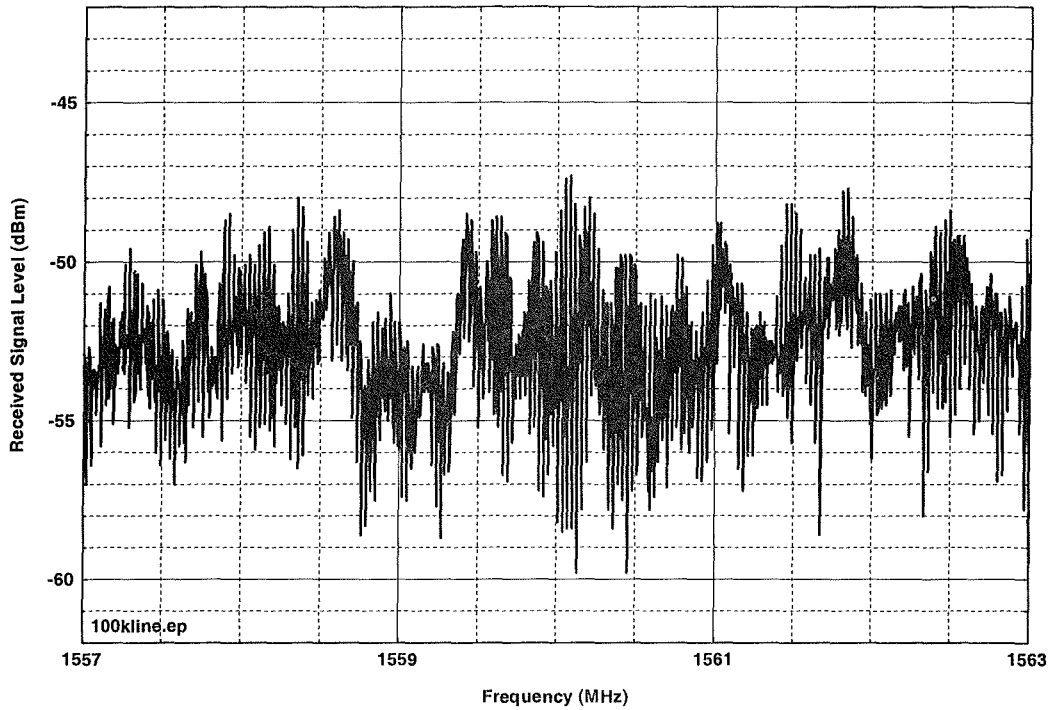

Figure D.D.21. Device D, 10-MHz nominal PRR, no gating, 25% dither, 100-kHz measurement bandwidth.

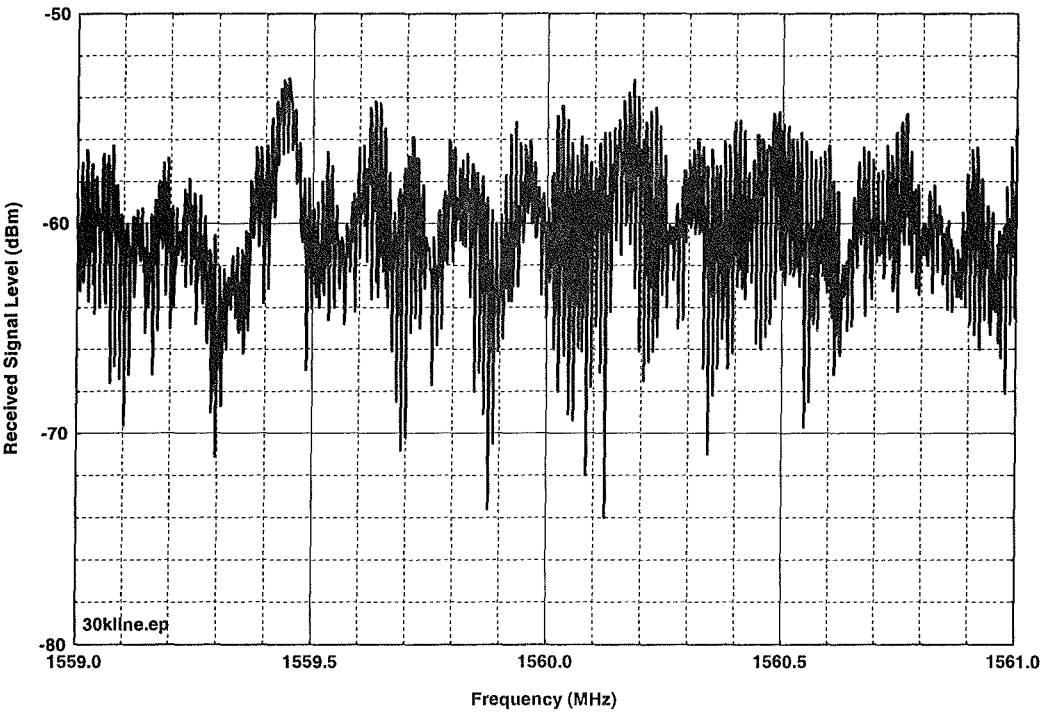

Figure D.D.22. Device D, 10-MHz nominal PRR, no gating, 25% dither, 30-kHz measurement bandwidth.

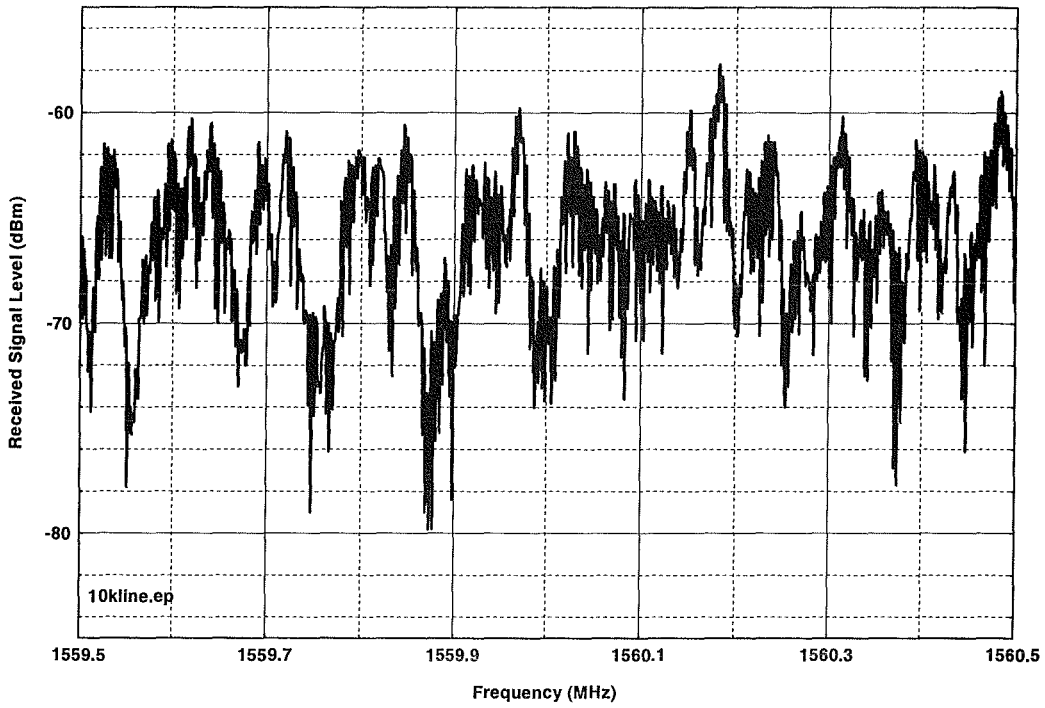

Figure D.D.23. Device D, 10-MHz nominal PRR, no gating, 25% dither, 10-kHz measurement bandwidth.

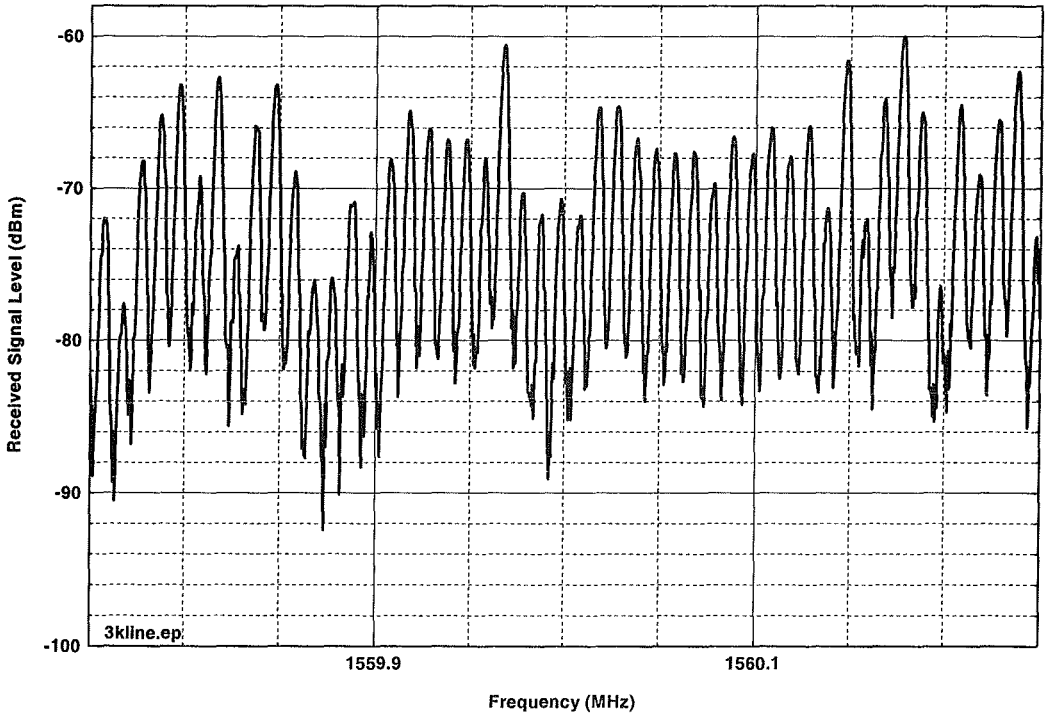

Figure D.D.24. Device D, 10-MHz nominal PRR, no gating, 25% dither, 3-kHz measurement bandwidth.

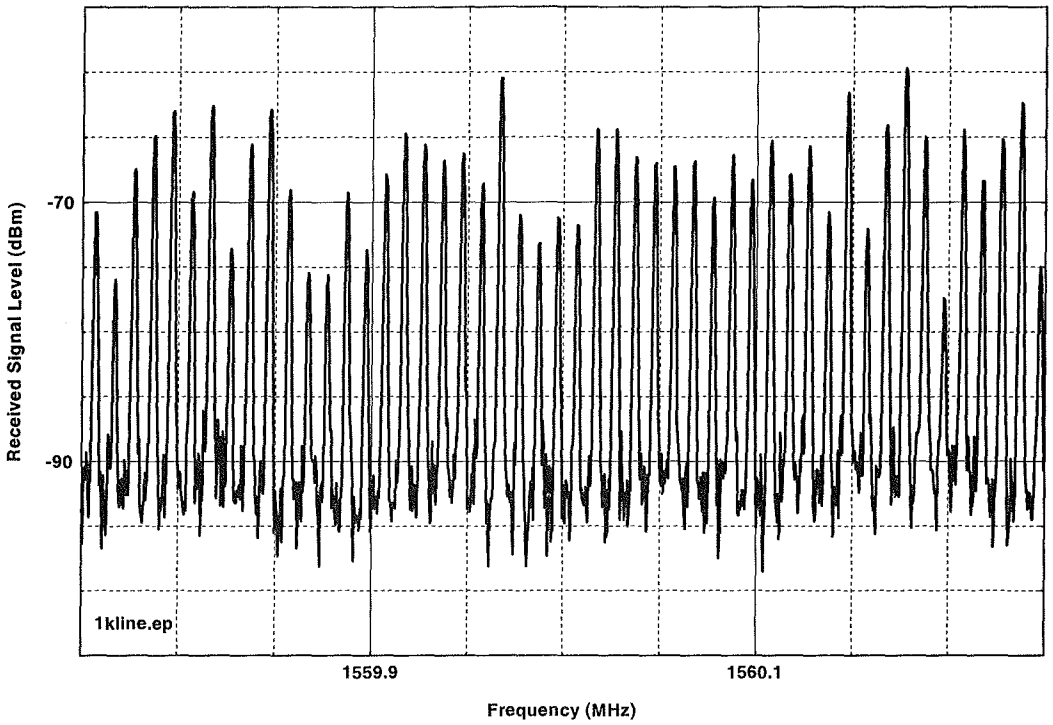

Figure D.D.25. Device D, 10-MHz nominal PRR, no gating, 25% dither, 1-kHz measurement bandwidth.

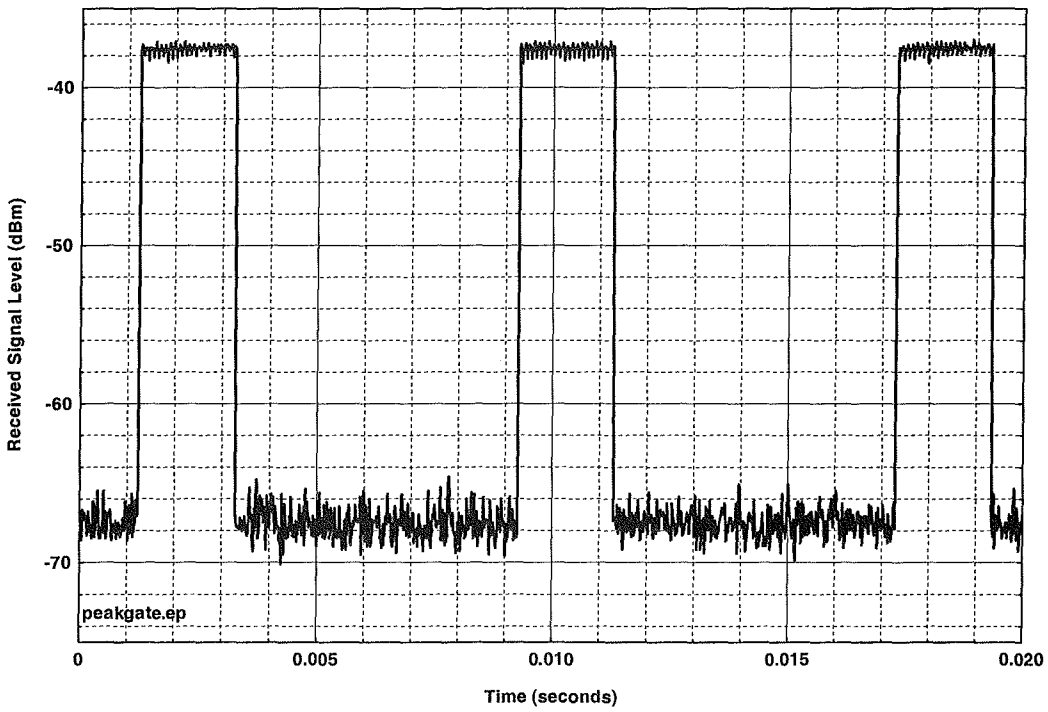

Figure D.D.26. Device D, 10-MHz nominal PRR, 25% gating, 25% dither, 3-MHz peak-detected bandwidth.

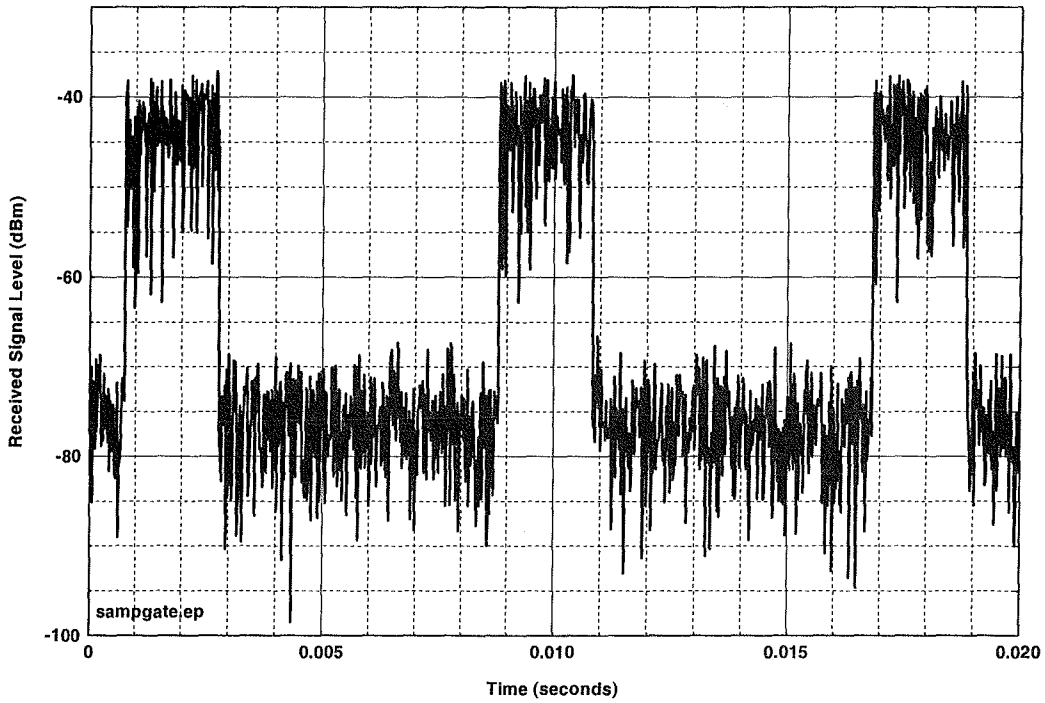

Figure D.D.27. Device D, 10-MHz nominal PRR, 25% gating, 25% dither, 3-MHz sample-detected bandwidth.

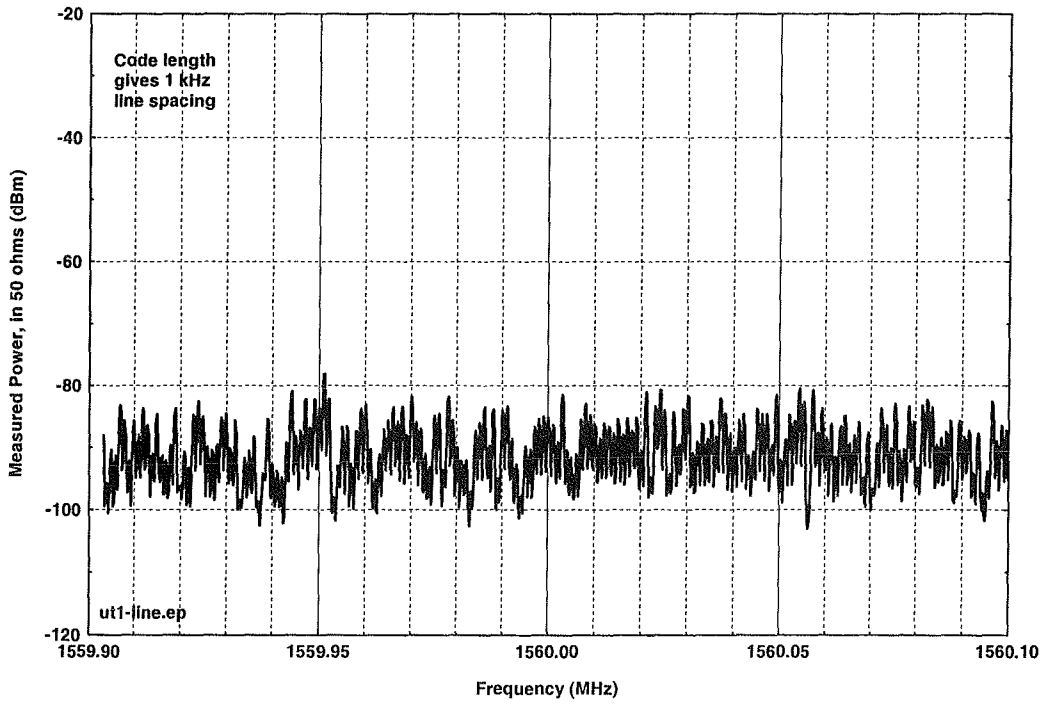

Figure D.D.28. Device D, 1-kHz emission lines with 1-MHz nominal PRR, no gating, 25% dither.

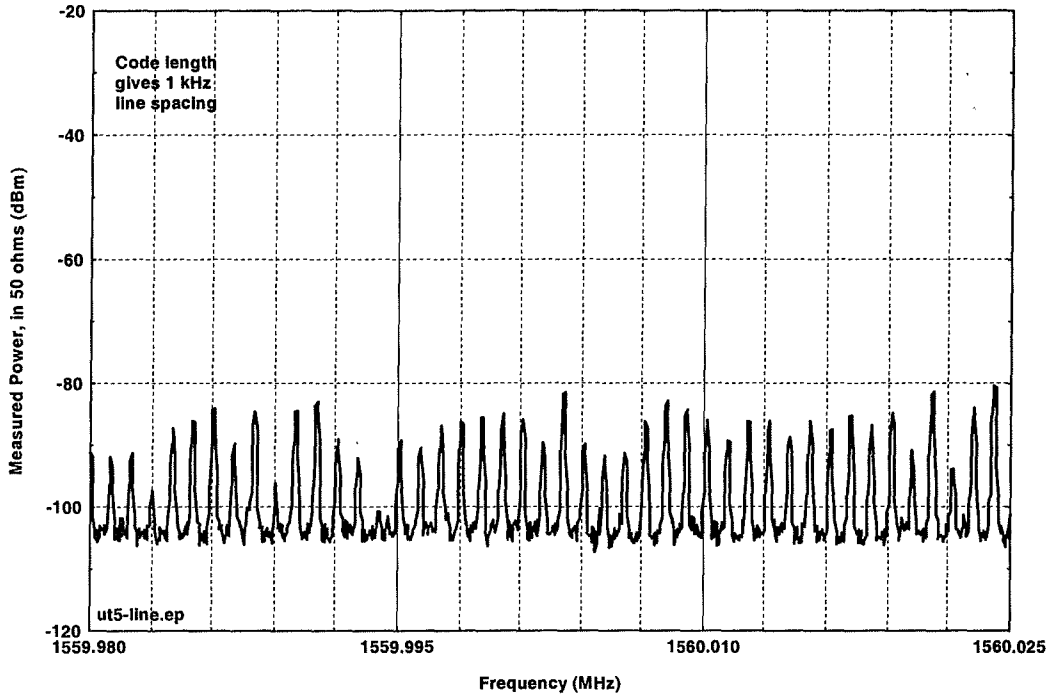

Figure D.D.29. Device D, 1-kHz emission lines with 1-MHz nominal PRR, 25% gating, 25% dither.

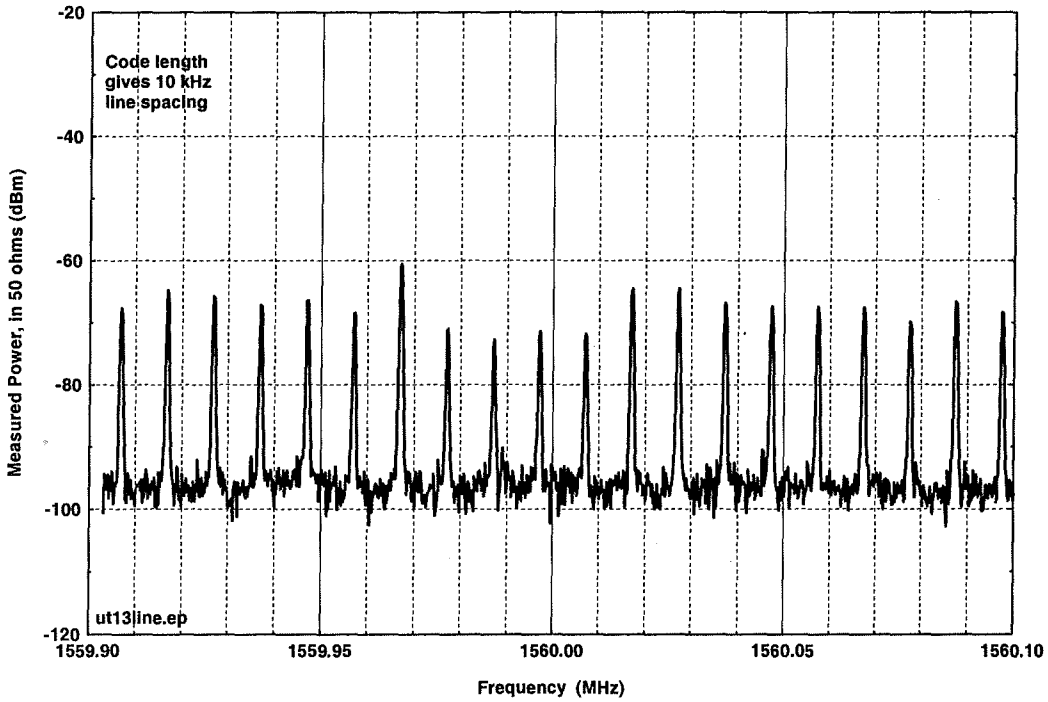

Figure D.D.30. Device D, 10-kHz emission lines with 10-MHz nominal PRR, no gating, 25% dither.

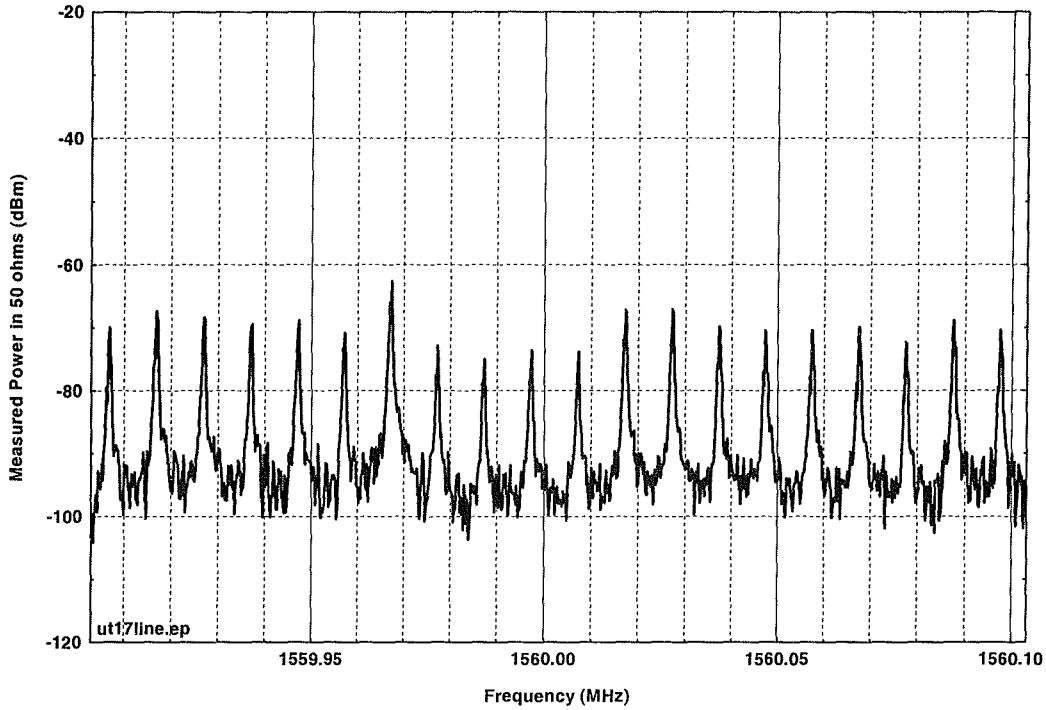

Figure D.D.31. Device D, 10-kHz emission line with 10-MHz nominal PRR, 25% gating, 25% dither.

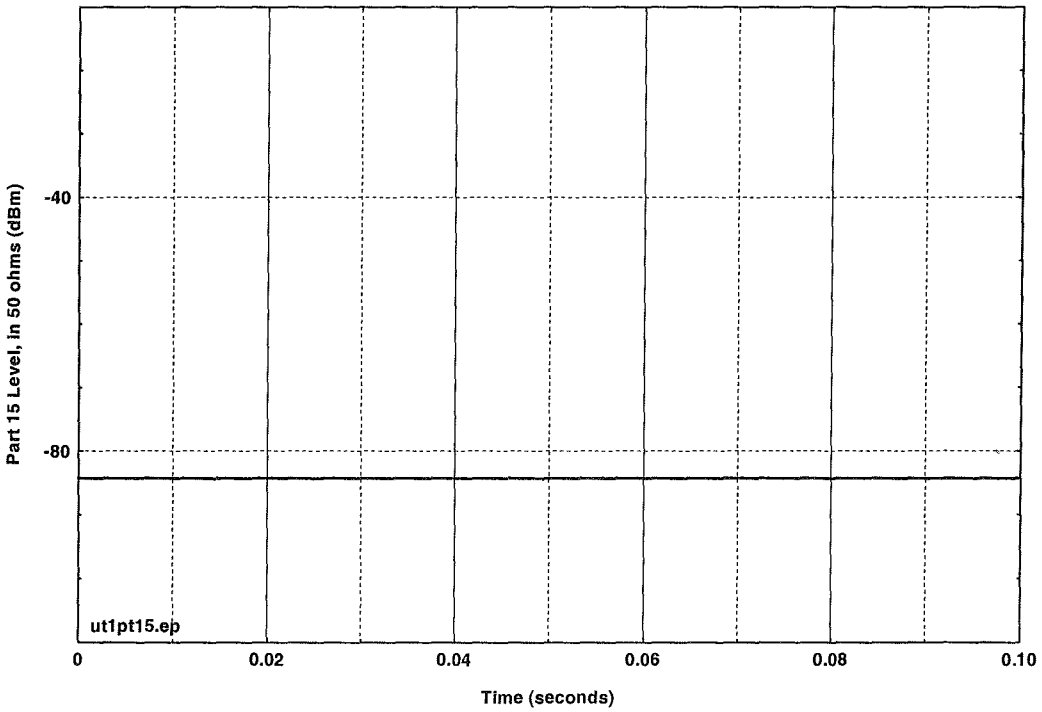

Figure D.D.32. Device D, Part 15, 1-MHz nominal PRR, no gating, 25% dither, 10-Hz video bandwidth.

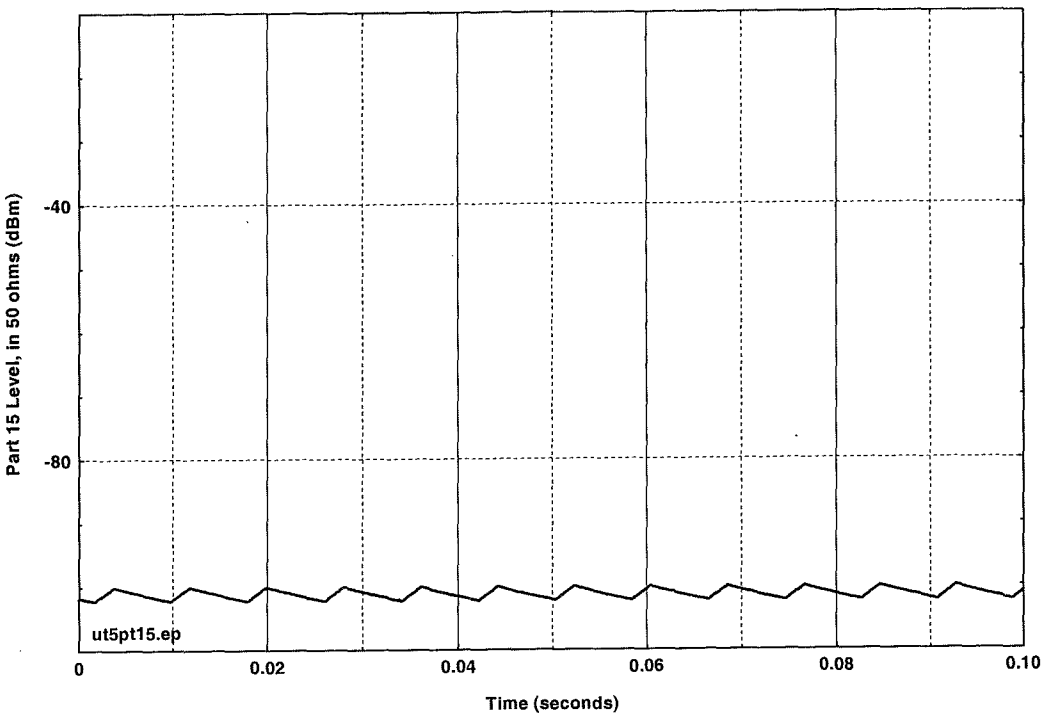

Figure D.D.33. Device D, Part 15, 1-MHz nominal PRR, 25% gating, 25% dither, 10-Hz video bandwidth.

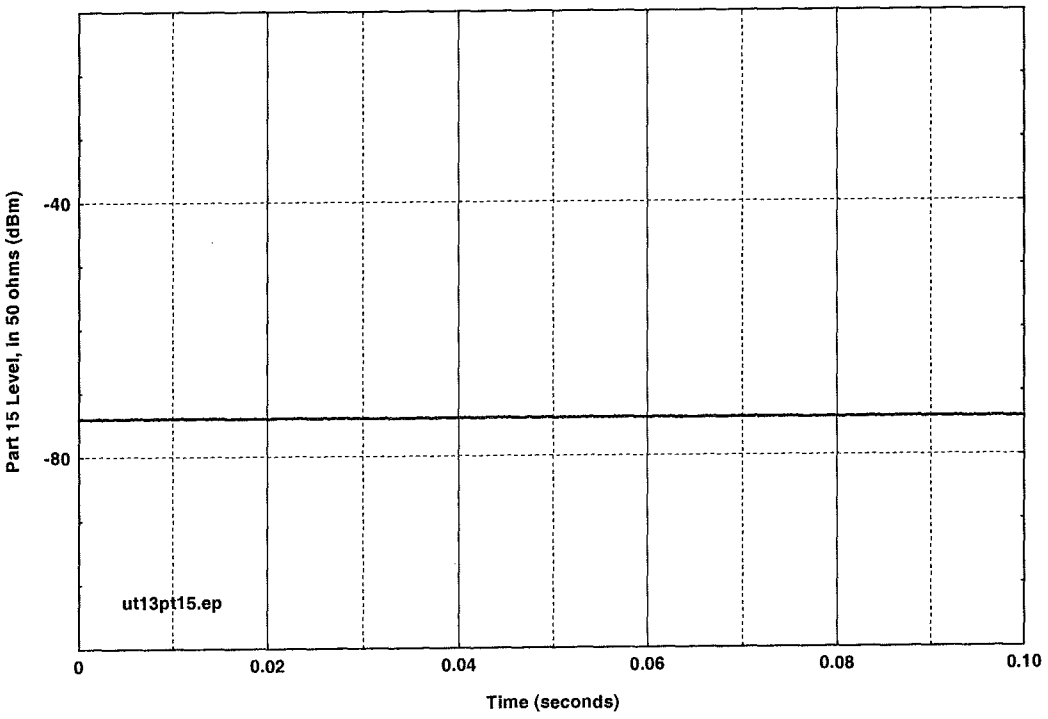

Figure D.D.34. Part 15, 10-MHz nominal PRR, no gating, 25% dither, 10-Hz video bandwidth.

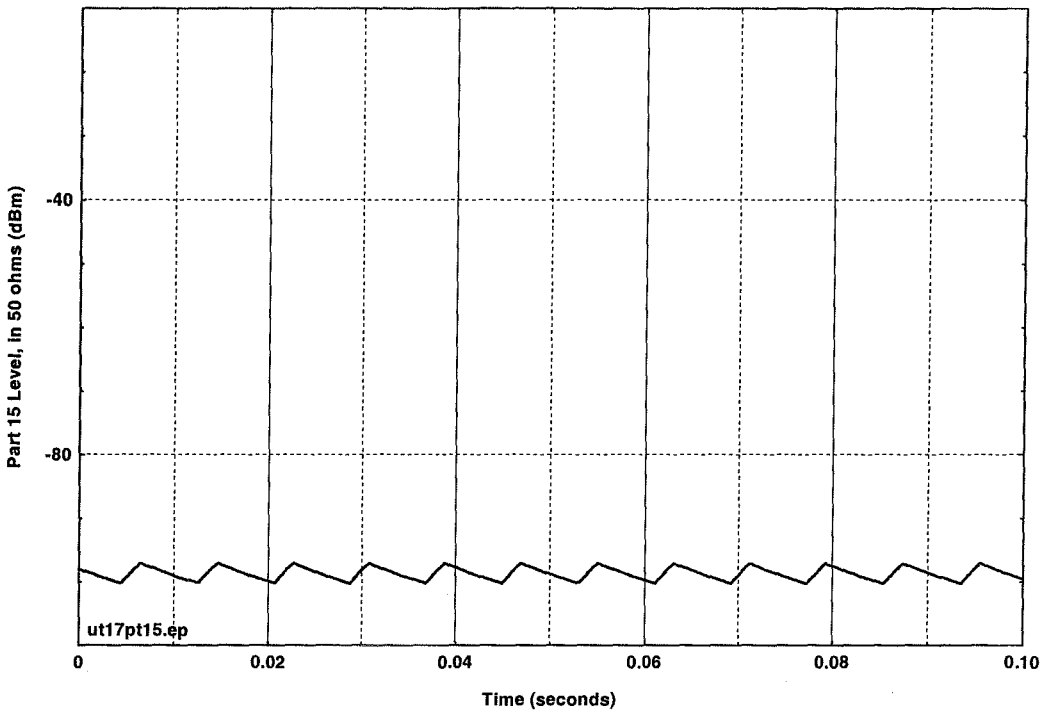

Figure D.D.35. Device D, Part 15, 10-MHz nominal PRR, 25% gating, 25% dither, 10-Hz video bandwidth.

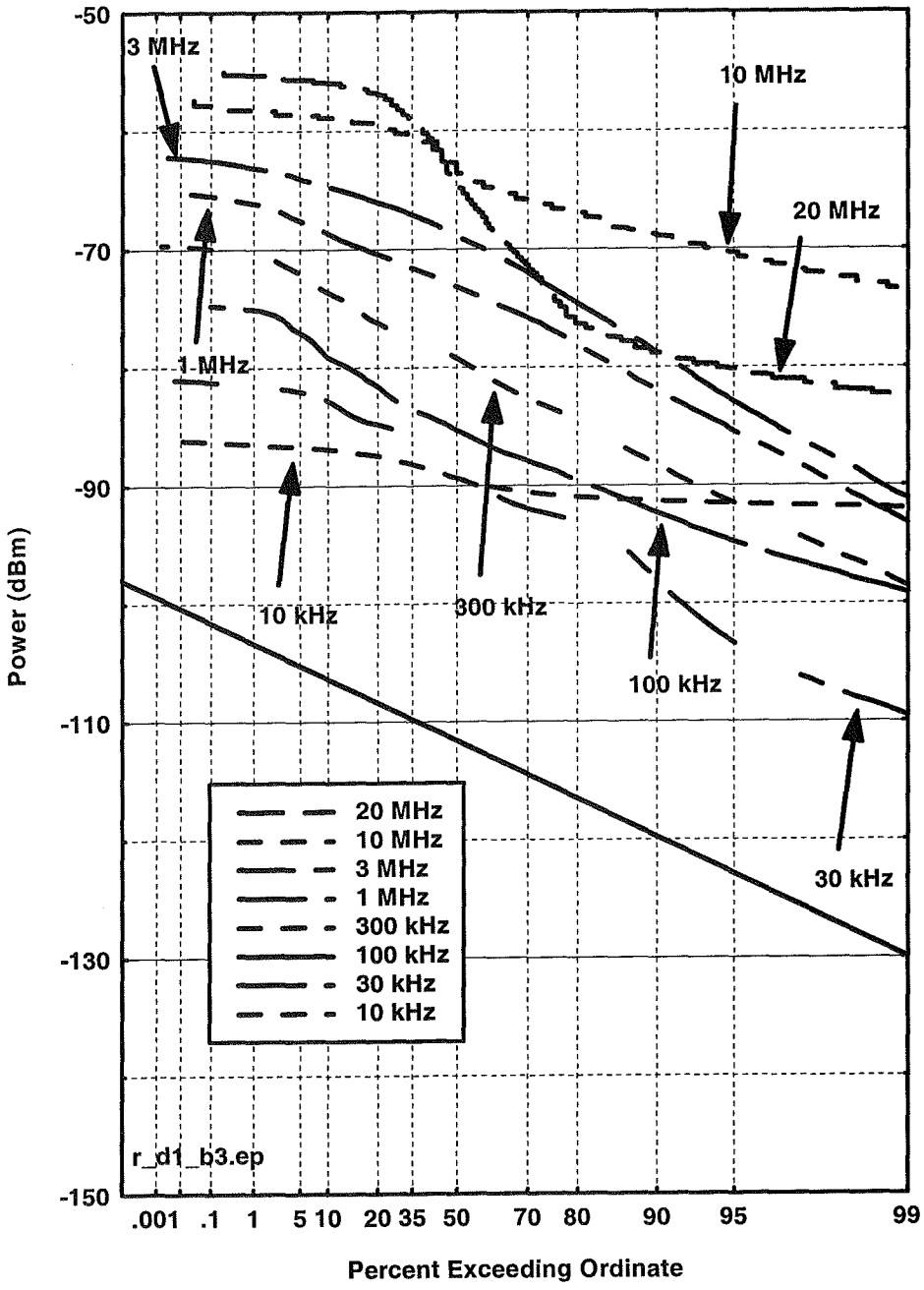

Figure D.D.36. Device D, 10-MHz PRR, 100% gating, APDs.

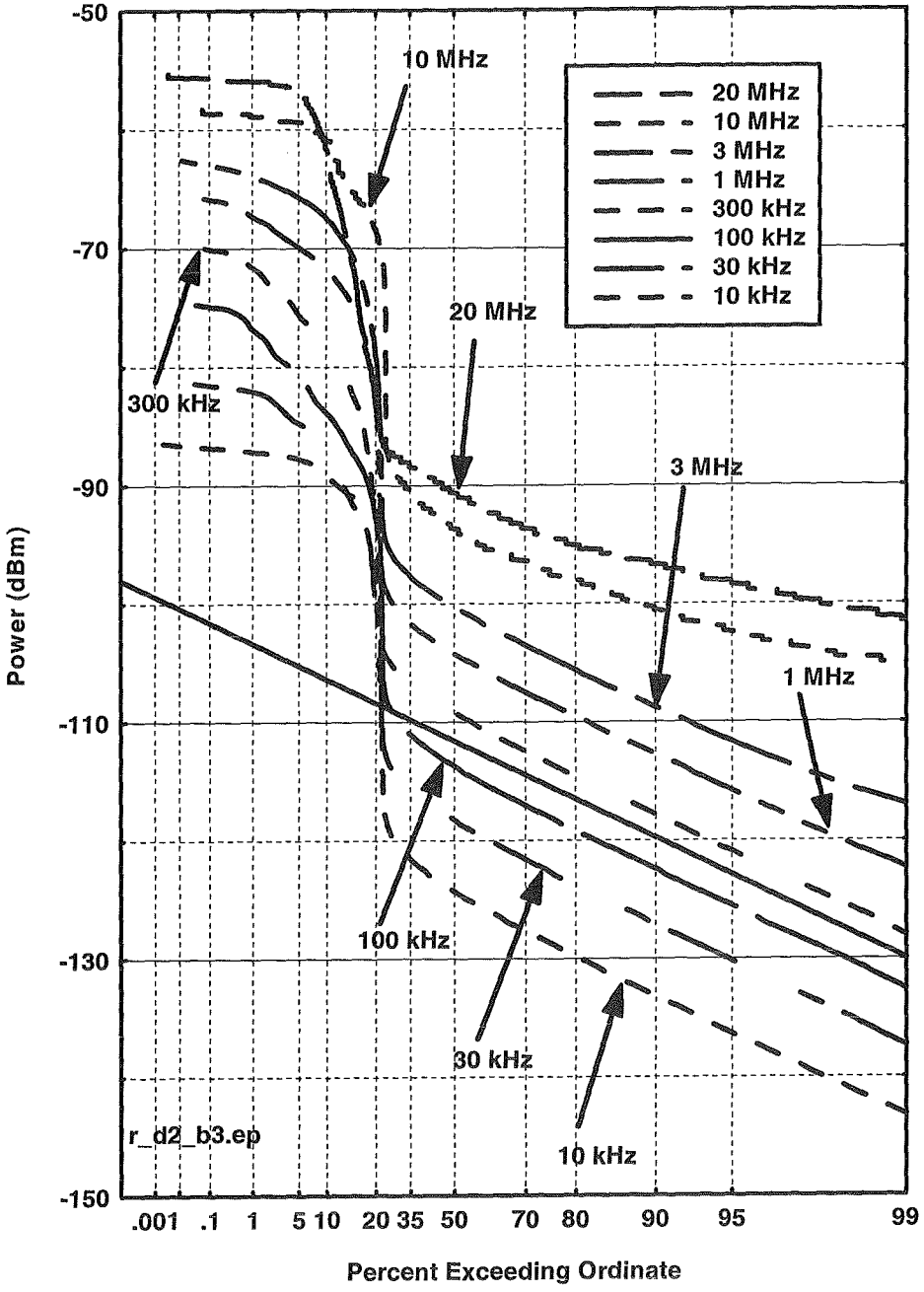

Figure D.D.37. Device D, 10-MHz PRR, 25% gating, APDs.

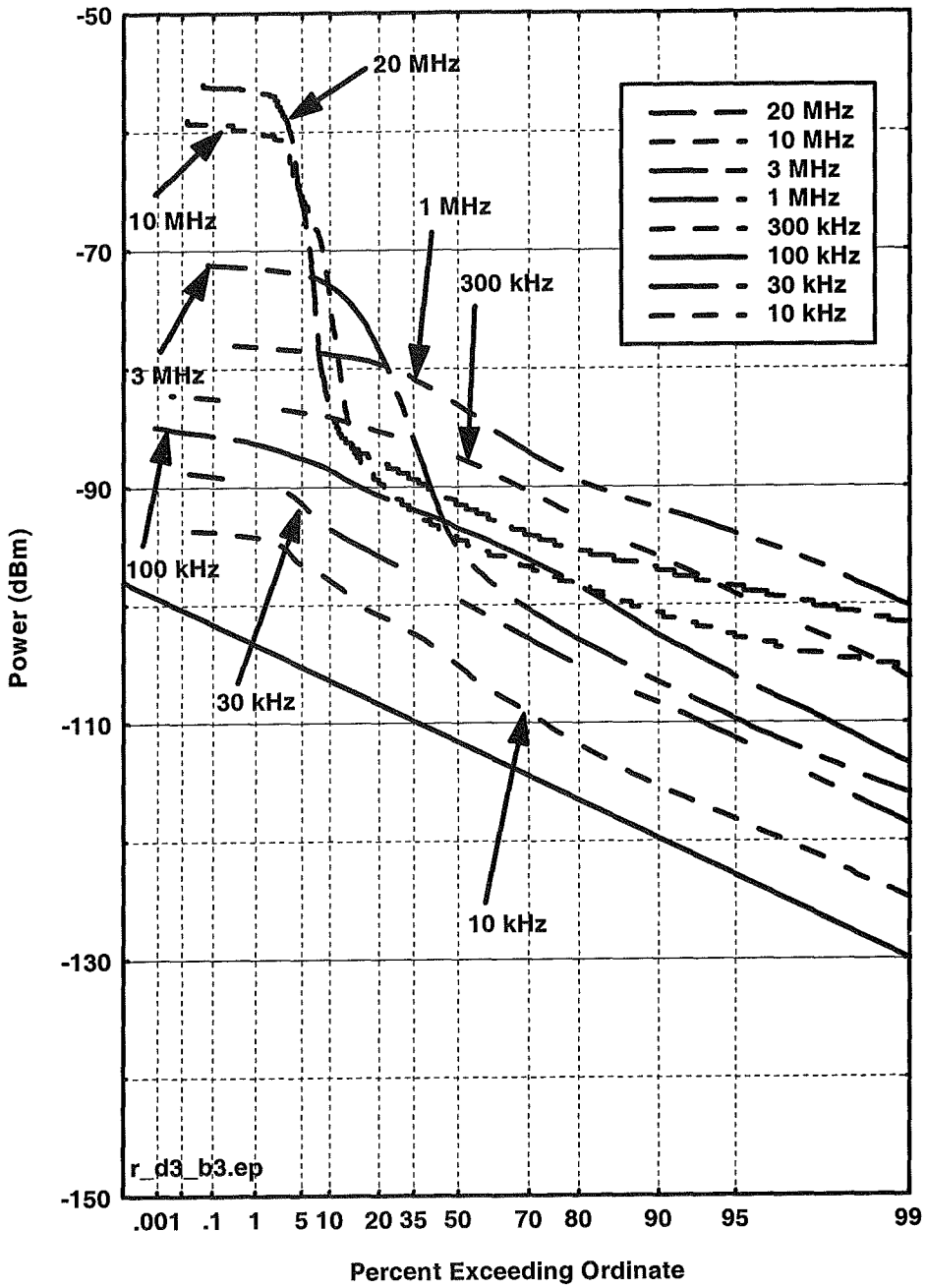

Figure D.D.38. Device D, 1-MHz PRR, 100% gating, APDs.

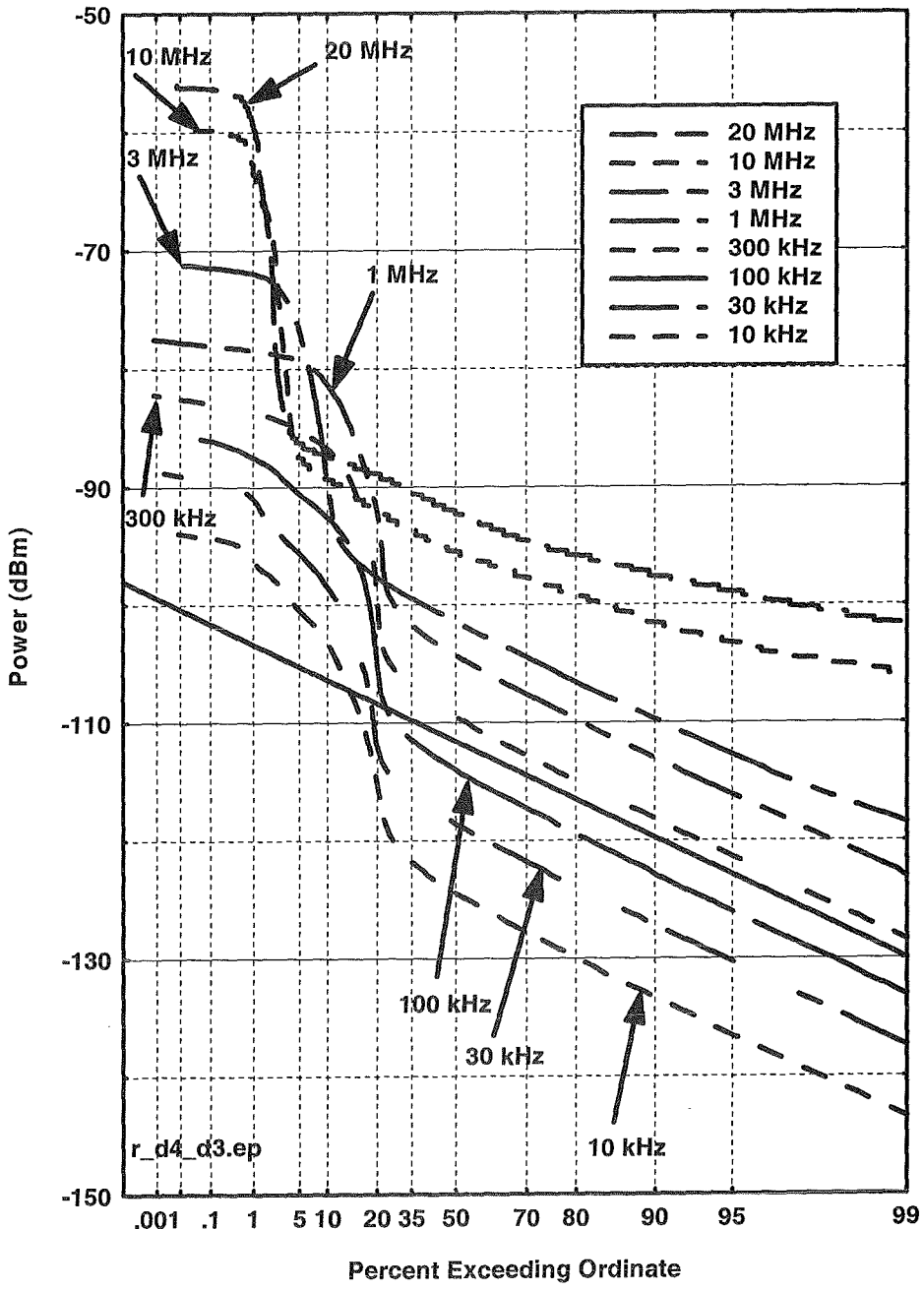

Figure D.D.39. Device D, 1-MHz PRR, 25% gating, APDs.

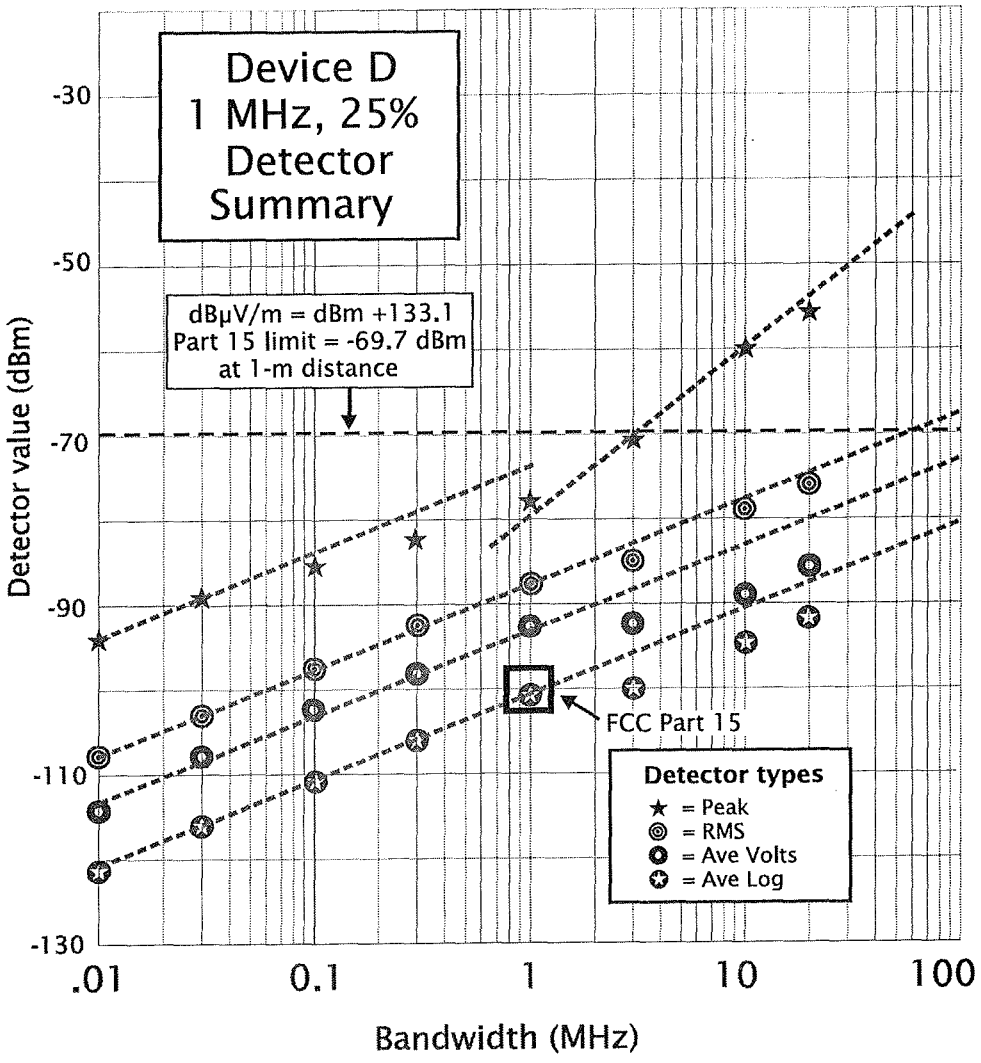

Figure D.D.40. Device D, 1-MHz PRR, 25% gating, detector summary.

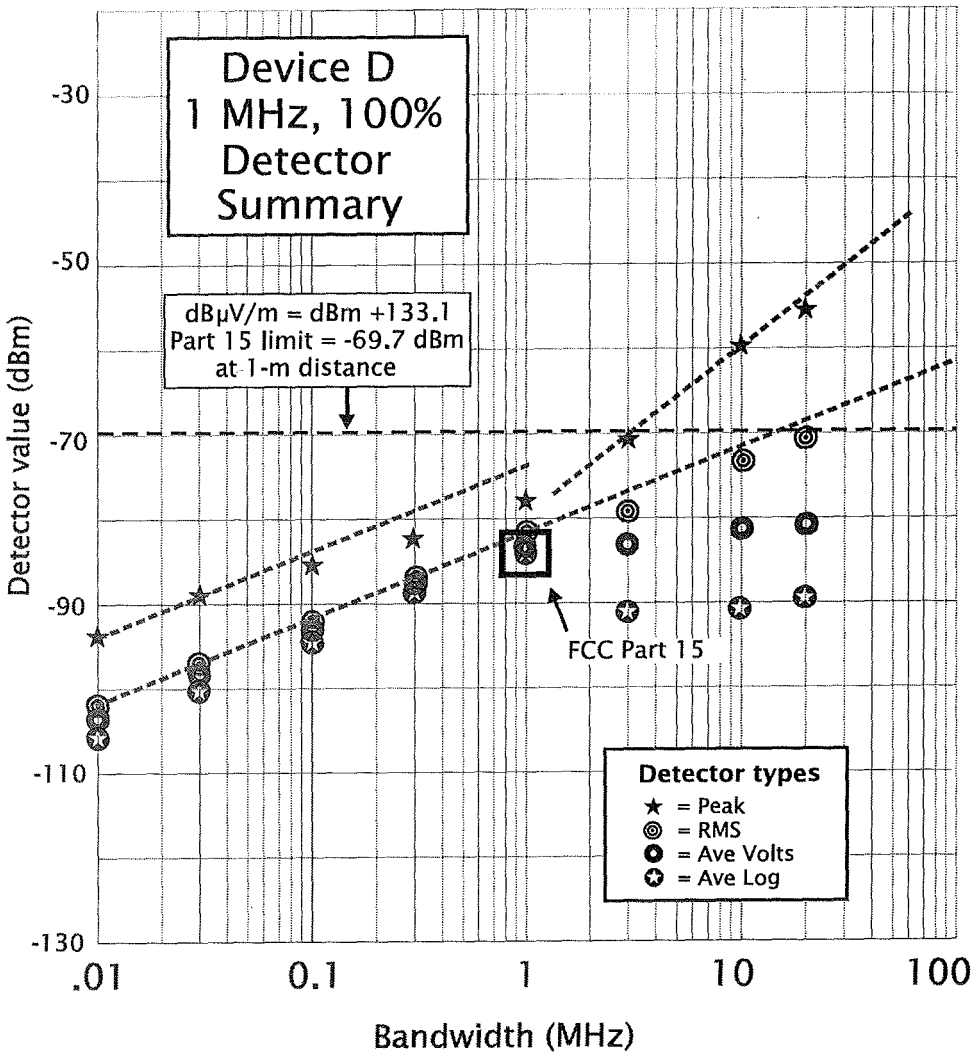

Figure D.D.41. Device D, 1-MHz PRR, 100% gating, detector summary.

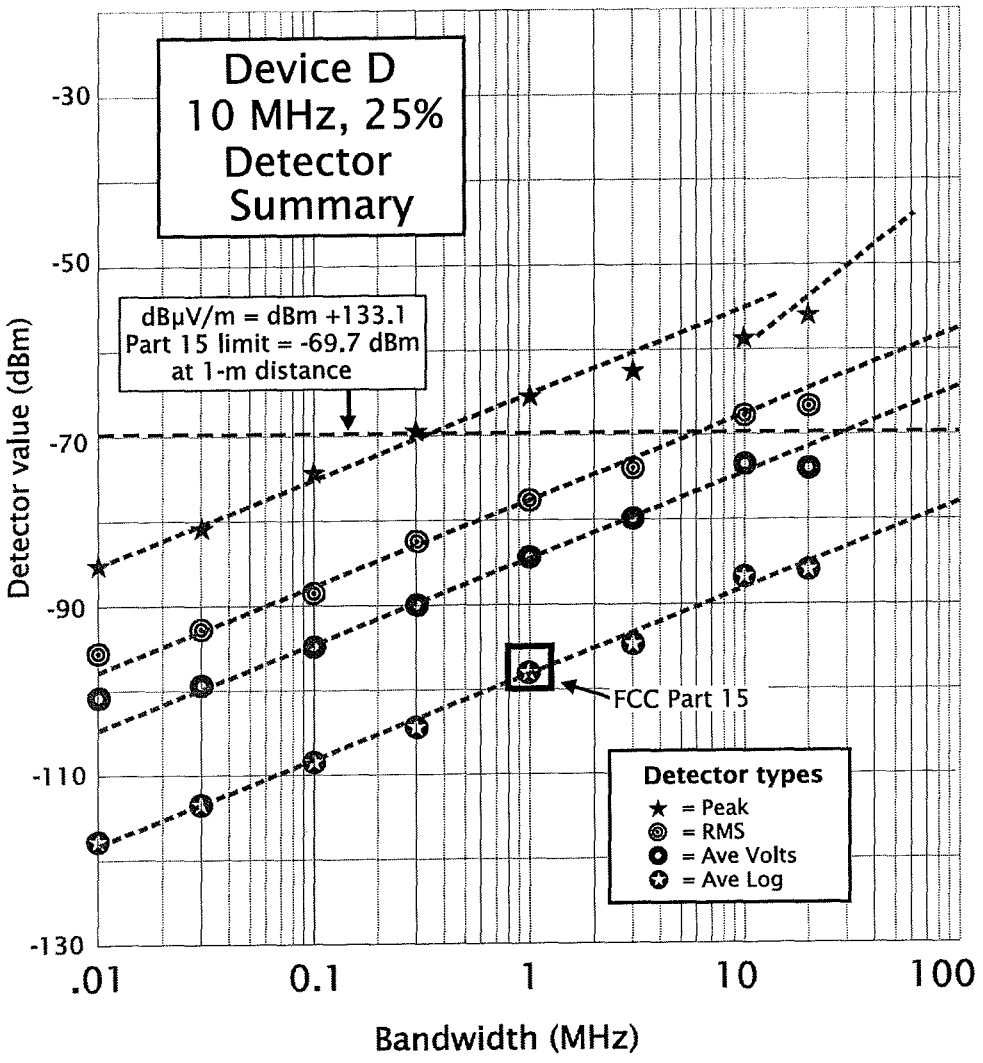

Figure D.D.42. Device D, 10-MHz PRR, 25% gating, detector summary.

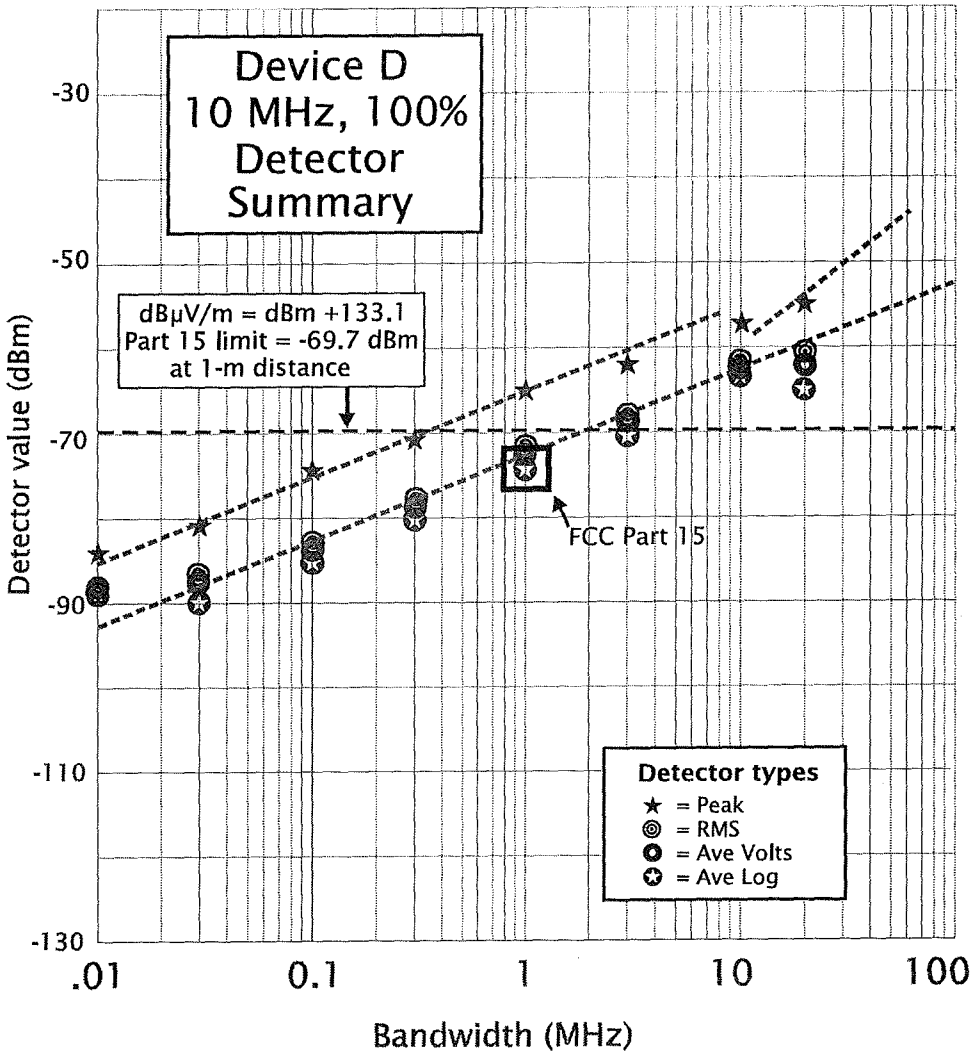

Figure D.D.43. Device D, 10-MHz PRR, 100% gating, detector summary.

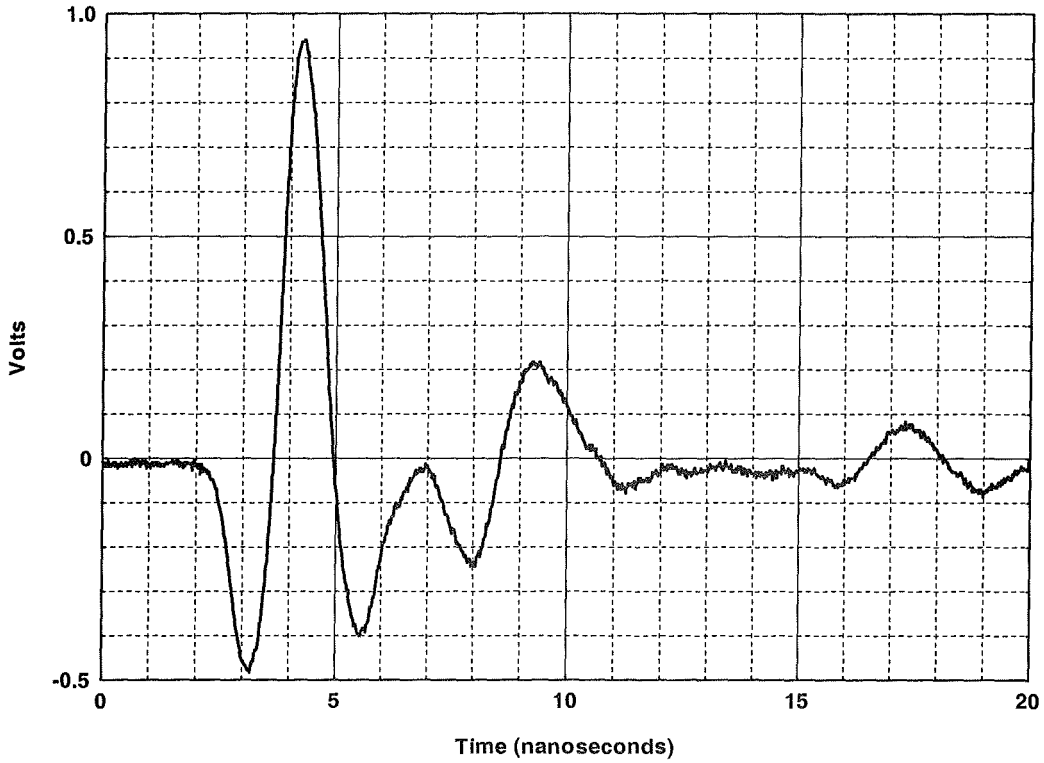

Figure D.E.1. Device E, (300 MHz) radiated time-domain waveform.

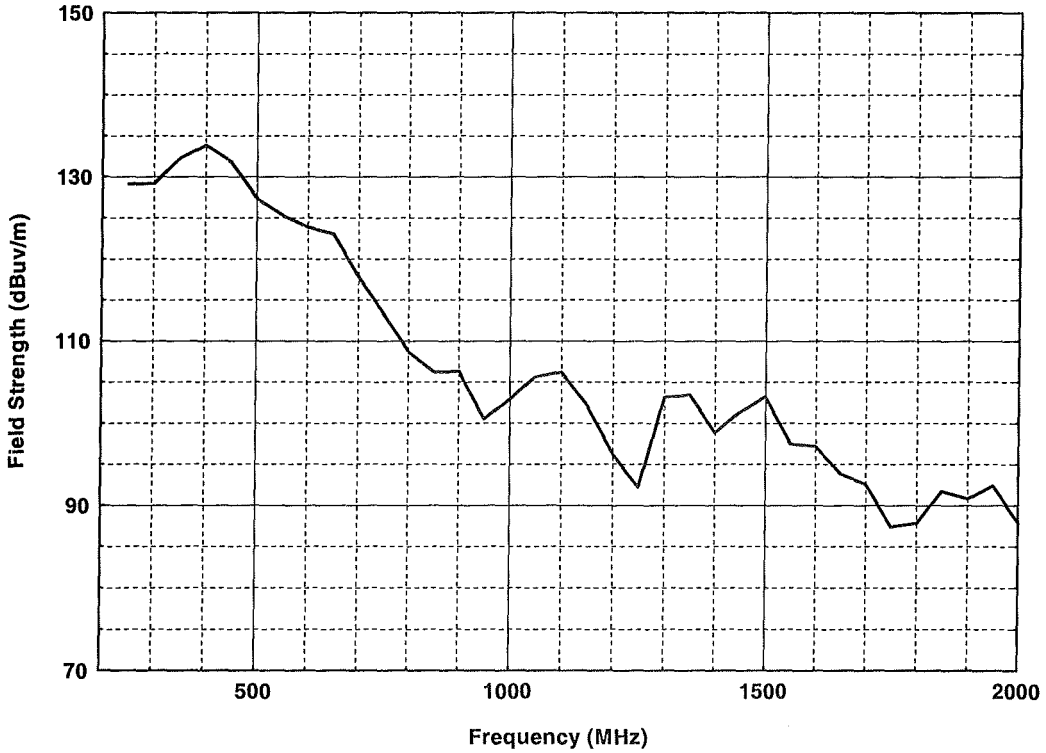

Figure D.E.2. Device E, (300 MHz) radiated peak field strength at 1 m, $\Delta f = 49.99$ MHz.

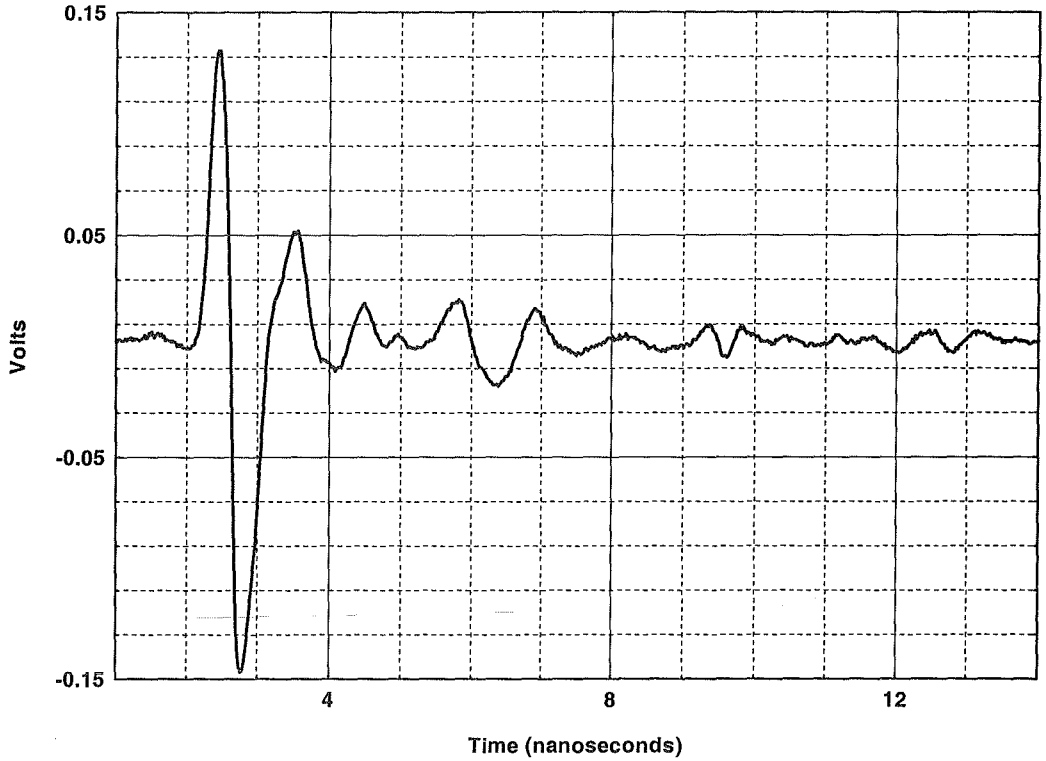

Figure D.E.3. Device E, (900 MHz) radiated time-domain waveform.

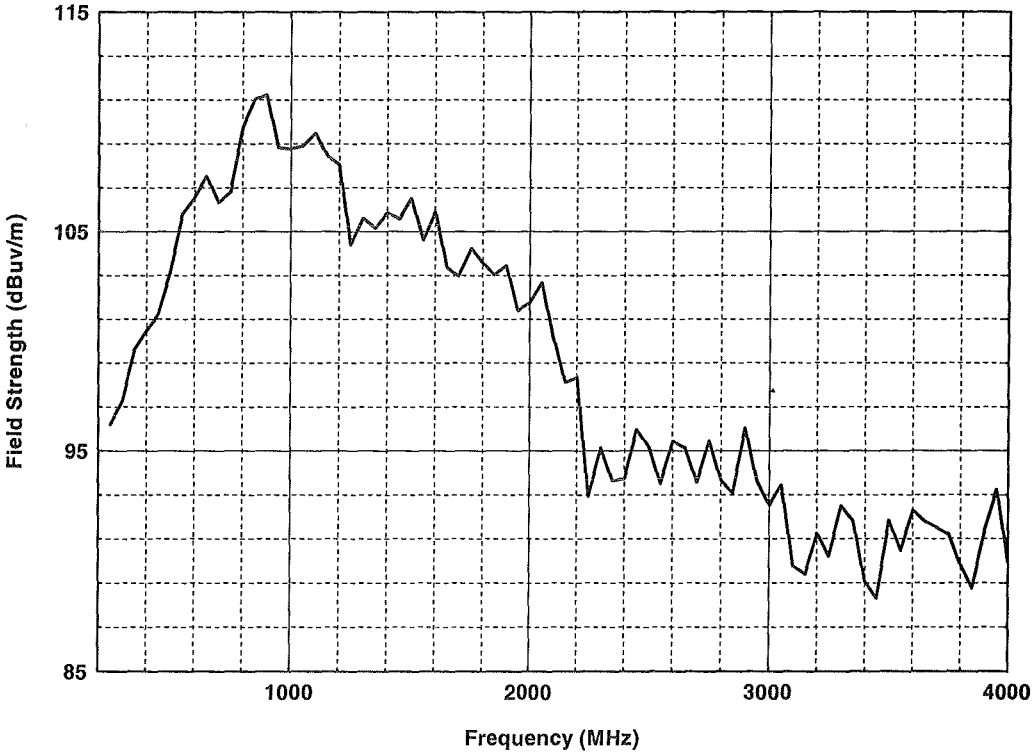

Figure D.E.4. Device E, (900 MHz) radiated peak field strength at 1 m, $\Delta f = 49.99$ MHz.

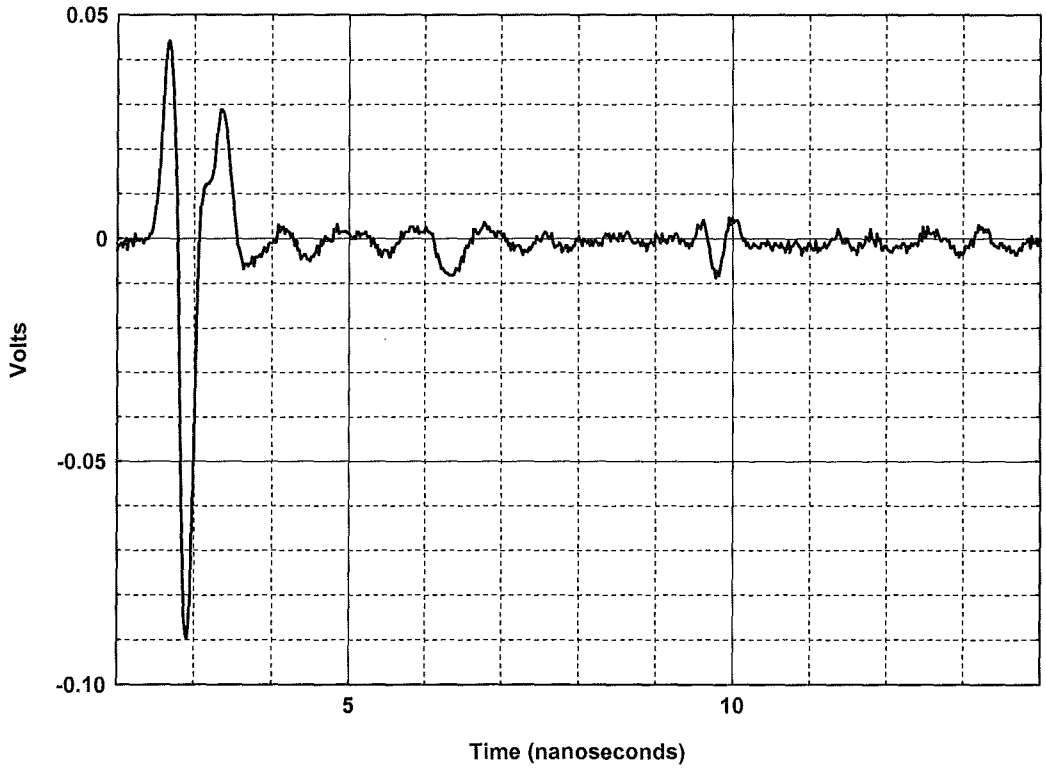

Figure D.E.5. Device E, (1500 MHz) radiated time-domain waveform.

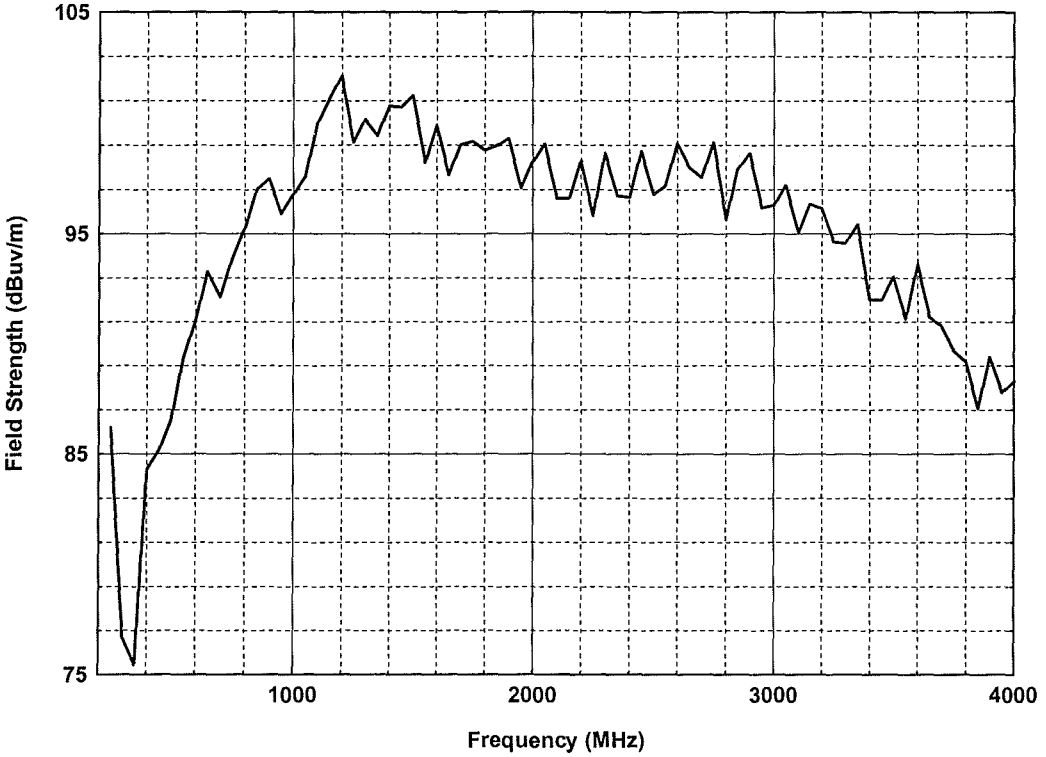

Figure D.E.6. Device E, (1500 MHz) radiated peak field strength at 1 m, $\Delta f = 49.99$ MHz.

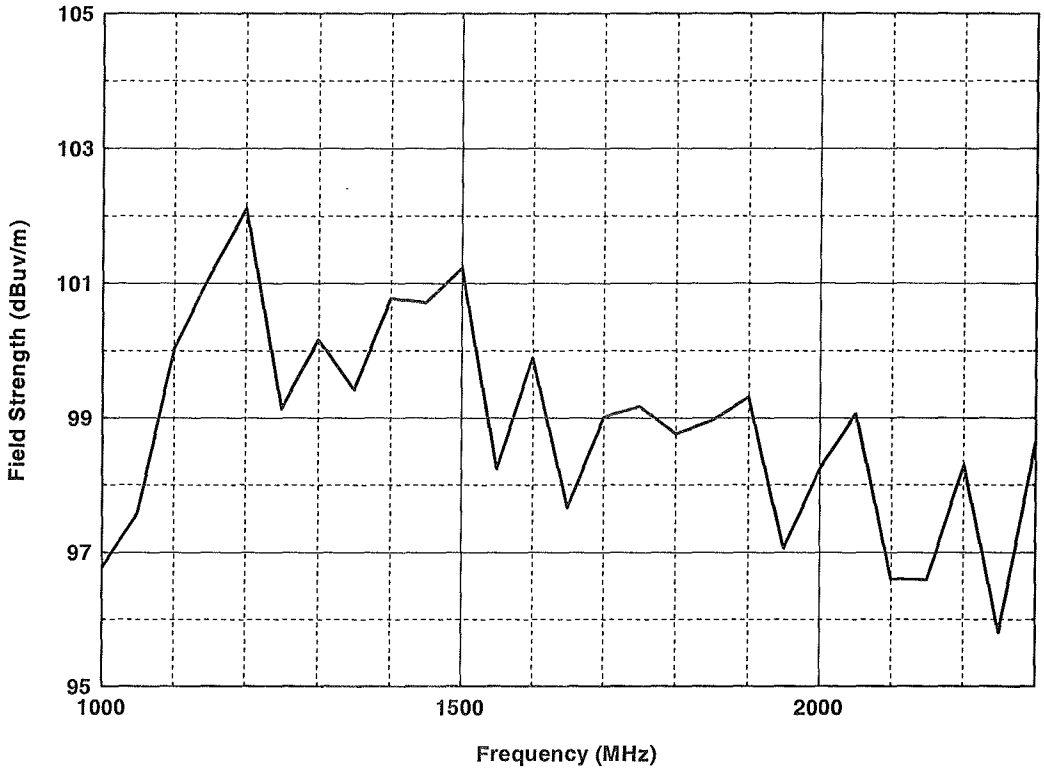

Figure D.E.7. Device E, (1500 MHz) radiated peak field strength at 1 m, $\Delta f = 49.99$ MHz.

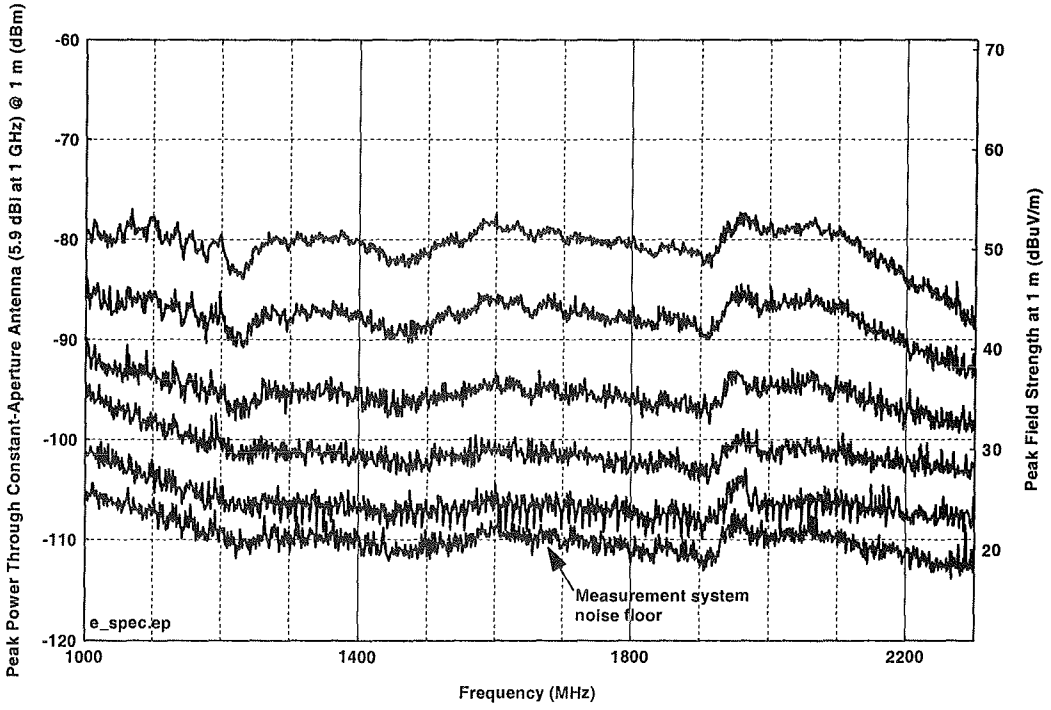

Figure D.E.8. Device E, (1500 MHz head) spectra as a function of measurement bandwidth.

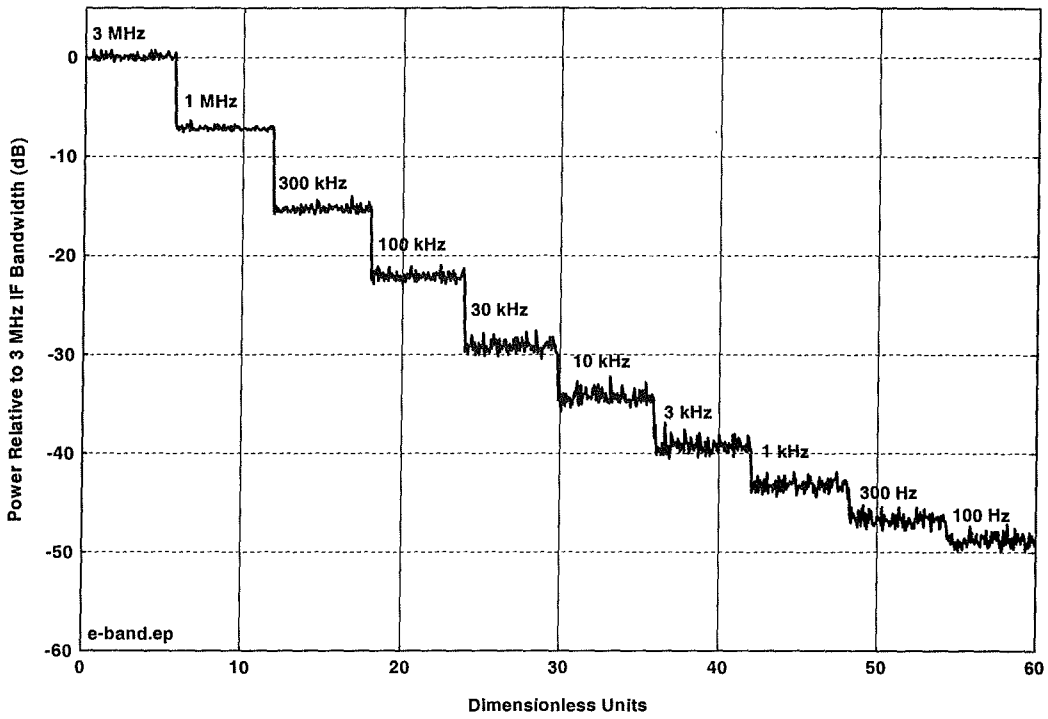

Figure D.E.9. Device E, power as a function of measurement bandwidth stairstep.

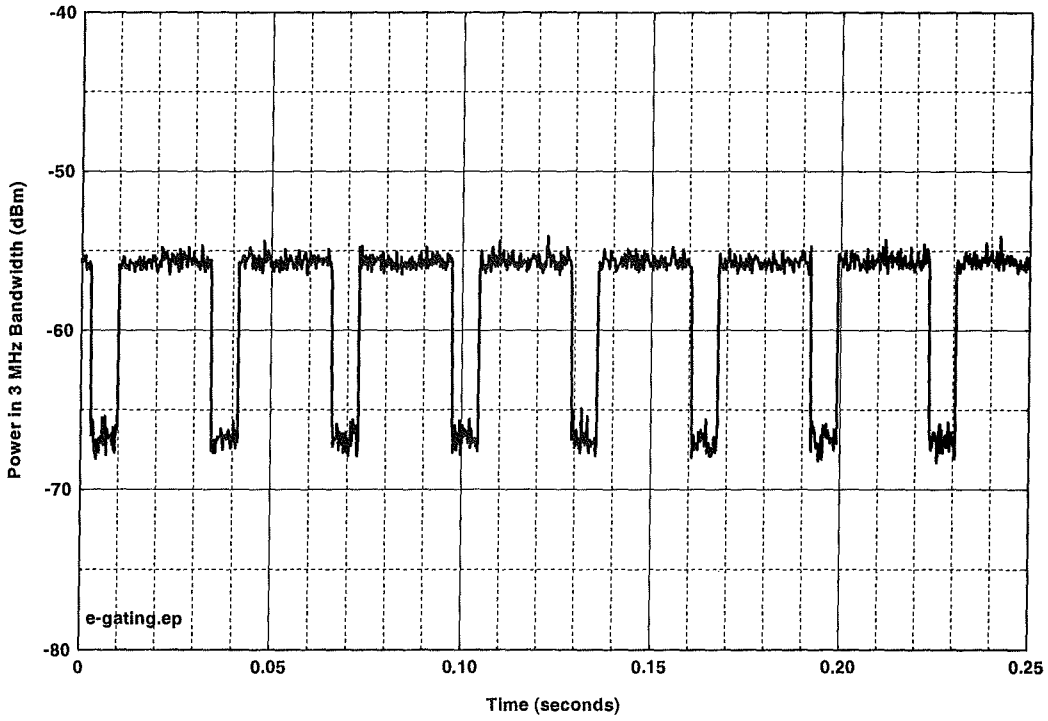

Figure D.E.10. Device E, gating behavior.

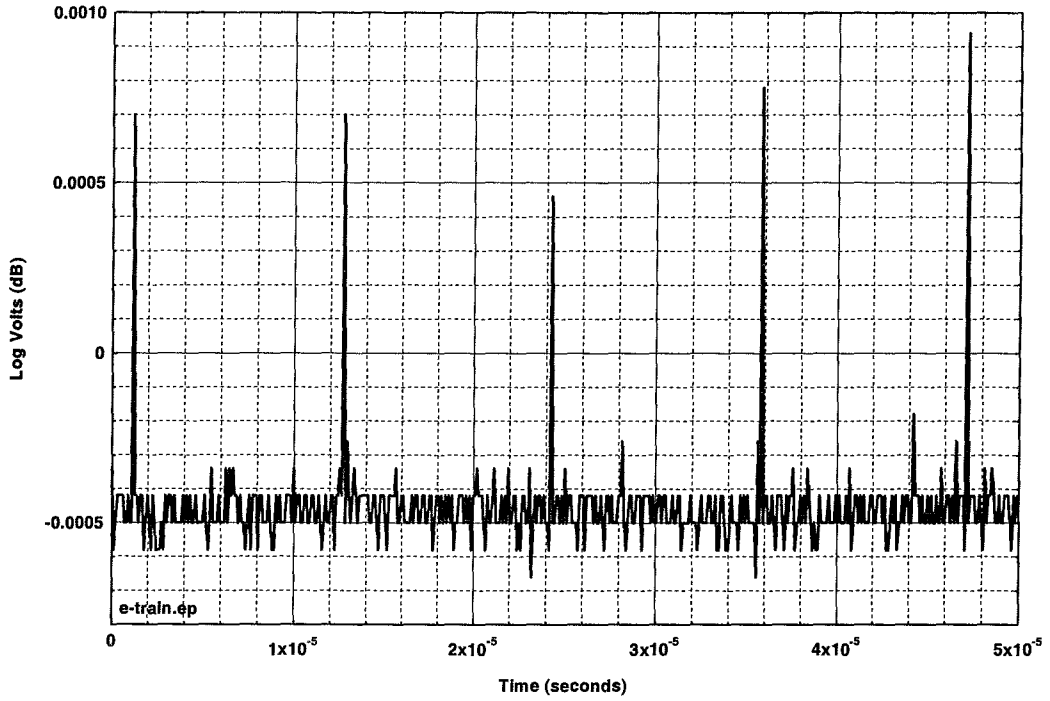

Figure D.E.11. Device E, pulse train.

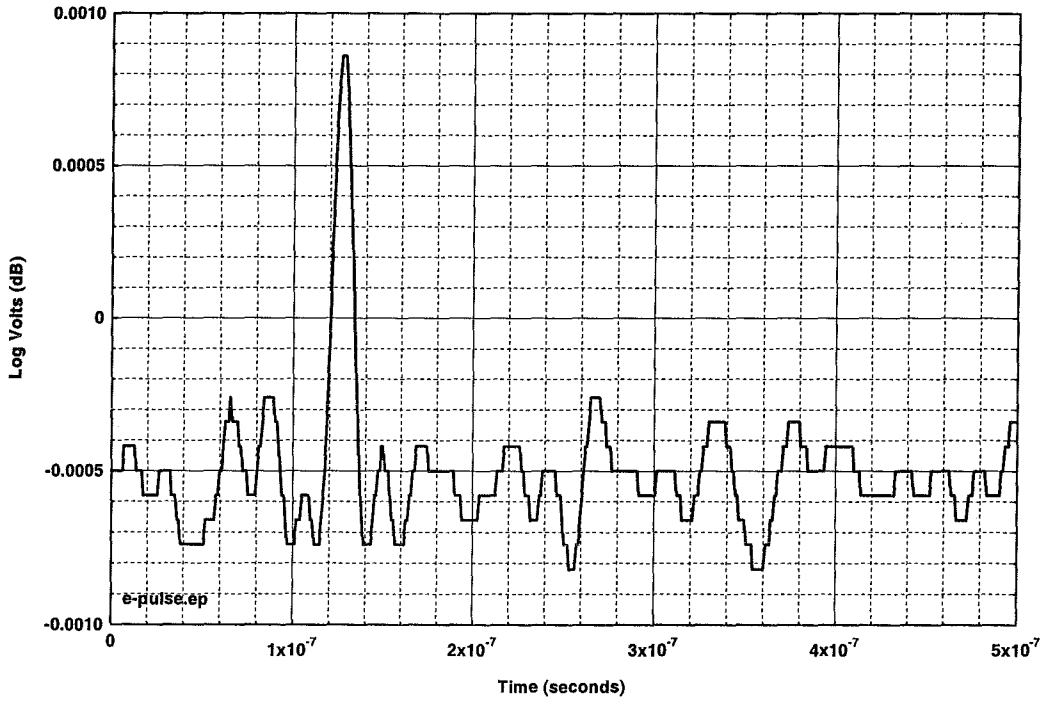

Figure D.E.12. Device E, individual pulse (bandwidth-limited at 50 MHz).

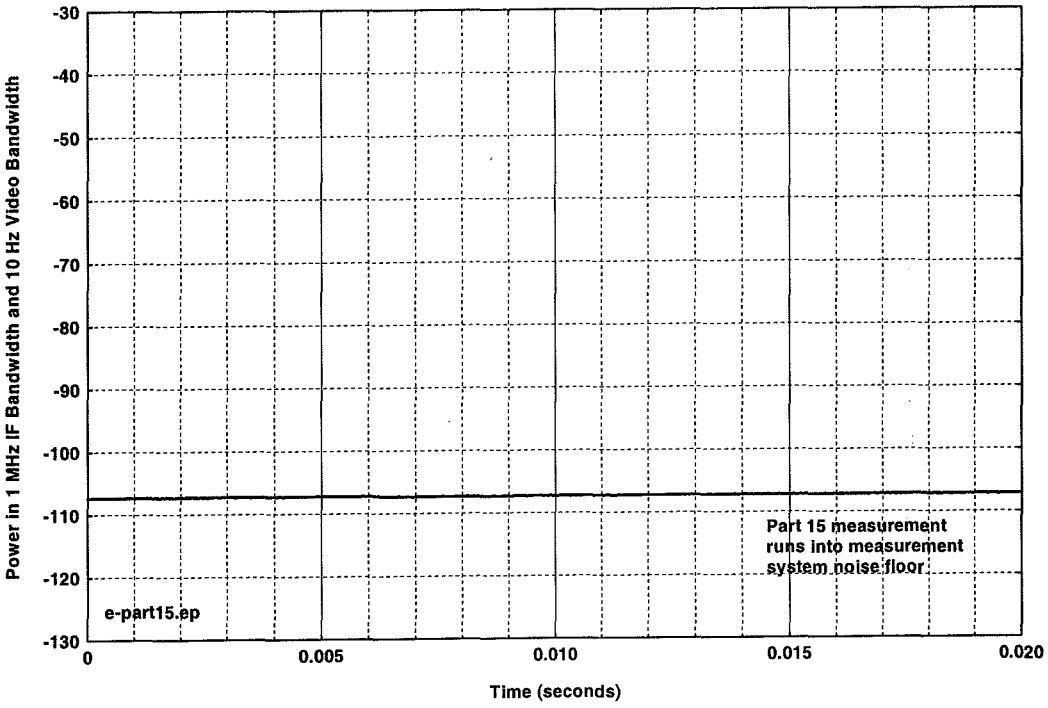

Figure D.E.13. Device E, Part 15 measurement.

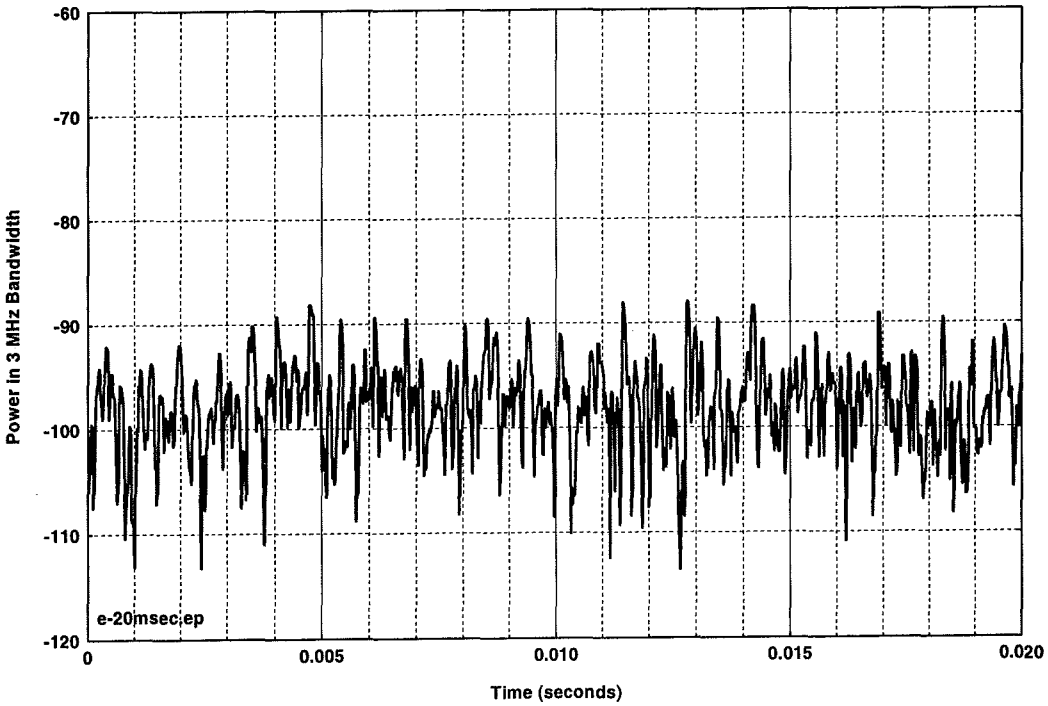

Figure D.E.14. Device E, 20-msec time waveform.

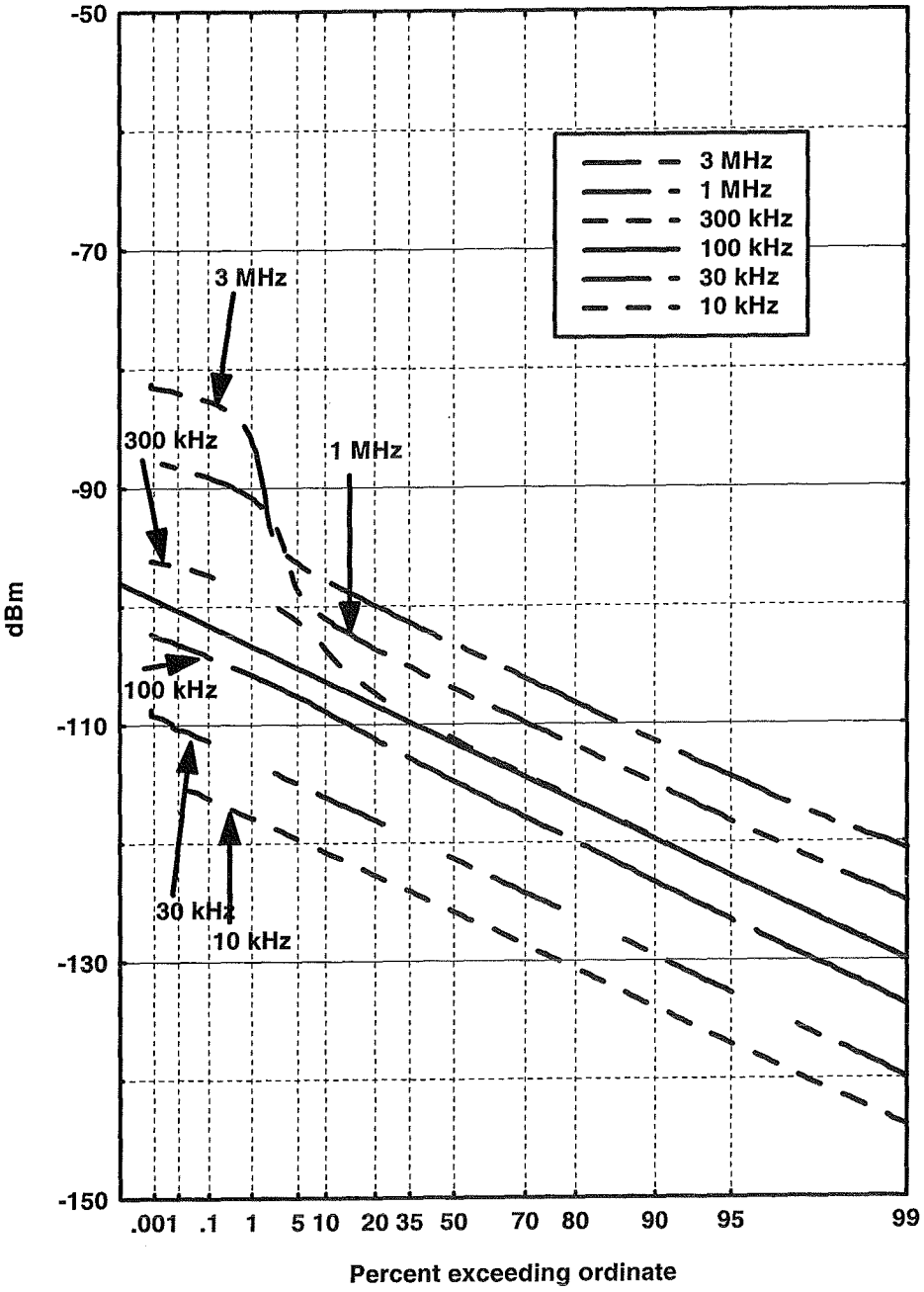

Figure D.E.15. Device E, APDs.

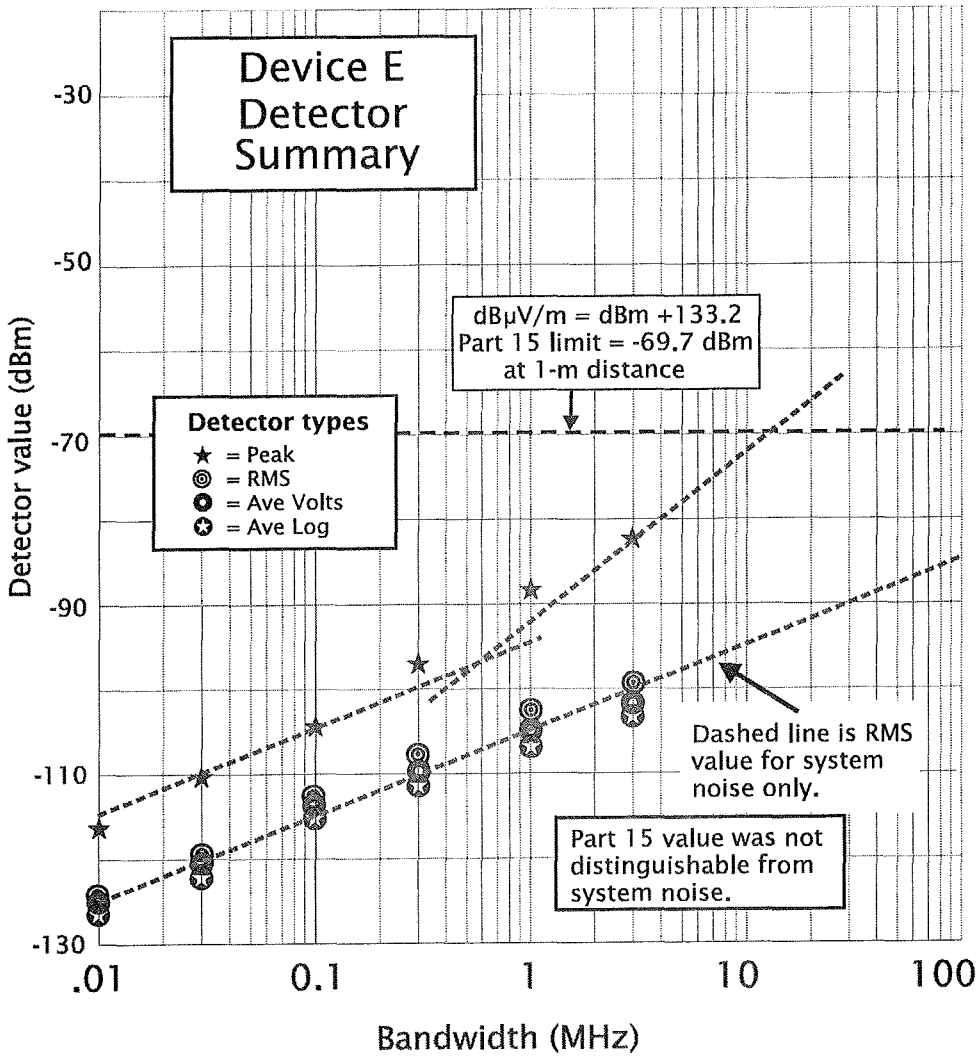

Figure D.E.16. Device E, detector summary.

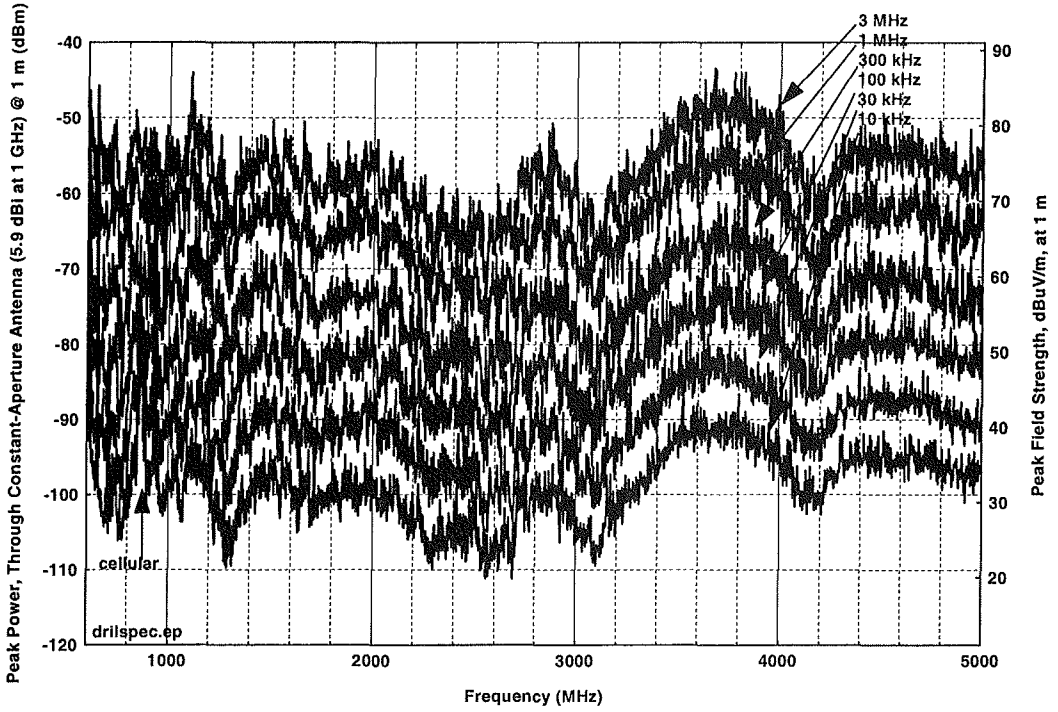

Figure D.F.1. Electric drill, emission spectrum as a function of bandwidth.

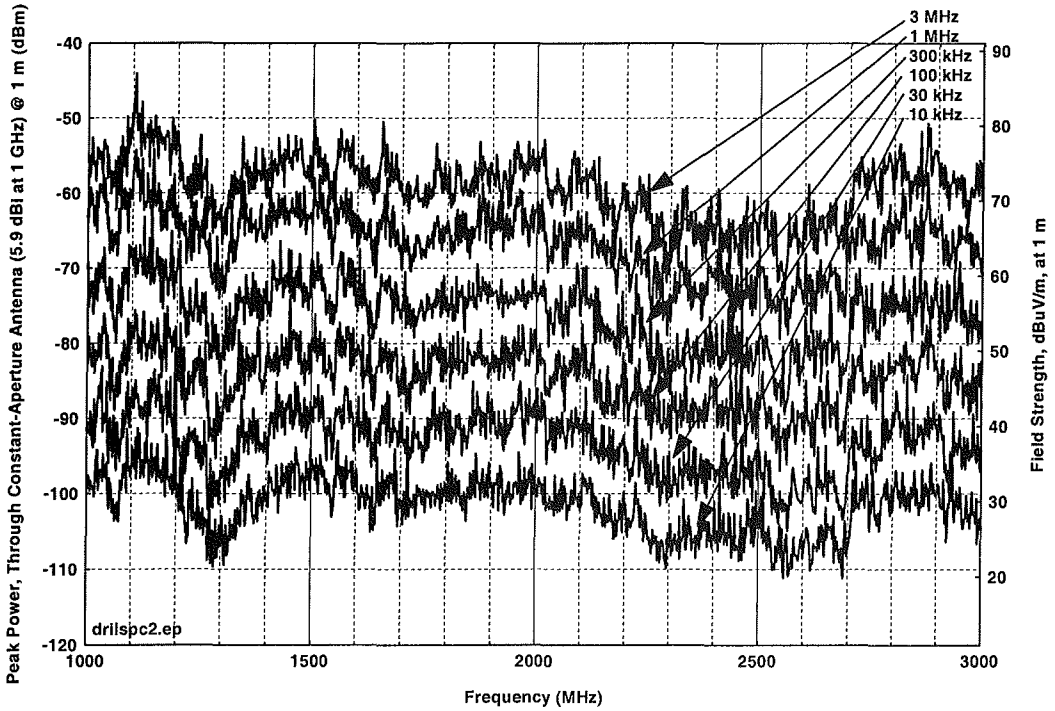

Figure D.F.2. Electric drill, emission spectrum from 1-3 GHz as a function of bandwidth.

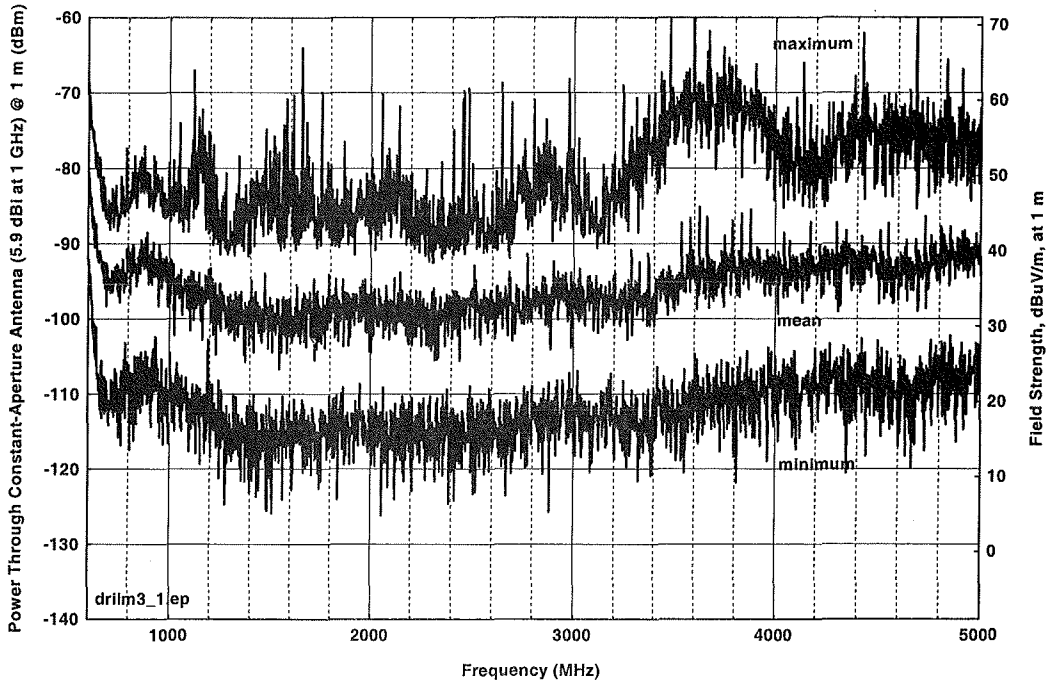

Figure D.F.3. Electric drill, sample-detected electric drill spectrum, 3 MHz bandwidth, max, mean, and min curves.

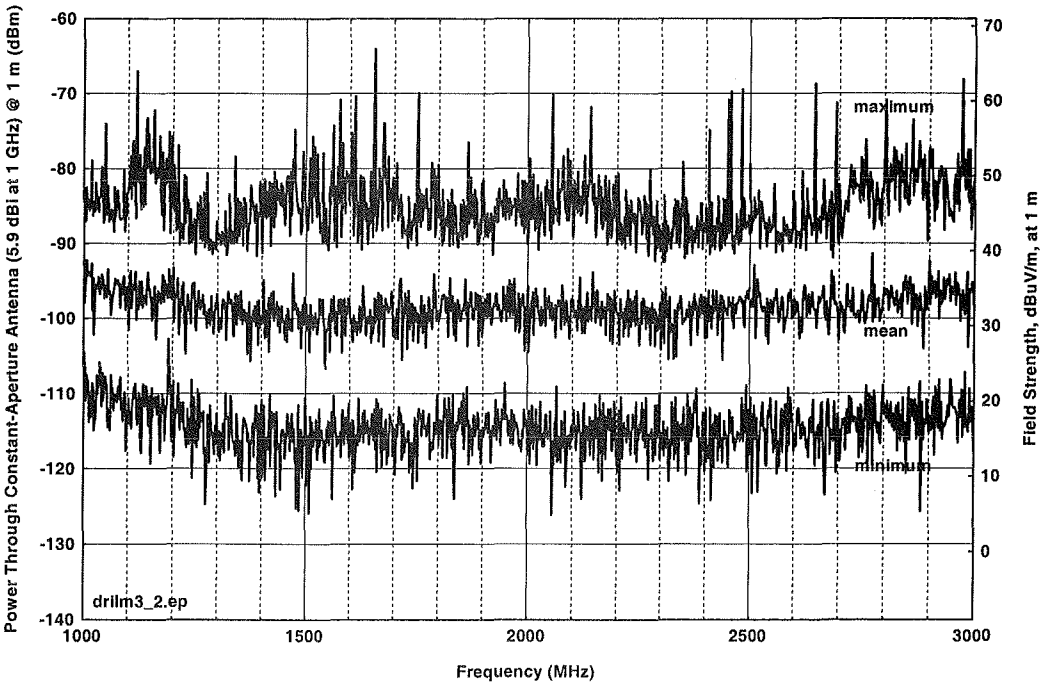

Figure D.F.4. Electric drill, sample-detected electric drill spectrum, 3 MHz bandwidth, max, mean, and min curves.

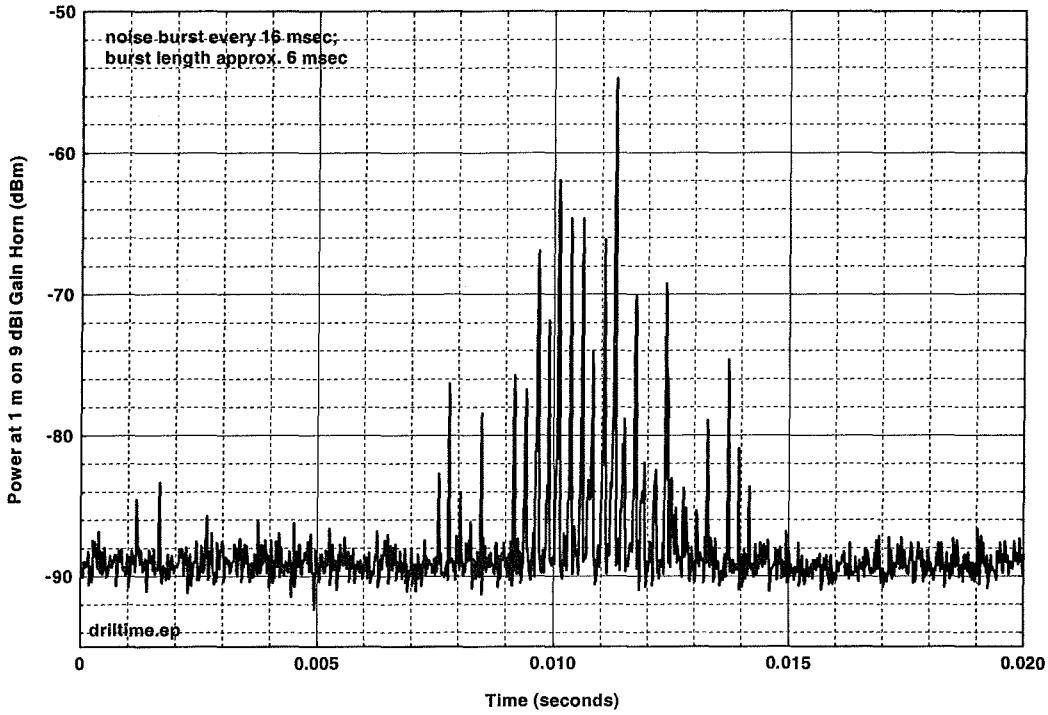

Figure D.F.5. Electric drill, time waveform in 3 MHz bandwidth, sample detected, for 20 msec.

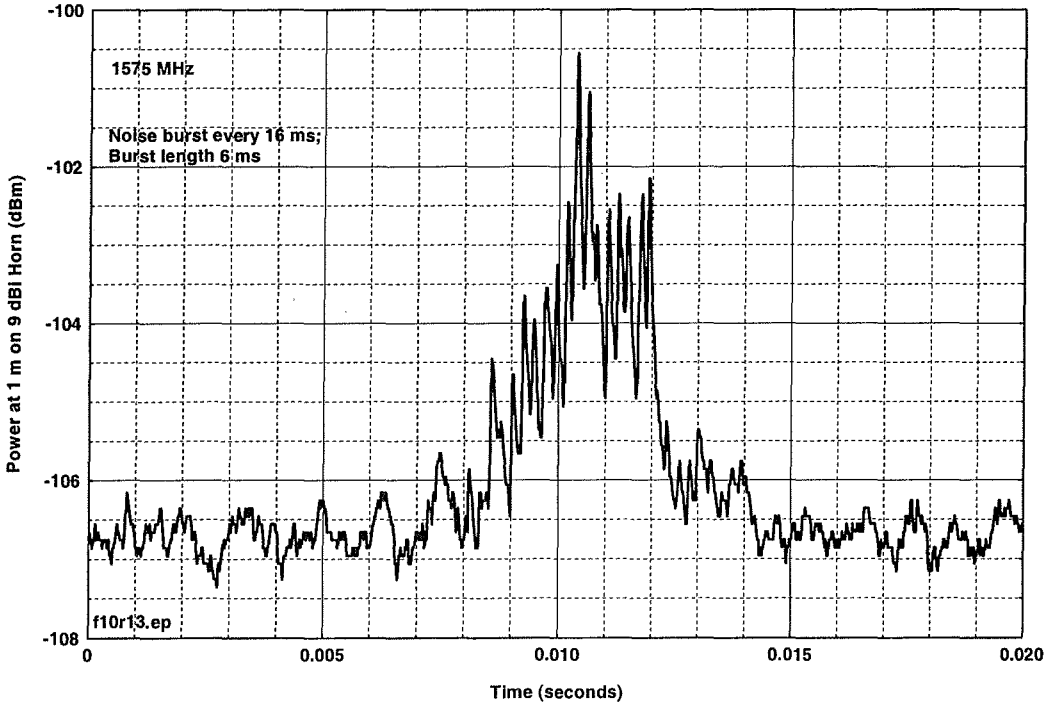

Figure D.F.6. Electric drill, Part 15 measurement, 1-MHz IF bandwidth, 1-kHz video bandwidth.

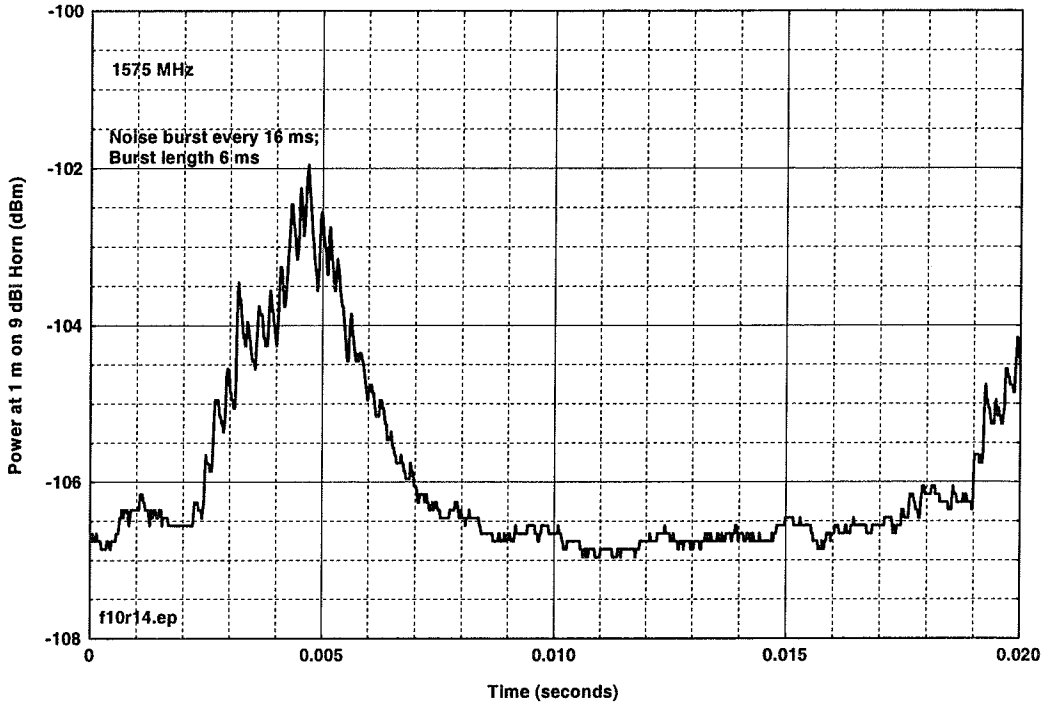

Figure D.F.7. Electric drill, Part 15 measurement, 1-MHz IF bandwidth, 300-Hz video bandwidth.

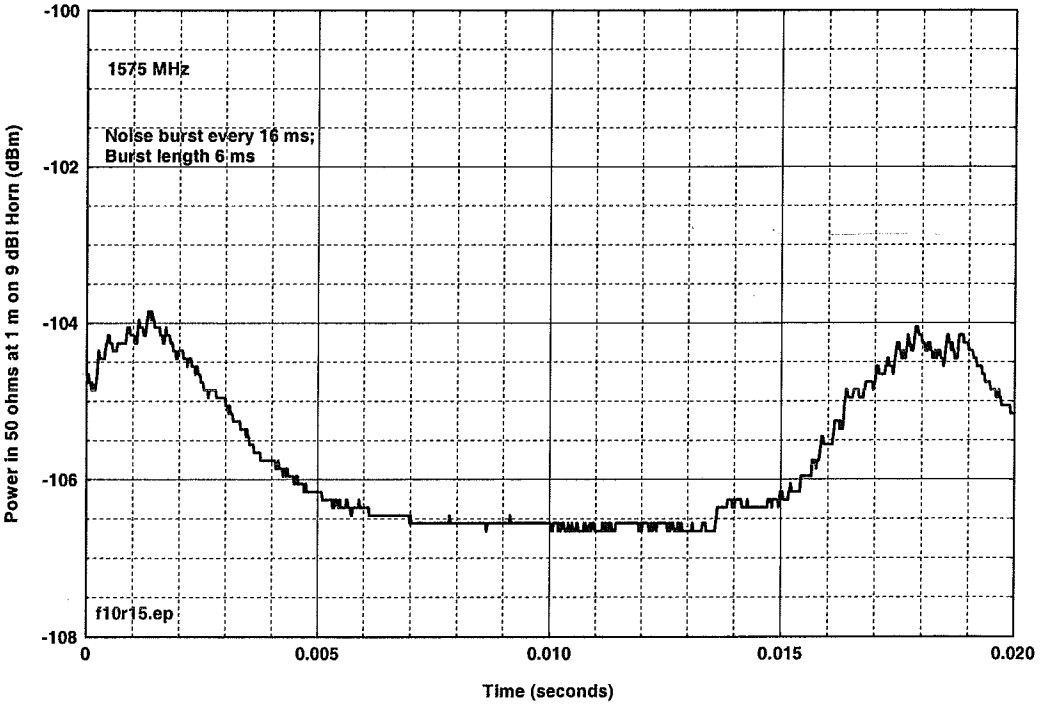

Figure D.F.8. Electric drill, Part 15 measurement, 1-MHz IF bandwidth, 100-Hz video bandwidth.

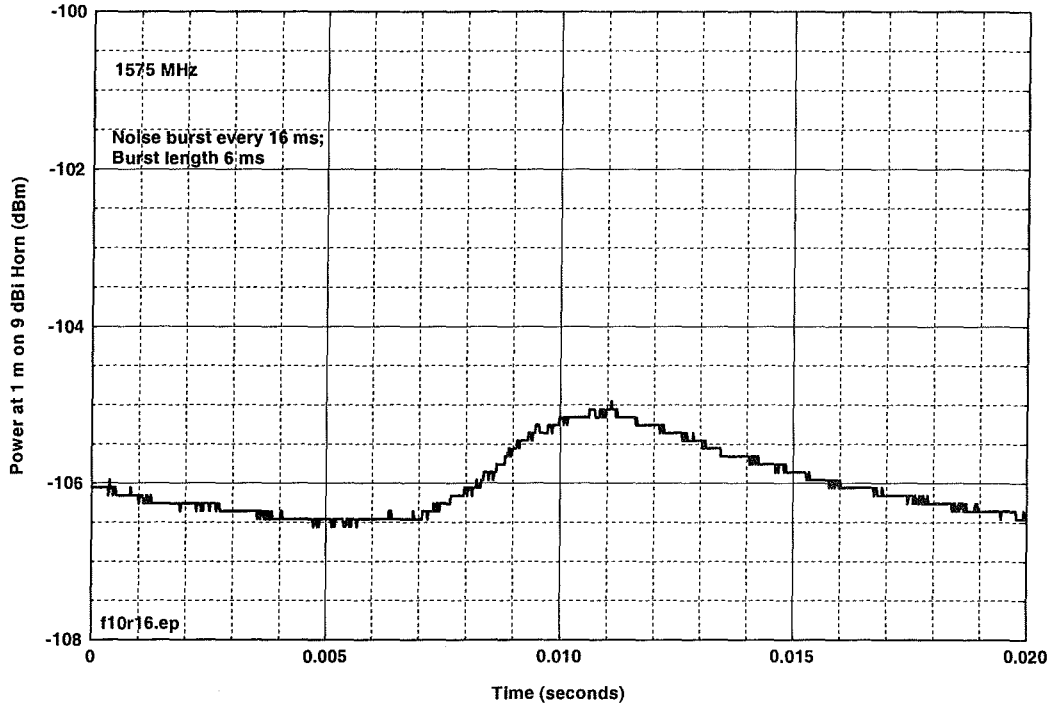

Figure D.F.9. Electric drill, Part 15 measurement, 1-MHz IF bandwidth, 30-Hz video bandwidth.

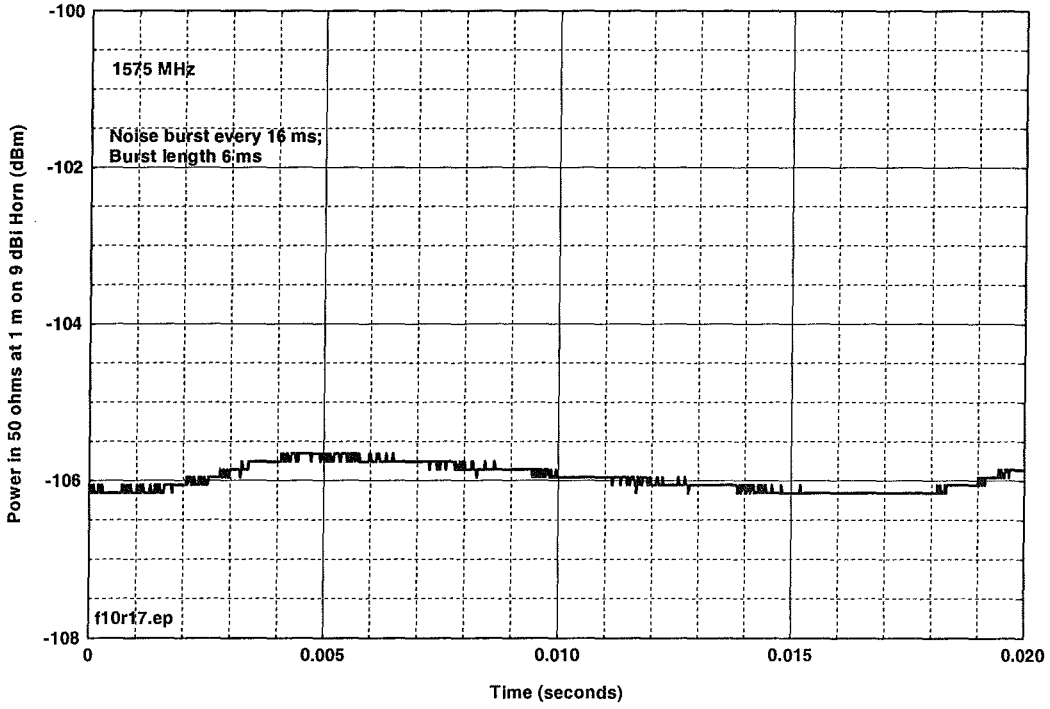

Figure D.F.10. Electric drill, Part 15 measurement, 1-MHz IF bandwidth, 10-Hz video bandwidth.

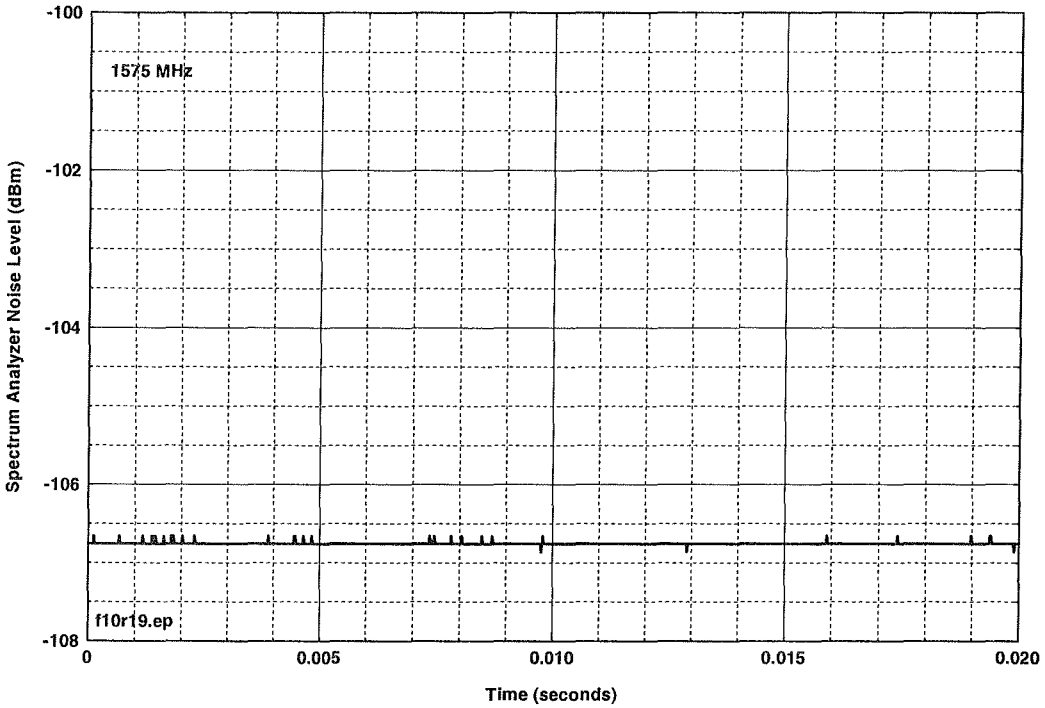

Figure D.F.11. Electric drill, terminated spectrum analyzer input with 1-MHz IF bandwidth, 10-Hz video bandwidth.

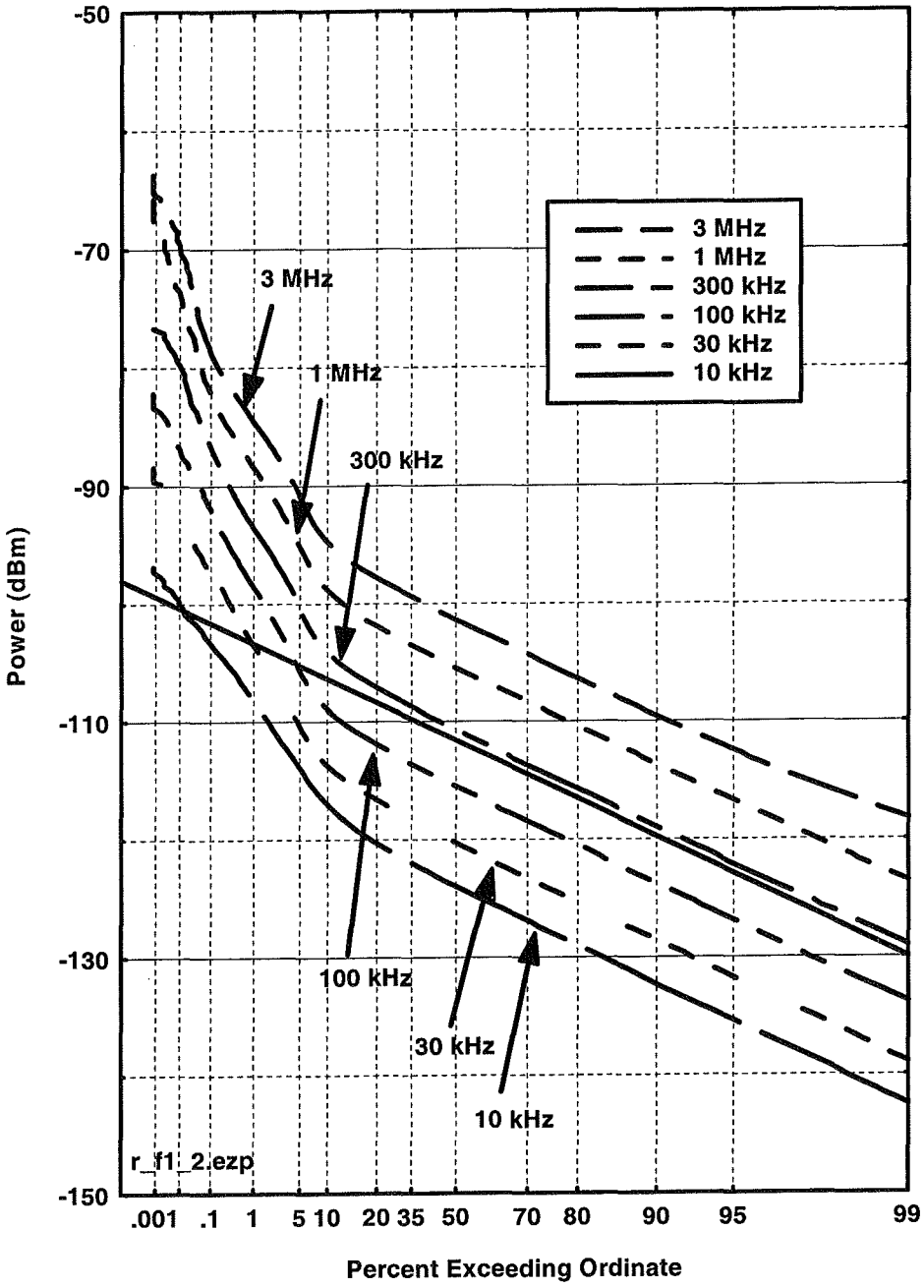

Figure D.F.12. Electric Drill, APDs.

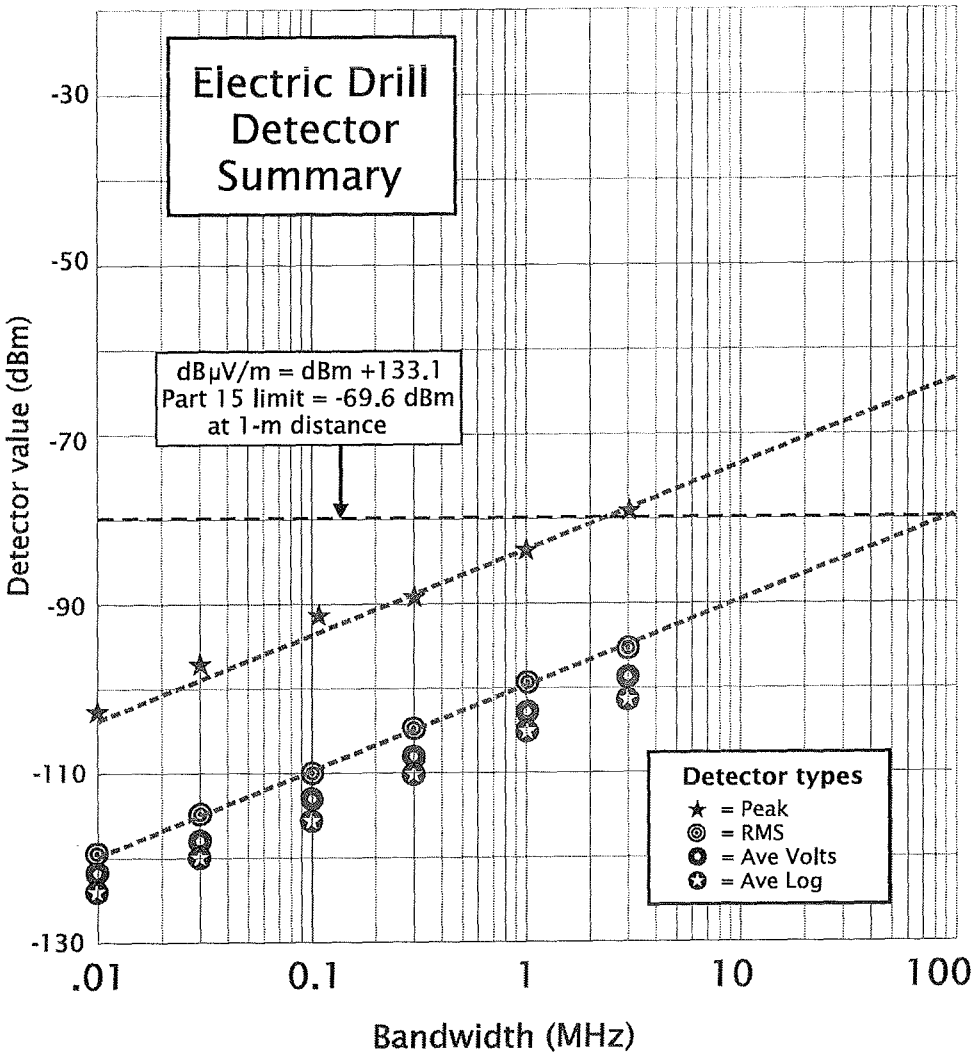

Figure D.F.13. Electric Drill, detector summary.

APPENDIX E. SUMMARY OF AGGREGATE MEASUREMENTS

Frank Sanders[1]

Device description. A pair of UWB pulsers were procured by ITS and operated for the purpose of assessing the emission levels in various IF bandwidths as a function of nominal pulse repetition rate (PRR), dither, and the number of pulsers in an aggregate. These pulsers produce UWB impulses at times precisely controlled by signals from an arbitrary waveform generator. Therefore, these pulsers can be controlled to provide a wide range of PRR, dither, and gating combinations, depending on the programming of the arbitrary waveform generators. An independent (and non-synchronized) generator was used to control each pulser.

Figure E.1 shows the measurement system used for the aggregate measurements.

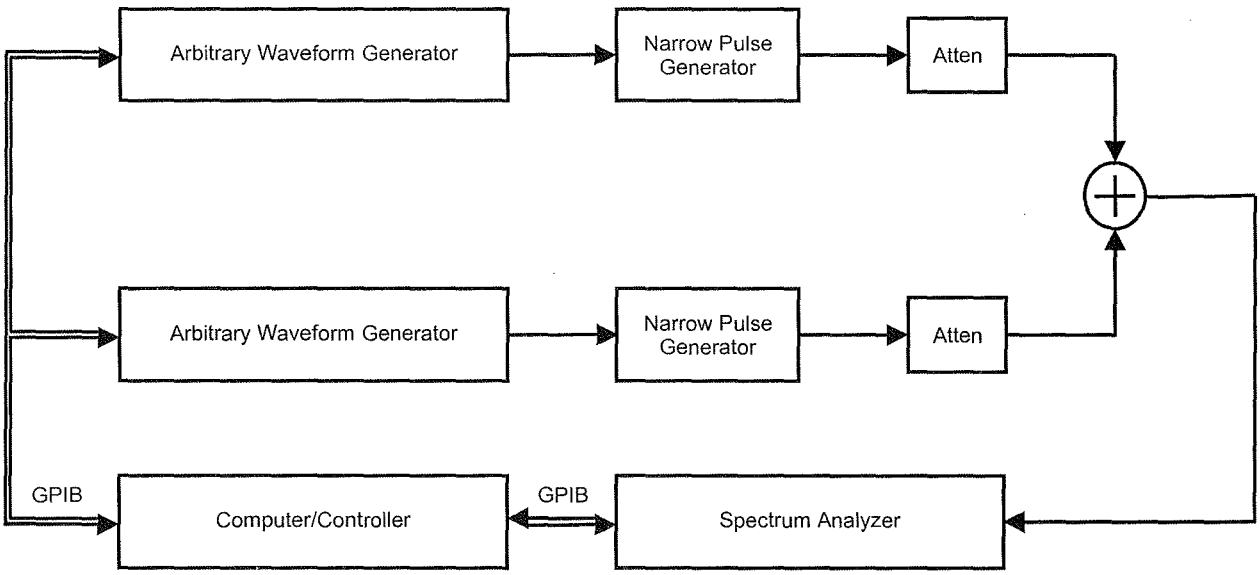

Figure E.1. Aggregate measurements block diagram.

Arbitrary waveform generators were programmed to give average PRRs of 100 kHz and 10 MHz, 50% dithered or non-dithered. This dithering is based on delay relative to a fixed time base. When both pulsers were in use, their respective wideband peak amplitudes were matched to within 0.2 dB.

---

[1]The author is with the Institute for Telecommunication Sciences, National Telecommunications and Information Administration, U.S. Department of Commerce, Boulder, CO 80305.

Measurement comments. The general technique for investigating aggregate UWB signals was to independently measure APDs from each of two UWB sources, then combine the UWB sources and measure an APD from the combined sources. This technique was followed for all of the aggregate measurements, with the only variable being the modulation parameters of two UWB signals.

Figures E.2 and E.3 show the wide range peak emission spectra of single pulsers using a 100-kHz PRR and 50% dithering, and a 10-MHz PRR and 50% dithering, respectively. Figure E.4 shows the peak bandwidth progression for a pulser with 10 MHz PRR and 50% dithering.

Figure E.5 shows video-averaged measurements for a single dithered pulser (10 MHz PRR, 50% dither) and for two such pulsers. The measured signal for two pulsers increased 2.6 dB over the level for a single pulser. This falls within the precision of the measurement for the expected 3-dB increase.

Figure E.6 shows APDs measured in a 1-MHz bandwidth for a single pulser and two pulsers. Each pulser produced a signal with10-MHz PRR and 50% dither. The APDs for the individual pulsers appeared Gaussian. The APD for the two pulsers also appeared Gaussian, but was raised about 3 dB from the individual pulser APD, as theory predicts.

Figure E.7 shows APDs measured in a 1-MHz bandwidth for a single pulser and two pulsers. Each pulser produced a non-dithered signal with 100-kHz PRR. The two-pulser APD shows a stepped high-amplitude plateau, where the lower step is equal in amplitude to the single pulser APD, but with about 1.5-2 times the percentage duration (depending on what amplitude is used to compare the duration). In addition, there is a very-small-percentage step that is about 6 dB higher than the single pulser maximum amplitude, which is consistent with impulses from the two pulsers occasionally overlapping and combining coherently.

Figure E.8 shows a 1-MHz APD that was derived from the combination of one pulser with 10-MHz PRR (dithered) and one pulser with 100-kHz PRR (non-dithered). The APD shows an approximately Gaussian character, which should be expected considering that the non-dithered 100-kHz pulser produced only 1% as many impulses as the 10-MHz dithered pulser.

Figure E.9 shows APDs measured in a 1-MHz bandwidth for a single pulser and two pulsers. Each pulser produced a signal with 100-kHz PRR and 50% dithering. Since the UWB pulses remain non-overlapping in the 1-MHz bandwidth, the resulting APDs are identical to the APDs measured in Figure E.7.

Table E.1 shows the detector values for the various APDs.

Table E.1 - Detector Values for Aggregate Tests

Figure	Source	PRR	Dither	Avg Log	Avg volt	RMS	Peak
Figure E.6	#1	10 MHz	50%	-49.2	-47.9	-46.9	-39
	#2	10 MHz	50%	-49.2	-47.9	-46.9	-39
	#1 & #2	- - -	- - -	-46.5	-45.1	-44.1	-36.5
Figure E.7	#1	100 kHz	none	-87.2	-76.6	-67.9	-54
	#2	100 kHz	none	-87.2	-76.6	-67.9	-54
	#1 & #2	- - -	- - -	-84.1	-72.1	-65.2	-49
Figure E.8	#1	10 MHz	50%	-49.2	-47.9	-46.9	-39
	#2	100 kHz	none	-87.2	-76.6	-67.9	-54
	#1 & #2	- - -	- - -	-49.2	-47.9	-46.9	-39
Figure E.9	#1	100 kHz	50%	-86.9	-76.6	-67.9	-54
	#2	100 kHz	50%	-86.9	-76.6	-67.9	-54
	#1 & #2	- - -	- - -	-84.0	-72.1	-65.2	-49

The measurement results can be summarized as follows:

1. Noise-like signals with Gaussian APD characteristics (10-MHz PRR, 50% dither) add together to give noise-like signals with Gaussian APD characteristics (Figure E.6). All detector values increased by approximately 3 dB when two equal UWB Gaussian signals were added.

2. A noise-like signal with Gaussian APD characteristics added to a weaker (20 dB weaker) impulsive signal produced a signal with a Gaussian APD characteristic (Figure E.8). The difference in detector values was not apparent, though this may have been caused by limited measurement system resolution.

3. Impulsive signals added to impulsive signals (Figures E.7 and E.8) produced APDs that were less impulsive that the original signals. Dithering of signals in an impulse environment (i.e., measurement bandwidth greater than the combined PRR) produced similar results to non-dithered signals. The combined signals produced APDs with approximately twice the total percentage pulse duration as the original pulses at the same amplitude, as well as a small percentage of pulses with amplitudes as much as 6 dB higher than the original pulses. The detector values were generally about 3 dB higher for the combined signals (except 6 dB increase for peak).

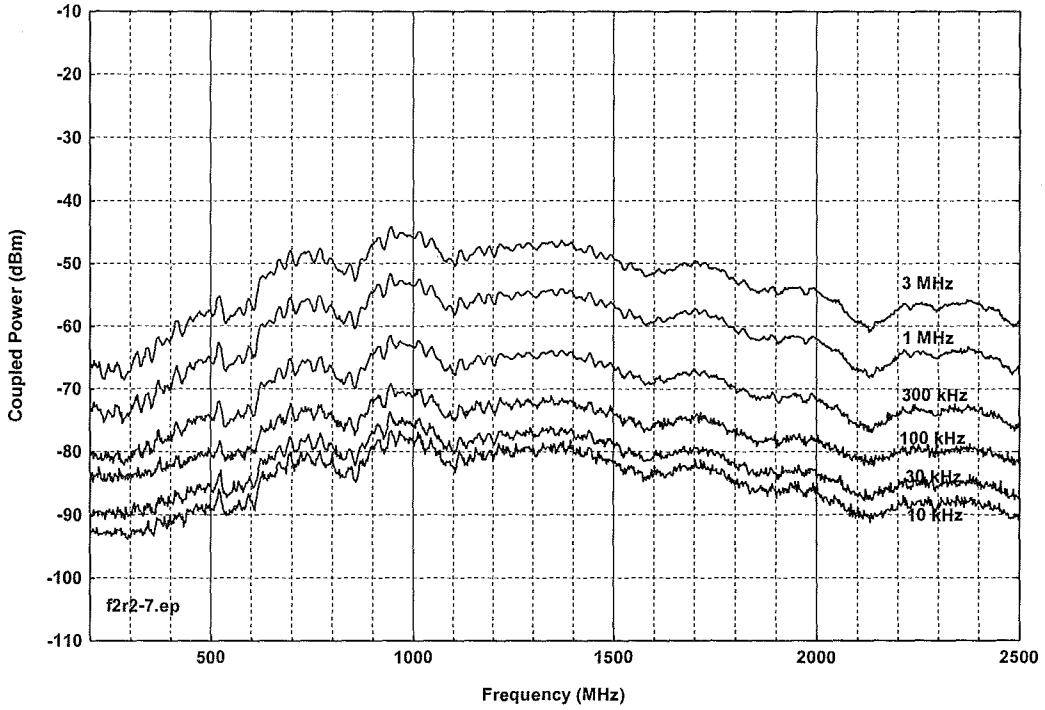

Figure E.2. Spectrum analyzer emissions spectra from 100-kHz PRR, 50% dither pulser.

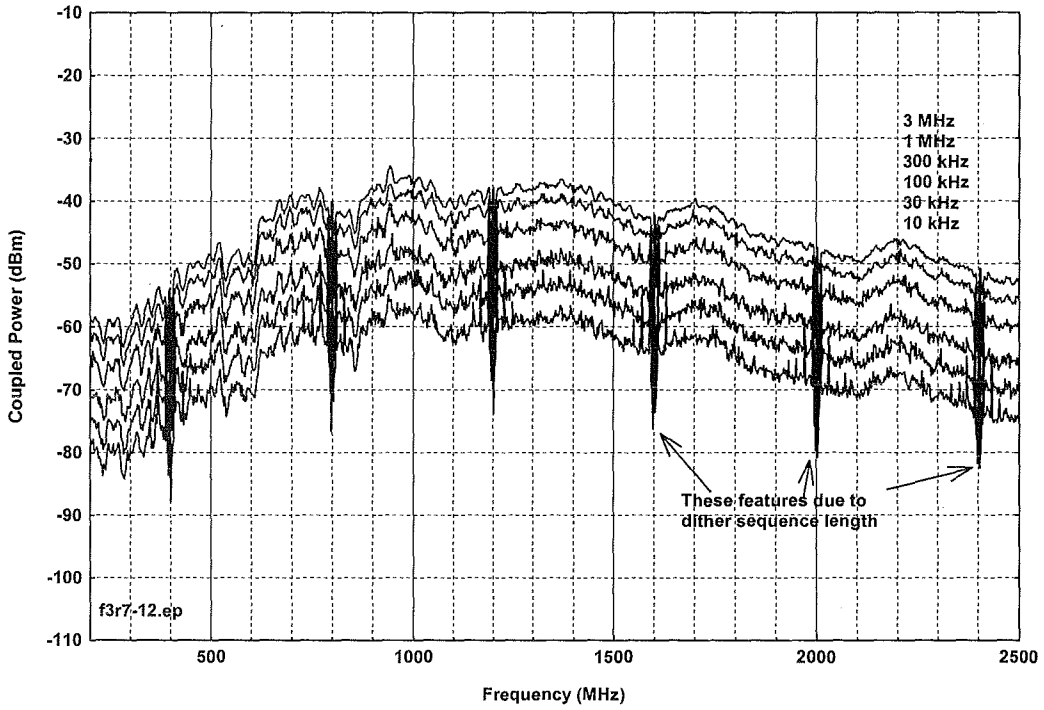

Figure E.3. Spectrum analyzer emission spectra from 10-MHz PRR, 50% dither pulser.

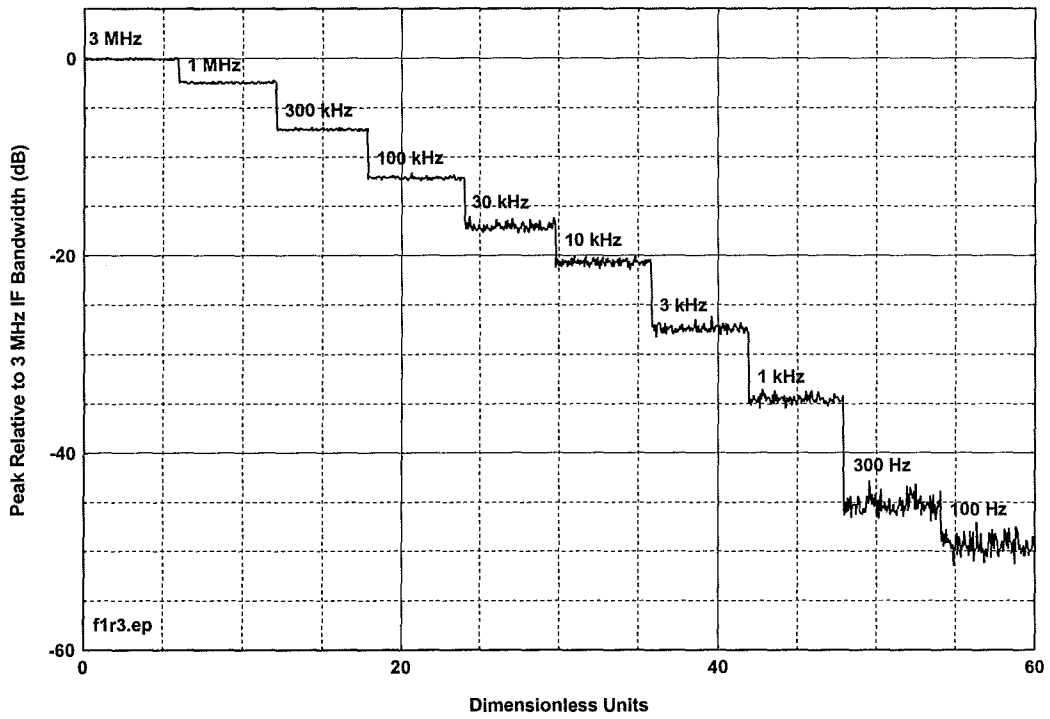

Figure E.4. Peak bandwidth progression stairstep for 10-MHz PRR, 50% dither pulser.

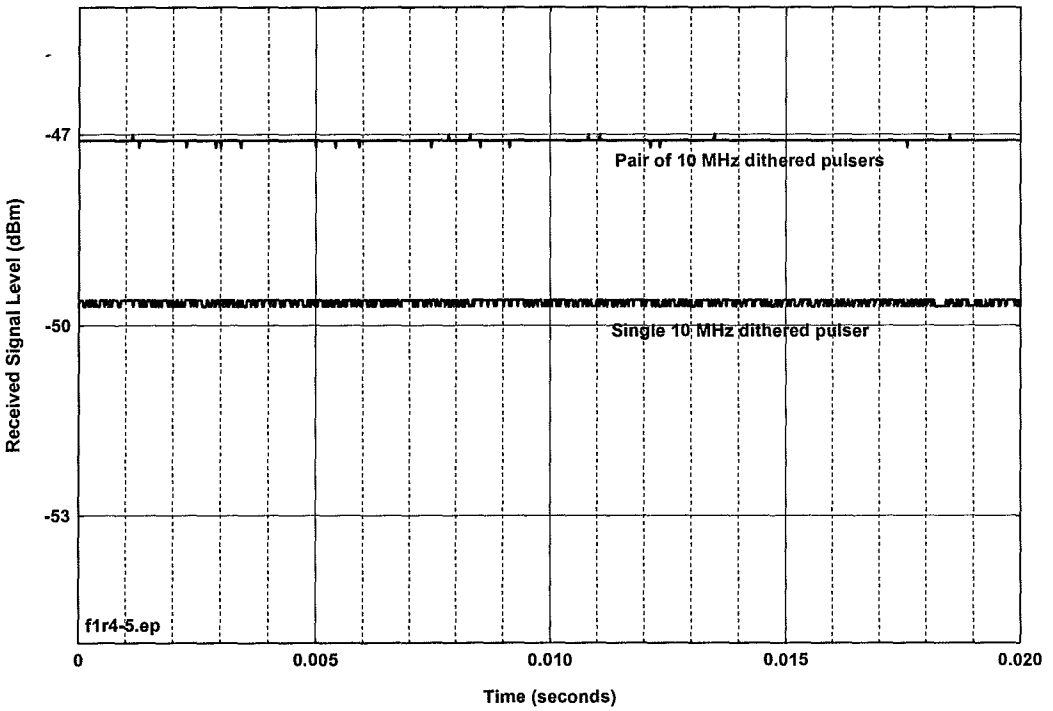

Figure E.5. Video signal from single and double pulsers, each at 10 MHz PRR, 50% dither.

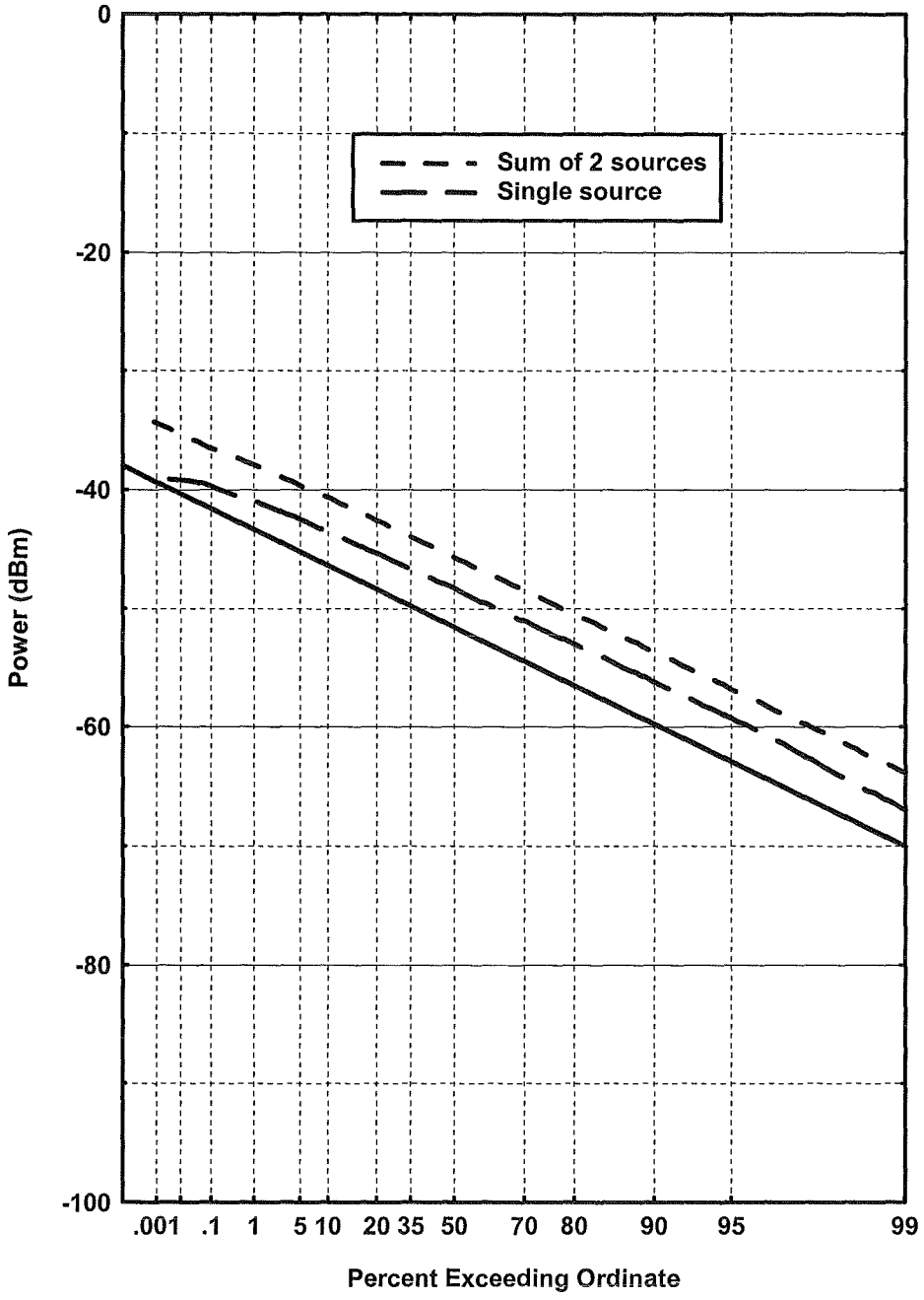

Figure E.6. 1-MHz APD for single and double 10-MHz, 50% dither pulser.

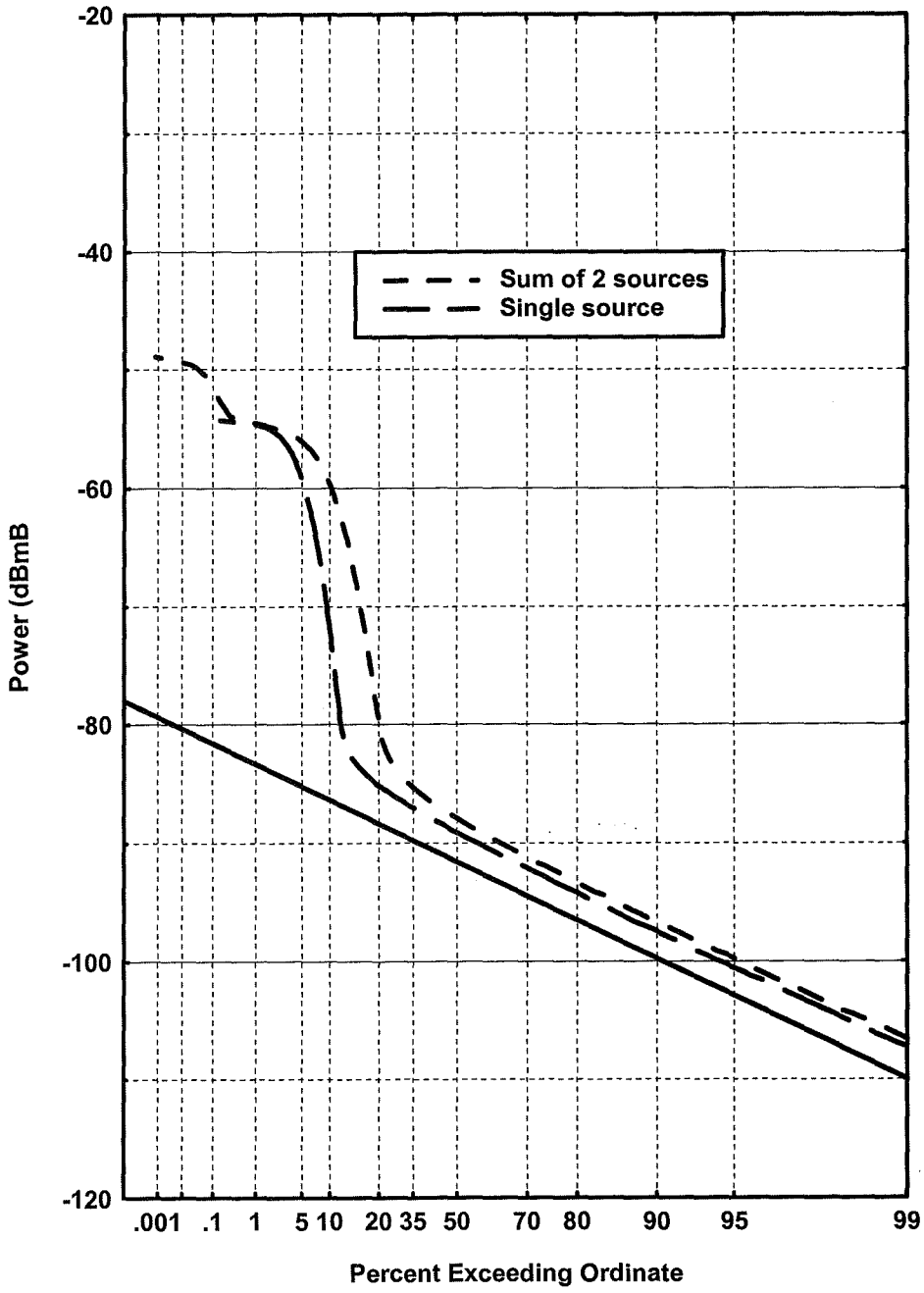

Figure E.7. 1-MHz APD for single and double 100-kHz PRR, non-dither pulsers.

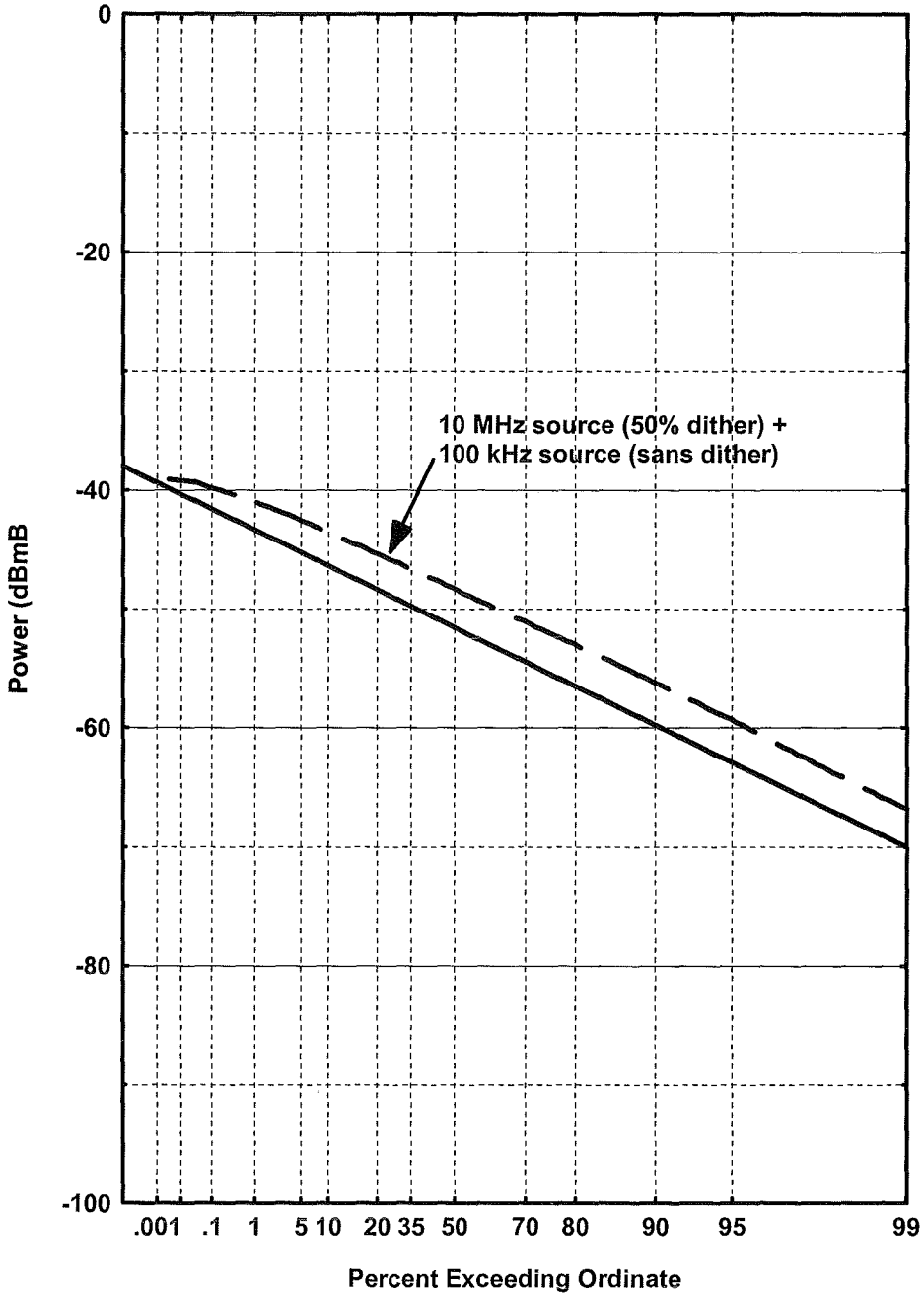

Figure E.8. 1-MHz APD for a 10-MHz PRR, 50% dither pulser and a 100-kHz, non-dithered pulser.

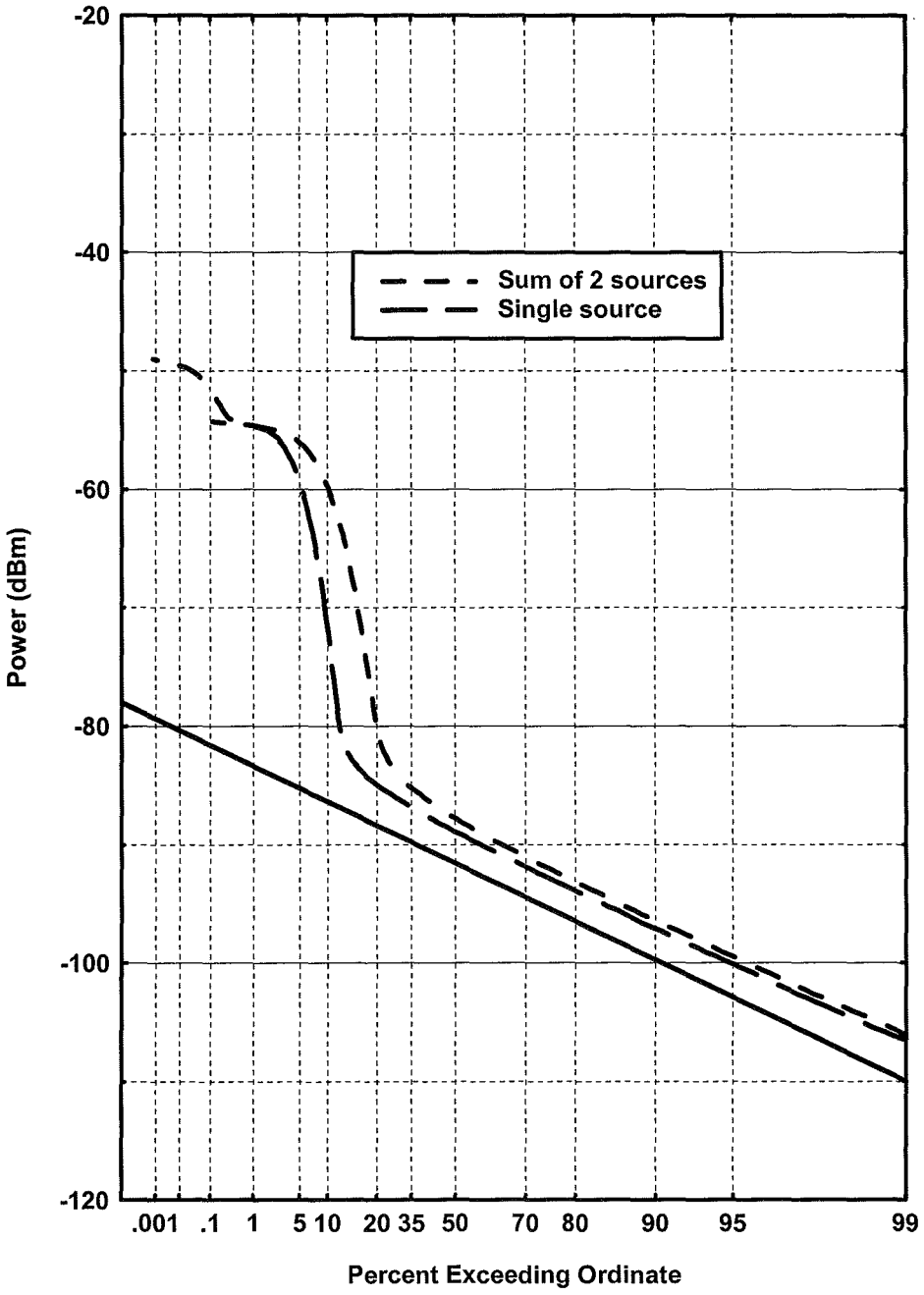

Figure E.9. 1-MHz APDs for single and double 100-kHz PRR 50% dithered pulsers.